Tissue engineering approaches to study biomechanical sensing in pseudoachondroplasia

Thais De Las Heras Ruiz

Thesis submitted for the degree of Doctor of Philosophy
Institute of Genetic Medicine
August 2020

Abstract

Articular cartilage is a dense and avascular tissue present at the ends of diarthrodial joints that protects the underlying bone from shear and compressive forces. Pseudoachondroplasia (PSACH) is a skeletal dysplasia resulting from mutations in cartilage oligomeric matrix protein (COMP), a large glycoprotein found in cartilage. The presence of mutant protein in the cartilage matrix affects tissue stability and mechanosensing, leading to early-onset OA, muscle weakness and tendon abnormalities, thus COMP mutations affecting the C-terminal domain represent a good model of musculoskeletal ageing. Cartilage disease and ageing studies are often hindered by the difficulty in obtaining human material and the use of costly animal models. The aim of this study was to create a model that could recapitulate this disease in a mechanosensing model for the very first time, that could be applied in further ageing and other disease studies.

In order to generate a novel mechanosensitive tissue-engineered model of cartilage that would allow the study of the pathomolecular mechanism of COMP PSACH, chondroprogenitor ATDC5 cells were seeded in pellets and 2% agarose constructs, cultured in chondrogenic medium with and without growth factor supplementation, and compared to the established 2D chondrogenesis model. ATDC5 cells transfected with wild type (WT) and mutant COMP constructs were then grown in pellets and 2% agarose cyclically compressed for 2 weeks for 30min/day at 10kPa 0.33Hz to mimic physiological compression of cartilage. Supplementation with both BMP7 and TGF-β3 improved ATDC5 chondrogenesis. Moreover, chondrogenic markers increased in ATDC5 cells upon compression, whilst dedifferentiation markers decreased.

The p.T585M COMP ATDC5 models recapitulated the phenotype of the disease, with abnormal ECM deposition, an increase in cell apoptosis and a decrease in cell proliferation also allowed us for the very first time to see its effects in a novel mechanosensitive compressed in vitro model. These data suggest that this novel mechanosensing 3-dimensional 2% agarose and pellet model could be employed to study and discover possible targets to treat rare skeletal diseases and reduce the use of animal sin research in the future.

Acknowledgements

Firstly, thank my supervisor, Dr Katarzyna Pirog, for all her support through these years, I would not be the person I am today if it were not for you. Prof David Young, for his support and key suggestions making the project into what it ended up being. To JGW Patterson foundation for the funding of this project. The previous and present members of the Briggs group and Professor Michael Briggs for their ideas and help through this PhD. Acknowledgement to the amazing staff from the centre for life, Ewa and Paul, for their hugs and awesomeness, making your days brighter, to Michelle, Lisa, Trish, Claire, and Debbie always ready to help any occasion they had.

To my Geordie family, I could not have gone through this PhD and illness without your help, you made Newcastle my home. To my wives, Ellie and Ines, for all those microscope emergency meetings, for your support and love through the darkest days, for always being there giving me strength to continue, I really couldn't have done without you.

To Marjolein, for her constant help, her supportive calls, her infinite kindness, you were there from the beginning and never left. You are a great example of success and compassion, thank you for never changing and be who you are.

To Beth, for your guidance and support since the beginning. Not only in the lab and through my PhD, but also with your friendship, especially at the beginning when I had no one. Thank you for always being there and never letting me give up.

To Helen and Adrian, for the many coffees/therapy, for sharing my pain and my difficult times, with you I felt understood and less lonely, thank you for always understand me, listen to me and support me through it all.

To Rob, for the many hours, he spent patiently teaching me new techniques and giving me ideas and advice. But also, for his support and his friendship, you made the days lighter full of laughter making the difficult days less challenging.

Thanks to my friends Mario, Alicia and Vero for their support, selflessness, and constant love through these years, despite the long-distance, you were always there supporting me and fighting my battles.

Special thanks to Miguel, you were my rock through the hardest bit of my PhD and the pandemic. Your support and attitude through life not only gave me the strength I needed to finish it but also the optimism and courage to do it. I will always be grateful for meeting you.

To my partner Dani, for being a source of inspiration and strength in the hardest times. For not letting me give up and making my life bright and colourful even in the most difficult and stressful periods. You pushed me and helped me to be better every day and without your endless support and love, I could not be where I am today. Thank you for being who you are, you are the best partner anyone could ask for.

Special thanks to my brother and parents, for their endless love, support, and sacrifice. I really could have not done it without your support, and I definitely would not be the person I am today if it wasn't for you.

To my parents, because not only have they supported me through my PhD, but they have sacrificed their whole life helping me and giving me the opportunities, they were deprived of.

To my mum, for not only being an amazing and selfless person but for leading by example and showing me that life is not fair, but despite it, you just dust off and never give up. I know life has not been easy on you, especially with your illness, but you never let that define you or let it stop you from being who you are and reaching your goals.

To my dad, for being always that ray of sunshine making the darkest days into the brightest. Your laugh is contagious, and I hope you keep infecting everyone with your brightness because during the toughest times of my PhD is what kept me going, knowing how many sacrifices you've done and how you've kept your smile at all times.

To my brother, for the endless calls, his thoughtfulness, for not allowing me to give up, ever, and for always being there, regardless of what he was going through. I am the luckiest person for having my brother and my best friend in the same person. I really could not have done this without your support, do not ever change the amazing person you are.

Finally, to my grandparents, Lorenzo and Ramira, wherever you are, I know you are still supporting me and taking care of me every step of the way.

This Page Intentionally Left Blank

Index

Index of Figures xiii
Index of Tables xvii
Abbreviations xviii
1 Introduction 2
1.1 Skeletal development 2
1.1.1. Endochondral ossification 4
1.1.2. Cartilage growth plate 6
1.1.2.1. SOX9 8
1.1.2.2. PTHrP and Ihh negative feedback loop 8
1.1.2.3. FGF signalling 10
1.1.2.4. WNT signalling 11
1.1.2.5. BMPs 11
1.1.2.6. VEGF 13
1.1.2.7. RUNX2 14
1.2 Articular Cartilage 14
1.2.1 Zonal stratification 17
1.2.2 Cartilage ECM regions 19
1.2.3 Chondrocytes 20
1.2.4 Extracellular Matrix (ECM) 21
1.2.4.1 Water 21
1.2.4.2 Collagen 21
1.2.4.3 Proteoglycans 23
1.2.4.4 Non-aggregating proteoglycans 25
1.2.4.5 Glycoproteins 26
1.3 Mechanical influences on cartilage 26
1.4 Chondrodysplasias 28
1.4.1 Pseudo-achondrodysplasia 29
1.4.1.1 Cartilage Oligomeric Matrix Protein 31
1.4.1.2 Type 3 repeats domain 33
1.4.1.3 C-terminal domain 33
1.4.1.4 T585M COMP Mutation 40
1.5 Cartilage ageing and injuries. 49
1.5.1 Repair strategies for damaged cartilage and their limitations 49
1.6 Regenerative medicine 51
1.6.1 Tissue engineering for cartilage repair and study 52
1.6.2 Scaffolds for tissue engineering 52

1.6.2.1 Meshes 53
1.6.2.2 Sponges 56
1.6.2.3 Hydrogels 57
1.6.2.4 Scaffold-free cartilage engineering 61
1.6.2.4.1 Pellet culture 62
1.6.2.4.2 Cell sheets 62
1.6.2.4.3 Cell Aggregate 62
1.6.3 Cell's source 63
1.6.3.1 Primary chondrocytes 64
1.6.3.2 Stem cells 64
1.6.3.3 ATDC5 cell line 65
1.6.4 Application of external stimulus to improve chondrogenesis 66
1.6.4.1 Growth Factor Supplementation 66
1.6.4.2 Dynamic compression 67
1.6.4.3 Hydrostatic pressure 69
1.6.4.4 Oxygen 69
1.6.5 In vivo and in vitro cartilage models 69
1.7 Aims of the project 73
1.7.1 Aims of each result chapter. 73
2 Materials and methods 75
2.1 Materials 75
2.1.1 Solutions 75
2.1.2 Antibodies 84
2.1.3 Immunohistochemistry controls 85
2.1.4 Primers 87
2.1.5 Embedding parameters 88
2.1.6 RT-PCR parameters. 89
2.1.7 QuikChange Mutagenesis PCR parameters. 89
2.1.8 Standards for DMMB assay 90
2.2 Methodology 90
2.2.1 Harvest of femoral heads 90
2.2.2 Cell Culture 91
2.2.2.1 Expansion of the ATDC5 cells 91
2.2.2.2 Culture of cells in well plates 91
2.2.3 Hydrogels 93
2.2.3.1 Low gelling temperature agarose 93

2.2.3.2 Basement-membrane extract - Matrigel 93
2.2.3.3 HyStem®-C Cell Culture Scaffold with modified HA 94
2.2.4 Pellets 94
2.2.5 Visualization of ECM and cell morphology 94
2.2.5.1 Cell and tissue harvest 94
2.2.5.2 Tissue staining 95
2.2.5.3 Immunohistochemistry staining 96
2.2.6 Protein extraction and Western blotting 97
2.2.6.1 Protein harvest and extraction 97
2.2.6.2 Protein measurement in models 98
2.2.6.3 Western blotting 98
2.2.7 Processing the 3D and 2D cultures for RNA extraction 99
2.2.7.1 RNA harvest and extraction 99
2.2.7.2 Homogenisation of Samples for RNA extraction 99
2.2.7.3 Purification and Measurement of RNA 99
2.2.7.4 Reverse transcription of RNA to cDNA 100
2.2.7.5 Real Time-Polymerase Chain Reaction (RT-PCR) 100
2.2.8 Terminal deoxynucleotidyl transferase dUTP nick end labelling (TUNEL) assay 101
2.2.9 Dimethyl-Methylene Blue (DMMB) assay 102
2.2.10 Thiazolyl Blue Tetrazolium Bromide (MTT) 102
2.2.11 Design of plasmids and transformation of ATDC5 cells 103
2.2.11.1 QuikChange Site-Directed Mutagenesis 103
2.2.11.2 Plasmid MiniPrep 104
2.2.11.3 Transfection of DNA plasmid to ATDC5 cells 104
2.2.12 Agarose hydrogel scaffolds compressed in the Flexcell® Compression System 105
2.2.13 ImageJ measurement 108
2.2.13.1 Measurement of the width in 3-dimension low gelling temperature agarose 108
2.2.13.2 Measurement of the clusters and pellets area in both pellet and 3-dimension low gelling temperature agarose models 108
2.2.13.3 Cell count for cell apoptosis and cell proliferation in both pellet and 3-dimension low gelling temperature agarose models 108
2.2.14 Analysis of data 109
2.2.15 Statistical analysis 109
3 Validation of the ATDC5 chondrogenesis line in a monolayer (2D model) 111
3.1 Introduction 111
3.2 Aims of the chapter 112
3.3 Results 112

3.3.1 Cell morphology, ECM deposition and cell metabolic activity 112
3.3.2 Gene expression of chondrogenic markers in the 2D culture of ATDC5 cells ... 118
3.4 Discussion 120
4 Development and characterisation of a 3-dimensional pellet culture of ATDC5 cells as a model of zonally stratified cartilage 124
4.1 Introduction 124
4.2 Aims of the chapter 125
4.3 Results 125
4.3.1 ECM deposition and area of pellets with no supplementation of growth factors 125
4.3.3 Cell apoptosis in pellets with and without growth factor supplementation 137
4.3.4 Cell proliferation and cell metabolic activity in pellets with and without growth factor supplementation 139
4.3.5 Gene expression in pellets with and without growth factor supplementation 142
4.4 Discussion 147
5 Development and characterisation of a 3-dimensional zonally stratified model of cartilage using ATDC5 cells and growth factor supplementation. 152
5.1 Introduction 152
5.2 Aims of the chapter 153
5.3 Results 154
5.3.2 Optimisation of the low gelling temperature agarose hydrogel at a different cell and hydrogel densities 155
5.3.3 Cell morphology differences between the ATDC5 cells in the 2-dimensional model compared to the optimised low gelling temperature agarose hydrogel. 159
5.3.4 ECM deposition in agar hydrogel with and without growth factor supplementation 161
5.3.5 Width of constructs and area of cell clusters in 1% agarose with and without growth factor supplementation 163
5.3.6 ECM deposition in 1% agarose constructs with and without growth factor supplementation 165
5.3.7 Cell apoptosis in 1% agarose constructs with and without growth factor supplementation 169
5.3.8 Cell proliferation and cell metabolic activity in 1% agarose constructs with and without growth factor supplementation 171
5.3.9 Gene expression of chondrogenic markers in 1% agarose constructs with and without growth factor supplementation 175
5.4 Discussion 180
6 Characterisation of the 3-dimensional hydrogel model under compression. 186
6.1 Introduction 186
6.2 Aims of the chapter 187

6.3 Results 187
6.3.1 ECM deposition in both uncompressed and compressed hydrogel constructs supplemented with BMP7 and TGF-β3 188
6.3.2 Proteoglycan deposition in uncompressed and compressed tissue-engineered constructs supplemented with BMP7 and TGF-β3 194
6.3.3 Collagen deposition in uncompressed and compressed hydrogel constructs supplemented with BMP7 and TGF-β3 196
6.3.4 Cell apoptosis in uncompressed and compressed hydrogel constructs supplemented with BMP7 and TGF-β3 202
6.3.5 Cell proliferation and cell metabolic activity in uncompressed and compressed hydrogel constructs supplemented with BMP7 and TGF-β3 204
6.3.6 Gene expression of chondrogenic markers in uncompressed and compressed hydrogel constructs supplemented with BMP7 and TGF-β3 208
6.4 Discussion 211
7 Characterisation of T585M COMP mutation in tissue-engineered models of cartilage . 217
7.1 Introduction 217
7.2 Aims of the chapter 218
7.3 Results 218
7.3.1 Morphology and ECM deposition in the 2-dimensional model of ATDC5 cells stably transfected with WT and p.T585M mutant COMP 219
7.3.2 Cell metabolic activity in the 2-dimensional model of ATDC5 cells stably transfected with WT and p.T585M mutant COMP. 223
7.3.3 Gene expression activity in 2-dimensional model of ATDC5 cells stably transfected with WT and p.T585M mutant COMP. 224
7.3.4 Morphology and area of pellets of ATDC5 cells stably transfected with WT and p.T585M mutant COMP 228
7.3.5 Proteoglycan deposition in pellets of ATDC5 cells expressing WT and p.T585M mutant COMP. 230
7.3.6 Collagen deposition in pellets of ATDC5 cells expressing WT and p.T585M mutant COMP 232
7.3.7 Cell apoptosis in pellets of ATDC5 cells expressing WT and p.T585M mutant COMP 238
7.3.8 Cell proliferation in the pellets of ATDC5 cells expressing WT and p.T585M mutant COMP. 241
7.3.9 Gene expression in pellets of ATDC5 cells expressing WT and p.T585M mutant COMP 244
7.3.10 Morphology in 3-dimensional 2% low gelling temperature agarose hydrogel seeded with ATDC5 cells expressing WT and p.T585M mutant COMP. 248
7.3.11 The width and zonal stratification of 3-dimensional 2% low gelling temperature agarose constructs seeded with ATDC5 cells expressing WT and p.T585M mutant COMP 250

7.3.12 Proteoglycan deposition in 3-dimensional 2% low gelling temperature agarose constructs seeded with ATDC5 cells expressing WT and p.T585M mutant COMP 252
7.3.13 Collagen deposition in 3-dimensional 2% low gelling temperature agarose constructs seeded with ATDC5 cells expressing WT and p.T585M mutant COMP 254
7.3.14 Cell apoptosis in 3-dimensional 2% low gelling temperature agarose hydrogel seeded with ATDC5 cells expressing WT and p.T585M mutant COMP 259
7.3.15 Cell proliferation and cell metabolic activity in 3-dimensional 2% low gelling temperature agarose constructs seeded with ATDC5 cells expressing WT and p.T585M mutant COMP..... 261
7.3.16 Gene expression in 3-dimensional 2% low gelling temperature agarose hydrogel seeded with ATDC5 cells expressing WT and p.T585M mutant COMP. 265
7.4 Discussion 270
7.4.1 2-dimensional monolayer model 271
7.4.2 Pellet model 271
7.4.3 3-dimensional 2% agarose model 273
Chapter 8. Discussion 276
8. Discussion..... 277
Chapter 9. Conferences and publications..... 280
9.1 Conferences: 281
9.2 Publications: 281
Chapter 10. Bibliography 282
10 Bibliography..... 283

Index of Figures

Figure 1. Schematic of the mechanisms involved in skeletal development.. 3
Figure 2. Alterations in skeletal development and patterning cause severe disorders. 4
Figure 3. Schematic diagram showing the development of long bones through the process of endochondral ossification. 6
Figure 4. Structure and localisation of the growth plate..... 7
Figure 5. Pathways and processes SOX9 is involved in. 8
Figure 6. IHH and PTHrP negative-feedback loop regulate the longitudinal bone growth. 9
Figure 7. FGF pathways regulate growth plate chondrocytes and bone growth.. 10
Figure 8. Representation of BMP and TGF-β activation pathway and functions. 13
Figure 9. Types of cartilage and the main fibrous component. 15
Figure 10. Joint anatomy and articular cartilage.. 16
Figure 11. Articular cartilage composition and schematic overview. 18
Figure 12. Pre-hypertrophic chondrocytes.. 20
Figure 13. Collagen fibril meshwork in the territorial ECM and Table summarising the collagen and their function and structure. 23
Figure 14. Proteoglycan structure. 25
Figure 15. Radiographs of pseudoachondroplasia and multiple epiphyseal dysplasia patients 30
Figure 16. Schematic of the structure of thrombospondin family subgroups. 31
Figure 17. Crystallography and rotary shadow structure from COMP. 32
Figure 18. Diagram of the pentameric structure of COMP 33
Figure 19. Composition of the T3 repeats 5 to 7 domains and CTD..... 34
Figure 20. Representation of three calcium-binding sites in the CTD globular domain..... 35
Figure 21. Schematic of some of the COMP ECM interactions. 36
Figure 22. Mapping of mutations located in T3 repeat domain and CTD..... 38
Figure 23. Mutant protein retention due to a mutation in the T3 repeats domain of COMP. .. 39
Figure 24. Alteration in the matrix secretions and organization of the CTD-COMP mutant growth plate 40
Figure 25. Radiographs of the T585M COMP mutation pathology in a seven-year-old boy. . 41
Figure 26. Diagram of the available options to restore articular cartilage 51
Figure 27. Graph showing the number of papers published in cartilage tissue engineering since 1992 52
Figure 28. Diagram showing the electrospinning technique with nanofibres 55
Figure 29. Schematic process of developing nanoporous scaffold sponge-like. 57

Figure 30. A representative of hydrogel constructs 59
Figure 31. Schematic representation of energy input needed to achieve a certain dimension and examples of pellets 63
Figure 32. Examples of cell types employed in articular cartilage models.. 65
Figure 33. Example of the loading regime used for this research. 68
Figure 34. Fast Read 102 W chamber. 92
Figure 35. Diagram explaining the collection and section of the hydrogel at each day point. 95
Figure 36. Representation of the washers with the agarose hydrogel seeded inside. 105
Figure 37. A BioPress™ 6-well plate with components 106
Figure 38. Loading regime. 107
Figure 39. Histological staining of ATDC5 cells following 1, 7, 14 and 21 days of culture and cell metabolic activity in the 2-dimensional model 114
Figure 40. Alcian blue and sGAG quantification for days 1 to 21 in the 2-dimensional model. GAG histology staining of ATDC5 for days 1 to 21 in the 2-dimensional model 115
Figure 41. Collagen histology staining along day points 1 to 21 in the 2-dimensional model.. 116
Figure 42. Calcium depositions during the 21 days incubation period in 2-monolayer model 117
Figure 43. mRNA expression after 21 days of culture... 119
Figure 44. Histology staining of ATDC5 cells following 1, 7, 14 and 21 days of pellet culture 127
Figure 45. Picrosirius histological staining and area measurements of pellets with growth factors. 130
Figure 46. Picrosirius histological staining of pellets with growth factors. 131
Figure 47. Immunohistochemistry for type II collagen in pellets with growth factor supplementation. 132
Figure 48. Immunohistochemistry for type I collagen in all conditions after 21 days. 133
Figure 49. Positive and negative controls for type I, II and X collagen and aggrecan. Positive and negative controls were done in 3-week-old mice femoral heads for type I, II and X collagen and aggrecan. Scale bar: 50 µm 134
Figure 50. Glycosaminoglycan analysis via staining and quantification. 135
Figure 51. Toluidine blue histological staining of pellets with growth factors. 136
Figure 52. Immunohistochemistry for cell apoptosis in all conditions after 21 days.. 138
Figure 53. Cell apoptosis at the surface and centre zones and numerical data presented in graphs 139

Figure 54. Immunohistochemistry for cell proliferation in all conditions after 21 days.....141
Figure 55. Cell metabolic activity and cell proliferation with its numerical data presented in graphs. 142
Figure 56. mRNA expression of cartilage differentiation markers in ATDC5 pellets cultured for 21 with growth factor supplementation. 146
Figure 57. Histological analysis of hydrogels HA/Gelatin, agar and matrigel at day 21.....155
Figure 58. Histological analysis for the different cell and gel densities and study of the area of clusters per zone at day 21.....157
Figure 59. Histological analysis of a 1-week-old femoral head, and 1% constructs at different cell concentrations and clusters area analysis for all conditions and zones. 159
Figure 60. Bright-field images comparing seeding ATDC5 cells in 2-dimensional models and hydrogel 3-dimensional models 160
Figure 61. Histological analysis after the addition of growth factor at days 7, 21 and 42. 162
Figure 62. Analysis of width and area of clusters in 1% agar constructs seeded with 10x106cells/ml and supplemented with BMP7, TGF-β3 or a combination of both 164
Figure 63. Immunohistochemistry against type I and II collagen and aggrecan.....166
Figure 64. Positive and negative controls for type I, II and X collagen and aggrecan.....167
Figure 65. Analysis of sGAG deposition.....169
Figure 66. TUNEL assay for cell apoptosis 170
Figure 67. TUNEL assay for cell apoptosis. 171
Figure 68. Immunohistochemistry for cell proliferation in all conditions after 21 days......173
Figure 69. Cell proliferation and cell metabolic activity of ATDC5 cells cultured in the 3-dimensional 1% agar scaffold with growth factor supplementation 174
Figure 70. qRT-PCR data showing gene expression in 3dimentional ATDC5 1% agar cell culture.. 179
Figure 71. Loading regimen used.. 188
Figure 72. Histological analysis when compressed and without compressing at day 21.....190
Figure 73. Analysis of width and area of clusters with a combination of BMP7 and TGF-β3 and uncompressed and compressed conditions 193
Figure 74. Histological and analysis of sGAG deposition via quantification via DMMB assay after the addition of growth factor at days 7, 14 and 21. 195
Figure 75. Histological analysis after the addition of both growth factor at days 7, 14 and 21 when compressing and no compressing. 197
Figure 76. Immunohistochemistry for type II collagen.....198
Figure 77. Immunohistochemistry for type X collagen.....199

Figure 78. Immunohistochemistry for type I collagen. 200
Figure 79. Positive and negative controls for type I, II and X collagen and aggrecan. 201
Figure 80. Immunohistochemistry for TUNEL assay. 203
Figure 81. Numerical data and statistical analysis in graph 204
Figure 82. Immunohistochemistry for cell proliferation assay for ATDC5 cells seeded. 206
Figure 83. Analysis in cell proliferation and cell metabolic activity. 207
Figure 84. mRNA expression after 21 days of culture. 210
Figure 85. Western blot showing WT and pT585M COMP mutant cells with the COMP protein. 218
Figure 86. Brightfield microscope analysis and alcian blue and alizarin red staining. 221
Figure 87. Alcian blue and calcium deposits for days 1 to 21 in the 2-dimensional model. . 222
Figure 88. Analysis of sGAG for WT and mutant model 223
Figure 89. Cell metabolic activity in WT and mutant model. MTT assay was performed in the monolayer culture after 7, 14 and 21 days. 224
Figure 90. Gene expression after 21 days of culture 227
Figure 91. Histology haematoxylin and eosin and measurement of area in the pellets. 229
Figure 92. Toluidine blue histological staining and sGAG quantification in pellets. 231
Figure 93. Picrosirius histological staining and cell metabolic activity of pellets. 233
Figure 94. Immunohistochemistry for type II collagen in all conditions after 21 days. 234
Figure 95. Immunohistochemistry for type X collagen in all conditions after 21 days. 235
Figure 96. Immunohistochemistry for type I collagen in all conditions after 21 days 236
Figure 97. Positive and negative controls for type I, II and X collagen and aggrecan 237
Figure 98. Immunohistochemistry for cell apoptosis in all conditions after 21 days 239
Figure 99. Cell apoptosis in surface and centre of the pellet 240
Figure 100. Immunohistochemistry for cell proliferation in all conditions after 21 days. 242
Figure 101. Cell proliferation in the surface and centre of the pellet.. 243
Figure 102. Cell metabolic activity with numerical data presented in graphs 244
Figure 103. Gene expression after 21 days of culture 247
Figure 104. Histological analysis at days 7, 14 and 21. 249
Figure 105. Analysis of width and area of clusters in WT and T585M models compressed. 251
Figure 106. GAG analysis at days 7, 14 and 21. 253
Figure 107. Analysis of sGAG deposition via quantification via DMMB assay after 21 days 254
Figure 108. Collagen analysis at days 7, 14 and 21 255
Figure 109. Immunohistochemistry for type II collagen in all conditions after 21 days. 256

Figure 110. Immunohistochemistry for type I collagen in all conditions after 21 days. 257
Figure 111. Positive and negative controls for type I, II and X collagen and aggrecan 258
Figure 112. Immunohistochemistry for cell apoptosis in all conditions after 21 days. 260
Figure 113. Cell apoptosis and numerical data and statistical analysis presented in graphs in the WT and T585M models uncompressed or compressed. 261
Figure 114. Immunohistochemistry for cell proliferation in all conditions after 21 days. 263
Figure 115. Cell proliferation and cell metabolic activity in WT and T585M models compressed and uncompressed. 264
Figure 116. Gene expression after 21 days of culture. 268
Figure 117. Gene expression after 21 days of culture. 269

Index of Tables

Table 1. Summary of the main outcomes of the in vitro models of COMP mutations. 45
Table 2. Summary of the main outcomes of the mouse models with COMP mutations 48
Table 3. Summarise of key finding in zonally stratified 3D models compressed or uncompressed found in literature 72
Table 4. Table of primary and secondary antibodies used (dilution, source and manufacturer). 97
Table 5. Table summarising the outcome of the gene expression 118
Table 6. Table summarising the outcome of the gene expression 145
Table 7. Table summarising the outcome of the gene expression 178
Table 8. Table summarising the outcome of the gene expression 209
Table 9. Table summarising the outcome of the gene expression 226
Table 10. Table summarising the outcome of the gene expression. 246
Table 11. Table summarising the outcome of the gene expression. 267

Abbreviations

(SDS)-PAGE	Sodium dodecyl suphate
ACI	Autologous chondrocytes implantation
ADA	Adenosine deaminase
ADAMTS	Disintegrins and metalloproteinase with thrombospondin motifs
ASOS	Antisense oligonucleotides
BAC	Bacterial artificial chromosome
BCA	Bicinchoninic Acid
BCL-2	Protein B-cell lymphoma-2
BM-MSC	Bone marrow mesenchymal stem cells
BMP	Bone morphogenetic proteins
BMPRI and BMPRII	BMP type I and II
BSA	Bovine serum albumin
CamKII	Calcium/calmodulin-dependent kinase II
CBFA1	Core-binding factor Subunit alpha-1
cDNA	Complementary DNA
CHOP	CCAAT-enhancer-binding protein homologous protein
CILP	Cartilage intermediate-layer protein
CMP	Cartilage matrix protein
COMP	Cartilage olimeric matrix protein
COS-7	African green monkey SV40-transformed fibroblast
Co-SMAD	Common-partner Smad
CTD	C-terminal domain
DAPI	4′,6-diamidino-2-phenylindole
DMEM	Dulbecco’s modified Eagle’s medium
DMMB	1,9-Dimethyl-Methylene Blue zinc chloride double salt
DMSO	Dimethyl sulfoxide
DPBS	Dulbecco’s phosphate-buffered saline
DTT	DL-Dithiothreitol
ECM	Extracellular matrix
EDTA	Ethylenediaminetetraacetic acid
EMT	Epithelial-mesenchymal transition
eIF2α	Eukaryotic initiation factor 2α
FBS	Fetal Bovine Serum
FCS	Foetal calf serum
FGF	Fibroblast growth factor
FGFR	Fibroblast growth factor receptor
FRZ	Receptor complex of frizzled
GAG	Glucosaminoglycans
GEP	Granulin-epithelin precursor
HA	Hyaluronic acid

HOXD13	Homeobox gene
IGF-1	Insulin-like growth factor 1
IHH	Indian hedgehog
iPSCs	Induced pluripotent stem cells
IPTG	Isopropyl-β-D-thiogalactoside
JNK	c-Jun N-terminal kinases
KIF22	Kinesin family member 22
LRP	Low density lipoprotein receptor-related protein
LXM1B	LIM homeodomain protein
MATN	Matrilin-
MED	Multiple epiphyseal dysplasia
MIDAS	Metal ion dependent adhesion site
MMPs	Metalloproteinases
MSC	Mesenchymal stem cells
MTT	3-(4,5-Dimethylthiazol-2-yl)-2,5-Diphenyltetrazolium Bromide
NCAD	Adhesion molecules such as neural cadherin
NCAM	Neural cell adhesion molecule
NEA	Non-essential amino acid solution
NSAIDS	Nonsteroidal anti-inflammatory drugs
NTD	N-terminal domain
OA	Osteoarthritis
OPN	Osteopontin
PAPSS2	Phosphoadenosine-phosphosulfate-synthase 2
PBS	Phosphate buffered saline
PCM	Pericellular Matrix
PDE	Phosphodiesterase
PGA	Polyglycolic acid
PKC	Protein kinase C
PLC	Phospholipase C
PLGA	Polylactic-co-glycolic acid
PLLA	Polylactic acid
POC	Poly(1,8 octanediol citrate)
PRELP	Proline/arginine-rich end leucine-rich repeat protein
PSACH	Pseudochondroplasia
Ptc-1	Receptor patched-1
PTHrP	Parathyroid Hormone-Related Protein
RCS	Swarm rat chondrosarcoma cells
rER	Rough endoplasmic reticulum
RGD	Arginine-glycine-aspartate
R-SMAD1, 5 and 8	Receptor-regulated Smad
RT-PCR	Reverse transcription polymerase chain reaction
RUNX2	Runt-related transcription factor 2

SCC	Saline sodium citrate
SCID	Immunodeficiency
SDSCs	Synovium-derived stem cells
SH3BP2	SH3 Domain Binding Protein 2
SLRPs	Small leucine rich proteoglycans
SMAD	Canonical mothers against decapentaplegic homolog
SMO	Smoothened factor
SOX9	Sex-determining region Y-Box 9
SSC	Saline sodium citrate
STAT1	Signal transducer and activator of transcription
T2	Type 2 epidermal growth factor-like repeats
T3	Type 3 calcium-binding repeat domain
TdT	Terminal Deoxynucleotidyl Transferase
TGF-β	Transforming growth factor beta
TIMP-1	tissue inhibitor of metalloproteinases 1
TLC	L-Cysteine hydrochloride anhydrous
Trizma®	TRIS base
TSP5	thrombospondin 5
TUNEL	Terminal deoxynucleotidyl transferase dUTP nick end labelling
UPR	Unfolded protein response
VDDR1	Vitamin D-dependent rickets type 1
VEGF	Vascular endothelial growth factor
WNT	Wingless-type MMTV integration site
WT	Wild type
X-Gal	5-Bromo-4-chloro-3-indolyl-β-D-galactopyranoside

Chapter 1. Introduction

1 Introduction

1.1 Skeletal development

The human skeleton is the framework of the body that protects, supports, and anchors vital organs such as the heart, brain, lungs, and muscle. It is mainly comprised of bone and cartilage, supported by tendons, ligaments, and muscles. Different types of cells contribute to the development of the skeleton, two of which derive from a mesenchymal progenitor: the chondrocytes producing cartilage and the bone-forming osteoblasts. The other cell type, the osteoclast, regulates the turnover of the bone and originates from a hematopoietic lineage (Ducy *et al.*, 1997).

Disorders affecting the skeleton are rare and comprise a vast and diverse group of conditions ranging from mild cases with growth retardation, arthropathy, etc as seen in Stickler dysplasia, to severe cases leading to neonatal lethality like lethal achondrogenesis, both diseases mentioned resulting from a mutation in COL2A1 (Kornak and Mundlos 2003). Due to the wide spectrum of disease, the disorders can be classified according to four major groups: disorders affecting skeletal patterning, differentiation of skeletal precursor structures, growth, and homeostasis (Spranger *et al.*, 2018). Mutations affecting patterning genes were called dysostoses (affecting skeletal elements), while those affecting the development and growth of the skeleton (developmental disorders) osteochondrodyspasias (Kornak and Mundlos 2003 and Zelzer and Olsen 2003). Traditionally, for the study of the pathogenesis mice models have been employed, however small animal models like mice are associated with fundamental limitations, such as, variation in their anatomical and histological structure (McCoy 2015), lower range of assays available comparable to humans such as synovial fluid collections (Teeple et al. 2013), shorter life span, therefore with faster disease progression which might not accurately mimic the human progression (Teeple et al. 2013), variation between mice strains (McCoy 2015), and small anatomical size which could hinder lesion and damage analysis (McNulty et al. 2012). Despite the previously mentioned, since these mutations are not a simple loss-of-function and are multifactorial, mice generated models are essential to decouple the pathogenesis and progression of these rare disorders (Zelzer and Olsen 2003). Some examples were mice have mimic accurately the disease is campomelic dysplasia, lethal in babies, where the heterozygous *Sox9*-null mice (*Sox9*$^{+/-}$) recapitulates most of the abnormalities found in humans (Bi et al. 2001); point mutations or deletions in *Pax3* display abnormalities found in Splotch phenotype (Epstein, Vekemans, and Gros 1991); disruption of the segmentation clock found in mutations in the Notch ligand delta-like3 in both humans and mice (Bulman et al. 2000); and a null mutation in Gdf5 leads to the development of brachypodism in homozygous mice, which

mimics the Hunter-Thompson type acromesomelic dysplasia abnormalities (Thomas et al. 1996).

The mature adult skeleton comprises 206 bones which are formed by two mechanisms, intramembranous ossification, and endochondral ossification (Figure 1). Intramembranous calcification is responsible for the formation of flat membranous bones, such as the facial and cranial bones, through a process in which the cranial neural crest cells differentiate through epithelial-mesenchymal transition (EMT) into mesenchyme stem cells that condense and then differentiate into osteoblasts to deposit bone extracellular matrix comprising mainly type I collagen (Jiang *et al.*, 2002; Percival and Richtsmeier, 2013). Endochondral ossification is responsible for the formation of long bones, such as femur or tibia, whereby a continuously growing cartilage template is gradually replaced by bone (Mackie, Tatarczuch and Mirams, 2011).

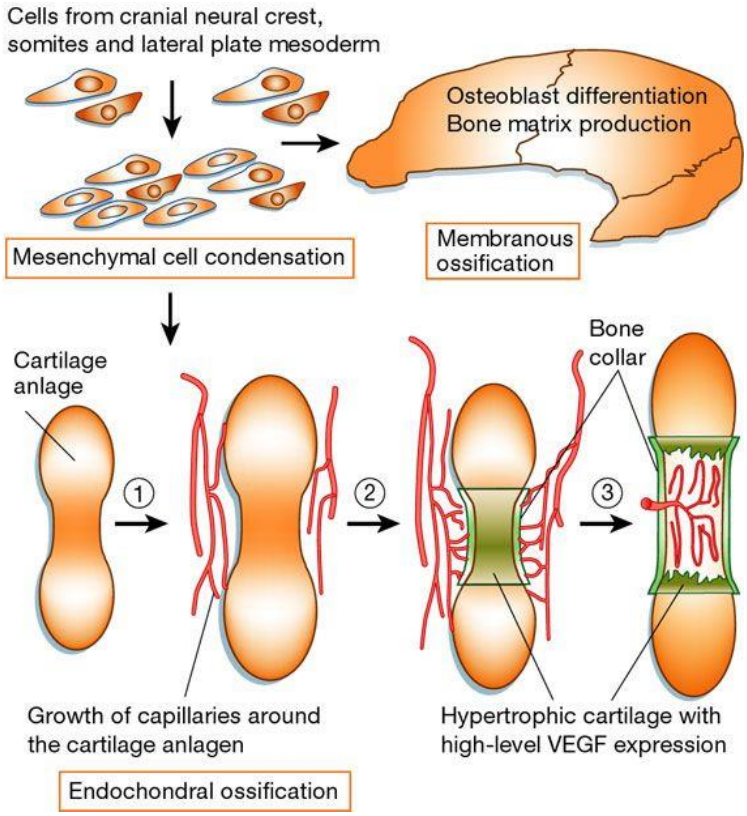

Figure 1. **Schematic of the mechanisms involved in skeletal development.** *Intramembranous ossification is responsible for the development of flat bones, and endochondral ossification leads to long bone development and growth. Somites and lateral plate mesoderm aggregate in certain zones of the developing embryo that will lead to future bones. During the intramembranous ossification, the mesenchymal stem cells differentiate into osteoblasts and start producing bone matrix. In the long bones, the process is more complex to allow for longitudinal growth. It includes the formation of the Anlagen (cartilage template) after differentiation of the stem cells into chondrocytes. The cartilage template is replaced by hypertrophic cartilage followed by a bone matrix with the formation of two endochondral ossifications centres and growth plate through the blood vessel invasion around the bone collar. Figure adapted from* (Kronenberg, 2003)**.**

1.1.1. Endochondral ossification

Endochondral ossification is a highly complex process, which involves the initiation of a cartilage template in the developing embryo that will be gradually replaced by bone. Alterations in this process lead to the development of many diseases, collectively known as skeletal dysplasias (Figure 2).

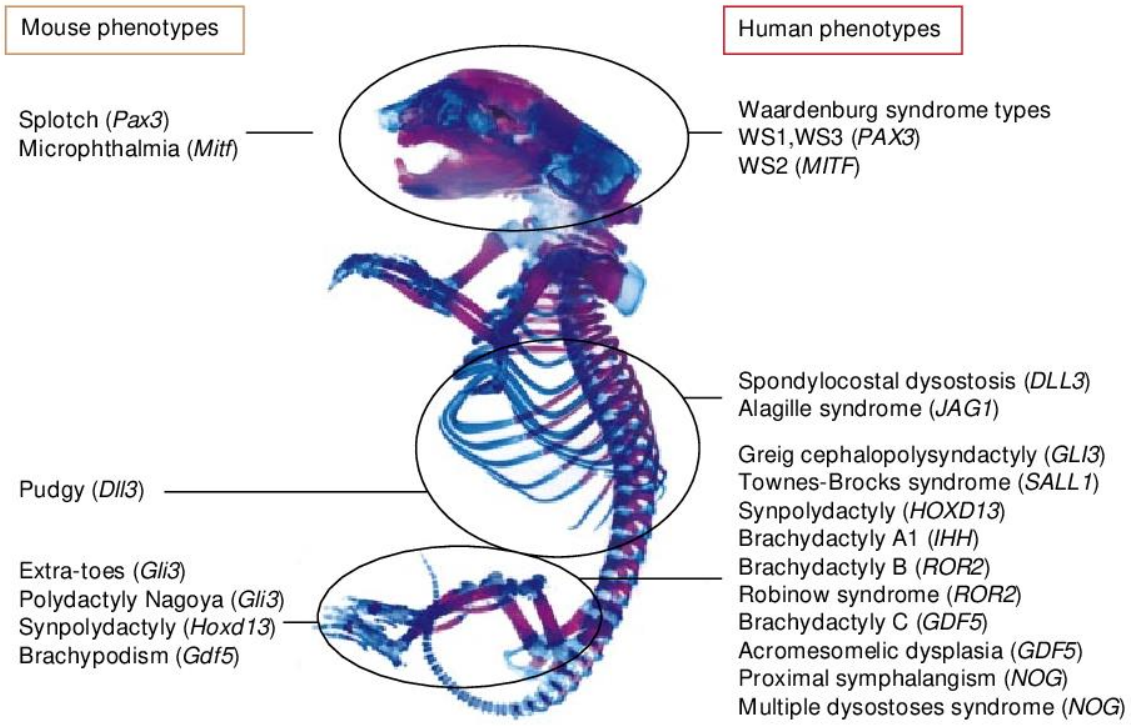

Figure 2. Alterations in skeletal development and patterning cause severe disorders. *This Figure represents the mouse and human phenotypes. Disorders are grouped depending on the origin of the progenitor cells, either from the cranial neural crest, the somites or the lateral plates mesoderm. The genes affected by each disease are specified in parentheses (Zelzer and Olsen, 2003).*

The process of endochondral ossification starts with mesodermal lineage cells, which were first described in 1976 by Alexander Friedenstein as "a population derived from the bone marrow capable of self-renewal and differentiation into a wide variety of cell types", such as chondrocytes, osteocytes and adipocytes, *in vitro* (Friedenstein, 1976; Andrzejewska, Lukomska and Janowski, 2019). Mesenchymal stem cells (MSCs) are closely regulated by many growth factors and signalling molecules, such as fibroblast growth factors (FGFs), Wingless-types MMTV integration site (WNTs), Indian hedgehog (IHH), Parathyroid Hormone-Related Protein (PTHrP), transforming growth factors beta (TGF-β) and bone morphogenetic proteins (BMPs), and proteins such as SRY-Box 9 (SOX9) and vascular endothelial growth factor (VEGF) (Bi *et al.*, 1999).

MSC migrate to aggregate and condense (Figure 3), the latter is facilitated by adhesion molecules such as neural cadherin (NCAD) and neural cell adhesion molecule (NCAM) (Karsenty, Kronenberg and Settembre, 2009; Mackie, Tatarczuch and Mirams, 2011). Cells within the condensate lead to the cartilage anlagen and differentiate into chondrocytes that secrete a cartilage extracellular matrix (ECM) rich in type II, IX, XI collagens and proteoglycans such as aggrecan and glycosaminoglycans such as hyaluronan (Karsenty, Kronenberg and Settembre, 2009; Mackie, Tatarczuch and Mirams, 2011). On the periphery of the anlage, the cells form the periosteum - a tissue collar that surrounds the cartilage anlage and after vascularisation and expression of RUNX2 induces proliferation of osteoblasts and the formation of the periosteum (Karsenty, Kronenberg and Settembre, 2009; Mackie, Tatarczuch and Mirams, 2011).

Chondrocytes in the diaphysis (mid-shaft) of the anlage undergo a process of differentiation through proliferation, hypertrophy and, eventually, cell death (Figure 3). Hypertrophic chondrocytes recruit blood vessel invasion into the anlage, with osteoblast and osteoclast precursors invading the centre of the anlage and forming the primary ossification centre. The hypertrophic chondrocytes increase the synthesis of proteins that stimulate vasculogenesis and angiogenesis and degrade the matrix, such as matrix metalloproteinases (MMPs), especially MMP13 and vascular endothelial growth factor (VEGF) (Tuckermann *et al.*, 2000; Mackie, Tatarczuch and Mirams, 2011; Staines *et al.*, 2013). The primary ossification centre enlarges towards the epiphysis (end of the bone) degrading the cartilage template matrix by osteoclasts and depositing bone through osteoblasts (Mackie, Tatarczuch and Mirams, 2011).

A secondary ossification centre forms at the epiphysis around human birth or in the first two years of life, depending on the bone. This centre is separated from the primary centre by the remaining chondrocytes that arrange into distinct zones forming the physis or cartilage growth plate, which is responsible for postnatal long bone growth until puberty (Karsenty, Kronenberg and Settembre, 2009; Staines *et al.*, 2013; Shim, 2015).

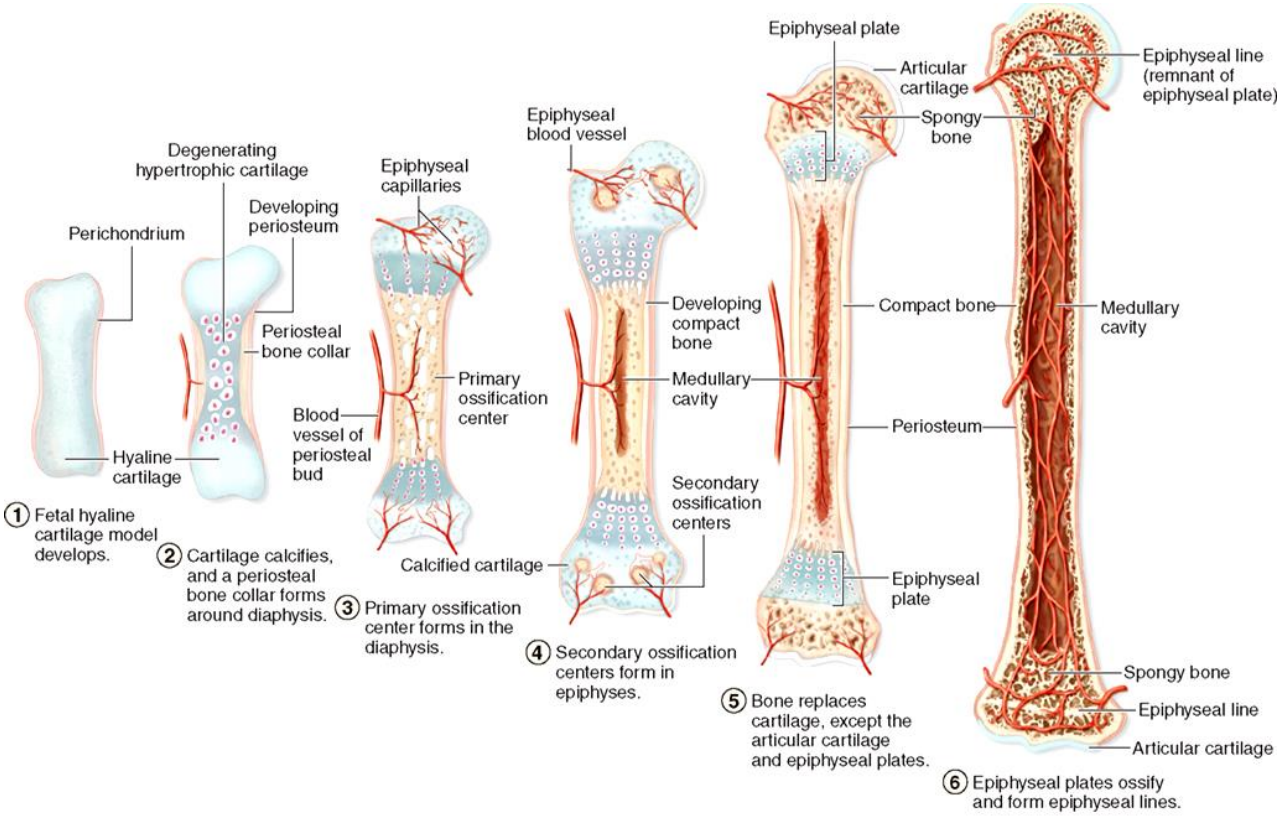

Figure 3. Schematic diagram showing the development of long bones through the process of endochondral ossification. *(1) Mesenchymal stem cells condense and differentiate into chondrocytes forming the cartilage template for bone. (2) Chondrocytes in the centre of the shaft mature and become hypertrophic leading to mineralisation of their ECM and recruitment of blood vessels thus forming the primary ossification centre (3-4) Osteoblasts enter the cartilage template through the blood vessels and start depositing bone matrix in the primary ossification centre, a secondary centre is formed in epiphysis leading to the development of the cartilage growth plate at the tip of the bone that drives the cartilage scaffold deposition and longitudinal bone growth until puberty (5-6) (McGurk, 2013).*

1.1.2. Cartilage growth plate

Cartilage growth plates (physes) are located at the proximal and distal ends of long bones. They are responsible for the longitudinal growth of bones through the differentiation of chondrocytes within the physis. The growth plate is organised in three characteristic zones (Figure 4): the resting zone, which contains rounded randomly distributed chondrocytes ready to differentiate with reduced proliferative capacity, the proliferative zone that contains flattened proliferating chondrocytes arranged in columns in the direction of the longitudinal growth and the hypertrophic zone where the cells enlarge and secrete molecules leading to the remodelling the ECM and blood vessel invasion. (Rochira *et al.*, 2001; Gentili and Cancedda, 2009). At the bottom of the growth plate, at the vascular invasion front, the cells produce alkaline phosphatase and other markers of terminal differentiation such as osteopontin (OPN) and MMP-13. These allow the cartilage template to become mineralised due to the accumulation of hydroxyapatite and increased alkaline phosphatase activity. In this calcified area, the chondrocytes are undergoing apoptosis due to the environment created by the mineralisation. The blood vessels

invade, attracted by VEGF secreted by the hypertrophic chondrocytes once the mineralised matrix has been degraded by MMP-13 and disintegrins and metalloproteinase with thrombospondin motifs' (ADAMTS) (Johansson *et al.*, 1997; Gerber *et al.*, 1999; Kuno *et al.*, 2000; Li *et al.*, 2009; Maes *et al.*, 2010).

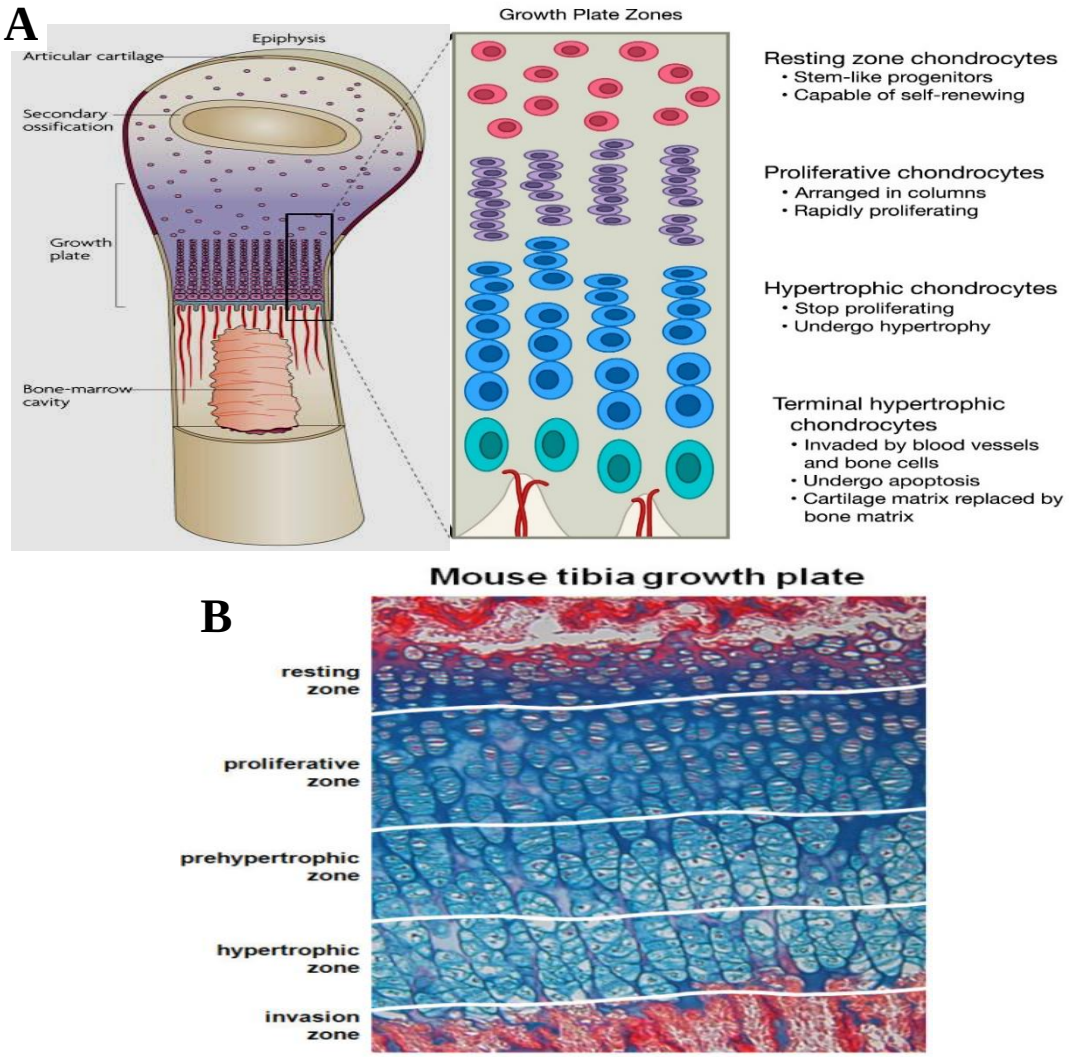

Figure 4. Structure and localisation of the growth plate. (A) *Longitudinal section of the growth plate, in which rounded randomly distributed chondrocytes with self-renewing properties lie in the resting zone (RZ). The proliferative zone (PZ) contains closely packed flat chondrocytes with high proliferation capacity and arranged in columns, closely followed by hypertrophic zone (HZ) in which chondrocytes mature and stop proliferating starting to undergo hypertrophy. Finally, the invasion zone or terminal hypertrophic zone forms a bridge between cartilage and bone (Lui, 2017; Page-McCaw et al., 2007).* ***(B)*** *Growth plate of a 15-month-old mouse showing the different zones by Weigert's haematoxylin and eosin, alcian blue and picrosirius red staining for ECM, proteoglycans and collagen respectively (Dreier, 2010).*

Skeletal development is a highly complex zonally stratified process regulated by a tight network of signalling pathways such as SOX9, IHH/PTHrP, FGF, BMP, WNT, VEGF, and TGF.

1.1.2.1. SOX9

Transcription factor SOX9 is implicated in the differentiation of condensed MSCs into chondrocytes and the expression of cartilage matrix components such as type II collagen and aggrecan in the proliferative zone of the growth plate. SOX5 and six indirectly enhance SOX9 action (Figure 5) (Han and Lefebvre, 2008; Ikegami et al., 2011). Other factors, such as IHH, BMPs and FGFs, are involved in the maintenance of SOX9 function in the growth plate (Kumar and Lassar, 2014). Mutations in *SOX9* gene lead to campomelic dysplasia, a disorder affecting skeletal development (Bell et al., 1997; Bi et al., 1999; Healy et al., 1999; Wagner et al., 1994).

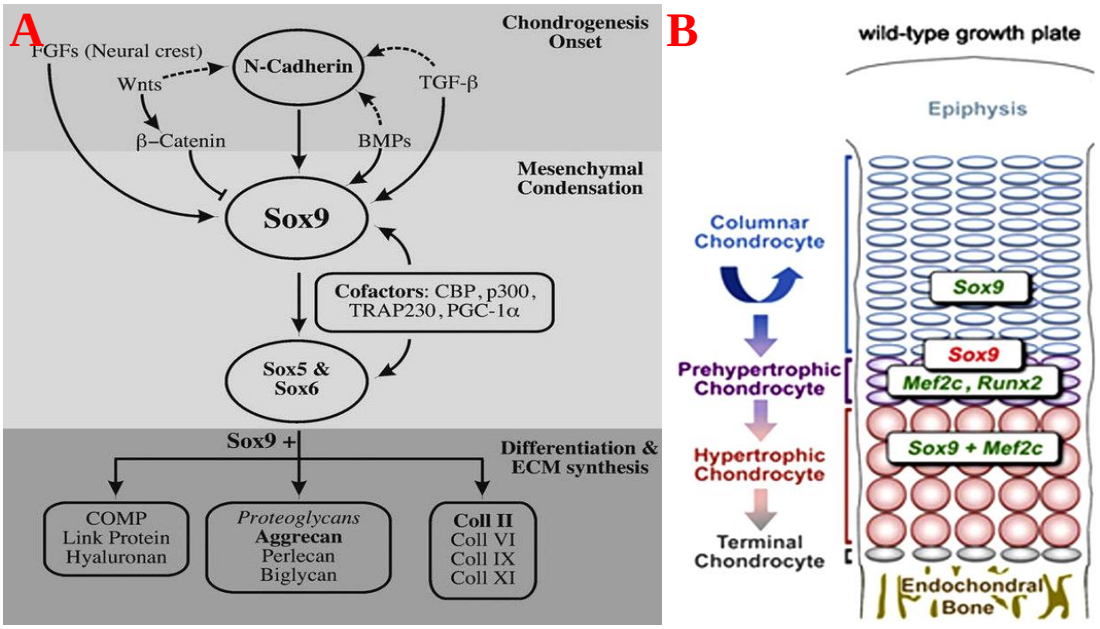

Figure 5. Pathways and processes SOX9 is involved in. ***(A)*** *N-cadherin and other factors such as TGF-β, BMPs and FGFs can upregulate SOX9, while β-catenin from WNT signalling pathway inhibits it leading to chondrogenesis and mesenchymal condensation. SOX9 with cofactors CBP, p300, TRAP230 and PGC-1α, induces the expression of SOX5 and SOX6 which in conjunction with SOX9 trigger the differentiation to chondrocytes and ECM synthesis (Quintana et al., 2009).* ***(B)*** *Moreover, SOX9 is involved in the growth plate development by regulating columnar cell proliferation and hypertrophy. SOX9 induces the proliferation (green SOX9) and delays hypertrophy (red SOX9) by decreasing β-catenin and RUNX2, however, in the hypertrophic zone, associated with MEF2C induces hypertrophy (Dy et al., 2012).*

1.1.2.2. PTHrP and Ihh negative feedback loop

PTHrP and IHH are involved in a negative feedback loop whose main function is to regulate the longitudinal bone growth through regulating chondrocyte proliferation in the growth plate (Figure 6) (Kronenberg *et al.*, 1997; Kronenberg, 2003; Oji *et al.*, 2007).

Proliferative chondrocytes produce parathyroid Hormone-related Protein (PTHrP). It inhibits hypertrophy by acting in a morphogen gradient, i.e. the closer the chondrocytes are to the hypertrophic zone, the less they are exposed to PTHrP. Pre-hypertrophic and hypertrophic chondrocytes express Indian Hedgehog (IHH) and Runt-related transcription factor 2 (RUNX2), which stimulates IHH in a negative loop. IHH signalling induces proliferation and

upregulates the expression of *PTHrP* gene thus creating a feedback signal and regulating the proliferative capacity of the growth plate (Figure 6) (Kronenberg *et al.*, 1997; Kronenberg, 2003; Oji *et al.*, 2007).

Pre-hypertrophic and hypertrophic chondrocytes express *IHH* and its signalling regulates PTHrP expression, differentiation of resting chondrocytes into proliferating ones and the rates of proliferation and hypertrophy by binding to the receptor patched- (PTC-1) which activates the membrane molecule smoothened (SMO) and a cascade triggering chondrocyte proliferation and activation of *IHH* (Denef *et al.*, 2000; Mariani and Martin, 2003).

PTHrP and IHH are therefore key in regulating the length of the proliferative columnar regions, and mutations in genes encoding one of these molecules cause skeletal dysplasia with abundant bone production, abnormal bone growth and premature hypertrophy (Karaplis *et al.*, 1994; Oji *et al.*, 2007). Interestingly, IHH has been proposed as a therapeutic target for osteoarthritis, since its expression is upregulated correlating with the progression of the disease (Wei *et al.*, 2012; Zhou, Wei and Wei, 2014).

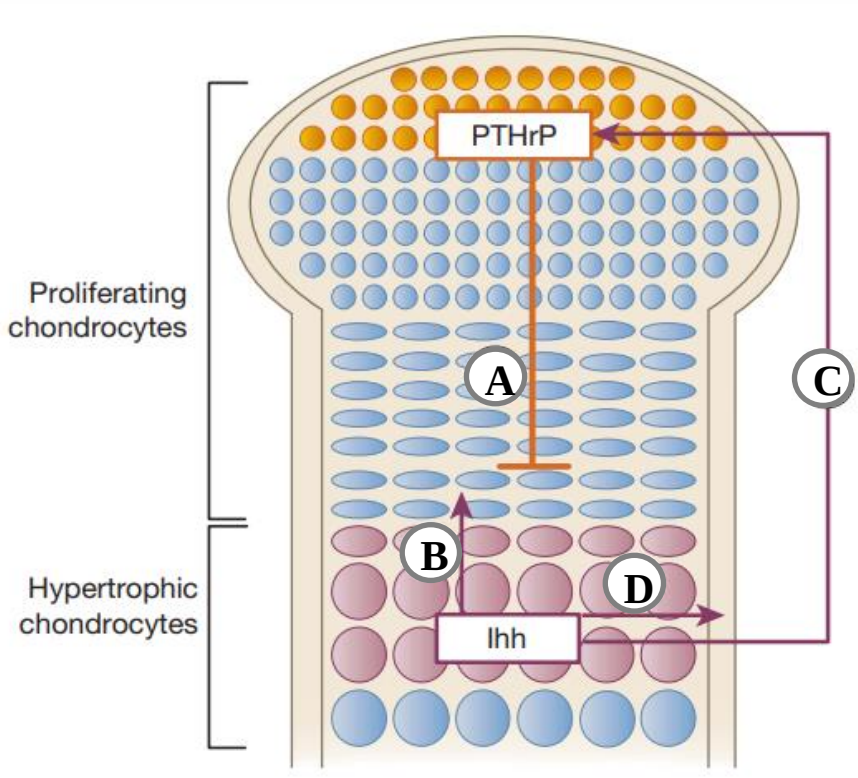

Figure 6. IHH and PTHrP negative-feedback loop regulate the longitudinal bone growth. ***(A)*** *PTHrP upregulates proliferation of the chondrocytes in the proliferative zone inhibiting IHH. However, the farther away the chondrocytes are the signal weakness.* ***(B)*** *IHH inhibits the proliferation of chondrocytes and supports their maturation and hypertrophy. IHH is also involved in stimulating the production of PTHrP at the ends of the bone* ***(C)*** *and in converting the perichondral chondrocytes into osteoblasts* ***(D)*** *(Kronenberg, 2003).*

1.1.2.3. FGF signalling

The development of cartilage is also regulated by fibroblast growth factors (FGFs). The FGF family of signalling molecules comprises 22 members and three FGFR receptors (Figure 7). The receptors, FGFR1, 2 and 3, are expressed in the growth plate, specifically, FGFR1 in the pre-hypertrophic and hypertrophic zones, FGFR2 in the perichondrium and FGFR3 in the proliferating and pre-hypertrophic zones (Delezoide *et al.*, 1998). Particularly FGFR3, a tyrosine kinase receptor for fibroblast growth factors, inhibits chondrocyte proliferation and expression of IHH affecting growth via signal transducer and activator of transcription (STAT1) activation. This receptor is regulated by herapan sulphate GAG (glucosaminoglycans), and its effect is counteracted by BMP signalling (Figure 7) (Delezoide *et al.*, 1998; Ornitz, 2005; Oji *et al.*, 2007). Mutations show the important role of this receptor, for instance, missense mutations in the FGFR3 lead to three human dwarfism syndromes, hypochondroplasia, achondroplasia, and thanatophoric dysplasia, furthermore, a deletion of FGFR3 in mice shows skeletal overgrowth with the expansion of the proliferative zone, whereas overexpression of this receptor causes achondroplasia, short-limbed dwarfism, and a decrease in chondrocyte proliferation (Bellus *et al.*, 1995; Oji *et al.*, 2007).

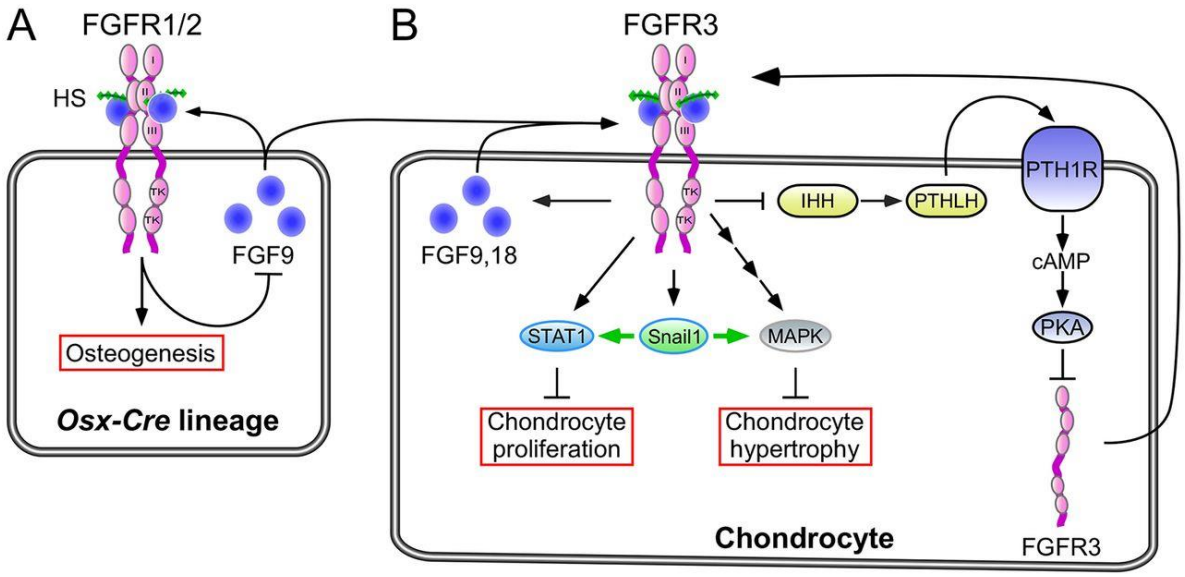

Figure 7. **FGF pathways regulate growth plate chondrocytes and bone growth.** ***(A)*** *FGFR1/2 are induced by FGF9 expression and express osteogenesis in the osteoprogenitor lineages* ***(B)*** *FGF-9 and -18 upregulate FGFR3 which indirectly activates Snail1 that indirectly inhibits the chondrocytes proliferation and hypertrophy through STAT1 and MAPK* (Karuppaiah *et al.*, 2016).

1.1.2.4. WNT signalling.

WNT family of signalling molecules comprises 19 secreted lipid-modified glycoproteins implicated in the development, growth and patterning of the skeleton via the activation of two pathways, canonical or non-canonical, dependent or independent of β-catenin, respectively (Komiya and Habas, 2008). The canonical β-catenin dependent pathway is initiated by canonical and non-canonical WNT molecules binding to the receptor complex of frizzled (FRZ)/low-density lipoprotein receptor-related protein (LRP) 5/6 and the accumulation of the transcription factor β-catenin which translocates to the nucleus inducing expression. The non-canonical pathway alters the levels of intracellular calcium by either activation of calcium/calmodulin-dependent kinase II (CamKII) and protein kinase C (PKC) or binding of heterotrimeric GTP-binding proteins to induce phospholipase C (PLC) and phosphodiesterase (PDE) (Kohn and Moon, 2005; Komiya and Habas, 2008).

Depending on the development stage, mouse models have shown that both pathways can have opposing roles. For example, during the mouse embryonic development the canonical β-catenin dependant pathway can inhibit development as opposed to non-canonical WTN signalling which promotes it, whereas, during the postnatal growth, both pathways are involved in chondrocyte differentiation and osteoblast regulation (Andrade *et al.*, 2007; Usami *et al.*, 2016). Mutations in this signalling pathway lead to delay in chondrogenesis, hypertrophy and endochondral bone development (Ma *et al.*, 2013).

1.1.2.5. BMPs

Bone Morphogenetic Proteins (BMPs) are members of the transforming growth factor-β (TGF- β) superfamily that are implicated in the formation of the skeleton and regulation of cell differentiation and maturation (Figure 8). Due to their unique ability to produce ectopic cartilage, BMPs have been widely studied. BMP2, 4, 5, and 7, in particular, are implicated in chondroprogenitor determination, condensation of MSC and differentiation into chondrocytes (Wozney *et al.*, 1988; Pizette and Niswander, 2000) and BMP2, 4 and 6 are highly expressed by the proliferating chondrocytes and involved in hypertrophy in contrast to BMP3 is expressed in the resting zone, as an antagonist of hypertrophy (Nilsson *et al.*, 2007).

BMPs exert their function via two types of transmembrane receptors that hold an intrinsic serine/threonine kinase activity, BMP type I and II (BMPRI and BMPRII) (Figure 8). hetero-dimerization of both receptors is achieved once the BMPs bind to the BMPRII, which

consequently phosphorylates BMPRI. This phosphorylation results in the recruitment and phosphorylation of signal transducers, R-SMAD1, 5 and 8 (receptor-regulated SMAD) which forms a heterocomplex with SMAD4 called Co-SMAD (Common-partner SMAD) that translocate into the nucleus inducing transcription of genes (Nishimura *et al.*, 2003).

Mice overexpressing *Noggin,* an antagonist of BMPs that inhibits cartilage formation, in the cartilage growth plate, develop shorter growth plate and higher amount of hypertrophic chondrocytes whereas *Noggin* knockout mice show exacerbated growth plate and skeletal bones and reduction of other signalling molecules such as IHH (Brunet *et al.*, 1998; Pizette and Niswander, 2000; De Luca *et al.*, 2001; Tsumaki *et al.*, 2002). Interestingly, BMPs, especially BMP2 and 4, maintain a positive feedback loop with IHH by inducing IHH gene expression, showing the high level of complexity and balance that is required to achieve a successful skeletal development (Figure 8) (Pathi *et al.*, 1999). Due to this and their implications in other tissues, certain mutations affecting BMPs or TGF-βs and their receptors or signal transducers, develop early embryonic lethality. For instance, Smad-1 and -2 knockout mice died during gestational periods, due to embryonic defects and failure to establish the anterior-posterior axis respectively. Interestingly, Smad3 null mice survive, however, develop impaired immunological functions, cancer and osteoarthritis later in life (Song, Estrada and Lyons, 2009).

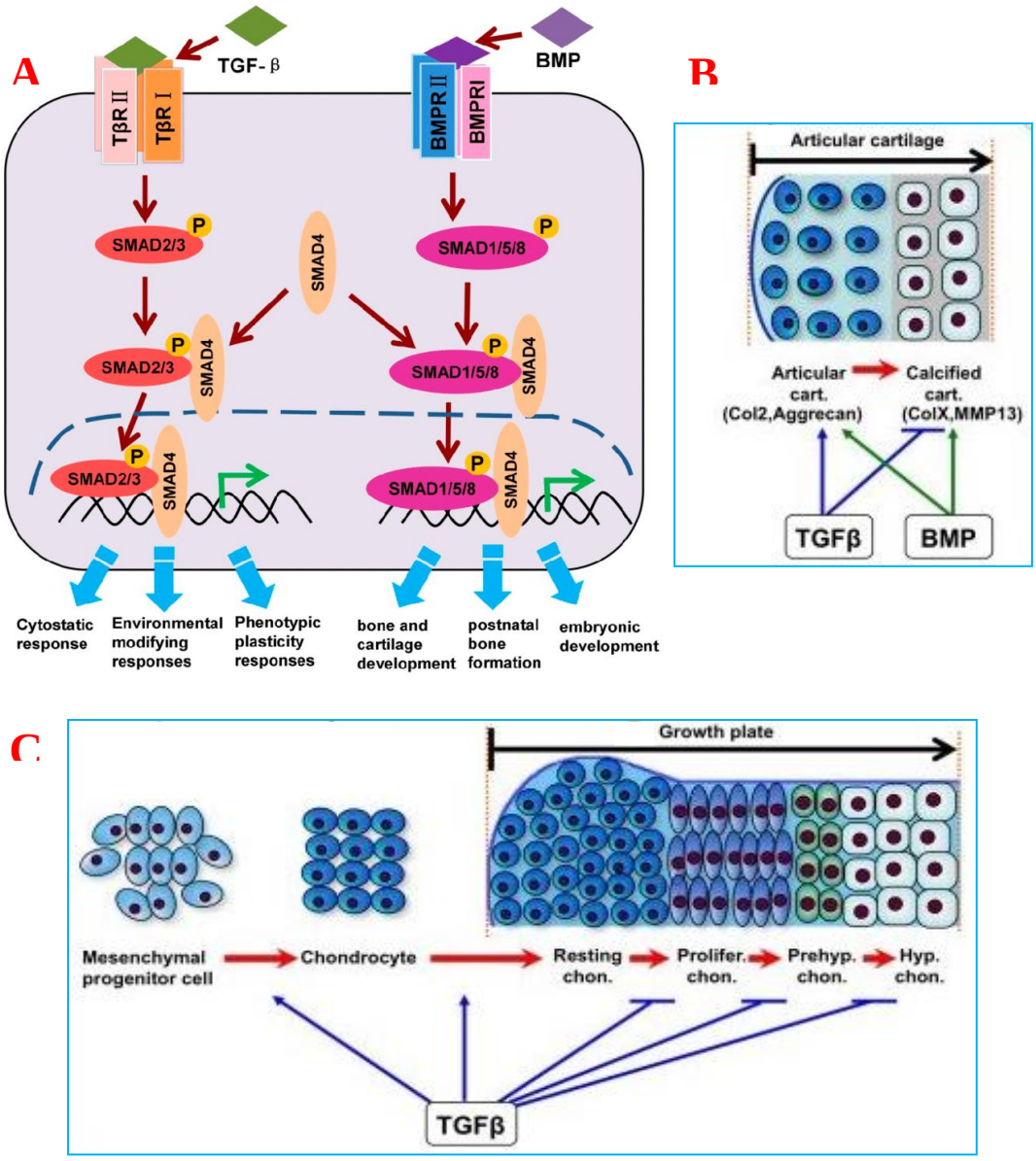

Figure 8. **Representation of BMP and TGF-β activation pathway and functions.** ***(A)*** *TGF-β and BMP bind its receptor (TβRI and II or BMPRI and II respectively) which phosphorylases SMAD2/3for TGFβ or SMAD 1/5/8 for BMP that joints SMAD4 and translocate to the nucleus increasing the transcription of genes for bone and cartilage development* (Xie *et al.*, 2014) ***(B)*** *TGF-β and BMP induce chondrogenesis and secretion of type II collagen and aggrecan. However, TGF- of type II collagen and aggrecan acts as an antagonist of BMP preventing hypertrophy* (Wang, Rigueur and Lyons, 2014) ***(C)*** *TGF- β is involved in the skeletal development inducing cell condensation and differentiation, in the growth plate inhibits proliferative and hypertrophic cell differentiation and stimulates, with BMP, ECM secretion* (Wang, Rigueur and Lyons, 2014)

1.1.2.6. VEGF

Vascular Endothelial Growth Factor (VEGF) is expressed by hypertrophic and perichondrium chondrocytes. It plays a key role during endochondral ossification allowing the invasion of the blood vessels into the perichondrium and cartilage, thus regulating the ossification centre formation and endochondral ossification (Dai and Rabie, 2007; Gerber et al., 1999). VEGF is also implicated in the proliferation and differentiation of osteoclasts and osteoblasts through the production of osteogenic factors, and during chondrogenic

differentiation, where it is upregulated by RUNX2, BMPs, TGF-β1 and MMP-9 (Dai and Rabie, 2007; Nakagawa et al., 2000; Wang et al., 1997). Knock-out mouse models for Vegf show the altered bone formation and an increase in the size of the hypertrophic zone in the growth plate (Gerber et al., 1999).

1.1.2.7. RUNX2

Pre-hypertrophic and hypertrophic chondrocytes express RUNX2, also known as core-binding factor Subunit alpha-1 (CBFA1) that promotes hypertrophy through regulating the expression of type X collagen and regulation of osteoblast differentiation. RUNX2 is part of the runt-domain gene family of transcription factors made of RUNX1, RUNX2, and RUNX3 (Enomoto *et al.*, 2000; Zheng *et al.*, 2003; Komori, 2015). A knockout out mouse for this gene produces a lethal phenotype with a lack of bone development, showing the importance of this transcription factor in skeletal development (Otto *et al.*, 1997).

1.2 Articular Cartilage

There are three types of cartilage tissue found in the human body: hyaline, fibrous, and elastic cartilage (Figure 9). This classification is based on the biochemical composition and the structural and mechanical properties of the respective tissues (Bhosale and Richardson, 2008). Whereas hyaline cartilage is the most abundant cartilage in the human body, fibrous cartilage is mainly found within the knee at the menisci and the intervertebral disc, and elastic cartilage is present in the outer ears, Eustachian tube and epiglottis (Roughley, 2006).

Hyaline cartilage is found in the nose, larynx, trachea, bronchi and end of ribs, where it provides flexible support, and at the end of long bones (articular cartilage) where it distributes and protects from the forces produced during joint motion (Watkins *et al.*, 2009).

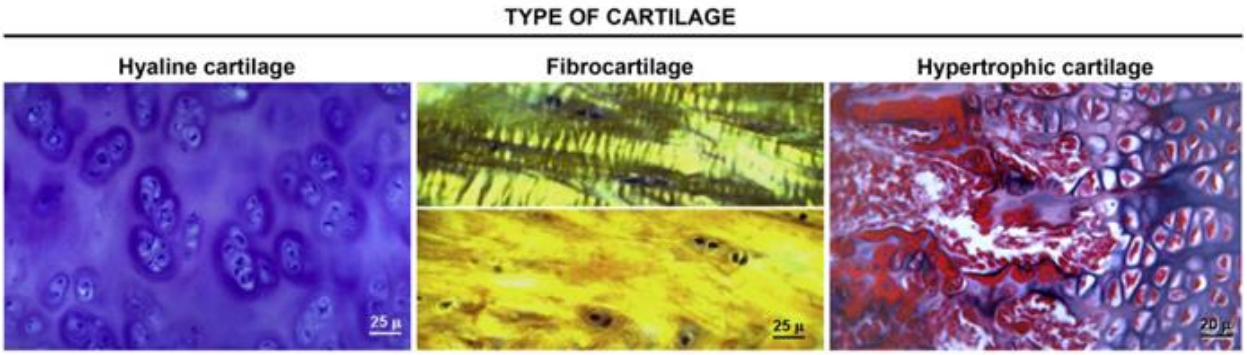

Figure 9. Types of cartilage and the main fibrous component. *Hyaline cartilage stained with haematoxylin & eosin, fibrocartilage with haematoxylin and tartrazine visualised under polarised light, and hypertrophic cartilage stained with AZAN trichrome stain. (Armiento, Alini and Stoddart, 2019)*

Articular cartilage is a highly specialized hyaline cartilage located at the ends of diarthrodial joints to provide a mechanically stable loadbearing template with high compressive strength and minimise friction coefficient by lubrication (Figure 10) (Lima *et al.*, 2008; Fox, Bedi and Rodeo, 2009). It is roughly 2 to 4 mm thick (depending on the joint) and composed of a dense extracellular matrix (ECM) and unique and specialised cells, the chondrocytes, that maintain the mechanical properties of the tissue by remodelling its ECM composition (Fox, Bedi and Rodeo, 2009). Cartilage lacks vascular, lymphatic and nervous system, which results in poor regenerative and healing capacity and leaves it vulnerable to degeneration and diseases (Klein *et al.*, 2009; Fox, Bedi and Rodeo, 2009).

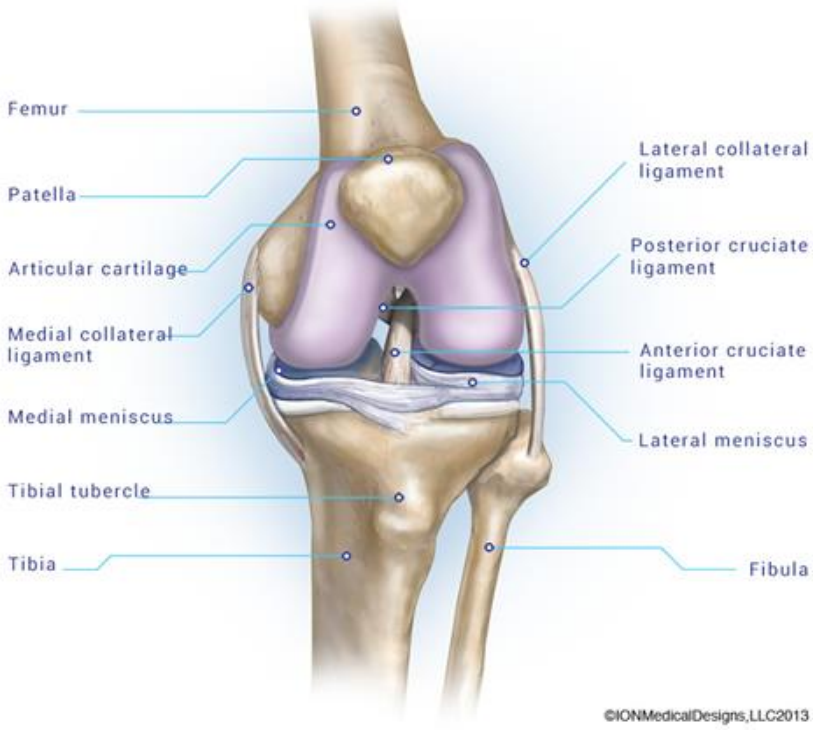

Figure 10. Joint anatomy and articular cartilage. *Right knee joint anatomy from IONMedicalDesigns, LLC2013.*

Hyaline articular cartilage is an avascular, alymphatic and aneuronal tissue mainly comprised of ECM, with chondrocytes representing 1-5% of the total tissue volume (Bhosale and Richardson, 2008). The ECM is a dynamic network of macromolecules that maintains the structure and mechanical properties of the tissue and provides mechanical stress transduction, protection for the chondrocytes against mechanical load and filtration of nutrients (Bhosale and Richardson, 2008; Fox, Bedi and Rodeo, 2009). Its composition is based on water, collagens, proteoglycans, glycoproteins, glucosaminoglycans (GAG) and non-collagenous proteins (Mow, Ratcliffe and Poole, 1992).

Articular cartilage is an anisotropic tissue characterised by a zonal stratification of macromolecular arrangement. Four different zones can be distinguished: superficial, middle, deep and calcified zone, each one with specific ECM composition, zone thickness, oxygen concentration and chondrocyte morphology that are of high importance for the integrity and biomechanical properties of the tissue (Klein *et al.*, 2009; Peng *et al.*, 2014).

The differential gradient of oxygen throughout the articular depth affects the cell function in each zone. Specifically, oxygen concentration varies from 5% of oxygen at the surface zone and decreasing to 1-2.5% in the middle and just 1% on the deep zone (Zhou, Cui and Urban, 2004).

1.2.1 Zonal stratification

The superficial zone of articular cartilage comprises 10-20% of the total cartilage thickness. Chondrocytes in this zone have a characteristic flattened ellipsoid shape and orientate parallel to the joint surface (Figure 11) (Bhosale and Richardson, 2008; Fox, Bedi and Rodeo, 2009). The cells in this zone produce lubricin, a glycoprotein whose main role is to reduce friction and wear by maintaining a lubricated joint surface (Schumacher *et al.*, 1994). The main ECM macromolecules in the superficial zone are collagen fibres, mainly type II collagen, which is arranged parallel to the articular surface, densely packed and stabilised by cross-linking with other molecules such as type IX collagen (Fox, Bedi and Rodeo, 2009; Peng *et al.*, 2014). The parallel arrangement of the collagen fibres and the lubrication contribute to the integrity of the layer and give it high mechanical stability, thus protecting the rest of the cartilage tissue and giving it resistance to bear the shear, tensile and compressive stresses exerted on it by the normal joint function (Bhosale and Richardson, 2008; Fox, Bedi and Rodeo, 2009). The characteristic arrangement and orientation of the collagen fibres in the different zones of the cartilage is described as 'Benninghoff arcades' (Klika *et al.*, 2016). Furthermore, due to the lack of blood vessels, the superficial zone protects the synovial tissue immune system and regulates the transport of large macromolecules and oxygen to underlying layers by osmosis and diffusion (Bhosale and Richardson, 2008; Bonnevie *et al.*, 2015).

The middle zone (Figure 11) represents 40-60% of the total cartilage thickness. However, the chondrocytes in this zone are scarcer, spheroidal and are arranged perpendicularly to the surface (Bhosale and Richardson, 2008; Peng *et al.*, 2014). The concentration of proteoglycans is higher in this layer, whereas the collagen fibres, mainly type II collagen, are found in a lower amount, larger diameter and randomly orientated. This specific composition allows the tissue to maintain compressive integrity and tensile resistant properties (Fox, Bedi and Rodeo, 2009; Becerra *et al.*, 2010).

The deep zone (Figure 11) is located farthest away from the joint surface and provides the tissue with additional resistance to compressive forces. This zone represents the remaining 30% of the articular cartilage thickness. The chondrocytes are rounded and arranged in perpendicular columns. In this zone, the ECM contains a high amount of glycosaminoglycans and perpendicularly oriented type II collagen fibres (Peng *et al.*, 2014; Zhang, Blalock and Wang, 2015).

A characteristic tidemark marks the transition to the calcified zone. The role of the calcified area is to act as a transition zone between the cartilage and the subchondral bone and to prevent the potential vascular invasion towards articular cartilage layers (Bhosale and Richardson, 2008). Chondrocytes in the calcified zone produce a calcified cartilage matrix, containing type X collagen. These chondrocytes present a hypertrophic phenotype and are larger than in any other zones. The calcified layer plays an important role in maintaining the structural integrity and absorbing impacts along the subchondral bone surface (Bhosale and Richardson, 2008; Fox, Bedi and Rodeo, 2009; Iwamoto *et al.*, 2013).

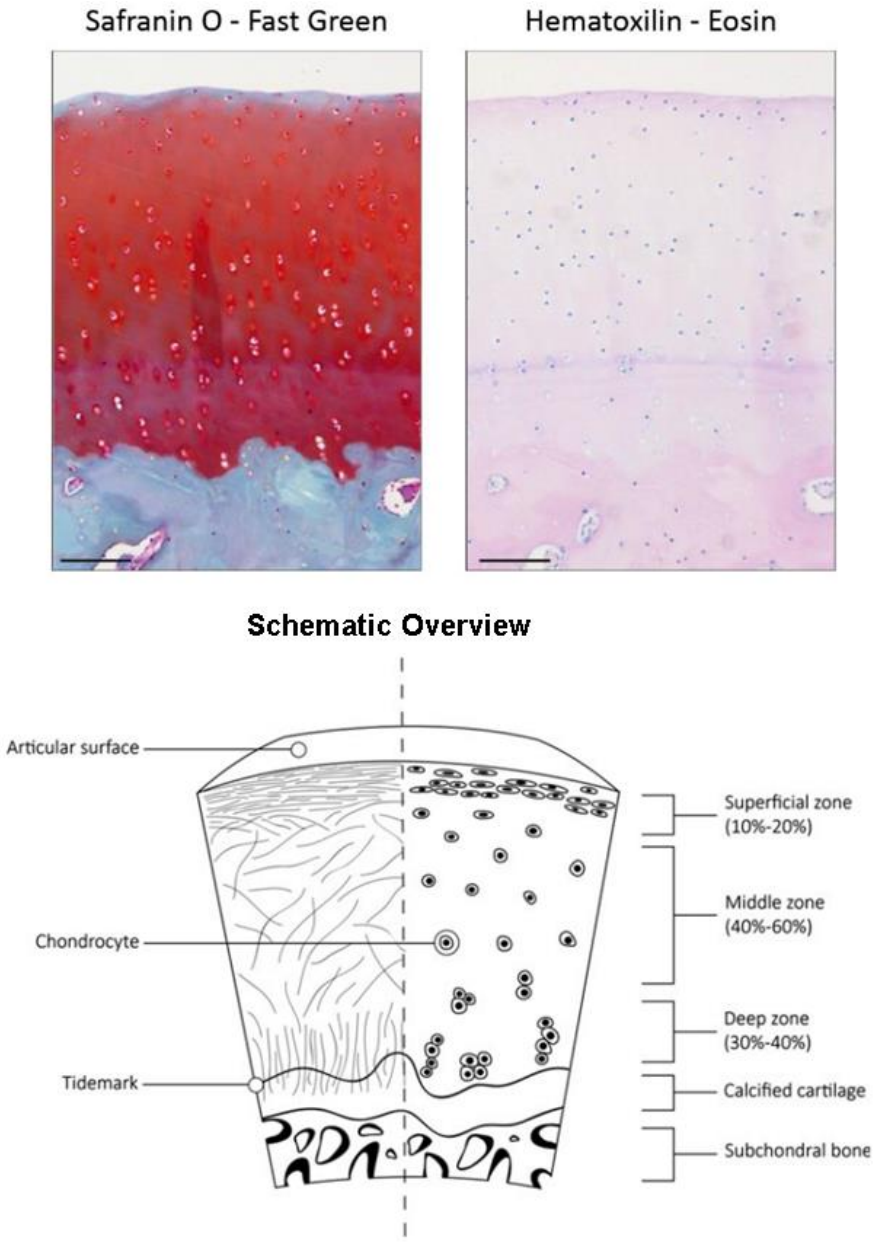

Figure 11. Articular cartilage composition and schematic overview. *Safranin O dye for cartilage proportional to its proteoglycan content, while Fast green stains for bone. Haematoxylin staining for nuclei while eosin for ECM. Scale bar = 100 µm.* (Thielen, van der Kraan and van Caam, 2019) *Schematic overview showing the different arrangement of the collagen fibres along with the tissue and its zone classification* (Ondrésik, Oliveira and Reis, 2017).

The ECM is a dynamic network of macromolecules that maintains the structure and mechanical properties of the tissue and provides mechanical stress transduction, protection for the chondrocytes against mechanical load, and filtration of nutrients (Bhosale and Richardson, 2008; Fox, Bedi and Rodeo, 2009). Its composition is based on water, collagens, proteoglycans, glycoproteins, glucosaminoglycans (GAG) and non-collagenous proteins (Mow, Ratcliffe and Poole, 1992).

1.2.2 Cartilage ECM regions

The cartilage ECM can also be divided into three regions of different function and properties based on the proximity to chondrocytes: pericellular - adjacent to the chondrocytes, interterritorial - contiguous to the pericellular region, and territorial - the farthest away from the chondrocyte (Goldring, 2012).

The pericellular ECM in articular cartilage is rich in proteoglycans and contains mainly type VI collagen, with a remarkable absence of collagen type II. Collagen fibres in the pericellular matrix produce a narrow filamentous network that connects the chondrocytes with the territorial matrix (Poole, Flint and Beaumont, 1984; Goldring, 2012). Besides, other non-collagenous molecules such as fibromodulin, decorin, and anchorin CII act as cell membrane-associated and collagen-anchoring molecules, playing an important role in the function of this region. The main purpose of the pericellular matrix is to contribute to the signal transduction after mechanical forces are applied to the tissue by propagating the mechanical loads from the ECM to the cell membrane, that will activate intracellular cascades and genes transcription (Bhosale and Richardson, 2008; Fox, Bedi and Rodeo, 2009; Goldring, 2012).

The territorial matrix is located adjacent to the pericellular matrix and is thicker than the latter. Thin collagen fibres, mainly type II collagen, are the principal component of this region. Their criss-cross like deposition leads to a basket-like network whose main function is to protect the chondrocytes from damages during mechanical impacts and deformation of the tissue (Poole, Flint and Beaumont, 1984; Fox, Bedi and Rodeo, 2009).

The interterritorial region comprises the majority of the ECM volume and is abundant in large diameter collagen fibrils, mainly types II, IX and XI. Besides collagen, non-collagenous proteins and large proteoglycan molecules such as aggrecan are present in the matrix (Poole, Flint and Beaumont, 1984; Goldring, 2012). The complexity of this structure contributes to the biomechanical properties of the cartilage and the ability to withstand mechanical loads (Bhosale and Richardson, 2008; Fox, Bedi and Rodeo, 2009).

1.2.3 Chondrocytes

Chondrocytes arise from mesenchymal stem cells (MSC) and are the only cell type found in articular cartilage, representing solely 1-5% of the total volume of the tissue (Figure 12). The environment surrounding the chondrocytes has a unique and precise structure easily disrupted by changes in oxygen levels or pH, and the normal state of the tissue is at a pH of 7.4 and low oxygen density. This microenvironment is essential for survival and function. Consequently, the main functions of chondrocytes are reliant on their interactions with the ECM and reaction to mechanical forces such as piezoelectric forces, hydrostatic pressures and mechanical loads or molecular stimulus by growth factors and pro-inflammatory cytokines (Fox, Bedi and Rodeo, 2009; Akkiraju and Nohe, 2015).

The main function of the articular chondrocytes is to provide the tissue with a complex ECM to withstand high loads. For instance, their mechanic sensitivity enables chondrocytes to detect shear stress and produce a higher amount of collagen in the superficial zone, while increasing the concentration of GAGs in the middle layer to withstand compression (Bhosale and Richardson, 2008; Fox, Bedi and Rodeo, 2009).

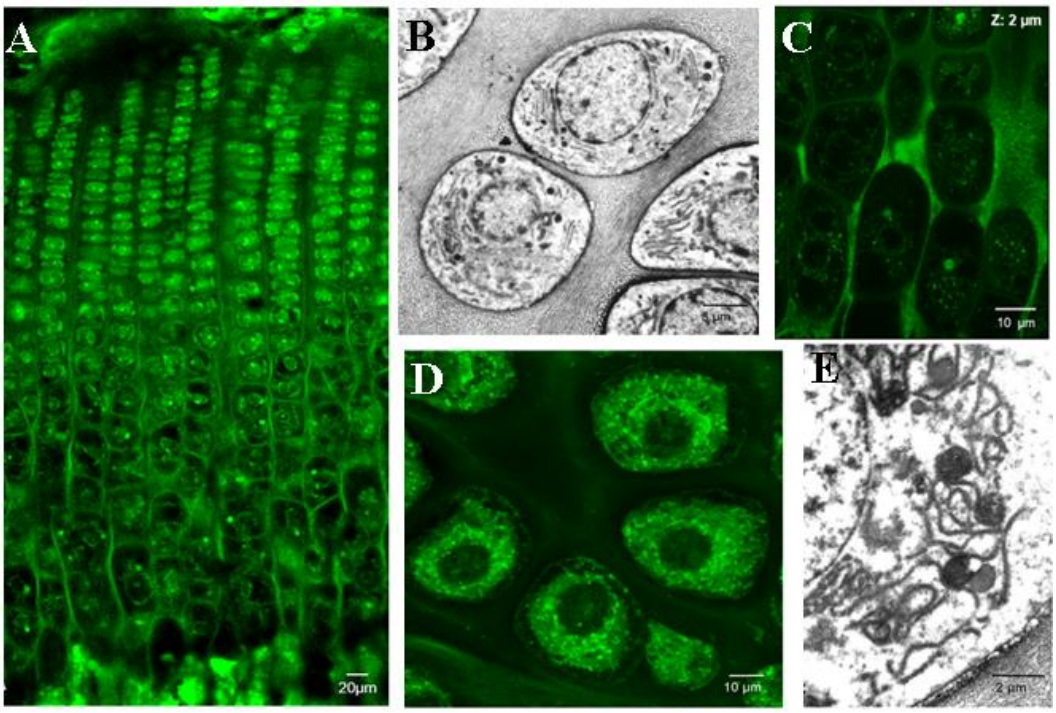

Figure 12. Pre-hypertrophic chondrocytes. A) *Low-power micrograph showing chondrocytes arranged in columns variating in size, shape, and cytoplasm density via immunohistochemistry staining. Scale bar: 20 µm.* ***B)*** *Pre-hypertrophic chondrocytes on transmission electron micrograph showing the rough endoplasmic reticulum via immunohistochemistry staining. Scale bar: 5 µm.* ***C)*** *Optical sections of the growth plate columns chondrons. Scale bar: 10 µm.* ***D)*** *Pre-hypertrophic chondrocytes labelled with fluorescence in a confocal micrograph. Scale bar: 10 µm.* ***E)*** *Rough endoplasmic reticulum, mitochondria and several lipid droplets in chondrocytes in a transmission electron micrographs. Scale bar: 2 µm. Images adapted from* (Fernández-Iglesias *et al.*, 2020).

1.2.4 Extracellular Matrix (ECM)

The cartilage ECM can be further divided into solid and fluid phase. The solid phase consists of collagen, proteoglycans, glycosaminoglycans and non-collagenous proteins. The fluid phase comprises 60-80% of the weight of the tissue and interacts with the macromolecules such as proteoglycans via negative electrostatic repulsion forces. This interaction between both phases is of high importance to allow the tissue to resist and absorb compressive loads by swelling pressure (Mow, Ratcliffe and Poole, 1992; Ateshian *et al.*, 1997).

1.2.4.1 Water

The water in cartilage tissue is of high importance for withstanding mechanical loads and preventing friction in the joint space. The flow of water aided by the low permeability of the tissue allows load-dependent deformation and frictional resistance by lubricating the tissue. In addition to the transport and distribution of nutrients, water reacts with the negatively charged glycosaminoglycans (GAGs), creating electrostatic repulsive forces that contribute to swelling pressure (Fox, Bedi and Rodeo, 2009; Akkiraju and Nohe, 2015).

Water comprises 60-80% of the total cartilage weight and is unequally distributed along with the tissue. There is up to 80% of the water in the superficial zone while in the deep zones, the water contents decrease to less than 60%. Besides water, the cartilage tissue fluid also comprises inorganic ions dissolved in it, such as sodium, calcium and potassium (Fox, Bedi and Rodeo, 2009). These inorganic ions are of high importance since a tissue under load will be affected not only by the loading rate and the load but also will depend on the Donnan osmotic effect (Lai, Hou and Mow, 1991).

Ageing and diseases such as osteoarthritis (OA) are related to disruption of the water content in cartilage affecting the biomechanical properties of the tissue. During healthy ageing, the water content decrease is induced by the reduction of GAG content in cartilage, in contrast, during OA, as the ECM deteriorates, greater permeability allows invasion of water from superficial layers deeper into the tissue (Bhosale and Richardson, 2008).

1.2.4.2 Collagen

Collagens are the most abundant proteins in the cartilage ECM and comprise 10-20% of the wet weight and up to 60% of the dry weight of the tissue (Figure 13) (Akkiraju and Nohe, 2015). Type II collagen is the dominant insoluble fibrous protein in the cartilage ECM and consists of 3 parallel polypeptide strands, two α1 chains and one α2 in a helical conformation coil forming a homotrimer (Lodish *et al.*, 2000).

The basic function of the collagen networks is to stabilise and provide tensile and compressive strength to cartilage as well as to protect the cells against high shear stress and interstitial swelling, to contribute to proteoglycans anchorage, and to attach the cartilage layer to the subchondral bone (Akkiraju and Nohe, 2015; Tsumaki, 2015).

Type I collagen is directly associated with disrupted and damaged articular cartilage, and is not present in the healthy cartilage but is highly abundant in bone (Tsumaki, 2015). Type II collagen is the main collagen found in cartilage comprising 90-95% of all collagen in the tissue. It is associated with type IX and XI collagens producing a meshwork that provides the tissue with tensile strength. At the same time, type IX and XI collagens regulate the collagen fibril diameters and support the networking function by respectively producing cross-links on the surface of the fibrils or within the macrofibres (Bhosale and Richardson, 2008; Akkiraju and Nohe, 2015). Type VI collagen is principally presented in the pericellular region where secures the attachment of chondrocytes to the macromolecules of the ECM. Finally, collagen X is localised in the deep zone and is synthesised specifically by hypertrophic chondrocytes (Choi *et al.*, 2010; Akkiraju and Nohe, 2015).

A

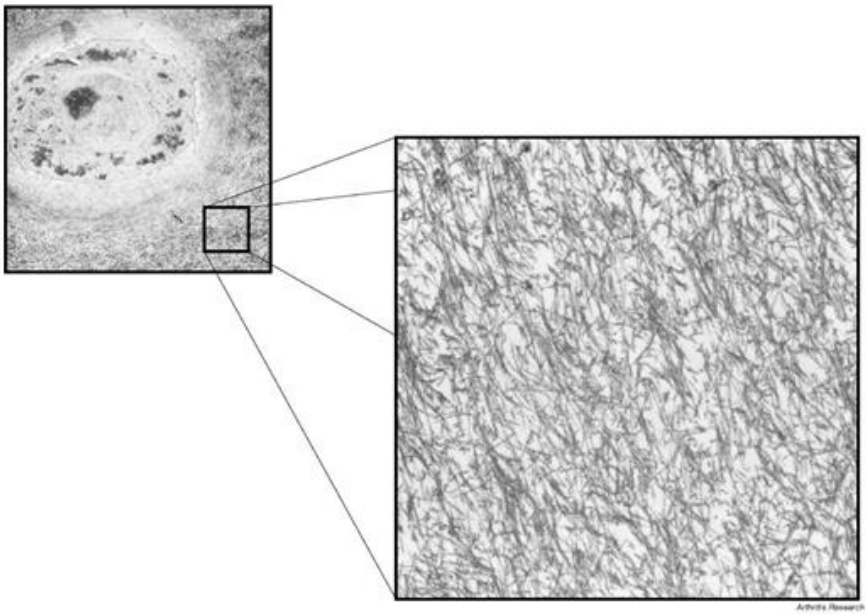

B

Fibril forming	Type I, II	Microfibrils; Collagen fibrils; Collagen fibers
Network forming	Type IV	Dimer; C-terminal; Tetramer; Network
	Type VI	Dimer; Tetramer; Beaded filament
FACITs	Type IX, XII, XIV	Monomer; Globular C-terminal; Collagen XII or XIV; Collagen type I fibrils; Collagen IX; Collagen type II fibrils
Transmembrane	Type XIII, XVII, XXIII, XXV	Cytoplasm; N-terminal NC; C-terminal
Multiplexin	Type XVIII	N-terminal NC; Globular C-terminal: Endostatin

Figure 13. Collagen fibril meshwork in the territorial ECM and Table summarising the collagen and their function and structure. A) *Transmission electron microscopy showing the complex collagen fibril meshwork found in the ECM of articular cartilage* (Eyre, 2002). ***B)*** *A Table summarising the main types of collagen and their various roles fibril formation, establishment a solid ECM network, anchorage to cell membrane and transduction of mechanical signals to the nucleus (Singh et al., 2012).*

1.2.4.3 Proteoglycans

Proteoglycans are the second most abundant group of macromolecules in cartilage ECM, and they represent 10-20% of the total wet weight of the tissue (Bhosale and Richardson, 2008; Akkiraju and Nohe, 2015). Proteoglycans consist of a vastly glycosylated protein monomer attached covalently to one or more highly anionic glycosaminoglycans linear polysaccharide chains (Fox, Bedi and Rodeo, 2009). Proteoglycans possess a heavily negatively charged structure derived from the GAG chains that can bind to large amounts of water resulting

in a high osmotic swelling pressure, which allows the tissue to withstand compressive loads (Figure 14) (Mow, Ratcliffe and Poole, 1992; Akkiraju and Nohe, 2015).

Proteoglycan function is dependent on their ability to aggregate. The type of the GAG chains and the core protein, thus are subdivided into two classes: large aggregating proteoglycans, such as aggrecan, which provide the tissue with resilience to compression and stiffness by recruiting large amounts of water, and small leucine-rich proteoglycans (SLRPs), such as decorin, biglycan and fibromodulin, which contribute to the stabilization of the matrix by binding and interacting with other matrix macromolecules (Sivan, Wachtel and Roughley, 2014).

The largest proteoglycan found in cartilage and the major non-collagenous component of the tissue is aggrecan, which is made up of numerous chondroitin sulphate and keratan sulphate GAG chains that form greater aggregates by binding non-covalently to linear hyaluronan (HA) (Fox, Bedi and Rodeo, 2009; Sivan, Wachtel and Roughley, 2014). Aggrecan aggregates play an important role in cartilage by maintaining the resilience to compressive loads, shear, hydraulic permeability and providing great swelling pressure (Jin and Grodzinsky, 2001; Han, Grodzinsky and Ortiz, 2011). HA is a long, linear and negatively charged GAG capable of binding more than 100 aggrecan monomers, leading to aggrecan aggregation. This GAG is known to play a role in lubrication (Han, Grodzinsky and Ortiz, 2011; Wu *et al.*, 2015). Diseases or ageing of the articular cartilage have been linked to a decrease and breakdown in proteoglycans, and as a result, a reduction in the load-bearing abilities (Han, Grodzinsky and Ortiz, 2011).

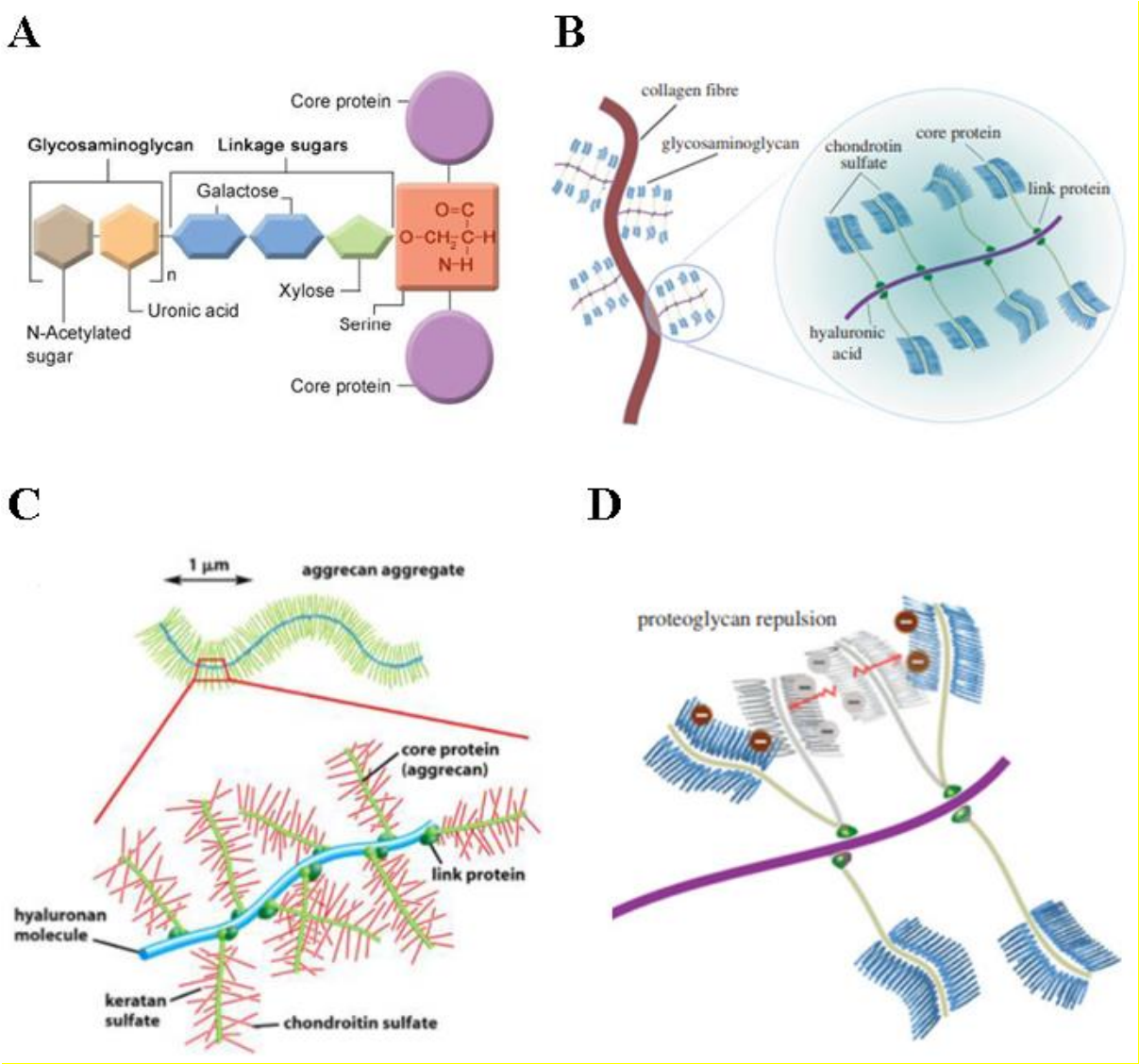

Figure 14. Proteoglycan structure. A) *Schematic of a basic structure of proteoglycans* (Fox, Bedi and Rodeo, 2009). ***B)*** *Schematic showing the cartilage network with proteoglycans aggregates interacting with type II collagen fibres* (Manzano *et al.*, 2015). ***C)*** *Structure of proteoglycan aggregates. The proteoglycans aggregate via GAGs which are made of chondroitin-sulphate and keratan sulphate-rich regions linked to hyaluronic acid* (Fox, Bedi and Rodeo, 2009). ***D)*** *Schematic showing the phenomenon of repulsion that takes place in proteoglycans with the surrounding water* (Manzano *et al.*, 2015).

1.2.4.4 Non-aggregating proteoglycans

The non-aggregating proteoglycans, also known as small leucine-rich proteoglycans (SLRPs), are distinguished by their smaller size and can bind collagen and other ECM molecules such as growth factors, potentially contributing to chondrocyte differentiation and function. The most common non-aggregating proteoglycans are decorin, biglycan and fibromodulin (Bhosale and Richardson, 2008; Fox, Bedi and Rodeo, 2009). Decorin consists of 1 dermatan sulphate chain and is involved in regulating collagen fibril arrangement by staying linked to mature collagen, and in the modulation of the function of transforming growth factor-beta (TGFβ). Biglycan comprises two dermatan sulphate chains and is involved in binding

collagen type II and VI acting as a coupler among different fibrils. Finally, fibromodulin contains keratan sulphate chains, and its main role is binding and modifying collagen fibres (Fox, Bedi and Rodeo, 2009; Aspberg and Aspberg, 2016).

1.2.4.5 Glycoproteins

Glycoproteins and non-collagenous proteins contribute to the organization and maintenance of the macromolecular structure of the extracellular matrix and the anchorage of chondrocytes. Some of these proteins such as lubricin, cartilage oligomeric matrix protein (COMP), cartilage matrix protein (CMP), cartilage intermediate-layer protein (CILP), fibronectin, proline and arginine-rich end leucine-rich repeat protein (PRELP) and anchorin CII, are made up of a protein core bound to monosaccharides and oligosaccharides (García-Carvajal *et al.*, 2013; Bonnevie *et al.*, 2015).

Lubricin is implicated in lubrication and wear protection, COMP in collagen fibrillogenesis and interaction, CMP in ECM stability by connecting to other ECM elements such as COMP, collagens and proteoglycans and PRELP in connecting the basement membrane to the connective tissue. Some of these are upregulated in disease, for instance, levels of CILP are increased during OA, and fragments of fibronectin and COMP are released from the tissue further enhancing the breakdown (Bonnevie *et al.*, 2015).

1.3 Mechanical influences on cartilage

As previously mentioned, the main function of articular cartilage is bearing the mechanical load applied to the tissue. Lubricin, in the surface, and hyaluronic acid, are some of the proteins that facilitate the low coefficient of friction allowing the absorption and dissipation of this mechanical load (Houard, Goldring and Berenbaum, 2013).

Contrary to initial beliefs, a moderate mechanical loading contributes to the maintenance of homeostasis and integrity of cartilage, favouring the increase in aggrecan and decreasing MMP-13 expression and reducing the incidence of osteoarthritis (Bader, Salter and Chowdhury, 2011; Houard, Goldring and Berenbaum, 2013). Chondrocytes are exposed to a wide variety of stress, such as, *in vivo* cyclically mechanical loading, which results in a composite of radial, tangential and shear stress on the cells, piezoelectric forces, and hydrostatic pressures (Fox, Bedi and Rodeo, 2009; Lee and Salter, 2015). Depending on the localisation, depth, and orientation relative to the joint surface, the loading capacity differs, for example, the load will generate a combination of tensile, compressive and shear stress in the tissue, and

depending on the area varies from 0.4-2.0MPa (compressive modulus) and 5-25MPa (tensile modulus) (Akizuki *et al.*, 1986; Armstrong and Mow, 1982; and Athanasiou *et al.* 1994).

When a mechanical load is applied to the tissue, the interstitial fluid or water within the matrix is pressurised and the reduction of the fluid flow rates delays the pressure loss from the surrounding matrix, this pressurisation is known as hydrostatic pressure, which ensures uniform stress (biphasic theory) avoiding cellular deformation and is one of the most influential stimuli during cartilage mechanical stress (Pattappa *et al.*, 2019). Despite the biphasic theory stating that the stress is distributed uniformly through the tissue, it has been shown that when a load is applied, the stress is distributed in gradients through the tissue, particularly on the joint surface (Lee and Salter, 2015). Hydrostatic pressure as mentioned previously is one of the most influential stimuli and has been predicted that approximately 90% of the load is withstood by fluid pressurisation within the tissue layers (Pattappa *et al.*, 2019). The ECM, mainly collagen and proteoglycan disperse the rate of fluid flow from pressurised regions, helping delay the pressure loss, although has been hypothesised that proteoglycans, due to their negative charged nature, attract the highest hydrostatic pressure (Pattappa *et al.*, 2019).

Chondrogenesis is affected by physiological stress, which plays an important role in regulating the metabolism and integrity of the tissue, as mechanical load maintains the fluid low and ion phase function stimulating chondrocyte metabolism (Lee and Salter, 2015). The low permeability of articular cartilage allows that under any pressure the interstitial fluid remains within the tissue avoiding mechanical deformation (Fox, Bedi and Rodeo, 2009). Articular cartilage viscoelasticity allows responding to any deformation via either flow-dependent or independent mechanism. The flow-dependant mechanism is characterised for presenting a biphasic viscoelastic behaviour, in which, the mechanism is caused by the interstitial fluid and frictional drag associated with it. However, the flow-independent component depends on macromolecular motion, specifically the intrinsic collagen-proteoglycan matrix viscoelastic behaviour and not the flow (Fox, Bedi and Rodeo, 2009).

During the loading of cartilage, mechanical signals generated are sensed by receptors located on the cell surface, such as primary cilium, integrin, syndecan, ion channels and other cell adhesion molecules that translated into chemical signals intracellularly, affecting the homeostasis and functional integrity (Deschner *et al.*, 2003; Houard, Goldring and Berenbaum, 2013).

Primary cilium functions as a mechano-receptor, among many other roles in cartilage homeostasis. It has been observed that the absence of the cilia produces defects in the matrix

deposition and the cellular organisation in both articular cartilage and growth plate tissues, suggesting its vast involvement in tissue integrity (Houard, Goldring and Berenbaum, 2013). Other mechanical sensors, integrin, function as mechanosensors, that through tyrosine phosphorylation activates cytoskeleton-associate enzymes at focal adhesion sites, which then activate in the nucleus transcription factors such as nuclear factor kappa B (NF-κB) and activator protein-1 (Deschner *et al.*, 2003). Therefore, cartilage integrity is maintained by the mechanical load applied to the tissue, resulting in a constant turnover of ECM components (Bader, Salter and Chowdhury, 2011).

1.4 Chondrodysplasias

Skeletal dysplasias are a group of over 450 heritable disorders affecting the development and growth of the skeleton. These diseases manifest in 1 in 5,000 births and vary in the clinical spectrum from mild to severe and lethal forms. Skeletal dysplasias are often characterised by disproportionate short stature, joint laxity, and skeletal deformations. Initial diagnosis and classification are based on clinical features and radiographic abnormalities (Krakow, 2015; Chen *et al.*, 2016).

Historically, the diagnosis of skeletal dysplasias was based on the radiographic features and patient examinations, and the diseases were often classes as "syndromes" based on pathogenetic similarities (Beighton *et al.*, 1992); however, thanks to advances in genetics, the more recent classifications focus on the class and function of the genes affected by the disease-causing mutations. This classification divides skeletal dysplasia into subgroups resulting from mutations in genes/proteins involved in the extracellular matrix, metabolic pathways, folding and degradation of macromolecules, hormones and signal transduction mechanisms, nuclear proteins and transcription factors, oncogenes and tumour suppressor genes and RNA and DNA processing and metabolism (Superti-Furga, Bonafé and Rimoin, 2001). A summary of examples of diseases depending on the gene affected is listed below (Superti-Furga, Bonafé and Rimoin, 2001):

1. Mutations in extracellular structural proteins
    a. COL1A1, COL1A2 (collagen1 α1, α2 chains), leading to Osteogenesis imperfecta disease.
    b. COL10A1 (collagen10 α1 chain), leading to Spondylometaphyseal dysplasia type Schmid.
    c. COMP (cartilage oligomeric matrix protein) leading to Pseudochondroplasia and Multiple epiphyseal dysplasias.

d. MATN3 (matrilin-3) leading to Multiple epiphyseal dysplasias
e. Perlecan leading to Schwartz-Jampel type 1.

2. Mutations in metabolic pathways
    a. PAPSS2 (phosphoadenosine-phosphosulfate-synthase 2) leading to Spondylo-epi-metaphyseal dysplasia Pakistani type.
    b. Vitamin K-epoxide reductase complex leading to Chondrodyssplasia punctate with vitamin K-dependent coagulation defects.
3. Mutations in folding and degradation of macromolecules
    a. Cathepsin K leading to Pysnodyostosis.
    b. MMP2 (matrix metalloproteinase 2) leading to Torg type osteolysis.
4. Mutations in hormones and signal transduction mechanism
    a. 25-α-hydroxycholecalciferol-hydroxylase leading to Vitamin D-dependent rickets type 1 (VDDR1).
5. Mutations in nuclear proteins and transcription factors
    a. LXM1B (LIM homeodomain protein) leading to Nail-patella syndrome.
    b. HOXD13 (homeobox gene) leading to Synpolydactyly.
6. Mutations in oncogenes and tumour suppressor genes
    a. SH3BP2 (c-Abl-binding protein) leading to Cherubism.
7. Mutations in RNA and DNA processing and metabolism
    a. RNAse MRP-RNA component leading to Cartilage-hair-hypoplasia.
    b. ADA (adenosine deaminase) leading to Severe combined immunodeficiency (SCID) with metaphyseal changes.

Mutations in group 1 affect extracellular structural proteins, such as collagens and proteoglycans. A broad variety of mutations have been identified in collagen types I, II, IX, X and XI and in genes encoding proteoglycans, leading to various diseases ranging from mild to severe phenotypes. Proteins serving as a link among extracellular matrix proteins are also affected, such as COMP resulting in Pseudoachondroplasia (PSACH) or MATN-3 resulting in and multiple epiphyseal dysplasias (MED) (Superti-Furga, Bonafé and Rimoin, 2001).

1.4.1 Pseudo-achondrodysplasia

PSACH is an autosomal dominant disease, with an incidence of 1 in 20,000 births, that results from mutations in the gene encoding cartilage oligomeric matrix protein (COMP) and characterised by short-limbed dwarfism, brachydactyly, deformity of legs and laxity of joints and ligaments (Briggs and Chapman, 2002; Tufan *et al.*, 2007). Radiographically the disease

shows irregular and small epiphyses and metaphyses, and a delay in the ossification of annual epiphyses (Figure 15). The patients often require bilateral hip replacement due to early-onset osteoarthritis (Briggs and Chapman, 2002). Mild forms of PSACH can phenotypically overlap with other chondrodysplasias such as multiple epiphyseal dysplasias (MED) (H.-C. Chen *et al.*, 2008).

Figure 15. **Radiographs of *pseudoachondroplasia* and multiple epiphyseal dysplasia patients**. ***(A)*** *For patient* ***ESDN-00521,*** *the radiography showed reduced and flat proximal femoral, distal femoral and proximal tibia epiphyses. Delayed ossification of the carpal bones and epiphyses in the wrist contrasted with normal phalanges, metacarpals and spine.* ***(B)*** *For patient* ***ESDN-01040****, at the age of 6 years, small hips and knees epiphyses and two round translucent areas in the distal femoral metaphysis similar to the ones in pseudoachondroplasia were observed.* ***(C)*** *Female patient with pseudoachondroplasia showing disproportion.* (Jackson *et al.*, 2012; Posey, Alcorn and Hecht, 2014).

MED results from mutations in genes encoding COMP, type IX collagen (chains α1, α2 and α3), MATN-3 and SLC26A2, however clinically the disease is less severe than PSACH (Superti-Furga *et al.*, 1999; Chapman *et al.*, 2001; Holden *et al.*, 2001). The disease is subdivided into two types, a milder type, Ribbing type, and a severe one, Fairbank type (Maddox *et al.*, 2000). In the mild form, patient height is not affected, but pain manifests in joints such as knees and ankles from year two to five. In the case of the more severe phenotype, debilitating hip pain and onset of osteoarthritis is visible in childhood and early adulthood (Maddox *et al.*, 2000). Radiographic studies of PSACH and MED patients show irregular and flat epiphyses in all weight-bearing joints, especially knees and hips, *genu varus* and *genu valgum* abnormalities and shorthands (Figure 15).

1.4.1.1 Cartilage Oligomeric Matrix Protein

COMP gene is localised on chromosome 19 (19p13.1). COMP is a 550kDa pentameric glycoprotein mainly found in cartilage, ligament and tendons, although *COMP* is also expressed in the synovium, smooth muscle and in fibrotic disease states (Briggs *et al.*, 1995; Coustry *et al.*, 2018). COMP, also referred to as thrombospondin 5 (TSP5), is a member of the thrombospondin family of multimeric matricellular proteins that can be either trimeric (A) or pentameric (B). Subgroup A comprises TSP-1 and -2 that form homotrimers with three identical units. TSP-3, -4 and -5 form homo-pentamers and belong to subgroup B (Figure 16) (Posey, Alcorn and Hecht, 2014). COMP's monomer is composed of an N-terminal oligomerisation domain (NTD), followed by four types 2 epidermal growth factor-like repeats (T2), eight highly conserved type 3 calcium-binding repeats (T3) and a highly conserved C-terminal globular domain (CTD) (Tan *et al.*, 2009).

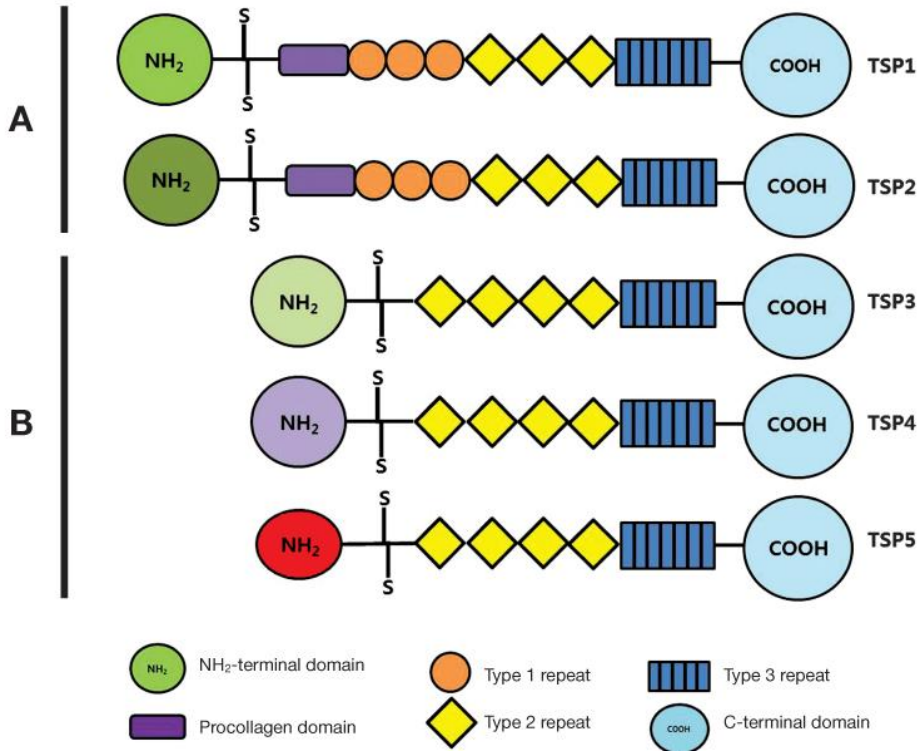

***Figure 16.* Schematic of the structure of thrombospondin family subgroups.** *In subgroup **A**, made up of TSP1 and -2, the monomer is made up of an N-terminal domain, followed by a procollagen domain, a type 1, 2 and 3 repeat domain and a C-terminal domain. These thrombospondins assemble into homotrimer. Subgroup **B**, converge into homo-pentamers, and their monomers are formed by an N-terminal domain, a type 2 and 3 repeat domain and a C-terminal domain* (Jeong, 2015).

The correct folding of the COMP protein (Figure 17) involves calcium and zinc ions that stabilise the structure. The highly conserved aspartic acid-rich T3 domain binds two calcium ions, whereas the CTD domain with a lectin-like-β sandwich structure binds four calcium ions (Posey, Coustry and Hecht, 2018). These two domains fold and form a tertiary

structure called the signature domain, which contributes to the correct folding and secretion of the protein (Posey, Coustry and Hecht, 2018). The monomer chains assemble into a pentamer via the NTD coiled-coil domain, which is stabilised by interchain disulphide bonds (Figure 18). This coiled domain has an affinity to hydrophobic molecules involved in skeletal development such as retinol and vitamin 1α,25(OH)2D3 (Malashkevich *et al.*, 1996; Ozbek, Engel and Stetefeld, 2002; Chen *et al.*, 2005).

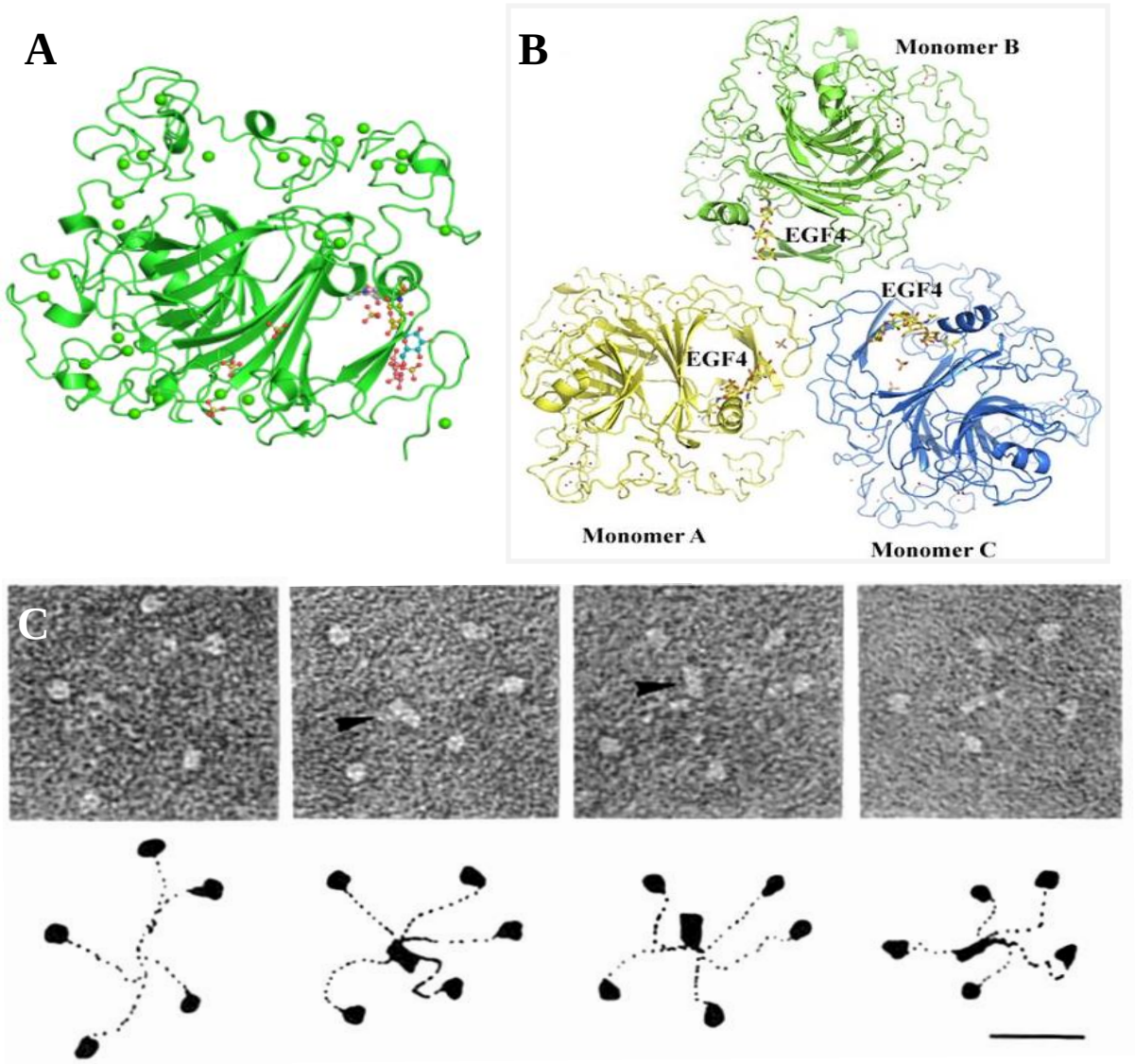

Figure 17. **Crystallography and rotary shadow structure from COMP.** ***(A)*** *Crystal structure of a single COMP monomer viewed from the signature domain* (Tan *et al.*, 2009). ***(B)*** *Crystal structure of three copies of COMP monomers interacting in an asymmetric unit viewed from the signature domain* (Tan *et al.*, 2009). ***(C)*** *Rotary shadow showing COMP in negative electron micrographs with its predicted pentameric assembling structure, scale bar: 25nm* (Mörgelin *et al.*, 1992).

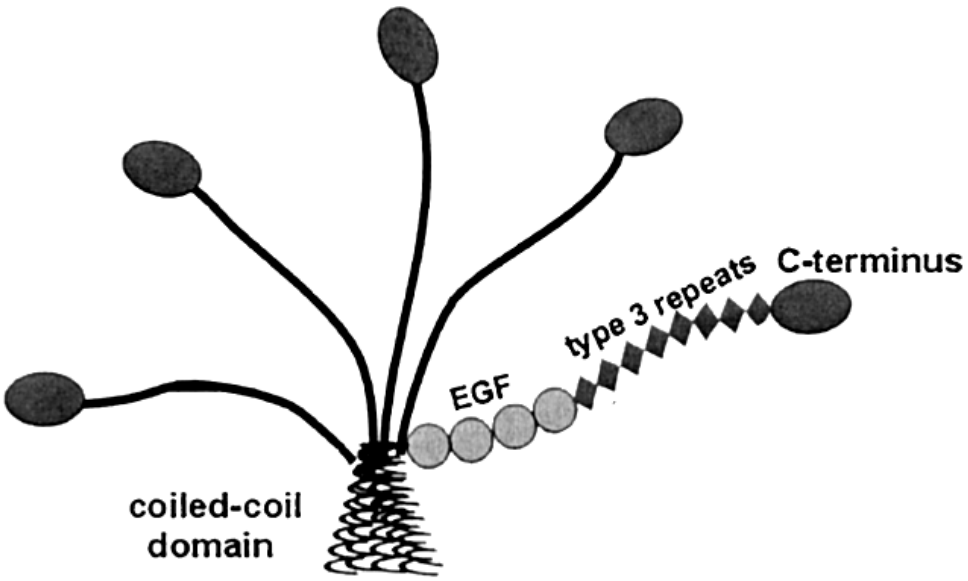

Figure 18. **Diagram of the pentameric structure of COMP.** *Five monomer chains are attached through their N-terminal domain forming a coiled-coil domain* (Maddox *et al.*, 2000)

1.4.1.2 Type 3 repeats domain

Type 3 repeats of COMP form an EF hand-like structure which consists of a helix-loop-helix structural domain mainly found in calcium-binding proteins (Figure 19). Not only the calcium binding helps to stabilise the protein and prevent proteolysis, but it also helps to maintain the structural conformation. Compared to an EF-hand structure, this domain lacks a secondary structure and contains 17 cysteines, a rich motif of aspartate, and 13 EF putative hands wrapped around the core of calcium ions (Misenheimer and Mosher, 1995; Maddox *et al.*, 2000; Kvansakul, Josephine C Adams and Hohenester, 2004).

1.4.1.3 C-terminal domain

The globular C-terminal domain is a β sandwich of two curved antiparallel β-sheets belonging to the family of lectin-like folds, differing in the shaping of the concave cleft (Figure 19 and 20). Eight of these β stranded sheets: β3-7, β11 and β14-15, form a jelly roll motif which consists of a deep concave cleft filled with a short α-helix that is buried by a prominent loop between β7-8, the other seven β stranded sheets are smaller. They produce a convex face to the solvent (Figure 19) (Kvansakul, Adams and Hohenester, 2004). This structure creates two hydrophobic cores, one within the concave cleft and another one between two β-sheets. The calcium ions bind to the structure through four sites (Figure 20). The first one on the side chains of aspartic acids in positions 956 and 975 in the β1- β2 loop coordinated by three carbonyl groups, the second and the third ones are close in proximity in the β5- β6 loop by aspartic acids

in positions 1001, 1002 and 1003. Finally, the fourth calcium-binding site is in the β5- β6 loop and side chains of glutamine and aspartic acid in positions 2024 and 1086 respectively binding to two carbonyl groups (Kvansakul, Adams and Hohenester, 2004). The importance of calcium (affinity of $K_D \approx 0.1$ mM) for the folding of the protein is shown in a study in which calcium was chelated by EDTA, affecting the conformation of the protein in which the C-terminal were elongated while the C-terminal globule shrunk (Kvansakul, Josephine C Adams and Hohenester, 2004).

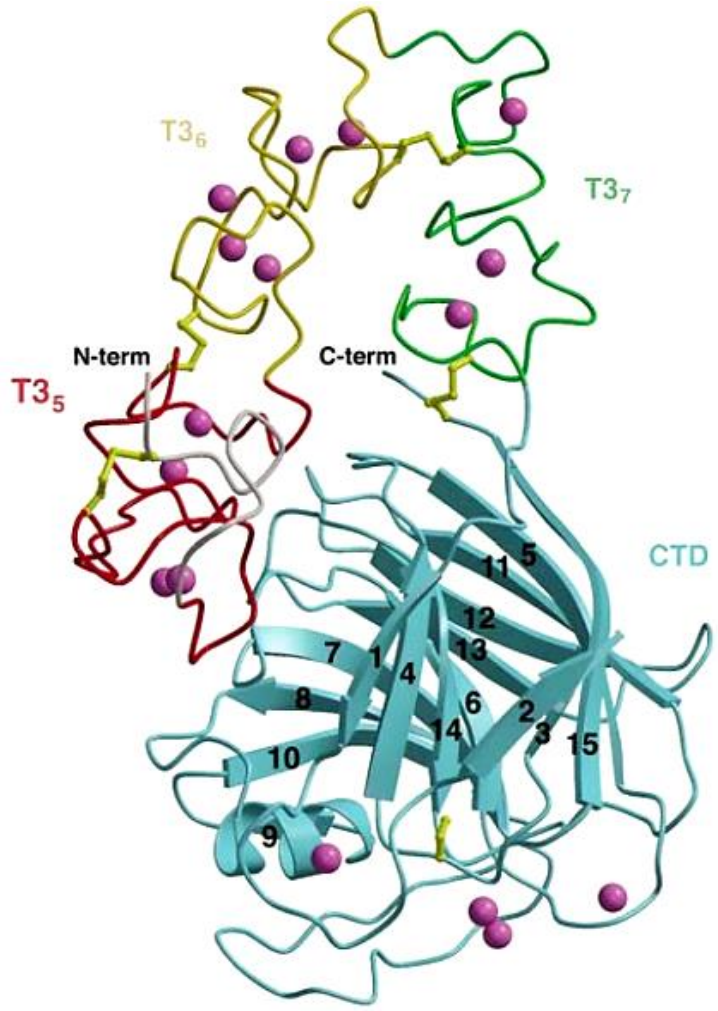

Figure 19. **The composition of the T3 repeats 5 to 7 domains and CTD.** *In red, the structure of T3 number 5 repeat followed by repeats 6 and 7 in yellow and green, respectively. In cyan the β sandwich structure formed by the 15 β-strands of the C-terminal domain labelled. The pink spheres represent the calcium ions, while the ball-and-sticks in yellow the disulphide bridges* (Kvansakul, Adams and Hohenester, 2004).

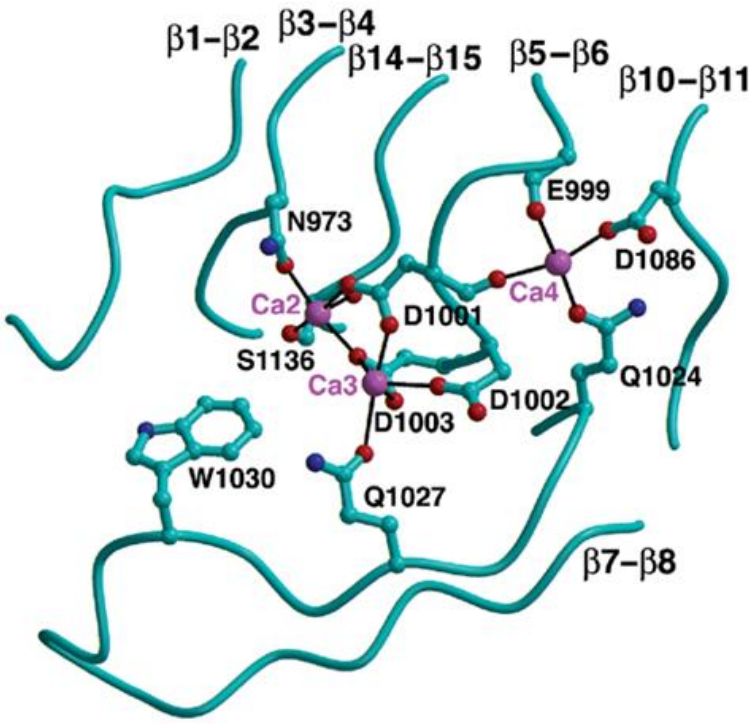

Figure 20. **Representation of three calcium-binding sites in the CTD globular domain.** *A simplified representation of the CTD domain to show the calcium-binding sites 2 to 4. In the diagram, the calcium ions are represented in purple spheres, and their calcium-ligand bonds in thin black lines. The residues involved in their binding are labelled and represented with ball-and-sticks* (Kvansakul, Adams and Hohenester, 2004).

C-terminal domain function is tightly linked to divalent cations which cause conformational changes in the CTD and can alter COMP-ECM interactions. COMP binding to fibronectin is supported by manganese and calcium cations (Figure 21). In contrast, zinc or nickel affect the binding to type I, II and IX collagen and type I and II procollagen. In the case of type, I and II collagen CTD attaches at the two ends of the molecule, while for type IX collagen to the NC4 and other domain (Rosenberg *et al.*, 1998; Holden *et al.*, 2001; Tan and Lawler, 2009). Other functions the CTD of COMP is involved in tissue homeostasis, fibril formation, cell adhesion and migration, collagen network and binding to fibronectin and matrilin-3 (Kvansakul, Adams and Hohenester, 2004; Mann *et al.*, 2004).

Apart from the specific functions that involve CTD, a wide range of other functions are controlled by COMP, such as, acting as catalyst regulating the organisation and assembly of collagen fibrils, interacting with other proteins from the ECM like types I, II, IX, XII and XIV collagen, matrilin-3, aggrecan, proteoglycans or fibronectin, regulating the incorporation of matrilin-3 into the ECM by binding type IX collagen, interconnecting various matrix components to each other and chondrocytes surface with the ECM via integrins, regulating chondrocyte proliferation by upregulating cell apoptosis inhibitors, adjusting the turnover of the ECM by interacting with proteins such as granulin-epithelin precursor (GEP) or

metalloproteinases (MMP) -9, -19 and -20 (Figure 21) (Stracke *et al.*, 2000; Holden *et al.*, 2001; Thur *et al.*, 2001; Di Cesare *et al.*, 2002; Dickinson *et al.*, 2003; Mann *et al.*, 2004; Chen *et al.*, 2007; Xu *et al.*, 2007; Blumbach *et al.*, 2009).

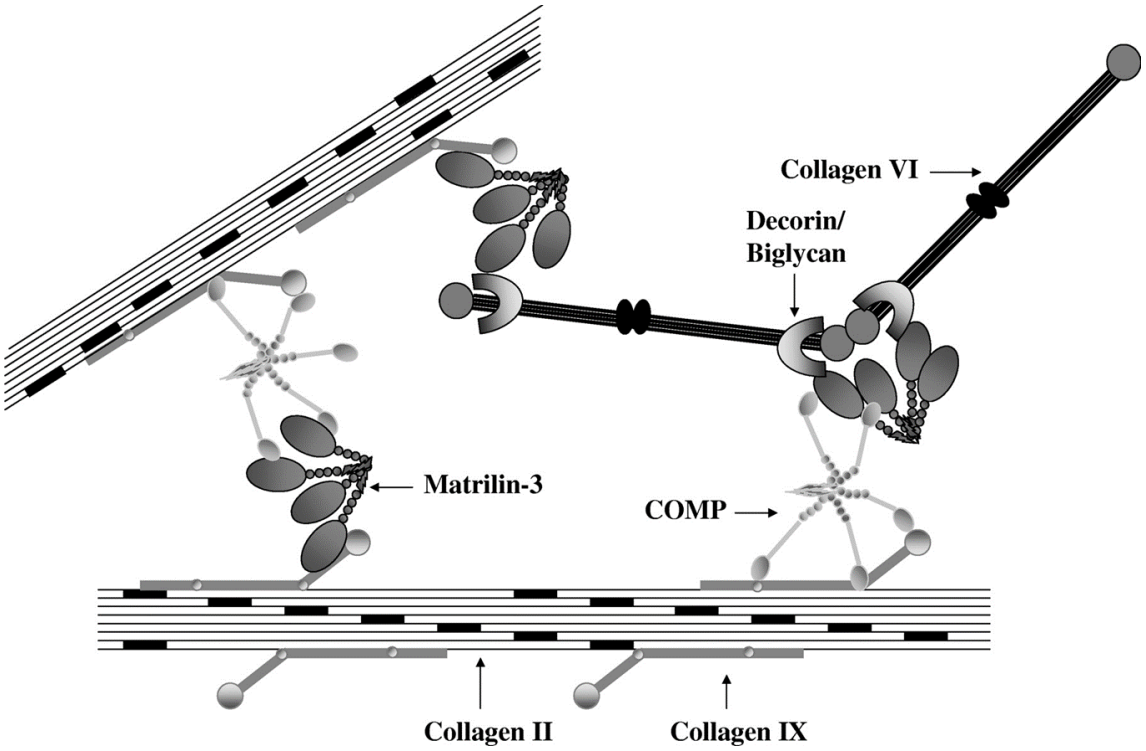

Figure 21. Schematic of some of the COMP ECM interactions*. In this diagram, COMP interacts through its CTD with type II, IV collagen, matrilin-3, and type VI collagen through decorin and biglycan. This Figure shows the complexity of the assembly of fibrillar networks* (Budde *et al.*, 2005).

COMP interactions with ECM components are regulated through divalent cations in the CTD domain. A highly conserved metal ion-dependent adhesion site (MIDAS) is potentially implicated in the interaction between COMP and collagens (Tan and Lawler, 2009). Furthermore, GAG affinity varies depending on the presence or depletion of calcium. The presence of calcium enhances the binding of COMP to low molecular weight heparin, chondroitin sulphate 4 and 6 and dermatan sulphate, and weakens or inhibits the binding to heparin sulphate and keratan sulphate. On the other hand, the absence of calcium decreases the binding of heparin and chondroitin sulphate 4 and 6. Interestingly, soluble chondroitin sulphate 4 and 6 and heparin affect negatively the binding to aggrecan, correlating the affinity for these molecules and inhibition for aggrecan (Chen *et al.*, 2007; Tan and Lawler, 2009).

Due to the involvement of COMP in many processes in the articular cartilage, mutations in this glycoprotein affect the normal function of the tissue. More than 100 mutations have been found in the *COMP* gene. PSACH results solely from mutations in *COMP*; however, only 66% of MED cases result from COMP mutations (Posey, Coustry and Hecht, 2018).

85% of the mutations resulting in PSACH are localised in the T3 domain, and 30% of those are in-frame deletions of five aspartic acid residues between amino acids 469 and 473 in the seventh T3 repeat (Figure 22) (Hecht *et al.*, 1995; Unger and Hecht, 2001; Briggs and Chapman, 2002; Mabuchi *et al.*, 2003). The majority of mutations in the T3 domain are missenses mutations and in-frame insertions or deletions of single residues affecting the fifth and seventh calcium-binding repeats. These mutations alter the tertiary structure resulting in misfolding of the protein and retention in the rER (rough endoplasmic reticulum) (Tan *et al.*, 2009; Suleman *et al.*, 2012; Posey, Coustry and Hecht, 2018). The resulting ER stress affects cell proliferation and induces apoptosis, disrupting tissue homeostasis.

The remaining 1% of the mutations are found in the type 2 repeat domain, and 14% in the C-terminal domain (Figure 22). These remain largely unstudied due to difficulty in obtaining patient samples. Some of these mutations are C1586T, C1665G, N555K, E583K, C1665A, T585M, T585R, H587R, R718P, G1813A, C2042G, G2153C, R718W, G719S, G719D, G2155A, N742fsX743, 1352-1353ins and generally produce a mild phenotype of the disease (Briggs and Chapman, 2002; Kennedy *et al.*, 2005; Suleman *et al.*, 2012; Briggs *et al.*, 2014). As previously mentioned, COMP mutations affect the tertiary structure and affecting the extracellular interactions of COMP (Chen *et al.*, 2000; Kvansakul, Josephine C Adams and Hohenester, 2004).

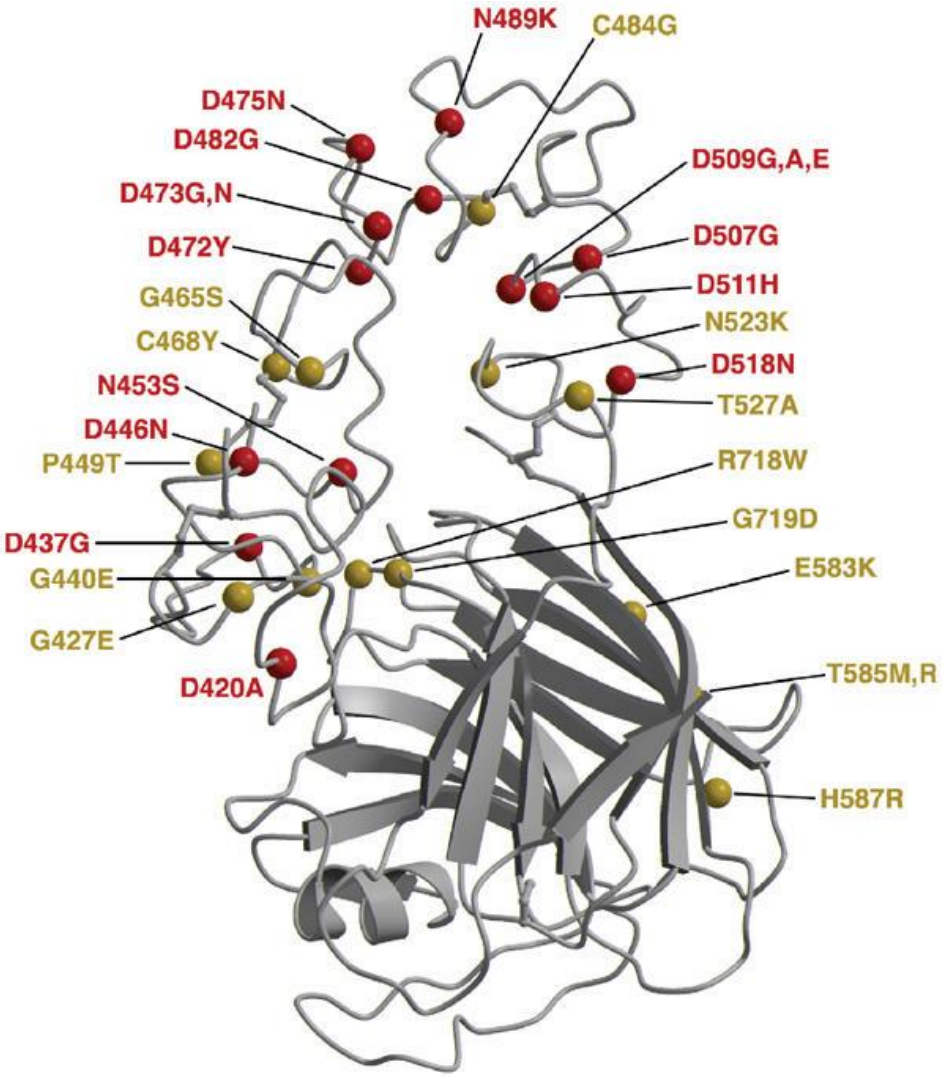

***Figure 22*. Mapping of mutations located in T3 repeat domain and CTD.** *The cartoon drawing is a composition of mutations affecting the 15 β-strands of the globular C-terminal domain and T2 domain in yellow spheres and red the ones located in the repetitions five to seven from the T3 repeats domain* (Kvansakul, Adams and Hohenester, 2004).

The cell-matrix pathology for mutations affecting the T3 domain has been studied in detail (Unger and Hecht, 2001). Patient chondrocytes show an aberrant concentration of the mutant protein retrained in the rER forming large inclusions of bodies occasionally with lamellar structures (Figure 23) (Hecht *et al.*, 1998, 2001). This, in turn, affects the tissue architecture, collagen fibril orientation and morphology, and binding and secretion of other molecules that interact with COMP in the ECM (Suleman *et al.*, 2012). In particular, type I, II and IX collagen binding is reduced, although type II collagen secretion is not affected (Délot *et al.*, 1999; Thur *et al.*, 2001; Vranka *et al.*, 2001). Interestingly, a putative collagen-binding site is located in the CTD, showing that there is an interaction between T3 domain and CTD (Délot *et al.*, 1999; Thur *et al.*, 2001; Vranka *et al.*, 2001). Finally, cell proliferation is decreased, and apoptosis is increased due to ER stress (Pirog-Garcia *et al.*, 2007).

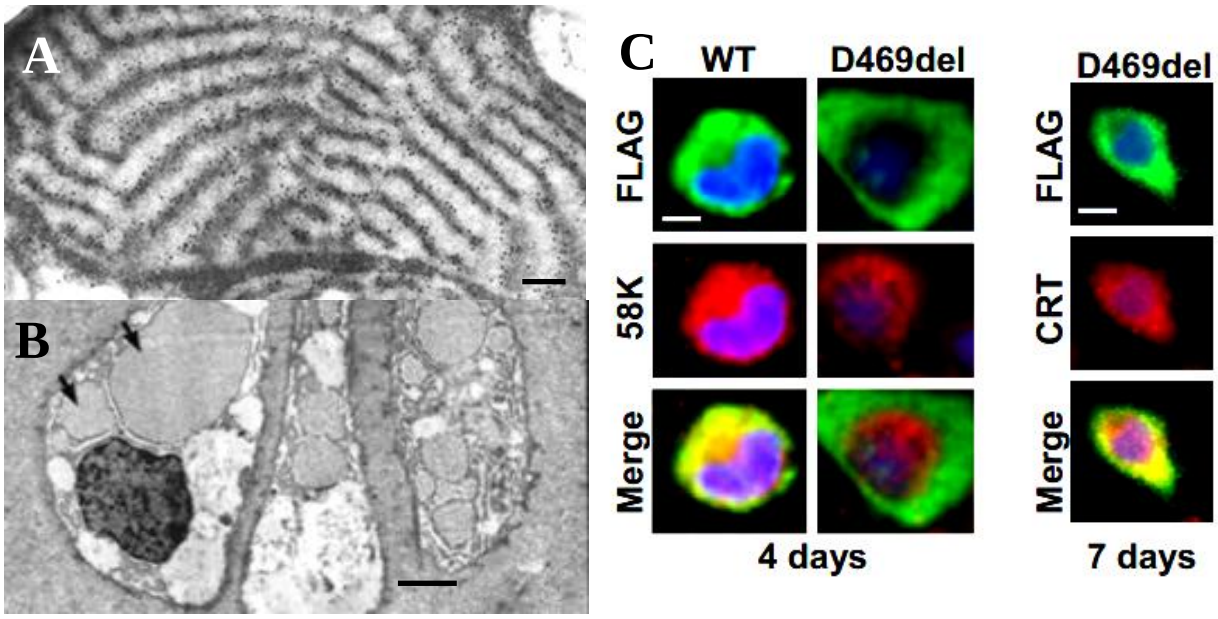

Figure 23. **Mutant protein retention due to a mutation in the T3 repeats domain of COMP**. ***(A)*** *Immunolocalization of COMP in the vesicles, specifically the dark rings of the lamellar structures, scale bar: 200 nm* (Maddox *et al.*, 1997) ***(B)*** *Ultrastructural changes in the cells with vesicles forming large inclusions of bodies indicated by arrows, scale bar 2µm* (Maddox *et al.*, 1997). ***(C)*** *Co-immunostaining of Rat Chondrosarcoma Swarm cells transfected with D469del COMP mutation (Flag tag on the recombinant protein –green) and with Golgi specific (58K – red) and ER (CRT – red) antibodies and nuclear staining with DAPI in blue. This image shows retention of the mutated protein COMP in the ER after seven days of culture and the lack of its secretion through the Golgi, in contrast to the WT model (co-localisation of red and green = yellow), scale bar 5µm* (Coustry *et al.*, 2012).

COMP C-terminal domain mutations have previously been studied *in vitro* (Posey, Alcorn and Hecht, 2014). Moreover, a CTD mutation (T585M COMP) mouse model was developed by Pirog-Garcia *et al.* in 2007. This model recapitulated the PSACH patient phenotype of short-limbed dwarfism and early onset osteoarthritis and interestingly showed no COMP mutant retention in the rER. Instead, mutant COMP was secreted into the ECM, thus affecting the organisation of several COMP-binding proteins and in turn, the organisation of the chondrocyte columns in the growth plate (Figure 24). Despite the protein being secreted, several cell stress response molecules were upregulated, potentially indicating a delay in secretion and folding, cell proliferation was decreased, and apoptosis increased and dysregulated. This model will be further discussed since gave an insight into the patients with mild PSACH (Pirog-Garcia *et al.*, 2007).

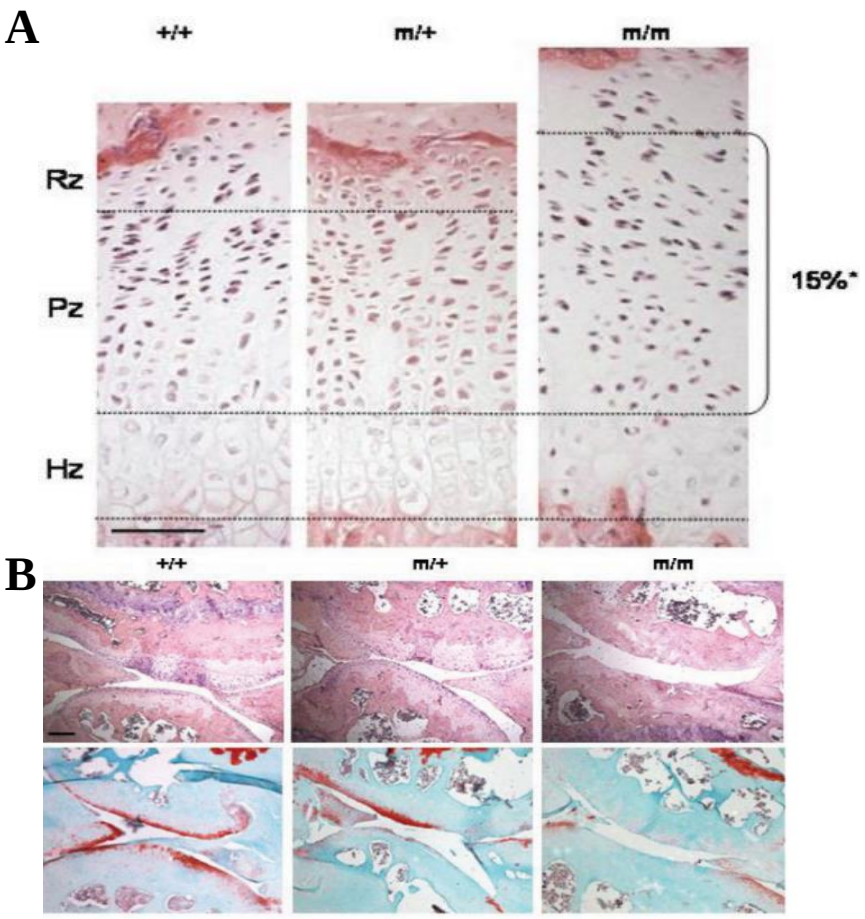

Figure 24. Alteration in the matrix secretions and organization of the CTD-COMP mutant growth plate. (A) *Haematoxylin-eosin staining of a three-week-old mouse growth plate showing disorganised and decreased columns of chondrocytes in the proliferative zone (PZ) of mutant growth plates, and in the case of homozygous mutant, an enlargement of PZ due to the disruption of the columnar organisation. Key legend: +/+ WT, m/+ mutant heterozygous, m/m homozygous mutant. Scale bar 100μm* ***(B)*** *Haematoxylin-eosin staining and Safranin-O (top and bottom panels respectively) of articular cartilage at 16 months mice showing the degradation of the ECM and GAG in CTD-COMP mutant mice. Scale bar: 100 μm* (Pirog-Garcia *et al.*, 2007)

1.4.1.4 T585M COMP Mutation

The T585M (Thr583Met equivalent in mouse) mutation is found in the CTD of COMP and was first reported by Briggs *et al.* in 1998 (Briggs *et al.*, 1998). A single nucleotide, threonine (a small polar amino acid), in position 585 of the C-terminal domain is mutated to another hydrophobic amino acid, methionine (a large nonpolar amino acid). The patients affected by this mutation present a mild form of PSACH with normal or mildly shorter stature, waddling gait and radiographic features with irregular epiphyses in hands and load bearing weight joints (Figure 25) (Rimoin *et al.*, 1994; J, J and JT, 1996; Briggs *et al.*, 1998; Spitznagel *et al.*, 2004; T.-L. L. Chen *et al.*, 2008).

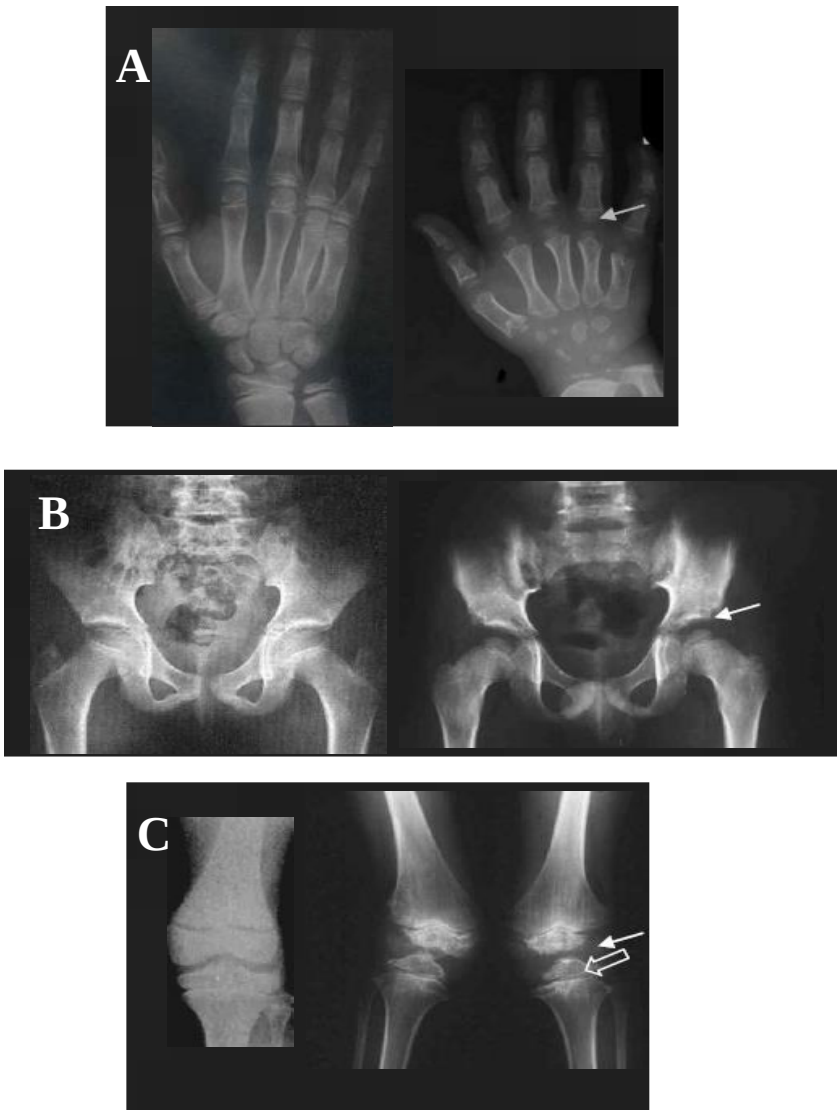

Figure 25. **Radiographs of the T585M COMP mutation pathology in a seven-year-old boy.** The X-rays showed o*n the left are of a healthy age-matched individual and on the right of the patient. For **A**, **B** and **C** the hands, pelvis and knee of the patient show a severe epiphyseal dysplasia with reduced and abnormal epiphyses respectively, especially in the portion pointed by the arrows. Images courtesy of International Skeletal Dysplasia Registry, Los Angeles (USA).*

T585M COMP is not retained in the rER. However, the delay in its secretion is enough to increase the rER stress via the unfolded protein response (UPR) leading to a reduction in chondrocyte proliferation, dysregulated apoptosis and affecting differentiation and hypertrophy of chondrocytes through Sox9, Ihh, BMP-2, RunX and HIF1/2α (Schmitz *et al.*, 2006b; Piróg *et al.*, 2014; Kung *et al.*, 2015; Yuan *et al.*, 2017). Activation of the UPR in T585M COMP chondrocytes leads to an increase in several chaperone proteins such as binding immunoglobulin protein (BiP) and calreticulin that in turn activate other ER stress mediators such as eIF2a, ATF6 and caspase-12. An increase of a pro-apoptotic transcription factor, CCAATenhancer-binding protein homologous protein (CHOP) and c-Jun N-terminal kinases

(JNK) was also found, with a decrease in the anti-apoptotic protein B-cell lymphoma-2 (bcl-2). Moreover, this trafficking defect affects the secretion of several ECM proteins such as collagens XIV, IX, XI, XII and VI, laminin β2, and fibronectin (Briggs, Bell and Pirog, 2015; Yuan *et al.*, 2017).

1.4.1.4.1 In vitro studies of COMP mutations

To further understand the PSACH disease aetiology and progression, *in vitro* models have been developed to recapitulate it. A model was developed using bovine articular cartilage chondrocytes transfected with several mutations affecting the T3 domain (D469del and D475N), and the CTD domain (H587R) (Dinser *et al.*, 2002; Schmitz *et al.*, 2006b). The first mutation is a deletion of one of the five sequential aspartic acid residues in position 469, the second one substitution of an aspartic acid residue in position 475 for an asparagine, lastly, H587R is a substitution of the histidine in position 587 for arginine in the C-terminal domain of COMP. To avoid the rapid dedifferentiation of chondrocytes grown in monolayer, the primary cells were seeded in alginate beads for 2-5 weeks. These models showed a decreased cell viability, disorganised ECM, and, in the case of T3 domain mutations, minor retention of mutant COMP, without a noticeable enlargement of the rER whereas a delayed COMP secretion was found in H587R mutations (Hecht *et al.*, 2001; Dinser *et al.*, 2002; Schmitz *et al.*, 2006b). Some limitations described in this model that may have affected the experimental outcomes are the use of a BM40 signal peptide, which could promote a more competent transcription, and the alginate bead matrix, which has been shown to alter collagen fibrils causing alterations in the ECM gene expression (Beekman *et al.*, 1997; Gregory *et al.*, 1999; Holden *et al.*, 2005; Schmitz *et al.*, 2008).

Apart from short stature, PSACH also affects joint and muscles (Unger and Hecht, 2001; Briggs and Chapman, 2002). In some studies, primary bovine tenocytes were transfected with three mutations, D469del and D473N (substitution of aspartic acid for asparagine in position 473) affecting the T3 domain and H587R in the CTD. In the T3 mutant cells, the mutant protein was retained in the rER while the trafficking in H587R was comparable to the wild type, and mutant COMP was found in the Golgi. The ECM ultrastructure was affected in all mutations, with a lesser amount of type I collagen fibrils and large COMP deposits, affecting the tenocyte proliferation and inducing apoptosis (Maddox *et al.*, 1997b; Weirich *et al.*, 2007). Interestingly, the phenotype described in these models contrasts with the phenotype found *in vivo* in patients with D346N mutations, where the COMP was released to the ECM. This could be due to an

overexpression of the mutated protein in the *in vitro* model compared to lower levels of endogenous synthesis. Furthermore, differences between the chondrocyte and tenocyte secretion of COMP, suggests a possible different secretory pathway (Maddox *et al.*, 1997b; Chen *et al.*, 2004).

Human chondrocytes were also used in 3D models of PSACH, cultured either in alginate beans, or non-adherent conditions (Beekman *et al.*, 1997; Gregory *et al.*, 1999; Hecht *et al.*, 2001; Hongisto *et al.*, 2013). Mutations expressed in these models were the T3-COMP mutations: D469del, G427E and D511Y. G427E and D511Y are a mutation in glycine and aspartic acid at positions 427 and 511 for glutamic acid and tyrosine respectively (Hecht *et al.*, 2001; Merritt *et al.*, 2006, 2007; Posey *et al.*, 2008). The chondrocytes grown in non-adherent conditions, and alginate beads were studied over 3-6 months of culture. The mutant cell culture affected secretion of type II and IX collagen and MATN3 while chaperone proteins such as Grp94 and BiP were found intracellularly (Merritt *et al.*, 2007). Intracellular retention and reduction in ECM, chondrocyte viability and nodule size were observable after one year of culture for the T522A COMP mutation (Duke *et al.*, 2003). However, human chondrocyte models require excessively long time cultures and special 3D conditions to achieve these results (Posey *et al.*, 2008).

Established cell lines were also explored as alternative options to primary cell culture. COS-7 (African green monkey SV40-transformed fibroblast) cells were used to express D472Y COMP mutation, a missense mutation in which an aspartic acid is substituted for tyrosine in position 472 of the T3 repeat domain (Hashimoto *et al.*, 2003). Interestingly, despite COS-7 cells not possessing chondrogenic potential, the system recapitulated the main phenotype of the disease. For instance, COMP was retained in the rER enlarging its size, whereas the wild type (WT) protein was localised in the Golgi and secreted into the ECM. Moreover, an increase in apoptosis and a stress response associated with an increase in phosphorylated eukaryotic initiation factor 2α (eIF2α) were detected solely in mutated COS-7 cells (Hashimoto *et al.*, 2003). Despite this, another study using COS-1 cells showed no retention of the mutated protein, in this case, D469del mutation, in the rER, with both WT and mutated COMP located in the Golgi. This shows inconsistency within similar cell lines and highlights the importance of the cell line of choice (Hashimoto *et al.*, 2003; Chen *et al.*, 2004).

Swarm rat chondrosarcoma cells (RCS), a chondrogenic cell line, were used in a larger study in which 11 mutations affecting COMP were studied. Three of these mutations affected type 2, and 3 repeat domains (D271H, L272P and P276R), six affected T3 domain (G299R,

D302V, G309R, D469del, D473N and D473G) and three mutations were located in the CTD (T585R, T585M and H587R) (Chen *et al.*, 2008). The mutants in T2 and T3 domains that resulted in MED (P276R and D302V) presented light intracellular retention of the mutant protein compared to the mutations occurring in PSACH that produced a more acute trafficking defect correlating with the clinical phenotype. On the other hand, all the mutations in CTD showed no correlation or abnormality in the protein folding. Therefore more studies decoupling the pathways affected in this disease are needed (Chen *et al.*, 2008).

Cell type	3D model	COMP mutation	Phenotypic outcomes	Reference
Bovine articular cartilage chondrocytes	Alginate beads	Mutations affecting: T3 domain (D469del and D475N), and CTD domain (H587R)	D469del and D475N: Decreased cell viability, disorganised ECM, and, in the case of T3 domain mutations, minor retention of mutant COMP, without a noticeable enlargement of the rER H587R: a delayed COMP secretion was found in H587R mutations	(Dinser *et al.*, 2002; Schmitz *et al.*, 2006a)
Primary bovine tenocytes	Monolayer	Mutations affecting: T3 domain (D469del and D473N), and CTD domain (H587R)	D469del and D473N: the protein was retained in the rER H587R protein was not retained and mutant COMP was found in the Golgi. The ECM ultrastructure was affected in all mutations, with a lesser amount of type I collagen fibrils and large COMP deposits, affecting the tenocyte proliferation and inducing apoptosis	(Maddox *et al.*, 1997b; Weirich *et al.*, 2007)
Human chondrocytes	Alginate beans, or non-adherent conditions	Mutations affecting: T3 domain (D469del, G427E and D511Y)	The mutant cell culture affected secretion of type II and IX collagen and MATN3 while chaperone proteins such as Grp94 and BiP were found intracellularly	(Merritt *et al.*, 2006, 2007; Hongisto *et al.*, 2013)
COS-7 cells	Monolayer	D472Y COMP mutation	COMP was retained in the rER enlarging its size. An increase in apoptosis and a stress response associated with an increase in phosphorylated eukaryotic initiation factor 2α (eIF2α) were detected solely in mutated COS-7 cells	(Hashimoto *et al.*, 2003)
COS-1 cells	Monolayer	D469del mutation	In the rER, with both WT and mutated COMP located in the Golgi	(Chen *et al.*, 2004)

Swarm rat chondrosarcoma cells	Monolayer	Three mutations affected type 2 domains: (D271H, L272P and P276R) Six affected T3 domain (G299R, D302V, G309R, D469del, D473N and D473G) Three mutations in the CTD (T585R, T585M and H587R)	The mutants in T2 and T3 domains that resulted in MED (P276R and D302V) presented light intracellular retention of the mutant protein compared to the mutations occurring in PSACH that produced a more acute trafficking defect correlating with the clinical phenotype. The mutations in CTD showed no correlation or abnormality in the protein folding.	(T.-L. L. Chen *et al.*, 2008)

Table 1. Summary of the main outcomes of the in vitro models of COMP mutations.

1.4.1.4.2 Mouse models of PSACH and MED

Cell culture models of skeletal disease present several disadvantages such as secretion differences depending on the cell type and promoter used, need for special 3D conditions due to dedifferentiation of primary cells and lack of recapitulation of mechanosensing properties of cartilage (Duval *et al.*, 2017). Therefore, animal models of disease are useful and provide a model in which the disease can be developed and observed with preserved systemic and biomechanical interactions.

The high level of genetic conservation and physiological similarities between mice and humans make this organism a useful model to study the progress of diseases. Compared to other mammals, mice possess a reduced gestational period and are simple to maintain in captivity. Therefore, mouse models facilitate elucidating the pathomolecular mechanism of diseases affecting development when human samples are not sufficient or available (Perlman, 2016).

Transgenic animals and knock-in and knock-out approaches are techniques that allow the introduction of genetic information or manipulate the correspondent targeting sequence in the mouse. Transgenic animals are developed by microinjecting the mutated gene of interest into the pronucleus of a fertilised oocyte or by using a retroviral vector to integrate the mutated DNA into pre- or post-implanted embryos (Horton, 2003). In contrast, a knock-out or knock-in mouse is developed by inserting the targeting mutated DNA into embryonic stem cells via electroporation. This allows for homologous recombination to occur, replacing the target gene with the engineered sequence. To ensure solely the cells that incorporated correctly, the target gene is selected, a resistance, for instance, neomycin or ganciclovir, is introduced in the target sequence. The selected cells are injected into a foster evolving mouse blastocyst which then

produces chimeric offspring that carries a mixture of the knockout cells and the normal ones and is crossed with a wild type animal of the correct genetic background to promote germline transmission (Hall, Limaye and Kulkarni, 2009).

The first mouse model generated to study the role of COMP in skeletal tissues was a knock-out of *Comp* gene. The study focused on decoupling the mechanism and molecules affected by the total absence of the protein. Surprisingly, mice lacking one or both copies of *Comp* gene showed no anatomical, histological or skeletal defects compared to the wild-type model, and the lack of COMP was not compensated for by other members of the thrombospondin family, suggesting that COMP is not required for the normal function of the ECM and that the intracellular stress driven by *COMP* mutations is the more likely disease mechanism leading to PSACH. The authors concluded that this study suggests that chondrodysplasias are potentially developed due to the retention of the mutant protein in the rER, upregulated stress response in the cells, and the dysfunctional miss-folding or defects assembling of the protein rather than the absence of COMP in the ECM (Liz Svensson *et al.*, 2002).

D469del COMP mutation was introduced into C57BL6/DBA2 mice blastocysts through microinjection (Lee *et al.*, 2001; Swaminathan *et al.*, 2001). In this case, only the females presented with PSACH phenotype, and from the 53 offspring, only 2 expressed the transgene, although one of them died in infancy and the other was collected as a 15-dpc (days *post coitum*) embryo. Some alterations in the mutant growth plate were found, its structure significantly thinner and with a reduction in chondrocytes (40-50%) and columnar structure (12-18%). Two ECM proteins and COMP interaction partners, MATN3 and type IX collagen, presented a normal distribution. However, immunostaining for mutant COMP was patchy and showed intracellular retention, similar to osteoarthritis articular cartilage (Hecht *et al.*, 2004; Koelling *et al.*, 2006; Posey *et al.*, 2008).

In a different study, COMP cDNA driven by a mouse type II collagen promoter and enhancer was used in a pKN185 vector containing the sequence of mutation D469del COMP (Tsumaki *et al.*, 2000). The offspring from this transgenic line weighed 16-18% less, and their lengths were 11-12% less compared to wild type littermate controls. Not only did they display the clinical phenotype of the short stature but also the growth plate showed disorganisation of the chondrocyte columns and patchy deposition of COMP protein in the matrix. However, despite that MATN3 and type IX collagen co-localised with COMP, and were not intracellularly retained (Tsumaki *et al.*, 2000; Posey *et al.*, 2008).

Another mouse model of D469del COMP mutation was generated with a myc-tag and under the type II collagen promoter in a transgenic mouse which was then crossed onto a COMP knockout background (Schmitz *et al.*, 2008). Only males developed the phenotype, showing an 8-10% decrease in bone length compared to the wild-type controls and disorganisation of the growth plate with interruptions within the chondrocyte columns and increased apoptosis. Mutant COMP was localised in the ECM presenting an irregular pericellular location, with no perturbed staining for MATN3 and collagen type II, IX and X. However, aggrecan ECM staining was decreased, and MATN1 was upregulated. Moreover, the transgenic mouse model showed intracellular protein retention and dilated rER cisternae, both hallmarks of PSACH patient cartilage, which recapitulated the clinical phenotype of D469del COMP patients (Posey *et al.*, 2008; Schmitz *et al.*, 2008).

The majority of the studies discussed above focused on the D469del mutation in the T3 domain of COMP protein. Interestingly, in 2007 Pirog-Garcia *et al.* described a homozygous mouse model carrying a T583M COMP mutation, an equivalent of the human T585M COMP change. At nine weeks of age, mutant mice were 6% lighter than their wild-type littermates, had 4% shorter tibias and hip dysplasia. Moreover, mutant mice showed loss of articular cartilage at 16 months of age, thus fully recapitulating the clinical mild PSACH phenotype. On a molecular level, the mutated protein trafficking was retarded with a mild upregulation of the UPR, but it was not retained in the rER. The growth plate presented a disorganised structure, with apparent lesser columns of chondrocytes, a reduction in cell proliferation and an increase in apoptosis.

Mice, therefore, are a good model to explore the mechanism of PSACH/MED resulting from the T585M COMP mutation and caused by secretion of the mutant COMP into the ECM affecting the molecular network.

Type	COMP mutation	Outcomes	Reference
Knock-out of *Comp* gene		No anatomical, histological or skeletal defects compared to the wild-type model, and the lack of COMP was not compensated for by other members of the thrombospondin family	(Svensson *et al.*, 2002)
The mutation was introduced into C57BL6/DBA 2 mice blastocysts through microinjection	D469del COMP mutation	Only the females presented with PSACH phenotype. Alterations in the mutant growth plate were found, its structure significantly thinner and with a reduction in chondrocytes (40-50%) and columnar structure (12-18%). Two ECM proteins and COMP interaction partners, MATN3 and type IX collagen, presented a normal distribution	(Lee *et al.*, 2001; Swaminathan *et al.*, 2001)
COMP cDNA driven by a mouse type II collagen promoter and enhancer was used in a pKN185 vector containing the sequence of mutation	D469del COMP mutation	The offspring weighed 16-18% less, and their lengths were 11-12% less compared to WT. The growth plate showed disorganisation of the chondrocyte columns and patchy deposition of COMP protein in the matrix. MATN3 and type IX collagen co-localised with COMP, and were not intracellularly retained	(Tsumaki *et al.*, 2000)
Myc-tag and under the type II collagen promoter in a transgenic mouse which was then crossed onto a COMP knockout background	D469del COMP mutation	Only males developed the phenotype. Mutant COMP was localised in the ECM presenting an irregular pericellular location, with no perturbed staining for MATN3 and collagen type II, IX and X. Aggrecan ECM staining was decreased, and MATN1 was upregulated. Intracellular protein retention and dilated rER cisternae, both hallmarks of PSACH patient cartilage was found in the mutant mouse.	(Schmitz *et al.*, 2008)
Homozygous mouse model carrying the mutation	T585M COM	Mutant mice showed loss of articular cartilage at 16 months of age. On a molecular level, the mutated protein trafficking was retarded with a mild upregulation of the UPR, but it was not retained in the rER. The growth plate presented a disorganised structure, with apparent lesser columns of chondrocytes, a reduction in cell proliferation and an increase in apoptosis.	(Pirog-Garcia *et al.*, 2007)

Table 2. Summary of the main outcomes of the mouse models with COMP mutations.

1.5 Cartilage ageing and injuries.

Articular cartilage has a low regeneration potential due to the lack of blood supply. This impedes the regeneration of the tissue after injuries and results in diseases such as osteoarthritis (OA), which represents one of the main health problems in developed countries (Lima *et al.*, 2008; Fox, Bedi and Rodeo, 2009). Early-onset OA is also a complication in many skeletal dysplasia.

1.5.1 Repair strategies for damaged cartilage and its limitations

The healing potential of articular cartilage is limited, making finding novel strategies to repair it of paramount importance (Akkiraju and Nohe, 2015). Current techniques to repair the damage and avoid the complete joint replacement are either endogenous or exogenous. Therapeutic approaches could be classified in intra-articular injections of various compounds, such as corticosteroid injections, hyaluronic acid injections, injection of autologous platelet-rich plasma; or surgical approaches, such as micro-fractures and chondroplasty; or regeneration medicine and cell-based approaches like autologous chondrocytes implantation or matrix-induced autologous chondrocyte implantation (tissue engineering) (Figure 26) (Medvedeva *et al.*, 2018).

Endogenous therapies are those that drive the repair by enhancing the innate properties of the tissue, such as introducing growth factors to promote the proliferation and differentiation of cells *in situ.* In contrast, exogenous approaches often use a cell type from another source or modify the cells harvested from the wounded region *ex vivo* before implanting them back into the joint (Moreira-Teixeira *et al.*, 2011; Tsumaki, 2015).

One of the oldest and most applied endogenous techniques is the application of a microfracture, in which a surgical penetration into the subchondral bone leads to the disruption of blood vessels that form a clot. This clot attracts bone marrow mesenchymal stem cells (BM-MSC) that invade the microfracture and eventually differentiate into neo-cartilage. Despite the huge success of this technique, the main issue is the development of fibrous cartilage whose mechanical properties differ from healthy tissue (Figure 26) (Bhosale and Richardson, 2008; Moreira-Teixeira *et al.*, 2011; Peng *et al.*, 2014). Another potential strategy for minor osteoarthritic lesions is mosaicplasty (Hangody *et al.*, 1998). This technique is based on extracting osteochondral plugs from zones that tolerate moderate weight within the joint structure and applying them to fill the injured regions. Unfortunately, the new tissue formed is also often fibrocartilaginous (Bhosale and Richardson, 2008; Moreira-Teixeira *et al.*, 2011).

Exogenous techniques comprise autologous chondrocytes implantation (ACI) and stem cells implantation. ACI was first mentioned by Brittberg et al. 1994 (Brittberg *et al.*, 1994), and is considered the first-ever tissue engineering approach in cartilage repair, consisting of extracting chondrocytes from less weight-bearing areas and expanding them *in vitro* in monolayer for up to 6 weeks, then transplanting them into the injured area (Moreira-Teixeira *et al.*, 2011; Tsumaki, 2015). Initially, this strategy showed great success in terms of expression makers of healthy cartilage; however, in time the tissue expressed type I collagen and produced fibrous cartilage (Bhosale and Richardson, 2008; Moreira-Teixeira *et al.*, 2011).

Another promising exogenous technique for cartilage regeneration is the implantation of stem cells (SC), owing to their pluripotency and the capacity to differentiate into other cell lineages. Suitable cells can be harvested from embryos, synovium or bone marrow (Figure 26). However, the use of human embryonic stem cells involves ethical issues, and thus they are not routinely employed (Bian *et al.*, 2011; Akkiraju and Nohe, 2015). Synovium-derived stem cells (SDSCs) retain their chondrogenic potential and display articular cartilage mechanical properties when seeded in 3D hydrogels. Despite this, cell senescence was highly notable, and further studies regarding the long term properties of SDSCs derived constructs are necessary (Sampat *et al.*, 2013; Akkiraju and Nohe, 2015). Bone marrow stromal cells preserve the ability to differentiate into chondrocytes and are a good candidate for cartilage repair. Early studies using these cells showed their potential to synthesise cartilage-like tissue comparable to healthy tissue, despite this other studies showed fibrocartilaginous formation and hypertrophy (Akkiraju and Nohe, 2015; Tsumaki, 2015).

Induced pluripotent stem cells (iPSCs) offer an autologous alternative to using stem cells. These cells were first mentioned in 2006 by Takahashi and Yamanaka whereby adult fibroblasts were dedifferentiated using four factors: OCT3/4, SOX2, c-MYC and KLF4 and thus generated cells were capable of re-differentiation into multiple other cell types (Takahashi and Yamanaka, 2006). A study since had differentiated skin and blood cells from patients with articular cartilage injuries and reintroduced them into the injuries showing a reparative potential (Tsumaki, 2015). This novel technique presents some advantages compared to the other cell sources by avoiding ethical issues and by the ease to harvest (Figure 26). However, its main limitation is the risk of teratoma development due to the presence of undifferentiated iPSCs at the implantation site (Tsumaki, 2015).

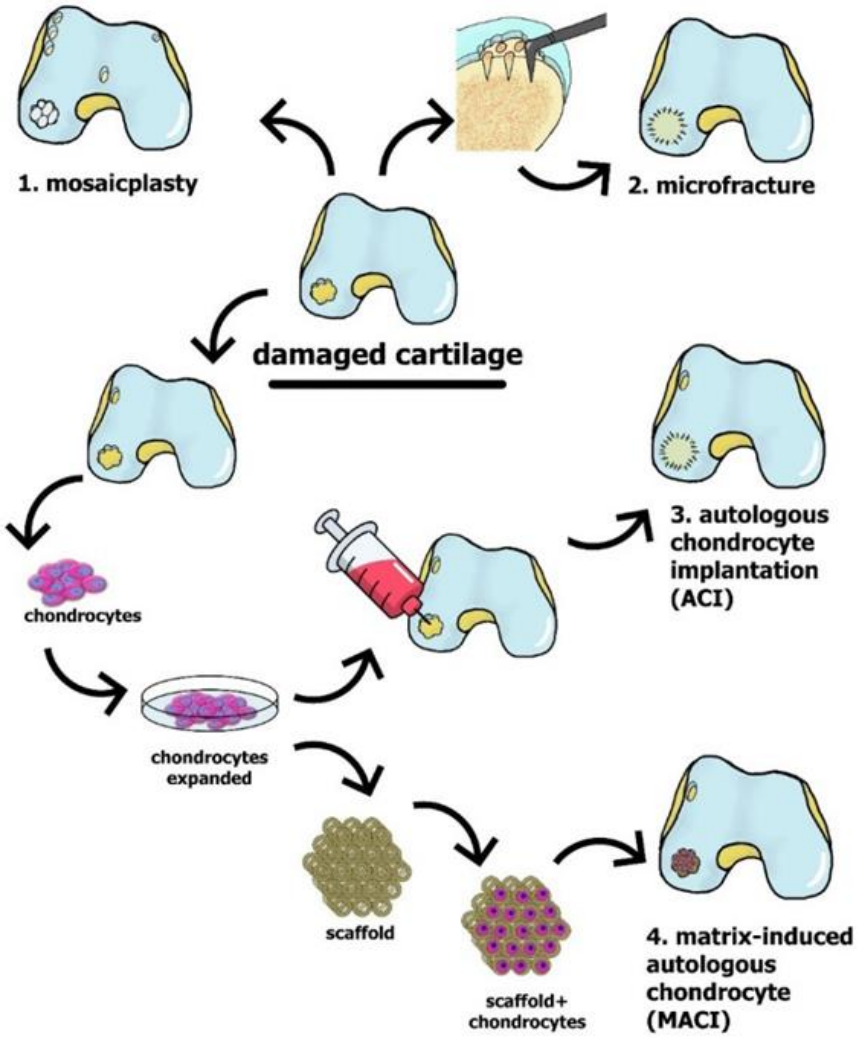

Figure 26. Diagram of the available options to restore articular cartilage. *Some of the approaches are intra-articular injections of various compounds, such as corticosteroid injections, hyaluronic acid injections, injection of autologous platelet-rich plasma, or surgical approaches, such as micro-fractures and chondroplasty, or regeneration medicine and cell-based approaches like autologous chondrocytes implantation or matrix-induced autologous chondrocyte implantation (tissue engineering). Diagram from* (Medvedeva *et al.*, 2018).

1.6 Regenerative medicine

Regenerative medicine and tissue engineering focus on developing strategies to effectively repair, replace, or assist the healing tissues both structurally and functionally (Mao and Mooney, 2015). Reliance solely on transplantation presents significant limitations such as limited donor supply where usually supply does not meet the demand, immune response complications, costs and organ or tissue failures (Mao and Mooney, 2015 and Dzobo *et al.*, 2018). Regenerative medicine has the potential to offer reliable sources of tissues and organs employing both engineering and biological principles showing promising preclinical and clinical data supporting the idea that tissues and organs can be regenerated when damaged, aged, diseased or suffered a traumatism (Dzobo *et al.*, 2018).

Tissue engineering is a combination of biomaterials and engineering and resulted from an initial necessity to approach the disparity between the rising number of patients that required a transplant and the limited number of organs available for donation. For instance, over 5 million patients in the United States suffer from congestive heart failure, and other chronic diseases affect main organs such as the liver, lungs and kidney (Furth and Atala, 2013; Sudhakar *et al.*, 2015). Interventions focused on the replacement of the damaged tissue or organ with an engineered scaffold that mimics the properties of the damaged tissue are therefore attractive and actively pursued in regenerative medicine research (Furth and Atala, 2013).

1.6.1 Tissue engineering for cartilage repair and study

The concept of applying tissue engineering to repair cartilage damage was first mentioned in 1993 by Langer and Vacanti (Langer and Vacanti, 1993). The cartilage engineering field has evolved drastically since 1992, where solely one paper was available on PubMed under the key search of "Cartilage scaffold tissue engineering", compared to 4521 papers in 2020 (Figure 27).

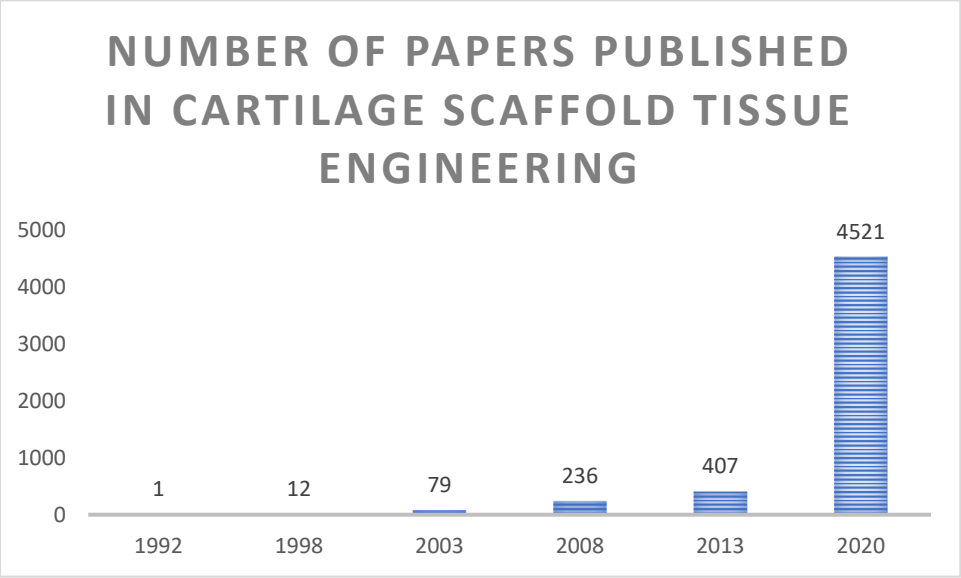

Figure 27. Graph showing the number of papers published in cartilage tissue engineering since 1992. *Representation of the number of papers published under the name of "cartilage tissue engineering" from 1992 to 2020 [Pubmed].*

1.6.2 Scaffolds for tissue engineering

The main challenge of tissue engineering is the selection of a suitable scaffold to provide cells with a proper attachment and a correct microenvironment. Depending on the tissue or organ to replace, constructs need to meet a long list of requirements such as matching the mechanical strength of the repaired tissue, permeability to nutrients, oxygen, metabolites, and waste products; they need to enhance or maintain the cell viability, phenotype and adhesion and to reproduce the biomechanical properties of the tissue. Moreover, scaffolds for clinical

applications require biocompatibility with biodegradability and lack of inflammation induction (Moreira-Teixeira *et al.*, 2011; García-Carvajal *et al.*, 2013). For articular cartilage, tissue engineering faces additional challenges due to the avascularity and the complex and zonally stratified nature of the tissue (Asadi *et al.*, 2018)

The architecture of the scaffold is of paramount importance since it affects cell behaviour and matrix deposition. Materials commonly used in tissue engineering are meshes, sponges and hydrogels. Meshes and sponges are more biomechanically resilient; however, hydrogels may support the cell phenotype better and can be engineered to retain growth factors and nutrients necessary for tissue differentiation (Chung and Burdick, 2008; Asadi *et al.*, 2018).

1.6.2.1 Meshes

Meshes are made up of polymer networks that allow for slight modifications in fibre diameter, volume and orientation that can influence cell morphology and differentiation (Figure 28) (Chung and Burdick, 2008). Depending on the method of manufacturing the meshes are divided into non-woven or woven. Woven fibres are arranged at certain angles in a set pattern, whereas non-woven meshes have randomly interlaced fibres with no discernible orientation (Müller *et al.*, 2015).

The organisation of fibres gives the scaffold variations in properties, for instance, higher strength and resilience was found in woven meshes, while non-woven meshes present a higher attachment surface and voids within contiguous fibres (Chung and Burdick, 2008; Edwards *et al.*, 2011).

A wide range of methods to fabricate meshes is currently available such as phase separation, self-assembly fibres, fibre bonding and electrospinning. Despite this variety, the most commonly used method is electrospinning, due to its capacity to reproduce the nanostructure of collagen fibres found in native cartilage (Mo *et al.*, 2004; Lu, Li and Chen, 2013). Electrospinning consists of a polymer solution that is injected into a high electric field. As the jet moves in the electric field, a charge evaporates the solvent, leaving highly charged fibres that are collected typically on a metal screen or a collector drum (Figure 29). The size of the fibres is variable, from nanoscales of 1000 nm to microscales of 1 µm, depending on the properties of the solution, such as conductivity of surface and tension, the diameter of the syringe, or electrical field applied (Chung and Burdick, 2008; Lu, Li and Chen, 2013).

Polymers applied in electrospinning are poly(α-hydroxy esters) including poly(lactic acid) [PLLA], poly(glycolic acid) [PGA] and poly(lactic-co-glycolic acid) [PLGA]. However,

natural fibres, such as collagen or silk fibroin, can also be used. The properties of each polymer, such as lateral groups or hydrophobicity may impact the properties of the scaffold, for instance, PGA hydrophilic structure is degraded into natural products that presented non-toxicity and are re-absorbed, whereas hydrophobicity in groups from PLA gives it a moderate degradation rate (Chung and Burdick, 2008; Lu, Li and Chen, 2013). Other methods, such as phase separation, consist of inducing instability in the thermodynamic properties of a polymer induced thermally or by non-solvent that leads to the division of the polymer in two phases, one rich in polymers and the other not. The rich phase produces a scaffold, and the poor phase is aspirated and eliminated (Liu and Ma, 2009; Lu, Li and Chen, 2013).

Several studies proved that using meshes to engineer cartilage *in vitro* can enhance cartilage regeneration and enhance mechanical properties of the tissue in vivo by providing a solid structure (Levenberg *et al.*, 2003; Jung *et al.*, 2008). Nevertheless, other studies suggest combining meshes with a hydrogel to maintain the cell phenotype (Moutos, Freed and Guilak, 2007; Moutos and Guilak, 2008).

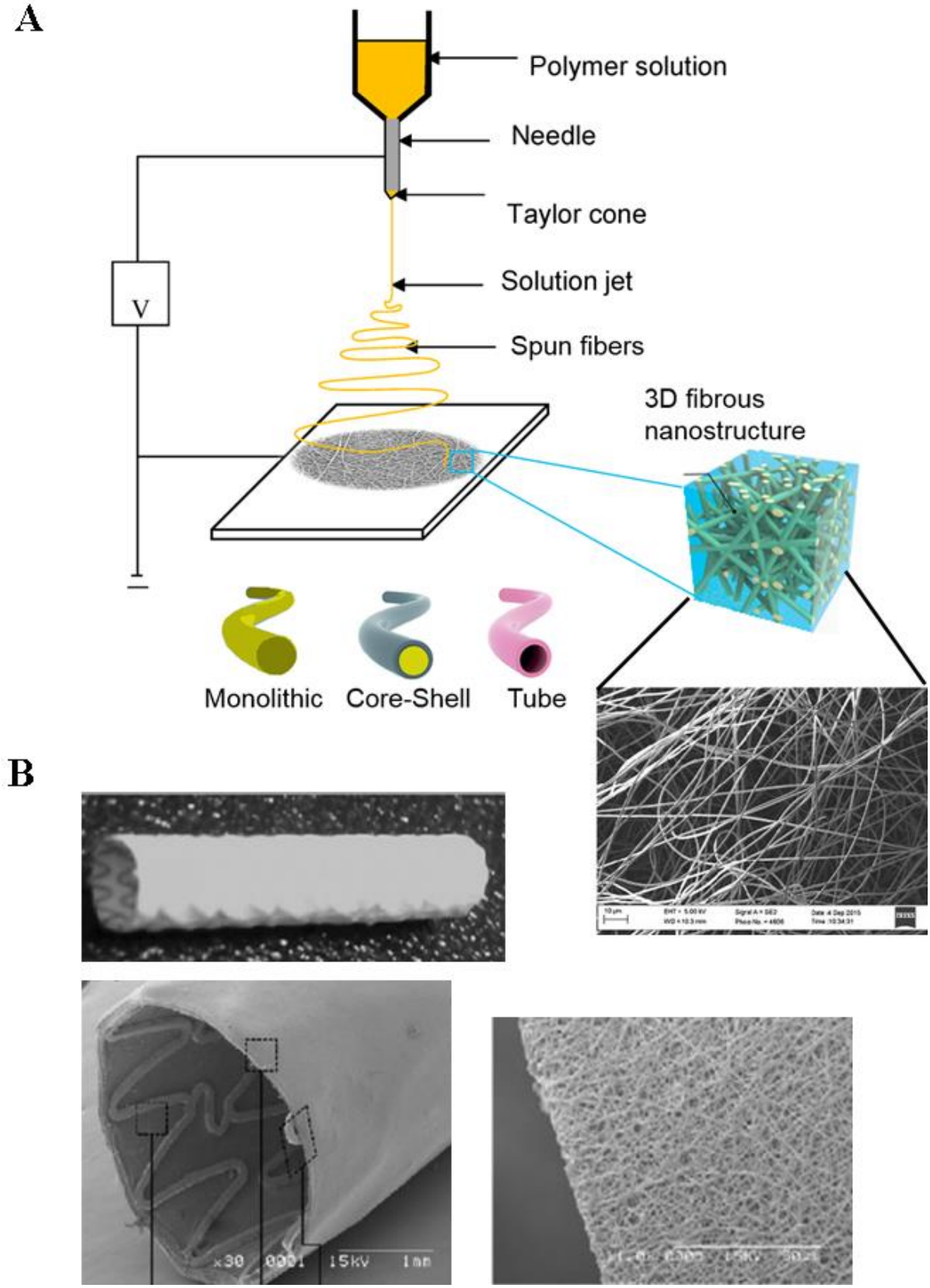

Figure 28. Diagram showing the electrospinning technique with nanofibres. A) *Diagram representing a normal electrospinning setup with the final 3D product and an amplified image of electrospun nanofibres, Scale bar: 10µm. Images from* (Alharbi *et al.*, 2016; Bonadies, 2018) ***B)*** *Composite of a tracheal scaffold made of the metal bare stent and bilayer nanofibres SEM micrographs. Image from* (Heo *et al.*, 2011)

1.6.2.2 Sponges

Sponges are another type of porous scaffold that can be used in tissue engineering. Sponges are defined as solid structures filled with pores whereby the porosity and interconnection of pores play a crucial role in the properties of the scaffold (Figure 29). The surface available for cell anchorage is determined by the number of pores, whereas the diameter of the pores and their interconnectivity decide the waste and nutrients diffusion and the dispersion of the matrix and cells (Chung and Burdick, 2008; Cho *et al.*, 2014). Methods to design sponges are divided into traditional and solid free-form technologies. Traditional methods include salt-leaching, phase separation, freeze-drying, gas foaming, and lyophilisation, whereas solid-free form fabrication comprises stereolithography, selective laser sintering and 3D printing. Despite the constantly growing variety of techniques, the traditional methods are the most commonly applied in tissue engineering (Cho *et al.*, 2014; Bhattacharjee *et al.*, 2015).

Salt-leaching is frequently used to manufacture sponges due to its simplicity (Figure 29). Salt particles are inserted within the polymer matrix, and the removal of these salt particles by water creates a porous structure. The porosity is directly related to the porogen particle size. However, the interconnectivity within the sponge is not controllable. This technique has been applied in wound healing and bone tissue engineering; however, some studies show increased toxicity from the leaching step (Tessmar, Holland and Mikos, 2005; Janik and Marzec, 2015; Liverani *et al.*, 2019). Freeze drying, phase separation and gas foaming can overcome the technical issues associated with leaching. Gas foaming reduces the toxic solvents; however, the pore size and interconnectivity are not controlled, and the results are heterogeneous from batch to batch (Gorth and J Webster, 2011; Liverani *et al.*, 2019). Another interesting technique is freeze-drying in which the polymer solution is initially frozen at low temperature, (-70 to -80^{o}C) and placed in a different compartment in which the pressure is reduced progressively up to nearly vacuum, leading to the evaporation of the ice and the removal of non-frozen particles, leaving behind a porous-intricate scaffold. The lack of high-temperature steps makes this method applicable for clinical applications, and it's been used in cartilage and osteochondral tissue engineering (Haugh, Murphy and O'Brien, 2010; Lu, Li and Chen, 2013; Liverani *et al.*, 2019).

Sponges made up of poly(1,8 octanediol citrate) (POC), chitosan, collagen and silk fibroin have been previously applied to tissue engineering, supporting cell growth in constructs with potential compressive strength and enhancement of ECM production after four weeks of seeding (Chung and Burdick, 2008; Bhattacharjee *et al.*, 2015). Despite these promising results, other studies suggest that the cells cultured in sponges grow on the pore surface, a 2D

microenvironment, and lose their rounded morphology, flatten and reduce ECM synthesis (Mauck and Burdick, 2011; Zhang, Yang, Li, Dou, Li, Thote, D. Wang, *et al.*, 2013)

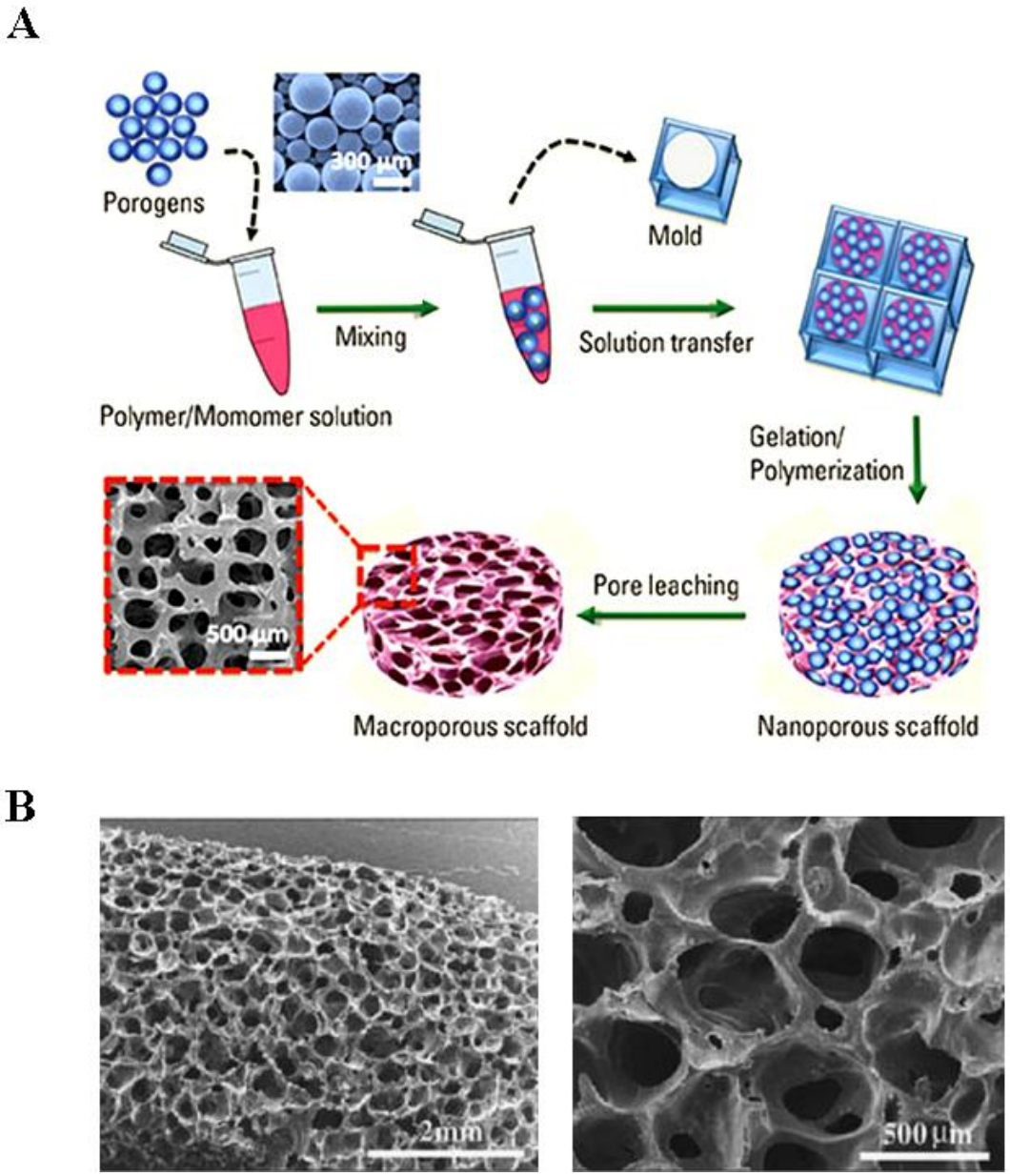

Figure 29. Schematic process of developing nanoporous scaffold sponge-like. A) *Steps to fabricate a macroporous scaffold via pore leaching. Schematic diagram from* (Bencherif, Braschler and Renaud, 2013) *B) Scanning electron microscopy (SEM) image of a sponge PLLA polymer after being processed via supercritical CO_2. Scale bar:2mm and 500µm Images from* (Jokanović *et al.*, 2019).

1.6.2.3 Hydrogels

Hydrogels (Figure 31) consist of highly hydrated and hydrophilic polymer networks mimicking the high-water content (up to 80%) present in articular cartilage and other tissues. This hydrophilic network is made of ionic crosslinks and hydrogen bonds, or chemical, as covalent bonds. The most frequently used hydrogels in tissue engineering are those with covalent or ionic bonds that provide a more stable structure (Chung and Burdick, 2008; García-Carvajal *et al.*, 2013). The hydrogel source can be natural or synthetic. Natural scaffolds, such

as collagen, gelatine, agarose, fibrin, chitosan and alginate, consist of proteins and polypeptides or polysaccharides, and are most commonly used due to the minimal development of inflammatory reaction upon grafting. Synthetic scaffolds can be biodegradable or non-biodegradable (García-Carvajal *et al.*, 2013). The hydrogels can also be divided into homopolymeric in which only one source of polymer is used, or co-polymeric, which is a combination of different polymers. Hydrogels can also vary in appearance, as a matrix, film, or microspheres, or even depending on the charge of the scaffold, being neutral, ionic amphoteric or zwitterionic (Chung and Burdick, 2008; Asadi *et al.*, 2018).

Hydrogels represent promising candidates for tissue engineering of articular cartilage due to their high content in water, biocompatibility, diffusion of oxygen, metabolites and waste, maintenance of the cellular phenotype and providing an adequate structure that bears with high mechanical loads (Chung and Burdick, 2008; Moreira-Teixeira *et al.*, 2011; García-Carvajal *et al.*, 2013). In addition to the desirable features of hydrogels, compared to sponges and meshes, the cell attachment in hydrogels is of a 3D nature and supports rounded morphology of the cells, similar to the microniches found in native tissue (Figure 30) (García-Carvajal *et al.*, 2013; Zhang, Yang, Li, Dou, Li, Thote, D. Wang, *et al.*, 2013).

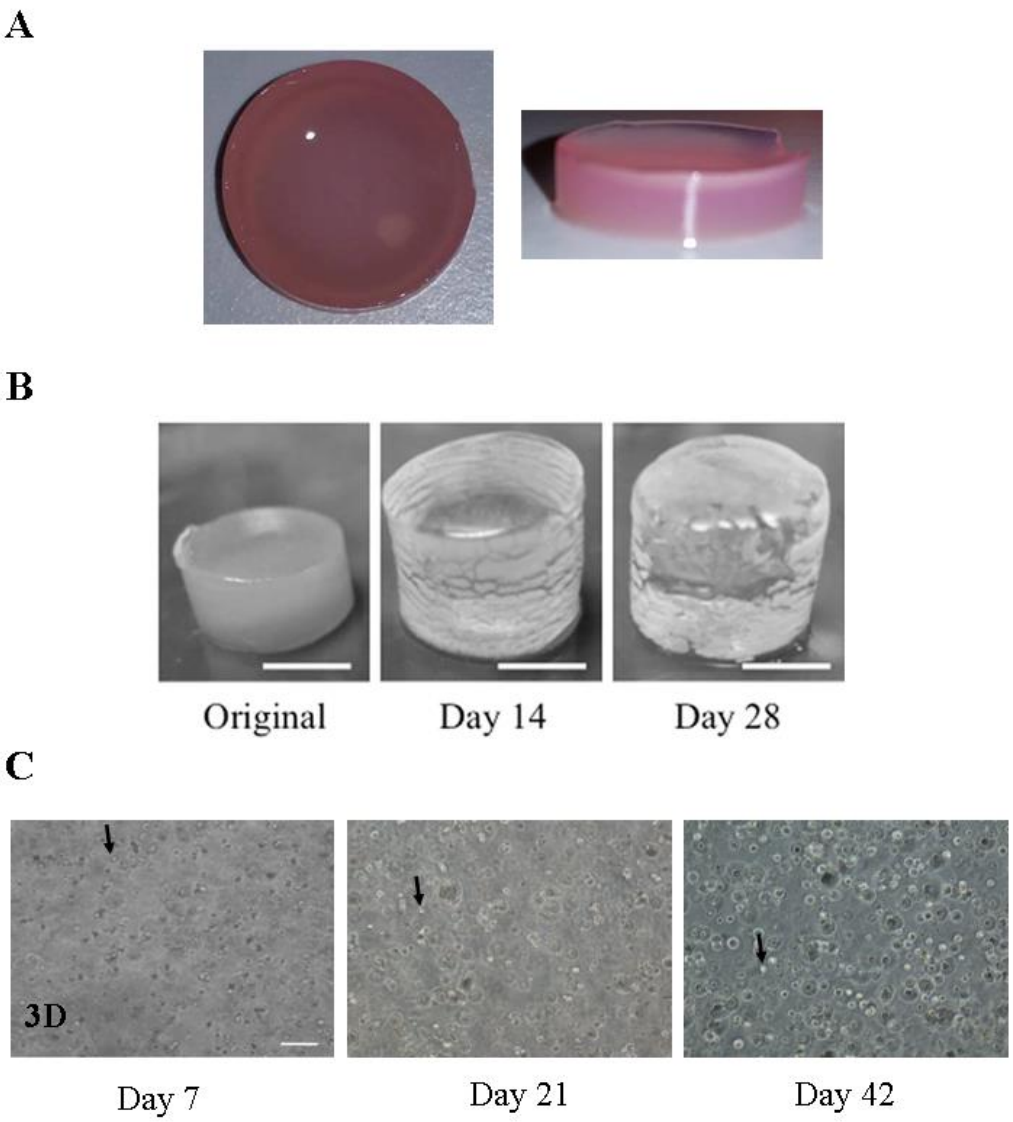

Figure 30. A representative of hydrogel constructs. A) *Agarose low-temperature hydrogel seeded with ATDC5 cells* ***B)*** *High-purity alginate during in vitro degradation Scale bars: 5 mm. Image from* (Shahriari *et al.*, 2016). ***C)*** *ATDC5 cells seeded in Agarose low-temperature hydrogel after 42 days of seeding showing rounded chondrocyte-like morphology throughout the time of culture. Scale bar: 100 µm*

1.6.2.3.1 Collagen

Type I and III collagen hydrogels are the main hydrogels that have been tested in tissue engineering of cartilage as they are present in the native tissue. Collagen-based natural scaffolds have been developed for clinical purposes, and collagen is also one of the main components in compositions such as Carticel® and Matricel®, both of which retain the chondrocyte phenotype and provide easy cell migration (Chung and Burdick, 2008; Bhattacharjee *et al.*, 2015). Gelatine is a collagen-derived scaffold obtained by denaturation and hydrolysis; however, even if its properties of higher water solubility (similar to proteoglycans found in the tissue) and low cost are attractive for cartilage engineering, further studies suggest that it is thermosensitive and shows unstable mechanical properties (Chung and Burdick, 2008; Hoch, Tovar and Borchers, 2016).

1.6.2.3.2 Alginate

Alginate is a natural polysaccharide polymer crosslinked by bivalent cations. Alginate is commonly used in tissue engineering and generation of organoids, and it can be further modified with short peptide sequences such as Arg-Gly-Asp (RGD), providing a greater scaffold-cell interaction (Chung and Burdick, 2008; Moreira-Teixeira *et al.*, 2011). In addition to this, alginate offers some important features such as high transport of nutrients, oxygen and waste, homogenous distribution, and efficacy synthesis of ECM. Despite this, other studies showed low mechanical stability and biocompatibility, in addition to this, the chondrocytes are usually embedded in alginate droplets and sponges rather than hydrogels. Therefore, more optimization or combination with other scaffolds is required (Chung and Burdick, 2008; Bernstein *et al.*, 2009; Kim, Mauck and Burdick, 2011; Bhattacharjee *et al.*, 2015).

1.6.2.3.3 Hyaluronic acid

Hyaluronic acid is present in the native cartilage and forms part of the natural polysaccharide polymers. This scaffold has been applied in tissue engineering for cartilage injuries, and currently, two scaffolds, Hyalograft-C® and Hyalgan® are being tested for clinical purpose. Hyalograft® has been supported by many studies showing promising properties to aid the repair of cartilage damages in the short and long term (García-Carvajal *et al.*, 2013; Brix *et al.*, 2014). Moreover, hyaluronic acid matrix enhances cell proliferation, wound repair, bioactivity, morphogenesis and viscoelastic features (Chung and Burdick, 2008; Huang, Hu and Athanasiou, 2016); however, other studies showed a poor proteoglycan deposition (Alini *et al.*, 2003).

1.6.2.3.4 Matrigel

Matrigel® is a natural and complex scaffold derived from Englebreth-Holm-Swarm tumours in mice that contains elastin, laminin and collagen type IV. Both laminin and type IV collagen are components of the articular cartilage ECM, making this matrix a desirable hydrogel for cartilage engineering. Several studies have used Matrigel® as a 3D model to stimulate chondrogenesis, and it has been shown to enhance the differentiation of stem cells, increase the cell attachment and help cells synthesise a complex ECM network (Levenberg *et al.*, 2003; Jukes *et al.*, 2008; Hughes, Postovit and Lajoie, 2010). Other studies suggest that the presence of several growth factors such as IGF or TGFβ could negatively affect tissue development, despite this, some of these factors are currently applied in scaffolds to enhance ECM production (Hughes, Postovit and Lajoie, 2010; Mauck and Burdick, 2011).

1.6.2.3.5 Agarose

Agarose is a natural hydrogel derived from seaweed and is made up of polysaccharides. It has been widely used since first mentioned in 1982 (Benya and Shaffer, 1982) due to its ability to reproduce the properties of articular cartilage, maintain the morphology of cells, phenotype, and mechanical strength during compression (Chung and Burdick, 2008; Huang, Hu and Athanasiou, 2016). Despite some limitations, such as lower tensile properties and non-degradability (Bian *et al.*, 2009; Huang, Hu and Athanasiou, 2016) most studies showed the ability of agarose constructs to produce an ECM similar to the one found in native cartilage in long-term cultures when seeded with either chondrocytes or stem cells (Lima *et al.*, 2008; Yuan, Serra and Yang, 2015).

Current scaffolds applied in the clinic include materials present in the native tissue, such as the previously mentioned Carticel® or Matricel® made up of type I and III collagen, Hyalograft-C® and Hyalgan® composed of hyaluronic acid, and Tisseel® and Cartipatch® that comprise a combination of alginate-agarose hydrogels. These constructs have been successfully used in clinic improving the functionality and reducing the pain of patients, but despite the initial successes, a long term follows up is necessary to ascertain the mechanical properties of grafted tissues (García-Carvajal *et al.*, 2013).

1.6.2.4 Scaffold-free cartilage engineering

Scaffold-free tissue engineering involves the self-assembly of the cells without any scaffold or external input (Figure 31). Self-assembly consists of depositing the cells on a non-adherent material, such as hydrophobic materials, or bio-inert scaffolds like agarose, in which cells minimize free energy by binding into an aggregate without the need for external energy. Advantages of this technique include the lack of toxicity or degradation from the scaffolds which makes this method favourable for clinical application, as well as the maintenance of the phenotype of the cells stopping dedifferentiation of the chondrocytes *in vitro* (Lee *et al.*, 2017). The cell density required for scaffold-free models is reduced compared to some tissue-engineered constructs, which require extended passaging and lengthy culture times (Bernstein *et al.*, 2009). Despite this, the consistency of the self-assembly aggregates is fragile with poor mechanical strength (Figure 32) (Tortelli and Cancedda, 2009; Lee *et al.*, 2017).

1.6.2.4.1 Pellet culture

Pellet culture involves the centrifugation of a cell suspension in a conical tube that leads to the formation of a solid aggregate of cells (Figure 31). As mentioned previously, this technique not only helps maintain the chondrocyte phenotype but also produces a zonal stratification inside the pellet, in which cells in the middle suffer higher hypoxia than the ones on the surface, leading to a differential gene expression along the zones and stratified ECM secretion, similar to what is seen *in vivo* in the tissue (Murphy *et al.*, 2015; Lee *et al.*, 2017). Despite this, pellets have limited dimensions compared to other tissue-engineered models, and mechanical stability limits them as tissue-engineered functional tissue (Rahul S. Tare *et al.*, 2005; Athanasiou *et al.*, 2015).

1.6.2.4.2 Cell sheets

Cell culture in sheets allows creating larger constructs by culturing the cells in a large monolayer surface which is either functionalised with substrates or thermo-responsive polymers. In both cases, the layer of cells could be shaped into different forms depending on the functionalisation or temperature. Despite the manufacturing being in monolayer lacking mechanical compression, this systems offers the possibility of building different layers creating thicker sheets or tissues (Figure 31) (Shimizu *et al.*, 2006; Lee *et al.*, 2017).

1.6.2.4.3 Cell Aggregate

Aggregates or spheroid culture are similar to pellet culture and have been employed as bioink in bioprinting. When printing, the aggregates or spheroids fuse and deposit, forming a larger 3-dimensional structure (Figure 31) (Bhumiratana *et al.*, 2014).

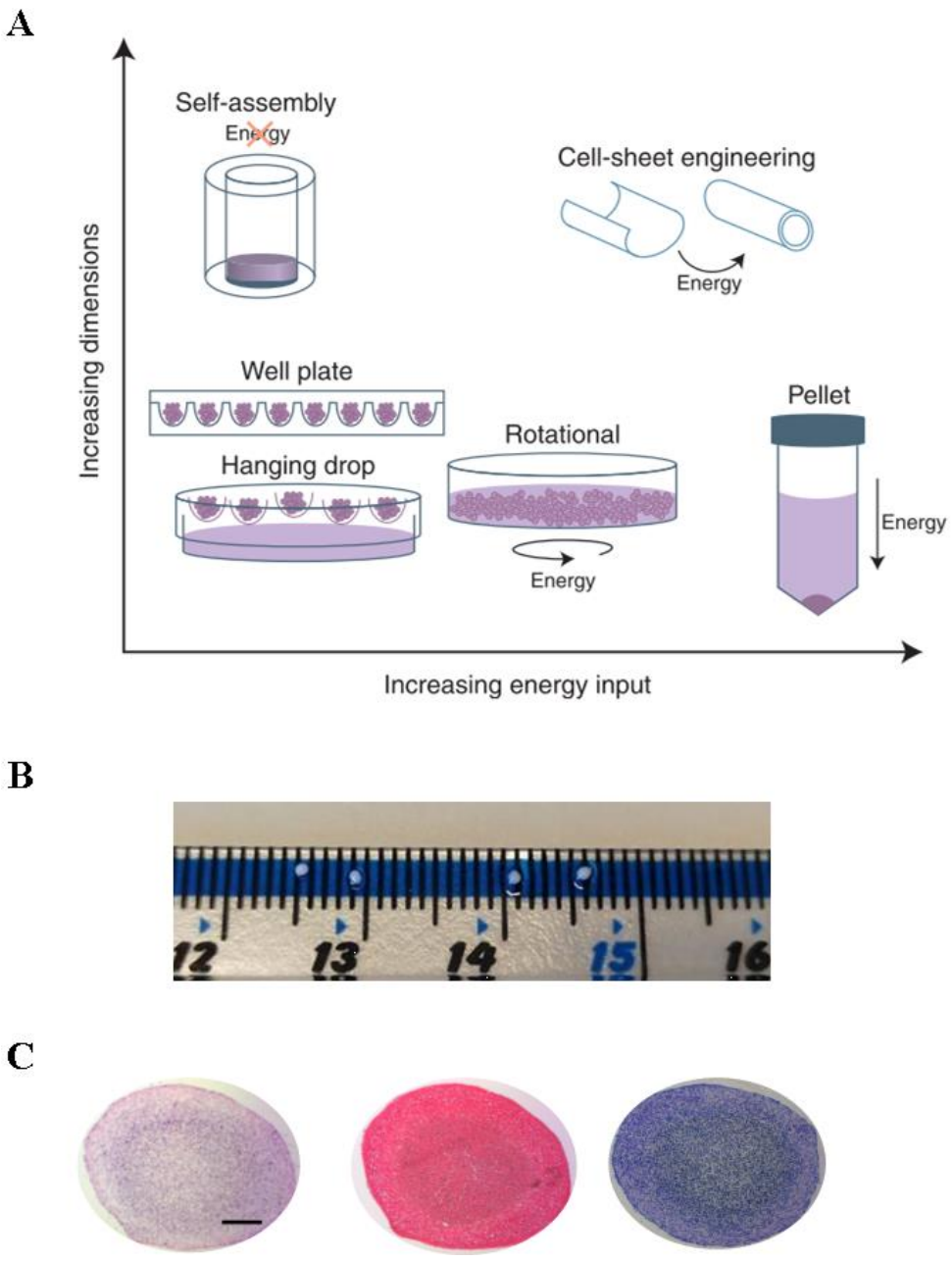

Figure 31. Schematic representation of energy input needed to achieve a certain dimension and examples of pellets. A) *Representation of the energy usage required for different dimensions for scaffold-free constructs. Image from* (Lee *et al.*, 2017). ***B)*** *ATDC5 cells processed into scaffold-free pellets on a ruler for size measurement* ***C)*** *Histology of haematoxylin and eosin (left), picrosirius red (centre), toluidine blue (right) of ATDC5 cells pellet showing matrix deposition and zonal stratification Scale bar: 200 µm*

1.6.3 Cell's source

Different sources of cells are available for studying chondrogenesis and cartilage homeostasis *in vitro* and for developing tissue-engineered constructs.

1.6.3.1 Primary chondrocytes

Articular cartilage tissue engineering traditionally employed autologous chondrocytes obtained from the patients to develop constructs, which could be grafted back into the damaged site (Figure 33) (Medvedeva *et al.*, 2018). However, the use of primary chondrocytes presented various limitations, from invasive procedures for harvesting to insufficient cell quantities for either implantation into the damaged area, or expansion in the complex 3-dimensional scaffolds, and disparity of the chondrogenic properties depending on the location of the cell harvest (Mauck *et al.*, 2003; Bhumiratana and Vunjak-Novakovic, 2015; Asadi *et al.*, 2018; Kisiday, 2019). Expanding chondrocytes *in vitro* to reach the required cell density presents several limitations, such as low cell proliferation and rapid loss of chondrogenic properties becoming fibroblast-like (Phull *et al.*, 2016; Kisiday, 2019).

1.6.3.2 Stem cells

The use of stem cells helps to overcome many of the issues associated with primary chondrocytes, and due to their differentiation capacity into several tissue lineages such as cartilage, bone and adipose tissues, are a promising alternative for cartilage tissue engineering (Figure 33) (Pelttari, Steck and Richter, 2008; Asadi *et al.*, 2018). Stem cells have a higher proliferative rate than chondrocytes while maintaining differentiation (Phull *et al.*, 2016). The main cell source in cartilage tissue engineering is mesenchymal stem cells (Phull *et al.*, 2016). Mesenchymal stem cells can be obtained from adipose tissue or bone marrow (Reppel *et al.*, 2015; Phull *et al.*, 2016). Embryonic stem cells (ESC) are an ethically controversial source of cells, despite the advantageous properties of cell proliferation and differentiation into many somatic lineages (Denker, 2006; Phull *et al.*, 2016). Induced pluripotent stem cells (iPSC) are also a novel promising cell type and have shown excellent properties at repairing cartilage damage. Despite this, iPSC could transmit diseases and adverse response (Phull *et al.*, 2016).

Genetic manipulation of stem cells presents several hurdles regarding the efficiency of transfection, preserving the expression, limiting mutagenic potential and reducing cytotoxicity all while maintaining their differentiation capability (Baek *et al.*, 2016; Tamm *et al.*, 2016). Viral transfection, a laborious technique, allow an 80% efficiency. In comparison, the other methods such as electroporation (40%), and cationic polymer and liposome (20-35%) have low efficiencies as well (Wang *et al.*, 2011; Baek *et al.*, 2016). The low efficiency of genetic modification makes primary cells and stem cells a difficult material to work with when studying the impact of novel genetic on chondrogenesis and cartilage stability in a laboratory setting.

1.6.3.3 ATDC5 cell line

ATDC5 cell line was first established in 1990 by Atsumi et al., and derives from AT805 mouse teratocarcinoma fibroblastic cells (Atsumi *et al.*, 1990) (Figure 32). Since then, the ATDC5 cells have been well characterised and have shown excellent potential for studying chondrogenesis, as with the right growth factor regime they are capable of recapitulating chondrocyte differentiation and mineralisation (Newton *et al.*, 2012; Kudva, Luyten and Patterson, 2018). ATDC5 cells showed high proliferation rates, maintenance of the phenotype when re-seeded in 3-dimensional models after expansion, and development of cartilage-like formation comparable to chondrocytes (Rahul S. Tare *et al.*, 2005; Seriwatanachai, Krishnamra and Charoenphandhu, 2012; Tare *et al.*, 2018). This cell line can easily be transfected using Lipofectamine 2000 Transfection Reagent (Morimoto and Obinata, 2011; Luan and Liang, 2018; Ying *et al.*, 2019).

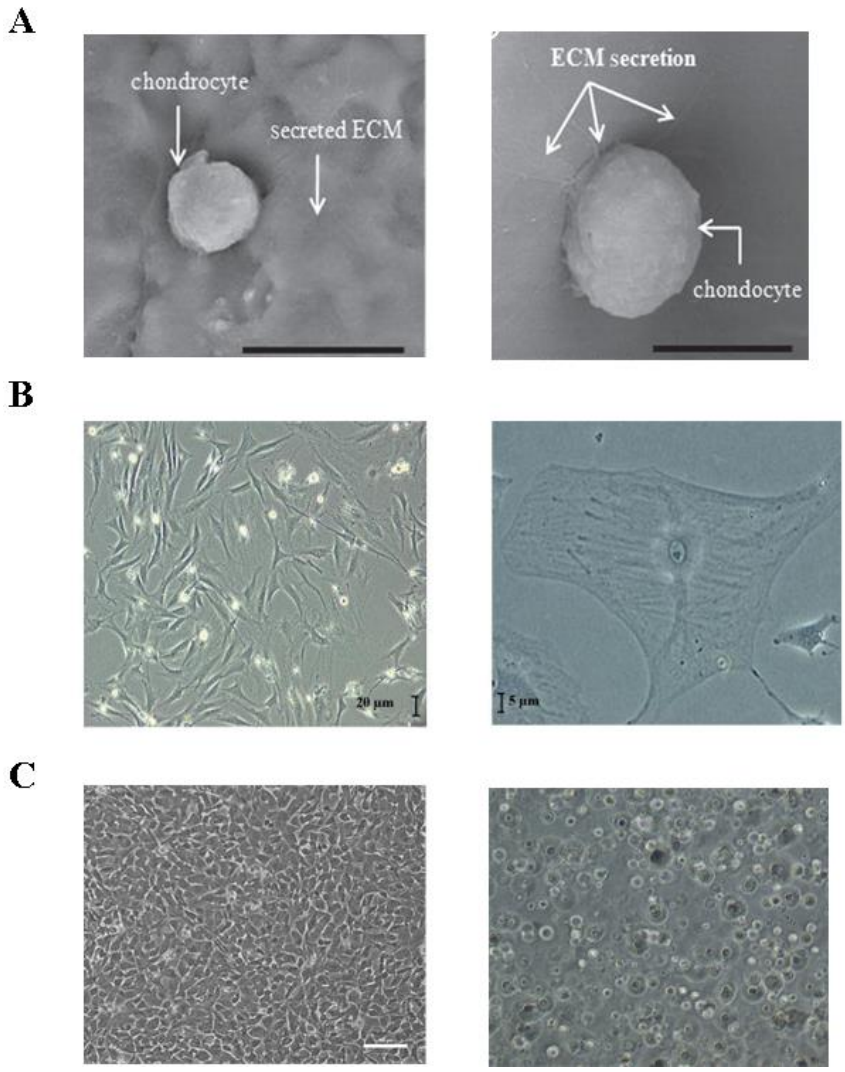

Figure 32. Examples of cell types employed in articular cartilage models. A) *Chondrocytes adhered to the surface of hydrogels after 24h via a scanning electron microscope, scale bar, left 20 µm, right 10 µm. Images from* (Bhat, Tripathi and Kumar, 2011). ***B)*** *Mesenchymal stem cells seeded in flasks (2D) Scale bars: left 20 µm, right 5 µm. Images from* (Rochefort *et al.*, 2005) ***C)*** *ATDC5 chondrogenic cell line seeded in monolayer (left) and 2% low-temperature agarose culture (right). Scale bar: 100 µm.*

1.6.4 Application of external stimulus to improve chondrogenesis

The use of the scaffold may not be sufficient to reproduce the complexity of cartilage ECM and zonal stratification. It has been shown that manipulating the constructs with external stimuli such as growth factor supplementation, varying the oxygen levels, or adding a mechanical stimulus (compression, shear stress etc.), can enhance the formation of ECM thus improving the construct's resemblance to native tissue (Chung and Burdick, 2008; Tur, 2009).

1.6.4.1 Growth Factor Supplementation

Studies confirm that anabolic growth factors combined with the scaffold can induce the production of ECM and promote chondrogenesis. The main growth factors applied in cartilage tissue engineering include transforming growth factor-beta (TGFβ), Bone morphogenetic proteins (BMPs) and Insulin-like growth factor 1 (IGF-1) (Mauck and Burdick, 2011; Moreira-Teixeira *et al.*, 2011).

IGF-1 has been shown to enhance the synthesis of proteoglycans and type II collagen when supplemented in the culture (Clemmons, 2004; Frenkel and Di Cesare, 2004; Bhattacharjee *et al.*, 2015). In addition to this, the TGF superfamily such as TGFβ1, TGFβ2, and TGF-β3 play the main role in the stimulation of chondrogenesis of embryonic and adult MSCs and the maintenance of chondrogenic phenotype and may amplify the ECM deposition (Bian *et al.*, 2011; Bhattacharjee *et al.*, 2015). Finally, the BMP group which is included within the TGF superfamily has shown potential to enhance the production of matrix and encourage chondrogenesis (Chung and Burdick, 2008; Chen, Li and Li, 2015). Specifically, BMP2 and BMP7 induced the expression of *Sox9* and tissue inhibitor of metalloproteinases type 1 (TIMP-1) synthesis, and the production of type II collagen, aggrecan and proteoglycans (Chung and Burdick, 2008; Scarfì, 2016). BMP4 contributed to the maintenance of the phenotype, whereas, BMP6 and BM7 induced chondrogenesis and synthesis of ECM molecules such as proteoglycans and type II collagen (Chen, Li and Li, 2015; Scarfì, 2016).

Several studies suggest that the combinatorial effect of TGF-β and BMPs is more beneficial in chondrogenesis than the addition of both growth factors on their own (Shen *et al.*, 2009; Shintani, Siebenrock and Hunziker, 2013). In particular, a study showed that combining BMP7 and TGF-β3 increased gene expression of type II collagen and *Sox9* and promotion of ECM deposition and inhibition of hypertrophy (Huang *et al.*, 2018).

1.6.4.2 Dynamic compression

As previously mentioned, compression is an essential parameter for articular cartilage. Native tissue is constantly compressed and bearing high mechanical loads and loading and mechano-responsiveness are highly implicated in the deposition and remodelling of the ECM. Several options to mimic this environment are applying hydrostatic pressure, static or dynamic compression and shear stress. However, experimental results may vary depending on the cycle of pressure, frequency and duration of stress (Lima *et al.*, 2007; García-Carvajal *et al.*, 2013).

Dynamic compression could be applied by compression systems like the one illustrated in Figure 33. Dynamic compression has been shown to enhance the production of ECM molecules such as proteoglycans and collagens and increase the tissue resilience bearing compressive stresses (Mauck *et al.*, 2000; Chung and Burdick, 2008; Huang, Hu and Athanasiou, 2016). Moreover, a combination of dynamic compression and other previously mentioned stimuli such as growth factors has been shown to combine synergistically and drastically enhance the resemblance of tissue-engineered constructs to complex native cartilage (Jin *et al.*, 2003; Robert L. Mauck *et al.*, 2003).

Despite the promising results, some studies show conflicting data, in which variations of the dynamic compression lead to differential expression of ECM molecules, MSCs chondrogenesis inhibition and poor mechanical properties of prolonged loading (Lee *et al.*, 2006; Thorpe *et al.*, 2008). Hence, further improvement of the technique is needed to achieve consistent results.

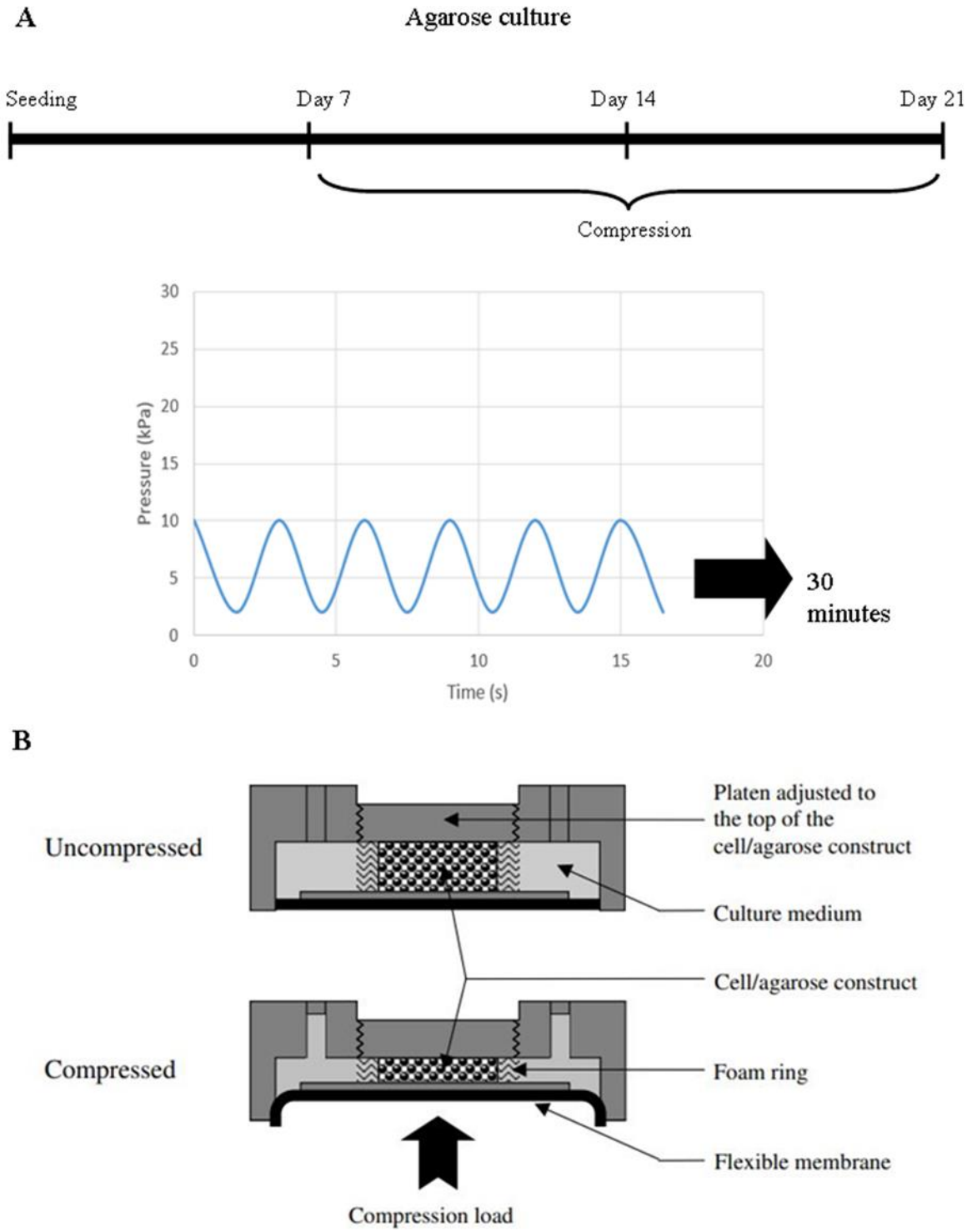

Figure 33. Example of the loading regime used for this research. A*) ATDC5 cells in the agarose construct were compressed for 14 days for 30min/day at 10kPa magnitude and a sinusoidal waveform and a frequency of 0.33Hz.* ***B)*** *Schematic diagram of the BioPress™ culture plate (Dunn Labortechnik GmbH) placed in the compression machine (Flexcell FX-500™) when compressed and uncompressed. (Bougault et al., 2008).*

1.6.4.3 Hydrostatic pressure

Hydrostatic pressure could be applied by transferring the load to the construct through a gas phase or compressing the 3D model. However, alteration of the gas concentration is visible inwardly in the culture medium, whereas the second option could not be applied in different oxygen concentrations studies (Elder and Athanasiou, 2009).

The application of hydrostatic pressure to 3D and 2D models has shown great improvement in ECM secretion and cell activity. Despite this, studies have shown large inconsistencies and low reproducibility depending on the loading rates (Chung and Burdick, 2008; Huang, Hu and Athanasiou, 2016).

1.6.4.4 Oxygen

Native articular cartilage exists in a largely hypoxic environment and presents with a low oxygen tension (less than 5%). Therefore, the application of hypoxia in cartilage tissue engineering is a promising stimulus that may help to replicate the properties of the native tissue. Studies that applied hypoxia reported induced chondrogenesis, and activation of pathways enhancing the production of matrix molecules as type II collagen and proteoglycans, in addition to other enzymes stimulated, such as lysyl-oxidase that enhanced the biomechanical properties by augmenting the crosslinking in collagen (Chung and Burdick, 2008; Makris, Hu and Athanasiou, 2013; Huang, Hu and Athanasiou, 2016). The combination of hypoxia with growth factors such as TGF-β3 had a synergic effect on the deposition of ECM, especially of collagen (Durant *et al.*, 2014).

1.6.5 In vivo and in vitro cartilage models

The employment of animal models for in vivo studies is integral and indispensable for medical research and regenerative studies. Animals provide essential insight into the ageing or disease process, evaluation of efficacy or adverse reactions of new drugs or developed biomaterials or devices prior to human clinical trials (Xing et al., 2016). Despite all the benefits that animal studies offer, there are considerable limitations such as ethical issues, cost-benefit, expenses, conflicting parameters, lengthy duration, and translational results to the human model (Xing et al., 2016). *In vitro* testing before animal application potentially provides insight and predicts *in vivo* results, contributing to a reduction in the amount and costs of animal studies (Nickien *et al.*, 2018).

Another consideration when using animal models is the interpretation and extrapolation of results to the human organism, this is why, the choice of the animal species matters (Xing *et al.*, 2016 and Nickien *et al.*, 2018). For example, small animals as the murine model present a short duration of the reproductive cycle and high reproductive capacity, however, the resemblance with human articular cartilage is lower and provides limited information if comparing to larger animals such as sheep or cows (Zhu et al. 2015; Fitzgerald et al. 2008; Malda et al. 2013). Rats, despite their bigger joints and ticker cartilage, possess a higher heal capacity therefore, extrapolating the results to human clinical models could be misleading (Sakata, Iwakura, and Reddi 2015; Lammi *et al.*, 2001; Oshima *et al.*, 2004). Employing large non-companion animals, like goat or pig, benefits the reduction of sampling and provides with more reliable results, however, might translate into higher costs of maintenance, and despite the higher resemblance to human cartilage, small animals are still required for initial stages of in vivo studies (Xing *et al.*, 2016).

Despite initial limitations (Doran 2015), the articular cartilage *in vitro* model's development allowed to overcome certain obstacles such as the lack of mechanical stimulation, growth factors, or maturation of the tissue (Thorpe *et al.*, 2013; Huang *et al.*, 2018). *In vitro* models offer advantages in comparison to *in vivo* models in the recapitulation of internal and external spatiotemporal signalling involved in embryonic development, and the study of regeneration via novel 3D cell culture systems, biomaterial scaffolds, shear/compression bioreactors, etc Xing *et al.*, 2016). Furthermore, no contradictions between *in vitro* and *in vivo* outcomes have been shown, suggesting a justification to further align both study methodologies. Some study methodologies that could be harmonised are the experimental timeframes (long-term animal models against short-term *in vitro* studies), analytical methods, such as *in vivo* studies only employing Mankin score as an outcome, and computational models to confirm the link between both studies (Nickien *et al.*, 2018). In table 3 a summary of recent zonally stratified *in vitro* cartilage models.

Cell type	3D scaffold	Compression	Outcomes	Reference
Mesenchymal stem cell	2% agarose concentration	Dynamic compressive loading sine wave of 10% strain amplitude 1 Hz frequency 4 hours/day 5 days/week.	Increased GAG exhibited in the deep zone of scaffolds with increased collagen and proteoglycan-4 (lubricin) deposition in the surface of the hydrogel, and a lack of hypertrophy and calcification throughout the scaffold.	(Thorpe *et al.*, 2013)

Chondrocyte subpopulations from bovine calf knees from the surface and middle zones	1.2% alginate forming alginate beads	Compression tests of 0.1 kPa for the sample geometry	Superficial zone chondrocytes presented less ECM and lower compressive properties than middle zone chondrocytes. The stratified superficial-middle scaffolds exhibited middle zone properties, and specific surface proteins were presented in the surface scaffolds.	(Klein et al. 2003)
Human adipose-derived stem cells	Hybrid bioprinting of a scaffold-free tissue strands	-	Collagen fibres were orientated resembling articular cartilage and matrix orientation of native tissue. Mechanical studies showed a compression modulus of ≈1.1 MPa, like human articular cartilage.	(Wu et al. 2020)
Bone marrow-derived mesenchymal stem cells	Press-molding of the cell pellet on the surface of a bone construct.	-	Lubricin was found at the surface, while proteoglycans and type II collagen in the bulk zone. Type X Collagen was deposited at the interface with the bone, and type I collagen in the bone.	(Bhumiratana and Vunjak-Novakovic 2015)
Bovine chondrocytes	Porous poly(ethylene glycol)-terephthalate – poly(butylene terephthalate) (PEGT/PBT) copolymer scaffolds by 3D fibre deposition (3DF) technique	-	Deposition and orientation of zonal GAG and type II collagen was similar to what found in native articular cartilage, however, the GAG:DNA content differed	(Woodfield et al. 2005)
Marrow stem cell	Chondroitin sulphate (CS) and matrix metalloproteinase-sensitive peptides (MMP-pep) into PEG hydrogels	-	Induced high deposition of type II collagen with low proteoglycan levels, which results in a low compressive modulus	(Nguyen et al. 2011)

	(PEG:CS:MMP-pep)			
Marrow stem cell	Chondroitin sulphate (CS) and matrix metalloproteinase-sensitive peptides (MMP-pep) into PEG:CS hydrogels	-	Intermediated deposition of both type II collagen and proteoglycans, as found in the middle zone	(Nguyen et al. 2011)
Marrow stem cell	Chondroitin sulphate (CS) and matrix metalloproteinase-sensitive peptides (MMP-pep) into PEG:hyaluronic acid (HA) hydrogels	-	High synthesis of proteoglycan and low type II collagen deposition with a high compressive modulus, similar to the deep zone found in native tissue	(Nguyen et al. 2011)

Table 3. Summarise key finding in zonally stratified 3D models compressed or uncompressed found in the literature

1.7 Aims of the project

Articular cartilage studies are often hindered by the difficulty in obtaining human material and the use of costly animal models. Tissue engineering is opening possibilities to develop zonally stratified models of cartilage that facilitate *in vitro* studies.

This project hypothesised that an articular cartilage model developed *in vitro* could be used to study the progression of cartilage-related diseases. The aim of this project was to create an *in vitro* zonally stratified articular cartilage model in which the disease mechanism of Pseudoachondroplasia (PSACH), a skeletal dysplasia in cartilage, could be replicated, using its applicability in the future to get further insight into potential treatments.

1.7.1 Aims of each result chapter.

- *Chapter 3:* Aimed to validate the chondrogenic potential of ATDC5 cells in monolayer culture.
- *Chapter 4:* To develop and characterise 3-dimensional pellet culture of ATDC5 cells as a model to study cartilage differentiation and disease *in vitro*.
- *Chapter 5:* Aimed to develop a 3D in vitro system that replicates the zonal stratification observed in vivo using ATDC5 cells in a hydrogel culture.
- *Chapter 6:* The aim of this chapter was to study the effect of dynamic compression on the agar-based *in vitro* 3D model of cartilage.
- *Chapter 7:* To study the pathological mechanism of the p.T585M COMP mutation during ATDC5 chondrogenesis in the conventional 2-dimensional culture and in the two developed in vitro 3D systems: pellets and hydrogels.

Chapter 2. Materials and Methods

2 Materials and methods

All experiments were carried out at room temperature unless specified otherwise.

2.1 Materials

2.1.1 Solutions

- **1% (v/v) Acetic Water:**

1.5mL Glacial acetic acid

300 mL of Deionised water

- **1% (v/v) acid alcohol:**

5mL Glacial acetic acid

995 mL Deionised water.

- **0.5% (v/v) Acidified water:**

990 mL of 70% EtOH

10 mL of 37% Concentrated HCl

- **2% (v/v) Agarose:**

1.2g of low melting point agarose

60 mL of dH_2O

- **Alizarin Red staining solution:**

5 mg (f.c 0.05 mg/mL) Alizarin Red S

100 mL (2% v/v) Potassium hydroxide

- **Alcian Blue pH 0.75**

15 mg of Alcian Blue

80 mL of 95% Ethanol

20 mL glacial acetic pH = 0.75

- **0.2% (w/v) Bovine hyaluronidase:**

100 mg Bovine hyaluronidase

50 mL x1 PBS

- **1% (w/v) Bovine Serum Albumin**

1g of Bovine serum albumin

100 mL of 1x PBS

- **10% Cetylpyridinium chloride:**

10g of Cetylpyridinium chloride

90 mL of Deionised water

- **0.1 M Citrate buffer pH 6:**

0.96g Citric acid (f.c 10mM)

250 µL Tween® 20(f.c 0.05%)

500 mL Deionised water

- **5mM Cysteine-HCl:**

0.078g Cysteine

10 mL phosphate buffer

- **1mg/mL Chondroitin sulphate**

1 mg Chondroitin sulfate A sodium salt from bovine trachea

1 mL 0.1M phosphate buffer

- **Differentiation medium:**

DMEM/F-12 with GlutaMAX I

5% FBS

1% insulin transferrin

1% sodium pyruvate

1% Penicillin-Streptomycin

10 mM β-glycerophosphate (βGP)

50 µg/ml L-ascorbate-2-phosphate

- **Dimethyl-methylene blue pH 3:**

3.04 g glycine

2.37 g Sodium Chloride

785 µL Hydrochloric acid 12.1M (36%)

1 litre deionised water

- **0.5M EDTA pH 8:**

800 mL Deionised water

146.12 g EDTA

- **5mM EDTA pH 6.5:**

0.078 g EDTA

10 mL Phosphate buffer

- **6 M Guanidine-HCl**

8.59g guanidine hydrochloride

15 mL deionised water

- **LB-Agar**

5g Tryptone

2.5 Yeast Extract

5g Sodium Chloride (NaCl)

7.5 Agar

Before its uses, agar was autoclaved and once the temperature was close to 37ºC 50µg/mL of Ampicillin were added.

- **LB-Broth**

5g Tryptone

2.5 Yeast Extract

5g Sodium Chloride (NaCl)

Before its uses, the broth was autoclaved and once the temperature was close to 37ºC 50µg/mL of Ampicillin were added.

- **Maintenance medium:**

Dulbecco's Modified Eagle's Medium (DMEM) high glucose pyruvate

10% Fetal Bovine Serum (FBS)

1% of Non-essential amino acid solution (NEAA)

1% Penicillin-Streptomycin

- **50:50 Matrigel**

250 µL of matrigel

250 µL of cells plus differentiation medium

- **X1 MES buffer**

50 mL of MES SDS running buffer (20x)

950 mL of deionised water

- **3% Milk in PBS-T**

1.5 g of skimmed milk

50 mL PBS-T

- **5% Milk in PBS-T**

2.25 g of skimmed milk

50 mL PBS-T

- **25mg/mL MTT**

5 mg/mL of MTT

250 µL of DPBS

- **0.85% (w/v) NaCl**

0.85g NaCl

100 mL Deionised water

- **Papain Solution pH 6.5**

0.1M sodium phosphate

5mM EDTA

5mM Cysteine-HCl

125µg/mL papain enzyme

- **PBS-T**

5 Tablets of Phosphate buffered saline

500 µL of Tween® 20

1 Litre of Deionised water

- **X1 PBS**

5 Tablets of Phosphate buffered saline

1 Litre of deionised water

- **PCR Control for QuikChange Mutagenesis**

5 µL of 10x reaction buffer

25 ng of pWhiteScript 4.5 kb control plasmid

125 ng of control primer 1

125 ng of control primer 2

1 µL of dNTP mix

1.5 µL of QuikSolution reagent

34 µL double deionised water

1 µL QuikChange Lightning Enzyme

- **PCR Proline for Leucine for QuikChange Mutagenesis**

5 µL of 10x reaction buffer

10, 25 or 50ng of ds DNA template

125 ng of Pro>Leu forward primer

125 ng of Pro>Leu reverse primer

1 µL of dNTP mix

1.5 µL of QuikSolution reagent

Up to 50 µL double deionised water

1 µL QuikChange Lightning Enzyme

- **PCR Arginine for Glutamine for QuikChange Mutagenesis**

5 µL of 10x reaction buffer

10, 25 or 50ng of ds DNA template

125 ng of Arg>Gln forward primer

125 ng of Arg>Gln reverse primer

1 µL of dNTP mix

1.5 µL of QuikSolution reagent

Up to 50 µL double deionised water

1 µL QuikChange Lightning Enzyme

- **0.1M Phosphate buffer pH 6.5**

Solution A

9.36g Sodium phosphate monobasic

600mL deionised water

Solution B

7.1 g Sodium phosphate dibasic

500 mL deionised water

Mix 137 mL of solution A and 63 mL of solution B, pH to 6.5

- **0.1 M Potassium phosphate buffer pH 7.5**

86.6 mL of 0.2M Potassium phosphate dibasic (K_2HPO_4)

13.4 mL of 0.2M Potassium phosphate monobasic (KH_2PO_4)

900 mL of Deionised water

- **20µg/mL proteinase K**

20µL of 10mg/mL Proteinase K

10mL Deionised water

- **RIPA buffer (1x)**

1 mL of 50mM Trizma-HCl pH 7.4 (f.c 50 mM)

1.5 mL of 1M NaCl (f.c 0.15M)

100 µL of Nonidet-P40 (f.c. 1%)

250 µL Sodium deoxycholate (f.c 10%)

20 µL of 0.5 mM EDTA pH 8 (f.c 1 mM)

4.28 mL of Deionised water (f.c 1mM)

A Tablet of EDTA-free protease inhibitor cocktail table was added once the buffer was made.

- **2D RNA-extraction solution:**

1mL of RLT buffer

10 µL of β-Mercaptoethanol

- **3D RNA-extraction solution**:

1 mL of RLT buffer

10 µL of β-Mercaptoethanol

1.5 mL of QG buffer

- **0.1 M sodium acetate buffer pH4**

8.2 g of Sodium acetate

1 litre of deionised water

- **5x Sodium dodecyl sulphate (SDS) loading buffer**

6 mL of 1M Tris-HCl pH 6.8 (f.c 0.3M)

2g Sodium dodecyl sulphate (f.c 10%)

10 mL of Glycerol (f.c 50%)

1mL of 1% Bromophenol blue (f.c 0.05%)

Add deionised water to a final volume of 20 mL

- **50x TAE**

242 g of Tris-base (f.c 2 M)

57.1 mL Glacial acetic acid

100 mL 0.5M EDTA pH8

Add deionised water to a final volume of 1L, and diluted to x1 TAE before use.

- **0.04% Toluidine blue pH 3.75**

0.04g of Toluidine Blue O (f.c 0.04%)

100 mL of 0.1 M Sodium acetate buffer pH4

Adjust the pH to 3.75 with HCl

- **0.2 % (v/v) Triton –X**

200 µL of Triton-X

200 mL of deionised water

- **1x Transfer buffer**

50 mL 20x Transfer buffer

200 mL of Methanol (f.c 1x)

750 mL Deionised water

- **20x Transfer buffer**

60.75 g Tris-Base (f.C 1M)

28.9 g of Glycine (f.c 0.77 M)

3.6 g sodium dodecyl sulphate (f.c 25 mM)

500 mL of deionised water

- **1 M Tris-HCl pH 6.8**

15.76 g of Tris-HCl

100 mL of Deionised water

Adjust the pH to 6.8

- Standard curve for protein measurement in 2D cultures:

Dilution	Abbreviation	**BSA**	**RIPA**
2 mg/mL	V_0	200µL	0µL
1.5 mg/mL	-	150µL of V_0	50µL
1 mg/mL	V_1	100µL of V_0	100µL
0.5 mg/mL	V_2	100µL of V_1	100µL
0.25 mg/mL	-	100µL of V_2	100µL
0.1 mg/mL	-	20 µL of V_0	180µL

Working solution 4.5 mL of Solution A

90 µL of solution B

- Combination of RNA and primers:

Component	**Volume**
Experimental RNA	4.5 µL
Random primer	1 µL
Nuclease-Free Water	0 µL
Final volume	**5.5 µL**

- Reverse transcription reaction mix:

Components	**Volume**
Nuclease-Free Water	X µL
GoScript™ 5X Reaction Buffer	4 µL
$MgCl_2$ (final concentration 1.5-5mM)	1.2-6.4 µL
PCR Nucleotide Mix	1 µL
Recombinant RNasin® Ribonuclease inhibitor	20 µL
GoScript™ Reverse Transcriptase	1 µL
Final volume	**15 µL**

2.1.2 Antibodies

Antibody Against	Dilution	Source	Obtained from
Acetylated α-Tubulin (Ab24610)	1:200	Mouse	Abcam
Type I Collagen (Ab34710)	1: 500	Rabbit	Abcam
Type II collagen (Ab34712)	1:250	Rabbit	Abcam
Type X collagen (Ab58632)	1:500	Rabbit	Abcam
Aggrecan	1:400	Rabbit	Professor Tim Hardingham (University of Manchester)
Recombinant Anti-Ki67 antibody (Ab92742)	1:500	Rabbit	Abcam
Mouse (Ab150113)	1:500	Goat	Abcam
Rabbit (Ab150075)	1:500	Donkey	Abcam

2.1.3 Immunohistochemistry controls

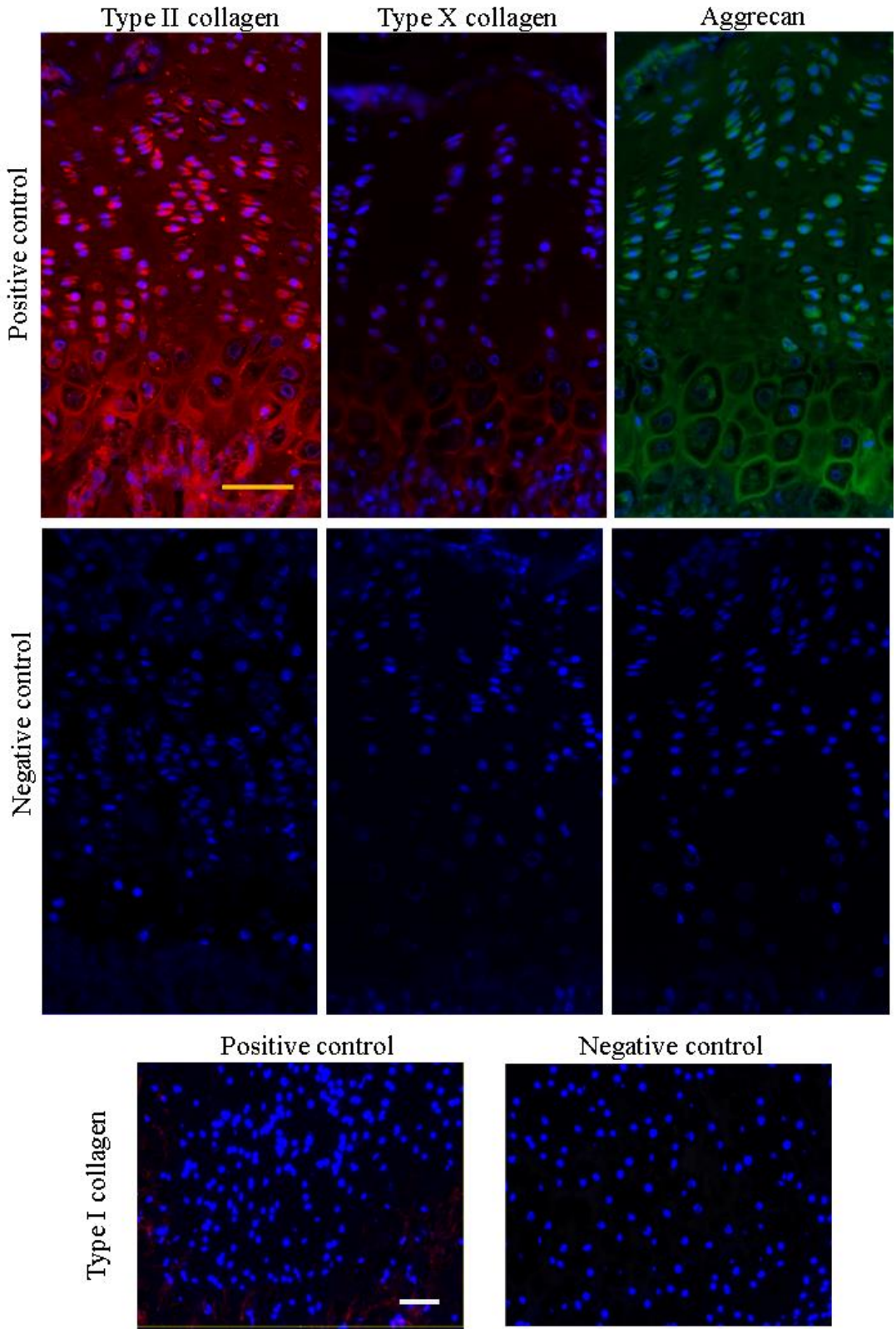

Positive and negative controls for type I, II and X collagen and aggrecan. *Positive and negative controls were done in 3-week old mice femoral heads for type I, II and X collagen and aggrecan. Scale bar: 50 µm*

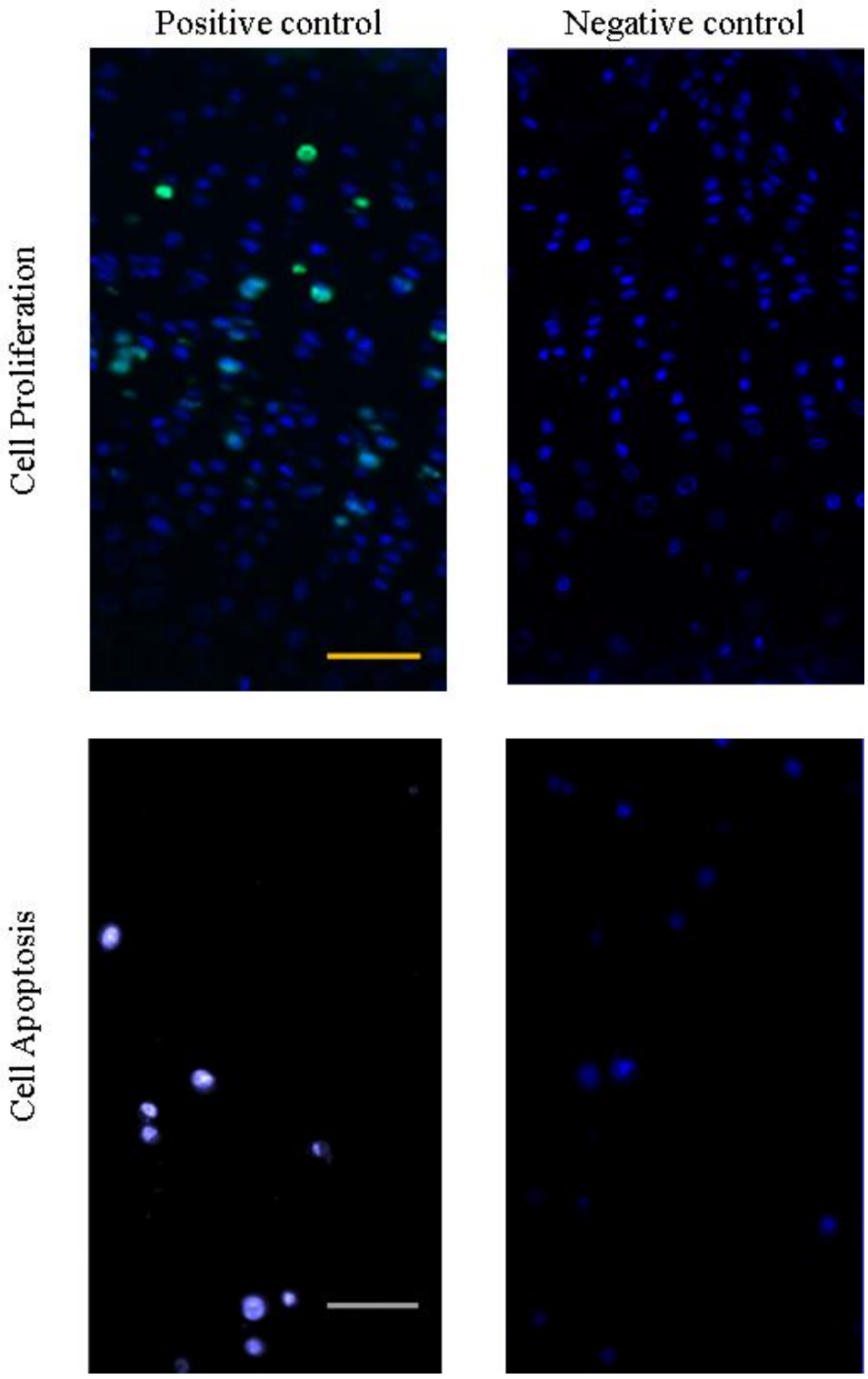

Positive and negative control for cell proliferation and cell apoptosis assay. *3-week old femoral head was used for a positive and negative control of cell proliferation assay (ki67), while for cell apoptosis (TUNEL assay low gelling temperature hydrogels were used (For the positive control of cell apoptosis the cells were seeded with 70% ethanol to assure death). Scale bar: 50 µm*

2.1.4 Primers

Primer for	Origen	Primer sequence 5`-3`
Sox9	Mouse	GTACCCGCATCTGCACAACCTCCTCCACGAAGGGTCTCT
Ihh	Mouse	TGCATTGCTCTGTCAAGTCTGGCTCCCCGTTCTCTAGGC
Type II Collagen isoform A1	Mouse	TGGTAACCCAGGGACTGATGCCAGCAATTCCAGGAGCA
Type X Collagen isoform A1	Mouse	GCATCTCCCAGCACCAGACCATGAACCAGGGTCAAGAA
Type I Collagen isoform A1	Mouse	CATGTTCAGCTTTGTGGACCTGCAGCTGACTTCAGGGATGT
Agreccan	Mouse	TGAAGCAGAAGGTCTGGACACCAGAAGGAATCCCACTAACA
18S	Mouse	GCCGCTAGAGGTGAAATTCTTCGTCTTCGAACCTCCGACT

2.1.5 Embedding parameters

Step	Solution	Duration (minutes)
First	70% Ethanol	360
Second	90% Ethanol	45
Third	95% Ethanol	45
Fourth	100% Ethanol	45
Fifth	100% Ethanol	45
Sixth	100% Ethanol	45
Seventh	Xylene	30
Eighth	Xylene	30
Ninth	Xylene	30
Tenth	Paraffin Wax	60
Eleventh	Paraffin Wax	60

2.1.6 RT-PCR parameters

Cycle	Temperature	Duration (seconds)
Denaturation	94°C	
Primer Annealing	55°C	
Elongation	72°C	
Repetition of cycles for 44		

2.1.7 QuikChange Mutagenesis PCR parameters

Name	Cycles	Temperature	Duration (Seconds)
Control and Mutagenesis	1	95 °C	120
Control and Mutagenesis	18	95 °C	20
Control and Mutagenesis		60 °C	10
Control		68 °C	150
Mutagenesis		68 °C	225
Control and Mutagenesis	1	68 °C	300

2.1.8 Standards for DMMB assay

Standard (µg/mL)	0.1 M Phosphate buffer (µL)	1 mg/mL Chondroitin sulphate (µL)
SC0	1000	0
SC5	995	5
SC10	990	10
SC15	985	15
SC20	980	20
SC25	975	25
SC30	970	30
SC35	965	35
SC40	960	40

2.2 Methodology

2.2.1 Harvest of femoral heads

Two wild-type C57BL6/J mice per age were sacrificed by Dr Pirog, at 1 and 3 weeks post-birth, and their femoral heads were extracted and immediately fixed in 10% formalin (Sigma-Aldrich®), for 24h. The femoral heads were then paraffin wax embedded (melting point 62^{o}C; Thermo- Fisher Scientific) and sectioned at 5 µm thickness in a sagittal plane in an HM 355S automatic microtome and STP 120 Spin Tissue Processor from Thermo-Fisher Scientific™. and placed into SuperFrost® Plus slides Adhesion (VWR™).

2.2.2 Cell Culture

2.2.2.1 Expansion of the ATDC5 cells

ATDC5 chondrogenic cell line (ECACC 99072806) was used in the initial optimisation of the chondrogenic 3D culture systems due to its low costs, easy transfection and high potential to differentiate into chondrocytes (Tare *et al.*, 2005; Newton *et al.*, 2012; Yao and Wang, 2013).

ATDC5 cells stored at -80ºC were gently defrosted from a Corning 2mL Cryogenic Vial Internal Thread PP with Round Bottom (Scientific Laboratory Supplies) in a 37ºC water bath and cultured in 75 cm^2 tissue culture flasks (VWR®) with 12 mL non-differentiating medium, at 5% CO_2 and 37ºC using a Safe 2020 Class II Biological Safety Cabinets and Heracell™ 150i CO_2 and Incubators with Stainless-Steel Chambers and Precision™ General-Purpose Water Baths from Thermo Scientific™. After 24h the medium was discarded to remove the residual DMSO (Sigma-Aldrich®), and another 12mL of fresh medium was added. Cells were placed in the incubator at 5% CO_2 and 37ºC until 90-100% confluency was reached. Media was replaced every 2-3 days. The maintenance medium was made up with Dulbecco's Modified Eagle's Medium (DMEM) high glucose pyruvate (Gibco™), 10% Fetal Bovine Serum (FBS) (Gibco™), 1% of Non-essential amino acid solution (NEAA) (Gibco™) and 1% Penicillin-Streptomycin (5,000 U/mL) (Gibco™).

2.2.2.2 Culture of cells in well plates

To passage and seed the cells, ATDC5 cells were detached from the flasks. Firstly, the medium was discarded, and cells were washed with Dulbecco's phosphate-buffered saline (DPBS) (Sigma-Aldrich®), and 5 mL of 1x trypsin-EDTA was added and incubated for 3 minutes at 5% CO_2 and 37ºC. The trypsin-EDTA (0.05%) (Gibco™) digestion was stopped by adding 5 mL of medium, the cells were collected, centrifuged, and counted using a FastRead 102 counting slides (VWR®) (Figure 34). The number of cells was determined by the following formula:

$$\frac{Total\ cell\ counted}{mL} = \left(\frac{Total\ cells\ counted}{Number\ of\ 4x4\ grids\ counted}\right) x\ 10{,}000\ x\ Sample\ dilution$$

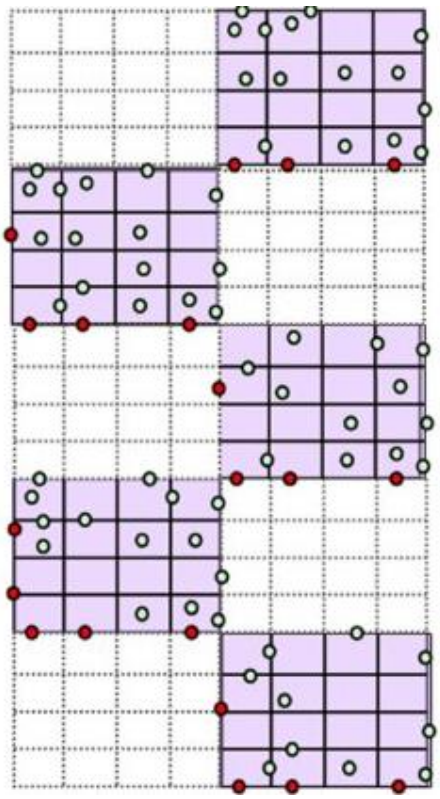

Figure 34. Fast Read 102 W chamber*. Plastic haemocytometer divided into 10 chambers, each containing a grid with 10 squares subdivided into 16 smaller squares* (Gunetti *et al.*, 2012)

Once the number of cells was calculated, the cell suspension was diluted depending on the number of cells required. Cells were cultured in a differentiation medium supplemented with 10 ng/ml BMP7, TGFβ3 (Peprotech), 1% (v/v) insulin-transferrin and 50 µg/ml ascorbic acid to promote chondrocyte differentiation. Different cell densities were cultured depending on the model and experiment. Differentiation medium was made up of DMEM/F-12 with GlutaMAX I (Gibco™), 5% FBS (Gibco™), 1% insulin transferrin (Thermo Scientific™), 1% sodium pyruvate (Thermo-Fisher Scientific™), 1% Penicillin-Streptomycin (Gibco™), 10 mM β-glycerophosphate (βGP) (Sigma-Aldrich®) and 50 µg/ml L-ascorbate-2-phosphate (Sigma-Aldrich®).

For the 2-dimensional (2D) model consisting of seeding cells on uncoated plastic, the cells were seeded at 6000 cells/cm^2 (Newton *et al.*, 2012). In contrast, for the 3D model different cell densities obtained from several tissue-engineering studies were tested to optimize the system - from 12,000 cells/cm^2 (Newton *et al.*, 2012), 1 million per ml (Bougault *et al.*, 2009), 2 million cells per ml (Bougault *et al.*, 2009), and 10 million cells per ml (Thorpe *et al.*, 2013). In the pellet model, the cell density seeded was 500,000 cells per pellet cultured in a universal tube. All models were incubated in 37ºC and 5% CO_2 for 21 days with regular media changes

and assessed on days 1, 7, 14, and 21 (Lewis *et al.*, 2016; Wu *et al.*, 2021), for pellets and 2D model. The optimisation 3D models with cell densities of 500,000 cells/cm^2 and 1 million cells/cm^2 were cultured for 21 days and assessed at day 21. And finally, the 3D model of 5 million cells/cm^2 was cultured for 42 days and evaluated at days 21 and 42, as previously seen in the study by Thorpe *et al.* (Thorpe *et al.*, 2013). The medium was substituted every 2-3 days. In the 2D model, the wells intended for histology were seeded on a sterile crystal coverslip of 13 mm diameter.

Every model was seeded in at least two to three technical replicates and three biological replicates. A biological repeat was considered when seeding another model (either, two-dimensional, pellet or low gelling temperature agarose) from a different batch of cells unfrozen on a different day and time. A technical repeat was considered when seeding the cells into a model the same day and at the same time from cells coming from the same batch of defrosted cells.

2.2.3 Hydrogels

2.2.3.1 Low gelling temperature agarose

Low gelling temperature 2.5% Agarose (w/v) (Sigma-Aldrich®) was autoclaved, re-melted at 60 ºC and cooled down to 39ºC in a temperature-controlled water bath prior to use. All plastics and medium were preheated to 39ºC as well. Agarose was mixed with cells in different final concentrations, 1% and 2% agarose (Bougault *et al.*, 2009; Gadjanski *et al.*, 2013; Thorpe *et al.*, 2013) was mixed with cells, seeded in 24-well plates in autoclaved steel washers of 2 mm height by 8 mm inner diameter and 13 mm out diameter, and left at room temperature to solidify before adding 500µL of differentiation medium.

2.2.3.2 Basement-membrane extract - Matrigel

Basement-membrane extract from Engelbreth–Holm–Swarm sarcoma with 9 mg/mL of protein content (Matrigel®) (BD Bioscience) was mixed 1:1 with cells in suspended differentiation medium at 10ºC (Basic *et al.*, 1996) and incubated at 5% CO_2 and 37ºC for an hour to solidify, before adding 500µL of differentiation medium on top of the construct. In this case, all equipment used was pre-chilled on ice to avoid the Matrigel® solidifying at room temperature.

2.2.3.3 *HyStem®-C Cell Culture Scaffold with modified HA*

HyStem®-C Cell Culture Scaffold Kit contained modified HA (Glycosil®) (synthetic), thiol-reactive crosslinker (Extralink®) (synthetic), thiol modified denatured collagen fibrils Gelin-S® to accommodate cell attachment, and degassed dH_2O (Sigma-Aldrich®). The hydrogel was prepared by following the manufacturer protocol. Both Glycosil® and Gelin-S® solutions were reconstituted by adding 1ml of degassed dH_2O, homogenised by vortexing and mixed 1:1. Media with the appropriate amount of cells was added to the mix and the well plates. Next, the Extralink® crosslinker was reconstituted by adding 0.5ml of degassed water and mixed with the Hystem solution of Glycosil® and Gelin-S® in a ratio of 1:4 (v/v). Hydrogel solidified after half an hour at room temperature, then the additional medium was added on top of the scaffolds.

2.2.4 Pellets

After counting the number of ATDC5 cells, the cells were centrifuged in the universal tubes for 10 minutes at 8000 g. The medium was changed the following day by gentle pipetting to increase the rotation and the rounded shape of the pellet and changed every two days to promote pellet formation.

2.2.5 Visualization of ECM and cell morphology

2.2.5.1 *Cell and tissue harvest*

Three technical replicates per condition were processed at each day point for histological analysis in three biological replicates. 3D constructs were extracted from the cell culture plate, as shown in Figure 35 with the help of a scalpel and forceps. To wax embed the hydrogels and pellets, the samples were fixed with 10% formalin (histology) (Sigma-Aldrich®) or 95% ethanol 5% acetic acid (immunohistochemistry) (Sigma-Aldrich®) for 24h at room temperature. 2D samples were fixed for 15-30 minutes with either solution directly in the cell culture well. The 3D models were processed overnight in a Thermo Scientific ™ STP 120 Spin Tissue Processor, and the UNISETTE™ Biopsy Processing/Embedding Cassettes (Sigma-Aldrich®) with pellets were covered with Tissuewrap (60mm x 60mm) – white (CellPath) to avoid losing the samples. The samples were then embedded in paraffin wax added polymers (melting point 62°C) (Thermo-Fisher Scientific™), and allowed to set overnight at room temperature, then stored at -20°C. All blocks were sectioned at 5 µm thickness with the HM

355S automatic microtome (Thermo-Fisher Scientific™) and collected on SuperFrost® Plus slide Adhesion (VWR™).

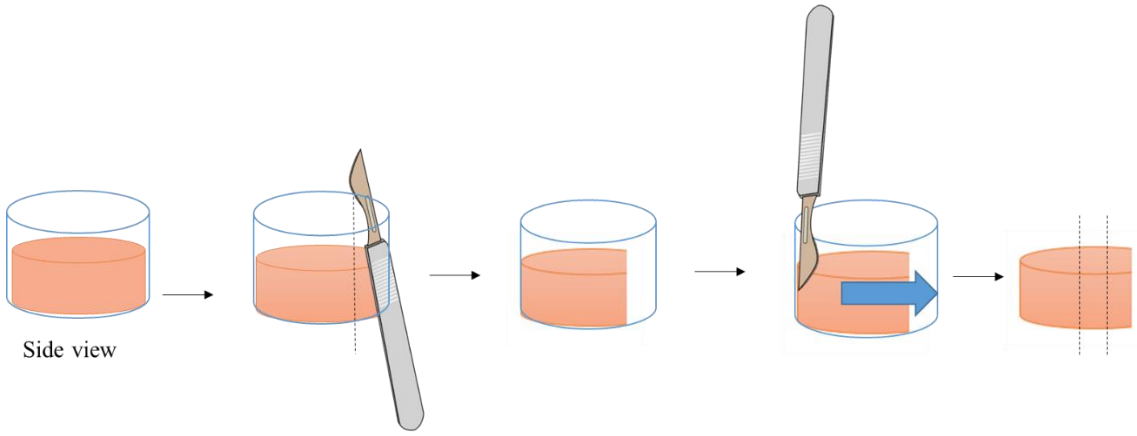

Figure 35. Diagram explaining the collection and section of the hydrogel at each day point.

2.2.5.2 Tissue staining

The slides were dewaxed in two changes of xylene (Sigma-Aldrich®) for 5 minutes. Following that, they were rehydrated through a series of decreasing concentrations of ethanol (Sigma-Aldrich®) (100%, 90%, 70% and 50%, 3 minutes each) followed by two rinses in deionised water (Sigma-Aldrich®). All steps were performed at room temperature.

Hematoxylin and eosin staining (VWR™) was carried out to study morphology. Hematoxylin stains the nucleus purple, whereas eosin stains the ECM pink (Duarte Campos *et al.*, 2012). Slides were stained using an automated stainer according to a standard protocol (Fischer *et al.*, 2008).

Toluidine Blue dye at a concentration of 0.04% (w/v) at pH 3.75 (Sigma-Aldrich®) was used to detect proteoglycan synthesis specific for cartilage ECM formation. All models were stained for 10 minutes, followed by 5 minutes staining of Fast Red nuclear (Sigma-Aldrich®) counterstain according to a standard protocol (Graeter *et al.*, 2014).

Picrosirius Red staining (Abcam) was used to assess the amount of collagen deposited by the cells in culture, and the rehydrated samples were incubated with the stain for 1h. Picrosirius red staining was performed following a standard protocol (Junqueira, Bignolas and Brentani, 1979).

Alcian Blue staining (Sigma-Aldrich®) was performed to study the sulphated proteoglycan synthesis; for this, cells seeded in the 2-dimensional model were seeded in a glass coverslip within the well plate. The cells were fixed in 95% methanol (Sigma-Aldrich®) for 20 min and stained overnight with 1% (w/v) Alcian blue in 0.1 M HCl at pH 0.75. After three washes with dH_2O, the dye was extracted with 6M guanidine-HCl (Sigma-Aldrich®) for 6h, and its optical density was measured at 630 nm by spectrophotometry.

Alizarin Red staining (Sigma-Aldrich®) to evaluate the calcium deposition of the cells. After fixing the cells in the coverslip with 10% formalin for 20 min, 2% alizarin red at a pH of 4.2 was added for 2 min. After three washes with dH_2O, the dye was extracted with 10% cetyl-pyridinium chloride (Sigma-Aldrich®) for 10 minutes, and its optical density was measured at 570 nm by spectrophotometry.

2.2.5.3 Immunohistochemistry staining

The slides were dewaxed twice for 5 minutes prior to rehydrating in decreasing concentrations of ethanol and two washes in dH_2O. Indirect immunohistochemistry was carried out using primary antibodies against acetylated tubulin (primary cilia), Ki67 (proliferation), type II, type I and type X collagen (Table 4) (Abcam). To stain the nucleus of the cells 4',6-diamidino-2-phenylindole (DAPI) (Abcam) was applied as a nuclear counterstain. To unmask epitopes, slides were incubated for 45 minutes at 37^{o}C with 0.2% (w/v) bovine hyaluronidase (Sigma-Aldrich®) in 1x PBS (Sigma-Aldrich®), followed by several PBS washes, incubation for 5 minutes of 1% (w/v) Triton-X in 1x PBS, and finally after several washes in PBS again a 5-minute incubation with 20 µg/mL proteinase K in 1x PBS. Unwanted cross-reaction was blocked using 1% (w/v) bovine serum albumin (BSA) (Sigma-Aldrich®) in PBS with donkey/goat serum for 1 hour. Incubation of the primary antibody diluted in 1% (w/v) BSA in PBS was carried overnight at 4^{o}C. In contrast, the secondary antibody at its respective dilution in 1% (w/v) BSA in PBS was incubated for 1h at room temperature. As a positive control, 1-week old femoral heads from wild type mice were used. In contrast, the negative control incubation was performed without the primary antibody.

All slides were mounted in Fluoroshield Mounting Media with DAPI (Abcam) and imaged using a fluorescence microscope.

Antibody Against	Dilution	Source	Obtained from
Acetylated α-Tubulin (Ab24610)	1:200	Mouse	Abcam
Type I Collagen (Ab34710)	1: 500	Rabbit	Abcam
Type II collagen (Ab34712)	1:250	Rabbit	Abcam
Type X collagen (Ab58632)	1:500	Rabbit	Abcam
Aggrecan	1:400	Rabbit	Professor Tim Hardingham (University of Manchester)
Recombinant Anti-Ki67 antibody (Ab92742)	1:500	Rabbit	Abcam
Mouse (Ab150113)	1:500	Goat	Abcam
Rabbit (Ab150075)	1:500	Donkey	Abcam

Table 4. *Table of primary and secondary antibodies used (dilution, source and manufacturer).*

2.2.6 Protein extraction and Western blotting

2.2.6.1 Protein harvest and extraction

The extraction of proteins from 2D cultures required a washing with DPBS and lysing the cells with 500µL of RIPA buffer (Sigma-Aldrich®) for 30 minutes on ice. After scraping the cells into an Eppendorf, the tubes were centrifuged for 10 minutes at 8000 g at 4^{o}C to pre-clear the lysates. The supernatant was then collected and stored at -20^{o}C.

Extraction of proteins for 3D scaffolds and pellets required a different approach. On the day of collection, the samples were previously washed in DPBS prior addition of 1 ml of trypsin

(Gibco™) for digestion of the ECM, then the collected media with cells was centrifuged at 8000 g for 5 minutes, discarding the suspension afterwards. RIPA buffer was added to the pellet obtained after centrifugation and incubated for 30 minutes at 4ºC in a rotator. After this, the eppendorfs with the samples were snap-frozen in liquid nitrogen, and quickly thaw in a water bath at 37ºC, repeating this step three times. Another centrifugation of the pellet for 10 minutes at maximum speed at 4ºC was carried out, as a final step. After the centrifugation, the supernatant was collected, and in the case of having high viscosity, the liquid was homogenised with a syringe and a small needle.

2.2.6.2 Protein measurement in models

Pierce™ Bicinchoninic Acid (BCA) Protein Assay Kit (ThermoFisher Scientific) was used to measure the protein content, the standard curve of known bovine serum albumin (BSA) (Sigma-Aldrich®) protein dilutions (mg/mL of protein). The assay was performed according to the manufacturer's instructions, and the absorbance was read in a Thermo Scientific™ Varioskan™ LUX multimode microplate reader at 562 nm.

2.2.6.3 Western blotting

Western blot is a widely used technique that allows the detection of specific proteins. To detect the protein expression, the samples were all standardised to 30 µg of protein, mixed with sodium dodecyl sulphate (SDS)-PAGE buffer (ThermoFisher Scientific), and denatured for 5 minutes at 95ºC. A 4-12% NuPAGE® Bis-Tris precast gel (ThermoFisher Scientific) was used to run the samples in NuPAGE® MES SDS Running Buffer (ThermoFisher Scientific) for 50 minutes at 200V. The samples were then transferred onto Nitrocellulose Membranes for Western Blotting (ThermoFisher Scientific) in 1x transfer buffer at 30V for 1 hour. The membrane was blocked in 3% (w/v) powdered semi-skimmed milk in PBS-T (Sigma-Aldrich®) for 1 hour, then incubated overnight at 4ºC with the primary antibody in 3% (w/v) milk/PBS-T solution. After the incubation, three washes of 5 minutes with PBS-T were carried out to discard any excess antibody, and the LICOR® IRDye® 800W secondary antibody (LICOR®) was added for 1 hour in a 5% (w/v) milk/PBS-T solution. The non-bound secondary antibody was removed by three washes of 15 minutes each with PBS-T, and then the membrane was analysed on the LI-COR® Odyssey CLx Imaging System.

2.2.7 Processing the 3D and 2D cultures for RNA extraction

2.2.7.1 RNA harvest and extraction

Before RNA extraction, the bench surfaces and equipment were wiped with RNaseZap™ (Sigma-Aldrich®), to eliminate RNAse contamination. Cells cultured in wells were washed with DPBS, and RNA was extracted using 500µL of 2D RNA-extraction solution (QIAGEN). The samples were then stored at -20^{o}C until further use. Extraction of RNA from scaffolds was performed after a DPBS wash and with 500µL of 3D RNA-extraction solution (QIAGEN). The hydrogel and pellet constructs were dissolved in the 3D RNA-extraction solution and snapped freeze.

2.2.7.2 Homogenisation of Samples for RNA extraction

To reduce risks of sample degradation, much faster isolation was carried out by disintegrating the samples using a high efficiency grinding Mikro dismembrator S (Sartorius).

All equipment from the dismembrator, sample vessel, grinding ball, spatula and forceps was autoclaved prior to RNA extraction and cleaned with RNaseZap™ between the samples to avoid contamination. Firstly, the vessel, grinding ball and samples were frozen in liquid nitrogen. The grinding ball and the sample that was previously snapped freeze with the RNA-extraction solution was then added to the vessel and were placed inside the dismembrator for 2 min at 1,500 rpm. The sample was harvested, thawed, set in a QIAshredder column (QIAGEN) and centrifuged 10 minutes at 8000 g. The flow-through solution was frozen at -80^{o}C.

2.2.7.3 Purification and Measurement of RNA

Following the extraction, the RNA was purified using the RNeasy® mini kit (QIAGEN) according to the manufacturer's protocol. All the surfaces and materials were wiped with RNaseZap™ to reduce RNA degradation. Each sample was mixed with an equivalent volume of 70% Ethanol made up with DEPC-treated water (Sigma-Aldrich®), placed in an RNeasy Mini Spin Column and centrifuged for 15 seconds at 8,000 g. The resulting flow-through was discarded and added to 700 µl RW1 which centrifuged for 15 seconds at 8,000 g in the column. The eluate was mixed again with another 500 µl of and RPE buffer and centrifuged. Both buffers were added to the column to purify the RNA and elute all the no-specific bindings. A second elution with 500 µl of RPE buffer was carried for 2 minutes at 8,000g, and finally, the RNA was eluted using 30 µl of DEPC-treated water.

The purity and concentration (ng/µl) of each RNA sample was measured using NanoDrop™ 2000/2000c Spectrophotometers (Thermo Scientific™). The purity was detected by the ratio of absorbance at 260 nm and 280 nm, where ratios within 1.80 to 2 were considered not contaminated and optimal for reverse transcription to cDNA.

2.2.7.4 Reverse transcription of RNA to cDNA

An equal concentration of RNA per sample, 30ng/µl was used in each reverse transcription reaction. This was performed with the GoScript™ Reverse Transcription System kit (Promega) according to the manufacturer's protocol. Firstly, the volume required of each RNA sample was mixed with 1 µL of Oligo$(dT)_{15}$ and 1 µL random primers, and the necessary amount of water for a final volume of 5 µL, the mixture was heated up at 70^{o}C for 5 minutes, followed by ice incubation for 5 minutes. After this, the 5 µL were mixed with a 15 µL solution made up of the following reagents: 3.0 mM of magnesium chloride, 5x GoScript™ reaction buffer, 20 units Recombinant RNasin® ribonuclease inhibitor, GoScript™ reverse transcriptase, and 0.5 µg of Oligo$(dT)_{15}$ and random primers, respectively. The final volume of 20 µL was then incubated at 25^{o}C for 5 minutes, 42^{o}C for 1 hour and 70^{o}C for 15 minutes for annealing, extension, and inactivation of the reverse transcriptase respectively in a MultiGene™ OptiMax Thermal Cycler (Labnet International). Finally, the resultant cDNA was treated with 1 µl of RNase H to remove residual RNA at 37^{o}C for 20 minutes.

2.2.7.5 Real Time-Polymerase Chain Reaction (RT-PCR)

The resulting cDNA was then subject to quantitative analysis by real-time polymerase chain reaction (RT-PCR) using primers (Eurofins Genomics) specifically designed for detection of chondrogenesis and ECM markers. Gene 18S was used as housekeeping for RT-PCR. Many studies have identified this gene as suitable and reliable for normalisation in chondrocytes and other cell types (Bas *et al.*, 2004; Pfander *et al.*, 2004; Pombo-Suarez *et al.*, 2008; Kuchipudi *et al.*, 2012; Peng *et al.*, 2012). Despite this, one study suggests its inability to be used in *in vitro* cartilage chondrocyte mechanobiology studies(Al-Sabah *et al.*, 2016).

For the detection of the cDNA, the SYBR™ Green PCR Master Mix was used according to the manufacturer's protocol. A final sample volume of 50 µL was made up of 10 pmol of forward and reverse primers, 25 µL of SYBR™ Green PCR Master Mix and Ribonuclease H (ThemoFisher Scientific), and 4.2 µL of cDNA of each sample, the volume of which was

adjusted by adding 18 MΩ ddH_2O. As controls, the samples were normalised to the levels of 18S as a housekeeping gene, and duplicates were run in each well plate. Negative control samples did not contain any cDNA to check for any potential contamination. The RT-PCR reaction was run in a DNA Engine Peltier Thermal Cycler, Chromo4™ real-time PCR detector (Bio-Rad). The results were used to calculate the C_t value for each sample and $2^{-\Delta\Delta Ct}$ to determine the gene expression relative to the housekeeping gene. To obtain the $2^{-\Delta\Delta Ct}$ first was calculated the difference between the gene tested experimental and the gene housekeeping experimental. The gene tested control, and the gene housekeeping control, obtaining the ΔCt. Then the ΔΔCt was calculated by the difference between the experimental and control ΔCT (RNA harvested after one day cultured). Finally, the expression fold change was estimated by calculating the value of $2^{-(\Delta\Delta Ct)}$.

2.2.8 Terminal deoxynucleotidyl transferase dUTP nick end labelling (TUNEL) assay

The DeadEnd™ Fluorometric TUNEL (TdT-mediated dUTP Nick-End Labelling) System (Promega) was used to quantify the apoptotic cells within the cell population or tissue. For this, the slides were fixed in 10% (w/v) formaldehyde as previously described, and the assay was carried out according to the manufacturer's protocol. Similarly to previously described immunostaining, the slides were dewaxed in xylene and rehydrated in decreasing concentrations of ethanol. The samples were then incubated for 5 minutes at room temperature with 0.85% (w/v) sodium chloride, followed by three washes for 5 minutes with 1x PBS. The samples were then fixed for 15 minutes in 4% (v/v) methanol-free formaldehyde in 1x PBS, then 5 minutes washes in 1x PBS was performed before the antigen unmasking via citrate buffer boiling was carried out. This step is a key substitution from the standard proteinase K unmasking protocol since the proteinase K has been shown to release endogenous endonucleases increasing the false-positive reactions (Stahelin et al. 1998). The samples were boiled in citric buffer (Sigma-Aldrich®) for 4 minutes at 800W, followed by 4 minutes at 400W and another 4 minutes at 200W. After boiling in the citrate buffer, the samples were left to cool down at room temperature for 30 minutes and washed once in x1 PBS for 5 minutes were performed. Slides were then again fixed in 4% (v/v) methanol-free formaldehyde (ThermoFisher Scientific) in 1x PBS for 5 minutes and washed in x1 PBS before proceeding with the equilibration buffer incubation for 10 minutes at room temperature. The samples were then incubated with the labelling buffer at 37ºC in a humidified chamber for 1h. The labelling

buffer is made up of the Terminal Deoxynucleotidyl Transferase (TdT), which forms a polymeric tail using the principle of the TdT-mediated dUTP Nick-End labelling (TUNEL). To stop the labelling the samples were submerged in 2x saline sodium citrate (SSC) buffer and rinsed in x1 PBS followed by a dehydration process in series of increasing ethanol concentrations and xylene, and finally mounted in Fluoroshield Mounting Media with DAPI (Abcam).

The samples were then imaged using a ZEISS Axio Imager 2 Research Upright Microscope (Carl Zeiss Microscopy) at 200x magnification, using the specific filters sets for DAPI and AlexaFluor™ 488 (Abcam).

2.2.9 Dimethyl-Methylene Blue (DMMB) assay

To assess the amount of proteoglycans in the collected samples, the 1,9-dimethyl methylene blue (DMMB) assay (Sigma-Aldrich®) was carried out by measuring the sulphated glycosaminoglycan (sGAG) secreted in the ECM of the 2D, 3D and pellets. For this, firstly a standard curve was carried out.

An amount of 40 µL of each standard was added per well of a 96-well plate in duplicate, then 250 µL of DMMB solution (Sigma-Aldrich®) was added and immediately read at a 530 nm.

Samples were digested with papain solution (Sigma-Aldrich®) for 16h at 65^{o}C. 40 µL of each digested sample was thoroughly mixed and added to a 96-well plates Clear Flat Bottom Polystyrene (Corning®), mixed with 250 µL of DMMB and read at 530 nm length wave in a Varioskan™ LUX multimode microplate reader (ThermoFisher Scientific).

To calculate the µg of sGAG, the standard curve was calculated using linear regression of the absorbance obtained for the standards and used to calculate the µg of sGAG secreted per sample.

2.2.10 Thiazolyl Blue Tetrazolium Bromide (MTT)

The MTT (4,5-dimethylthiazol-2-yl-2,5-diphenyltetrazolium bromide) assay (Sigma-Aldrich®) was used to assess the cell metabolic activity. MTT is a colourimetric assay whereby the mitochondrial dehydrogenases from the cells reduce the tetrazolium dye to its insoluble form, formazan, which then is solubilized with dimethyl sulfoxide (DMSO) anhydrous, ≥99.9% (Sigma-Aldrich®) and spectrophotometrically measured. MTT was mixed with fresh media

into a 1:4 proportion and left for 24 hours on the cells. The MTT and the media were removed and washed once gently with PBS. The formazan crystals were then solubilized with 200 µL of DMSO and read at 550 nm length wave in a Varioskan™ LUX multimode microplate reader (ThermoFisher Scientific). The agarose hydrogels were dehydrated at 60ºC for 1h after the 24h incubation with MTT and the remaining crystals were solubilised by DMSO and read.

2.2.11 Design of plasmids and transformation of ATDC5 cells

The mutation T585M was introduced into a full-length COMP from *Mus musculus* (house mouse) was purchased from GeneScript® cDNA using site-directed mutagenesis, where was cloned into pEGFP-N3 vector that leads into the fusion protein COMP-GFP. As control wild-type COMP was generated introducing full-length versions of WT COMP. The mutation of COMP was introduced using QuikChange Lightning Site-Directed Mutagenesis Kit from Agilent Technologies following the manufacturer's protocol. Both WT and mutant constructs were introduced into ATDC5 cells via transfection, and recombinant cells were selected using Geneticin™ Selective Antibiotic (G418 Sulfate) (50mg/mL) (Gibco™).

2.2.11.1 QuikChange Site-Directed Mutagenesis

Three PCR reactions were set up, a control, and one for each mutation using PCR QuikChange Mutagenesis Kit (Agilent Technologies). Following the PCR, *Dpn*I enzyme digestion (New England Biolabs® Inc.) took place in a 14-mL BD Falcon polypropylene round-bottom tube by adding 2 µL of *Dpn*I to each amplification reaction and incubating for 5 minutes at 37ºC. Transformation of the ultracompetent cells was carried out by mixing 45 µL of XL10-Gold Ultracompetent *E. coli* Cells from Agilent Technologies, 2 µL of β-Mercaptoethanol (β-ME) (Sigma-Aldrich®) and 2 µL of the previous mix digested with *Dpn*I for 30 minutes on ice, followed by a heat-pulse at 42ºC on the water bath for 30 seconds. Following this, the samples were incubated on ice for 2 minutes and then 0.5 mL of preheated LB Broth (Sigma-Aldrich®) was added to each tube and incubated for 1 hour at 37ºC with shaking (225rpm). The mix of each tube was seeded in LB Agar plates with 100 mg/L of ampicillin, X-gal and IPTG (Sigma-Aldrich®) overnight. The following day, the colonies that grew in blue were picked up with a tip and incubated with LB Broth and ampicillin (100mg/mL) overnight.

2.2.11.2 Plasmid MiniPrep

The DNA of picked colonies was extracted using a QIAprep Spin miniprep kit (QIAGEN). From each culture, 1 mL was used to create a glycerol stock, whereby the samples were centrifuged for 3 minutes at 4ºC at 13,000 g, and 300 µL LB Broth was replaced by autoclaved glycerol for molecular biology (Sigma-Aldrich®). The stocks were then stored at -80ºC. The remaining 9 ml of LB Broth cultures were centrifuged for 6 minutes at 3,000 g, and the DNA was extracted following the manufacturer's instructions using the Qiagen Spin Miniprep kit. Resuspension of the bacteria pellet in 250 µL of Buffer P1 was followed by the lysis of the bacteria in 250 µL of buffer P2 and the inhibition of the reaction and precipitation of proteins by 350 µL of Buffer N3. The mixture was then centrifuged for 10 minutes at 19,000 g, and most of the supernatant was removed and place in a QIAprep 2.0 spin column and centrifuged for 1 minute at 19,000 g. Following this, the DNA was washed with 300 µL Buffer PE and centrifuged for 1 minute at 19,000 g. Finally, the elution of the DNA was carried out by the addition of 30 µL of Buffer EB and centrifugation for 1 minute at 19,000 g.

2.2.11.3 Transfection of DNA plasmid to ATDC5 cells

The plasmid DNA quality and quantity (ng/ µL) were measured using NanoDrop™ 2000 (Thermo Scientific™). The quality was as previously mentioned detected within the 1.80 to 2 for the ratio of absorbance at 260 nm and 280 nm.

Transfection of the ATDC5 cells with the plasmid DNA was performed once the cells reached 70% confluency. 2 µg of Plasmid DNA was mixed with 200 µL of Opti-MEM™ serum-free medium (Gibco™) and incubated for 15 minutes at room temperature. In parallel, another tube with 200 µL of Opti-MEM™ and 16 µL Lipofectamine200® (ThermoFisher Scientific) was incubated similarly. Both tubes were mixed and incubated for 30 minutes at room temperature. The reaction mixture was then added to the ATDC5 cells for 24h at 37ºC and 5% CO_2 with a posterior culture with normal media for 24h at 37ºC and 5% CO_2 and split into 1/3 flasks. Finally, cells were selected with 400 µg/mL of Geneticin® and seeded into the models.

2.2.12 Agarose hydrogel scaffolds compressed in the Flexcell® Compression System

Stationary platens with an adjustable centre and 13 mm metallic washer. All removable components were autoclaved for disinfection. A 110 µl of agarose hydrogel with ATDC5 cells were poured inside a 13 mm sterile metallic washer and cultured for 7 days in a 6 well-plate prior compression (Figure 37).

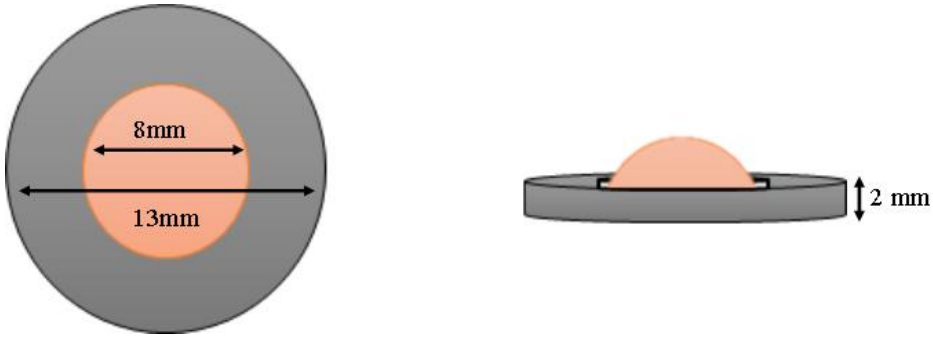

Figure 36. Representation of the washers with the agarose hydrogel seeded inside.

To compress the scaffold with the washer was placed inside the larger sample holder (Figure 38A) of the BioPress™ plate and placed facing the acrylic sample holder and adhering to the silicone elastomer on the bottom of the plate to ensure the compression of the free-swelling portion of the construct (Figure 38E). Following this, the sterilised stationary platers with adjustable centres were placed on top of the well to secure the hydrogel while compressing (Figure 38. B and C). The adjustable centres were tightened with sterile forceps following the equation below based on the known thickness of the hydrogel:

Where x is the number of 180º clockwise turns required so that the bottom of the centre screw is in contact with the gel, and h is the known height of the chondrocyte-agarose construct in millimetres (Flexcell, 2015).

$$x = \frac{(3.11 - h)}{0.62}$$

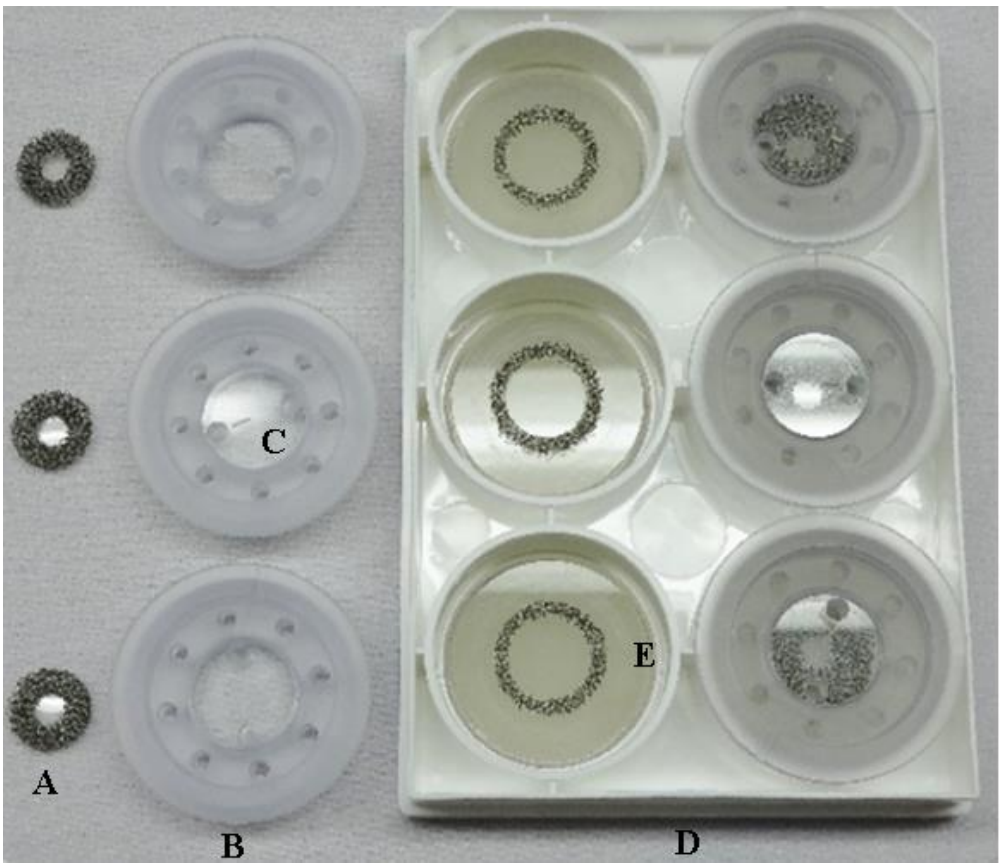

Figure 37. A BioPress™ 6-well plate with components. A) *Foam sample holders (two different sizes removable).* ***B)*** *Stationary platers.* ***C)*** *Adjustable centre.* ***D)*** *BioPress™ 6-well plate with* ***E)*** *acrylic pistons adhere to the silicone elastomer well bottom. Adapted from* (Flexcell, 2015).

After the addition of 5 ml of differentiation media to cover the wells of the BioPress™ 6-well plate using the holes in the stationary platens, the plates were placed in the Flexcell® FX-5000™ Compression System (Flexcell International Corporation) by locating the plates over the gaskets in the baseplate and clamping the plates with the help of the wing nuts on the clamping system until an airtight seal is formed between the BioPress™ plate and the baseplate of the Flexcell system (Figure 39B) (Flexcell, 2015). The compression system is computer-controlled by software with the loading regime. This increases the air pressure in the baseplate below the BioPress™ 6-well plate, displacing the silicone elastomer well bottom and compressing the hydrogel against the stationary platen (Flexcell, 2015). ATDC5-agarose constructs were compressed for 14 days for 30min/day at 10kPa magnitude and a sinusoidal wave frequency of 0.33Hz (Figure 39A).

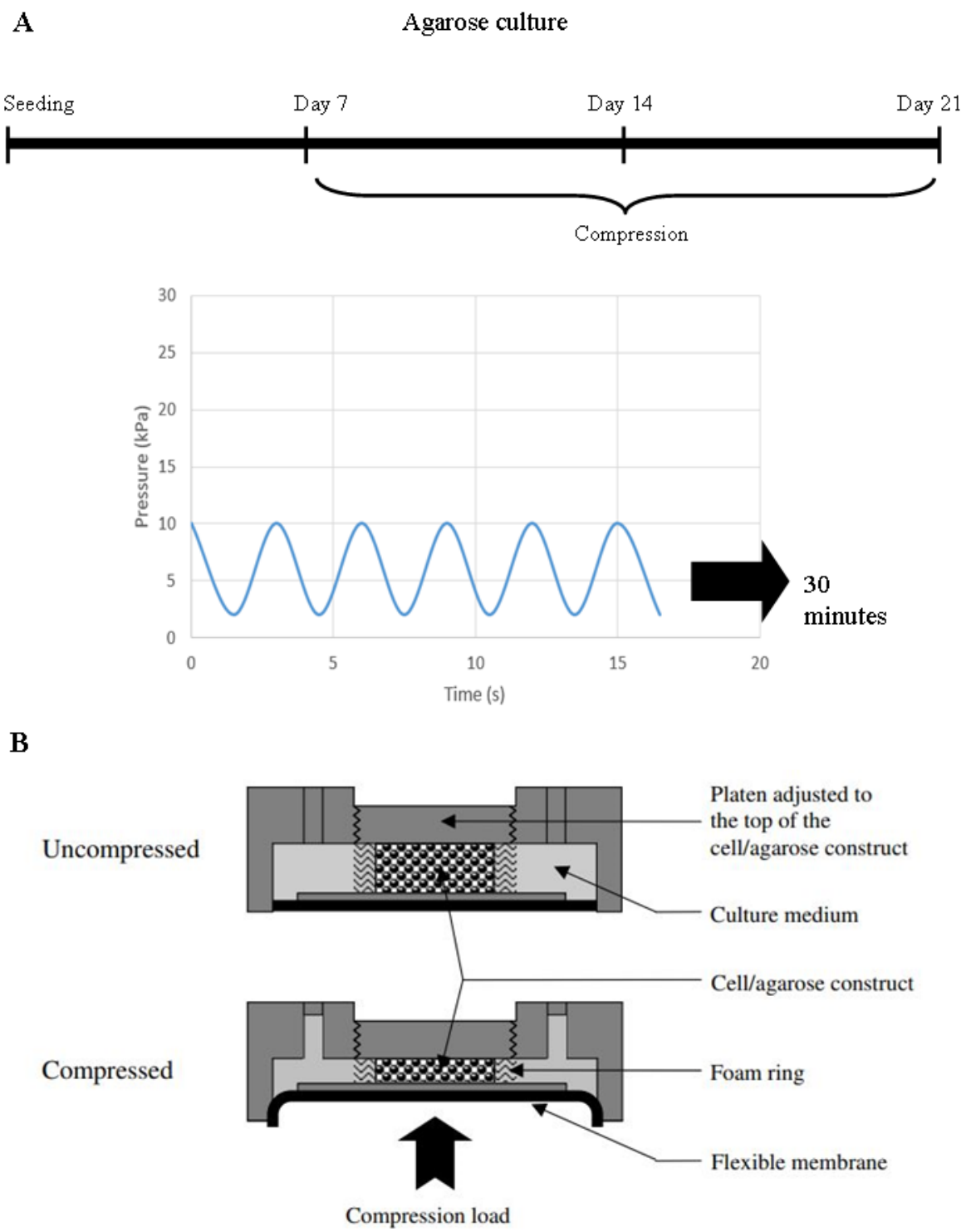

Figure 38. Loading regime. A) *ATDC5 cells in the agarose construct were compressed for 14 days for 30min/day at 10kPa magnitude and a sinusoidal waveform and a frequency of 0.33Hz.* ***B)*** *Schematic diagram of the BioPress™ culture plate placed in the compression machine when compressed and uncompressed.* (Bougault *et al.*, 2008).

2.2.13 ImageJ measurement

NIH ImageJ software (Schneider, Rasband and Eliceiri, 2012) was used for the following measurements.

2.2.13.1 Measurement of the width in 3-dimension low gelling temperature agarose

The width of the 3D low gelling temperature agarose hydrogel was measured using ImageJ measurement tools and converting the pixels (a standard unit of measurement of ImageJ) to µm using the scale bar as a reference.

2.2.13.2 Measurement of the clusters and pellets area in both pellet and 3-dimension low gelling temperature agarose models

The area of the clusters and pellets was measured using ImageJ measurement tools. For this, the area was selected, and the colour inverted, making the background white and pellets or the cluster's dark. Watershed plug-in (Soille and Vincent, 1990) allowed a marked differentiation and quantification of the clusters and pellets with the background facilitating the outline analysis. Pellets at 1 day of seeding could not be measured due to the fragility and lack of rounded shape.

2.2.13.3 Cell count for cell apoptosis and cell proliferation in both pellet and 3-dimension low gelling temperature agarose models

Cell counting in pellets and low gelling temperature agarose models for cell apoptosis (TUNEL assay) and cell proliferation (Ki67) was carried out using ImageJ. For the counting of the cells, the cell counter (Schneider, Rasband and Eliceiri, 2012) and the watershed plug-in (Soille and Vincent, 1990) were used along with the outline analysis. After this, the number of cells positive for cell apoptosis or cell proliferation was divided by the total number of cells in each model (counted by the total number of cells positive for DAPI counterstaining).

2.2.14 Analysis of data

All data were collected on days 1, 7, 14 and 21, and for one model on day 42. When analysing the data, all the results were expressed in fold change, with all-day points (7, 14, 21 and 42) against data collected at day 1 and resulting in day 1 being the value 1 in every graph.

When discussing the results obtained in every graph despite day 1 gene expression used as a reference for fold change, day point 1 would be equivalent to 1, being anything below that a reduction of gene expression compared to the baseline. Despite this, the results were analysed and discussed having in mind the overall trajectory, for example, if within the reduction (any data below 1) the data was increasing or decreasing along 21 days of seeding.

2.2.15 Statistical analysis

Statistical analysis performed was either a two-way ANOVA or a three-way ANOVA. The comparisons tests used were turkey's multiple comparisons test and Bonferroni's multiple comparisons tests, depending on the number of factors compared. For 2-dimensional, pellets, and 3-dimensional with and without compression, two-way ANOVA was performed. However, when comparing within different supplemented models, for different day points and different locations within the model (surface vs deep zone) a three-way ANOVA was carried out. All analysis performed in chapter 7 were a three-way ANOVA. In concordance with conventional statistical significance, a p-value below 0.05 (threshold of significant level) was considered statistically significant and was represented with an asterisk(s). The symbols in the figure legends and graphs to describe level of statistical significance as follow: * = $p<0.05$, ** = $p<0.01$, *** = $p<0.001$, and **** = $p<0.0001$.

Chapter 3. Validation of the ATDC5 Chondrogenesis in a Monolayer

3 Validation of the ATDC5 chondrogenesis line in a monolayer (2D model)

3.1 Introduction

Mouse teratocarcinoma stem cells can differentiate into all types of somatic and germ cells. However, was not until 1985, when PCC3/A/1 cells derived from a teratocarcinoma were firstly reported in a serum-free medium to differentiate in vitro into various types of somatic cells, such as chondrocytes or adipocytes (Atsumi, Ikawa and Noguchi, 1985). ATDC5 cell line was isolated from mouse teratocarcinoma stem cell line AT805 and was first reported to have chondrogenic potential in 1975 (Martin, 1975). However, *in vitro* differentiation of the cell line was not reported until 1990 and was induced by a modified culture medium that was a 1:1 mixture of Dulbecco's modified Eagle's medium (DMEM) and Ham's F12 (F12) medium containing 10 µg/ml human transferrin, 10 µg/ml bovine insulin and $3x10^{-8}$M of sodium selenite supplemented with 5% foetal calf serum (FCS) (Atsumi *et al.*, 1990). Since then, many studies have focused on enhancing the differentiation of ATDC5 cells, reducing the time to achieve mineralisation, increasing the deposition of ECM with either growth factors or by seeding the cells in hydrogels or microtopography (Altaf *et al.*, 2006; Newton *et al.*, 2012; Le *et al.*, 2017).

Modulation of ATDC5 chondrogenic differentiation was achieved either varying the topography of the material that the cells were seeded on, inducing late chondrogenesis or enhancing viability (Le *et al.*, 2017; Deliormanlı and Atmaca, 2018). Other studies varied the media composition to modulate mineralisation, some without adding the mineralisation-inducing β-glycerophosphate (Shukunami *et al.*, 1997), others by adding collagen-promoting ascorbic acid and 10 mM β-glycerophosphate (Newton *et al.*, 2012). Magnesium and magnesium alloy (Martinez Sanchez *et al.*, 2017) and leptin were implemented to induce osteogenic markers (Han *et al.*, 2016) and tetradecylthioacetic acid to increase ECM production (Le *et al.*, 2015). Different hydrogels, such as glycosaminoglycans or hyaluronic acid, were also applied to enhance chondrogenesis and differentiation (Sato *et al.*, 2014; Moulisová *et al.*, 2017).

The use of ATDC5 cell line to study chondrogenesis possess many advantages compared to primary cell lines, such as high proliferation rate, immortality, homogeneity and consistency which makes them an ideal model for the study of the molecular mechanism of development and disease (Yao and Wang, 2013). Another characteristic of the ATDC5 cell line is that with the right media components, such as insulin, transferrin and selenium, and ascorbic acid the cells undergo the different stages of chondrocyte differentiation *in vitro*: from the initial phases of differentiation to condensation in which ATDC5 cells form a cartilage nodule, to then

maturation progressing into hypertrophic chondrocytes and expressing type X collagen and alkaline phosphate activity and matrix mineralisation, a late stage of differentiation (Shukunami *et al.*, 1997; Akiyama *et al.*, 2000; Tare *et al.*, 2005; Phull *et al.*, 2016). ATDC5 cells are therefore a good model to study the process of mineralisation through the endochondral bone formation and key regulators in chondrogenesis (Newton *et al.*, 2012; Xu *et al.*, 2019; Wilhelm *et al.*, 2020).

3.2 Aims of the chapter

This chapter aimed to validate the chondrogenic potential of ATDC5 cells in monolayer culture, setting up a system with which to compare further developed 3D models to study the limitations of all and discuss the best model for studying diseases *in vitro*.

3.3 Results

In order to reproduce and test the chondrogenic potential of the ATDC5 line, cells were seeded in a 24 well-plate, at the density of 12,000 cells per ml for 21 days and collected every 7 days and after 24h (day 1). The collected cells were used for histological analysis, RNA extraction, and analysis of the sGAG content, calcium deposition analysis and cell metabolic activity studies. The media used to induce chondrogenesis was Gibco Dulbecco's Modified Eagle Medium: Nutrient Mixture F-12 (DMEM/F-12) with 10% (v/v) foetal calf serum, 1% (v/v) non-essential amino acids (NEAA) and 1% (v/v) penicillin/streptomycin in addition to 1% (v/v) Insulin-Transferrin-Selenium (ITS -G) (100X), 50 μg/ml of l-Ascorbic acid and Sodium Pyruvate (100 mM) (Temu *et al.*, 2010; Newton *et al.*, 2012) at 37 °C and 5% CO_2. All results represented in graphs were calculated via fold change using data obtained after 24h of seeding as a reference. Therefore, day point 1 has the value of 1 in all graphs. Every graph is accompanied by its fold change values and the p-values calculated when comparing all day points.

3.3.1 Cell morphology, ECM deposition and cell metabolic activity

Haematoxylin-eosin staining stains nuclei of the cells purple and the cytoplasm pink and was used to study the morphology of the cells during chondrogenic differentiation (Figure 40A). On day 1 cell presented an elongated fibroblast-like morphology. A dramatic difference was seen in the cell density and morphology during differentiation, with an increase in cell-

matrix deposition and cell proliferation (Figure 39B) that towards the end of the experiment impeded the assessment of cell morphology. A significant increase in fold change when comparing the cell metabolic activity at day 1 against the other day points was observed. Specifically, metabolic activity increased by 44, 46 and 47-fold between days 14 and 21 (Figure 39B). After 21 days, the fold change was nearly 50 times higher compared to day 1, showing a correlation with Figure 40A, in which the cell density increased after only 7 days of culture.

Having shown that the cells were producing ECM, further, the analysis focused on the type of the secreted matrix. Sulphated proteoglycan deposition was studied using Alcian blue staining (Figure 40.A) and showed a progressive increase in glycosaminoglycan deposition from day 14 and 21. To validate these results, the Alcian blue stain was extracted, and quantitative measurement of sulphated glycosaminoglycan was carried out (Figure 40.A). A significant increase when comparing day 7 against days 14 and 21 by 8.25-fold change ($p=0.0021$) and 13.07-fold change ($p=0.0002$) respectively. When comparing day 14 against day 21 a significant increase was also visible by 1.58-fold change ($p=0.027$) (Figure 41.A).

For further confirmation, the Dimethylmethylene Blue Assay (DMMB) assay was performed to analyse the amount of sGAG produced in the model (Figure 40.B). A significant increase in sGAG deposition comparing day 7 to days 14 and 21 was noted by a 3.61-fold change ($p=0.0003$) and 4.99-fold change ($p=0.0007$) respectively. Comparing day 14 against 21 showed a significant increase by 1.38-fold change ($p=0.049$) (Figure 40.B). red staining. Deposition of collagen, one of the major components of the cartilage ECM, was analysed using Picrosirius red staining. As shown in Figure 41.A, cells at day 1 did show pericellular collagen deposition, peaking in a deposition at day 21, forming darker collagen-rich nodules (arrows).

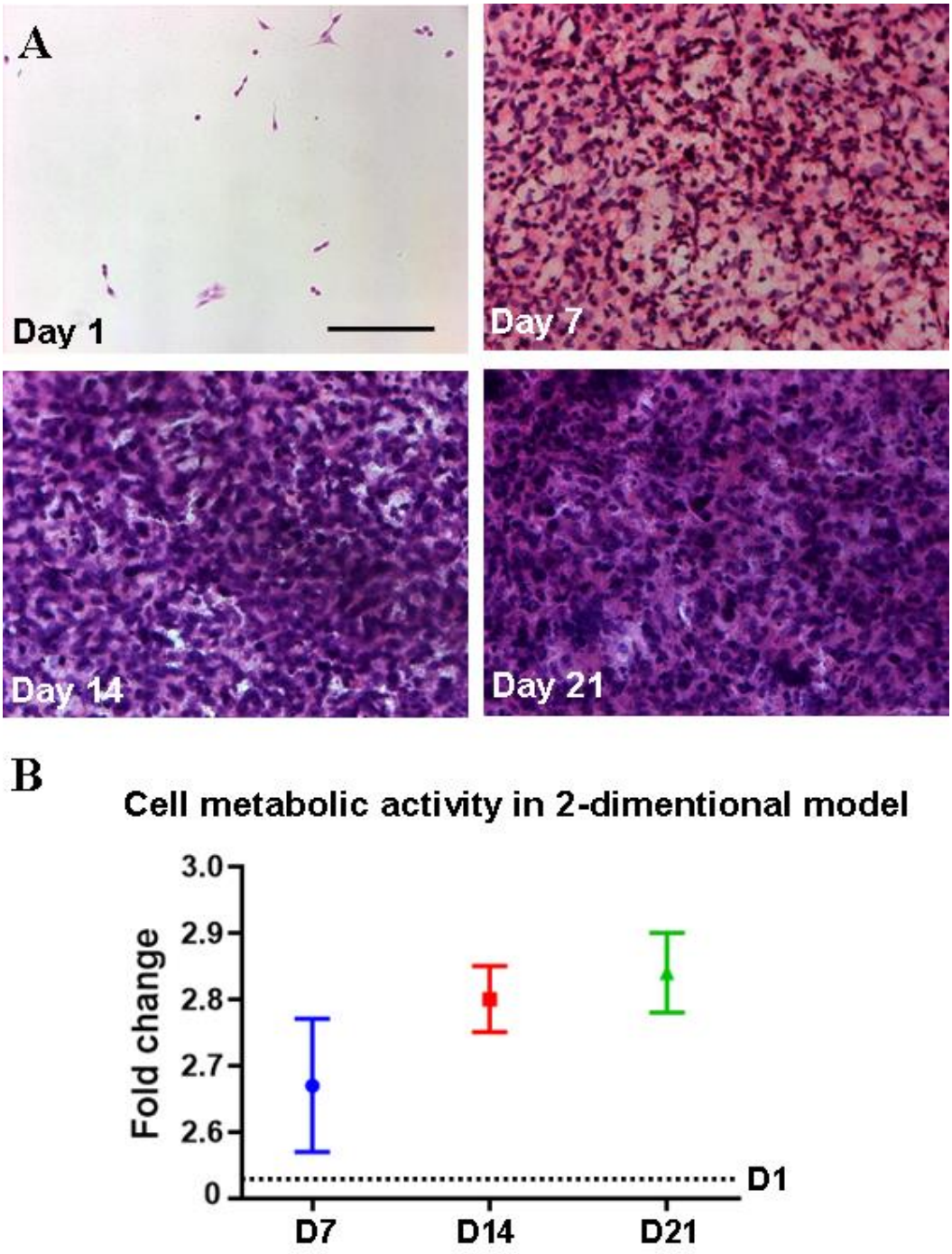

Figure 39. Histological staining of ATDC5 cells following 1, 7, 14 and 21 days of culture and cell metabolic activity in the 2-dimensional model. (A) *Haematoxylin and eosin staining performed in the monolayer culture on every harvest to stain ECM with eosin and nuclei studies with haematoxylin. Scale bar = 100µm.* ***(B)*** *Cell metabolic study was performed using the MTT assay and normalised to the levels after seeding 12,000 cells per ml in a monolayer (Day 1). * $p<0.05$, ** $p<0.01$, *** $p<0.001$, and **** $p<0.0001$ two-way ANOVA statistical analysis. N=3 and n=3.*

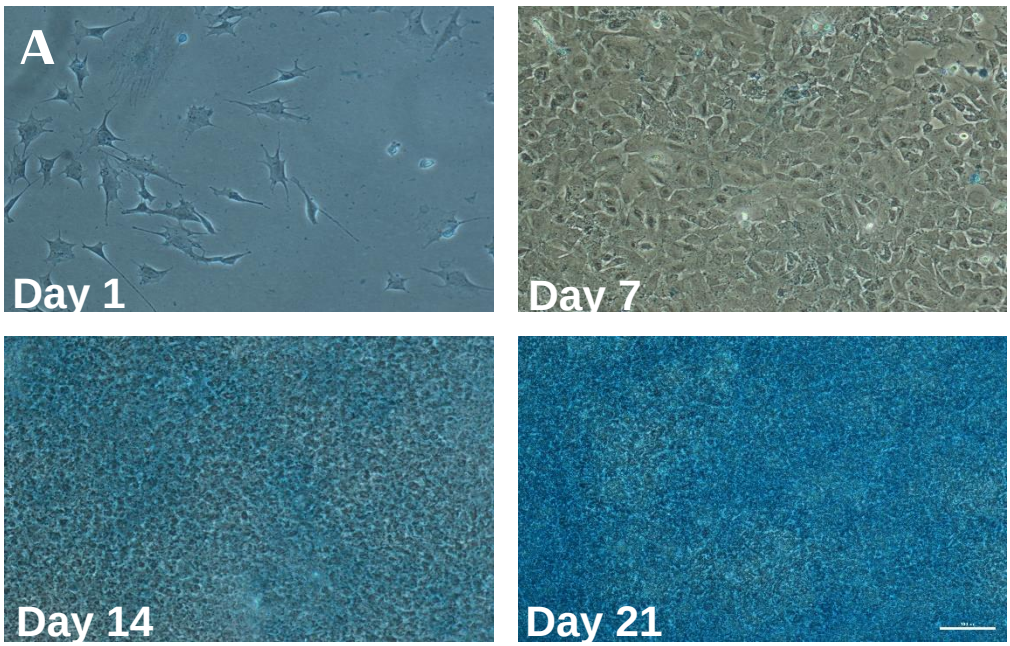

B

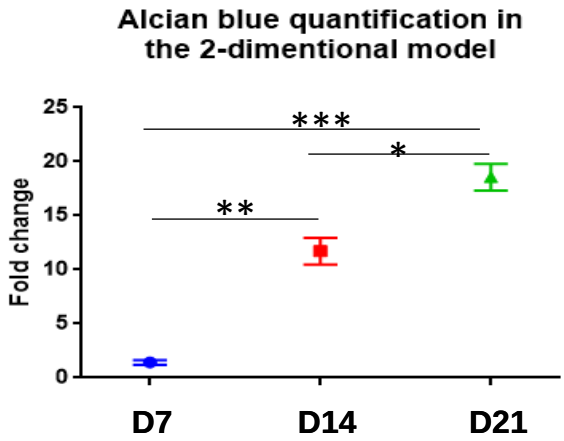

C

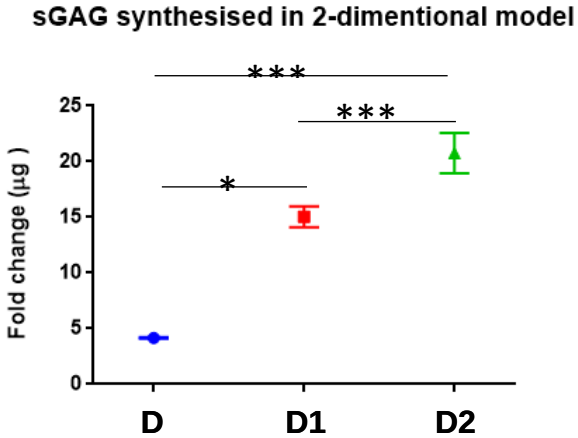

Figure 40. Alcian blue and sGAG quantification for days 1 to 21 in the 2-dimensional model. GAG histology staining of ATDC5 for days 1 to 21 in the 2-dimensional model. (A) *Alcian blue staining was performed to detect sulphated proteoglycans deposition during the ATDC5 chondrogenesis. Scale bar=100µm.* ***(B)*** *Quantification of the Alcian blue dye extracted by 4 M guanidine HCI overnight at 4°C and measured by optical density at 595nm* ***(C)*** *µg of sGAG produced quantify via DMMB assay. Both normalised to the levels after seeding 12,000 cells per ml on monolayer (Day 1). * p<0.05, **p<0.01, ***p<0.001, and ****p<0.0001 two-way ANOVA statistical analysis. N=3 and n=3.*

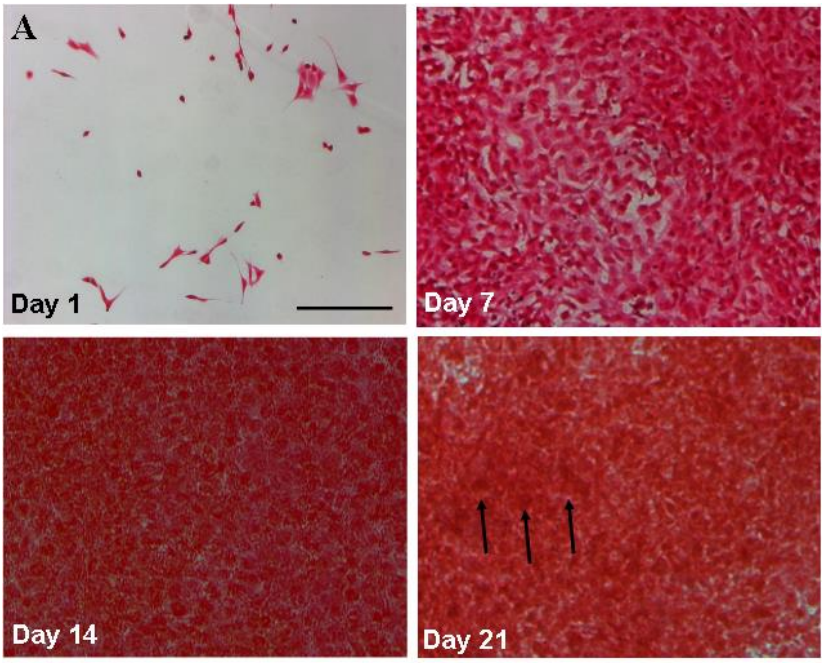

Figure 41. Collagen histology staining along day points 1 to 21 in the 2-dimensional model. *Picrosirius red staining was performed to detect sulphated proteoglycans deposition during the ATDC5 chondrogenesis. Scale bar=100µm. N=3 and n=3.*

Calcium deposition was studied using Alizarin red staining (Figure 42.A), which was extracted, and its optical density was measured at 570nm. A progressive increase of mineralisation within the ECM was observed from day 14. This deposition intensified at day 21, showing pericellular accumulation and nodule formation (Figure 42.A; arrows). Quantitative measurement of the stain (Figure 43.B) showed mineralisation at all day points. A significant increase when comparing day 7 against days 14 and 21 by 82.73-fold change ($p=0.05$) and 5.47-fold change ($p=0.00045$) respectively. When comparing day 14 against day 21 a significant increase was also visible by 1.99-fold change ($p=0.009$) (Figure 42.B). Therefore, the ATDC5 2D model did not only show deposition of sGAG and collagen, two of the main components of the cartilage ECM *in vivo* but also showed mineralisation, as seen in deeper layers in the stratified calcified cartilage tissue.

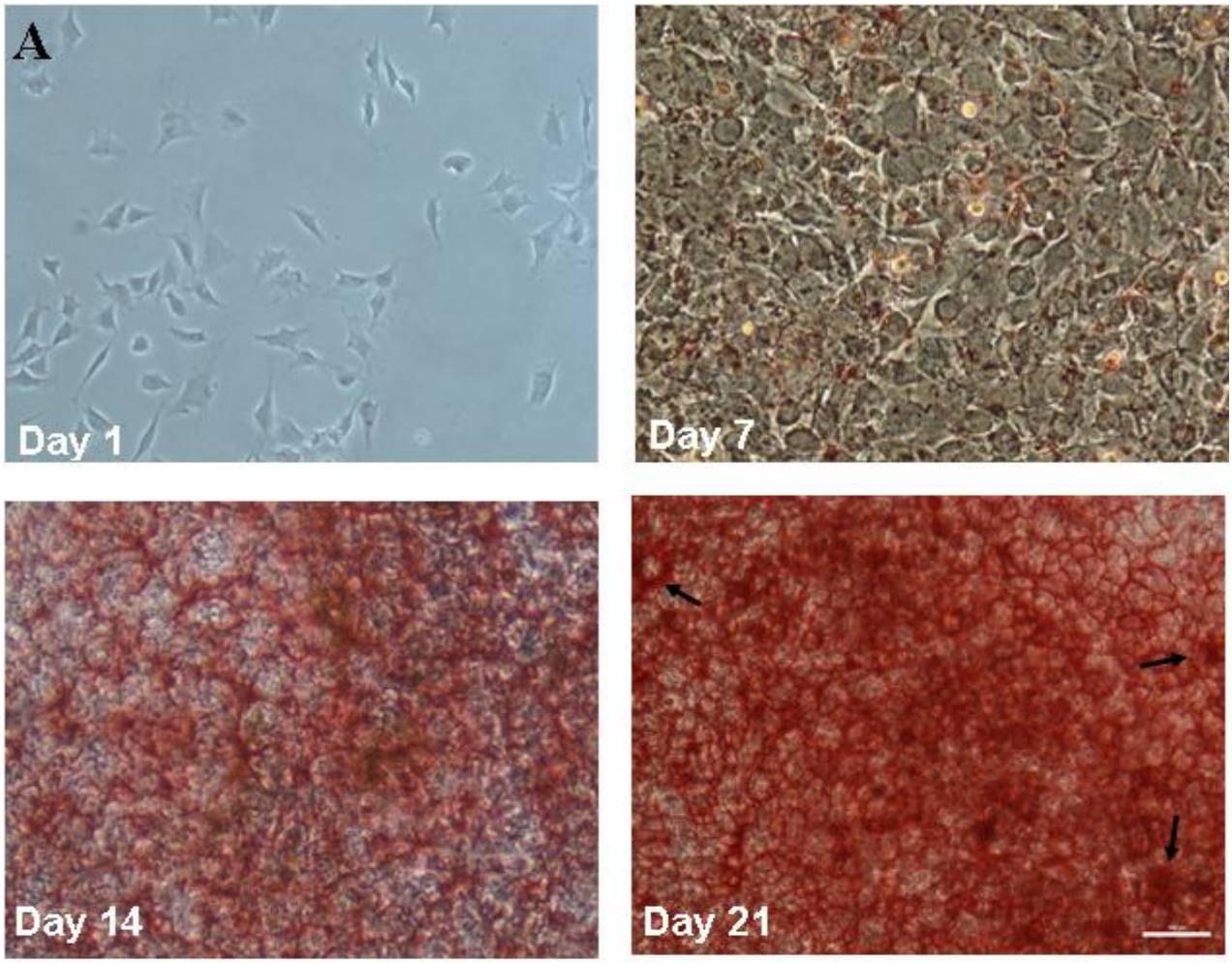

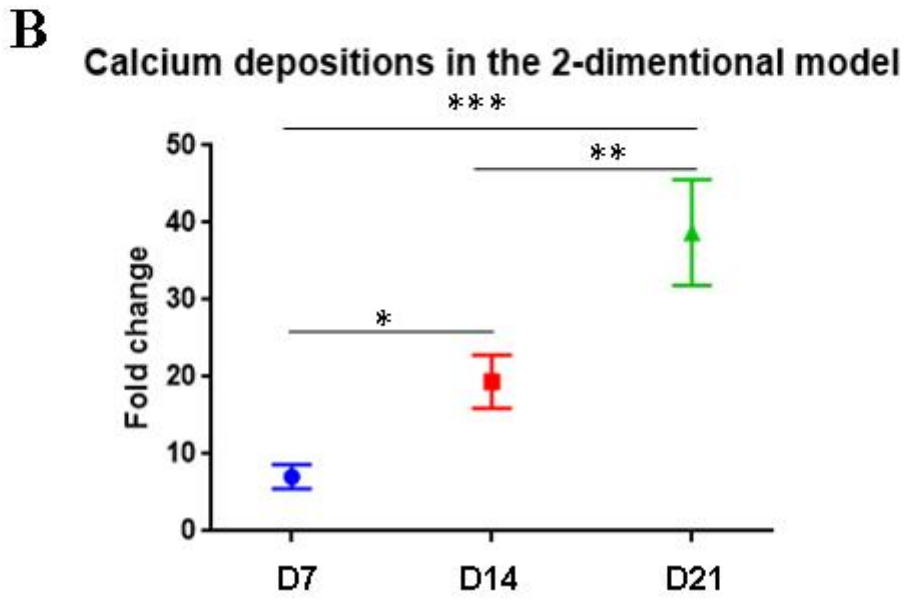

Figure 42. Calcium depositions during the 21 days incubation period in the 2-monolayer model. (A) *Alizarin red staining (red) to detect mineralisation during the ATDC5 monolayer. Arrows are pointing out at the nodule formation. Scale bar=100µm.* ***(B)*** *Quantification of the Alizarin red dye extracted by cetylpyridinium chloride and measured at 405nm. Quantification levels normalised to the levels after seeding 12,000 cells per ml on a monolayer (Day 1* $p<0.05$, ** $p<0.01$, *** $p<0.001$, and **** $p<0.0001$ two-way ANOVA statistical analysis. N=3 and n=3.*

3.3.2 Gene expression of chondrogenic markers in the 2D culture of ATDC5 cells

To further study the chondrogenesis in ATDC5 cells, real-time quantitative polymerase chain reaction (q-PCR), using *18S* as the house-keeping gene, was performed for chondrogenic markers such as *Sox9* (early chondrogenesis), *Ihh*, type II (*Col2a1*) and type X (*Col10a1*) collagen and aggrecan (*Acan*). Type I collagen (*Col1a1*) expression was used as a marker of de-differentiation and bone formation. The expression levels were normalised to the levels of gene expression at day 1 (pre-differentiation) (Figure 43).

Expression of *Sox9* significantly decreased by 0.49-fold change when comparing day 7 against day 14 (p=0.041) whereas when comparing day 14 against day 21 a significant increase was visible by 1.49-fold change (p=0.002). Interestingly, another chondrogenic marker, biomechanically regulated *Ihh*, did not increase during differentiation (Figure 43).

Expression of *Col2a1*, encoding type II collagen, one of the main components of the cartilage ECM, significantly increased by 17.29-fold change (p=0.011). The gene expression of type X collagen, a marker of hypertrophic chondrocytes was found significantly decreased when comparing day 7 against day 14 by 0.37-fold change (p=0.049) however, a significant increase when comparing day 14 to day 21 by 3.84-fold change (p=0.004) (Figure 43).

Type I collagen was studied to examine the quality of the collagen and ECM formed by the differentiating ATDC5 cells. Type I collagen is linked to osteoarthritis, low-quality cartilage or bone formation, and fibrosis, therefore it is of no interest in a model of chondrogenesis, although certain studies claim to be found on the surface (Duance, 1983). Type I collagen expression was consistent without any significant variation (Figure 43).

Finally, to study glycosaminoglycan, aggrecan (*Acan*) gene expression was analysed. The gene expression significantly increased from day 7 to day 21, by a 23.15-fold change (p=0.05) (Figure 43).

		Sox9	***Ihh***	***Col2a1a***	***Col10a1***	***Col1a1***	***Acan***
No growth factors	Day 7	↑	↑	↓	↓	↑	↓
	Day 14	↑	↑	↓	↓	↑	↓
	Day 21	↑	↑	↓	↔	↑	↓

Table 5. Table summarising the outcome of the gene expression *of Sox9, Indian hedgehog (Ihh), collagen II (Col2a1), collagen X (Col10a1), collagen I (Col1a1) and aggrecan (Acan) after 21 days of culturing ATDC5 in a 2-dimensional culture compared to day 1 gene expression. N=3 and n=3.*

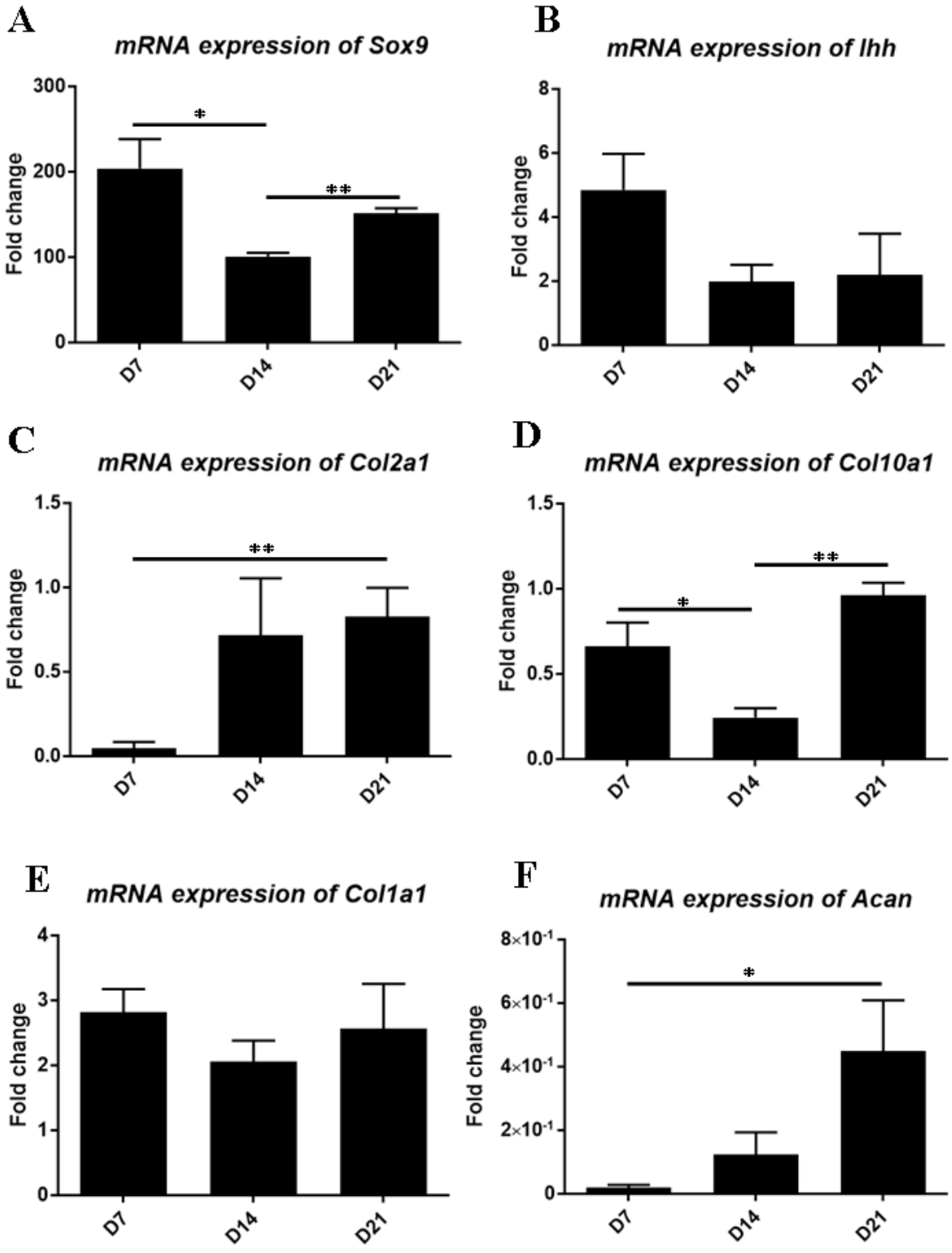

Figure 43. mRNA expression after 21 days of culture. *Gene expression of Sox9* ***(A)****, Indian hedgehog (Ihh)* ***(B)****, type II collagen (Col2a1)* ***(C)****, type X collagen (Col10a1)* ***(D)****, type I collagen (Col1a1)* ***(E)****, aggrecan (Acan)* ***(F)*** *after 21 days of culturing ATDC5 in a 2-dimensional culture. Quantification levels were normalised to the levels after seeding 12,000 cells per ml on monolayer (day 1). Two-way ANOVA statistical analysis where * p<0.05, **p<0.01, ***p<0.001, and ****p<0.0001. N=3 and n=3.*

3.4 Discussion

Work presented in this chapter validated the ATDC5 cell line as a chondrogenic cell line and was used for further comparison with the 3-dimensional models developed in this thesis. Cells at a density of 12,000 per ml were seeded in a 6 well-plate for 21 days and analysed at 1, 7, 14, and 21 days.

Tissue engineering requires large cell quantities, either for implantation in the damaged area or for the generation of complex 3-dimensional scaffolds (Mauck *et al.*, 2003; Kisiday, 2019). Primary chondrocytes present various limitations, not only the need for invasive harvesting but also the insufficient quantity and variations depending on the location source cells (Bhumiratana and Vunjak-Novakovic, 2015; Asadi *et al.*, 2018). Moreover, primary chondrocytes often lose their phenotype and have reduced proliferation rates when expanded in monolayer (Kisiday, 2019). Stem cells, due to their differentiation capacity into several tissue lineages such as cartilage, bone and adipose tissues, offer a promising alternative to primary chondrocyte in cartilage tissue engineering (Pelttari, Steck and Richter, 2008; Asadi *et al.*, 2018). Despite this, their collection can be painful and invasive with low availability, such as for bone marrow stem cells (Reppel *et al.*, 2015). Genetic manipulation of stem cells to facilitate studies of disease mechanisms also presents several challenges such as the efficiency of transfection and preserving the expression of transgenes, all while maintaining their differentiation capability (Baek *et al.*, 2016; Tamm *et al.*, 2016). iPSCs presents some advantages compared to the other cell sources by avoiding ethical issues and by the ease to harvest. However, its main limitation is the risk of teratoma development due to the presence of undifferentiated iPSCs at the implantation site (Tsumaki, 2015).

On the other hand, the ATDC5 cell line is a well characterised murine cell line that can recapitulate development steps seen during chondrocyte differentiation and cartilage mineralisation (Atsumi *et al.*, 1990; Kudva, Luyten and Patterson, 2018). This cell line can also be easily transfected using lipofectamine making it a good model to study cartilage disease mechanisms and progression (Morimoto and Obinata, 2011; Luan and Liang, 2018; Ying *et al.*, 2019). A progressive increase in proliferation, measured using the MTT metabolic assay, was seen through the ATDC5 cell culture and correlated with the increased cell density seen with haematoxylin-eosin staining. The cells growing in a 2-dimensional layer have equal access to nutrients which results in homogenous growth and ECM deposition (Duval *et al.*, 2017). However, this leads to the absence of the stratification typically found in articular cartilage, as mature chondrocyte phenotypes are often induced by depleted access to nutrients and changes in oxygen tension (Hsieh-Bonassera *et al.*, 2009; Fox, Bedi and Rodeo, 2009).

GAGs contribute to mechanical load support and act as signalling mediators in charge of cellular processes such as adhesion, cell proliferation and differentiation (Silva *et al.*, 2020). In the ATDC5 monolayer model, Alcian Blue staining for proteoglycan synthesis showed a significant increase in deposition of sGAG in 2-dimensional ATDC5 cell culture, especially after 21 days of culture with an 18.56-fold increase compared to day 1. Similar results were seen when quantifying sGAG deposition using DMMB assay. Aggrecan (*Acan*) gene expression was also upregulated at all day points. This is consistent with previous studies that have reported comparable results when seeding ATDC5 cells in monolayer, with increasing sGAG deposition and aggrecan gene expression, proving the chondrogenic potential of ATDC5 cells (Caron *et al.*, 2012; Newton *et al.*, 2012). GAGs *in vivo* have been shown to increase significantly through MSC chondrogenic differentiation, correlating with our results and supporting ATDC5 cell culture as a model of chondrogenesis (Silva *et al.*, 2020).

Following that, collagen expression and synthesis were analysed using Picrosirius Red. Pericellular matrix (PCM) was deposited by the cells at day and 14, and after 21 days of culture, the cells formed some nodules increasing the deposition and forming interterritorial deposition of collagen in the 2D culture. Type II collagen is one of the major components of ECM in cartilage, while *Col10a1* expression is associated with hypertrophy and mineralisation linked to chondrocyte maturity (Fox, Bedi and Rodeo, 2009; Caron *et al.*, 2012). Interestingly, gene expression of type II collagen (*Col2a1*) decreased initially in the 2D culture and was upregulated to basal levels after 2 weeks of culture, while type X collagen (*Col10a1*), peaked significantly after 21 days compared to days 7 and 14, indicating hypertrophic potential. High expression of hypertrophic markers by the differentiating ATDC5 cells has also been shown in other studies, whereby the cells became hypertrophic in the first two weeks of culture. Moreover, the addition of β-glycerophosphate (β-GP) or inorganic phosphate to the culture media upregulates the expression of hypertrophic markers and mineralisation (Caron *et al.*, 2012; Wu *et al.*, 2017a), and ATDC5 2D cultures have been previously shown to be mineralising after 4 weeks of culture (Magne *et al.*, 2003; Caron *et al.*, 2012). This hypertrophy and mineralisation apart from being detected in our study were also detected when seeding other cells in monolayer, but not in a 3-dimensional culture (Caron *et al.*, 2012; Duval *et al.*, 2017). One study reported mineralisation after 29 days (Magne *et al.*, 2003), the cells in this study presented calcium deposits after only 14 days, increasing significantly after 21 days, similar to what found by Newton *et al*. (Newton *et al.*, 2012). The reduced time for mineralisation could be due to the addition of 10 mM of β-GP, as indicated in other studies, which accelerates the expression of the hypertrophic marker (Newton *et al.*, 2012). ATDC5 are therefore a versatile

cell line, allowing the study of not only early chondrogenesis but also hypertrophy and mineralisation, making them a promising cell line for 3D modelling zonally stratified cartilage.

Sox9 is a chondrogenesis marker highly expressed at the beginning during the differentiation of condensed MSCs into chondrocytes and during the expression of ECM such as type II collagen and aggrecan (Han and Lefebvre, 2008; Ikegami *et al.*, 2011). *Sox9* expression in monolayer culture of ATD5 cells increased significantly at the start of the culture, which could represent the condensation stage, and after 3 weeks of culture, which could correlate to cartilage deposition *in vivo*.

PTHrP and IHH are involved in a negative feedback loop that regulates the longitudinal bone growth through regulating chondrocyte proliferation in the growth plate (Kronenberg *et al.*, 1997; Kronenberg, 2003; Oji *et al.*, 2007). The IHH signalling is associated with primary cilium and regulated by mechanosensing. Gene expression of chondrogenic marker *Ihh* appeared stable through the 21 days of chondrogenic culture of ATDC5 cells, and where these results have been previously shown in other studies where ATDC5 cells exhibited the *Ihh* and *PTH/PTHrP* signalling pathways (Kudva, Luyten and Patterson, 2018) and chondrogenic markers as *Sox9* (Caron *et al.*, 2012).

Interestingly, expression of type I collagen (*Col1a1*) remained high through the ATDC5 culture in monolayer compared to day 1. This was also observed in the primary chondrocyte monolayers, where the cells lose their phenotype and become more fibroblast-like after multiple passages (Hsieh-Bonassera *et al.*, 2009; Vinatier and Guicheux, 2016). The upregulation of type I collagen is linked in many studies with the downregulation of type II collagen, which was also visible in this experiment (Schuh *et al.*, 2010; Anderson and Johnstone, 2017). Interestingly, ATDC5 cells lack their rounded morphology that is typical for chondrocytes, further confirming the loss of phenotype in monolayer. Other studies, however, linked the expression type I collagen with later stages of osteoarthritis (Lahm *et al.*, 2010).

The lack of significant increase in some of the key cartilage matrix components and a steady high level of type I collagen expression highlight the limitation of using ATDC5 cells to study chondrogenesis despite the correct *Sox9* expression pattern increased sGAG deposition and end-stage mineralisation. Despite this, the simplicity of the 2D models allows quick characterisation of the effect of novel mutations on chondrogenesis, and they continue to be used as a model to study the effects of novel genetic variants discovered in the next-generation sequencing projects.

Chapter 4. Development and Characterisation of a 3-Dimensional Pellet Culture of ATDC5 Cells as a Model of Zonally Stratified Cartilage

4 Development and characterisation of a 3-dimensional pellet culture of ATDC5 cells as a model of zonally stratified cartilage

4.1 Introduction

Pellet culture proved to be an established gold standard for the study of mesenchymal stem cell (MSC) chondrogenesis, mimicking stem cell condensation during skeletal development and producing hyaline cartilage pellets (Bosnakovski et al., 2004; Bernstein et al., 2009). The model is highly reproducible and replicates the intimate interaction between neighbour cells synthesising stratified ECM (Yung Lee et al., 2001; Tare et al., 2005; Babur et al., 2013). Therefore, it can be implemented in studies in disease modelling, drug screening and regenerative medicine (Nam, Rim and Ju, 2017).

This model has been highly used with stem cells and chondrocytes due to its simplicity, using centrifugation to form the pellets in either polypropylene tubes or v-bottom plates (Babur et al., 2013). However, the formation of pellets and their mechanical properties varied between cell types and growth factors addition, and optimisation of the system is often required. For example, using too many cells may result in an uneven pellet with excessive cell death occurring in the centre due to the depletion of nutrients and an overdeveloped surface. In contrast, using a small number of cells results in an equal distribution of nutrients and a homogenous ECM deposition, but with no zonal stratification (Lewis et al., 2016). The perfect diameter of the pellet produces a gradient diffusion of nutrients developing a radial variation in the ECM synthesis and a zonal stratification of the tissue (Babur et al., 2013)

Pellet system compared to 2-dimensional culture systems allows the retention of the cell phenotype over culture time (Babur et al., 2013), higher expression of chondrogenic factors such as SOX9, aggrecan and type II collagen (Yung Lee et al., 2001; Tare et al., 2005), superior sensitivity and reliability (Prosser et al., 2019). Several studies show higher rates of transcription of *Sox9* and type II collagen in pellets than in alginate, alginate-chitosan and alginate-fibrin hydrogels (Bernstein et al., 2009).

Pellet models of stem cells have been used as a model to understand the differentiation potential of different stem cells *in vitro* in a serum-free medium or without the addition of differentiation factors (Bosnakovski et al., 2004; Murdoch et al., 2007; Gale et al., 2019), to study hypoxia activation of PTHrP-MEF2C pathways (Browe et al., 2019). ATDC5 have also been cultured in a pellet system to model the exogenous cues during differentiation, maturation and mineralisation with the addition of inorganic phosphate (Tare et al., 2005; Wu et al., 2017), and study the canonical Wnt signalling during chondrogenesis (Wang et al., 2019).

4.2 Aims of the chapter

The aim of this chapter was to develop and characterise 3-dimensional pellet culture of ATDC5 cells as a model to study cartilage differentiation and disease *in vitro* and to use the model to optimise a growth factor regime in order to improve the standard chondrogenesis protocol. The ideal model will recreate the zonal stratification presented in the human articular cartilage to allow *in vitro* studies of the healthy and diseased tissue.

4.3 Results

Due to the lack of literature regarding ATDC5 cells in pellets at the start of the project, different cell densities (from 1 to 2 million per pellet) were tested. These densities, despite working for other cell types, such as different types of stem cells and primary human chondrocytes (Bosnakovski *et al.*, 2004; Watts, Ackerman-Yost and Nixon, 2013), resulted in a disintegration of the ATDC5 pellet. The diameter of the seeding tube was also optimised, testing normal centrifuge falcon tubes, hydrophobic walls Eppendorf to finally sample transport tubes with a skirt. Subsequently, ATDC5 cells were seeded at a density of 500,000 cells per pellet and incubated for 21 days. Pellets were collected every 7 days (day 1, 7, 14 and 21) from the day of seeding and used for RNA extraction, proliferation and sGAG assays, and histology and immunohistochemistry studies. All results represented in graphs were calculated as a fold change over 24h of seeding (day 1). Therefore day point 1 has the value of 1 in all graphs. Every graph is accompanied by its fold change values and the p-values calculated when comparing all day points.

The Pellet system was used to optimise the growth factor regime necessary for optimal growth and zonal stratification of the developing cartilage before moving onto the compressible hydrogel system (chapter 5). BMP7, TGF-β3 either individually or together were added to the pellet culture at a concentration of 10ng/ml 24h after the seeding of the pellets (Knippenberg *et al.*, 2006; Dahlin *et al.*, 2014; Huang *et al.*, 2018).

4.3.1 ECM deposition and area of pellets with no supplementation of growth factors

ATDC5 pellets grown without any additional growth factors were stained with haematoxylin and eosin to study the morphology of the cells and the pellet. Picrosirius Red was used to detect collagen deposition, and toluidine blue was used to study sGAG deposition during the 21-day chondrogenic differentiation of ATDC5 cells in pellets (Figure 44A).

Stratification of the pellets and cell morphology throughout the differentiation process. Interestingly, the pellet centres became fragile on day 7 and 14 but filled with ECM and cells on day 21. The deposition of collagen was increased on the surface of the pellet by days 7 and 14; however, by day 21 there was a more homogenous distribution. On the other hand, GAG detected by toluidine blue staining were deposited primarily in the centre of the pellet on day 7 and 14, the production was even at day 21 however the centre remained richer in the deposition. Furthermore, the area of the pellets at each day point was quantified (Figure 44B), showing a lack of significant increase of pellet size during differentiation.

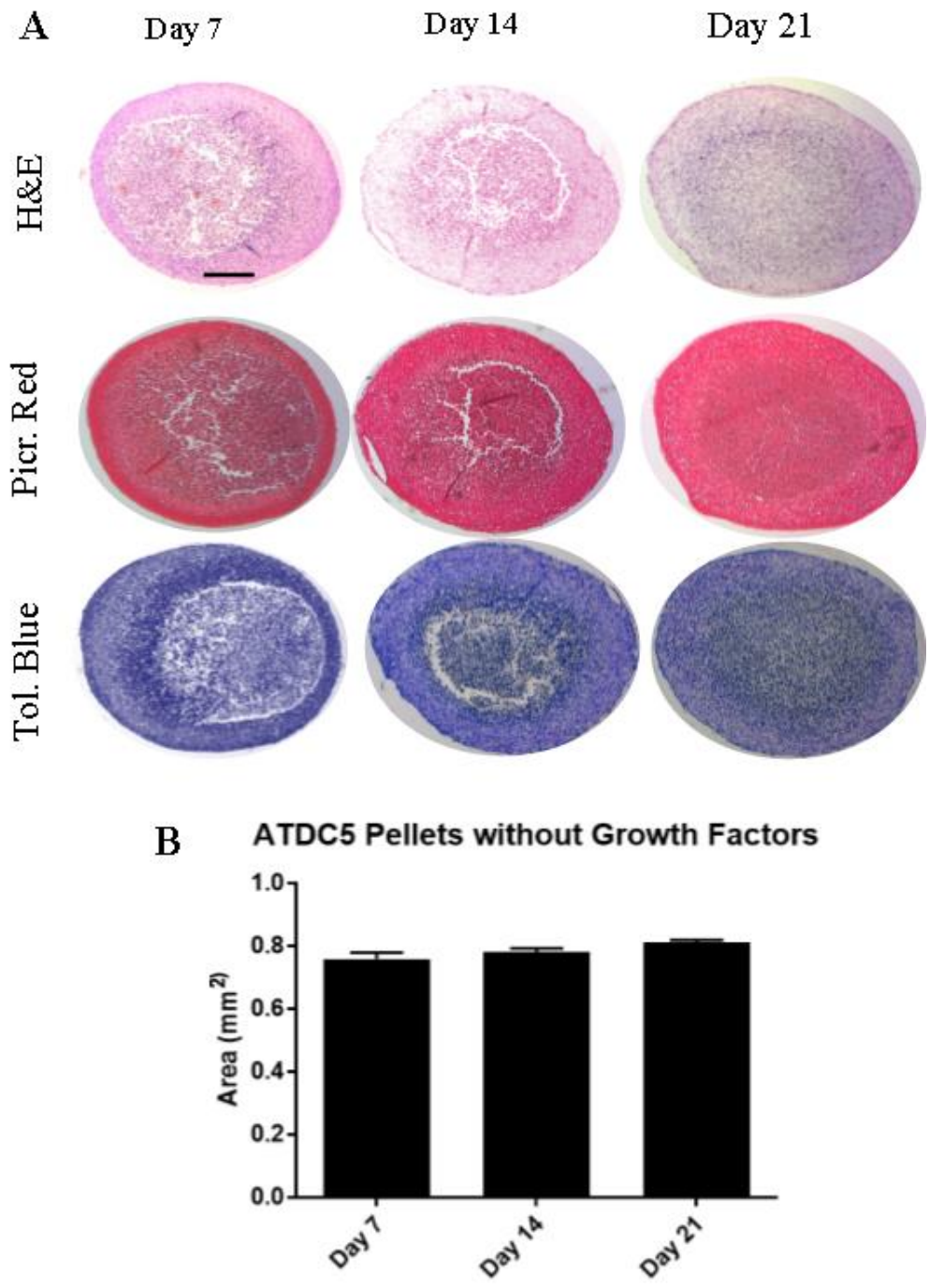

Figure 44. Histology staining of ATDC5 cells following 1, 7, 14 and 21 days of pellet culture. (A) *Top row: Haematoxylin and eosin staining was performed in the pellet model to study cell and pellet morphology. Middle row: Picrosirius staining for collagen deposition in red. Bottom row: Toluidine Blue staining for sulphated glycosaminoglycan in blue. N=3 and n=3. Scale bar= 200 µm* ***(B)*** *Area of pellets at each day point was measured with ImageJ and represented in mm^2. * p<0.05, **p<0.01, ***p<0.001, and ****p<0.0001 two-way ANOVA statistical analysis. N=3 and n=3.*

4.3.2 ECM deposition and area in pellets with growth factor supplementation

Pellet culture was supplemented with growth factors, either BMP7 or TGF-β3 individually or together at a concentration of 10ng/ml 24h after the seeding (Knippenberg *et al.*, 2006; Dahlin *et al.*, 2014; Huang *et al.*, 2018).

The area of pellets grown with and without the addition of growth factors was measured and compared (Figure 45.B). The area of the pellets cultured without growth factor supplementation did not change during the chondrogenesis protocol. Interestingly, BMP7 supplementation led to a significant increase ($p>0.0001$) by 2.4-fold change and 1.84-fold change from day 7 to days 14 and 21, respectively. The addition of TGF- β3 showed no significant variability. Finally, when adding both growth factors significantly increased pellet size when comparing day 7 to day 21 by 2 ($p>0.0001$) potentially indicating higher ECM deposition or increased proliferation. (Figure 45.B).

Initially, the collagen deposition (Picrosirius Red, Figure 45A and 46) was increased in the superficial zone of the pellets grown with both growth factors and with TGF- β3 alone at day 7 and increased at day 14 for the pellets grown with BMP7 addition. Finally, on day 21, the combination of both growth factors and the TGF-β3 treatment alone led to higher intensity of collagen staining in the superficial zone compared to the pellets grown with BMP7 and with no addition of growth factors (Figures 45.A and 46). The deposition of collagen in the middle and deep zones of the pellets appeared lighter, especially on day 7 and 14.

Type II and I collagen deposition in the engineered pellets was studied using immunohistochemistry to determine the quality of the ECM produced (Figure 47 and 48). Negative controls for respective antibodies can be found in Figure 49. Type II collagen showed more pericellular deposition at day 14 compared to the other conditions when adding both growth factors. After 21 days, the addition of BMP7 and TGF-β3 showed the highest deposition of type II collagen, now visible in all zones, especially on the surface. For the other conditions, the pericellular deposition of type II collagen was still detectable, however less visible within the depth in the zones (Figure 47). Type I collagen showed an initial lack of any deposition on day 7 for all conditions (Figure 48). The deposition of type I collagen was first detected on day 14 on the surface of all pellets; this deposition was higher for TGF-β3 and the addition of both growth factors. Interestingly, type I collagen was no longer detected at the surface for TGF-β3 and no addition of growth factors after 21 days, in the case of the latter the synthesis is more pericellular, while for the TGF-β3 condition is predominantly in the surface and surface-middle zone. In the pellets grown with the addition of BMP7 and with both growth factors, the synthesis

of type I collagen was limited to the surface but expressed densely, showing a zonally stratified ECM.

Analysis of the proteoglycan deposition in the ECM was performed using Toluidine blue staining and quantitative DMMB assay (Figure 50.A and 51). Toluidine blue showed a higher deposition of sGAG initially in the surface and deep zones of the pellet with the addition of BMP7 at day 7 compared to the other conditions. TGF- β3 supplementation led to a lower deposition of sGAG at day 7 and day 14. In contrast, culture with both growth factors led to sGAG deposition initially focused in the middle zone, but by day 14 and 21 localised in the middle and centre of the pellet. Interestingly, BMP7 supplemented pellets appeared to show lower deposition of sGAG and lighter Toluidine Blue staining. These results were verified by the quantitative measurement of sulphated GAG using the DMMB assay (Figure 50.B). In pellet cultures without growth factor supplementation, the synthesis of sGAG was not increased during the chondrogenesis.

In contrast, comparison of no growth factors against the rest of the conditions showed a significant increment comparing day 14 when adding TGF- β3 and both growth factors by 1.52-fold increment ($p=0.0078$ and 0.0077 respectively). On day 21 the sGAG was significantly increased with any supplemented condition, by 2.9, 3.4 and 3.93-fold change increment ($p<0.0001$). Comparing across supplements, deposition at day 21 was significantly increased when adding TGF- β3 or both growth factors compared to BMBP7, by increments of 1.17- and 1.36-fold change ($p<0.0001$ and $p=0.0147$ respectively). When comparison was done within each condition, day 21 presented a significant increment when compared to days 7 and 14, by 2.4- and 2.06-fold change for BMP7 ($p<0.0001$), 3.8- and 2-fold change for TGF- β3 ($p<0.0001$) and 3- and 2.35-fold change for the addition of both growth factors ($p<0.0001$) respectively.

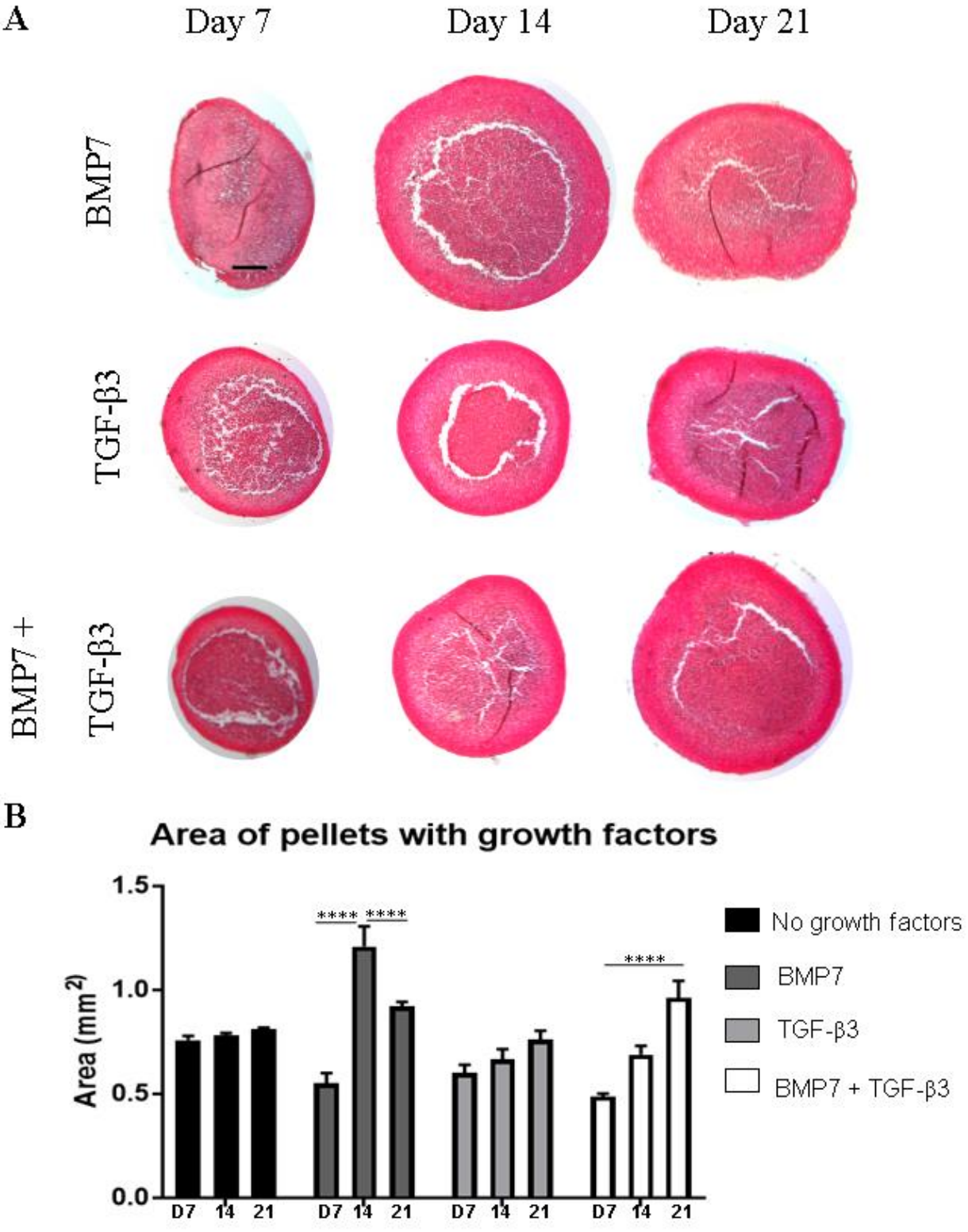

Figure 45. Picrosirius histological staining and area measurements of pellets with growth factors. (A) *Pellets seeded at a density of 500,000 ATDC5 cells per pellet were grown for 21 days withBMP7, TGF-β3 and addition of both factors (X2-GF) and stained with picrosirius red with Scale bar = 200 µm.* ***(B)*** *Pellet area was measured and compared at all day points, where * p<0.05, **p<0.01, ***p<0.001, and ****p<0.0001 two-way ANOVA statistical analysis. D=day. N=3 and n=3*

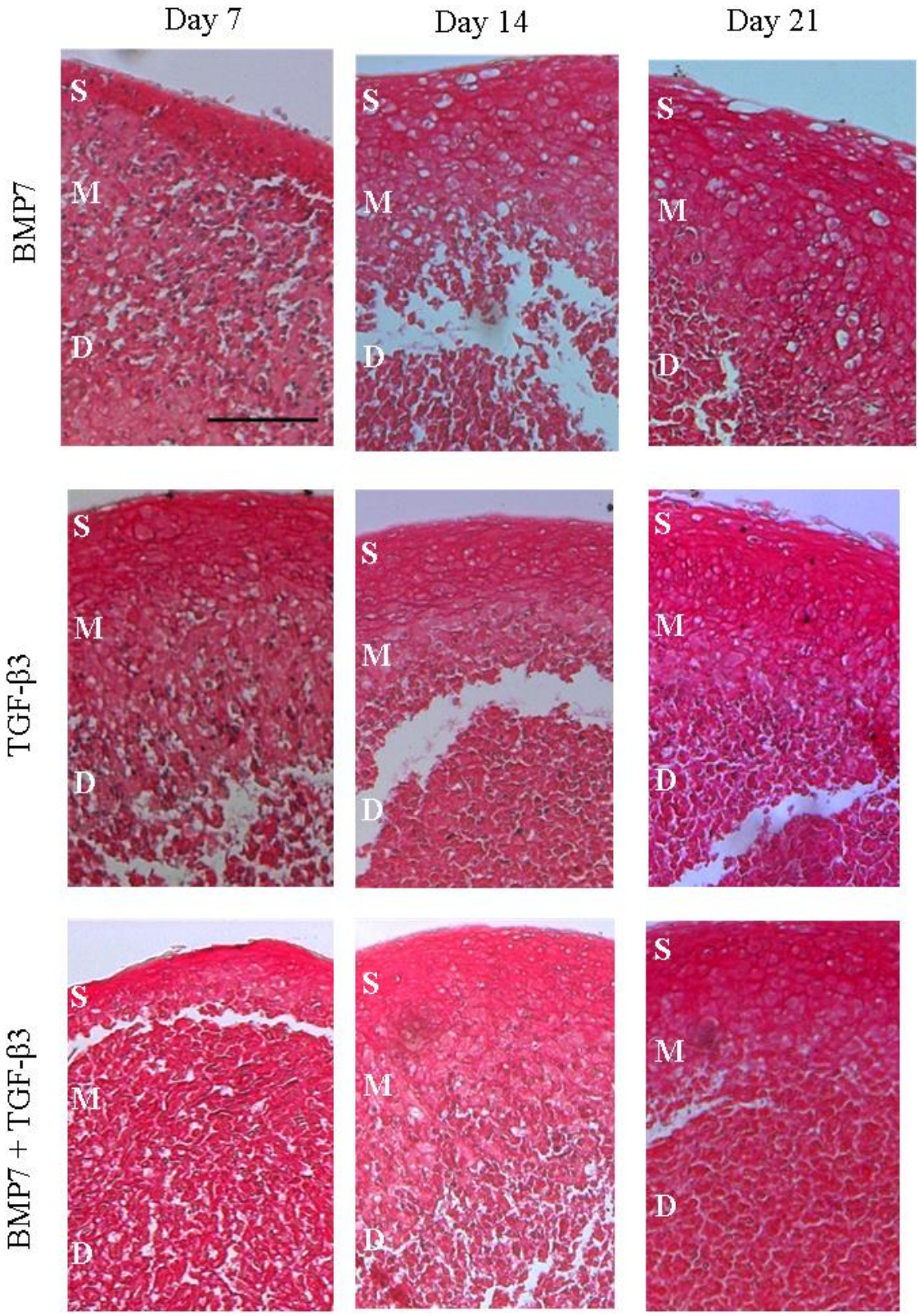

Figure 46. Picrosirius histological staining of pellets with growth factors. *(A) Pellets seeded at a density of 500,000 ATDC5 cells per pellet were grown for 21 days with BMP7, TGF-β3 and addition of both factors (X2-GF) and stained with picrosirius red with Scale bar = 100 µm.*

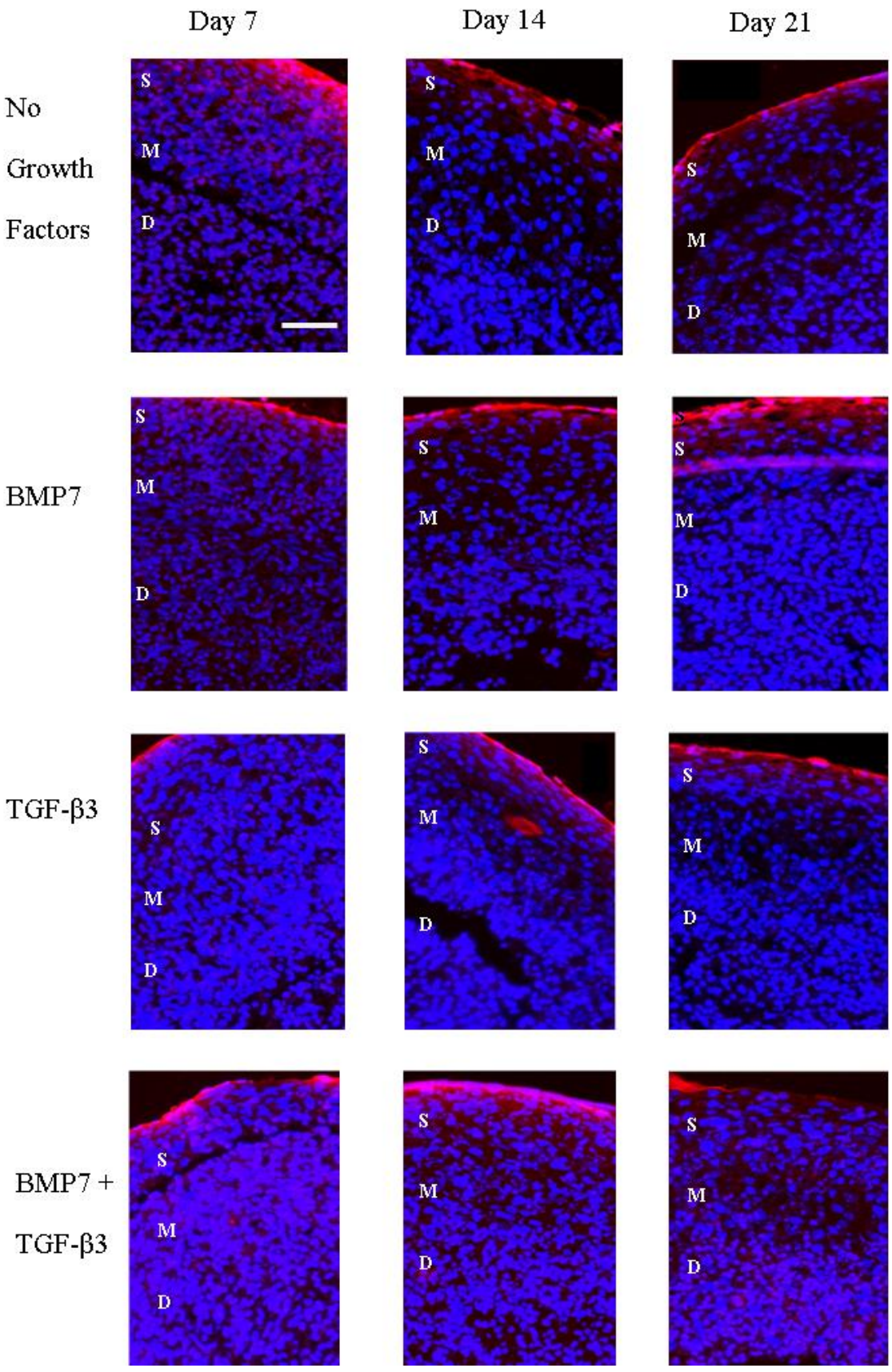

Figure 47. Immunohistochemistry for type II collagen in pellets with growth factor supplementation. *Pellets of ATDC5 cells were grown for 21 days with no addition of growth factors, BMP7, TGF-β3 and addition of both factors (BMP7 + TGF-β3) and used for immunohistological staining. Blue staining = DAPI nuclei staining. Red staining = type II collagen staining. S = Surface zone, M=Middle zone, D=Deep zone. Scale bar = 200 µm. N=3 and n=3.*

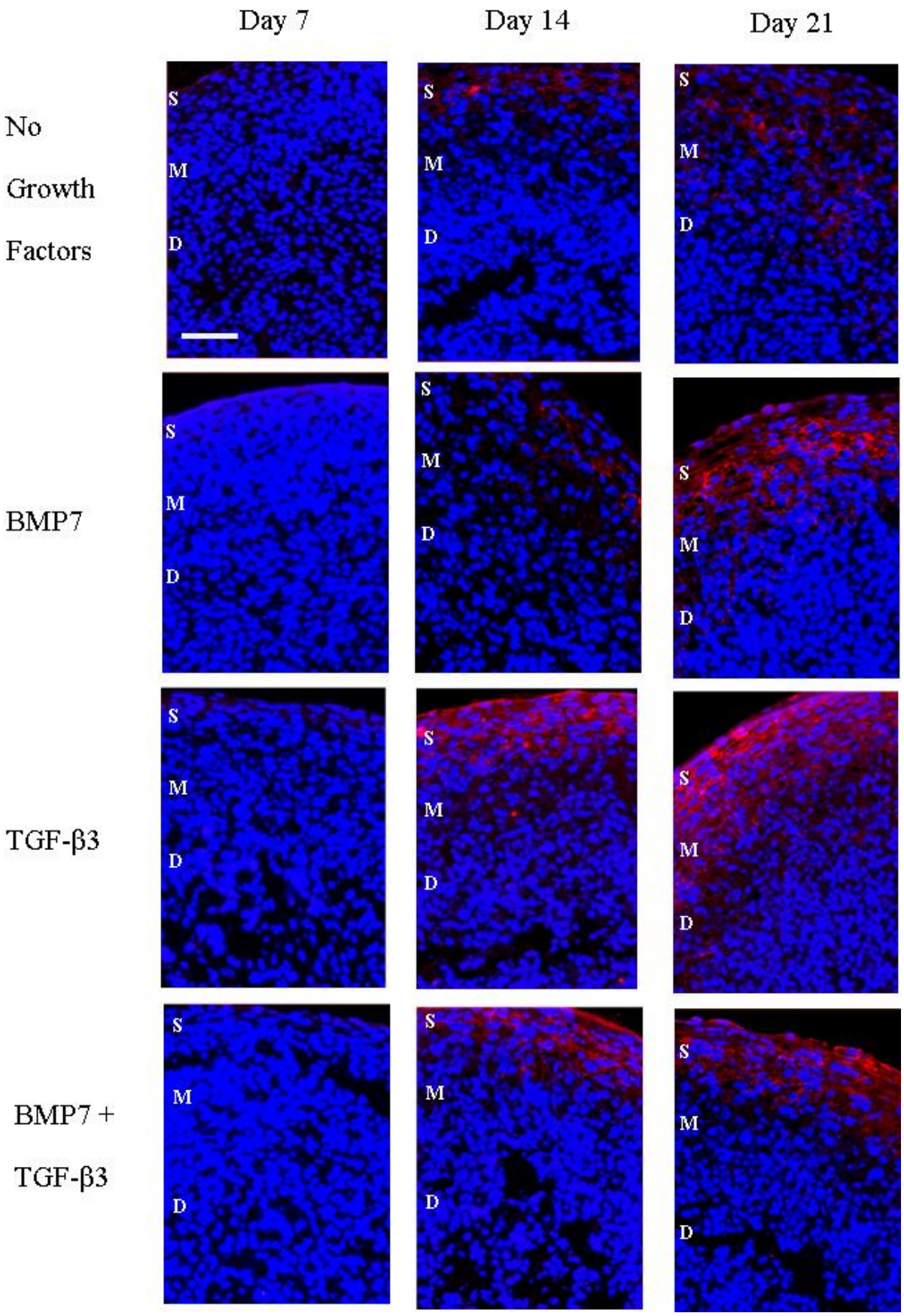

Figure 48. Immunohistochemistry for type I collagen in all conditions after 21 days. *Pellets seeded for 21 days for immunohistological staining with no addition of growth factors, BMP7, TGF-β3 and addition of both factors (BMP7 + TGF-β3). Blue staining = DAPI nuclei staining. Red staining = type II collagen staining. Scale bar = 200 µm. N=3 and n=3*

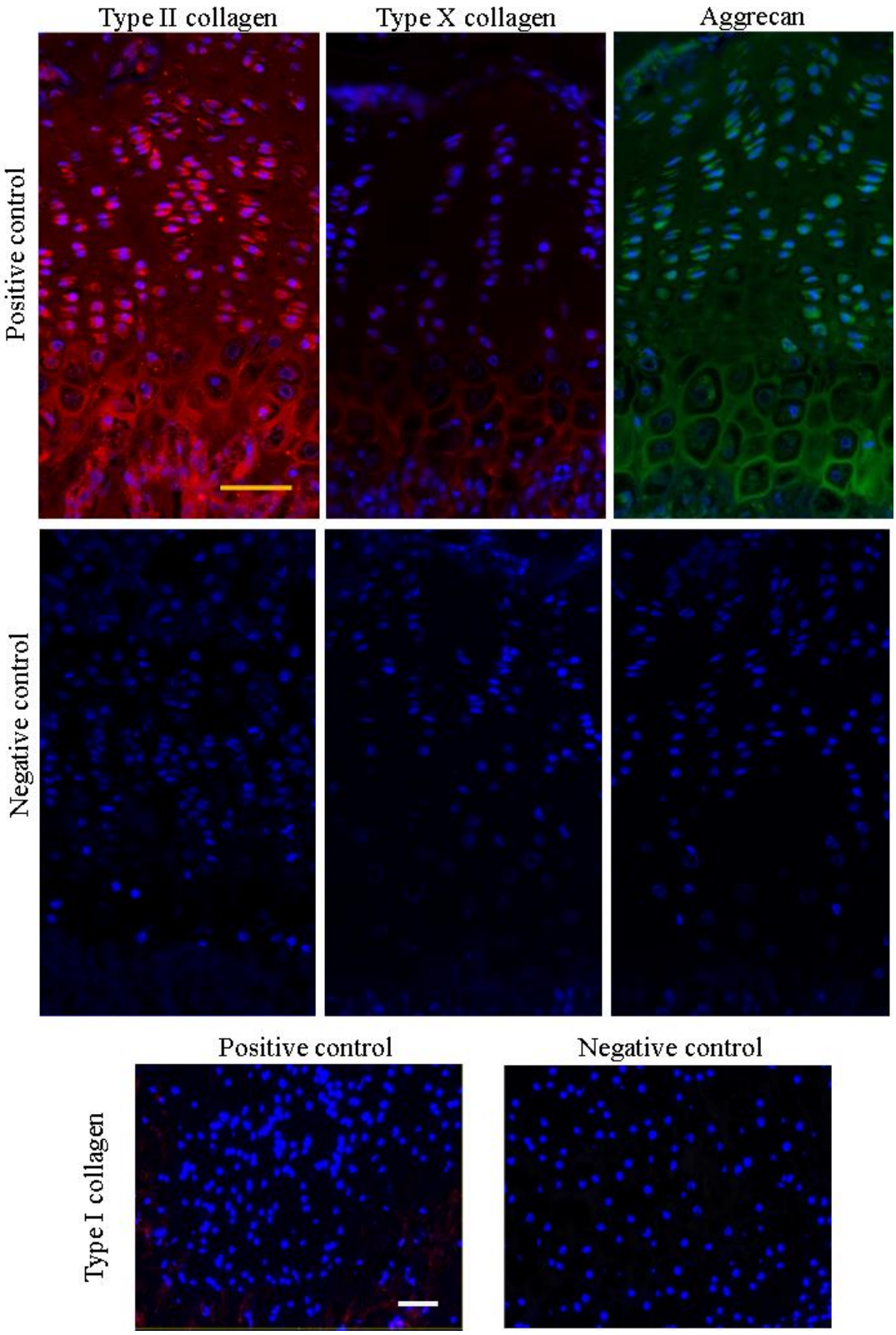

Figure 49. Positive and negative controls for type I, II and X collagen and aggrecan. *Positive and negative controls were done in 3-week-old mice femoral heads for type I, II and X collagen and aggrecan. Scale bar: 50 µm*

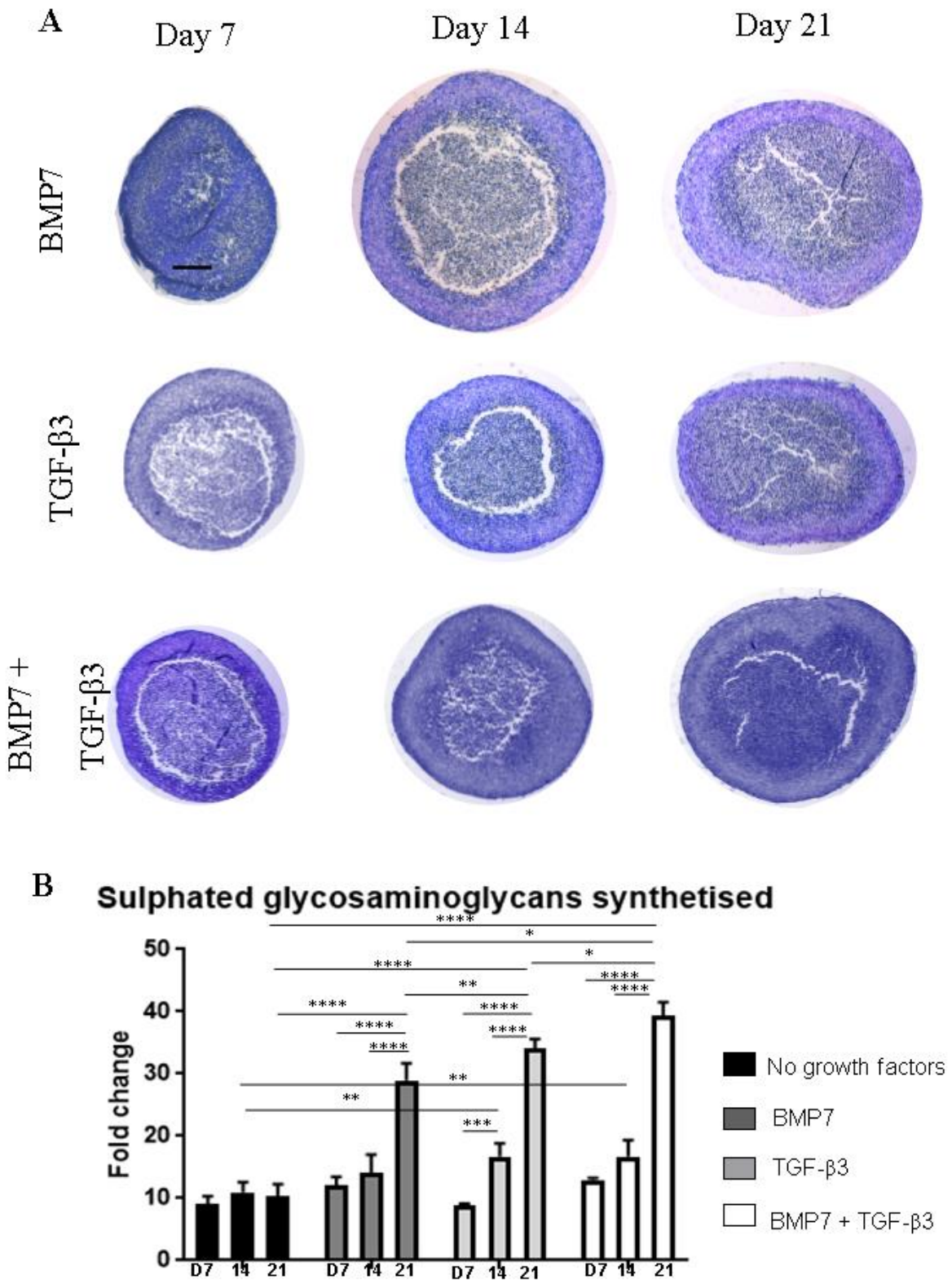

Figure 50. Glycosaminoglycan analysis via staining and quantification. *Pellets seeded for 21 days for histological staining for toluidine blue with no addition of growth factors, BMP7, TGF-β3 and addition of both factors (BMP7 + TGF-β3) Scale bar = 200 µm. N=3 and n=3* ***A).*** *Dimethyl methylene Blue (DMMB) assay for quantification of the sulphated glycosaminoglycan where * p<0.05, **p<0.01, ***p<0.001, and ****p<0.0001 two-way ANOVA statistical analysis. N=3 and n=3.****B).***

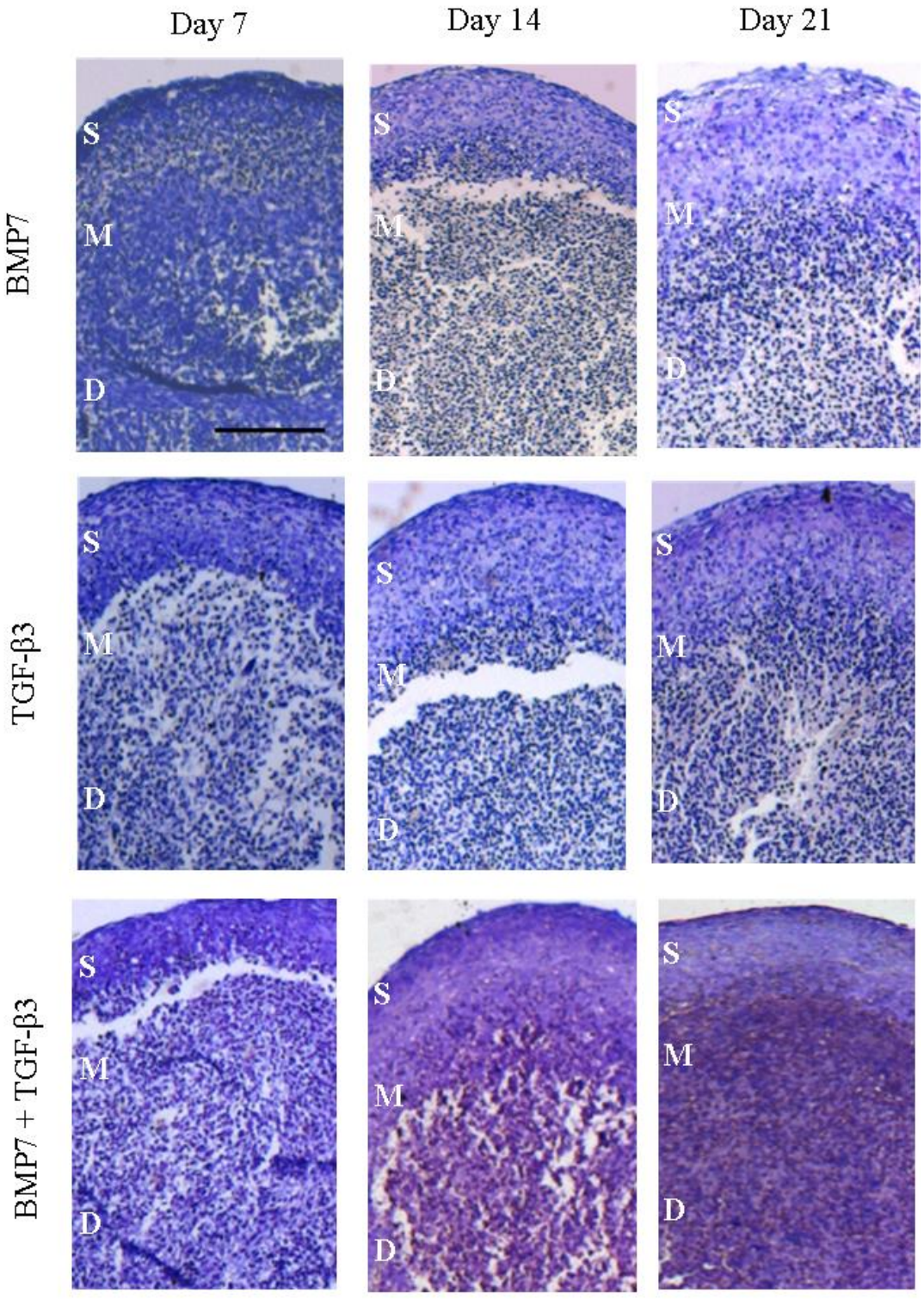

Figure 51. Toluidine blue histological staining of pellets with growth factors. *(A) Pellets seeded at a density of 500,000 ATDC5 cells per pellet were grown for 21 days with BMP7, TGF-β3 and addition of both factors (X2-GF) and stained with Toluidine blue with Scale bar = 100 µm.*

4.3.3 Cell apoptosis in pellets with and without growth factor supplementation

Apoptosis in the cultured pellets was assessed using the quantitative TUNEL assay (standardised to the cell apoptosis found after 24h of seeding (Figures 52 and 53). Supplementing the growth medium with two growth factors led to a steady level of apoptosis throughout the differentiation process. There was a significant increase in cell apoptosis in the surface of the pellets with supplementation of BMP7, from day 14 to 21 by a 2.73-fold change increase ($p=0.0343$) (Figure 53). However, the main variation was found in the centre of the pellet when comparing no addition of growth factors at day 7 against BMP7 and both growth factors supplementation with significant reduction by 0.57- and 0.50-fold change ($p= 0.0067$ and $p=0.0014$). Apoptosis comparing the surface against the centre of the pellet showed a significant increase of apoptosis in the centre at day 7 without supplementation of growth factors by 1.79-fold change ($p=0.0111$) (Figure 53).

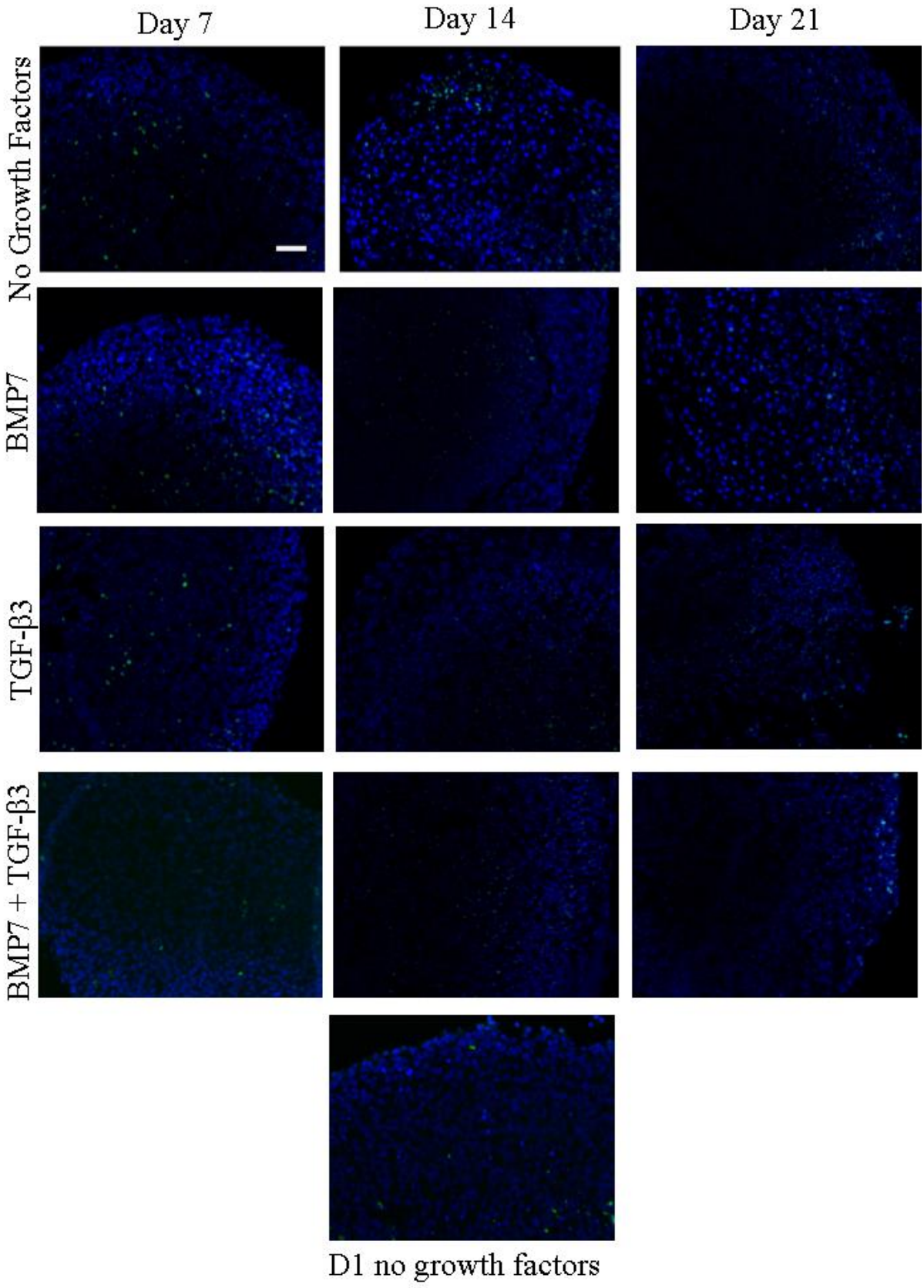

Figure 52. Immunohistochemistry for cell apoptosis in all conditions after 21 days. *Pellets seeded for 21 days for TUNEL staining with no addition of growth factors, BMP7, TGF-β3 and addition of both factors (BMP7 + TGF-β3). Blue staining = DAPI, nuclei staining. Green staining = cell apoptosis. Scale bar = 200 µm. N=3 and n=3.*

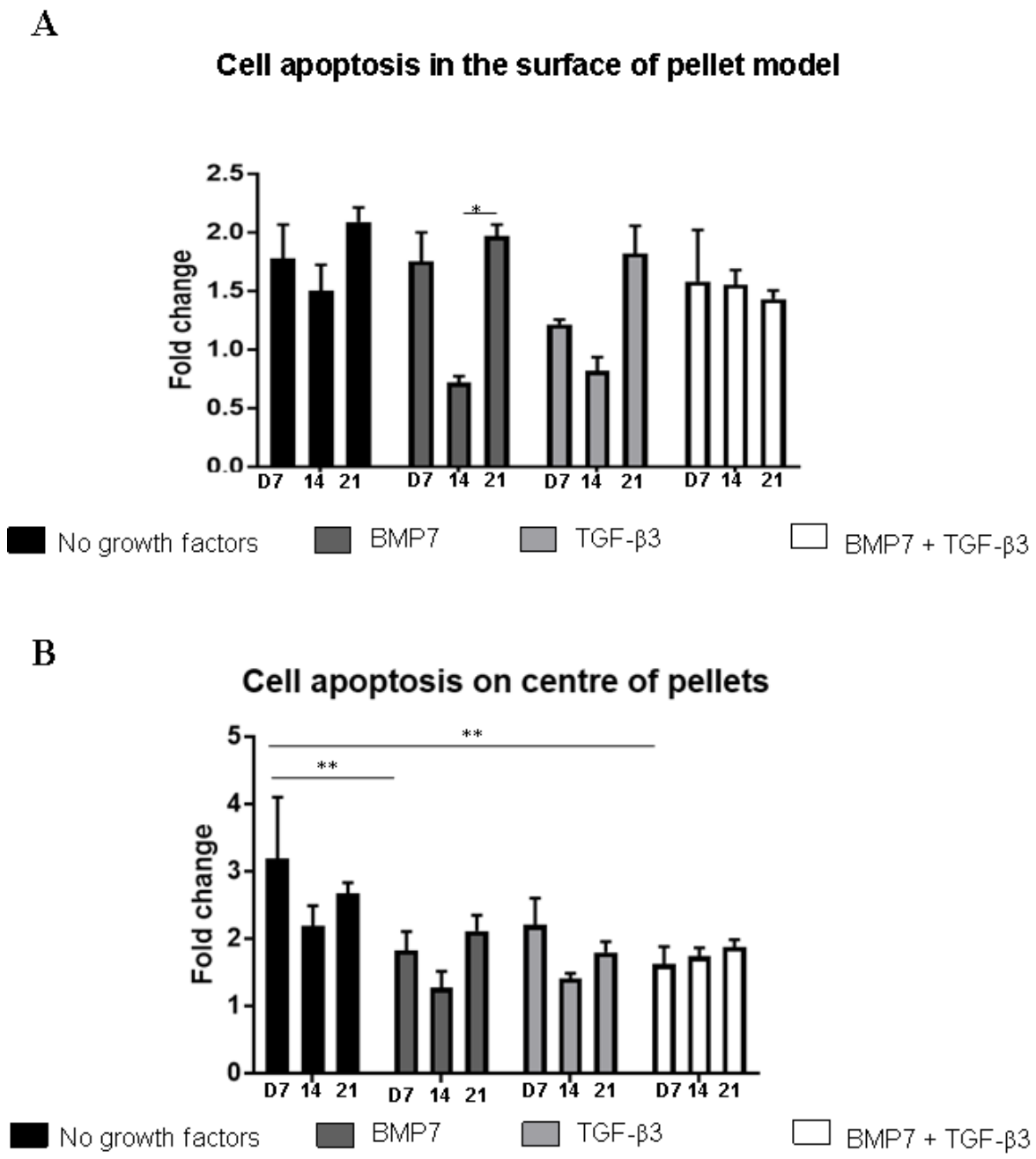

Figure 53. Cell apoptosis at the surface and centre zones and numerical data presented in graphs. *Cell apoptosis folds change of quantification with ImageJ for all conditions along the 21 days compared to day 1. Where * p<0.05, **p<0.01, ***p<0.001, and ****p<0.0001 two-way ANOVA statistical analysis. N=3 and n=3*

4.3.4 Cell proliferation and cell metabolic activity in pellets with and without growth factor supplementation

Cell proliferation and cell metabolic activity were validated using Ki67 immunohistochemistry and 3-[4,5-dimethylthiazole-2-yl]-2,5-diphenyltetrazolium bromide (MTT) assay, respectively, for all conditions during the 21 days of culture. All data were normalised to data collected after 24h of seeding (D1) and expressed as fold change (Figures 54 and 55). ImageJ was used to count the amount of proliferating (Ki67 positive) cells against total (DAPI positive) cells.

Cell metabolic activity (Figures 55A) showed significant variation when comparing in between all condition. No addition of growth factors against the addition of BMP7 and TGF-β3 resulted in a significant increase by 1.60- and 1.73-fold change ($p=0.0163$ and $p=0.003$). On day 21 when no addition of growth factors the cell metabolic activity was significantly decreased compared to an addition of TGF- β3 and both growth factors, by 1.31- and 1.59-fold change ($p=0.0392$ and $p<0.001$). Despite this, a significant increase was observed when comparing day 7 against day 21 with no supplementation, by a 1.64-fold change ($p=0.0053$).

Comparison in between the growth factor supplemented conditions showed that at day 14 adding BMP7 showed a significantly higher cell metabolic activity compared to TGF- β3 and addition of both growth factors by 0.70- and 0.59-fold change respectively ($p=0.0354$ and $p=0.0032$). Comparing TGF- β3 against supplementation of both growth factors for day 7 showed a significant decrease by 0.65- and 0.84-fold change respectively ($p=0.015$). Finally, comparison when the addition of BMP7 and TGF- β3 together showed a significant increase after 21 days of seed, by 2.31-fold change against day 7 ($p <0.0001$) and 2.44-fold change against day 14 ($p <0.0001$) (Figures 55A).

Cell proliferation quantified using Ki67 immunohistochemistry was not affected by the growth factor supplementation or the length of culture, suggesting that the increase in the pellet size seen was largely due to an increase in ECM deposition (Figures 55B).

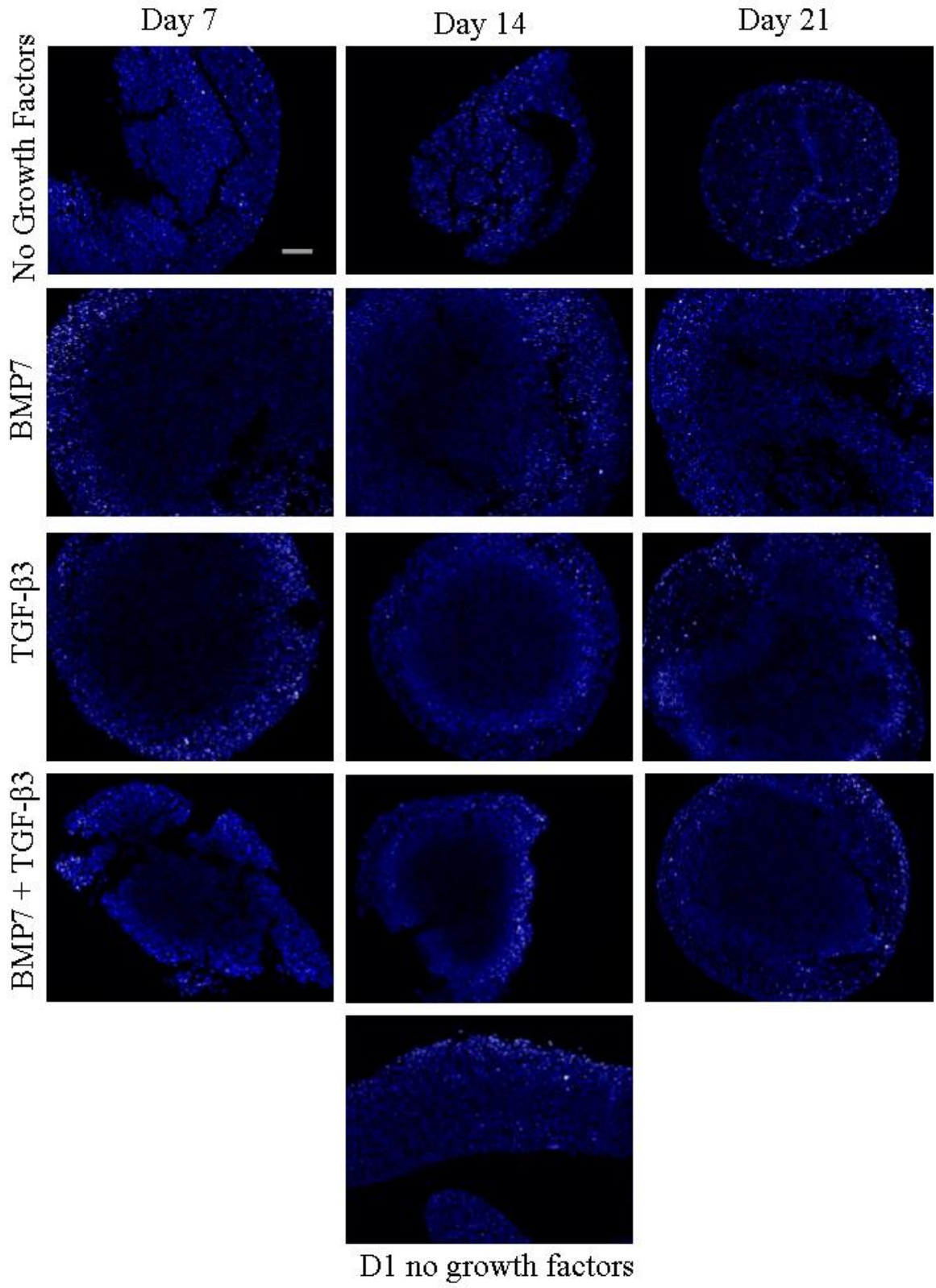

Figure 54. Immunohistochemistry for cell proliferation in all conditions after 21 days. *Pellets seeded for 21 days for ki67 staining with no addition of growth factors, BMP7, TGF-β3 and addition of both factors (BMP7 + TGF-β3). Blue staining = DAPI, nuclei staining. Yellow staining = cell proliferation. Scale bar = 200 µm. N=3 and n=3.*

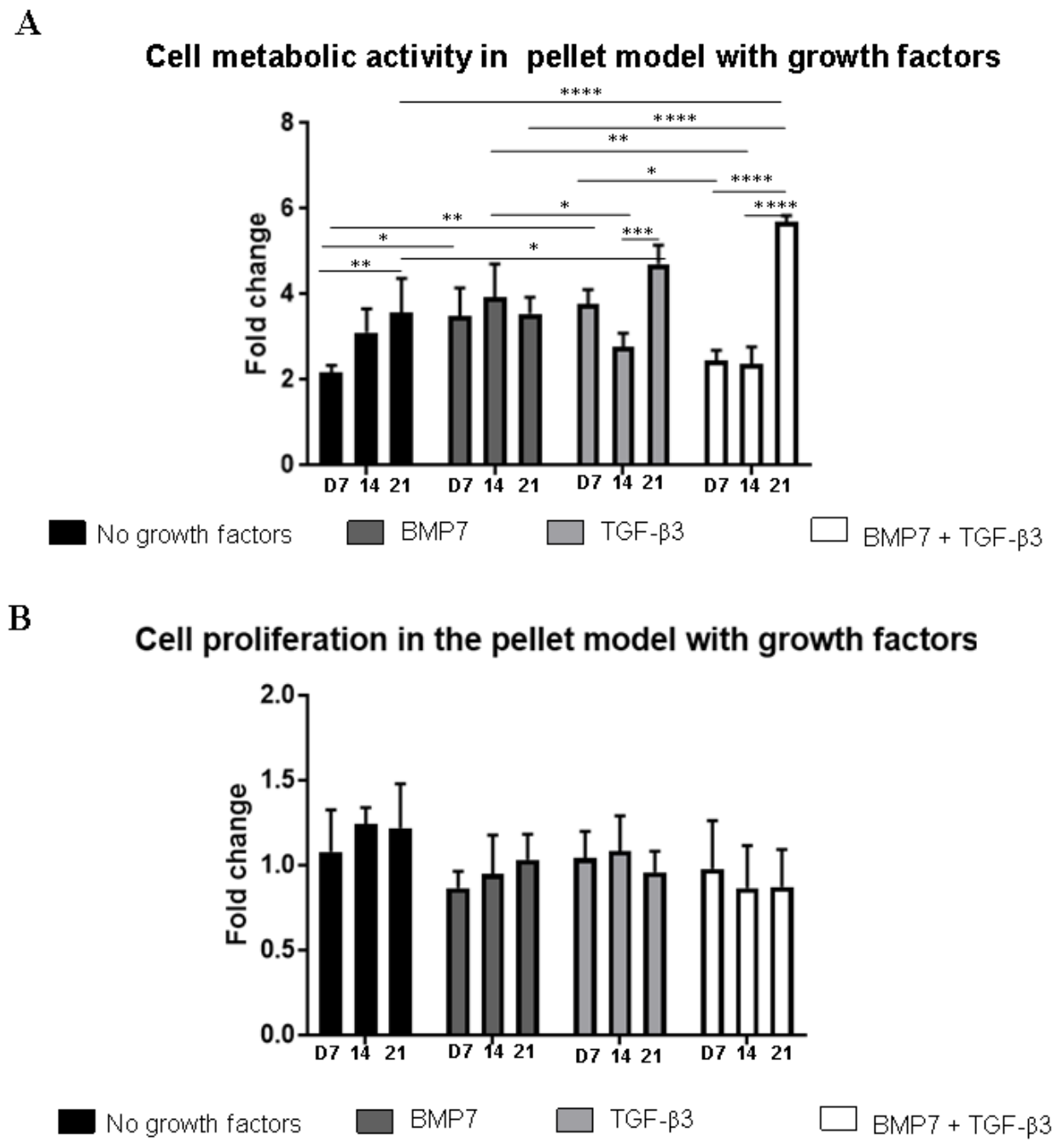

Figure 55. Cell metabolic activity and cell proliferation with its numerical data presented in graphs. (A) *Cell metabolic activity fold change compared to day 1.* ***(B)*** *Cell proliferation folds change of quantification with ImageJ for all conditions along the 21 days compared to day 1. Where * p<0.05, **p<0.01, ***p<0.001, and ****p<0.0001 two-way ANOVA statistical analysis. N=3 and n=3*

4.3.5 Gene expression in pellets with and without growth factor supplementation

Gene expression (Figure 56 A-F and Table 6) of several differentiation markers were measured using qPCR with *18S* as housekeeping gene and gene expression at day 1 was used as the baseline to verify the differentiation of the cells in the pellets. *Sox9* and *Ihh* were used as a measurement of chondrogenesis. Type II (*Col2a1*) and X (*Col10a1*) collagen and aggrecan

(*Acan*) were used as markers of healthy cartilage, and type I (*Col1a1*) collagen was used as a marker of de-differentiation and mineralisation.

Gene expression of *Sox9* (Figure 56 A) comparing no growth factors against BMP7 and TGF-β3 showed a significant increase in *Sox9* expression by 7.84- and 7.61-fold change respectively ($p=0.0048$ and $p=0.0065$) at day 7. Gene expression after 21 days significantly increased as well when comparing no addition of growth factors to supplementation of both, by 14.07-fold change ($p<0.0001$) Comparison between the supplemented conditions showed a significant increase in gene expression at day 21 when adding both growth factors, compared to BMP7, 8.63-fold change ($p<0.0001$) and TGF-β3 by 17.27-fold change ($p<0.0001$). Comparing within each condition, TGF-β3 presented a significant reduction comparing day 7 against days 14 and 21, by 0.33- and 0.22-fold change respectively ($p=0.027$ and $p=0.008$). Finally, day 21 when supplementing with both growth factors showed a significant increase when compared to day 7 by 9.74-fold change ($p<0.0001$) and day 14 by 4.93-fold change ($p<0.0001$).

Gene expression of *Ihh* (Figure 56 B) showed a significant increase when adding two growth factors against no supplementation by 153.5-fold change ($p<0.0001$), BMP7 by 5.94-fold change ($p<0.0001$), TGF-β3 by 51.11-fold change ($p<0.0001$). When comparing the gene expression within the day points when adding BMP7 and TGF-β3 simultaneously, a significant increment was observed when comparing days 7 and 14 against 21, by 15.6- and 70.8-fold change respectively ($p<0.0001$).

Expression of type II collagen (Figure 56 C) decreased in the pellets cultured without growth factor, BMP7 and TGF-β3 supplementation compared to the addition of both growth factors at day 21, by 42-, 4.6- and 22.9-fold change respectively ($p<0.0001$). When comparing within the seeding period, the addition of both growth factors showed a significant increase after 21 from day 7 by 14.8-fold change ($p<0.0001$) and by 42-fold change at day 14 ($p<0.0001$).

Potential hypertrophy in the centre of the generated cell pellets was verified by analysing type X collagen gene expression (Figure 56 D). When comparing no addition of growth factors against BMP7 and supplementation of both a significant increase of type X collagen expression was observed at day 21, by 9.65-fold change ($p<0.0001$) and by 12.85-fold change ($p<0.0001$) respectively. The highest significant variation within the supplemented conditions was found at day 21, where comparing BMP7 against TGF-β3 presented a significant reduction in the gene expression by 0.21-fold change ($p<0.0001$) whereas, if BMP7

and TGF-β3 were compared at day 21 to the addition of both growth factors, a significant increase was observed by 1.33-fold change ($p=0.0181$) and 6.11-fold change ($p<0.0001$) respectively.

When comparison was done within every condition along with the day points, no growth factors supplementation presented an initial significant increment from day 7 to day 14 by 8.11-fold change ($p<0.0001$) and a significant reduction from day 14 to day 21 by 0.14-fold change ($p<0.0001$). Adding BMP7 produced a significant increase of gene expression when comparing day 7 to days 14 and 21 by 8.15- and 10.15-fold change ($p<0.0001$). Supplementation of TGF-β3 presented an initial insignificant increase from day 7 to day 14 by 6-fold change ($p<0.0001$) and a decrease by 0.29-fold change ($p<0.0001$) comparing day 14 to day 21. Finally, the addition of both growth factors led to a significant increase of gene expression from day 7 to 14 and 21 by 5.88- ($p=0.0006$) and 14.27-fold change respectively ($p<0.0001$). A significant increase was also accounted for from day 14 to 21by 2.42-fold change ($p<0.0001$).

Type I collagen gene expression (Figure 56 E) was highly increased especially without the addition of growth factors. A significant decrease was visible at day 14 when comparing no growth factors against BMP7, TGF-β3 and both growth factors by 0.47-, 0.21- and 0.01-fold change respectively ($p<0.0001$). When comparison was done for the same day point but within the supplemented conditions, a significant reduction in gene expression was observed when comparing BMP7 against TGF-β3 by 0.44-fold change ($p=0.0043$) and against the addition of both growth factors by 0.03-fold change ($p<0.0001$). On day 14 TGF-β3 also presented a significant reduction in gene expression compared to supplementation of both growth factors by 0.07-fold change ($p=0.039$).

A significant decrease was visible at day 21 when comparing no growth factors against BMP7, TGF-β3 and both growth factors by 0.101-, 0.136- and 0.035-fold change respectively ($p<0.0001$). When comparison was done for the same day point but within the supplemented conditions, a significant increase in gene expression was observed when comparing BMP7 against TGF-β3 by 1.34-fold change ($p=0.0043$) and against the addition of both growth factors by a significant decrease 0.34-fold change ($p<0.0001$). On day 21 TGF-β3 also presented a significant reduction in gene expression compared to supplementation of both growth factors by 0.257-fold change ($p=0.039$).

When comparison was done within every condition along with the day points, no growth factors supplementation presented an initial significant increment from day 7 to day 14 by 48.78-fold change ($p<0.0001$) and from day 7 to day 21 by 51-fold change ($p<0.0001$). Adding

BMP7 produced a significant increase of gene expression when comparing day 7 to days 14 by 15.94-fold change ($p<0.0001$) and a significant decrease comparing day 14 against 21 by 0.22-fold change ($p<0.0001$).

Finally, aggrecan expression (Figure 56 F) was analysed as a marker of the GAG deposition in the ECM. The gene expression for aggrecan (*Acan*) was significantly increased when comparing no addition of growth factors against TGF-β3 by 3.07-fold change ($p=0.045$) and by 3.2-fold change ($p=0.029$) against the addition of both growth factors. When comparison was done within every condition along with the day points, no growth factors supplementation presented a significant decrease by 0.35-fold change comparing day 7 against 14 ($p=0.048$). In the case of the addition of TGF-β3, a significant decrease was also observed comparing days 14 against 21 by 0.39-fold change ($p=0.0483$). The only condition that presented a significant increase along the incubation period was when supplementing with both growth factors, in which day 21 presented an increase by 4.28- and 2.37-fold change against days 7 and 14 respectively ($p<0.0001$).

		Sox9	***Ihh***	***Col2a1a***	***Col10a1***	***Col1a1***	***Acan***
No growth factors	Day7	↓	↓	↓	↓	↓	↓
	Day14	↓	↓	↓	↑	↑	↓
	Day21	↓	↓	↓	↓	↑	↓
BMP7	Day7	↔	↓	↓	↓	↓	↓
	Day14	↓	↓	↓	↑	↑	↓
	Day21	↓	↑	↓	↑	↓	↓
TGF-β3	Day7	↔	↓	↓	↓	↓	↓
	Day14	↓	↓	↓	↑	↓	↓
	Day21	↓	↓	↓	↓	↓	↓
BMP7 + TGF-β3	Day7	↓	↓	↓	↓	↓	↓
	Day14	↓	↓	↓	↔	↓	↓
	Day21	↑	↑	↑	↑	↓	↓

Table 6. Table summarising the outcome of the gene expression *of Sox9, Indian hedgehog (Ihh), collagen II (Col2a1), collagen X (Col10a1), collagen I (Col1a1) and aggrecan (Acan) after 21 days of culturing ATDC5 in a pellet culture compared to day 1 gene expression. N=3 and n=3.*

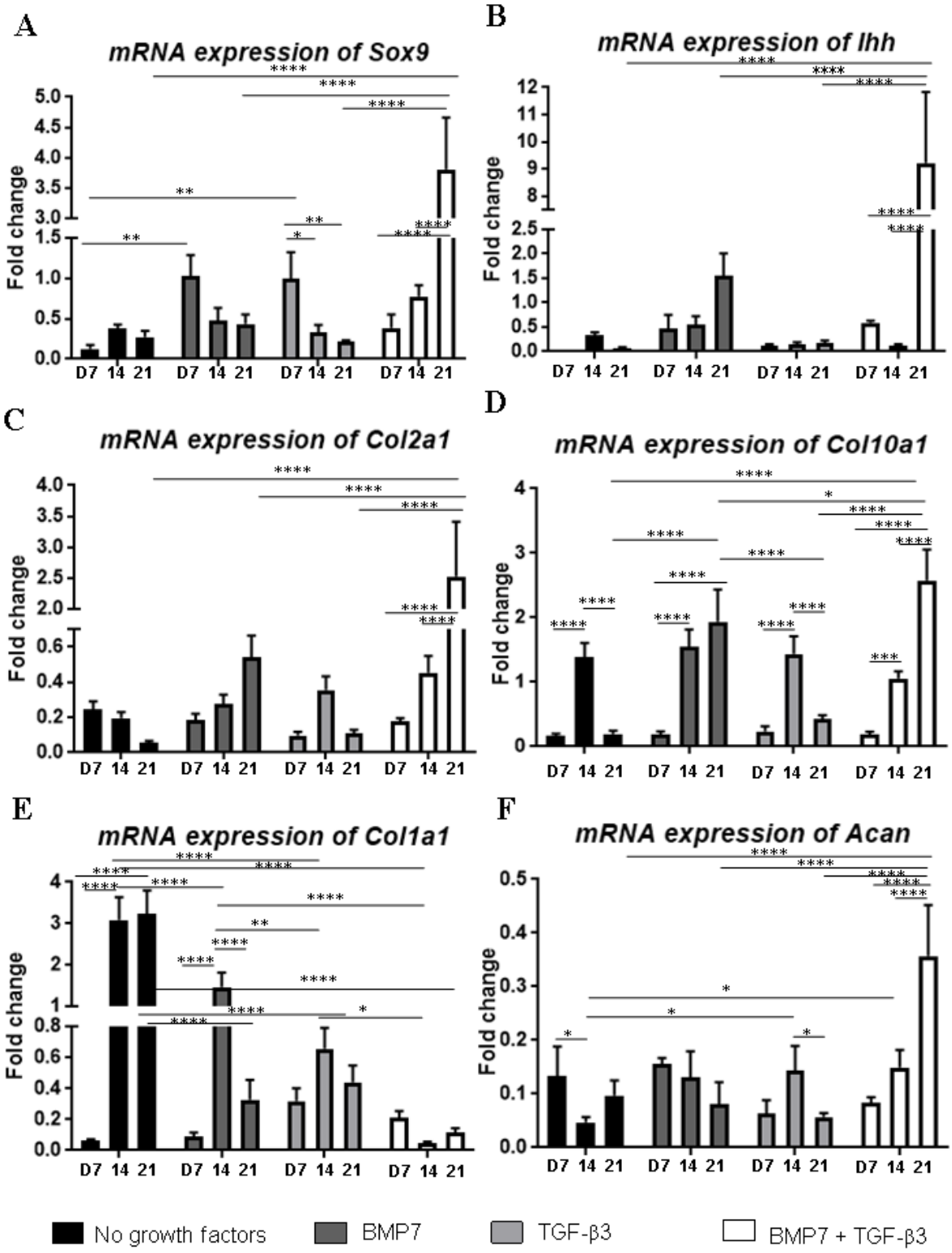

Figure 56. mRNA expression of cartilage differentiation markers in ATDC5 pellets cultured for 21 with growth factor supplementation. *Gene expression of Sox9* ***(A)****, Indian hedgehog (Ihh)* ***(B)****, type II collagen (Col2a1)* ***(C)****, type X collagen (Col10a1)* ***(D)****, type I collagen (Col1a1)* ***(E)****, aggrecan (Acan)* ***(F)*** *were measured using relative expression quantification and normalised to day 1 Where * p<0.05, **p<0.01, ***p<0.001, and ****p<0.0001 two-way ANOVA statistical analysis. N=3 and n=3.*

4.4 Discussion

Work presented in this chapter assessed the differences in the gene expression and extracellular matrix deposition in ATDC5 cells seeded in 3-dimensional pellet culture with and without growth factor supplementation, in comparison to the conventional 2D model. Four conditions were studied, no additional growth factors, the addition of 10 ng/ml of BMP7, 10ng/ml of TGF-β3, and both growth factors (BMP7 + TGF-β3) at 10 ng/ml after 24h (day 1) of culture.

Pellet culture is considered a gold-standard model widely used to re-establish and maintain chondrogenic differentiation after the expansion of primary chondrocytes in monolayer (Rahul S. Tare *et al.*, 2005). This system has been employed for chondrocytes, stem cells and ATDC5 cells in the past (Rahul S. Tare *et al.*, 2005; Watts, Ackerman-Yost and Nixon, 2013; Montagne, Furukawa and Ushida, 2019). ATDC5 cells seeded in pellet culture are a versatile model that could be used to study the effect of hypoxic conditions on chondrogenesis (Rahul S. Tare *et al.*, 2005), the effects of drugs and molecules on mechanically induced damaged cells (Montagne, Furukawa and Ushida, 2019) and even the process of endochondral ossification or chondrogenic differentiation (Weiss *et al.*, 2012; Kudva, Luyten and Patterson, 2018).

Cells were initially seeded at $5x10^5$, $1x10^6$ and $2x10^6$ per ml; however, the concentration that resulted in the formation of a rounded pellet with maintained integrity was $5x10^5$ of cells per ml. Interestingly, differences in cell density in the literature varied from $5x10^5$ cells (Rahul S. Tare *et al.*, 2005), to $8x10^5$ cells (Lewis *et al.*, 2016), $1x10^6$ cells (Weiss *et al.*, 2012) and $2x10^6$ cells per ml (Watts, Ackerman-Yost and Nixon, 2013). The cell density used in Watts *et al*. was intended for MSC pellets, and therefore variation between the size of MSC and ATDC5 cells could have led to instability when forming a solid pellet (Watts, Ackerman-Yost and Nixon, 2013). Another pellet model that used ATDC5 cells did not show integrity which could be a result of different media supplementation, with dexamethasone and TGF-β1 (Weiss *et al.*, 2012)

A wide variation in growth factors used in chondrogenic pellet culture in literature made the choice of parameters for this study difficult (Shukunami C, Ohta Y, Sakuda M, 1998; Han *et al.*, 2005). Moreover, several studies pointed out the beneficial effect of combining various growth factors to aid chondrogenesis (Shen *et al.*, 2009; Shintani, Siebenrock and Hunziker, 2013; Huang *et al.*, 2018). Type X collagen is associated with hypertrophy and mineralisation linked to chondrocyte maturity in the growth plate, and the mineralised zone in the articular

cartilage (Fox, Bedi and Rodeo, 2009; Caron et al., 2012) and type II collagen is the main component of the cartilage ECM (Fox, Bedi and Rodeo, 2009). BMP7 has previously been shown to prevent hypertrophy and maintain cell phenotype in ATDC5 cell culture (Caron *et al.*, 2013), and TGF-β3 has been shown to increase ECM deposition of type II collagen and maintained chondrogenesis phenotype in pellets (Huang *et al.*, 2004). Both growth factors have been tested in different studies (Asahina, Sampath and Hauschka, 1996; Caron *et al.*, 2013; Zhai, Yao and Wang, 2013; Wang *et al.*, 2014; Yao, Zhai and Wang, 2014; Scarfì, 2016).

The model supplemented with BMP7, and both growth factors gave a progressive increase in the ATDC5 cell pellet area along the 3 weeks of culture, indicating that the cells were synthesising ECM. ATDC5 cells showed an increase in proteoglycan deposition and synthesis when grown in the pellet culture and supplemented with growth factors. Interestingly, there was an increase in sGAG deposition in pellets cultured in the presence of BMP7 or both growth factors compared to the pellets grown in a non-supplemented growth medium. The sGAG appeared to be mainly deposited in the centre of the pellets and faintly in the other zones. Moreover, aggrecan (*Acan*) gene expression showed a highly significant increase in pellets cultured with both growth factors, supporting previously discussed benefits when combining growth factors to support chondrogenesis (Huang *et al.*, 2018). High levels of proteoglycan synthesis have been already shown in the ATDC5 pellet model that developed aggrecan deposits after 21 days of seeding (Wu *et al.*, 2017a; Tare *et al.*, 2018). It has also been shown that seeding MSC in a pellet culture increased sGAG deposition, and specifically, the concentration of $5x10^5$ cells per ml showed the highest aggrecan gene expression (Watts, Ackerman-Yost and Nixon, 2013). Interestingly, MSC pellets cultured with TGF-β3 showed higher aggrecan expression, similar to what was found in supplemented ATDC5 pellets in this study (Huang *et al.*, 2004).

Collagen synthesis in the ATDC5 pellets was analysed using Picrosirius Red staining. It showed a higher deposition of collagen fibres on the surface of the pellets, especially in the presence of both growth factors and TGF-β3 alone after 3 weeks of culture or in the presence of BMP7 after 2 weeks of culture. This observation correlated with the area of the pellets. In the pellets cultured with no additional growth factors, collagen deposition was limited to the surface at day 7 mainly, and the distribution became more homogenous through the pellet after 21 days of culture. Collagen synthesis in the pellets was verified by analysing gene expression. Interestingly, type II (*Col2a1*) and X (*Col10a1*) collagens were upregulated in all pellets when compared to the other day points, especially pellets cultured with both growth factors. This was further confirmed by immunohistochemistry, which showed type II collagen mainly at the

surface of the pellets which is comparable to the expression of these collagens in native cartilage (Fox, Bedi and Rodeo, 2009). Other studies of pellets of ATDC5 cells have also shown deposition of type II collagen with variations in its distribution (Wu *et al.*, 2017b; Tare *et al.*, 2018; Montagne, Furukawa and Ushida, 2019). Interestingly, in one study, the pellet became hypertrophic, *Sox9* expression decreased simultaneously with an upregulation in *Col10a1* expression (Tare *et al.*, 2018). In this study, culturing the pellets in the presence of BMP7 followed a similar pattern, in contrast, when the pellets were cultured with both growth factors, both *Sox9* and *Col10a1* expression increased concurrently, and both genes were downregulated in pellets growth with TGF-β3 and no growth factor supplementation. *Sox9* expression is a marker of immature chondrocytes in the early stages of chondrogenesis, whereas *Col10a1* expression is a hallmark of hypertrophy and maturation of chondrocytes (Leung *et al.*, 2011). Both genes were simultaneously upregulated in the pellets grown in the combination of growth factors, potentially reflecting the zonal stratification of the pellet with an area of immature chondrocytes, and cells in the deeper zones transitioning into hypertrophy. IHH is a marker of pre-hypertrophic and hypertrophic chondrocytes (Mariani and Martin, 2003), and increased expression of *Ihh* has been linked to late stages of OA and chondrocyte hypertrophy (Wei *et al.*, 2012; Thompson *et al.*, 2015). However, another study suggests that upregulation of *Ihh* alone cannot produce degradation of ECM (Thompson *et al.*, 2015). Interestingly, Ihh gene expression was highly upregulated at day 21 in pellets cultured with both growth factors, suggesting the development of hypertrophy. This was further confirmed by a decrease in type I collagen expression in pellets cultured with both growth factors (Lahm *et al.*, 2010). Interestingly, type I collagen (*Col1a1*) expression was highly upregulated in pellets grown without growth factor supplementation, which could be an indication of a loss of the phenotype, an OA-like dedifferentiation, or fibrosis (Lahm *et al.*, 2010; Vinatier and Guicheux, 2016).

Interestingly, cell metabolic activity was only increased in pellets grown with added TGF-β3 or with both growth factors. Variations in cell proliferation within day points or conditions were not significant, indicating that potentially the cells going through hypertrophy were not as many, since an increase in proliferation has been linked to the process of maturation and hypertrophy in chondrocytes (Bohme *et al.*, 1992). Ki67 immunohistochemistry showed the majority of the proliferating cells localised on the surface area of the pellets. Cells in this area of the pellet were subjected to a hydrostatic pressure every day during the media change, visibly modifying their rounded morphology into a flatter shape, resembling chondrocytes on the surface in articular cartilage (Fox, Bedi and Rodeo, 2009). Cartilage is exposed to many mechanical stimuli, and hydrostatic pressure is one of the important forces in native cartilage

(Elder and Athanasiou, 2009). It is interesting to hypothesise that the chondrocytes on the surface of the pellets are more immature and, being exposed to the hydrostatic pressure, develop a higher turnover capacity, thus increasing their proliferative activity.

Finally, the cell apoptosis was analysed using TUNEL assay and showed an increase at the surface of the pellet after 21 days of culture in pellets cultured with BMP7 or TGF-β3 alone. Apoptosis levels were not affected in pellets cultured without growth factor supplementation or with both growth factors together. Cell apoptosis was higher in the centre of the pellets compared to the surface, which may be correlated with increased cell apoptosis. An increase in cell apoptosis in the centre of the pellet and a decrease in ECM deposition have been reported previously (Dashtdar *et al.*, 2016; Lewis *et al.*, 2016). Some studies suggest that the increased cell death in the centre of the pellets may be due to hypertrophy and cell death resembling the events seen during endochondral ossification (Dashtdar *et al.*, 2016), while others link it to a nutrient deficiency or hypoxia (Lewis *et al.*, 2016).

One of the main goals of tissue engineering is to mimic native tissue *in vitro*, including the zonal stratification, which is impossible to achieve in monolayer (Bhumiratana and Vunjak-Novakovic, 2015). Pellet culture is easily reproducible and can reproduce the development of cartilage tissue, matrix synthesis and turnover, and allow the study of the effect of growth factor supplementation, and other pro-anabolic stimuli (Lübke *et al.*, 2005). ATDC5 cells cultured in pellets with a combination of BMP7 and TGF-β3 developed a stratified-like tissue similar to articular cartilage *in vivo* (Huang *et al.*, 2018).

Chapter 5. Development and Characterisation of a 3-Dimensional Zonally Stratified Hydrogel Model of Cartilage Using ATDC5 Cells and Growth Factor Supplementation

5 Development and characterisation of a 3-dimensional zonally stratified model of cartilage using ATDC5 cells and growth factor supplementation.

5.1 Introduction

Monolayer cultures were historically used as a model of cartilage differentiation due to their inexpensive, homogeneous distribution of nutrients and growth factors, simplicity and high proliferation rate (Duval *et al.*, 2017). However, expansion of the cartilage cells in monolayer (2D) results in dedifferentiation and loss of the chondrocyte phenotype (Benya and Shaffer, 1982), affecting the shape, development of stress fibres and the cytoskeleton (Archer, Rooney and Wolpert, 1982) and the gene profile expression, with an increase in type I and X collagen expression and a reduction in the synthesis of type II collagen and aggrecan (Schnabel *et al.*, 2002). These issues can be reversed using 3-dimensional (3D) approaches, such as pellet cultures explored in Chapter 4 and the use of scaffolds that mimic the cartilage environment. Moreover, growth factor and co-factor supplementation can improve the maintenance of the chondrogenic potential and chondrocyte phenotype *in vitro* (Caron *et al.*, 2012; Duval *et al.*, 2017)

Scaffolds and hydrogels provide a micro-environment for the cells that can affect gene expression, modify the phenotype, cytoskeletal organisation, ECM deposition, proliferation and affect mechanical properties (Zhang, Yang, Li, Dou, Li, Thote, D. A. Wang, *et al.*, 2013). 3-dimensional scaffolds are often used to replicate the conditions and interactions found in tissues *in vivo* (Duval *et al.*, 2017). Some of these methods have been well-established and popularised to support chondrogenesis, such as bioreactors, for larger-scale culture, and hydrogels (Duval *et al.*, 2017).

In a study comparing two different 3-dimensional models to the monolayer model, dedifferentiated human primary chondrocytes were allowed to re-differentiate between 14 and 28 days and have been shown to maintain their phenotype, producing high amounts of type II collagen, aggrecan and SOX9. In contrast, monolayer culture induced the synthesis of type X collagen, ALP and RUNX2, markers of hypertrophy and mineralisation associated with chondrocyte maturity, showing how the 3D model allowed the maintenance of phenotype and replicate closely the behaviours *in vivo* (Caron *et al.*, 2012).

Hydrogels have been used widely in the development of chondrogenic models (Schuh *et al.*, 2010). A study comparing different scaffolds showed that hydrogels maintain the chondrogenic phenotype keeping their high expression of type II collagen, aggrecan and *Sox9*,

high proliferation rates, and lower synthesis of type I collagen. However, other scaffolds such as sponges, due to their micro-fibrous character, increase cells attachment promoting the fibroblast-like morphology, the loss of phenotype, increased proliferative rates and the increase in type I collagen expression (Zhang, Yang, Li, Dou, Li, Thote, D. A. Wang, *et al.*, 2013).

One of the first hydrogels that were shown to reverse the dedifferentiation of chondrocytes *in vitro* was agarose (Benya and Shaffer, 1982). This hydrogel comes from a natural source and consists of polysaccharide. Agarose is considered a bio-inert scaffold; it does not interact with or affects, the cells. Despite the fact that chondrocytes are unable to turn over agarose, agarose constructs support chondrogenesis and maintain the cell phenotype better than other polymers such as type I collagen, alginate, fibrin and polyglycolic acid (Benya and Shaffer, 1982; Jacek *et al.*, 2018). Due to the negatively charged matrix in the assembled hydrogel, agarose resembles proteoglycans in the native cartilage tissue and its high water content and hydrophilic nature increase the diffusion of nutrients and waste, enhancing the cell performance depositing ECM (Jacek *et al.*, 2018). Agarose hydrogels have been used as a model to study chondrogenic induction, proliferation and differentiation of stem cells and cell lines (Thompson, Piez and Seyedin, 1985); however, they have never been used with ATDC5 cells before.

5.2 Aims of the chapter

This chapter aimed to develop a 3D *in vitro* system that replicates the zonal stratification observed *in vivo* in articular cartilage, using ATDC5 cells in a hydrogel culture, to further the understanding of inter and intramolecular signalling in developing and diseased cartilage.

5.3 Results

5.3.1 Selection of optimal hydrogel scaffold

As mentioned previously, hydrogels offer an environment similar to the native tissue avoiding the formation of 2-dimensional microenvironments found in sponges and fibres that can lead to dedifferentiation. Several hydrogels were therefore tested in order to develop a 3-dimensional *in vitro* model comparable to articular cartilage using commercially available ATDC5 cells. According to the literature, the most commonly used hydrogels in cartilage tissue engineering are low gelling temperature agar, and collagen or GAG derivate scaffolds.

One million ATDC5 cells per ml were seeded in HyStem®-C Cell Culture Scaffold, Matrigel® and low gelling temperature agarose hydrogels (Figure 57.A). HyStem®-C Cell Culture Scaffold and Matrigel® hydrogels were made up by mixing the solution purchased 1:1 (v/v) with dH_2O, while in the case of low gelling temperature agarose, 1% (w/v) of the powder was mixed with dH_2O (for more information refer to the Materials and Methods section of the thesis).

Matrigel® and HyStem®-C Cell Culture Scaffold have been previously shown to mimic properties of the native tissue; however, despite presenting a thicker and denser ECM surrounding the cells, the constructs made with both hydrogels were brittle and shrunk after 21 days of culture (Figure 56.A). In contrast, low gelling agarose presented an uneven distribution of clusters and cells (Figure 57.A). However, the agarose hydrogel did not appear to support interterritorial matrix deposition, and the cell distribution was much denser in the mouse articular cartilage (positive control) (Huang *et al.*, 2004, 2018; Thorpe *et al.*, 2013).

To further verify whether the low gelling point agarose could maintain the chondrocyte phenotype human adult chondrocytes (Sigma Aldrich) were grown in 1% agar constructs at 1 million cells per ml (Figure 57.B). Similar to the ATDC5 cells, the chondrocytes showed a pericellular matrix deposition. The differentiation profile of the cells was verified using quantitative RT-PCR (Figure 57.B). In this case, the cells gene expression was expressed by fold change, using as a baseline the expression after seeding the cells on the hydrogel. The upregulation of *SOX9*, *IHH*, *COL2A1* and *ACAN* showed that the cells maintained their phenotype. However, due to the costs of primary cells required for further optimisation of the model, ATDC5 cells were chosen for further studies in this chapter.

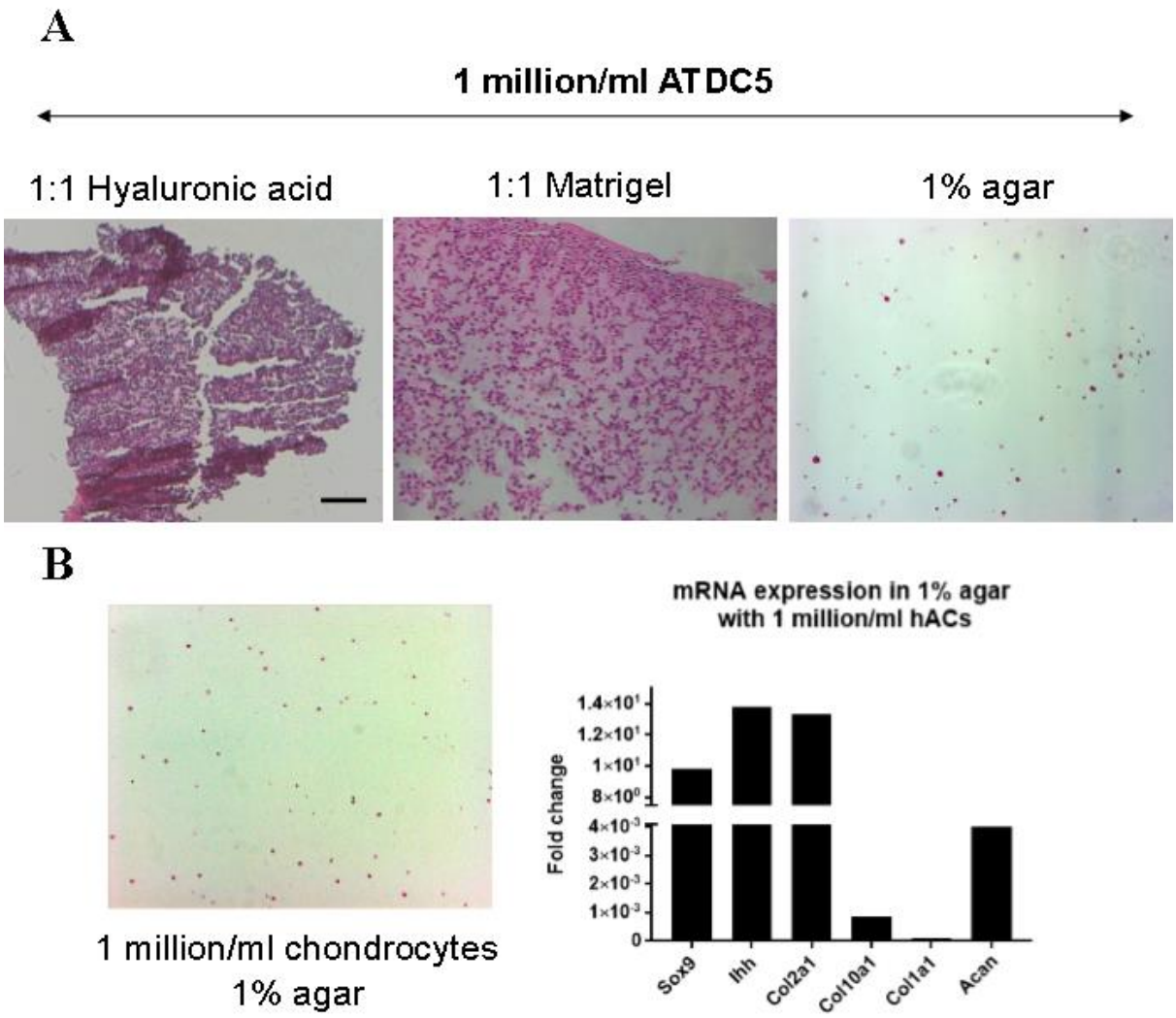

Figure 57. Histological analysis of hydrogels HA/Gelatin, agar and matrigel at day 21. *1 million ATDC5 cells per ml cultured after 21 days on HyStem®-C Cell Culture Scaffold, 1% agarose and 1:1 Matrigel® were stained with haematoxylin-eosin staining (H+E) being purple the nuclei, and pink the ECM. Scale bar=200µm. N=2.* ***(A)*** *Human adult chondrocytes seeded at a density of 1 million per ml in 1% of low gelling temperature agarose for 21 days, haematoxylin-eosin staining was performed, and gene expression of Sox9, Ihh, type II, I and X collagen and aggrecan were analysed using RT-PCR to assess chondrogenesis and maintenance of the phenotype. Scale bar=200µm. N=1. Where * p<0.05, **p<0.01, ***p<0.001, and ****p<0.0001 two-way ANOVA statistical analysis.* ***(B)***

5.3.2 Optimisation of the low gelling temperature agarose hydrogel at a different cell and hydrogel densities

To further optimise the model, a different range of cell densities and agar percentages were tested for 21 days in low gelling temperature agar (Figure 58).

Haematoxylin-eosin staining of the models showed that 2% agarose with either 1 or 2 million cells per ml produced big clumps of cells surrounded by randomly distributed cells and not a zonally stratified model. In contrast, 1% of agarose constructs were closer to the zonally stratified organisation resembling native tissue. The middle zone of the hydrogel presented a more random distribution of the clusters and the bigger clusters of cells appear to be deposited

in the deep zone arranged in columnar orientation, these results correlate with the area of clusters per zone (Figure 58B).

The area of cluster per zones was measure via Image J, when comparison was done for the same area of the scaffold but within the different conditions, a significant increase in cluster area was observed at the surface when comparing the addition of 2% agar with 2 million/ml cells against 1% agar with 1 or 2 million cells/ml by 1.73-fold change ($p=0.0008$) and by 1.52-fold change ($p=0.007$) respectively. In the middle zone, the scaffold seeded with 2% agar with 2 million/ml cells showed significantly increased cluster area compared to 1% agar with 1 or 2 million cells per ml and 2% agar with 1 million cells per ml, by 1.4- ($p=0.044$), 1.4- ($p=0.043$) and 1.76-fold change ($p=0.0015$) respectively. The deep zone showed a significant increase of clusters area when comparing the scaffold seeded with 2% agar and 1 million/ml cells against 1% agar with 1 or 2 million cells per ml, by 3.16-fold change and 3.20-fold change ($p<0.0001$) and a significant decrease in the area when comparing 2% agar with 2 million per ml cells against 2% agar with 1 million/ml cells by 0.39-fold change ($p<0.0001$). Comparing within each scaffold but different zones showed a significant reduction of clusters area when adding 2% agar with 1 million cells per ml when comparing middle zone against the surface zone by 0.68-fold change ($p=0.0409$), however, when comparing the deep zone against the surface and middle a significant increase was observed by 2.95-fold change and 4.32-fold change respectively ($p>0.0001$).

Further histological analysis was performed in the 1% agar constructs seeded with 2 million cells per millilitre as these showed the most potential for zonal stratification. Picrosirius Red (Figure 58C) and toluidine blue (Figure 58D) staining for collagen and GAG respectively were performed and showed that the ECM was synthesised in the model and deposited within the cell clusters pericellularly.

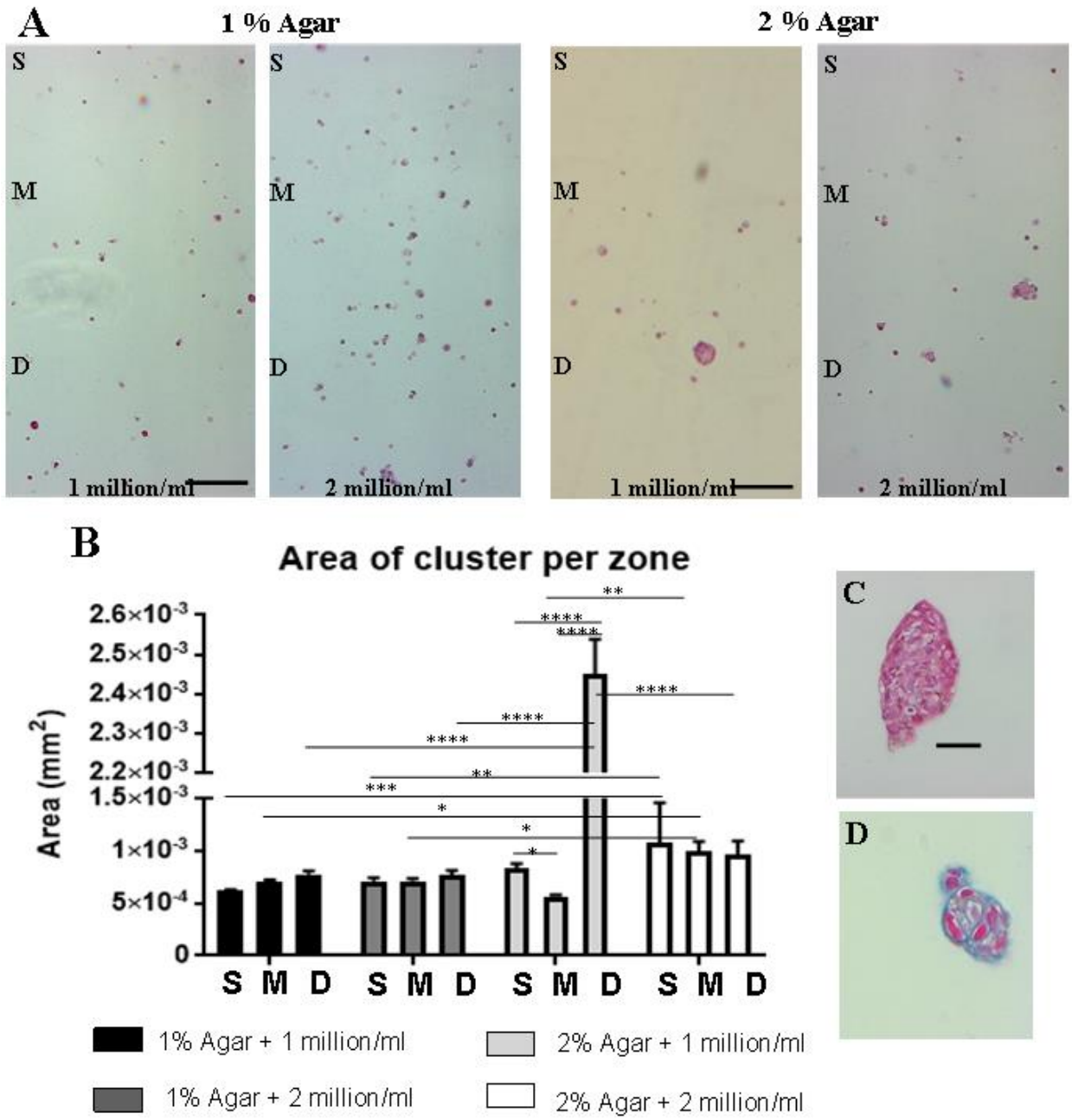

Figure 58. Histological analysis for the different cell and gel densities and study of the area of clusters per zone at day 21. ***A)*** *Haematoxylin-eosin staining of the 3D agar models at different cell densities and different agarose content at day 21. Scale bar=200µm. N=3 and n=3.* ***B)*** *Area of the clusters per zone (superficial, Middle, and Deep layer) at 21 days for all conditions, S=Surface zone, M= Middle zone, D=Deep zone. Where * p<0.05, **p<0.01, ***p<0.001, and ****p<0.0001 two-way ANOVA statistical analysis.* ***C)*** *Picrosirius Red staining (collagen) at day 21 when supplementing with both growth factors. Scale bar=50µm.* ***D)*** *Toluidine blue staining (sulphated proteoglycans) with nuclear fast red counterstain at day 21 when supplementing with both growth factors. Scale bar=50µm. N=3 and n=3.*

Despite the adequate cluster arrangement in the 1% constructs compared to 2%, due to the lack of ECM deposits, further optimisation was required. Cell number was therefore increased to 10 million per ml to improve ECM deposition.

The constructs with 10 million cells per ml in 1% agarose showed areas of cell clusters and localised tissue nodule formation (arrows in Figure 59A) compared to the models with lower cell density. Moreover, the model presented with a more discernible column-type arrangement

(rectangular boxes on Figure 59A) of the cells in the deep zone, resembling a 1-week-old femoral head from a mouse (in rectangular boxes). To further confirm the increase of the area of cellular clusters ImageJ measurements of area extrapolated to mm^2 were carried out (for more information refer to Materials and Methods section).

The area of cluster per zones was measure via Image J, when comparison was done for the same area of the scaffold but within the different conditions, a significant increase in cluster area was observed at the surface when comparing the addition of 1% agar with 1 million/ml cells against 1% agar with 10 million cells/ml by 1.77-fold change ($p=0.041$). In the middle zone, the scaffold seeded with 1% agar with 10 million/ml cells showed significantly increased cluster area compared to 1% agar with 1 or 2 million cells per ml by 2.17-fold change ($p=0.0006$) and 2.17-fold change ($p=0.0006$) respectively. The deep zone showed a significant increase of clusters area when comparing the scaffold seeded with 1% agar and 10 million/ml cells against 1% agar with 1 or 2 million cells per ml, by 4.56-fold change and 4.62-fold change ($p<0.0001$). Comparing within each scaffold but different zones showed a significant reduction of clusters area when adding 1% agar with 10 million cells per ml when comparing the deep zone against the surface and middle a significant increase was observed by 3.21-fold change and 2.28-fold change respectively ($p>0.0001$).

Despite this, in all cases, the ECM deposition was pericellular and did not recapitulate the complex interterritorial ECM found in a 1-week-old mouse femoral head suggesting further optimisation was required.

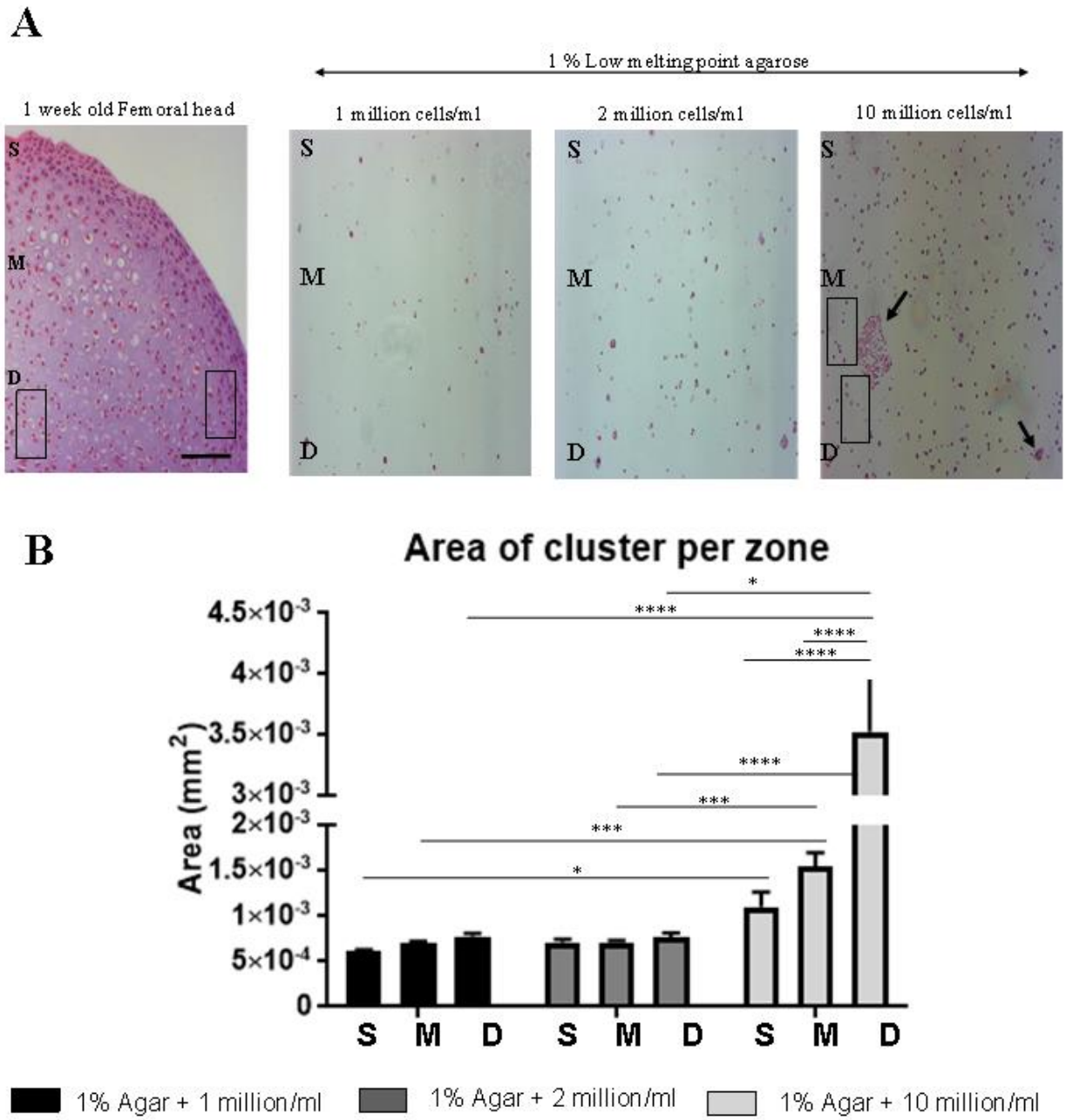

Figure 59. Histological analysis of a 1-week-old femoral head, and 1% constructs at different cell concentrations and clusters area analysis for all conditions and zones. (A) *Haematoxylin-eosin staining was performed in the femoral head from a 1-week-old mouse and in all three different constructs of 1% hydrogel seeded with either 1, 2 or 10 million ATDC5 cells per ml. Scale bar=100µm. N=3 and n=3. S=Surface zone, M= Middle zone, D=Deep zone.* ***(B)*** *Area of the clusters per zone (Surface, Middle, and Deep zones) for 21 days for all conditions, 1% agarose with 1 million, 2 million and 10 million cells per ml where * p<0.05, **p<0.01, ***p<0.001, and ****p<0.0001 two-way ANOVA statistical analysis. S=Surface zone, M= Middle zone, D=Deep zone. N=3 and n=3.*

5.3.3 Cell morphology differences between the ATDC5 cells in the 2-dimensional model compared to the optimised low gelling temperature agarose hydrogel.

A visual comparison of the morphology of the cells seeded in a 2-dimensional model compared to the cell-seeded in the 3-dimensional 1% agar model was performed by taking bright-field microscope images at each day point of the chondrogenesis protocol (Figure 60A).

The cells seeded in a monolayer showed an elongated morphology at day 7 (Figure 60B), with fusiform (arrows), fibroblast-like shape. In contrast, in the 3-dimensional model (1% agarose at a density of 10 million cells per ml) the cells showed rounded morphology, suggesting that the cells in hydrogel retained their chondrogenic phenotype (arrows).

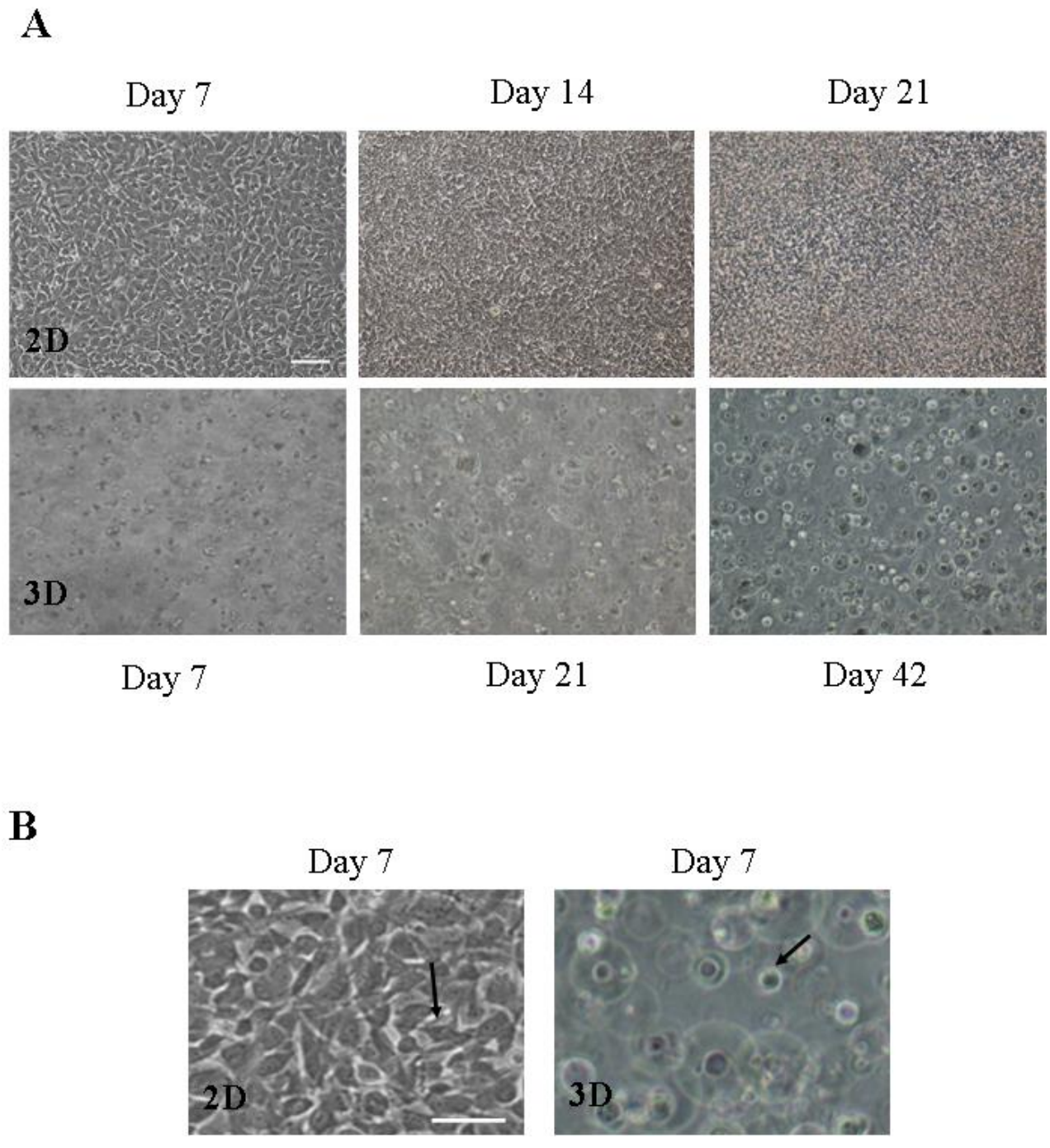

Figure 60. Bright-field images comparing seeding ATDC5 cells in 2-dimensional models and hydrogel 3-dimensional models. A) *Bright-field images of the cells at day 7, 14, and 21 (seeded at a density of 12,000 per ml for the 2-dimensional model) compared to day 7, 21 and 42 in 1% agarose at 10 million cells per ml. Scale bar=100µm B) Bright-field images of the cells at day 7 with ATDC5 seeded at a density of 12,000 per ml for the 2-dimensional model compared to 1% agarose at 10 million cells per ml. Arrows are pointing out to the elongated cells and the rounded shape cells. Scale bar=100µm. N=3 and n=3.*

5.3.4 ECM deposition in agar hydrogel with and without growth factor supplementation

Based on the data obtained in Chapter 4, growth factor treatment was added in order to improve the ECM production in the hydrogel constructs. Previous studies have suggested that the addition of growth factors to damaged tissue decreases the timeframe of repair, greatly increasing the secretion of matrix proteins. BMP7 and TGF-β3 were added to the medium 24h after seeding the constructs at a concentration of 10 ng/ml (Knippenberg *et al.*, 2006; Dahlin *et al.*, 2014; Huang *et al.*, 2018). Constructs of 10 million per ml of ATDC5 cells seeded in 1% agarose were cultured for 42 days, with data collection points of 1, 7, 21 and 42 days (Figure 61A).

The first visible change in the hydrogels that were not supplemented with growth factors was the collapse of the hydrogel after 42 days of culture. This could be related to a loss of phenotype of the cells, becoming fibroblast-like and being unable to support the integrity of the matrix. In contrast, growth factor supplementation (BMP7, TGF-β3 or a combination of both growth factors) resulted in an adequate distribution of the cells (Figure 61A). Haematoxylin-eosin (Figure 60.B), Picrosirius Red (Figure 60.B) and Toluidine Blue (Figure 61B) staining was used to visualise the construct morphology and matrix deposition at day 42 and showed pericellular accumulation of ECM, especially inside and around the cell clusters.

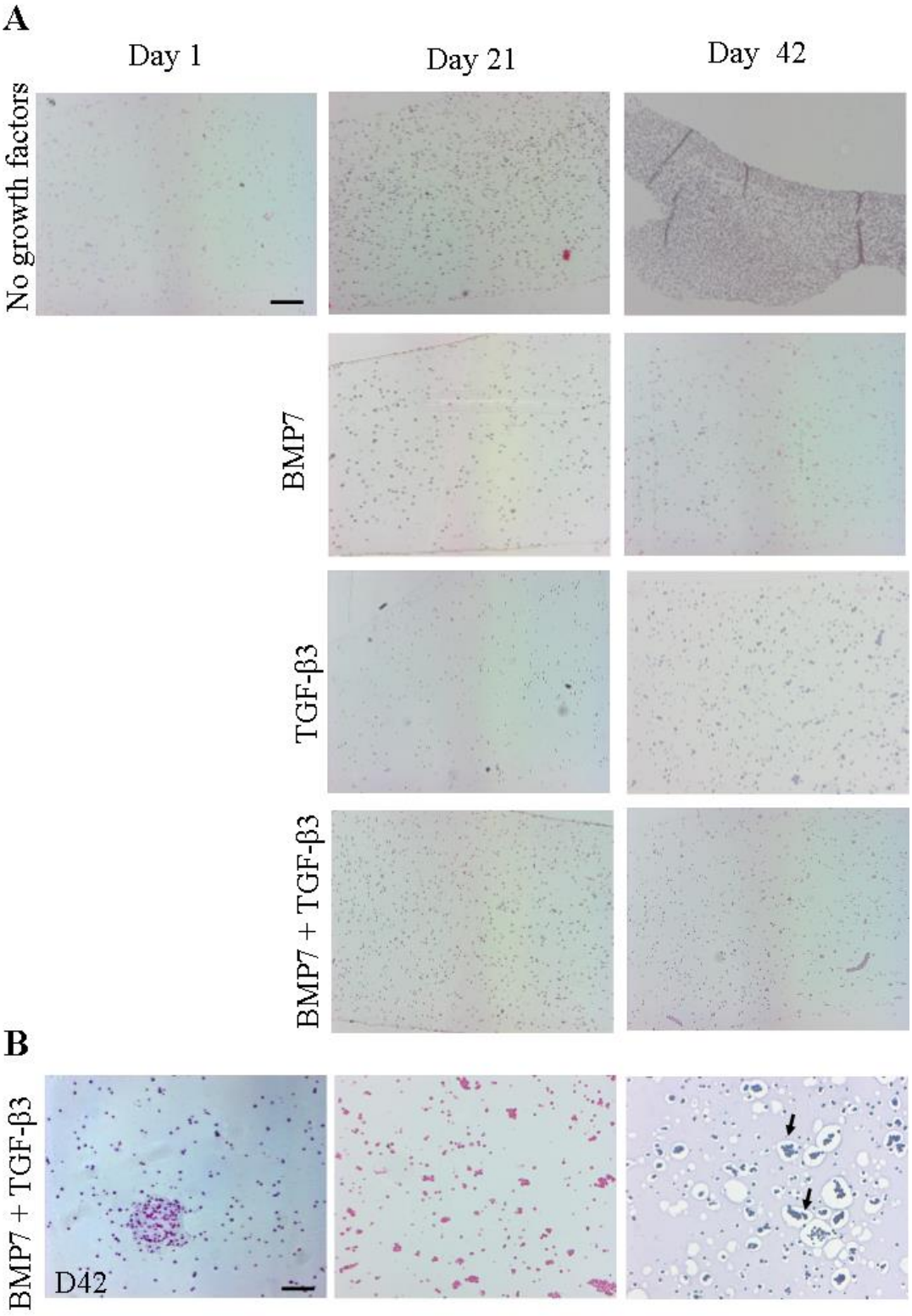

Figure 61. Histological analysis after the addition of growth factor at days 7, 21 and 42. A) *Haematoxylin-eosin staining of 3-dimensional ATDC5 culture in 1% low gelling temperature agarose with no-growth factors, BMP7, TGF-β3 and BMP7 + TGF-β3. N=3 and n=3. Scale bar 200 µm* ***B).*** *Haematoxylin-eosin staining for cell morphology analysis (left), picrosirius red for collagen deposition (middle), and toluidine blue staining for GAG deposition (right)) when supplementing with both growth factors at day 42. Scale bar 100 µm. N=3 and n=3.*

5.3.5 Width of constructs and area of cell clusters in 1% agarose with and without growth factor supplementation

The width of the hydrogels was measured from top to bottom and compared (Figure 62A). When comparison was done for the same day point but within the different supplemented conditions, a significant increase was observed at day 21 when comparing no addition of growth factors against the addition of TGF-β3 and both growth factors by 1.13-fold change ($p=0.0112$) and by 1.355-fold change ($p<0.0001$) respectively. A significant increase was visible when comparing adding both growth factors against the addition of only BMP7 or TGF-β3 by 1.35-fold change ($p<0.0001$) and by 1.19-fold change ($p<0.0001$) respectively. A significant increase was observed at day 42 comparing no addition of growth factors against the addition of BMP7, TGF-β3 and both growth factors by 2.59-fold change ($p<0.0001$), by 254-fold change ($p<0.0001$) and 2.44-fold change ($p<0.0001$) respectively.

When comparing within every condition along with the day points, no growth factors supplementation presented a significant decrease from day 42 to days 7 and 21 by 0.44- and 0.44-fold change respectively ($p<0.0001$). Adding BMP7 produced a significant increase of gene expression when comparing day 7 to day 42 by 1.20-fold change ($p=0.0009$) and comparing day 21 against 42 by 1.14-fold change ($p=0.0041$). Supplementation of TGF-β3 presented a significant increase when comparing day 7 against days 21 and 42 by 1.167-fold change ($p=0.001$) and by 0.0021-fold change ($p=0.0021$) respectively. Finally, the addition of both growth factor presented a significant increment from day 7 to days 21 by 1.3-fold change ($p<0.0001$), and a significant decrease from day 21 to day 42 by 0.79-fold change ($p<0.0001$).

Measurement of the area of the cluster for each condition and each zone, surface, middle or deep after 42 showed no statistical difference between the conditions and between the different zones of individual constructs except with a significant increase when supplementing with BMP7 and comparing the area of the clusters in the surface against middle and deep zones by 1.06-fold change ($p=0.018$) and by 1.204-fold change ($p=0.04$) respectively (Figure 62B).

A

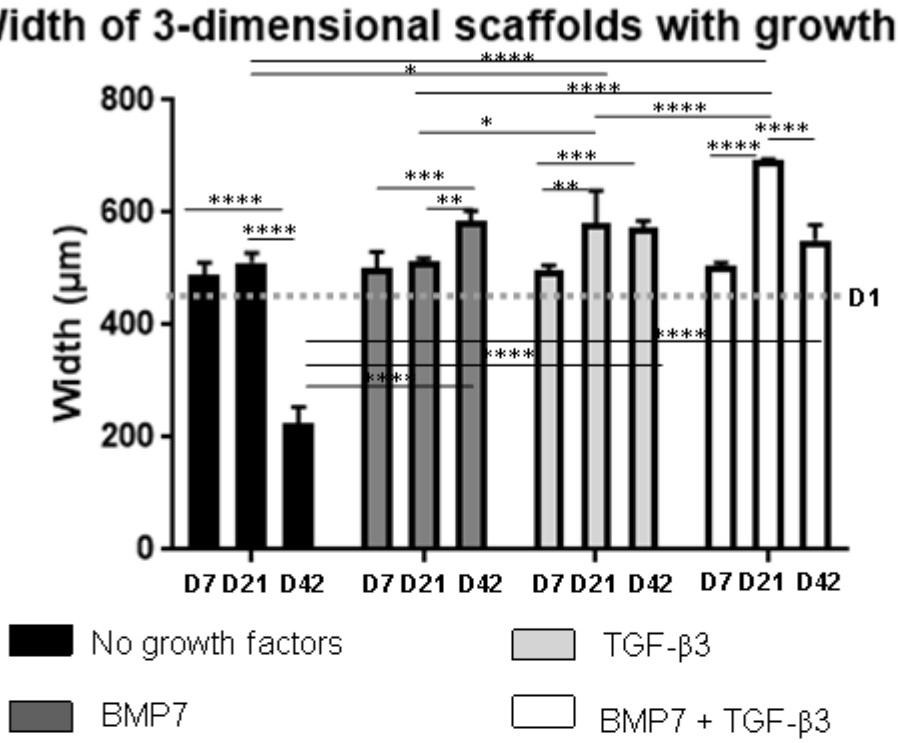

B

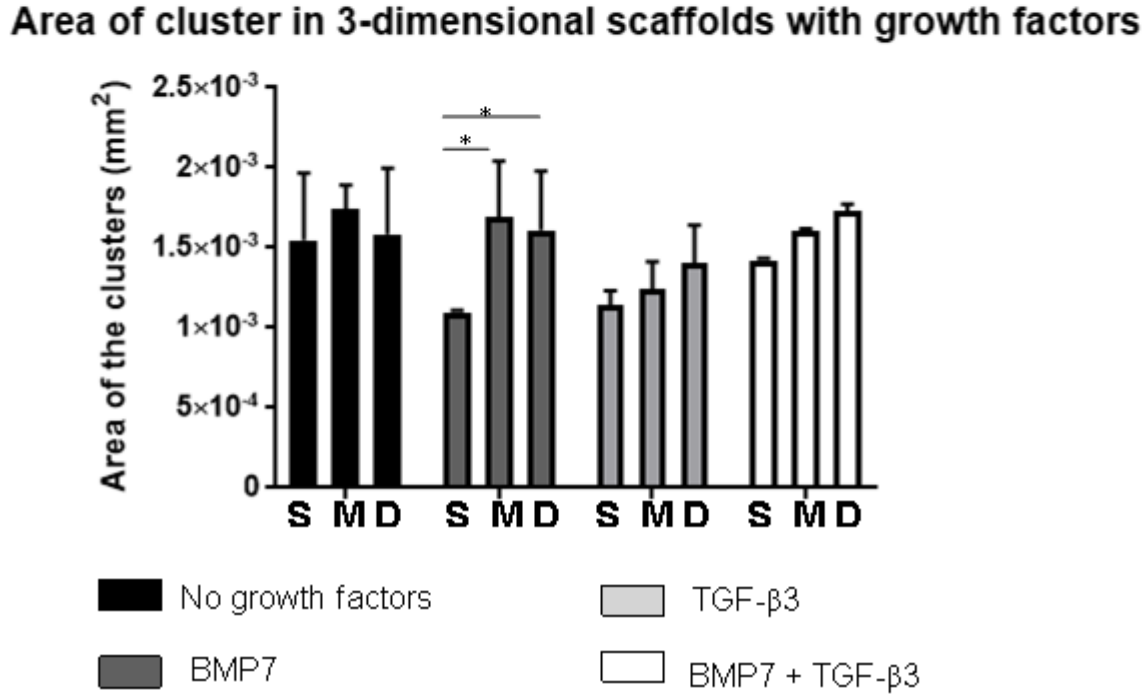

Figure 62. Analysis of width and area of clusters in 1% agar constructs seeded with 10x106cells/ml and supplemented with BMP7, TGF-β3 or a combination of both. (A) *Width (µm) was measured using ImageJ for all the conditions. Two-way ANOVA statistical analysis where * and # p<0.05. N=3 and n=3.* ***(B)*** *The area of clusters (mm2) for each zone after 42 days was measured via ImageJ. Two-way ANOVA statistical analysis where * p<0.05, **p<0.01, ***p<0.001, and ****p<0.0001. N=3 and n=3.*

5.3.6 ECM deposition in 1% agarose constructs with and without growth factor supplementation

Immunochemical staining was performed to detect matrix deposition in the engineered tissues (Figure 63), negative and positive control for the immunohistochemistry in Figure 64. As suggested by the Picrosirus Red staining, the type II collagen (main collagen in the cartilage ECM) deposition after 42 days of culture was mostly pericellular and the highest in the constructs cultured without growth factors, followed by supplementation with both growth factors. However, the combination of both growth factors appeared also to induce a more interterritorial localisation of type II collagen in the ECM (Figure 63). Type I collagen was slightly visible after 42 days pericellularly in constructs cultured without growth factor supplementation, and with BMP7 or TGF-β3. However, both growth factors combined led to no visible deposition of type I collagen in the ECM (Figure 63). Aggrecan immunostaining (Figure 63) showed a pericellular localisation for all conditions which strongly increased in the constructs cultured with a combination of BMP7 and TGF-β3. The higher density of the cells observed in the constructs with no growth factors is most likely due to the collapse and shrinkage of the constructs, which will be discussed in the Discussion section.

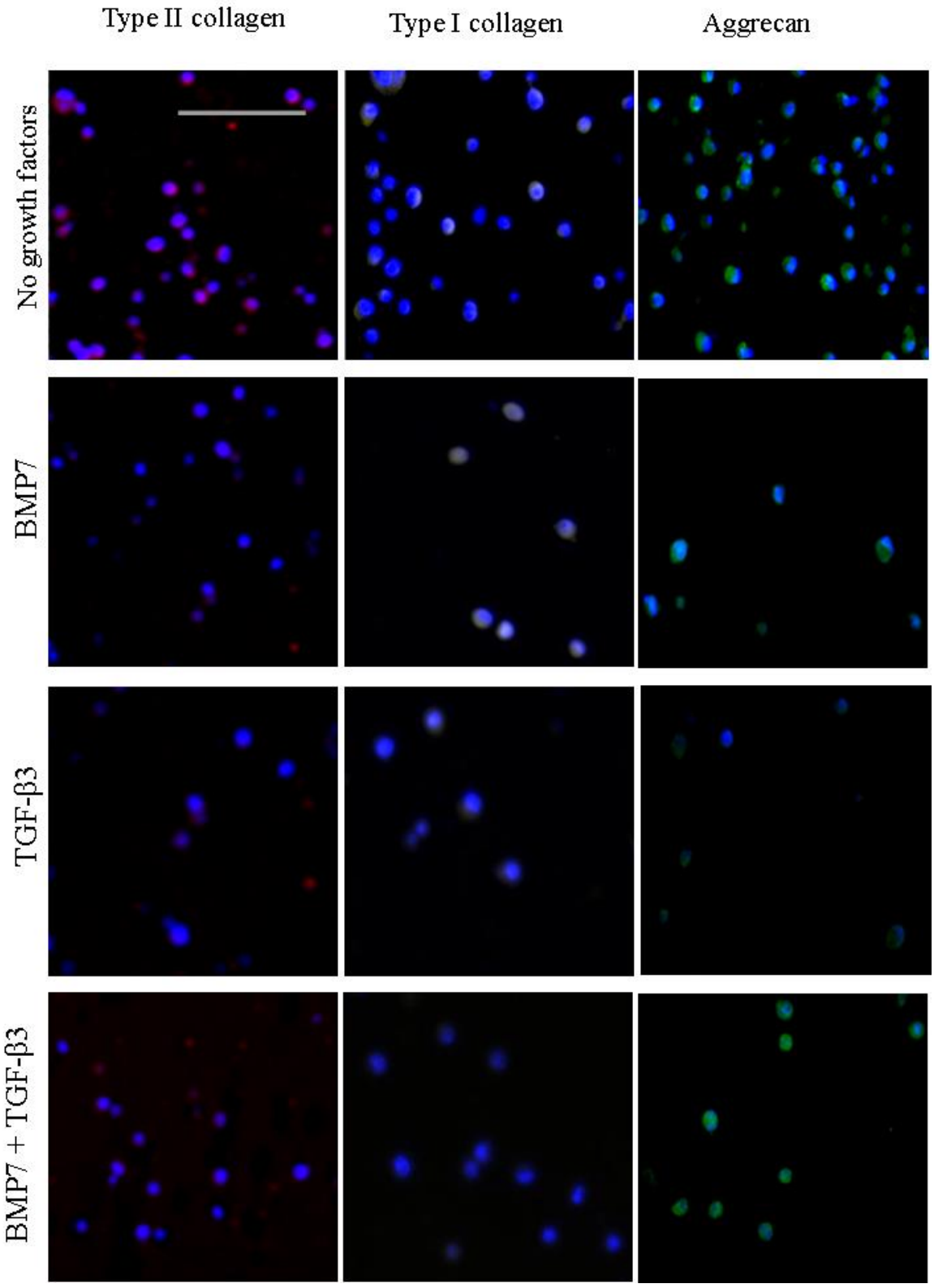

Figure 63. Immunohistochemistry against type I and II collagen and aggrecan *for ATDC5 cells seeded in a 3-dimensional culture in low gelling temperature agarose for 42 days, for non-growth factors, added,), BMP7 growth factor, TGF-β3 growth factor and combination of both growth factors added. Red staining = type II collagen. Green = type I collagen and aggrecan. Blue staining = nuclear staining. Scale bar 50 µm. N=3 and n=3.*

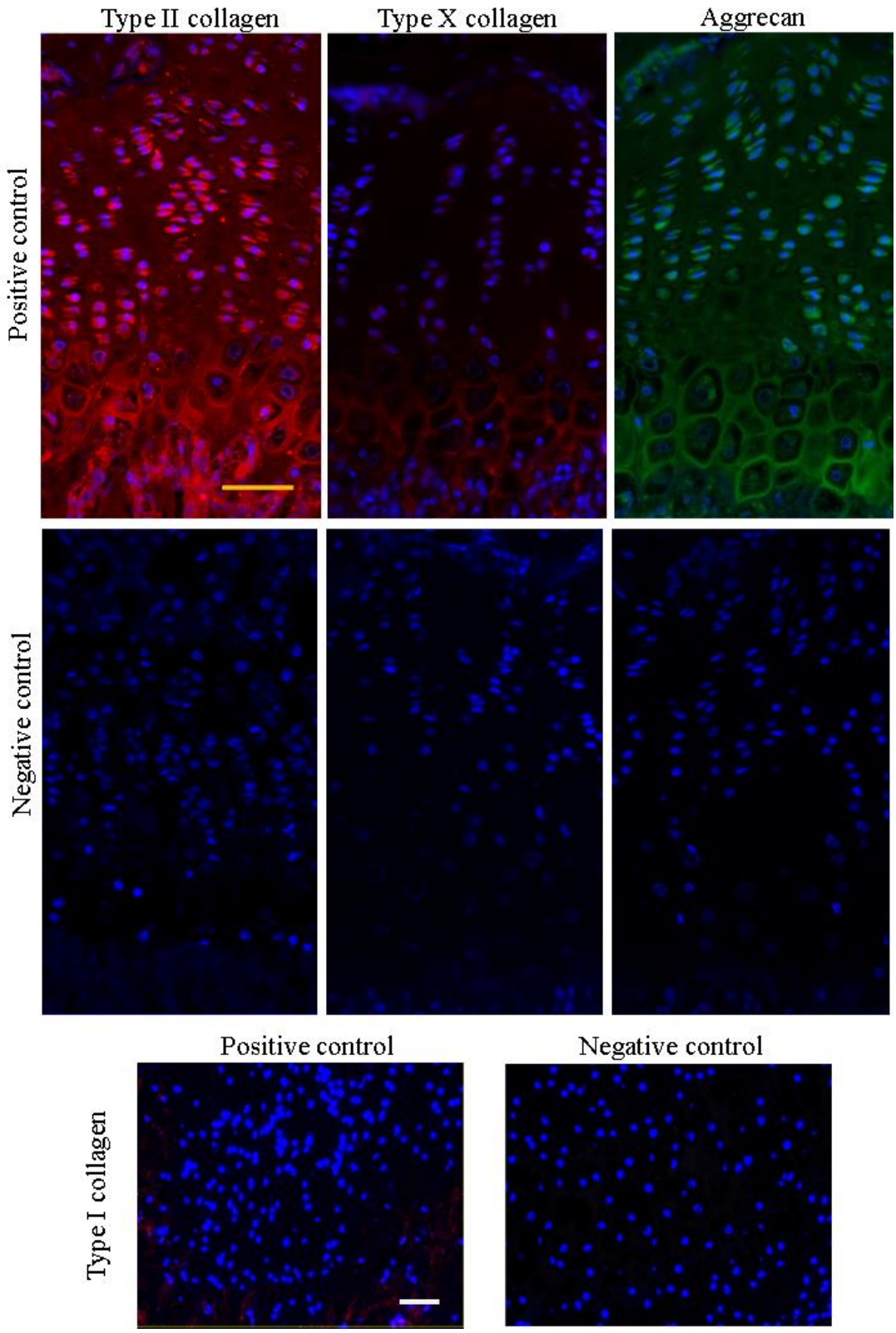

Figure 64. Positive and negative controls for type I, II and X collagen and aggrecan. *Positive and negative controls were done in 3-week-old mice femoral heads for type I, II and X collagen and aggrecan. Scale bar: 50 µm*

Deposition of sulphated GAGs was quantified using DMMB assay and compared to the amount of sGAG after 24h of seeding and before the addition of growth factors (day 1) (Figure 65). Interestingly when comparison was done within every condition along with the day points, no growth factors supplementation presented a significant increment from day 7 to days 21 and 42 by 2.09- and 2.69-fold change respectively ($p<0.0001$), and from day 21 to day 42 by 1.28-fold change ($p=0.0086$). Adding BMP7 produced a significant increase of sGAG deposition when comparing day 7 to day 42 by 2.52-fold change ($p<0.0001$) and comparing day 21 against 42 by 2.49-fold change ($p<0.0001$). Supplementation of TGF-β3 presented a significant increase when comparing day 7 and against days 21 and 42 by 1.94-fold change ($p=0.0016$) and by 1.59-fold change ($p=0.049$). Finally, the addition of both growth factor presented a significant increment from day 7 to days 21 and 42 by 1.58- ($p=0.0127$) and 3.53-fold change ($p<0.0001$) respectively, and from day 21 to day 42 by 2.22-fold change ($p<0.0001$).

Comparison within the different condition for the same day points showed a significant decrease at day 21 when comparing no addition of growth factors against BMP7, TGF-β3 and both growth factors by 0.41- ($p<0.0001$), 0.71- ($p=0.0153$) and 0.73-fold change ($p=0.026$) respectively. When comparison was done for the same day point but within the supplemented conditions, a significant increase in gene expression was observed when comparing BMP7 against TGF-β3 by 1.74-fold change ($p=0.0094$) and against the addition of both growth factors by a significant increase 1.79-fold change ($p=0.0053$). A significant decrease at day 42 when comparing no addition of growth factors against BMP7 and TGF-β3 by 0.11- ($p=0.0265$), 0.455- ($p<0.0001$) respectively, however, a significant increase was found when compared against supplementation of both growth factors by 1.27-fold change ($p=0.0025$). When comparison was done for the same day point but within the supplemented conditions, a significant increase in gene expression was observed when comparing BMP7 against TGF-β3 and addition of both growth factors by 1.60-fold change ($p<0.0001$) and by a significant increase 2.79-fold change ($p<0.0001$) (Figure 65).

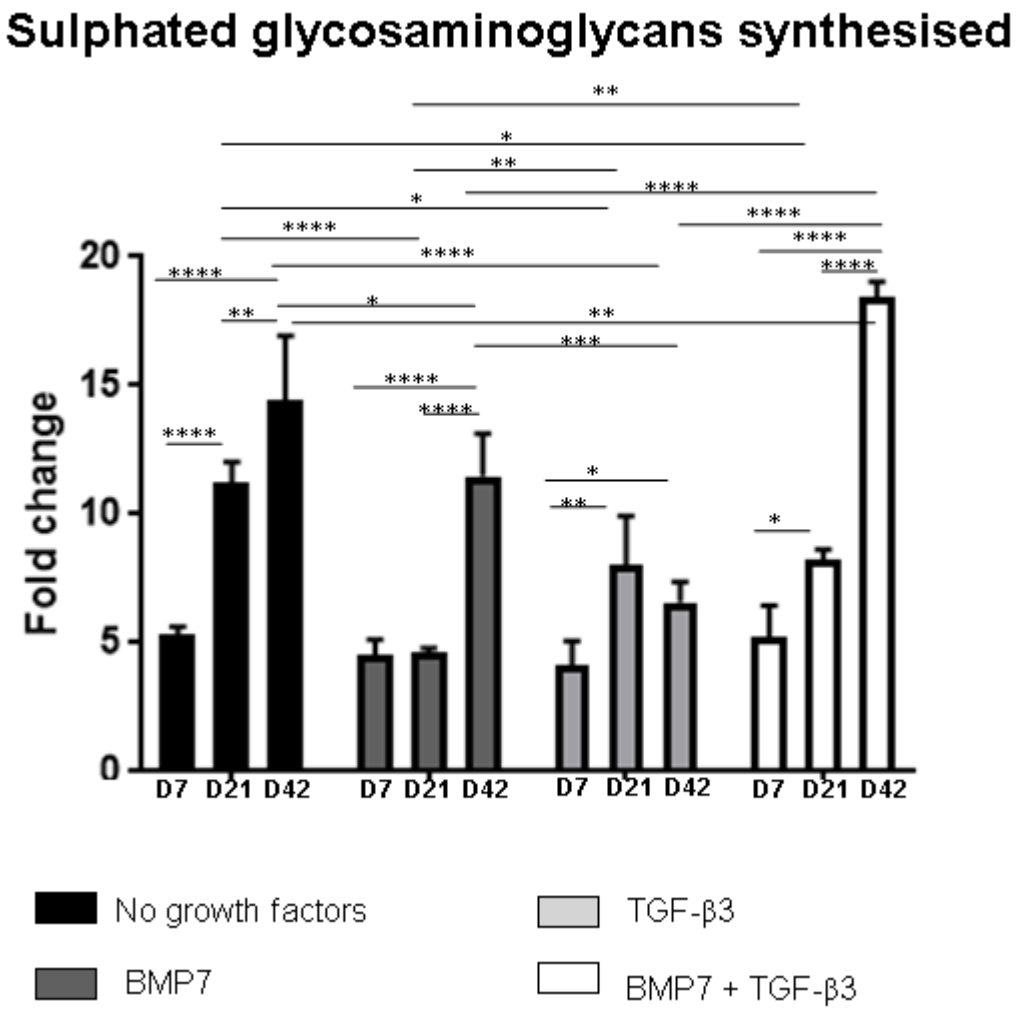

***Figure 65. Analysis of sGAG deposition** in 3D ATDC5 1% agar constructs with no growth factor supplementation and with the addition of BMP7, TGF-β3 and a combination of both. Two-way ANOVA statistical analysis where * p<0.05, **p<0.01, ***p<0.001, and ****p<0.0001. N=3 and n=3.*

5.3.7 Cell apoptosis in 1% agarose constructs with and without growth factor supplementation

Cell apoptosis was assessed using the TUNEL assay (Figure 66 and 67). Interestingly, the only significant difference was found when comparing at day 42 no addition of growth factors against BMP7, TGF-β3 and both growth factors by 0.69- (p=0.029), 0.687- (p=0.022) and 0.698-fold change (p=0.029) respectively.

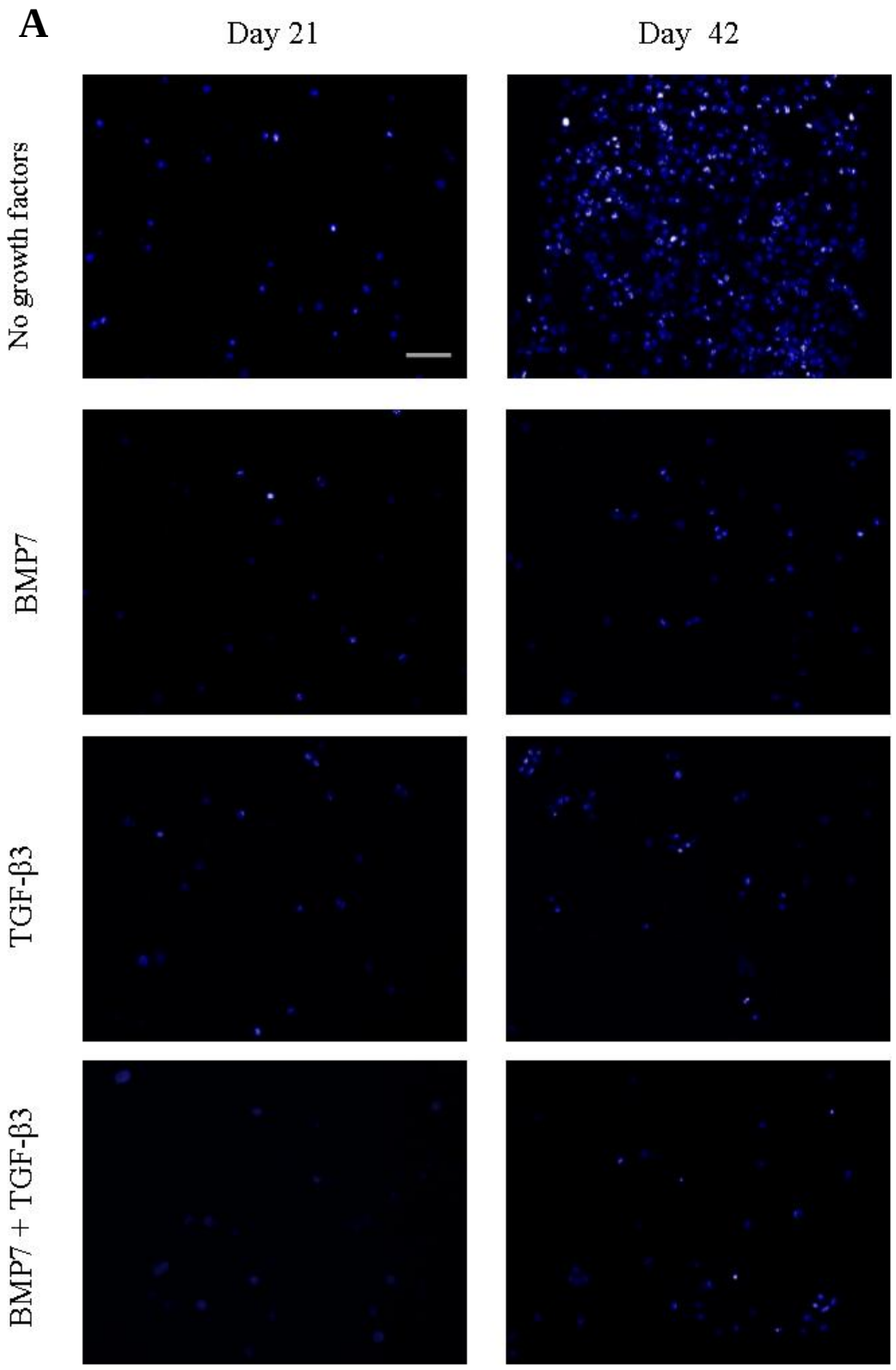

Figure 66. TUNEL assay for cell apoptosis *for ATDC5 cells seeded in a 3-dimensional culture in low gelling temperature agarose at 21 and 42 days, for non-growth factors, added, BMP7 growth factor, TGF-β3 growth factor and combination of both growth factors added. Cyan staining = cell apoptosis. Blue staining = nuclear staining. Scale bar 50 µm.. Quantification of cell apoptotic cells. N=3 and n=3.*

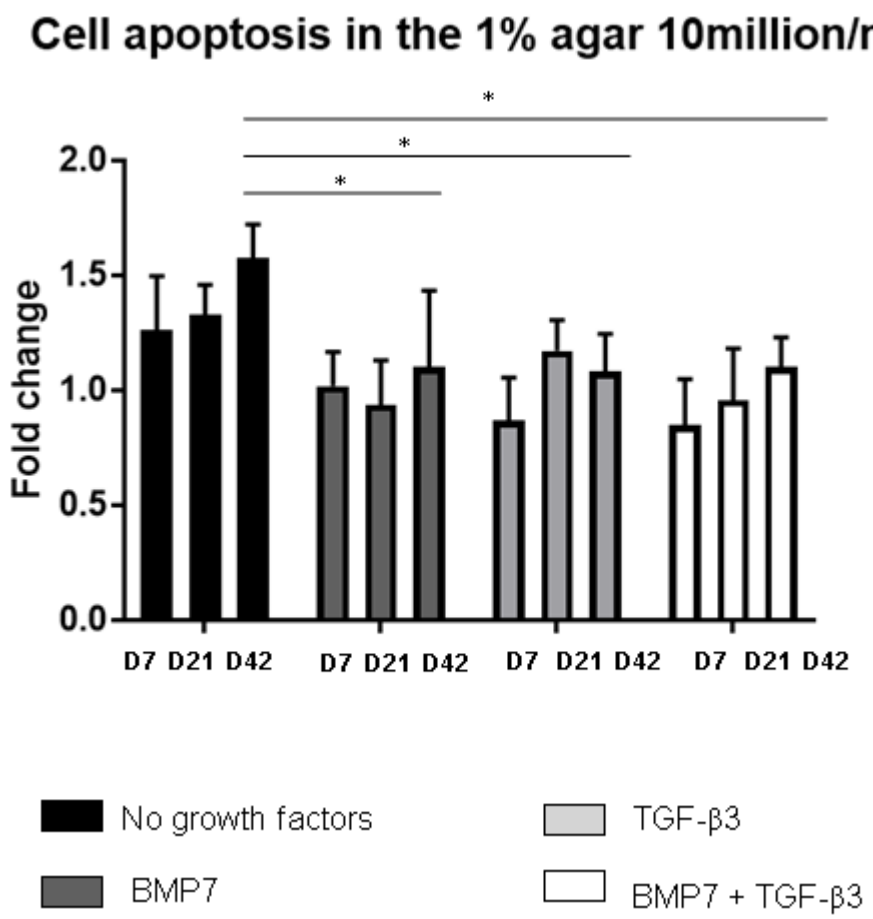

Figure 67. TUNEL assay for cell apoptosis *for ATDC5 cells seeded in a 3-dimensional culture in low gelling temperature agarose at 21 and 42 days, for non-growth factors, added, BMP7 growth factor, TGF-β3 growth factor and combination of both growth factors added. Yellow staining = cell apoptosis. Blue staining = nuclear staining. Scale bar 50 µm. Quantification of cell apoptotic cells. Two-way ANOVA statistical analysis where * p<0.05, **p<0.01, ***p<0.001, and ****p<0.0001. N=3 and n=3.*

5.3.8 Cell proliferation and cell metabolic activity in 1% agarose constructs with and without growth factor supplementation

Cell proliferation levels were measured using immunohistochemistry for Ki67, as described previously (Figures 68 and 69A). When comparison was done within every condition along with the day points, no growth factors supplementation presented a significant increment from day 7 to days 21 and 42 by 1.58- ($p=0.039$) and 4.19-fold change ($p<0.0001$) respectively, and from day 21 to day 42 by 2.65-fold change ($p<0.0001$). Adding BMP7 produced a significant increase of cell proliferation when comparing day 7 to days 21 and 42 by 2.08-fold change ($p=0.0001$) and 2 by 2.24-fold change ($p<0.0001$) respectively. Supplementation of TGF-β3 presented a significant increase when comparing day 7 and against days 21 and 42 by 2.37-fold change ($p<0.0001$) and by 2.35-fold change ($p<0.0001$) respectively. Finally, the addition of both growth factor presented a significant increment from day 7 to days 21 and 42 by 1.91- ($p=0.0282$) and 1.96-fold change ($p=0.0202$) respectively.

Comparison within the different condition for the same day points showed a significant decrease in cell proliferation at day 21 when comparing both growth factors against BMP7 and TGF-β3 by 0.61- ($p=0.0059$) and 0.63-fold change ($p=0.0151$) respectively. A significant decrease at day 42 when comparing no addition of growth factors against BMP7, TGF-β3 and both growth factors by 0.54- ($p<0.0001$), 0.478- ($p<0.0001$) and 0.315- ($p<0.0001$) respectively. A significant decrease was found when comparing supplementation of both growth factors against BMP7 and TGF-β3 by 058-fold change ($p=0.0014$) and by 0.65-fold change ($p=0.0257$) respectively.

Cell metabolic activity was assessed using the MTT assay (Figure 69B). Metabolic activity when compared within the same conditions but different day points, a significant increment from day 7 to day 21 by 1.379-fold change ($p<0.0001$) and a significant decrease when comparing day 42 against day 21 by 0.81-fold change ($p=0.0001$). Adding BMP7 produced a significant increase of cell proliferation when comparing day 7 to days 21 and 42 by 2.08-fold change ($p<0.0001$) and 2 by 2.39-fold change ($p<0.0001$) respectively. Supplementation of TGF-β3 presented a significant increase when comparing day 7 and against days 21 and 42 by 2.67-fold change ($p<0.0001$) and by 2.94-fold change ($p<0.0001$) respectively. Finally, the addition of both growth factor presented a significant increment from day 7 to days 21 and 42 by 2.35- ($p<0.0001$) and 2.78-fold change ($p<0.0001$) respectively. Day 21 against day 42 presented a significant increase by 1.18-fold change ($p=0.015$).

Comparison within the different condition for the same day points showed a significant decrease in cell proliferation at day 7 a significant decrease when comparing no addition of growth factors against BMP7, TGF-β3 and both growth factors by 0.40- ($p<0.0001$), 0.304- ($p<0.0001$) and 0.361- ($p<0.0001$) respectively (Figure 69B). At day 21 when comparing no addition of growth factors against BMP7, TGF-β3 and both growth factors by 0.60- ($p<0.0001$), 0.58- ($p<0.0001$) and 0.61- ($p<0.0001$) respectively. Finally, at day 42 when comparing no addition of growth factors against BMP7 and TGF-β3 a significant decrease was observed by 0.857-fold change ($p=0.022$) and by 0.80- ($p=0.0012$).

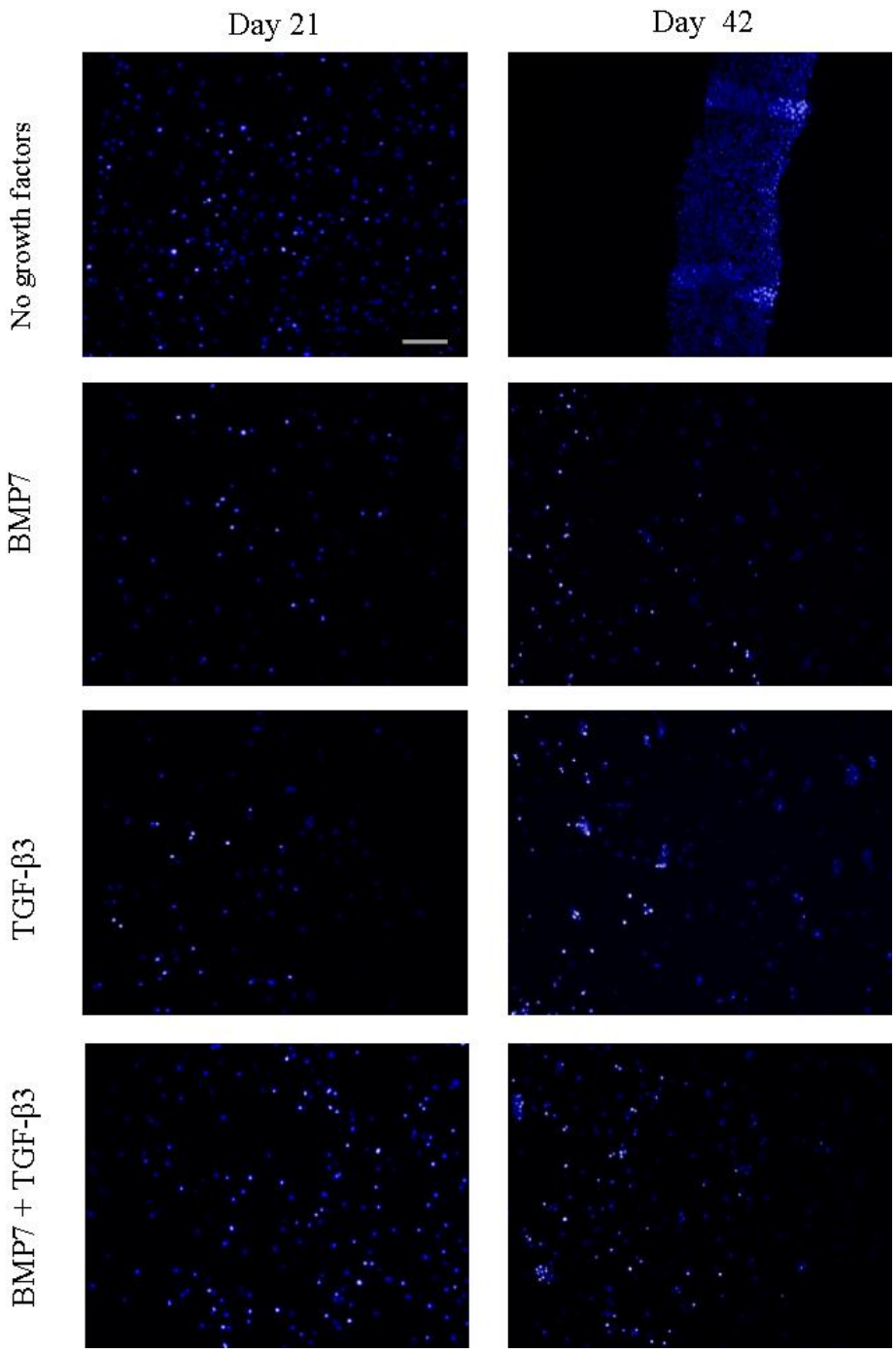

Figure 68. Immunohistochemistry for cell proliferation in all conditions after 21 days. *3-dimensional hydrogels were seeded for 21 days for ki67 staining with no addition of growth factors, BMP7, TGF-β3 and addition of both factors (BMP7 + TGF-β3). Blue = DAPI staining for nuclei. Green = Cell proliferation. Scale bar = 100 µm. N=3 and n=3.*

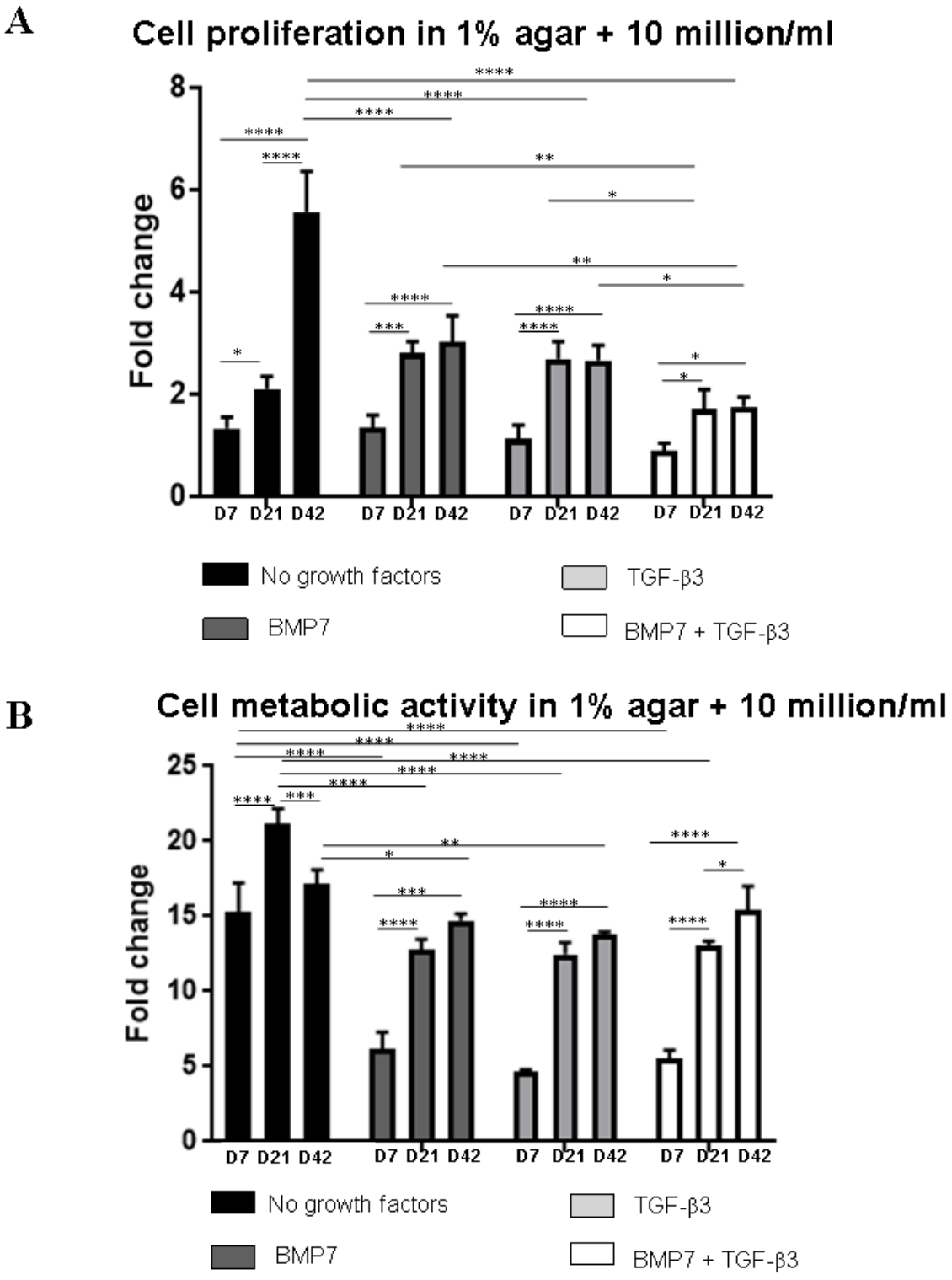

Figure 69. Cell proliferation and cell metabolic activity of ATDC5 cells cultured in the 3-dimensional 1% agar scaffold with growth factor supplementation. *Cell metabolic activity fold change* ***(B)*** *and cell apoptosis fold change* ***(A)*** *of quantification with ImageJ when no addition of growth factors, the addition of BMP7, TGF-β3 and combination of both along the 21 days compared to day 1. . Two-way ANOVA statistical analysis where * p<0.05, **p<0.01, ***p<0.001, and ****p<0.0001. N=3 and n=3.*

5.3.9 Gene expression of chondrogenic markers in 1% agarose constructs with and without growth factor supplementation

Gene expression of ECM and chondrogenic differentiation-related genes was examined using quantitative RT-PCR using mRNA extracted from the 1% agarose based ATDC5 constructs (Figure 70 and Table 7).

The expression of the early chondrogenesis marker, *Sox9*, was increased in all culture conditions when compared to day 1, indicating that agar hydrogel is supportive of chondrogenesis (Figure 70A). A significant increase was visible at day 7 when comparing no growth factors against BMP7 by 6.26-fold change respectively ($p<0.0001$). When comparison was done for the same day point but within the supplemented conditions, a significant reduction in gene expression was observed when comparing BMP7 against TGF-β3 by 0.39-fold change ($p=0.0007$) and against the addition of both growth factors by 0.10-fold change ($p<0.0001$). On day 21 supplementation of both growth factor presented a significant increase in gene expression compared to no supplementation by 5.80-fold change ($p<0.0001$). When comparison was done for the same day point (21) but within the supplemented conditions, a significant increase in gene expression was observed when comparing BMP7 and TGF-β3 against the addition of both growth factors by 9.77-fold change ($p<0.0001$) and by 5.1-fold change ($p<0.0001$) respectively.

A significant increase was visible at day 42 when comparing no growth factors against BMP7 and both growth factors by 37.37- ($p<0.0001$) and 20.94-fold change ($p=0.034$) respectively. When comparison was done for the same day point but within the supplemented conditions, a significant decrease in gene expression was observed when comparing BMP7 against TGF-β3 by 0.219-fold change ($p=0.0013$). When comparison was done within every condition along with the day points, no growth factors supplementation presented an initial significant increment from day 7 to day 21 by 3.08-fold change ($p=0.048$) and a significant reduction from day 21 to day 42 by 0.0395-fold change ($p=0.0042$). Adding BMP7 produced an initial significant decrease of gene expression when comparing day 7 to day 21 by 0.292-fold change ($p<0.0001$) and a significant increase comparing day 21 against 42 by 2.48-fold change ($p=0.0084$). Supplementation of TGF-β3 presented a significant decrease when comparing day 21 against day 42 by 0.285-fold change ($p=0.0156$). Finally, the addition of both growth factor presented an initial significant increment from day 7 to day 21 by 27.74-fold change ($p<0.0001$) and a significant reduction from day 21 to day 42 by 0.1426-fold change ($p<0.0001$).

Following the expression of *Sox9*, expression levels of another chondrogenesis marker, *Ihh*, were examined (Figure 70B). As can be seen in Figure 68 a significant increase was visible at day 42 when comparing no growth factors against BMP7, TGF-β3 and both growth factors by 1.28- ($p=0.0168$), 1.80- ($p<0.0001$) and 1.93-fold change respectively ($p<0.0001$). When comparison was done for the same day point (42) but within the supplemented conditions, a significant increase in gene expression was observed when comparing BMP7 against TGF-β3 by 1.41-fold change ($p<0.0001$) and against the addition of both growth factors by 1.506-fold change ($p<0.0001$). When comparison was done within every condition along with the day points, no growth factors supplementation presented a significant increment from day 7 to day 42 by 330.34-fold change ($p<0.0001$) and from day 21 to day 42 by 16.65-fold change ($p<0.0001$). Adding BMP7 produced a significant increase of gene expression when comparing day 7 to day 21 by 27.084-fold change ($p<0.0001$) and comparing day 21 against 42 by 20.128-fold change ($p<0.0001$). Supplementation of TGF-β3 presented a significant increase when comparing day 7 and day 21 against day 42 by 134.35- ($p<0.0001$) and 34.186-fold change ($p<0.0001$) respectively. Finally, the addition of both growth factor presented an initial significant increment from day 7 to day 42 by 244.3-fold change ($p<0.0001$) and from day 21 to day 42 by 26.017-fold change ($p<0.0001$).

Gene expression of *Col2a1* (Figure 70C) showed a similar trend to the one seen for the other two chondrogenic markers *Sox9* and *Ihh* and gradually increased in all conditions, further confirming that agarose hydrogel has the potential to support cartilage development. A significant increase was visible at day 42 when comparing no growth factors against TGF-β3 and both growth factors by 1.4- ($p=0.0031$) and 1.82-fold change respectively ($p<0.0001$). When comparison was done for the same day point but within the supplemented conditions, a significant increase in gene expression was observed when comparing BMP7 and TGF-β3 against the addition of both growth factors by a significant increase by 1.51-fold change ($p<0.0001$) and 1.30-fold change ($p=0.0017$) respectively. When comparison was done within every condition along with the day points, no growth factors supplementation presented a significant increment from day 7 to day 42 by 69.37-fold change ($p<0.0001$) and from day 21 to day 42 by 13.63-fold change ($p<0.0001$). Adding BMP7 produced a significant increase of gene expression when comparing day 7 to day 42 by 10.30-fold change ($p<0.0001$) and comparing day 21 against 42 by 16.41-fold change ($p<0.0001$). Supplementation of TGF-β3 presented a significant increase when comparing day 7 and day 21 against day 42 by 61.76- ($p<0.0001$) and 24.10-fold change ($p<0.0001$) respectively. Finally, the addition of both growth

factor presented an initial significant increment from day 7 to day 42 by 191.97-fold change ($p<0.0001$) and from day 21 to day 42 by 18.73-fold change ($p<0.0001$).

Similarly, to type II collagen expression, collagen X (Figure 70D) showed a progressive increase along with the day points. A significant decrease was visible at day 42 when comparing no growth factors against BMP7 + TGF-β3 addition by 1.56-fold change respectively ($p=0.02$). When comparison was done for the same day point but within the supplemented conditions, a significant increase in gene expression was observed when comparing TGF-β3 against the addition of both growth factors by 1.6-fold change ($p=0.014$). When comparison was done within every condition along with the day points, no growth factors supplementation presented a significant increment from day 7 to day 42 by 18.49-fold change ($p<0.0001$) and from day 21 to day 42 by 21.44-fold change ($p<0.0001$). Adding BMP7 produced a significant increase of gene expression when comparing day 7 to day 42 by 17.98-fold change ($p<0.0001$) and comparing day 21 against 42 by 39.316-fold change ($p<0.0001$). Supplementation of TGF-β3 presented a significant increase when comparing day 7 and day 21 against day 42 by 91.44- ($p<0.0001$) and 38.60-fold change ($p<0.0001$) respectively. Finally, the addition of both growth factor presented an initial significant increment from day 7 to day 42 by 275.93-fold change ($p<0.0001$) and from day 21 to day 42 by 34.09-fold change ($p<0.0001$).

Type I collagen expression (Figure 70E) was assessed to determine the quality of the ECM deposited after 42 days of seeding. The *Col1a1* mRNA expression showed a significant decrease was visible at day 7 when comparing BMP7 against TGF-β3 by 0.55-fold change ($p=0.0026$) and against both growth factors by 0.420-fold change ($p=0.001$). A significant decrease was visible at day 21 when comparing no growth factors against BMP7, TGF-β3 and both growth factors by 0.598- ($p=0.012$), 0.455- ($p=0.0006$) and 0.411-fold change ($p=0.0002$) respectively. When comparison was done within every condition along with the day points, no growth factors supplementation presented a significant decrease from day 7 to day 42 by 0.0048-fold change ($p<0.0001$) and from day 21 to day 42 by 0.0036-fold change ($p<0.0001$). Adding BMP7 produced a significant decrease of gene expression when comparing day 7 to days 21 and 42 by 0.56-fold change ($p=0.0017$) and 0.0038-fold change ($p<0.0001$) respectively, and comparing day 21 against 42 by 0.0068-fold change ($p=0.0001$). Supplementation of TGF-β3 presented a significant decrease when comparing day 7 and day 42 against day 42 by 0.0054- ($p=0.0001$) and 0.00712-fold change ($p=0023$) respectively. Finally, the addition of both growth factor presented a significant decrease from day 7 to day 42 by 0.00225-fold change ($p=0.0026$) and from day 21 to day 42 by 0.00244-fold change ($p=0.0054$).

Gene expression of aggrecan (*Acan*) (Figure 70E) followed the trend seen for the other chondrogenic markers. A significant increase was visible at day 7 by 66.83-fold change ($p<0.0001$) when comparing no growth factors addition against the addition of BMP7. At day 42, a significant increase was observed when comparing no growth factors against TGF-β3 and both growth factors by 1.586- ($p=0.0015$) and 1.958-fold change($p<0.0001$) respectively. When comparison was done for the same day point but within the supplemented conditions, a significant increase in gene expression was observed when comparing BMP7 against TGF-β3 by 1.5-fold change ($p=0.0041$) and against the addition of both growth factors by 1.85-fold change ($p<0.0001$). When comparison was done within every condition along with the day points, no growth factors supplementation presented a significant increment from day 7 to days 21 and 42 by 79.67- and 1186.74-fold change respectively ($p<0.0001$), and from day 21 to day 42 by 14.89-fold change ($p<0.0001$). Adding BMP7 produced a significant increase of gene expression when comparing day 7 to day 42 by 18.77-fold change ($p<0.0001$) and comparing day 21 against 42 by 21.266-fold change ($p<0.0001$). Supplementation of TGF-β3 presented a significant increase when comparing day 7 and day 42 by 152.-066-fold change ($p<0.0001$) and day 21 against day 42 by 23.62- ($p<0.0001$). Finally, the addition of both growth factor presented a significant increment from day 7 to days 21 and 42 by 21.43- ($p=0.0361$) and 109.67.74-fold change ($p<0.0001$) respectively, and from day 21 to day 42 by 5.11-fold change ($p<0.0001$).

		Sox9	***Ihh***	***Col2a1a***	***Col10a1***	***Col1a1***	***Acan***
No growth factors	Day 7	↑	↓	↑	↑	↑	↓
	Day 21	↑	↑	↑	↑	↑	↑
	Day 42	↓	↑	↑	↑	↓	↑
BMP7	Da y7	↑	↑	↑	↑	↑	↑
	Day 21	↑	↑	↑	↑	↑	↑
	Day42	↑	↑	↑	↑	↓	↑
TGF-β3	Day 7	↑	↓	↑	↑	↑	↑
	Day 21	↑	↑	↑	↑	↑	↑
	Day 42	↑	↑	↑	↑	↓	↑
BMP7 + TGF-β3	Day 7	↑	↓	↑	↑	↑	↑
	Day 21	↑	↑	↑	↑	↑	↑
	Day 42	↑	↑	↑	↑	↓	↑

Table 7. Table summarising the outcome of the gene expression *of Sox9, Indian hedgehog (Ihh), collagen II (Col2a1), collagen X (Col10a1), collagen I (Col1a1) and aggrecan (Acan) after 21 days of culturing ATDC5 in a 3-dimensional culture compared to day 1 gene expression. N=3 and n=3*

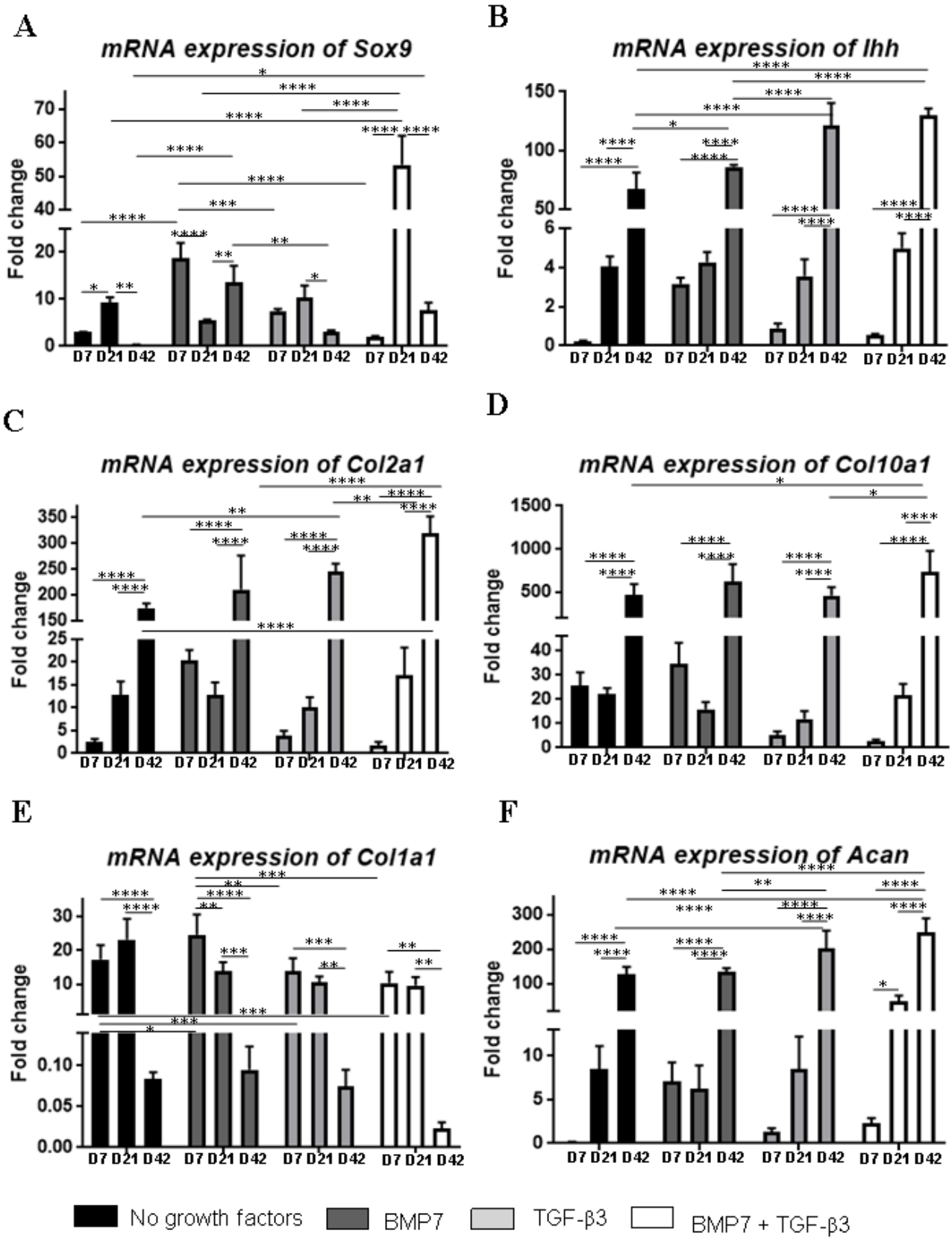

Figure 70. qRT-PCR data showing gene expression in 3dimentional ATDC5 1% agar cell culture. *Gene expression of Sox9* ***(A)****, Indian hedgehog (Ihh)* ***(B)****, type II collagen (Col2a1)* ***(C)****, type X collagen (Col10a1)* ***(D)****, type I collagen (Col1a1)* ***(E)****, aggrecan (Acan)* ***(F)*** *were normalised to the levels of 18S and the gene expression levels at day 1 (24h after seeding 10 million cells per ml and before growth factor addition). Two-way ANOVA statistical analysis where * p<0.05, **p<0.01, ***p<0.001, and ****p<0.0001. N=3 and n=3.*

5.4 Discussion

Work presented in this chapter studied the changes in gene expression and extracellular matrix deposition that resulted from culturing ATDC5 cells in different hydrogels, at different cell densities and with and without growth factor supplementation. The absence of blood vessel supply hinders the regeneration process of articular cartilage (Fox, Bedi and Rodeo, 2009). Current strategies employed for its repair lead to the formation of neocartilage, which in time express type I collagen and becomes less stable fibrous-like cartilage (Bhosale and Richardson, 2008; Moreira-Teixeira et al., 2011). A novel method pioneered for cartilage repair is tissue engineering, which initially showed great potential when cells were seeded into a scaffold and injected directly into cartilage lesion (Chuang et al., 2018). Hydrogels are a type of scaffold that creates a water-soluble polymeric network that mimics the high-water content environment that proteoglycans provide in the native cartilage tissue (Dhote and Vernerey, 2014). However, some studies suggest that without further modifications, the mechanical loading capabilities of hydrogels may not be sufficient to support cartilage formation (Chuang et al., 2018).

When chondrocytes are seeded in monolayer, expression of chondrogenic markers is lost and accompanied by an expression of type I collagen, which has been linked to later stages of osteoarthritis (Lahm et al., 2010; Vinatier and Guicheux, 2016). The hydrophilic nature of agarose hydrogel prevents cell attachment via integrins, which leads to dedifferentiation (Guilak and Hung, 2005; Vinatier and Guicheux, 2016). In this chapter, we compared the morphology of the cells seeded in monolayer (2-dimension) and 1% agarose hydrogel. ATDC5 cells in monolayer started to lose their morphology after 7 days in culture, expressing an elongated fibroblast-like phenotype. On the other hand, ATDC5 cells seeded in agarose hydrogel displayed a rounded morphology characteristic of chondrocytes for 42 days of culture. Agarose hydrogels have been proved by numerous studies to maintain the cell phenotype, by impeding cell binding and dedifferentiation, and to restore the phenotype of dedifferentiated chondrocytes (Benya and Shaffer, 1982; Guilak and Hung, 2005).

ATDC5 cells were cultured in different types of hydrogel, HyStem™ C (a mix of thiol modified hyaluronic acid (Glycosil®) with a thiol-reactive crosslinker (Extralink®) and a thiol modified denatured collagen fibrils called Gelin-S®) from Sigma-Aldrich®, Matrigel® Matrix Basement Membrane HC from Corning®, and low gelling temperature agarose from Sigma-Aldrich®. ATDC5 cells were seeded into the hydrogels at a density of 1 million cells per millilitre, in final mixtures of 1:1 (v/v) with dH_2O Matrigel, 1:1 (v/v) with dH2O HyStem™ C and 1.5% (w/v) of the agarose powder with dH_2O. Unfortunately, only agarose hydrogel maintained the framework and integrity of the scaffold after 21 days of seeding the cells.

HyStem™ C and Matrigel after 21 days of seeding lost the ability to support the cells and collapsed shrinking and disintegrating. The increase of brittleness in these hydrogels could be explained by a decrease in pH in the media, as a result of the high product waste created by a high cell density. Structural failure has been widely reported, where acidic environments of pH<4, resulted in the degradation of HA hydrogels (Maleki, Kjøniksen and Nyström, 2008; Kim et al., 2012). The polymerisation of Matrigel is also affected by pH variations (Slater, Partridge and Nandivada, 2019). Degradation of hydrogels has shown in GC/poly(EO-co-Gly) hydrogels of different densities collapsing at 5 and 14 weeks post-incubation (Cao et al., 2015). Gel formation is affected by many factors, such as gelation temperature, density, temperature, changes in proteins, water content, and, especially in collagen related hydrogels, the pH (Koutsopoulos and Zhang, 2013; Jin and Kim, 2017; Slater, Partridge and Nandivada, 2019). Moreover, the cells were visibly smaller in HyStem™ C and Matrigel after 21 days of seeding, compared to the cells grown in agarose. Chondrocytes have been shown to shrink when undergoing apoptosis (Visser et al., 2015). Cell death affects the ECM deposition and the sustainability of the scaffold. Comparison of agarose against multiple hydrogels such as type I collagen, alginate, fibrin and polyglycolic acid has shown that agarose hydrogels can best support chondrogenesis achieving the highest deposition of sGAG (Huang et al., 2004; Kim, Mauck and Burdick, 2011).

Low melting agarose was selected based on the maintained cellular phenotype and sustained integrity of the scaffolds. Properties such as the diffusion mechanism, are affected by pore size and hydrogel density. Generally, the lower the density of the hydrogel the better transport of nutrients towards the deeper areas, however, a higher density could potentially create disparity within the scaffold, leading to the development of a zonally stratified tissue. In this study, 1% and 2% (w/v) agarose constructs were examined to determine the optimal agarose concentration. A hydrogel density of 1% low-temperature agarose has been previously employed in the development of a model to study the induction, proliferation and differentiation of mesenchymal stem cells (MSCs) (Thompson, Piez and Seyedin, 1985). The study showed that agarose is a useful hydrogel to study the effect of soluble factors on chondrogenesis (Thompson, Piez and Seyedin, 1985). Increasing the hydrogel density to 2% significantly increased the mechanical stiffness of the scaffold under free-swelling conditions (Ng et al., 2006). Under compression, many studies show that a 2% agarose system is the lowest hydrogel density that could withstand mechanical compression (Buschmann et al., 1992; Mauck et al., 2003; Thorpe et al., 2013). Clusters area at each zone was following measured to replicate the increasing clusters with depth that is found in vivo (Lotz et al., 2010). Interestingly, a hydrogel

with a density of 2% showed a slightly uneven distribution of cells and clusters. At 1 million cells per ml, the bigger cellular clusters were restricted to the deeper zone, with no clusters in the middle or surface zones. However, at 2 million cells per ml, the cells were equally distributed along the zones, leading to a uniform scaffold. Hydrogel density of 1%, showed a preferable distribution of cells and clusters for both cell densities, with bigger cell clusters in the deeper zone, resembling hypertrophy in the native cartilage.

Different cell densities, from 1 to 2 and 10 million cells per ml, were tested in 1% low melting agarose. The constructs seeded with a higher cell density of 10 million cells/ml showed a larger area of clusters per zone, increasing significantly in the deep zone compared to middle and surface zones, creating a zonally stratified tissue. Cell seeding of 1 and 2 million cells per ml did not show significant variation within the zones, leading to a more homogenous construct probably due to the low density of cells seeded and the dimensions of the hydrogel. Several studies used a seeding density of 10 million cells per ml and showed an increase of the matrix content and improved gel biomechanics (Guilak and Hung, 2005; Dekosky et al., 2010; Mauck and Burdick, 2011). Even higher seeding densities, such as 60 million cells per ml have also been shown to significantly increase the mechanical and biomechanical properties of scaffolds (Ng et al., 2006; Erickson et al., 2009; Thorpe et al., 2013). In contrast, another study that compared 10 million cells per ml and 60 million cells per ml, at different FBS concentrations either, 10% or 20% showed that media composition and loading influenced more significantly the scaffold stiffness (Mauck et al., 2003).

Literature does not only vary on the type of growth factor used but also on the time it is added and its concentration. Variations in the concentration of the same growth factor have been shown to be key in the development of hypertrophy (Yao, Zhai and Wang, 2014). Several studies support the concentration of 10 ng/ml for both growth factors used in our study (Tare et al., 2005; Jiang et al., 2009; Caron et al., 2013; Yao, Zhai and Wang, 2014). The addition of BMP7 and TGF-β3 varied after seeding the cells, but studies agree on the addition after 24h of seeding (Asahina, Sampath and Hauschka, 1996; Akiyama et al., 2000; Palmer et al., 2000; Yao, Zhai and Wang, 2014). Constructs of 1% low melting agarose hydrogel with 10 million ATDC5 cells per millilitre were therefore tested without growth factors, and with the addition of 10 ng/ml of BMP7, TGF-β3 and addition of both (BMP7 + TGF-β3), to develop a zonally stratified compressible tissue.

Analysis of the synthesised ECM showed deposition of proteoglycans that was further confirmed by the analysis of a DMMB assay and immunohistochemistry. Firstly, aggrecan gene expression was significantly increased compared to the ATDC5 cells prior to differentiation,

reaching peaks in the culture supplemented with both growth factors. Moreover, a significant increase in *Acan* gene expression was detected in constructs grown with both growth factors in comparison to BMP7 and TGF-β3 alone. Similarly, the deposition of sGAG in the PCM was increased after 42 days of culture in non-supplemented constructs and constructs grown with both growth factors. This finding is supported by another study showing the beneficial effect when combining both growth factors rather than on their own (Huang et al., 2018).

When analysing the deposition of collagens in the hydrogel constructs, gene expression analysis showed a significant increase of type X collagen (Col10a1) expression and hypertrophy after 42 days of culture for all conditions. Several studies show that different growth factors and concentrations may increase the hypertrophy of human chondrocytes and ATDC5 cells (Caron et al., 2013; Yao, Zhai and Wang, 2014). Interestingly, expression of type II collagen (Col2a1) was upregulated up to 300-fold after culture of $10x10^6$ cells/ml bovine articular chondrocyte in 2% agarose being pericellular deposition visible by immunohistochemistry. A further increase in type II collagen deposition could be achieved by subjecting the constructs to mechanical loads. Despite the disparity in studies, cells seeded in agarose hydrogel have been shown to increase their deposition when compressed (Kaupp, Weber and Waldman, 2012; Omata et al., 2012; Kelly et al., 2013; Mesallati et al., 2013). Interestingly, type I collagen (Col1a1) expression was maintained through the first 3 weeks of culture, however, significantly decreased after 42 days of cultures in constructs grown with no growth factors or with a combination of both. However, it was not detectable by immunohistochemistry.

Interestingly, the scaffolds without supplementation collapsed after 42 days of culture, reducing in width to nearly half. However, cell proliferation and cell metabolic activity increased significantly. As previously mentioned, the shrinkage of the scaffold could be related to many factors, such as pH, which may be due to the increase in cell proliferation (Maleki, Kjøniksen and Nyström, 2008; Kim et al., 2012; Slater, Partridge and Nandivada, 2019).

Interestingly chondrocytes do not present high cell proliferation rates, however, when the maturation process and hypertrophy start the cells become more proliferative, which could be comparable to the construct cultured for 42 days with no growth factors (Bohme et al., 1992). An increase in proliferation and mineralisation is also linked with chondrocytes in disease cartilage (Dreier, 2010). As the articular cartilage is a mechanosensitive tissue, its turnover and maintenance of a healthy tissue rely on mechanical load (Fox, Bedi and Rodeo, 2009), we hypothesised that the loading of the system would improve its matrix deposition.

Finally, BMP7 or TGF-β3 did not promote ECM deposition and enhance chondrogenesis as much as the combinatorial effect of TGF-β and BMPs, which is similar to what previous studies found (Shen et al., 2009; Shintani, Siebenrock and Hunziker, 2013). In particular, a study showed the beneficial effect of combining BMP7 and TGF-β3 (Huang et al., 2018), increasing gene expression of type II collagen and Sox9 through the addition of TGF-β3, while BMP7 promoting ECM deposition and inhibition of hypertrophy (Huang et al., 2018).

Supplementation of ATDC5 hydrogel cultures with both growth factors showed an increment of the ECM deposition and a significant decrease in type I collagen indicating maintained chondrocyte phenotype. To further increase ECM deposition and considering articular cartilage is a mechanosensitive tissue, the next step focused on compressing the scaffold in order to intensify the gene expression and study whether the tissue-engineered model is mechanoresponsive.

Chapter 6. Characterisation of the 3-Dimensional Hydrogel Model Under Compression.

6 Characterisation of the 3-dimensional hydrogel model under compression.

6.1 Introduction

The main function of the articular cartilage is to provide a mechanically stable template that withstands high compressive strengths and minimises friction in the joint by providing lubrication (Lima *et al.*, 2008; Fox, Bedi and Rodeo, 2012). The tissue *in vivo* is exposed to multiaxial compressive and shear strains, and hydrostatic and osmotic pressures, which all play a role in ECM homeostasis (Anderson and Johnstone, 2017). The pressures that the tissue is exposed to can reach between 3-10 MPa depending on the articulation, and up to 18MPa in the hip joint (Elder and Athanasiou, 2009). Most *in vitro* models require months of culture periods increasing the cost and do not fully mimic the morphological and biomechanical composition of hyaline cartilage, however, only one study attempted to resemble the mechanical properties that the natural tissue exhibits (Mauck *et al.*, 2000). Compressing scaffolds in rudimentary and self-made bioreactors was implemented in order to mimic the mechanical properties and environment of the tissue (Mauck *et al.*, 2000). Several studies to date, using either static or dynamic compression, in a confined or free-swelling scaffold, with or without additional hydrostatic or shear stress, show an increase in deposition and formation of cartilage-like tissue with resembling native cartilage (Mauck *et al.*, 2000; Lee *et al.*, 2006; Responte *et al.*, 2012; Johnstone *et al.*, 2013; Thorpe *et al.*, 2013).

It is well established that the scaffold stiffness regulates stem cell differentiation (Park *et al.*, 2011) and that different types of loads enhance the deposition of different ECM proteins, for instance, dynamic compression has been linked to increased sGAG production, and fluid-induced shear stress leads to increased collagen synthesis (Mesallati *et al.*, 2013). In a study by Tariq *et al.*, dynamic compression was found to increase the sGAG deposition and synthesis compared to free-swelling controls (Mesallati *et al.*, 2013); however, another study from Kelly *et al.*, showed how dynamic loading presented no significant difference in the ECM deposition when comparing to free-swelling (Kelly *et al.*, 2006). Despite the biomechanical studies contributing to a better understanding of the mechanosensitive mechanisms mediating tissue remodelling, variability in conditions between the studies makes their comparison difficult (Mauck *et al.*, 2002; Elder and Athanasiou, 2009).

6.2 Aims of the chapter

The aim of this chapter was to study the effect of dynamic compression on the agar-based *in vitro* 3D model of cartilage with the aim to replicate physiological loading in articular cartilage *in vivo*. Developing a compressible zonally stratified model of cartilage will ultimately help to further understand the role of mechanosensing in musculoskeletal homeostasis and disease.

6.3 Results

As discussed previously, articular cartilage is a biomechanically sensitive tissue that is constantly bearing loads. Therefore, we hypothesised that the application of compression to our 3D engineered would increase the deposition of ECM and zonal stratification of the model.

After initial testing, the percentage of hydrogel was modified from 1% to 2% of low gelling temperature agarose, due to the collapsing of the scaffold when exposed to high compression. Furthermore, the hydrogel experiment was reduced from 42 days to days 7, 14 and 21, to allow direct comparison with the pellet model, since previous chapters have shown that adding a combination of growth factors to the pellet model showed increased cartilage marker gene expression and ECM deposition at day 21 of culture. All results represented in graphs were calculated as fold change normalised to data obtained after 24h of seeding as reference. Therefore, day point 1 has the value of 1 in all graphs. Every graph is accompanied by the calculated fold change values and the p-values.

In order to increase the synthesis of ECM, the optimised 3-dimensional model (2% agar, 10 million cells per ml, 10ng/ml of a combination of BMP7 and TGF-β3) was cultured with a

dynamic compression regime of 30min a day sinusoidal wave compression of 10kPa at 0.33Hz frequency for 21 days (Figure 71).

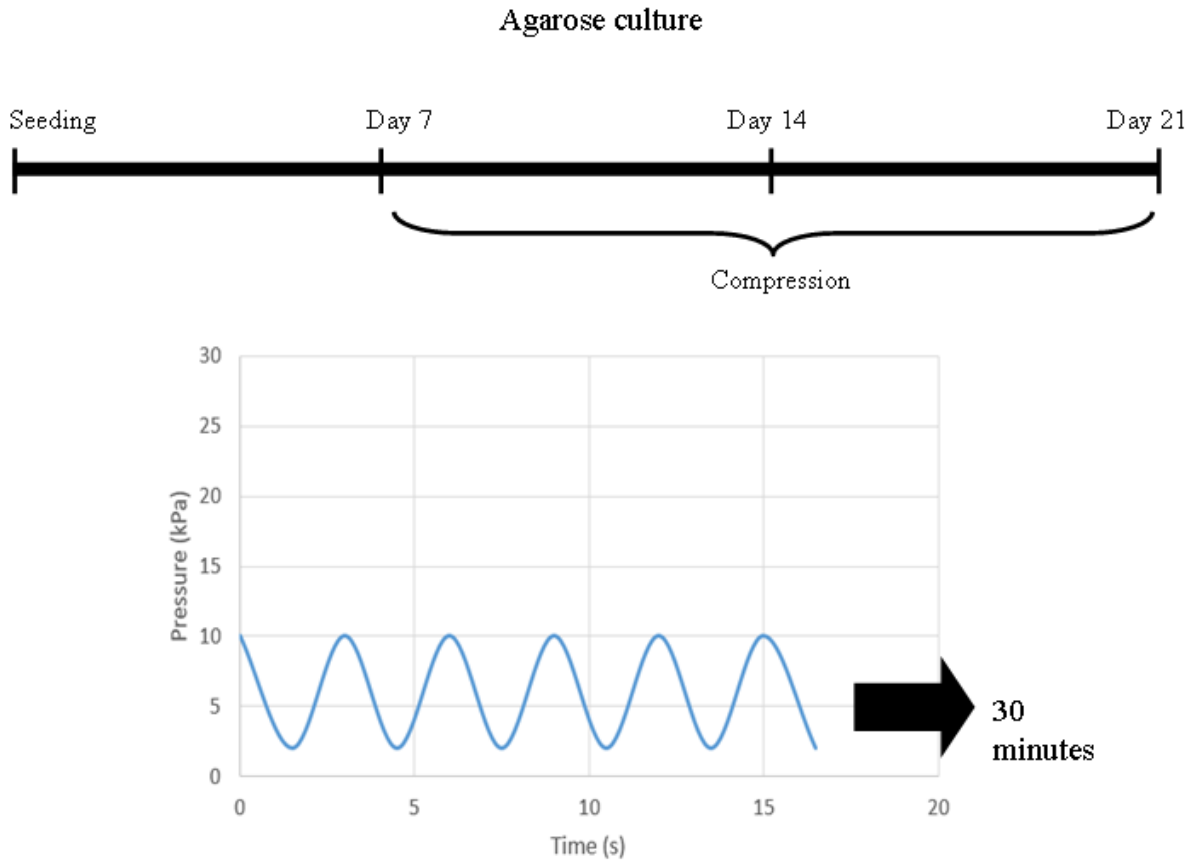

Figure 71. Loading regimen used. *ATDC5 cells in the agarose construct were compressed for 14 days for 30min/day at 10kPa magnitude and a sinusoidal waveform and a frequency of 0.33Hz.*

The hydrogels were cultured for 21 days and compressed after 7 days (including day 7) of culture for 30 minutes every day, at the same time each day (12 PM, to account for the circadian rhythms), and with a resting period of one hour prior to the collection of the samples.

6.3.1 ECM deposition in both uncompressed and compressed hydrogel constructs supplemented with BMP7 and TGF-β3

Haematoxylin-eosin staining was used to visualise the cells and the ECM in both compressed and uncompressed models, of 2% agarose, 10 million ATDC5 cells per ml, grown in a combination of BMP7 and TGF-β3 growth factors at a concentration of 10ng/ml each. Initially, there was no visual difference between the uncompressed and compressed samples on day 7. However, the compressed cells appeared to deposit more ECM at days 14, and especially 21, compared to the uncompressed controls. The distribution of the cells, despite changing the

percentage of the hydrogel to 2%, remained similar to the 1% model, where the cells on the deep zone (D) arranged in columns (rectangles) and the middle zone (M) randomly (Figure 72).

To confirm that the area of the cell clusters and the ECM deposition were increasing with compression, the width of the constructs and the area of the clusters per zone were analysed using ImageJ. A progressive increase in the width of the constructs was visible along with all-day points and conditions, in particular from day 7 to day 21 for uncompressed constructs, and day 7 to day 14 for the compressed samples (Figure 73.A) Interestingly, compression appeared to have no effect on the thickness of the scaffolds, indicating that 2% agarose was resilient to compression and supported tissue development.

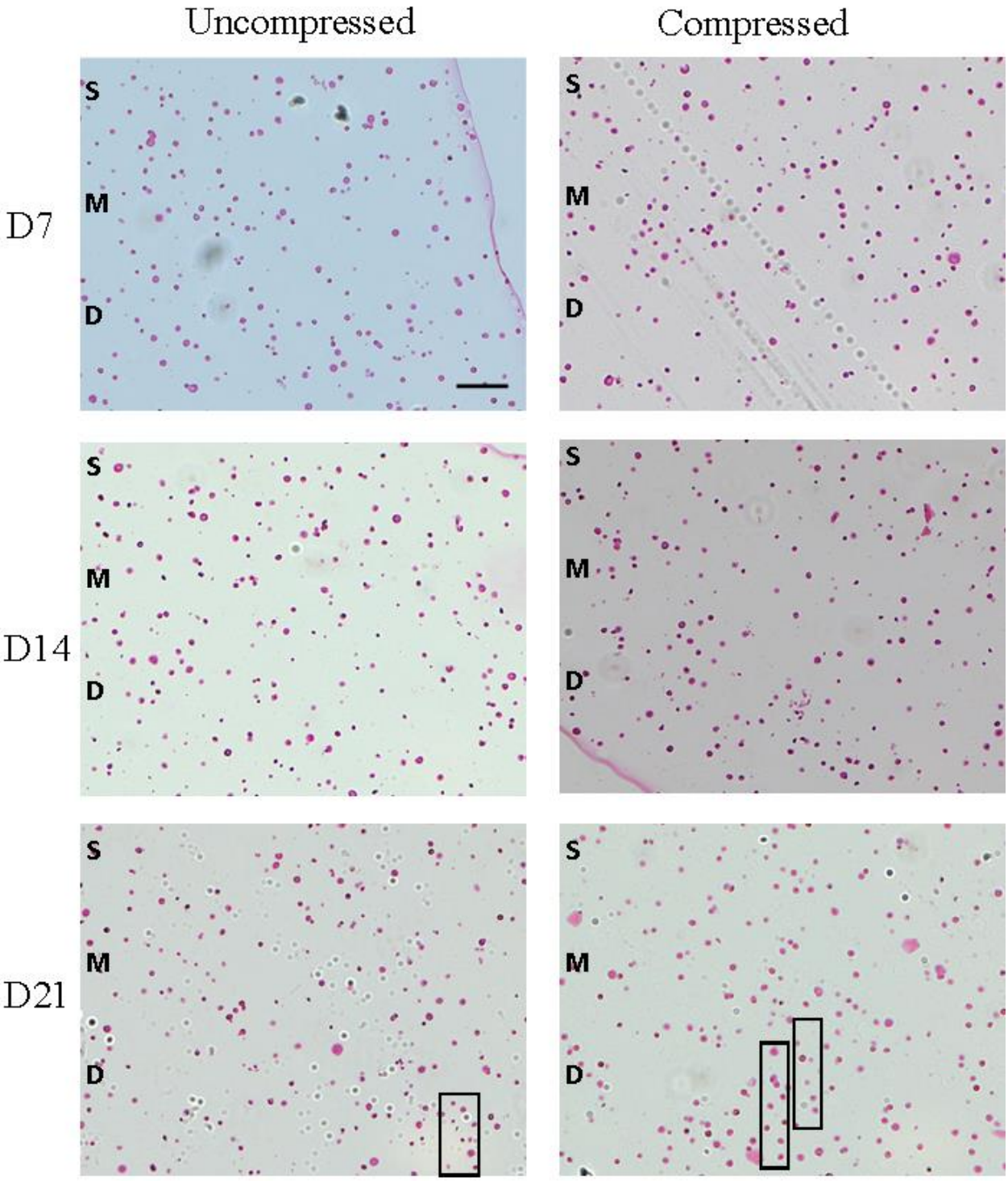

Figure 72. Histological analysis when compressed and without compressing at day 21. *Haematoxylin-eosin staining (H+E), purple-stained the nuclei, and pink the ECM 3D model of ATDC5 cultured at 10 million per ml, 2% agarose and with and without compression. S=Surface zone, M= Middle zone, D=Deep zone. Scale bar= 100 µm. N=3 and n=3.*

The width of the scaffolds (Figure 73A) presented a significant increase was visible uncompressing the scaffolds when comparing day 7 against days 14 and 21 by 1.06-foldchange ($p=0.0066$) and by 1.10-fold change ($p=0.0002$). A significant increase was noticed when compressing the scaffolds when comparing day 7 against days 14 and 21 by 1.11-fold change ($p<0.0001$), and by 1.078-fold change ($p=0.0019$). When comparison was done within each day point comparing uncompressed scaffolds versus compressed ones, a significant increase was visible at 14 by 1.053-fold change ($p=0.0221$).

Analysis of the area of the cellular clusters per zone showed an increase in the deposition of PCM, especially in the compressed constructs (Figure 73B). The area of cluster per zones was measure via Image J, when comparison was done for the same incubation day and zone of the scaffold but within the different conditions (compressed vs uncompressed), a significant increase in cluster area was observed at day 14 in the deep zone when comparing uncompressed against compressed by 77.5-fold change ($p<0.0001$). This significant increase was also observed when comparing different zones within the same day point, 14 and for compressed scaffold, when comparing deep zone against the surface and middle zones a significant increase was observed by 5.52-fold change ($p<0.0001$) and 2.34-fold change ($p=0.0052$) respectively. The comparison was done for the same incubation day and zone of the scaffold but within the compressed vs uncompressed conditions, a significant increase in cluster area was observed at day 14 in the deep zone when comparing uncompressed against compressed by 1.65-fold change ($p=0.0086$).

Comparing within each scaffold (compressed or uncompressed) (Figure 73 A and B) and zone (surface, middle or deep zone) but different day points showed a significant increase of clusters area when non compressing the scaffold at the surface zone when comparing day 21 against days 7 and 14 by 4.92-fold change ($p=0.0003$) and by 170-fold change ($p<0.0001$). Middle zone when no compressing showed a significant increase as well when comparing day 21 against days 7 and 14 by 7.68-fold change ($p<0.0001$) and by 242.46-fold change ($p<0.0001$). Deep zone when uncompressing, presented a significant decrease when comparing day 14 against day 7 by 0.03-fold change ($p=0.0211$) however when comparing the day 21 against days 7 and 14 a significant increase was observed by 1.96-fold change ($p=0.0227$) and 65.21-fold change respectively ($p<0.0001$).

Comparing within each scaffold (compressed or uncompressed) and zone (surface, middle or deep zone) but different day points showed a significant increase of clusters area when compressing the scaffold (Figure 73B) at the surface zone when comparing day 21 against days 7 and 14 by 196.91-fold change ($p<0.0001$)) and by 5.85-fold change ($p<0.0001$). Middle

zone when compressed showed a significant increase as well when comparing day 21 against days 7 and 14 by 1443.82-fold change ($p<0.0001$) and by 2.99-fold change ($p<0.0001$) and by 482.022-fold change ($p=0.0188$) when comparing day 14 against 7. Deep zone when uncompressing, presented a significant increase when comparing day 14 against day 7 by 115.47-fold change ($p<0.0001$) and when comparing the day 21 against days 7 and 14 was observed by 160.46-fold change ($p<0.0001$) and 1.39-fold change respectively ($p=0.0324$).

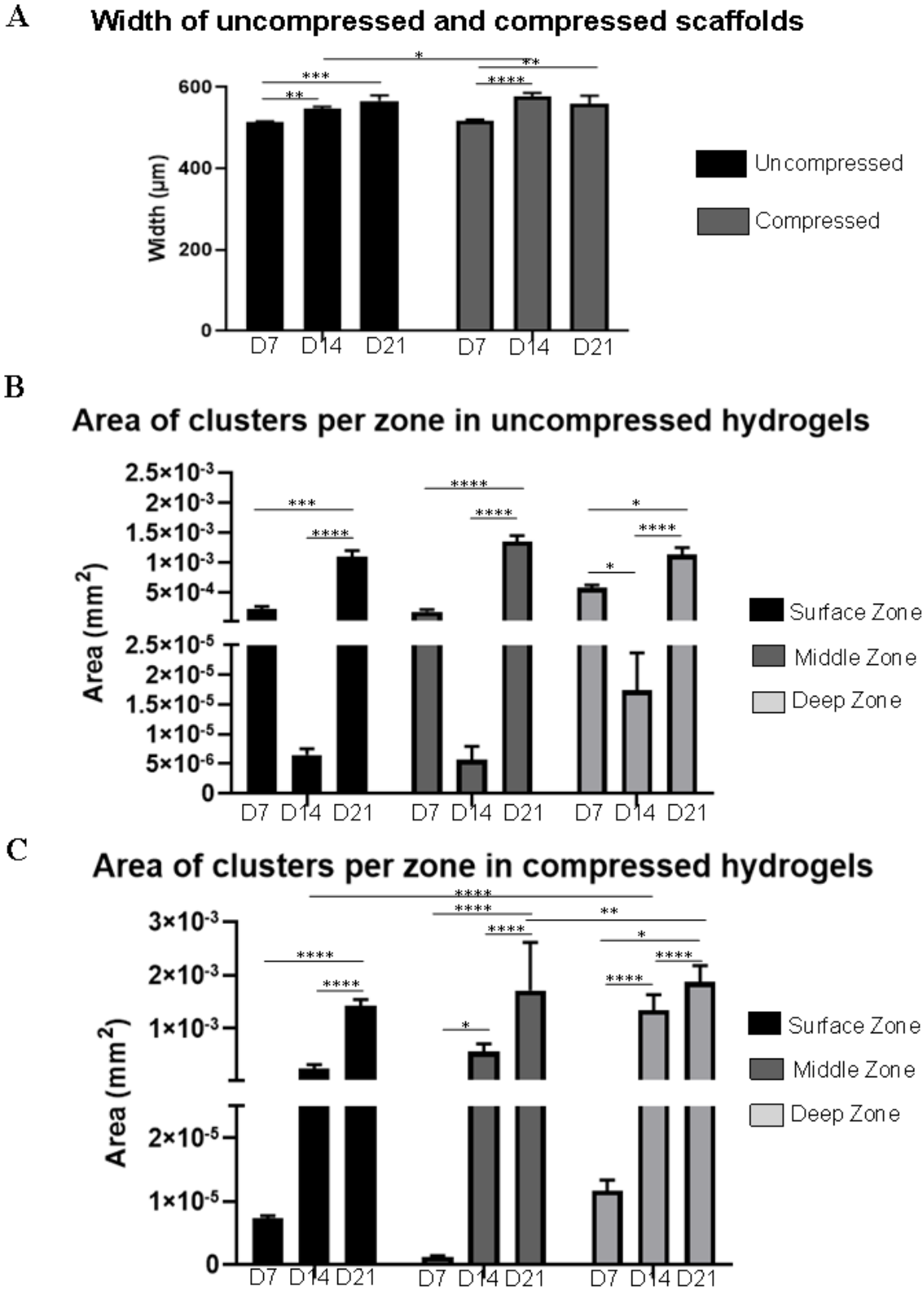

Figure 73. Analysis of width and area of clusters with a combination of BMP7 and TGF-β3 and uncompressed and compressed conditions. (A) *Width (µm) was measured via ImageJ for all the conditions at each day point. Two-way ANOVA statistical analysis where * = p<0.05. N=3 and n=3.* ***(B-C)*** *The area of clusters (mm2) for each zone after 21 days and no compressing (B) and after compressing* ***(C)*** *was measured via ImageJ. Two-way (A) and three-way (B-C) ANOVA statistical analysis where * p<0.05, **p<0.01, ***p<0.001, and ****p<0.0001. N=3 and n=3.*

6.3.2 Proteoglycan deposition in uncompressed and compressed tissue-engineered constructs supplemented with BMP7 and TGF-β3

The deposition of the cartilage ECM was investigated further by Toluidine Blue staining for sulphated GAGs and a quantitative DMMB assay (Figure 74).

As can be seen in Figure 74A, initially at day 7 for both conditions, there was a small amount of ECM deposited around the cellular clusters. However, the pericellular matrix deposition and the area of the clusters increased after 14 and 21 days of seeding in the compressed model (Figure 71.C). The clusters of the cells in the compressed hydrogel showed a higher deposition of GAGs with a dense colouration of toluidine blue after 2 weeks of culture, mainly at the pericellular location (Figure 71).

Deposition of sGAG was quantified using DMMB assay (Figure 74B), in which the matrix and hydrogel were digested, and the amount of sGAG was measured against a standard curve using as baseline the amount of sGAG synthesised after 24h. Interestingly when comparison was done within every condition along with the day points, no compressing the scaffolds showed a significant increase comparing days 14 and 21 against day 7 by 1.76- ($p=0.0197$) and 1.854-fold change ($p=0.0099$) respectively. Compressing the scaffold resulted in a significant increase of sGAG deposition when comparing day 7 to days 14 and 21 by 2.59-fold change ($p<0.0001$) and by 2.89-fold change ($p<0.0001$) and when comparing day 14 against 21 by 1.12-fold change ($p=0.0303$). Comparison within both conditions compressed against uncompressed for different day points showed a significant increase at days 7, 14 and 21 by 2.36- ($p=0.0003$), 3.47- ($p<0.0001$) and 3.69-fold change ($p<0.0001$) respectively (Figure 74B).

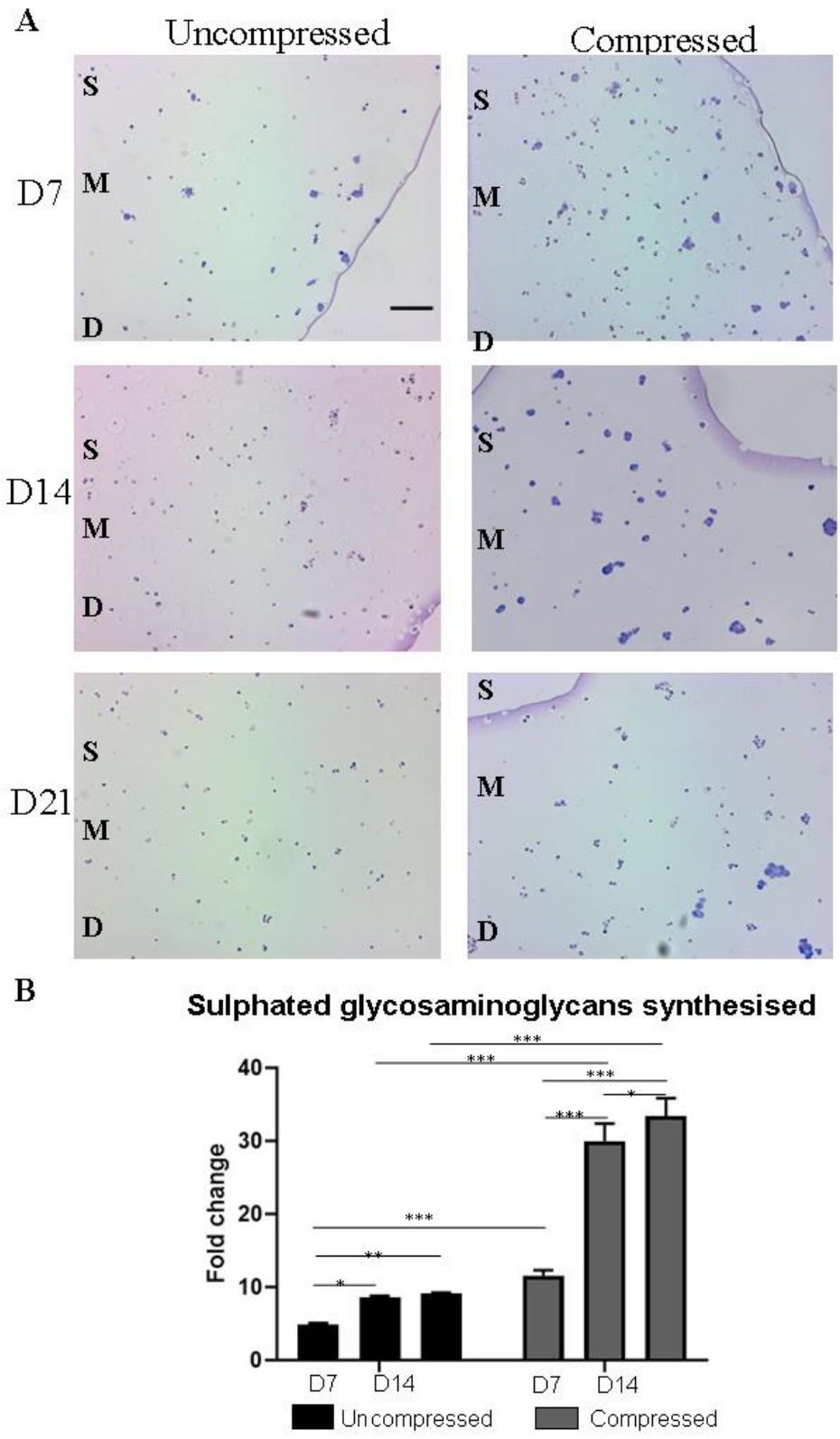

Figure 74. Histological and analysis of sGAG deposition via quantification via DMMB assay after the addition of growth factor at days 7, 14 and 21. *Toluidine blue staining for sGAG analysis for 3-dimensional culture in low gelling temperature agarose of ATDC5 when adding BMP7and TGF-β3 growth factors when compressing and uncompressing the model. S=Surface zone, M= Middle zone, D=Deep zone. Scale bar 100 µm. sGAG production for both conditions at each day point. Two-way ANOVA statistical analysis where * p<0.05, **p<0.01, ***p<0.001, and ****p<0.0001. N=3 and n=3.*

6.3.3 Collagen deposition in uncompressed and compressed hydrogel constructs supplemented with BMP7 and TGF-β3

Collagen deposition was analysed using Picrosirius Red histological stain (Figure 74). There was a visual increase in the pericellular matrix surrounding the cellular clusters with time. Interestingly, the compressed clusters had a larger area at day 7 but not as much ECM deposition as the uncompressed. However, on day 21, the compressed clusters were larger and showed an increased pericellular synthesis of collagen (Figure 75).

For assessment of the collagen deposited in the constructs, immunohistochemistry was performed using primary antibodies against type I, II and X collagen. Type II collagen is a marker of chondrogenesis, type X a marker of hypertrophy and chondrocyte maturation, and type I collagen is a potential marker of osteoarthritis, ossification, and tissue damage (Figures 76-79). Type II collagen deposition was not detectable in the uncompressed samples. In contrast, pericellular type II collagen was visible at all time points in the compressed constructs (Figure 76). Interestingly, type X collagen also appeared more abundant in the compressed samples, especially pericellularly after 21 days of culture (Figure 77). Finally, for further validation of the model, immunohistochemistry for type I collagen was performed (Figure 78). Deposition of type I collagen was not detectable in the compressed scaffold; however, in the uncompressed samples, faint pericellular staining was visible after 21 days of culture. Positive and negative controls in Figure 79.

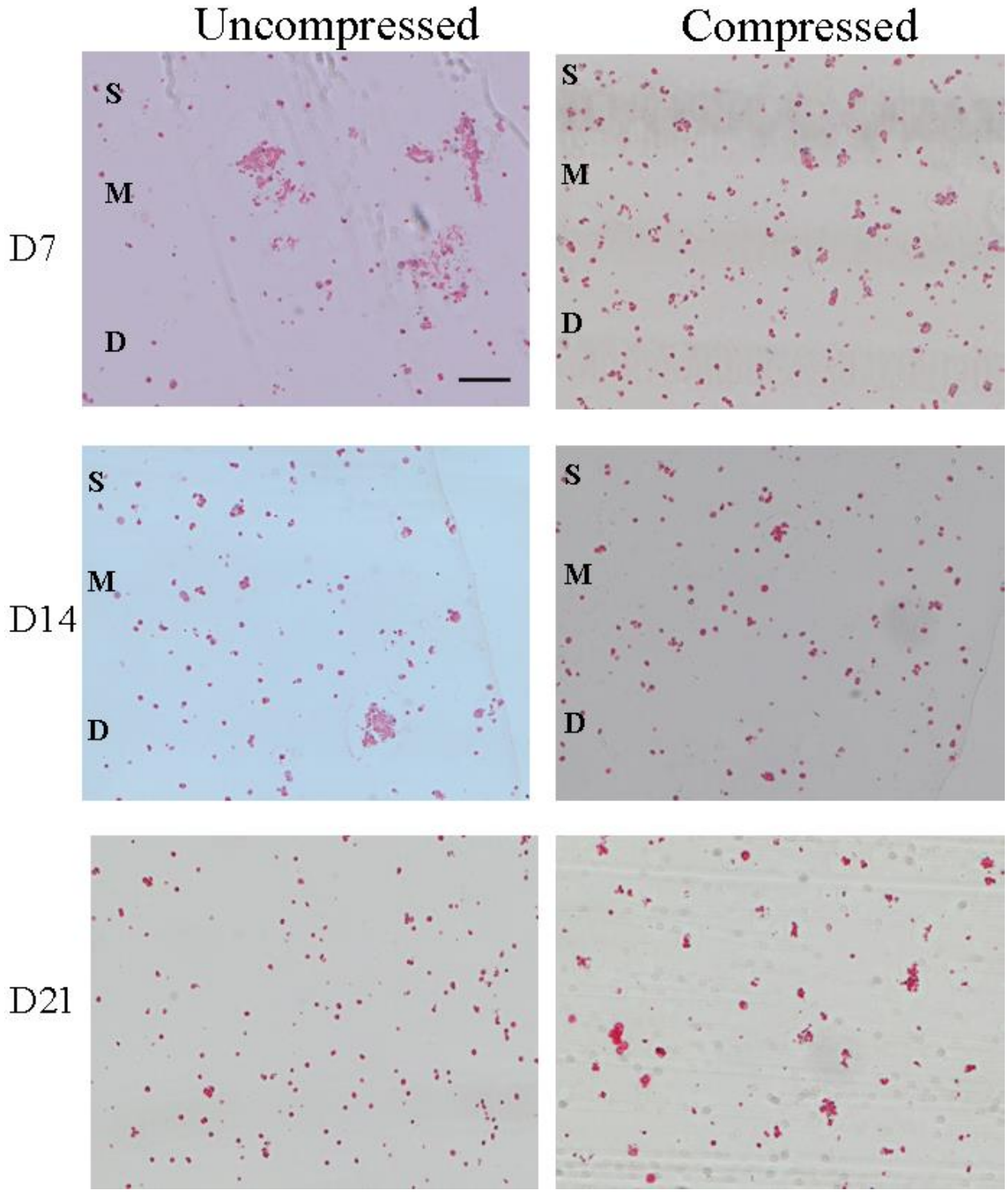

Figure 75. Histological analysis after the addition of both growth factor at days 7, 14 and 21 when compressing and no compressing. *Picrosirius Red for deposition of collagen for 3-dimensional culture in low gelling temperature agarose of ATDC5 for BMP7 and TGF-β3 growth factors. S=Surface zone, M= Middle zone, D=Deep zone. Scale bar 100 µm. N=3 and n=3.*

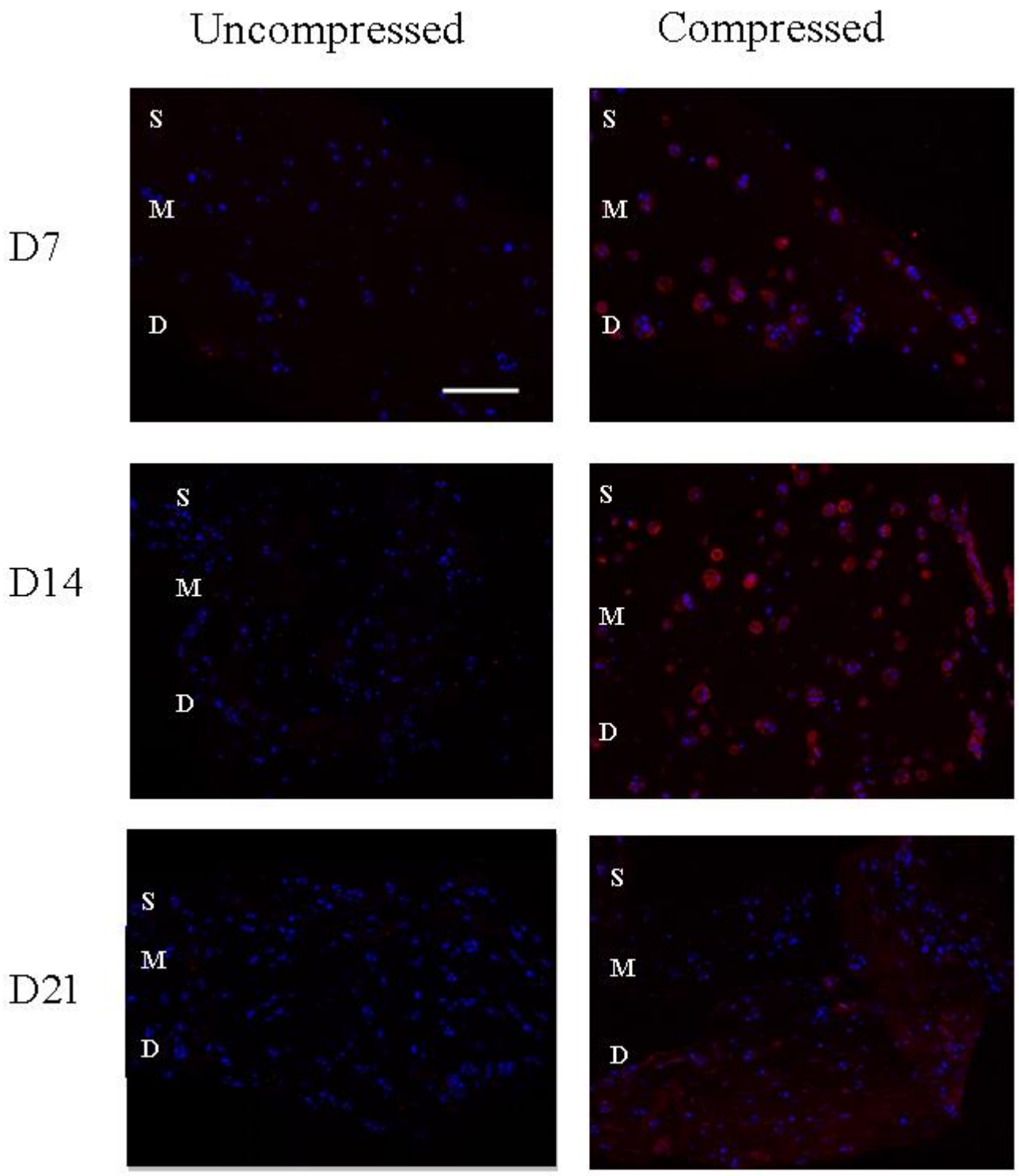

Figure 76. Immunohistochemistry for type II collagen. *ATDC5 cells seeded in a 3-dimensional culture in low gelling temperature agarose for 21 days, with the addition of BMP7 and TGF-β3 growth factors. Red staining = type II collagen. Blue staining = nuclear staining. S=Surface zone, M= Middle zone, D=Deep zone. Scale bar 100 µm. N=3 and n=3.*

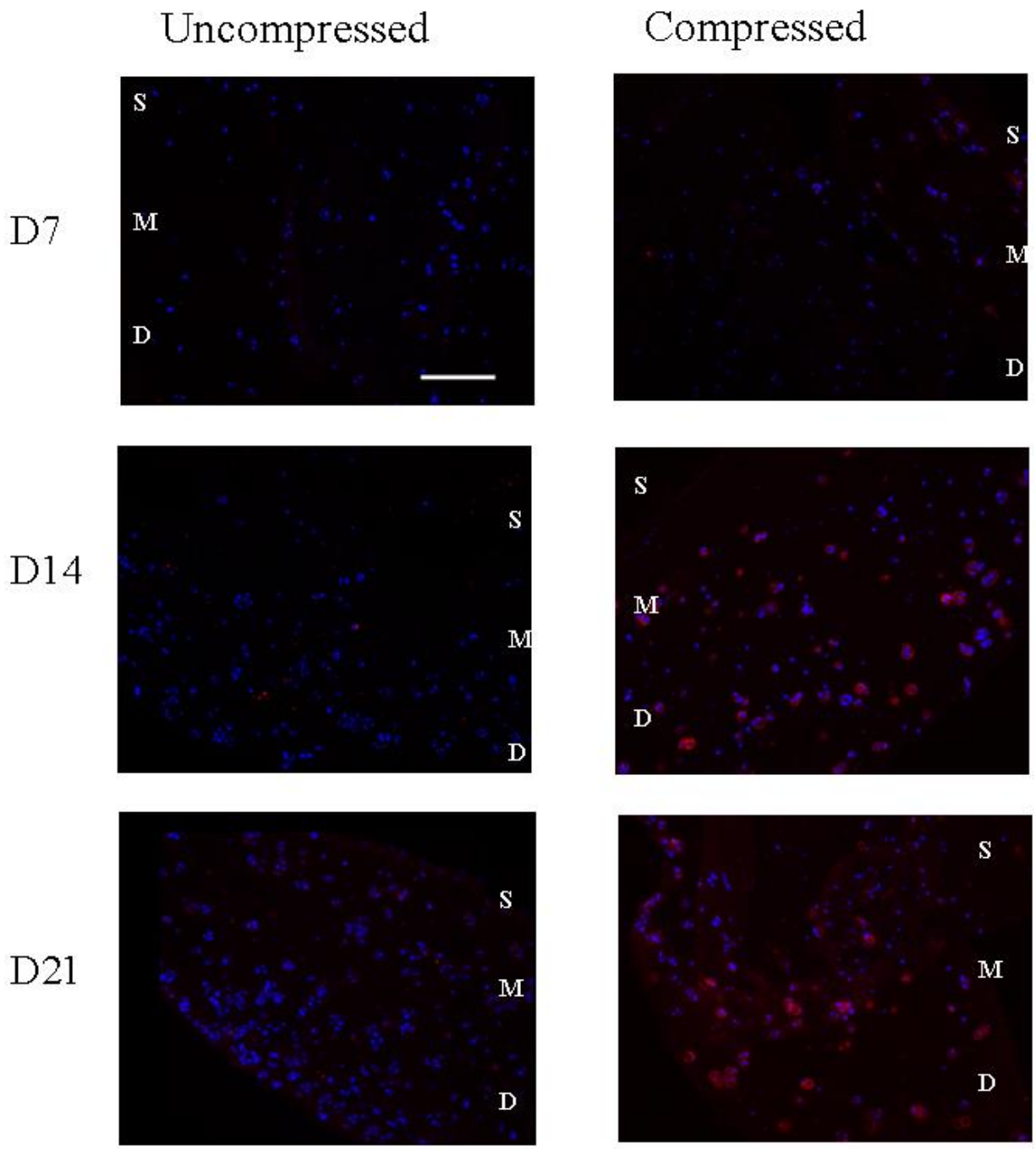

Figure 77. Immunohistochemistry for type X collagen. *ATDC5 cells seeded in a 3-dimensional culture in low gelling temperature agarose for 21 days, with the addition of BMP7 and TGF-β3 growth factors. Red staining = type X collagen. Blue staining = nuclear staining. S=Surface zone, M= Middle zone, D=Deep zone. Scale bar 100 µm. N=3 and n=3.*

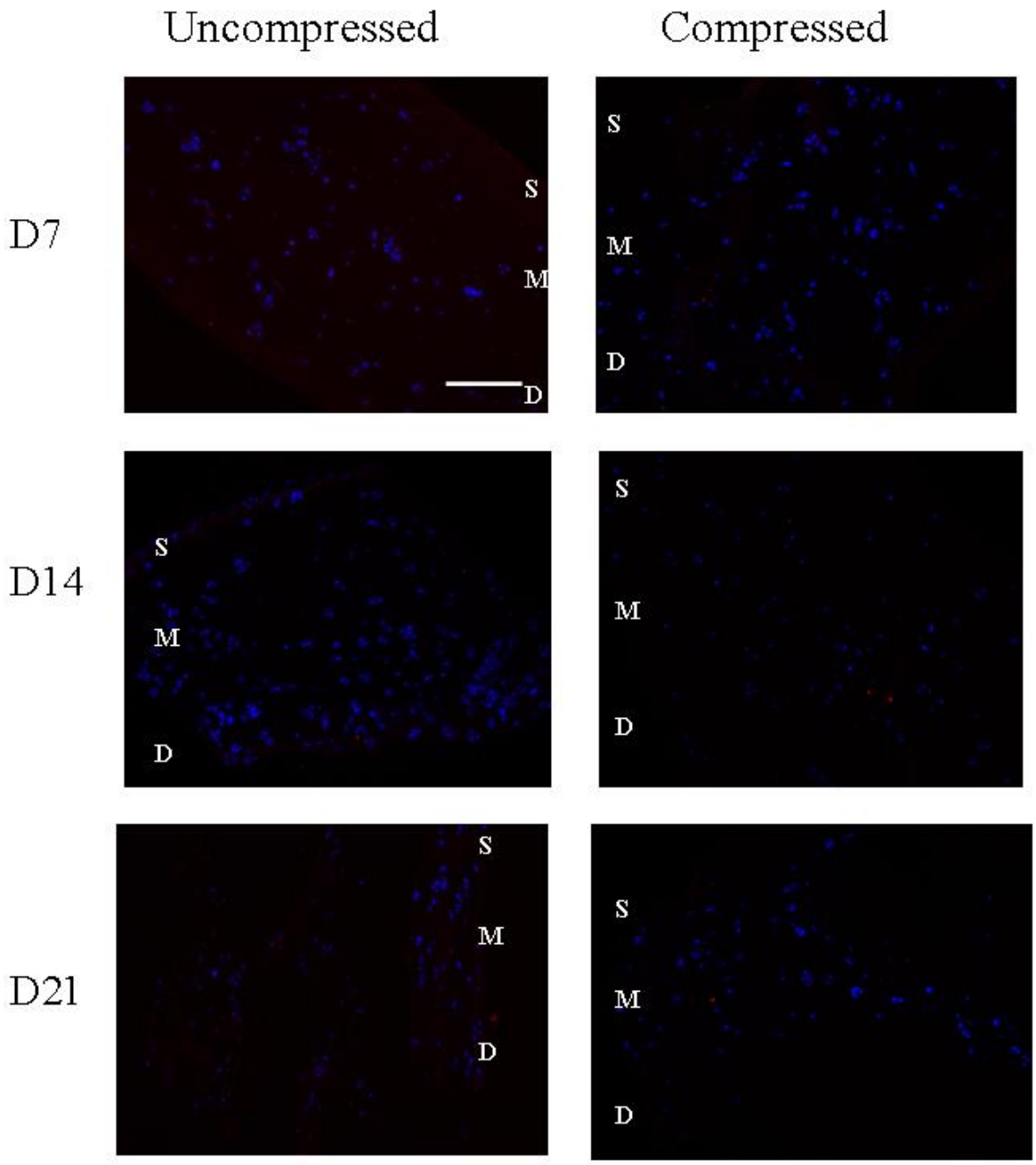

Figure 78. Immunohistochemistry for type I collagen. *ATDC5 cells seeded in a 3-dimensional culture in low gelling temperature agarose for 21 days, with the addition of BMP7 and TGF-β3 growth factors. Red staining = type I collagen. Blue staining = nuclear staining. S=Surface zone, M= Middle zone, D=Deep zone. Scale bar 100 µm. N=3 and n=3.*

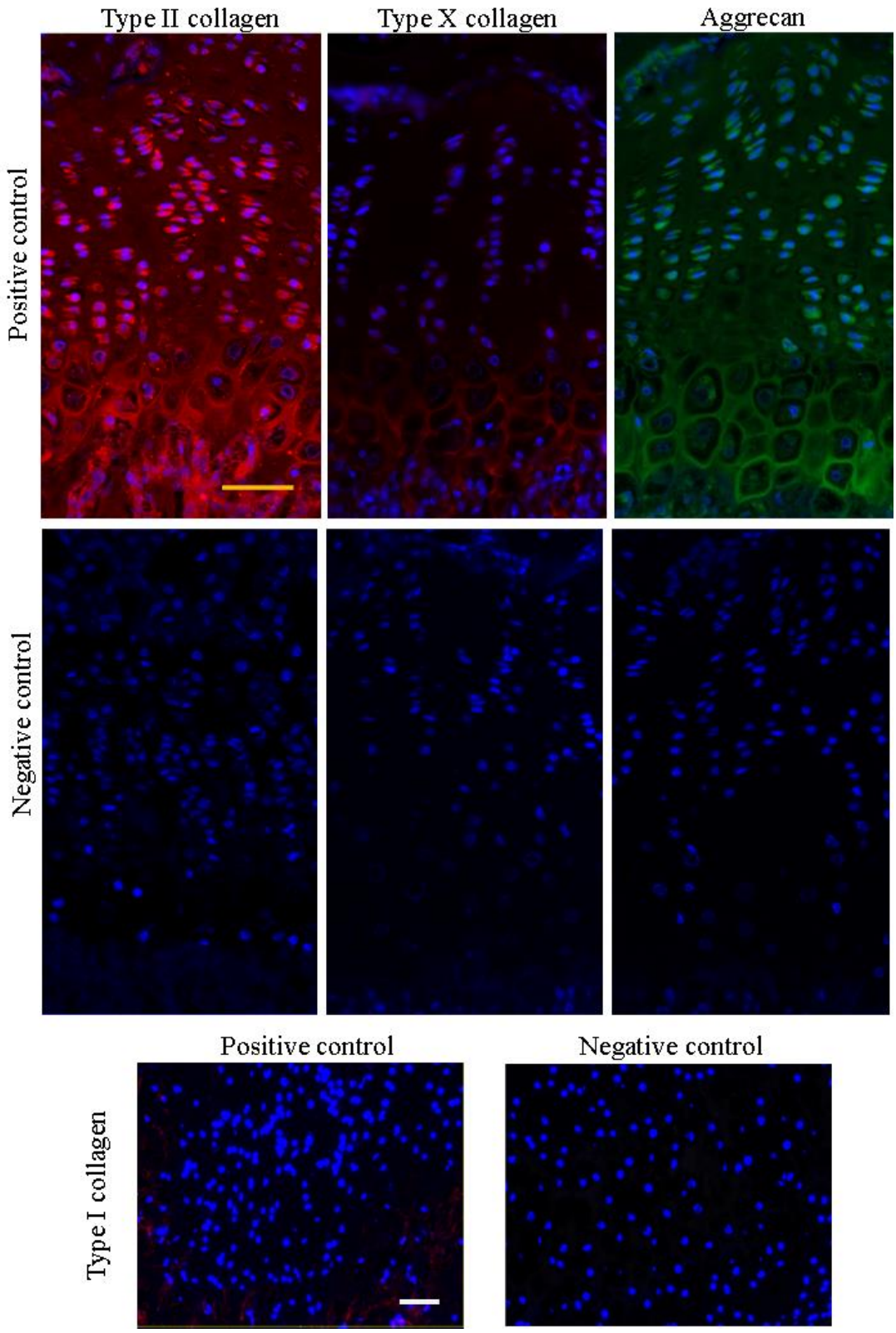

Figure 79. Positive and negative controls for type I, II and X collagen and aggrecan. *Positive and negative controls were done in 3-week-old mice femoral heads for type I, II and X collagen and aggrecan. Scale bar: 50 µm*

6.3.4 Cell apoptosis in uncompressed and compressed hydrogel constructs supplemented with BMP7 and TGF-β3

The histological and immunohistochemical analysis confirmed that compression could augment the deposition of the cartilage-like extracellular matrix in the tissue-engineered agar constructs. However, mechanical stress is known to affect cell survival. Therefore, cell apoptosis and proliferation were measured in the uncompressed and compressed constructs in order to analyse the effect of compression on cell viability (Figure 80 and 81).

Cell apoptosis was measured using the TUNEL assay (Figure 81). Apoptosis when comparison was done within every condition (compressed or uncompressed) along with the day points, no compressing the scaffolds showed a significant decrease comparing days 7 and 14 against day 21 by 0.68- ($p=0.007$) and 0.48-fold change ($p<0.0001$) respectively. A significant increase was visible when comparing day 14 against 7 by 1.422-fold change ($p=0.0008$). Compressing the scaffold resulted in a significant decrease of sGAG deposition when comparing day 21 to days 7 and 14 by 0.66-fold change ($p=0.0085$) and by 0.60-fold change ($p=0.0013$) respectively. Comparison within compressed against uncompressed for different day points showed a significant decrease at days 14 by 0.70-fold change ($p=0.001$).

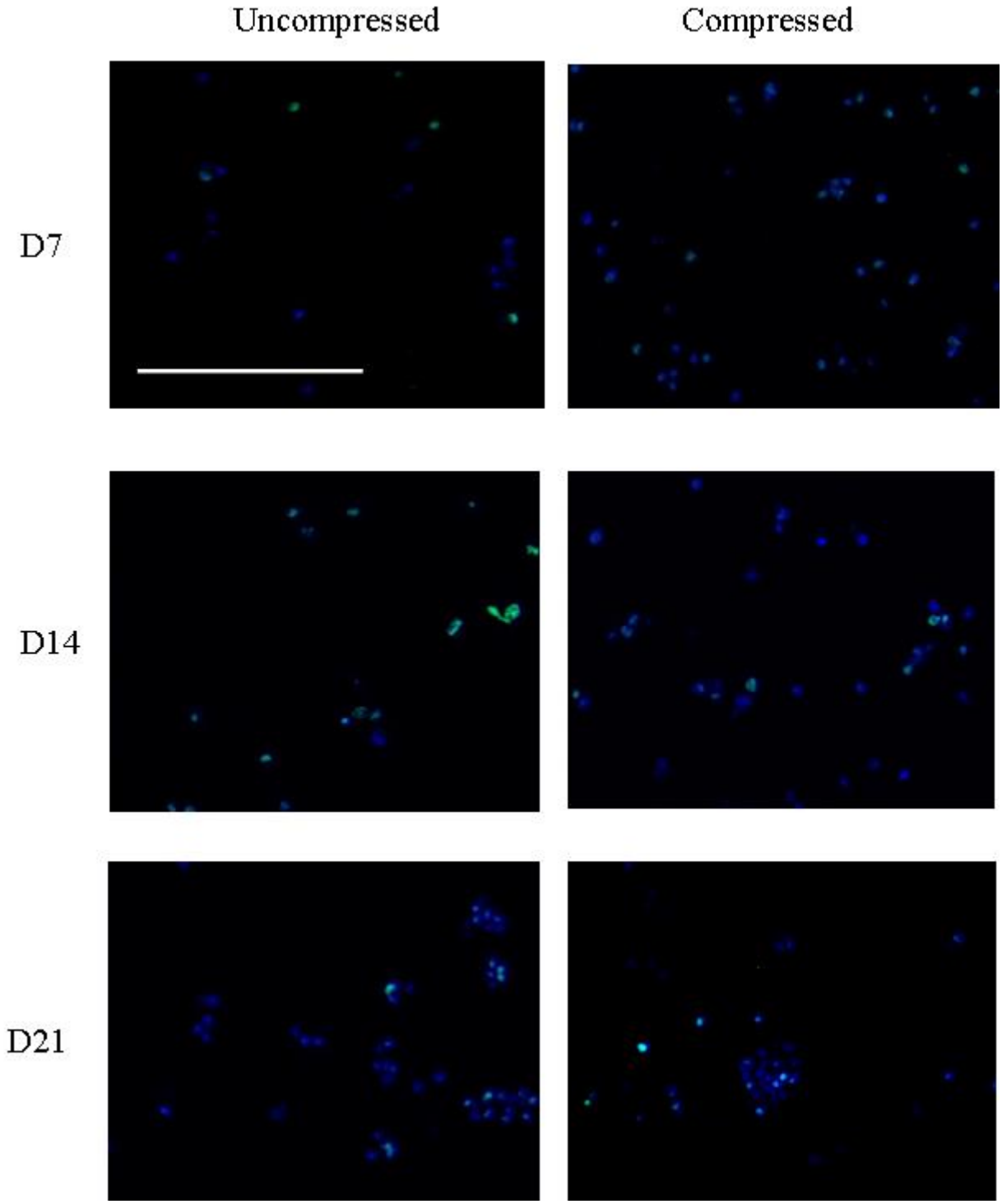

Figure 80. Immunohistochemistry for TUNEL assay *for cell apoptosis for ATDC5 cells seeded in a 3-dimensional culture in low gelling temperature agarose at 7, 14 and 21 days, for combination BMP7 and TGF-β3 growth factor, compression and with no compression. Yellow staining = cell apoptosis. Blue staining = nuclear staining. Scale bar 50 µm. N=3 and n=3.*

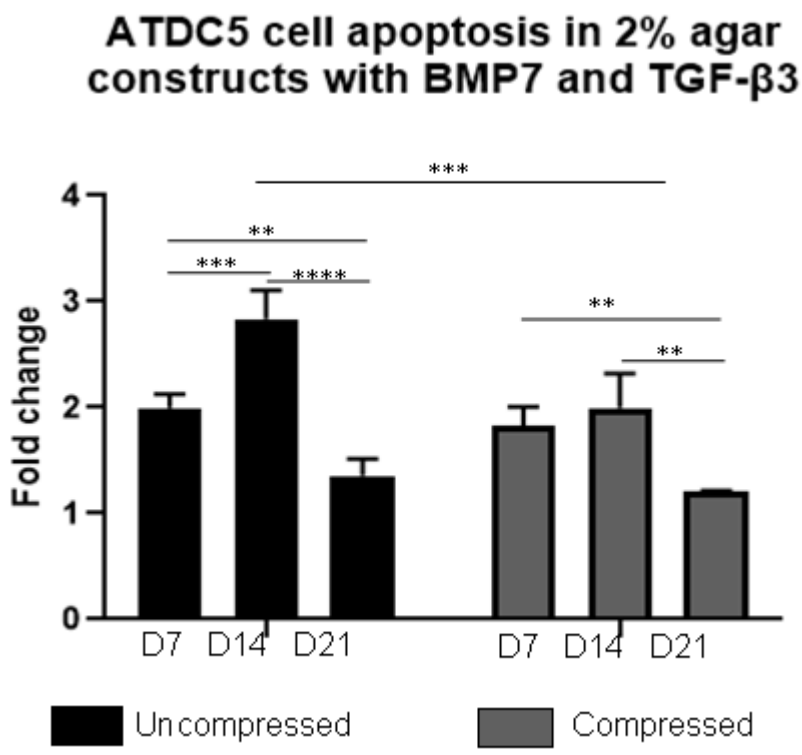

Figure 81. **Numerical data and statistical analysis in the graph.** Cell apoptosis after 21 for the addition of both growth factor compressing and no compressing. Two-way ANOVA statistical analysis where * p<0.05, **p<0.01, ***p<0.001, and ****p<0.0001. N=3 and n=3.

6.3.5 Cell proliferation and cell metabolic activity in uncompressed and compressed hydrogel constructs supplemented with BMP7 and TGF-β3

Cell proliferation was assessed using immunohistochemistry against Ki-67, a nuclear protein expressed during cell proliferation (Figure 82 and 83A) and quantified against all cells in the constructs (DAPI positive) then expressed against the proliferation at day 1 after seeding.

There was a progressive increase in cellular proliferation along the culture time for both conditions, especially when comparing day 7 against day 14 when no compression was done in the scaffold presented a significant increase in cell proliferation by 1.76-fold change (p=0.0341). When compressed the scaffold showed a significant increase comparing day 21 against day 7 by 1.53-fold change (p=0.0207). when comparing uncompressed against compressed for day 21, a significant increase in cell proliferation was observed when compressing the scaffolds by 1.46-fold change (p=0.0392) (Figure 83A).

Further analysis of the condition of the cells in the agar constructs was conducted by validating their metabolic activity using MTT assay (Figures 83B). The cell metabolic activity showed a similar tendency for both conditions when no compressing and comparing day 7 against days 14 and 21 a significant increase in cell metabolic active it was visible by 2.50-fold

change ($p<0.0001$) and 2.66-fold change ($p<0.0001$) respectively. When compressed the scaffold showed a significant increase comparing day 21 against days 7 and 14 by 3.42-fold change ($p<0.0001$) and 1.46-fold change ($p=0.0006$) respectively. A significant increase was also visible when comparing day 14 against 7 by 2.34-fold change ($p<0.0001$). Comparison uncompressed against compressed at day 21, a significant increase in cell metabolic activity was observed when compressing the scaffolds by 1.39-fold change ($p=0.0015$).

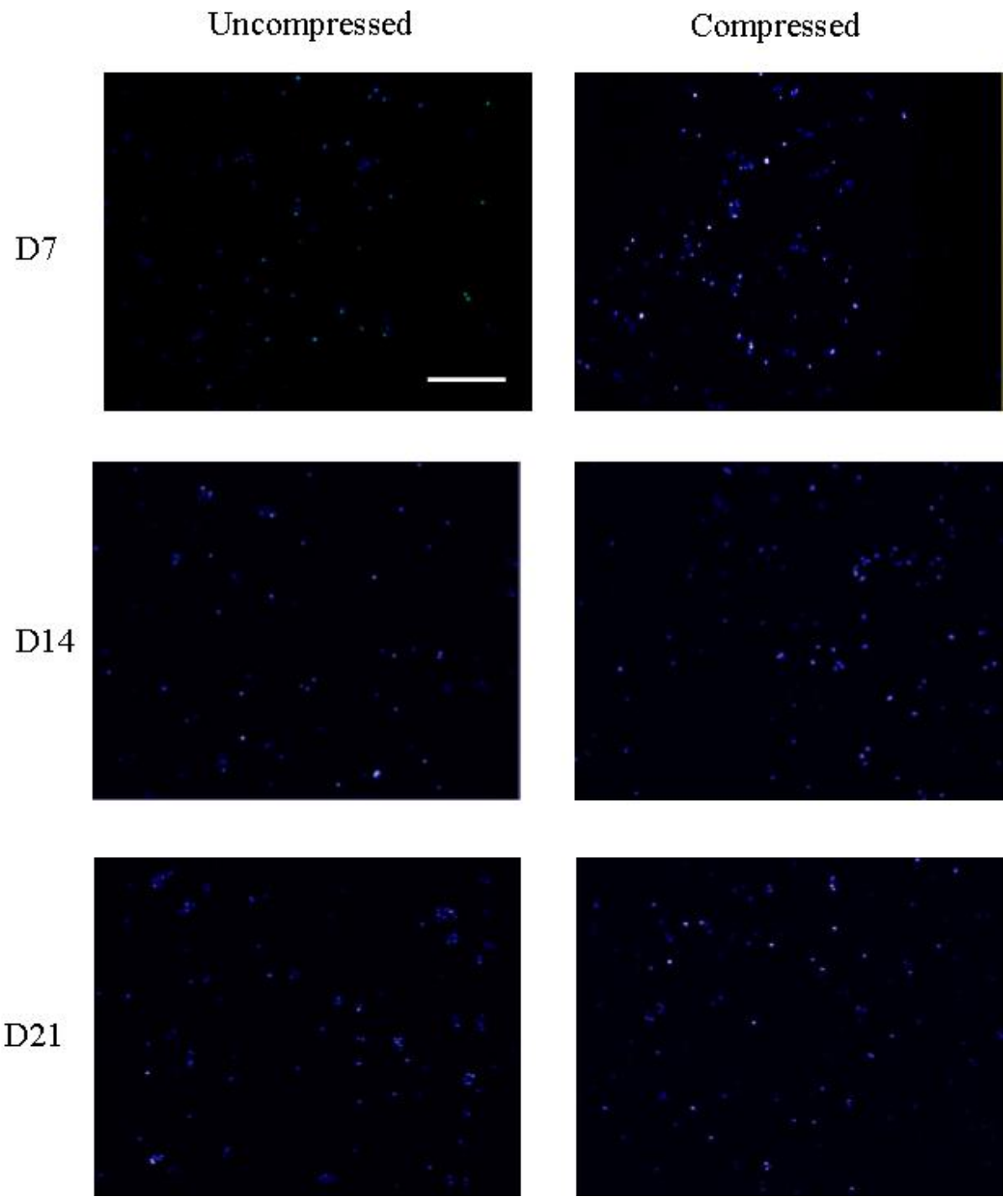

Figure 82. Immunohistochemistry for cell proliferation assay for ATDC5 cells seeded. *in a 3-dimensional culture in low gelling temperature agarose at 7, 14 and 21 days, for combination BMP7 and TGF-β3 growth factor, compression and with no compression. Yellow staining = cell apoptosis. Blue staining = nuclear staining. Scale bar 50 µm. N=3 and n=3.*

A

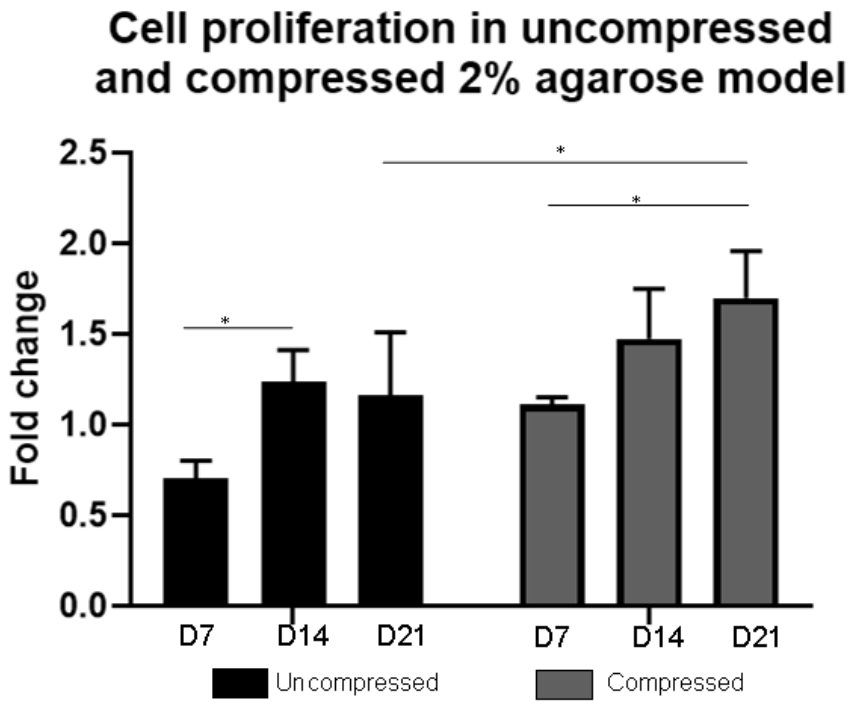

B

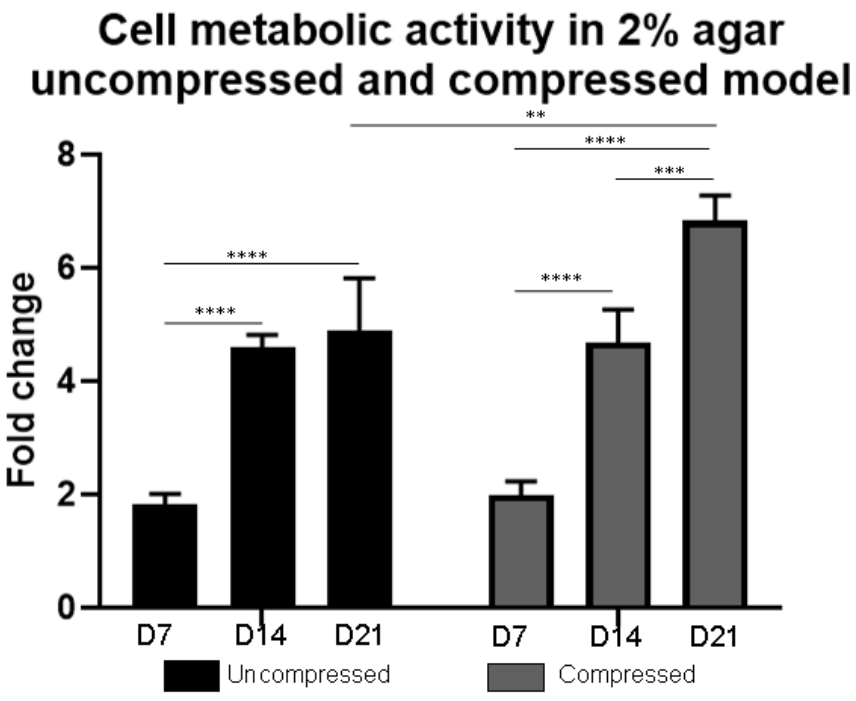

Figure 83. Analysis in cell proliferation and cell metabolic activity. A) *Cell proliferation via Ki-67 after 21 for the addition of both growth factor compressing and no compressing.* ***B)*** *Cell metabolic activity via MTT after 21 for the addition of both growth factor compressing and no compressing. Two-way ANOVA statistical analysis where * $p<0.05$, ** $p<0.01$, *** $p<0.001$, and **** $p<0.0001$. N=3 and n=3.*

6.3.6 *Gene expression of chondrogenic markers in uncompressed and compressed hydrogel constructs supplemented with BMP7 and TGF-β3*

The effect of mechanical compression on chondrogenesis was verified by measuring gene expression of *Sox9* and *Ihh*, and the ECM synthesis and cartilage differentiation by examining type I (*Col1a1*), II (*Col2a1*) and X collagen (*Col10a1*) and aggrecan (*Acan*) via quantitative RT-PCR over the 21 days of culture (Figure 84 and Table 8). All results represented in graphs were calculated as a fold change normalised to data obtained after 24h of seeding as a reference. Therefore, day point 1 has the value of 1 in all graphs. Every graph is accompanied by its fold change values and the p-values.

Sox9, a marker of early chondrogenesis, remained at baseline levels in the uncompressed cultures (Figure 84A). Only a significant increase was visible compressing the scaffolds when comparing day 7 against days 14 and 21 by 95.4- and 61.41-fold change respectively ($p<0.0001$). A significant reduction in gene expression was observed when comparing day 14 against day 21, by 0.643-fold change ($p<0.0001$). When comparison was done within each day point comparing uncompressed scaffolds versus compressed ones, a significant increase was visible at 14 and 21 by 76688.9-fold change and 230204-fold change respectively ($p<0.0001$).

Ihh is a mechanosresponsive gene and part of the IHH-PTHrP signalling pathway that regulates cartilage growth and proliferation (Figure 84B). A significant increase was visible uncompressing the scaffolds when comparing day 7 against day 14 by 15.05-foldchange ($p<0.0001$) and comparing day 14 against day 21 by 11.08-fold change ($p<0.0001$). A significant increase was noticed when compressing the scaffolds when comparing day 7 against day 14 by 11.24-fold change ($p<0.0001$), and a significant decrease when comparing day 14 against day 21, by 0.24-fold change ($p<0.0001$). When comparison was done within each day point comparing uncompressed scaffolds versus compressed ones, a significant increase was visible at 14 by 222.771-fold change ($p<0.0001$).

Col2a1 gene expression (Figure 84C) was significantly increased when compressing the scaffolds when comparing day 7 against days 14 and 21 by 65.354-fold change and 20.41-fold change respectively ($p<0.0001$), and a significant decreased when comparing day 14 against day 21, by 0.31-fold change ($p<0.0001$). When comparison was done within each day point comparing uncompressed scaffolds versus compressed ones, a significant increase was visible at 14 and 21 by 280.337-fold change and 55.01-fold change respectively ($p<0.0001$).

Col10a1 gene expression (Figure 84D) was significantly increased when compressing the scaffolds when comparing day 7 against days 14 and 21 by 86.78-fold change and 136.62-

fold change respectively ($p<0.0001$), and when comparing day 14 against day 21, by 1.57-fold change ($p<0.0001$). When comparison was done within each day point comparing uncompressed scaffolds versus compressed ones, a significant increase was visible at days 7 and 21 by 42.48-fold change and 81.28-fold change respectively ($p<0.0001$).

Type I collagen (Figure 84E) correlates with unhealthy and damaged cartilage. Uncompressed models showed a significant increase in *Col1a1* expression when comparing day 7 against day 21 by 5.2-foldchange ($p<0.0001$) and comparing day 14 against day 21 by 136.248-fold change ($p<0.0001$). When comparison was done within each day point comparing uncompressed scaffolds versus compressed ones, a significant decrease was visible at 21 by 0.062-fold change ($p<0.0001$).

Acan gene expression (Figure 84F) showed a significant increase when compressing the scaffolds at day 7 against days 14 and 21, by 67.23- and 106.68-fold change ($p<0.0001$) and comparing day 14 against day 21 by 1.58-fold change ($p<0.0001$). When comparison was done within each day point comparing uncompressed scaffolds versus compressed ones, a significant increase was visible at days 14 and 21 by 246.68- and 151.608-fold change respectively ($p<0.0001$).

Overall, compressed constructs showed a significant increase in expression of genes related to chondrogenesis and ECM synthesis, indicating that compression has a beneficial effect on chondrogenic differentiation of ATDC5 cells in low gelling agar tissue-engineered constructs (Figure 84).

		Sox9	***Ihh***	***Col2a1a***	***Col10a1***	***Col1a1***	***Acan***
Uncompressed	Day7	↓	↑	↑	↑	↓	↑
	Day14	↓	↑	↑	↑	↓	↑
	Day21	↓	↑	↑	↑	↓	↑
Compressed	Day7	↑	↑	↑	↑	↓	↑
	Day14	↑	↑	↑	↑	↓	↑
	Day21	↑	↑	↑	↑	↓	↑

Table 8. Table summarising the outcome of the gene expression *of Sox9, Indian hedgehog (Ihh), collagen II (Col2a1), collagen X (Col10a1), collagen I (Col1a1) and aggrecan (Acan) after 21 days of culturing ATDC5 in a 3-dimensional culture compressed and uncompressed compared to day 1 gene expression. N=3 and n=3.*

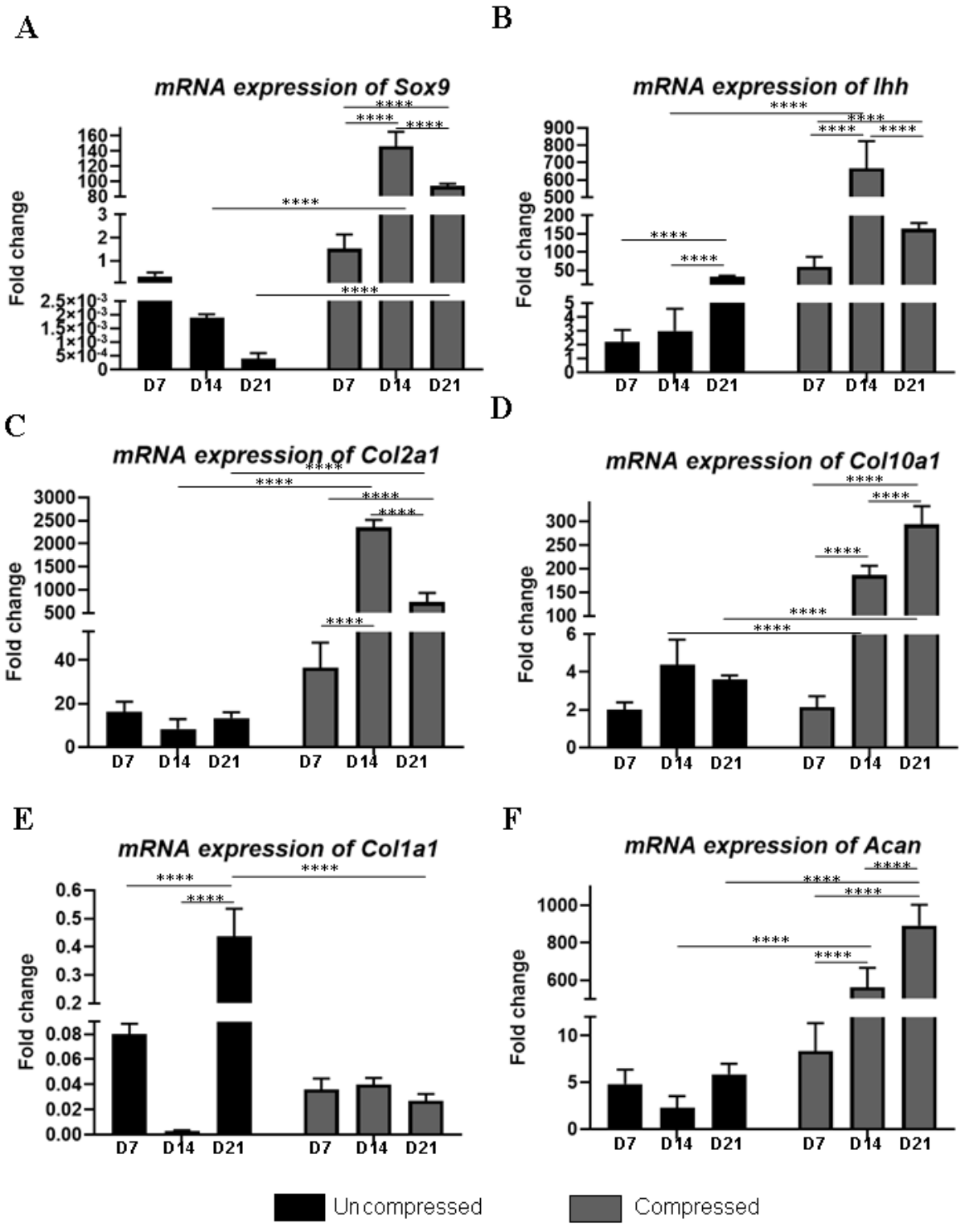

Figure 84. mRNA expression after 21 days of culture. *Gene expression of Sox9* ***(A)****, Indian hedgehog (Ihh)* ***(B)****, type II collagen (Col2a1)* ***(C)****, type X collagen (Col10a1)* ***(D)****, type I collagen (Col1a1)* ***(E)****, aggrecan (Acan)* ***(F)*** *after 21 days of culturing ATDC5 in a 3D hydrogel culture compressing and no compressing. Quantification levels were normalised to the levels after seeding 10 million cells per ml before being differentiated (Day point 1). Three-way ANOVA statistical analysis where * p<0.05, **p<0.01, ***p<0.001, and ****p<0.0001. N=3 and n=3.*

6.4 Discussion

Work presented in this chapter studied the differences in the extracellular matrix deposition and gene expression that resulted from mechanical loading of ATDC5 cells cultured in agarose hydrogels.

Articular cartilage is exposed to a combination of different types of mechanical stimulation, such as strain, shear stress and compressive forces, that not only serve as a stimulus to remodel the extracellular matrix but also regulate chondrogenic differentiation (Masuda et al., 2008; Bougault et al., 2009). For example, it has been shown that applying tensile strain inhibits the differentiation of ATDC5 cells, compared to compression, which enhances chondrogenic differentiation (Masuda et al., 2008). Not only does compressing contribute to the differentiation of the cells, but also dynamic compression enhances the synthesis of the cartilage ECM (Tsuang et al., 2008).

In articular cartilage, PCM serves as a biomechanical and biochemical transducer for the chondrocytes (Wilusz, Sanchez-Adams and Guilak, 2014). Pericellular matrix (PCM) was deposited in ATDC5 agarose constructs after 21 days of culture, the constructs were therefore grown for 21 days, with 15 days of compression. The compression regime was started a week after the constructs were seeded, based on literature studies such as a study by Lima et al. which showed that compressing immediately after seeding the cells leads to a significant decrease in sGAG deposition, collagen synthesis and Young's compressive modulus (Lima et al., 2007) and by Falconer et al. showing high rates of cell apoptosis when SW1353 chondrocyte-like cells in agarose constructs were compressed in the FX-5000C Flexcell® Compression Plus™ System immediately after seeding (Falconer, 2017). Despite this, another study suggests a minimal benefit of delaying the compression to ECM deposition (Bian et al., 2010).

Compression regimes with both sinusoidal and square waves have been widely used *in vitro* in articular cartilage modelling (Ridler, Plewes and Henkelman, 2001; Bevill et al., 2009; Engstrøm et al., 2018, 2019; Dolzani et al., 2019). Square waves retain longer periods of the pressure applied in the scaffold, not allowing time for the tissue to relax (Goseet et al., 2008), therefore, a sinusoidal wave was chosen for the current study, to mimic physiological impacts on the tissue.

Agarose hydrogels have been extensively used in numerous studies (Hung et al., 2004; Mauck et al., 2007; Chokalingam et al., 2009; Wu et al., 2013; Jacek et al., 2018). Not only have they been shown to maintain the phenotype of the cells (Chapter 3), but also to be an excellent model to replicate *in vitro* mechanical responses that the tissue goes through

(Bougault et al., 2009; Jin and Kim, 2018). Agarose hydrogels allow an adequate transmission of the mechanical forces and growth factors across the matrix via diffusion, similarly to what happens in vivo (Tsuang et al., 2008). An increase in the density of the hydrogel, from 1% to 2% was necessary since the initial optimisation experiments showed that 1% of agarose hydrogels were too brittle to bear with the compressive forces. The increase of the density of the hydrogel to 2% (w/v) was also applied in other studies for chondrogenesis using 2% agarose showing an optimised nutrient transport while preserving the ECM deposited (Bougault et al., 2008; Ng, Ateshian and Hung, 2009; Nims et al., 2014; Cigan et al., 2016).

FX-5000C Flexcell® Compression Plus™ System was used to compress the scaffold. It has been widely used in other studies, not only for cartilage (Bougault et al., 2008; Nakagawa et al., 2012; Falconer, 2017; Luo et al., 2018) but also for other organs, such as skin (Hara et al., 2014) or bone (Zaky et al., 2017).

The type of load, static or dynamic, but also the duration and frequency affect the biosynthetic cell response (Bougault et al., 2008). The compression regime is highly variable in many studies, with different cell types, hydrogel types, and type and frequency of loading (Anderson and Johnstone, 2017). In this study, a short-duration dynamic loading was chosen since it has been shown to stimulate the synthesis of ECM components, especially proteoglycans (Mauck et al., 2000; Tsuang et al., 2008; Anderson and Johnstone, 2017). The intermittent load allows the cells to respond to the stimulus and increase the deposition of ECM in response (Anderson and Johnstone, 2017).

Interestingly, toluidine blue staining showed a higher deposition of PCM in the cell clusters of compressed constructs when compared to the model without compression. This was verified by measuring the area of the clusters per zone, which increased over 21 days of culture, especially in the deeper zone of the compressed model. These structural changes were further substantiated by sGAG quantification, in which the compressed model synthesised significantly more sGAG at each day point than the uncompressed control. Previous studies in which dynamic compression was applied in chondrocytes seeded in agarose hydrogels also presented a higher deposition of sGAG when compressed (Tsuang et al., 2008; Anderson and Johnstone, 2017). Not only a higher sGAG deposition is linked to the pressure applied, but also, this PCM deposited prior to compression and encouraged while compressing has been associated with reduced cell apoptosis and deformation (De Vries et al., 2014). The ATDC5 seeded compressed model presented lower cell apoptosis at all day points when compared to the uncompressed model, with a significant decrease in apoptosis from day 7 to day 21. In contrast, other studies

showed an increase in cell apoptosis induced by mechanical stress-induced apoptosis in hydrogels (Falconer, 2017) and spheroids (Cheng et al., 2009).

The deposition of collagen, one of the main components of the ECM, was also analysed using Picrosirius Red staining. Similarly, to previous sGAG deposition, there was an increase in the PCM deposition of collagen, especially after 21 days of seeding. To get further insight into the type of PCM synthesised, immunohistochemistry for type II, X and I collagen was performed. Type II and X collagen immunohistochemistry demonstrated that compression increased the deposition of both cartilage-specific collagens after 14 and 21 days of culture, in contrast to the uncompressed scaffold, which did not show an increase in staining. These results contradict some studies that showed that compression did not affect the deposition of collagen (Kaupp, Weber and Waldman, 2012; Omata et al., 2012), while other studies suggest that this is dependent on the cells age/passage, in which juvenile chondrocytes showed a reduction of type II collagen deposition. In contrast, adult chondrocytes increased type II collagen after compression in 2% agarose hydrogels (Farnsworth, Antunez and Bryant, 2013). However, several studies of chondrocytes in 2% agarose showed an increase in type II collagen and proteoglycan deposition (Kelly et al., 2013; Mesallati et al., 2013).

Gene expression of chondrogenesis related genes (*Col2a1, Ihh, Acan*) was increased upon compression. Interestingly, type II collagen expression decreased after 1 week of compression, in time for type X collagen to reach its peak after 3 weeks of culture, suggesting that the cells were becoming more mature and hypertrophic. On the other hand, early chondrogenesis and cartilage formation and markers of chondrogenic proliferation and differentiation markers, *Sox9* and *Ihh* gene expression peaked after 2 weeks in the compressed samples (Guilak and Hung, 2005; Bougault et al., 2012). In mouse chondrocytes, high levels of *Sox9* correlate with a higher expression of type II collagen (Bougault et al., 2012). Interestingly, a steady level of *Sox9* expression concomitant with *Col10a1* expression has been linked to hypertrophic chondrocytes (Bougault et al., 2012), supporting the idea that the ATDC5 cells after 3 weeks of culture with dynamic compression were maturing and becoming more hypertrophic. Gene expression in the uncompressed scaffold showed high variation and lower mRNA synthesis. *Ihh, Col2a1 and Acan* genes have been shown to be mechanosensitive (Zhao et al., 2020), and (Fox, Bedi and Rodeo, 2009). A study using type I collagen gel showed upregulation of aggrecan and collagen (Ando et al., 2009) while another study using 2% agarose only showed upregulation of aggrecan when a dynamic load was applied (Mauck et al., 2007). Culturing bovine chondrocytes in 2% agarose led to upregulation of aggrecan but also downregulation of type II collagen when pre-culturing for 3 days before applying compression

and applying different compression forces (Hung et al., 2004; Mauck et al., 2007). In contrast, murine chondrocytes cultured in 2% agarose presented upregulated type II collagen expression without any pre-culturing (Chokalingam et al., 2009; Wu et al., 2013). Likewise, this variability was found in other hydrogels, such as alginate, in which, seeding adult human chondrocytes at 2% alginate with 1 Hz dynamic compression showed increased gene expression of aggrecan and type II and I collagen (Jeon et al., 2012, 2013), however, another study with the same cell source and hydrogel type and density, but compressed only 0.5 Hz resulted in no variation on aggrecan, type II or X collagen (Grogan et al., 2012). In two other studies using a polyurethane scaffold, with a frequency of 0.5 Hz and an amplitude of 10% ±25° oscillation, minimal alterations in the duration of compression led to either downregulation of type I collagen or maintenance of its gene expression (Wang et al., 2013; Hilz et al., 2014).

The cell proliferation and cell metabolic activity of ATDC5 cells grown in the agarose constructs were increased upon compression compared to the uncompressed scaffolds at all day points. These results are similar to a study by Shukunami et al. in which the cartilage nodules continued increasing for 3 weeks in culture, ceasing after that and becoming hypertrophic with a marked expression of type X collagen (Shukunami et al., 1997). Interestingly, the gene expression analysis of the compressed model showed a decrease in type II collagen after 14 days of seeding and an increase of type X collagen expression after 14 days, which could be linked to the hypertrophy of the chondrocytes and a reduction in proliferative capacity (Shukunami et al., 1997), indicating terminal differentiation and zonal stratification. A study of ATDC5 cells encapsulated in agarose hydrogel alone showed fairly consistent levels of metabolic activity thought the culture period (Pauly et al., 2017). However, this proliferative capacity varied when ATDC5 cells were encapsulated in alginate hydrogels with and without RGD groups (Yao, Zeng and Huang, 2016). The cell proliferation potential and cell metabolic activity are affected by parameters such as the hydrogel composition, density and compression showing the complexity and challenge when replicating the models and comparing them to other studies (Ahearne, 2014; Anderson and Johnstone, 2017).

As pointed out by Anderson and Johnstone, the large variety of parameters employed in the tissue engineering field results in different outcomes that often make comparison difficult (Anderson and Johnstone, 2017). These variations not only come from types of hydrogel and cell and their density, and application of different mechanical forces and loading regimes, but also, variability in gel preparation, such as the use of an autoclave, or the polymerization temperature of the hydrogel that may affect the stiffness and mechanical properties of the hydrogel (Buckley et al., 2009). The disparity in hydrogel stiffness directly influences cell

activity and phenotype (Ahearne, 2014). The large variety hinders reaching a consensus that would help the development of the field. Finally, growing ATDC5 cells in agar with cyclic physiological compression supported chondrocyte-like differentiation, zonal stratification, and decreased dedifferentiation, inducing the expression of mechanoresponsive genes and presenting a good model to study mechanosensing in developing and diseased cartilage.

Chapter 7. Characterisation of T585M COMP Mutation in Tissue Engineered Models of Cartilage

7 Characterisation of T585M COMP mutation in tissue-engineered models of cartilage

7.1 Introduction

Skeletal dysplasias are 450 hereditable bone and cartilage disorders (Krakow, 2015) that affect the development and growth of the skeleton. Currently, there are not many treatments available for skeletal dysplasias, due to the rarity of individual conditions, difficulty in obtaining the clinical material and the cost of animal studies required to test potential interventions. A better understanding of the molecular pathways involved in the disease progression is required to improve the treatment of the patients and accurate diagnosis (Krakow, 2015).

Work presented in this chapter focused on a point mutation in the gene encoding cartilage oligomeric matrix protein (COMP) and leading to an autosomal dominant condition called pseudoachondroplasia, with an incidence of 1 in 20,000 and a dwarfism phenotype (Briggs and Chapman, 2002; Tufan *et al.*, 2007). This phenotype is characterised by shorter limbs, brachydactyly, deformity of legs and laxity of joints and ligaments (Briggs and Chapman, 2002; Tufan *et al.*, 2007).

Mutations affecting the C-terminal domain (CTD) account for 15% of all mutations found in *COMP* and have been less characterised than the ones affecting the T3 domain (85%) (Briggs *et al.*, 1998). The p.T585M mutation in COMP affects a single amino acid Threonine in the position 585 in the C-terminal domain that is mutated to Methionine, a hydrophobic amino acid (T585M) (Spitznagel *et al.*, 2004; Pirog-Garcia *et al.*, 2007; T.-L. L. Chen *et al.*, 2008) and does not affect the secretion of mutant protein into the ECM, in contrast to the pathomolecular mechanism of PSACH resulting from mutations in T3-COMP, in which retention of mutant protein causes intracellular stress and subsequent cell death. It has been postulated that p.T585M COMP mutation may affect mechanosensing in the cartilage growth plate (Pirog, unpublished data); however, due to the lack of a suitable experimental model, this could not be studied in detail.

While some studies suggest that cell culture models might not be able to recapitulate some of the pathological features *in vitro* (Suleman *et al.*, 2012), other studies suggest that both mouse models and *in vitro* models may generate crucial information regarding the pathological features and cellular mechanisms of the disease development (K L Posey *et al.*, 2008). The

work presented in previous chapters shows that culturing ATDC5 cells in compressible hydrogel offers the potential of studies of mechanosensing and biomechanic outcomes *in vitro*.

7.2 Aims of the chapter.

This chapter aimed to study the pathological mechanism of the p.T585M COMP mutation during ATDC5 chondrogenesis in the conventional 2-dimensional culture and in the two developed *in vitro* 3D systems: pellets and hydrogels. The study of the disease progression in all the models would further decouple the signalling and pathological features of CTD-COMP PSACH in cartilage.

7.3 Results

For the study of pseudoachondroplasia (PSACH) development, p.T585M COMP mutation was introduced into the ATDC5 cells by stable transfection, and the cells were stably transfected, FACS sorted and established in the laboratory prior to this project (Figure 85). The p.T585M COMP cells were cultured in the models developed in previous chapters; 2-dimensional model, pellet, and 3-dimensional hydrogel.

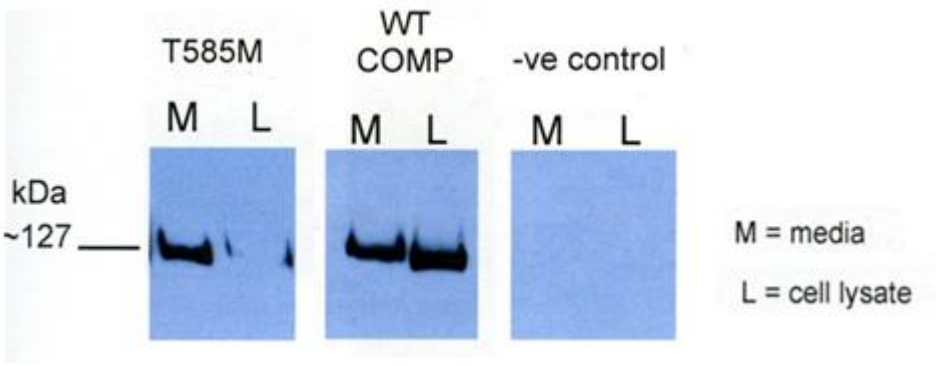

Figure 85. Western blot showing WT and pT585M COMP mutant cells with the COMP protein. *COMP was introduced into the ATDC5 cells by stable transfection and selected by FACS.*

All results represented in graphs were calculated as fold change using data obtained after 24h of seeding untransfected ATDC5 cells as a reference. Therefore, day point 1 has the value of 1 in all graphs. In the case of WT and p.T585M COMP ATDC5 cells, the day point 1 used was obtained from untransfected ATDC5 cells. Every graph is accompanied by its fold change values and the p-values.

7.3.1 Morphology and ECM deposition in the 2-dimensional model of ATDC5 cells stably transfected with WT and p.T585M mutant COMP

The morphology of untransfected, WT COMP and p.T585M COMP cells was fusiform, fibroblast-like and comparable across all conditions. However, in the 2-dimensional model after 7 days of culture, the p.T585M COMP ATDC5 cells showed a slower cell proliferation rate when compared to the cells transfected with the wild-type COMP (Figure 86A) and the untransfected controls (Chapter 3). Moreover, after 21 days, the mutant cells showed lower cell numbers, whereas the wild-type model presented a similar phenotype and proliferation rate as found for untransfected cells in chapter 3 (Figure 84.A). p.T585M COMP ATDC5 cells appeared rounded, detached from the plastic surface and dead after 21 days of culture.

Alcian blue staining for sulphated glycosaminoglycans was performed on day 21 (Figure 86B and 87A). WT cells showed patches of sGAG deposition similar to the deposition seen in the untransfected ATDC5 cultures, while the mutant cells did not show any visible stain. Similarly, when staining for calcium deposits via alizarin red (Figures 86C and 87B), the p.T585M COMP cells showed no staining, whereas the wild type staining showed small deposits of calcium (Figure 84.C). Alcian Blue and Alizarin Red stains were extracted from the stained cell layers and quantified using a spectrophotometer.

Quantification of the Alcian blue deposition (Figure 87A) showed a significant decrease was visible at days 14 and 21 when comparing WT-COMP against p.T585M-COMP by 0.0437-fold change ($p<0.0001$) and by 0.016-fold change ($p<0.0001$) respectively. When comparison was done for the same condition, but within different day points, a significant increase in gene expression was observed in WT-COMP cultures when comparing day 7 against day 14 and 21 by 12.69-fold change ($p<0.0001$) and 16.47-fold change ($p<0.0001$) respectively and when comparing day 14 against day 21 by 1.29-fold change ($p=0.0023$).

Alizarin Red of calcium deposition (Figure 87B) showed a similar tendency as found in Alcian Blue quantification. Cells showed a significant decrease was visible at days 14 and 21 when comparing WT-COMP against p.T585M-COMP by 0.050-fold change ($p<0.0001$) and by 0.012-fold change ($p<0.0001$) respectively. When comparison was done for the same condition, but within different day points, a significant increase in gene expression was observed in WT-COMP cultures when comparing day 7 against day 14 and 21 by 9.33-fold change ($p<0.0001$) and 11.86-fold change ($p<0.0001$) respectively and when comparing day 14 against day 21 by 1.27-fold change ($p=0.0023$). Comparing day points within the p.T585M-COMP condition showed a significant decrease by 0.144-fold change ($p=0.01$) when comparing day 7 against day 21.

Following analysis of sGAG via alcian blue and optical density, DMMB assay was performed to validate the quantity of sGAG synthesis in the ECM (Figure 88). Cells showed a significant decrease in sGAG deposition visible at days 14 and 21 when comparing WT-COMP against p.T585M-COMP by 0.217-fold change ($p<0.0001$) and by 0.0445-fold change ($p<0.0001$) respectively. When comparison was done for the same condition, but within different day points, a significant increase was observed in WT-COMP cultures when comparing day 7 against days 14 and 21 by 1.91-fold change ($p<0.0001$) and 3.01-fold change ($p<0.0001$) respectively and when comparing day 14 against day 21 by 1.57-fold change ($p=0.0023$). Comparing day points within the p.T585M-COMP condition showed a significant decrease by 0.174-fold change ($p=0.0021$) when comparing day 7 against day 21.

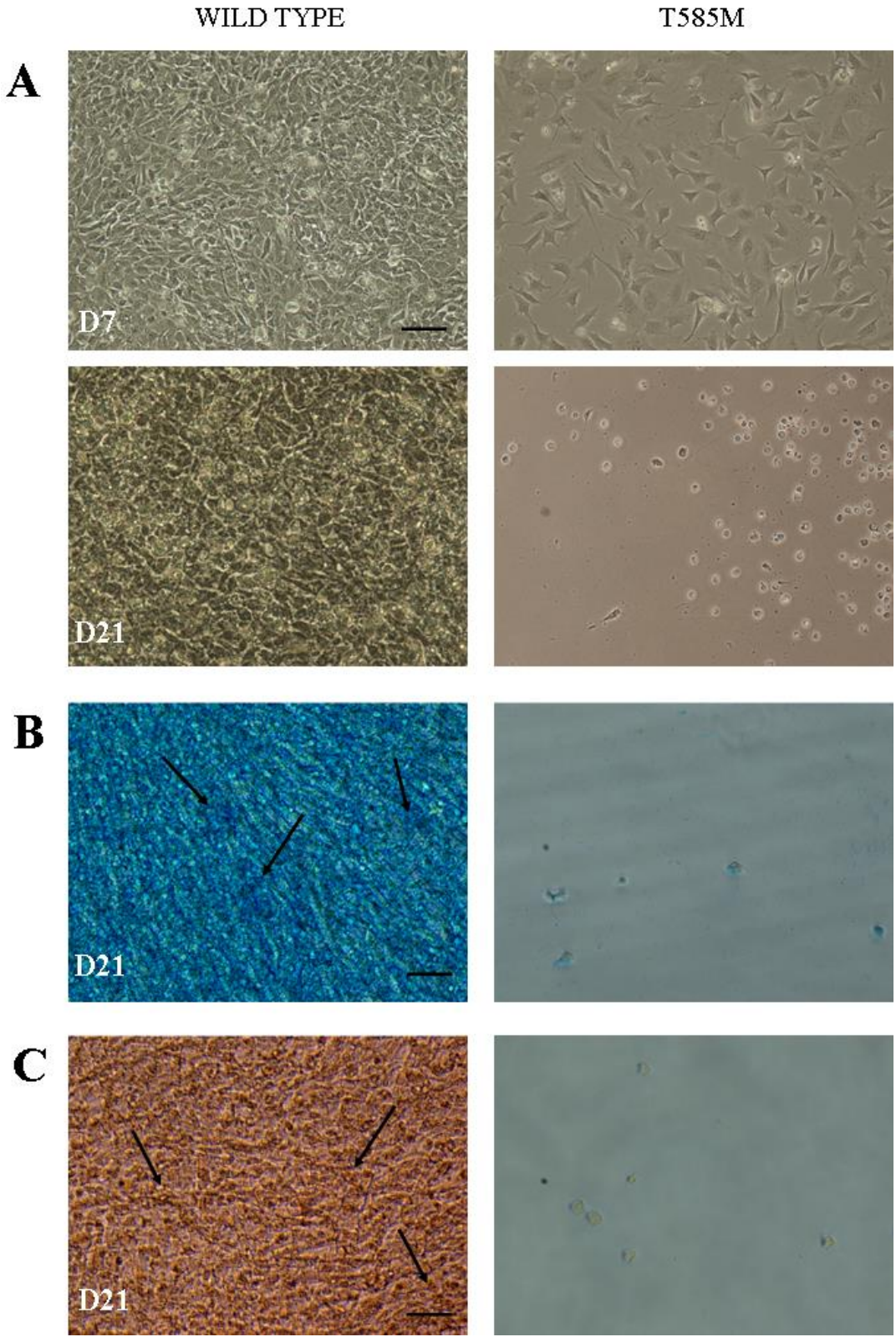

Figure 86. Brightfield microscope analysis and alcian blue and alizarin red staining. A) *Brightfield microscope images were taken at days 7 and 21 for both conditions, WT transfected cells and T585M mutated Scale bar: 100 µm. N=3 and n=3.* ***B)*** *Alcian blue staining at day 21 for sulphated glycosaminoglycan. Rows pointing at the alcian blue deposits. Scale bar: 200 µm. N=3 and n=3.* ***C)*** *Alizarin red staining for calcium deposits, at day 21 for both conditions. Scale bar: 200 µm. N=3 and n=3.*

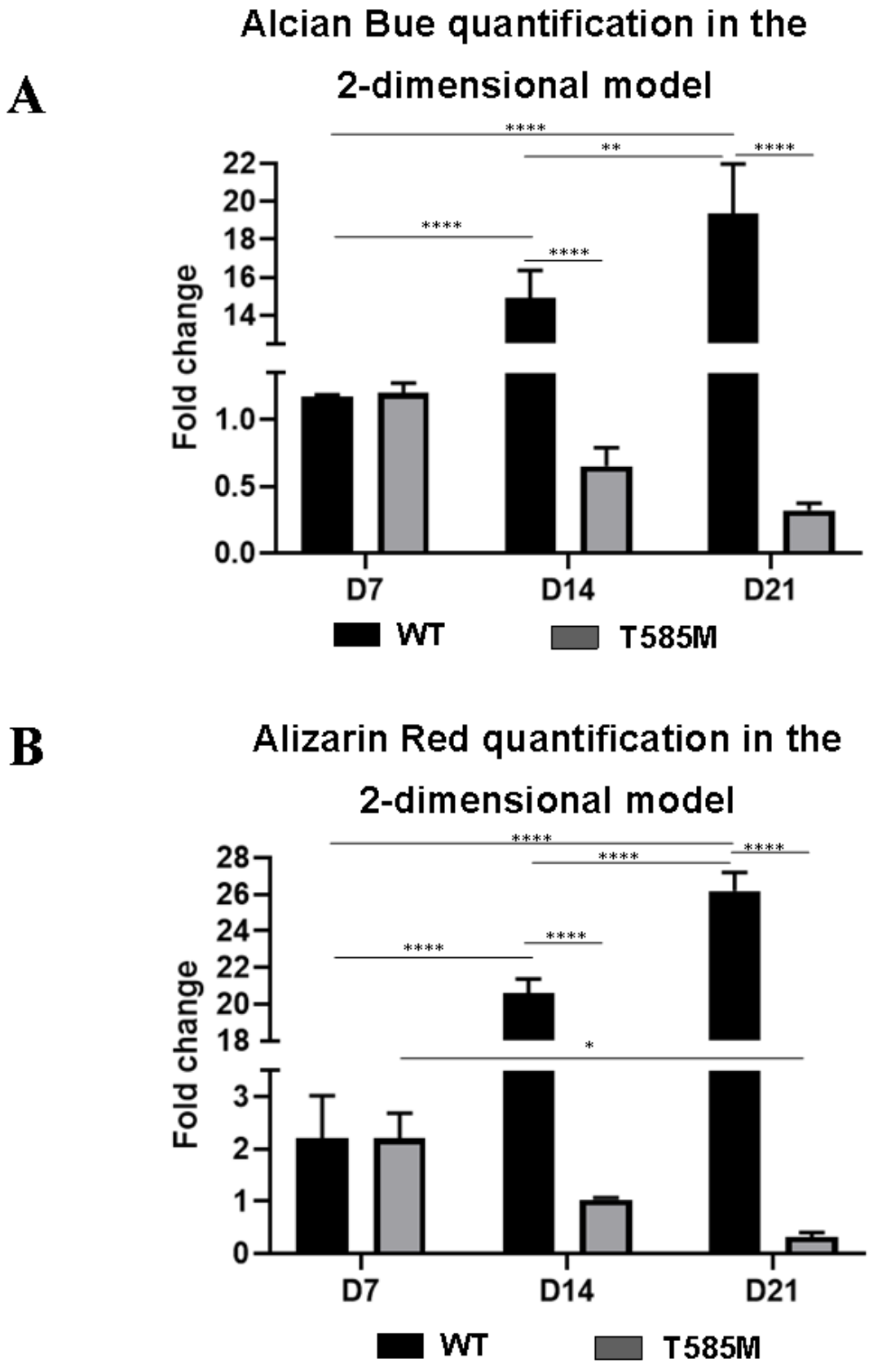

Figure 87. Alcian blue and calcium deposits for days 1 to 21 in the 2-dimensional model. (A) *Quantification of the Alcian blue dye extracted by 4 M guanidine HCI overnight at 4°C and measured by optical density at 595nm for both models (**B**) Quantification of the Alizarin red dye extracted by cetylpyridinium chloride method and measured by optical density at 405nm. All quantification levels normalised to the levels 24h after seeding 12,000 cells per ml on a monolayer (Day point 1). Two-way ANOVA statistical analysis where * p<0.05, **p<0.01, ***p<0.001, and ****p<0.0001. N=3 and n=3.*

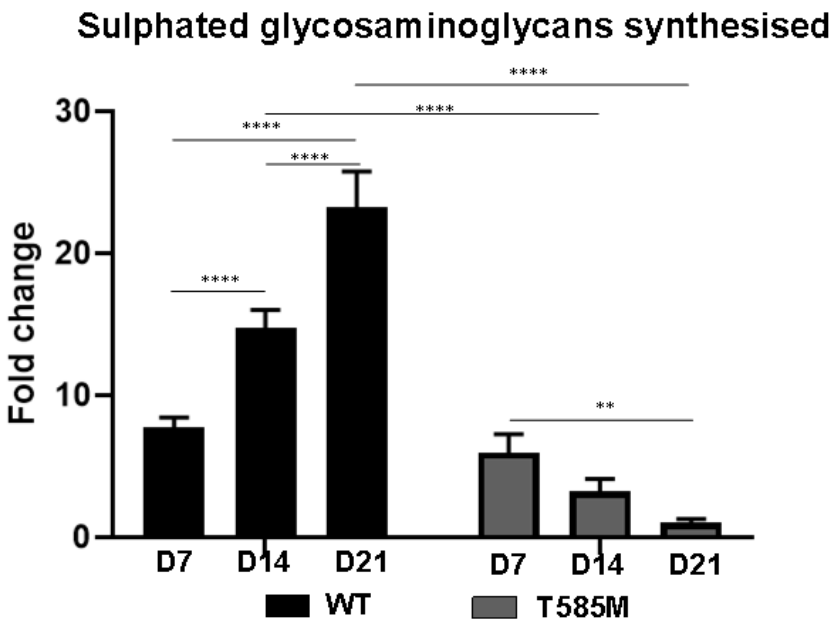

Figure 88. Analysis of sGAG for WT and mutant model. *sGAG production for all the conditions at each day point. Two-way ANOVA statistical analysis where * p<0.05, **p<0.01, ***p<0.001, and ****p<0.0001. N=3 and n=3.*

7.3.2 Cell metabolic activity in the 2-dimensional model of ATDC5 cells stably transfected with WT and p.T585M mutant COMP.

Assessment of the cell metabolic activity in the 2-dimensional model was performed via MTT assay (Figure 89). Interestingly, the cells that express the WT copy of COMP showed normal cell metabolic activity, increasing steadily over time, and similar to the metabolic activity seen in the untransfected cells. In contrast, cells expressing the p.T585M COMP mutation presented a marked reduction in metabolic activity after day 7 (Figure 88). Cells showed a significant decrease in sGAG deposition visible at days 7, 14 and 21 when comparing WT-COMP against p.T585M-COMP by 0.83-fold change ($p=0.001$), 0.35-fold change ($p<0.0001$) and by 0.097-fold change ($p<0.0001$) respectively. When comparison was done for the same condition, but within different day points, a significant increase in gene expression was observed in WT-COMP cultures by 1.128-fold change ($p=0.0055$) when comparing day 7 against day 21. Comparing day points within the p.T585M-COMP condition showed a significant decrease when comparing day 7 against days 14 and 21 by 0.45-fold change ($p<0.0001$) and 0.13-fold change ($p<0.0001$) respectively and when comparing day 14 against day 21 by 0.29-fold change ($p=0.0023$) (Figure 89).

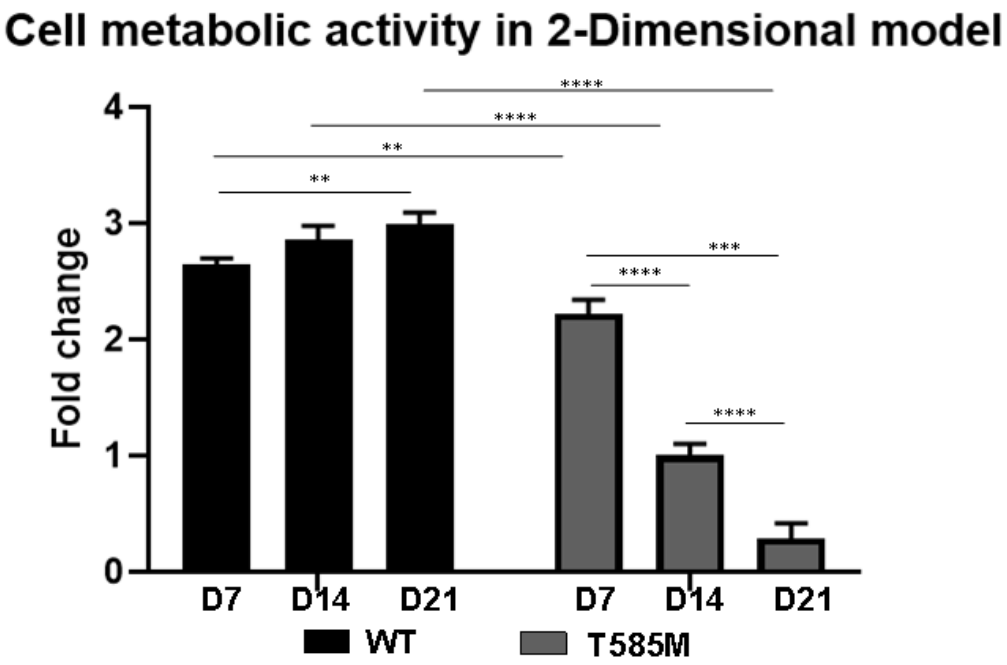

Figure 89. Cell metabolic activity in WT and mutant model. MTT assay was performed in the monolayer culture after 7, 14 and 21 days. *Quantification levels normalised to the levels after seeding 12,000 cells per ml on a monolayer (Day point 1). Two-way ANOVA statistical analysis where * p<0.05, **p<0.01, ***p<0.001, and ****p<0.0001. N=3 and n=3.*

7.3.3 Gene expression activity in a 2-dimensional model of ATDC5 cells stably transfected with WT and p.T585M mutant COMP.

Gene expression of articular cartilage markers for chondrogenesis (*Sox9* and *Ihh*) and ECM (*Col2aI*, C*ol1a1* and *Acan*) was assessed using quantitative RT-PCR on mRNA extracted from 2D ATDC5 cultures (Figure 90 A-F and Table 9).

Sox9 expression was noticeably different between the cell lines (Figure 90A). A significant decrease was visible at day 14 when comparing WT-COMP against p.T585M-COMP by 0.00059-fold change ($p<0.0001$). When comparison was done for the same condition, but within different day points, a significant increase in gene expression was observed in WT-COMP cultures when comparing day 7 against day 14 by 13.74-fold change ($p<0.0001$) however, a significant decrease was observed when comparing day 14 against day 21 by 0.08-fold change ($p<0.0001$) respectively.

Similarly, *Ihh* expression showed notable differences between the cell lines for all-day points (Figure 90B). A significant decrease was visible at day 21 when comparing WT-COMP against p.T585M-COMP by 0.0000000094-fold change ($p=0.0006$). Comparing within the same condition, but within different day points, a significant increase in gene expression was observed in WT-COMP cultures when comparing day 7 against day 21 by 110.99-fold change

(p=0.0006) and when comparing day 14 against day 21 by 30.62-fold change (p=0.0007) respectively.

Expression of *Col2a1* (Figure 90C) showed a significant decrease visible at day 21 when comparing WT-COMP against p.T585M-COMP by 0.0000041-fold change (p<0.0001). When comparison was done for the same condition, but within different day points, a significant increase in gene expression was observed in WT-COMP cultures when comparing day 7 against day 21 by 11.54-fold change (p<0.0001), and when comparing day 14 against day 21 by 4.59-fold change (p<0.0001) respectively.

Expression of *Col10a1* (Figure 90D) was significantly decreased was visible at day 21 when comparing WT-COMP against p.T585M-COMP by 0.00000019-fold change (p=0.0005). When comparison was done for the same condition, but within different day points, a significant increase in gene expression was observed in WT-COMP cultures when comparing day 7 against day 21 by 747158-fold change (p=0.0004) however, a significant decrease was observed when comparing day 14 against day 21 by 38.16-fold change (p=0.0005) respectively.

Interestingly, expression of type I collagen (*Col1a1*) (Figure 90E) a significant increase was visible at day 14 when comparing WT-COMP against p.T585M-COMP by 143.36-fold change (p<0.0001). When comparison was done for the same condition, but within different day points, a significant increase in gene expression was observed in p.T585M-COMP cultures when comparing day 7 against day 14 by 54.38-fold change (p<0.0001) however, a significant decrease was observed when comparing day 14 against day 21 by 0.131-fold change (p<0.0001) respectively.

Finally, aggrecan (*Acan*) gene expression (Figure 90F) showed a significant increase was visible at days 14 and 21 when comparing WT-COMP against p.T585M-COMP by 0.00000074-fold (p=0.008) change and by 0.0000089-fold change (p<0.0001) respectively. When comparison was done for the same condition, but within different day points, a significant increase in gene expression was observed in WT-COMP cultures when comparing day 7 against days 14 and 21 by 1051.61-fold change (p=0.007) and 2591.74-fold change (p<0.0001). Day 14 against day 21 showed a significant increase by 2.464-fold change (p=0.0004).

		Sox9	***Ihh***	***Col2a1a***	***Col10a1***	***Col1a1***	***Acan***
WT	Day7	↓	↑	↑	↓	↓	↓
	Day14	↑	↑	↑	↑	↓	↑
	Day21	↓	↑	↑	↑	↓	↑
T585M	Day7	↓	↓	↓	↓	↓	↓
	Day14	↓	↓	↓	↓	↑	↓
	Day21	↓	↓	↓	↓	↓	↓

Table 9. Table summarising the outcome of the gene expression *of Sox9, Indian hedgehog (Ihh), collagen II (Col2a1), collagen X (Col10a1), collagen I (Col1a1) and aggrecan (Acan) after 21 days of culturing ATDC5 in a 2-dimensional culture compared to day 1 gene expression. N=3 and n=3.*

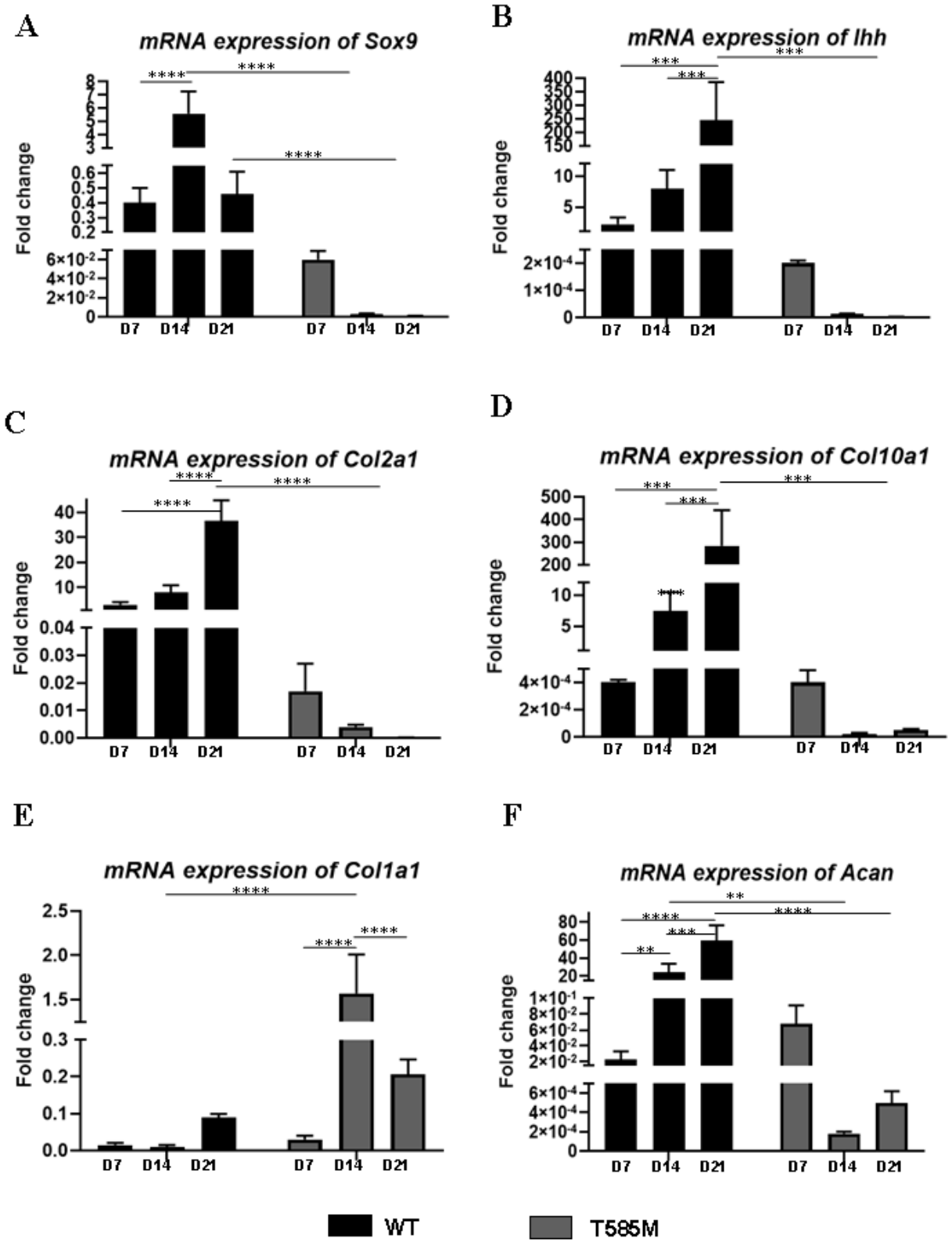

Figure 90. Gene expression after 21 days of culture. *Gene expression of Sox9* ***(A)****, Indian hedgehog (Ihh)* ***(B)****, type II collagen (Col2a1)* ***(C)****, type X collagen (Col10a1)* ***(D)****, type I collagen (Col1a1)* ***(E)****, aggrecan (Acan)* ***(F)*** *after 21 days of culturing ATDC5 in a monolayer expressing WT and T585M mutation. Quantification levels were normalised to the levels after seeding cells per ml before being differentiated (Day point 1). Two-way ANOVA statistical analysis where * p<0.05, **p<0.01, ***p<0.001, and ****p<0.0001. N=3 and n=3.*

7.3.4 Morphology and area of pellets of ATDC5 cells stably transfected with WT and p.T585M mutant COMP

The cells stably transfected with the mutation p.T585M COMP and the WT COMP were cultured in the pellet model with growth factor supplementation for further investigation of the impact of the C-terminal COMP mutation on chondrogenesis. The pellets were grown for 21 days, as described previously.

Firstly, haematoxylin and eosin histological staining was performed to study the overall structure and deposition of ECM in the developing cartilage pellets (Figure 91A). On day 7 there were no structural differences noticeable between the cell lines; however, on day 14 and 21 hallmarks of cell hypertrophy were observable at the centre of the p.T585M COMP pellet compared to the WT COMP pellet. Interestingly, the area of the pellets (Figure 91B) showed a significant decrease visible at day 7 when comparing WT-COMP against p.T585M-COMP by 0.69-fold change ($p=0.0432$). When comparison was done for the same condition, but within different day points, a significant increase was observed in WT-COMP cultures when comparing day 7 against days 14 and 21 by 1.33-fold change ($p=0.024$) and 1.56-fold change ($p=0.0006$) respectively. Comparing day points within the p.T585M-COMP condition showed a significant increase by 1.56-fold change ($p=0.0094$) and by 2.109-fold change ($p<0.0001$) when comparing day 7 against days 14 and 21 respectively and when comparing day 14 against day 21 by 1.35-fold change ($p=0.0105$).

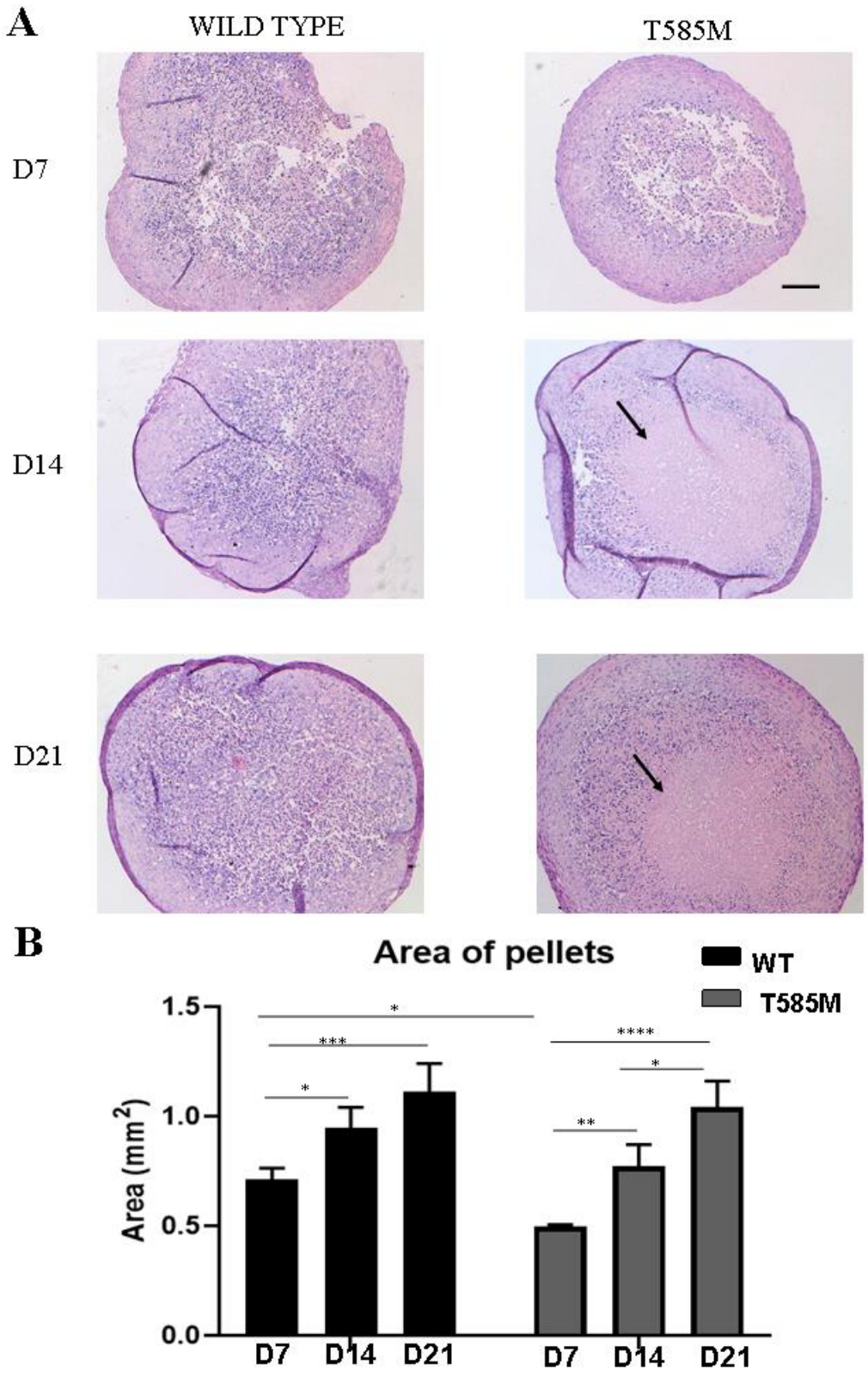

Figure 91. Histology haematoxylin and eosin and measurement of area in the pellets. *Haematoxylin staining was performed in both WT and T585M pellet model on every harvest to stain ECM and eosin for nuclei studies following 7, 14 and 21 days of pellet culture N=3 and n=3. Scale bar= 100 µm (**A**). Area of pellets at each day for the T585M and WT expressed models point measured with ImageJ and represented in mm2. Two-way ANOVA statistical analysis where * p<0.05, **p<0.01, ***p<0.001, and ****p<0.0001 **(B)**. N=3 and n=3.*

7.3.5 Proteoglycan deposition in pellets of ATDC5 cells expressing WT and p.T585M mutant COMP.

GAG deposition was studied in the pellets using Toluidine Blue staining, as described previously (Figure 92). There were apparent differences in GAG deposition between the COMP cell lines (Figure 92A), which showed a significant decrease in sGAG deposition visible at days 14 and 21 when comparing WT-COMP against p.T585M-COMP by 0.36-fold change ($p<0.0001$) and by 0.143-fold change ($p<0.0001$) respectively. When comparison was done for the same condition, but within different day points, a significant increase was observed in WT-COMP cultures when comparing day 7 against days 14 and 21 by 1.39-fold change ($p=0.0139$) and 2.483-fold change ($p<0.0001$) respectively and when comparing day 14 against day 21 by 1.778-fold change ($p<0.0001$). Comparing day points within the p.T585M-COMP condition showed a significant decrease by 0.512-fold change ($p=0.0304$) when comparing day 7 against day 21.

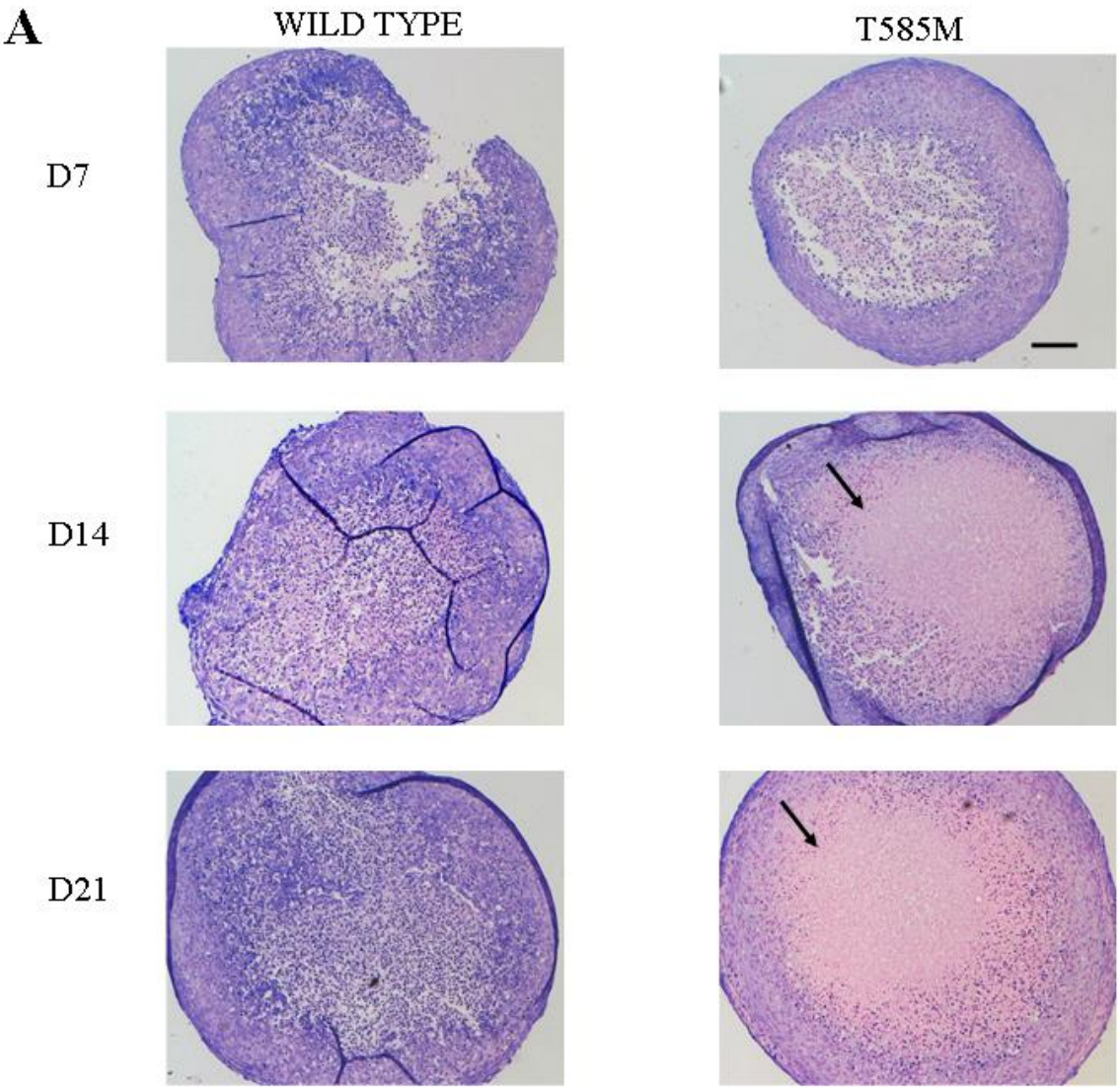

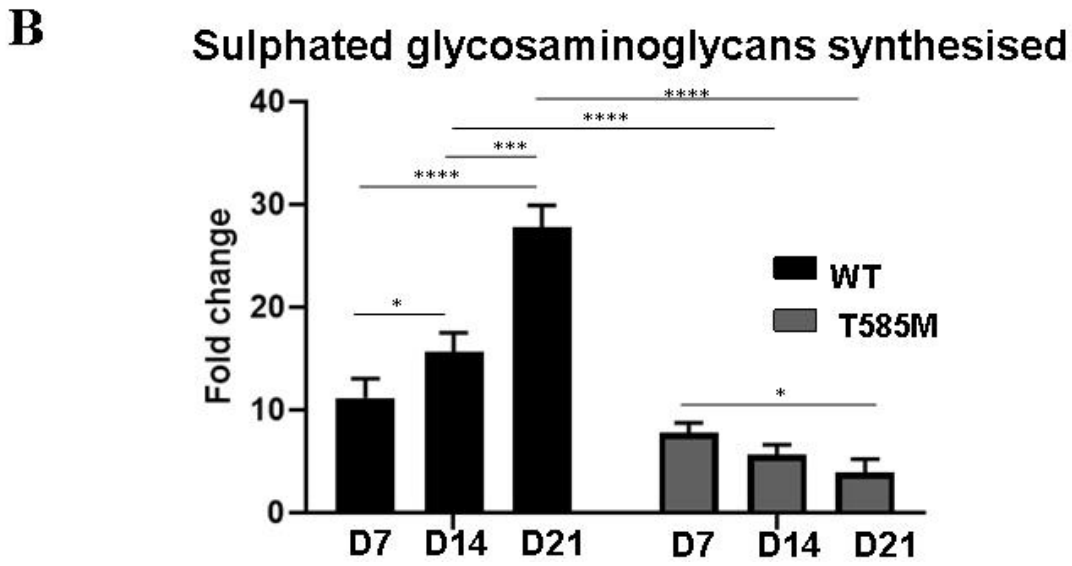

Figure 92. Toluidine blue histological staining and sGAG quantification in pellets. *Pellets seeded at a density of 500,000 ATDC5 cells per ml for 21 days for histological staining for toluidine blue for GAG in pellet mode expressing l WT and T585M. Scale bar = 100 µm (A). Study of the variation of quantification in sGAG at all day points for both conditions. Two-way ANOVA statistical analysis where * p<0.05, **p<0.01, ***p<0.001, and ****p<0.0001.* ***(B).*** *N=3 and n=3.*

7.3.6 Collagen deposition in pellets of ATDC5 cells expressing WT and p.T585M mutant COMP

Further analysis of the ECM deposition was performed using Picrosirius Red staining for collagen deposition (Figure 93). Collagen deposition, illustrated by red staining, was visible on the surface of the pellet of both wild type and mutant pellets, especially after 21 days of culture. Interestingly, even though both wild type and mutant pellets showed zonal stratification, in the p.T585M COMP pellets an increased deposition appeared increased in the centre of the pellet after 14 and 21 days of culture (Figure 93).

Further analysis of the ECM deposition in both models was performed using immunohistochemistry for type II, X and I collagen (Figures 94-96), with negative and positive control in figure 97. Wild type pellets showed staining for type II collagen at all stages, especially after culturing for 21 days, where collagen was deposited in the deeper layers. Interestingly, in the p.T585M COMP pellets, the initial type II collagen deposition found in the surface zone after 7 days disappeared after 14 and 21 days, suggesting that the mutation has a detrimental effect on the ECM deposition (Figure 94). Type X collagen immunohistochemistry (Figure 95) showed an increased deposition in the centre of the pellet for the wild-type model, particularly after 21 days. In contrast, the p.T585M COMP pellet model did not stain positive for type X collagen along any of the day points.

Type I collagen staining (Figure 96) did not show any positive staining in the WT pellets after 21 days. However, p.T585M COMP model showed deposition of type I collagen pericellularly initially after 14 days in the deeper layer of the pellet, and after 21 days of seeding over the whole ECM particularly in the surface.

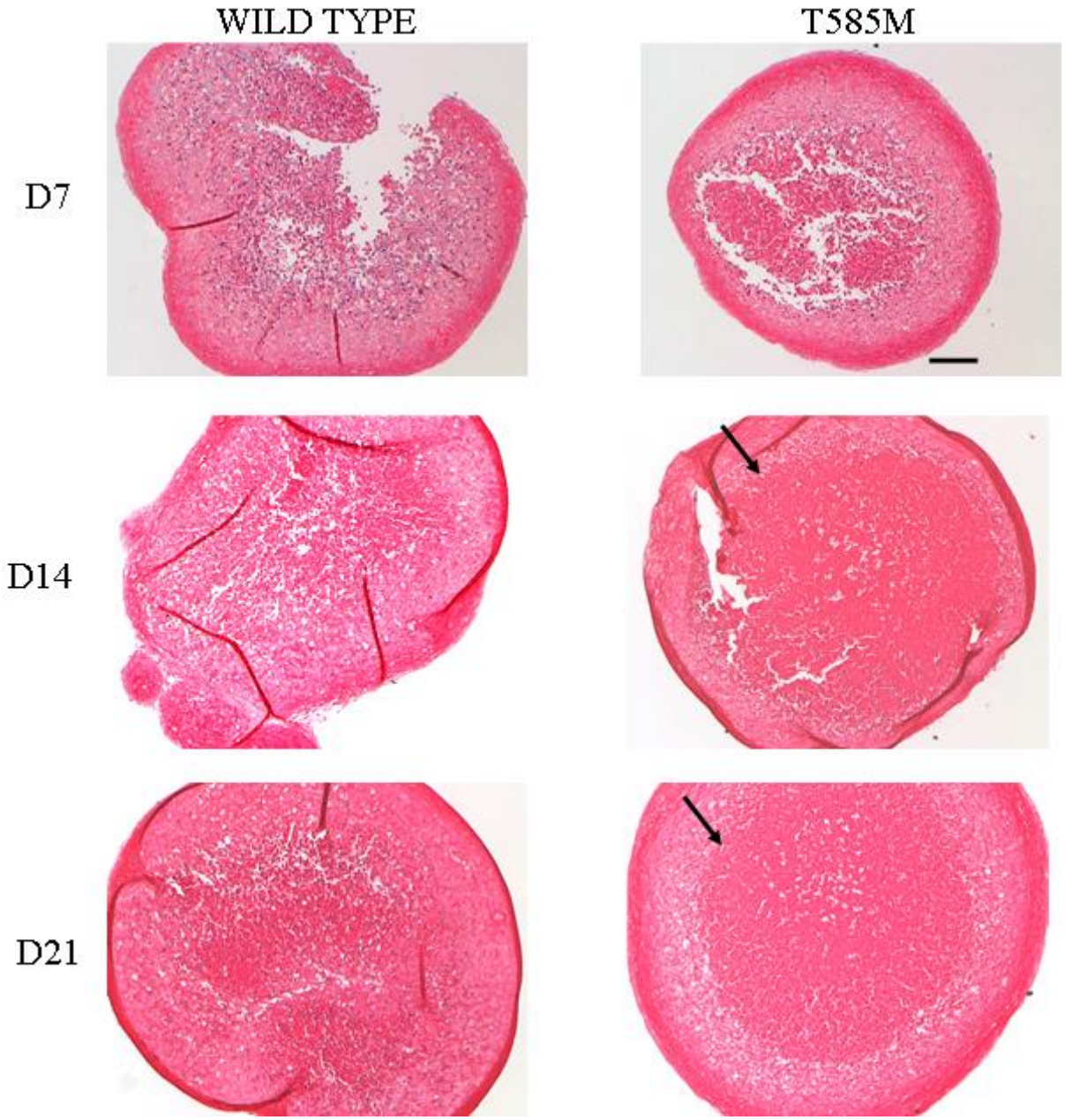

Figure 93. Picrosirius histological staining and cell metabolic activity of pellets. A) *Pellets seeded at a density of 500,000 ATDC5 cells per ml for 21 days for histological staining for Picrosirius Red for collagen in expressing WT and T585M models Scale bar = 100 µm. N=3 and n=3.*

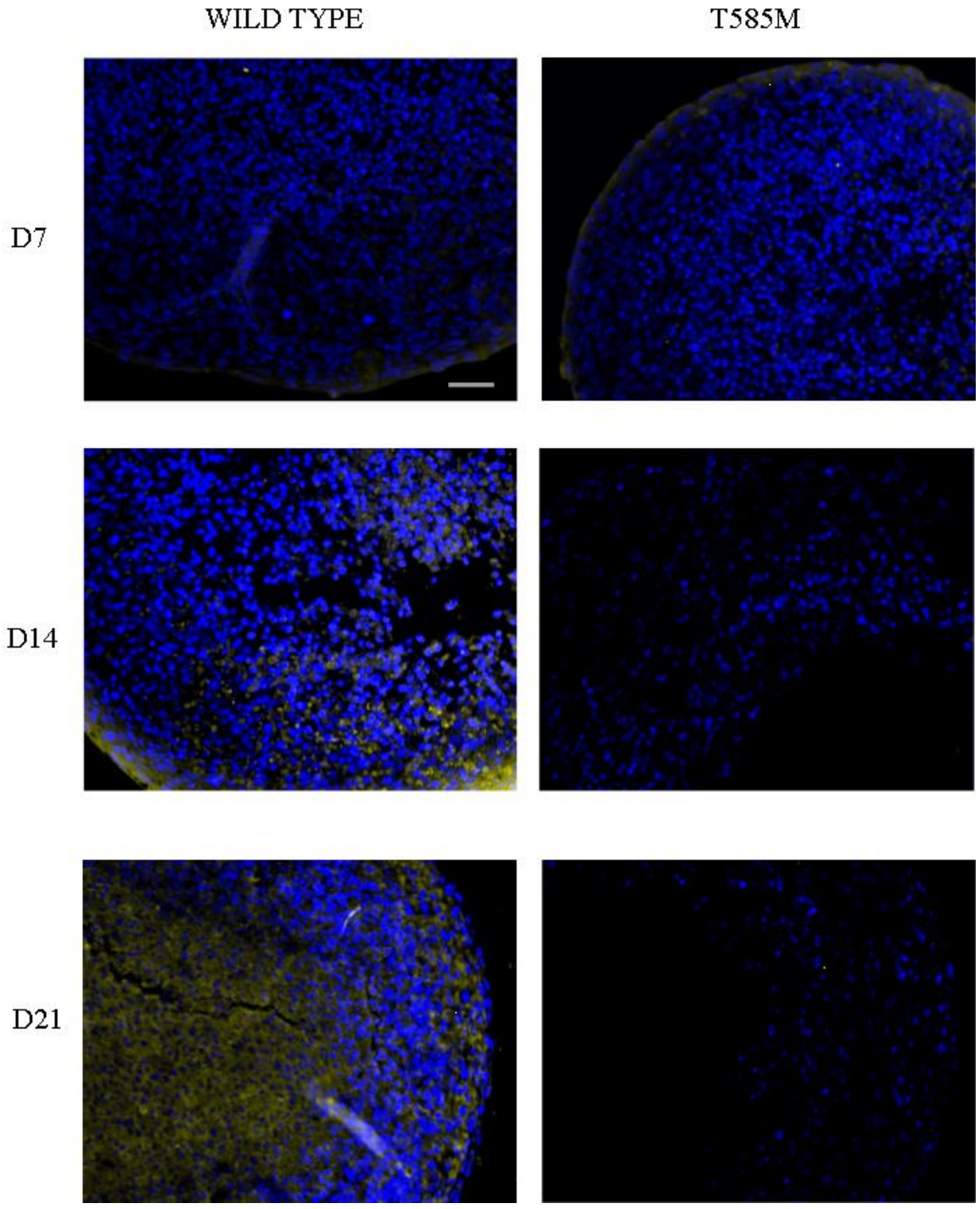

Figure 94. Immunohistochemistry for type II collagen in all conditions after 21 days. *Pellets seeded for 21 days for immunohistological staining type II collagen in models expressing WT and T585M. DAPI (nuclei) =blue. Type II collagen = yellow. Scale bar = 200 µm. N=3 and n=3*

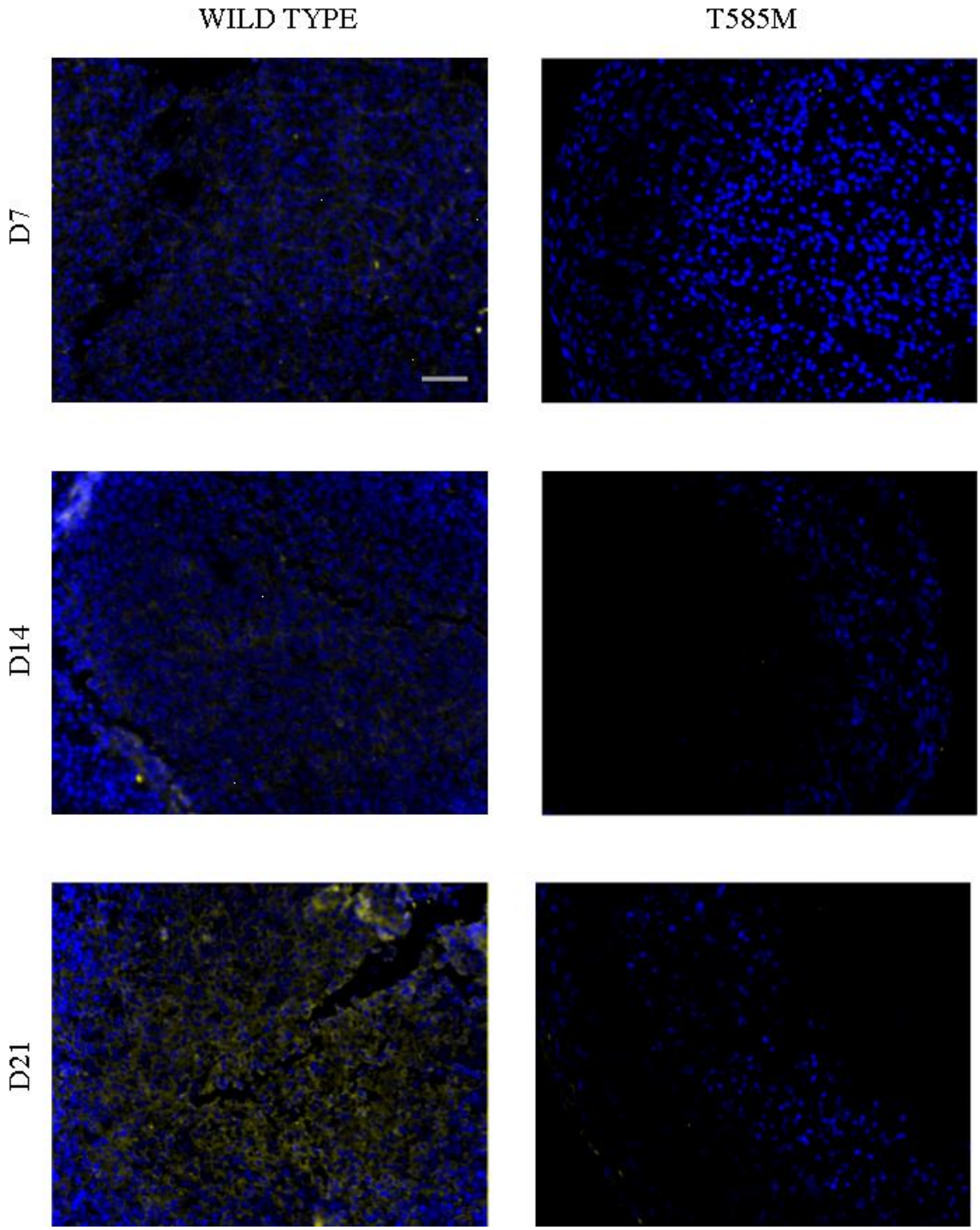

Figure 95. Immunohistochemistry for type X collagen in all conditions after 21 days. *Pellets seeded for 21 days for immunohistological staining type X collagen in models expressing WT and T585M. DAPI (nuclei) =blue. Type X collagen = yellow. Scale bar = 200 µm. N=3 and n=3.*

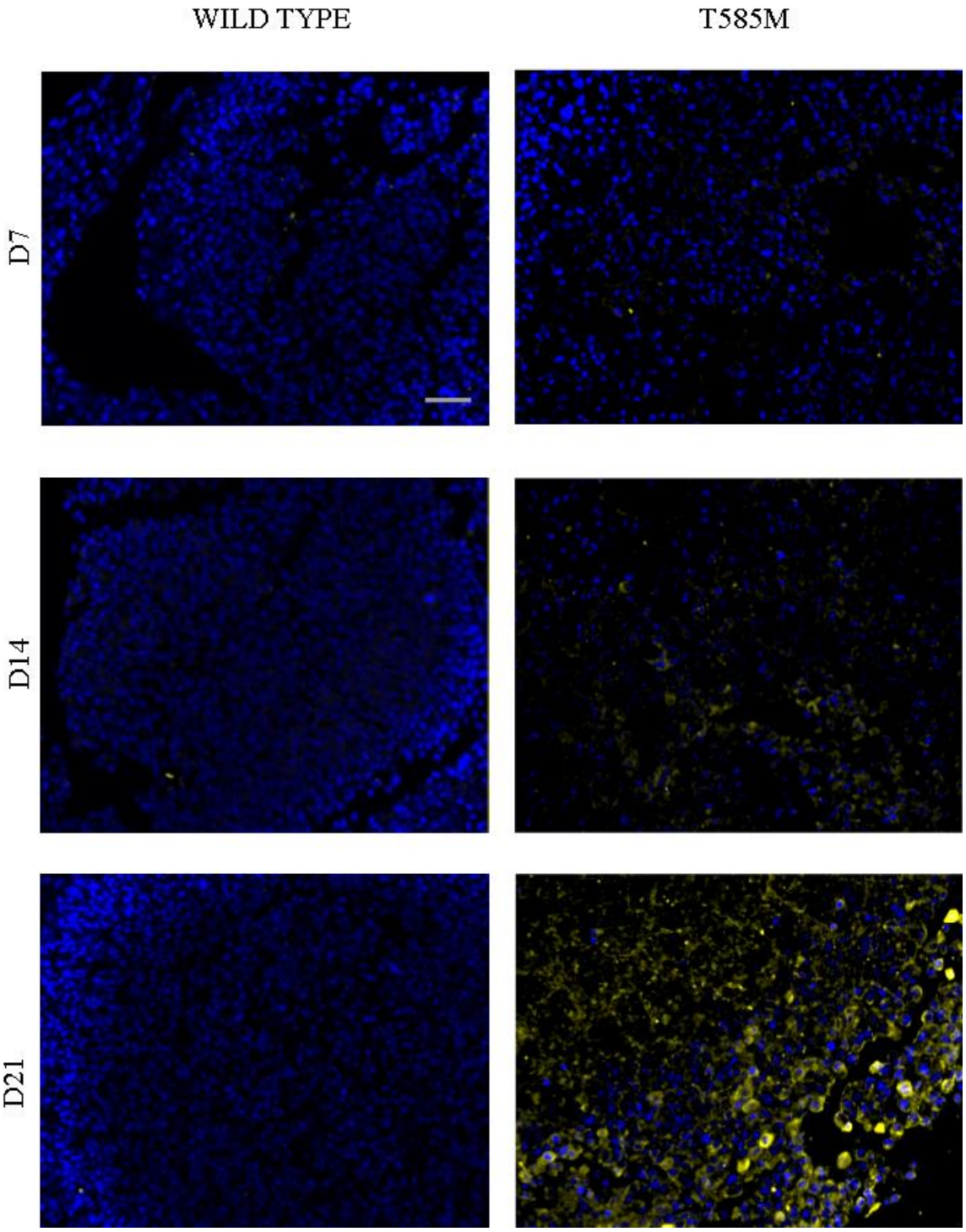

Figure 96. Immunohistochemistry for type I collagen in all conditions after 21 days. *Pellets seeded for 21 days for immunohistological staining for type I collagen in a model expressing WT and T585M. DAPI (nuclei) =blue. Type I collagen = yellow Scale bar = 200 µm. N=3 and n=3.*

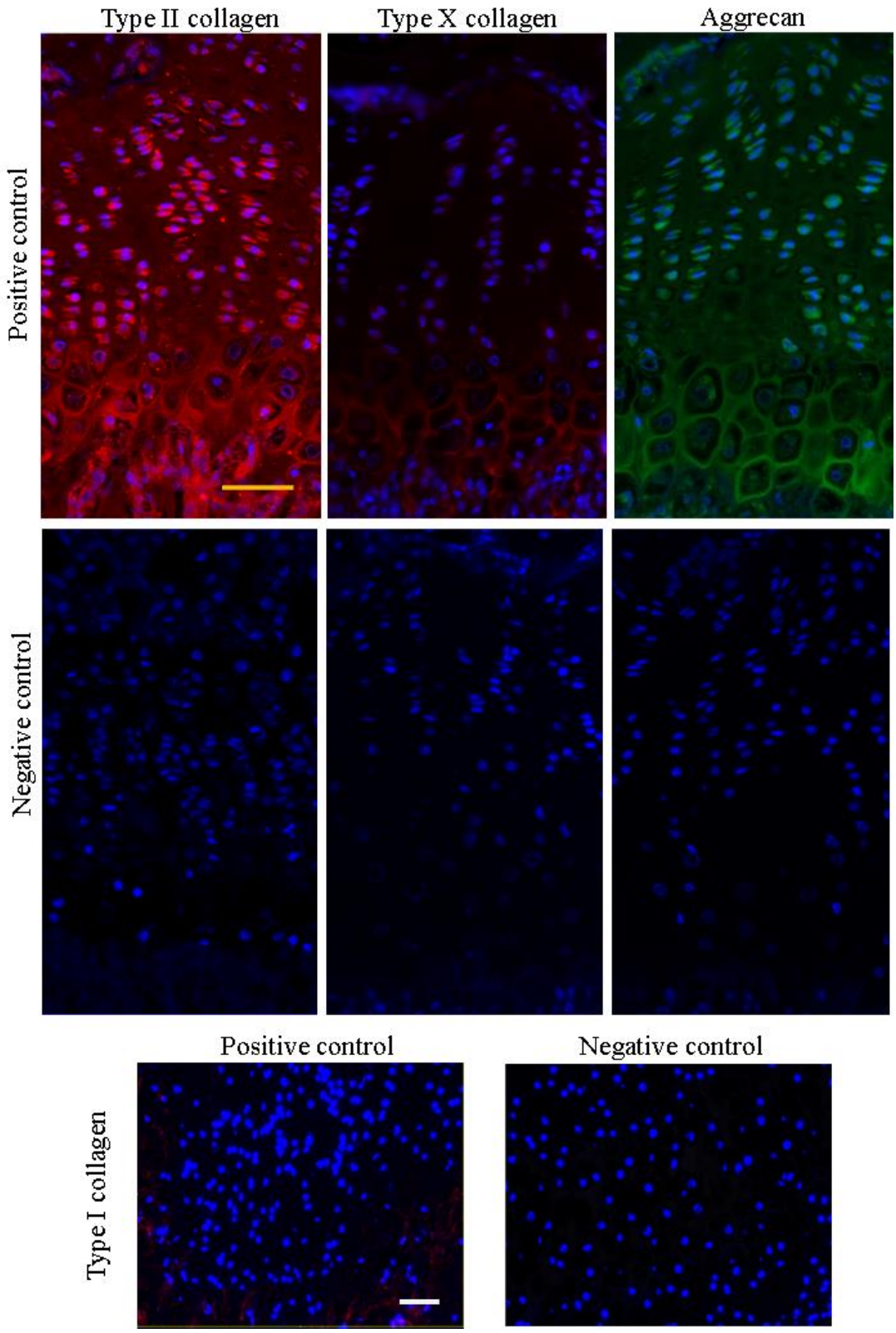

Figure 97. Positive and negative controls for type I, II and X collagen and aggrecan. *Positive and negative controls were done in 3-week-old mice femoral heads for type I, II and X collagen and aggrecan. Scale bar: 50 µm*

7.3.7 Cell apoptosis in pellets of ATDC5 cells expressing WT and p.T585M mutant COMP

Cell apoptosis was analysed using the TUNEL assay. Positive apoptotic cells were normalised with the total cell number (DAPI positive) in Figures 98 and 99. Apoptosis in the wild type pellets was not abundant and increased towards the centre of the pellets. In contrast, there was a notable increase in cell apoptosis at the centre of the mutant pellets after 14 and 21 days of culture (Figures 98 and 99). Upon quantification, via ImageJ, there was no difference in the levels of apoptosis on the surface or centre of wild type pellets throughout the culture. However, there was a significant increase in apoptosis within the mutant model in the centre of the pellet when comparing within day points, day 7 against days 14 and 21 by 7.64-fold change ($p<0.0001$) and 7.48-fold change ($p<0.0001$) respectively.

Comparison in between day points and comparing conditions showed at day 14 a significant increase when comparing cell apoptosis at the centre of the pellets of the WT cell model against p.T585M model by 5.77-fold change ($p<0.0001$) (Figure 99B). For the same day point, comparison within the p.T585M model showed a significant reduction of cell apoptosis when comparing the surface against the centre of the pellet by 0.144-fold change ($p<0.0001$). On day 21 significant increase when comparing cell apoptosis at the centre of the pellets of the WT cell model against p.T585M model by 5.90-fold change ($p<0.0001$). For the same day point, comparison within the p.T585M model showed a significant reduction of cell apoptosis when comparing the surface against the centre of the pellet by 0.134-fold change ($p<0.0001$).

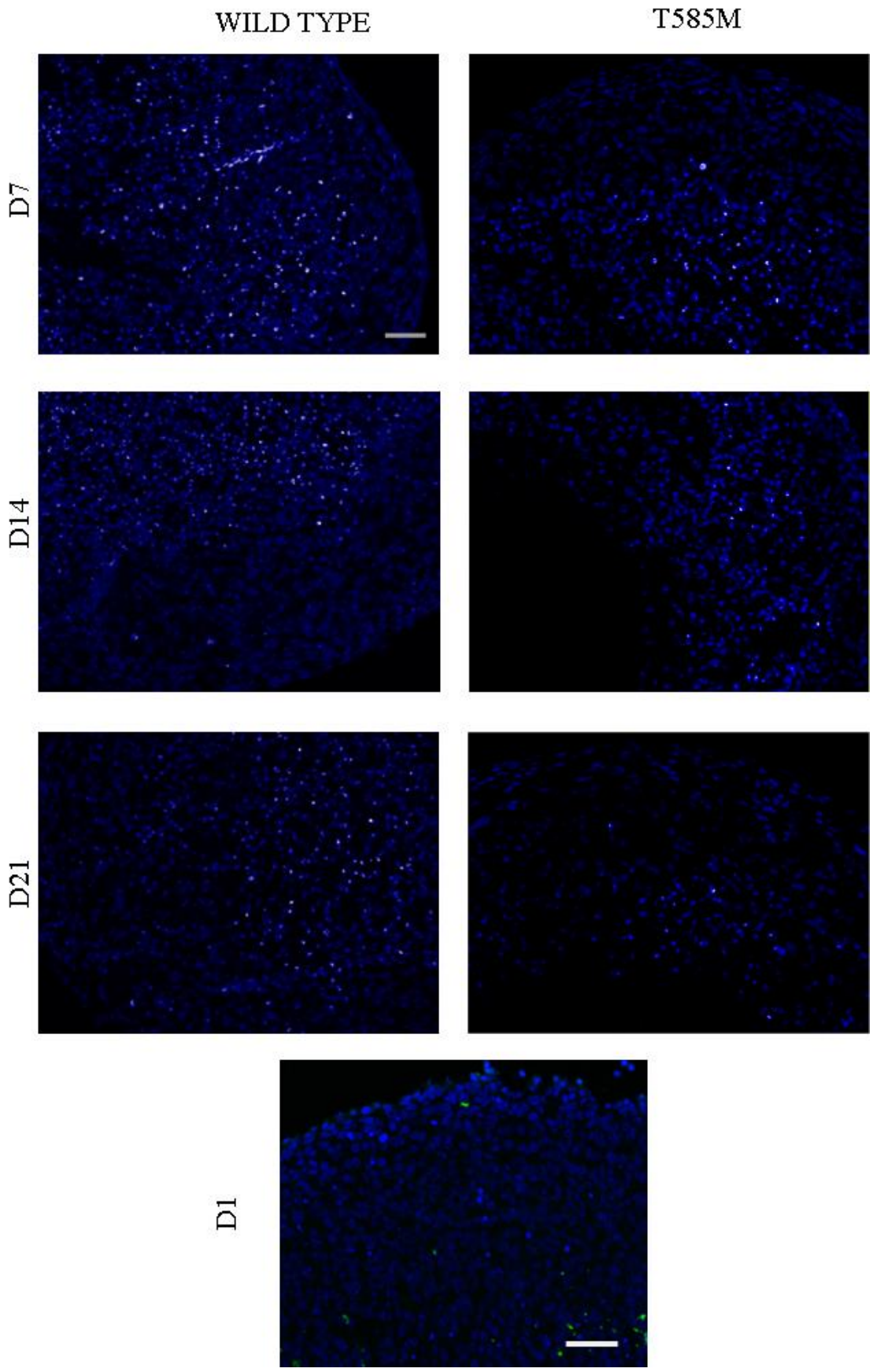

Figure 98. Immunohistochemistry for cell apoptosis in all conditions after 21 days. *Pellets seeded for 21 days were analysed via TUNEL staining to study cell apoptosis when expressing WT and T585M mutation. Blue= DAPI nuclei. Yellow = apoptotic cells. Scale bar = 200 µm. N=3 and n=3.*

A

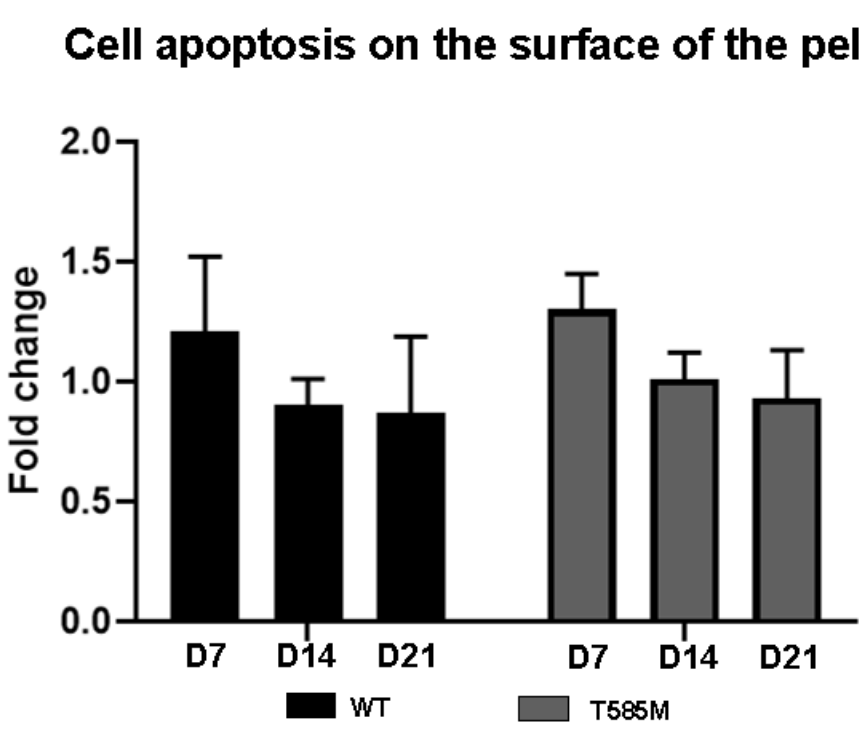

B

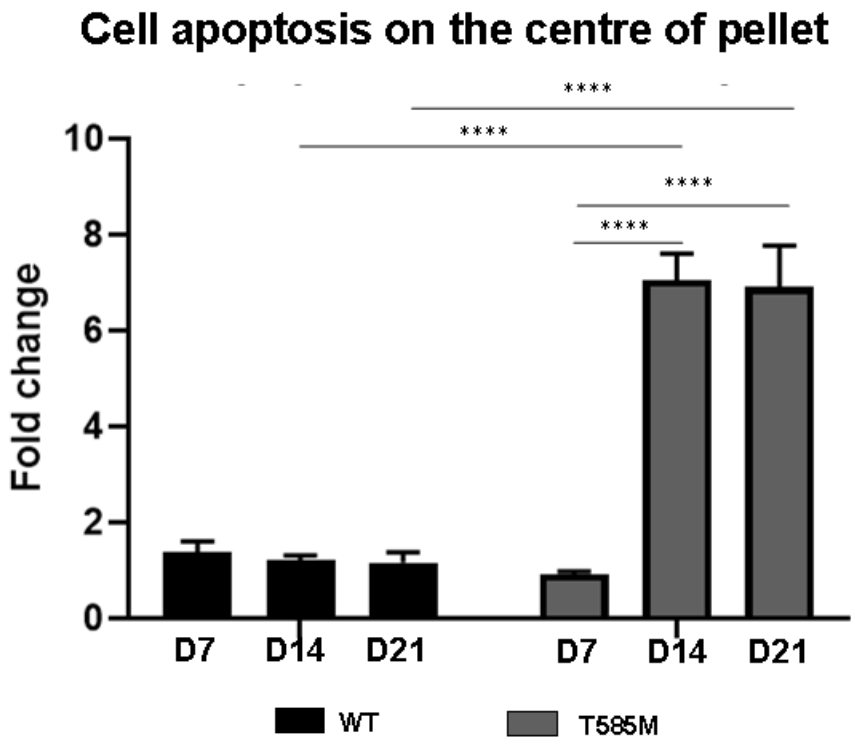

Figure 99. Cell apoptosis in the surface and centre of the pellet. *Cell apoptosis of quantification with ImageJ for all conditions along the 21 days normalised to day 1 at the surface of the pellet (A) and centre of the pellet (B) for expressed WT and T585M models. Three-way ANOVA statistical analysis where * p<0.05, **p<0.01, ***p<0.001, and ****p<0.0001. N=3 and n=3.*

7.3.8 Cell proliferation in the pellets of ATDC5 cells expressing WT and p.T585M mutant COMP.

Proliferation in the engineered pellets was assessed via immunohistochemistry against Ki67 (Figure 100 and 101) and quantified against all cells in the pellets (DAPI positive).

There was a significant decrease in cell proliferation within the WT model in the surface (Figure 101A-B) of the pellet when comparing within day points, day 7 against day 14 by 0.655-fold change ($p=0.0489$). Comparison in between day points and comparing conditions showed at day 7 a significant decrease when comparing cell proliferation at the centre and surface of the pellets of WT cell model against p.T585M model by 0.186-fold change ($p<0.0001$) and by 0.53-fold change ($p=0.001$) respectively. Comparison in the same day points within the p.T585M but between centre and surface showed a significant increase by 2.26-fold change ($p=0.0396$). Day 14 a significant decrease when comparing cell proliferation at the centre by 0.1295-fold change ($p<0.0001$) (Figure 101A-B). For the same day point, comparison within the WT model showed a significant reduction of cell proliferation when comparing the centre against the surface of the pellet by 0.617-fold change ($p=0.001$) and a significant increase in the p.T585M model when comparing surface vs centre of the pellet by 3.87-fold change ($p=0.0017$). On day 21 a significant increase in cell proliferation when comparing the surface against the centre of the pellet was observed in the p.T585M model by 6.39-fold change ($p=0.0004$), whereas a significant decrease was visible in the WT model by 0.71-fold change ($p=0.0076$). Comparing the centre and surface of the pellets of the WT cell model against p.T585M model showed a significant reduction by 0.0709-fold change ($p<0.0001$) and by 0.63-fold change ($p=0.0177$) respectively.

To assess the cell metabolic activity in the generated pellets, an MTT assay was performed (Figure 102). Interestingly, there was a significant increase in cell metabolic activity at day 7 when comparing the WT model against the p.T585M model, by 3.48-fold change ($p<0.0001$). For days 14 and 21 a significant decrease was visible when comparing both conditions by 0.215-fold change ($p<0.0001$) and 0.1279-fold change ($p<0.0001$) respectively. Within the WT model, there was a significant increase in the cell proliferation when comparing days 7 and 14 against day 21 by 1.435-fold change ($p=0.0012$) and by 1.346-fold change ($p=0.0042$) respectively.

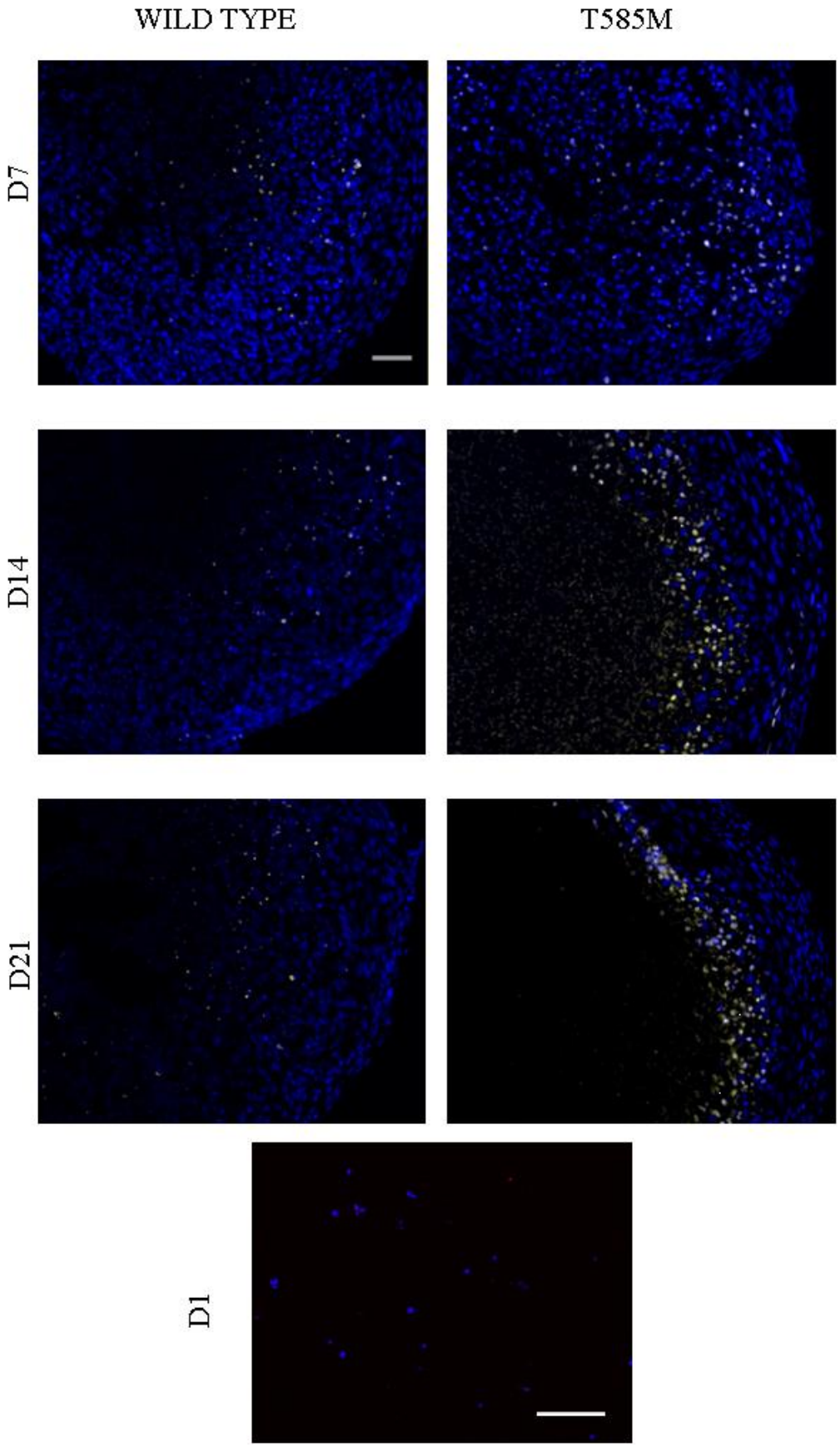

Figure 100. Immunohistochemistry for cell proliferation in all conditions after 21 days. *Pellets seeded for 21 days were analysed via ki67 staining to study cell proliferation when expressing WT and T585M mutation. Blue = DAPI (nuclei). Yellow = Cell proliferating (ki67). Scale bar = 200 µm. N=3 and n=3.*

A

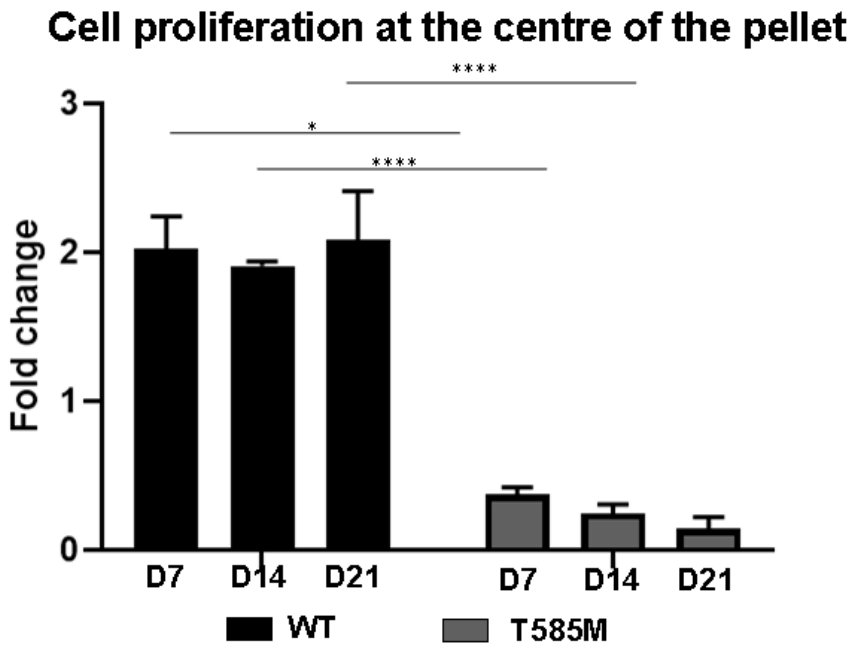

B

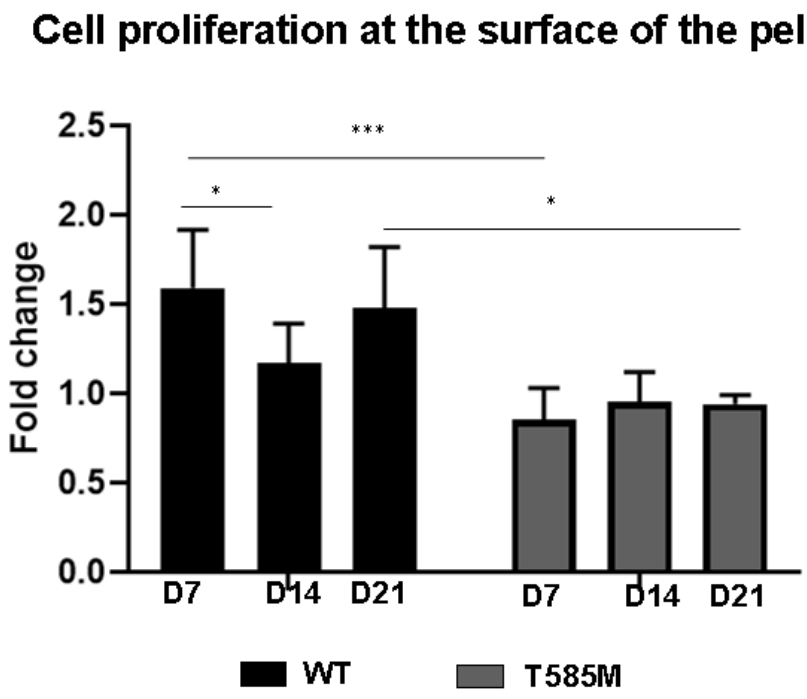

Figure 101. Cell proliferation in the surface and centre of the pellet. *Cell proliferation of quantification with ImageJ for all conditions along the 21 days compared to day 1 at the surface of the pellet* ***(A)*** *and centre of the pellet* ***(B)*** *for expressed WT and T585M models. Three-way ANOVA statistical analysis where * p<0.05, **p<0.01, ***p<0.001, and ****p<0.0001. N=3 and n=3.*

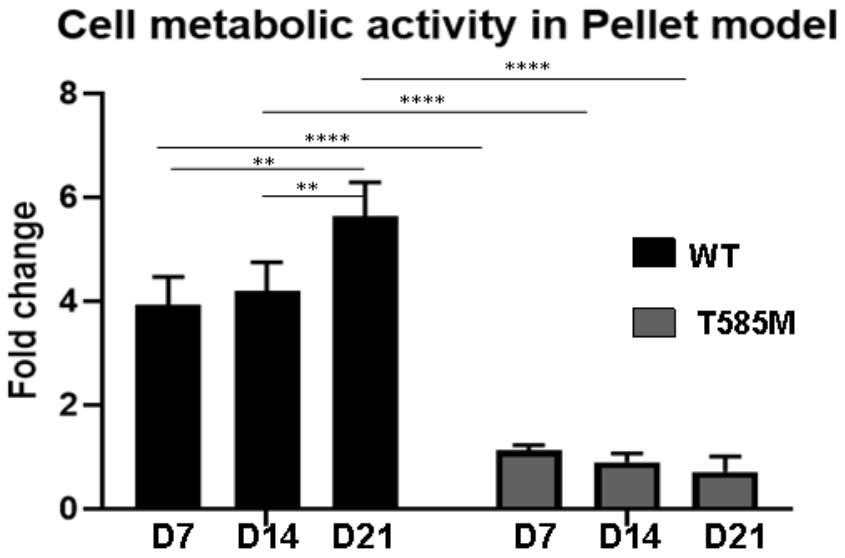

Figure 102. Cell metabolic activity with numerical data presented in graphs. *Study of the variation of cell metabolic activity at all day points for both conditions. Two-way ANOVA statistical analysis where * p<0.05, **p<0.01, ***p<0.001, and ****p<0.0001. N=3 and n=3.*

7.3.9 Gene expression in pellets of ATDC5 cells expressing WT and p.T585M mutant COMP

Gene expression for chondrogenesis markers and ECM synthesis was tested via qPCR for *Sox9*, *Ihh*, type II (*Col2a1*), X (*Col10a1*) and I collagen (*Col1a1*) and aggrecan (*Acan*) along with both models at day 1, 7, 14 and 21 (Figure 103 A-F).

Sox9 expression (Figure 103A) showed a significant decrease was visible at days 7, 14 and 21 when comparing WT-COMP against p.T585M-COMP by 0.4798-fold (p=0.0121), by 0.1077-fold change (p<0.0001) and by 0.0133-fold change (p<0.0001) respectively. When comparison was done for the same condition, but within different day points, a significant decrease in gene expression was observed in p.T585M-COMP cultures when comparing day 7 against day 21 by 0.0298-fold change (p=0.0203).

WT pellets showed a significant decrease in *Ihh* expression (Figure 103B) throughout the culture, at days 14 and 21 when comparing WT-COMP against p.T585M-COMP by 0.0022-fold (p<0.0001) change and by 0.0005-fold change (p<0.0001) respectively. When comparison was done for the same condition, but within different day points, a significant increase in gene expression was observed in WT-COMP cultures when comparing day 7 against days 14 and 21

by 487.93-fold change ($p<0.0001$) and 1335.2-fold change ($p<0.0001$). Day 14 against day 21 showed a significant increase by 2.736-fold change ($p<0.0001$).

Following the analysis of the chondrogenesis markers, the ECM markers were studied. *Col2a1* gene expression (Figure 103C) a significant decrease was visible at days 7, 14 and 21 when comparing WT-COMP against p.T585M-COMP by 0.2447-fold ($p=0.0142$), by 0.2119-fold change ($p=0.0031$) and by 0.41-fold change ($p<0.0001$) respectively.

Type X collagen expression (Figure 103D) showed a significant decrease was visible at day 21 when comparing WT-COMP against p.T585M-COMP by 0.0384-fold ($p<0.0001$) change. When comparison was done for the same condition, but within different day points, a significant increase in gene expression was observed in WT-COMP cultures when comparing day 7 against days 14 and 21 by 3.55-fold change ($p<0.0001$) and 8.84-fold change ($p<0.0001$). Day 14 against day 21 showed a significant increase by 2.488-fold change ($p<0.0001$). A significant increase in gene expression was observed in p.T585M-COMP cultures when comparing day 7 against day 14 by 13.339-fold change ($p<0.0001$), however, comparing day 14 against day 21 showed a significant decrease by 0.1204-fold change ($p<0.0001$).

Type I collagen (*Col1a1*) expression (Figure 103E) showed a significant increase was visible at days 14 and 21 when comparing WT-COMP against p.T585M-COMP by 1.57-fold ($p=0.0006$) change and by 3439.3-fold change ($p<0.0001$) respectively. When comparison was done for the same condition, but within different day points, a significant increase in gene expression was observed in WT-COMP cultures when comparing day 7 against day 14 by 3.488-fold change ($p<0.0001$). However, comparing days 7 and 14 against 21 a significant decrease was observed by 0.0017-fold change ($p=0.0468$) and by 0.0005-fold change ($p<0.0001$). A significant increase in gene expression was observed in p.T585M-COMP cultures when comparing day 7 against days 14 and 21 by 2.7118-fold change ($p<0.0001$) and by 2.832-fold change ($p<0.0001$).

Finally, *Acan* expression (Figure 103F) showed a significant decrease was visible at days 14 and 21 when comparing WT-COMP against p.T585M-COMP by 0.0596-fold ($p=0.0007$) change and by 0.0071-fold change ($p<0.0001$) respectively. When comparison was done for the same condition, but within different day points, a significant increase in gene expression was observed in WT-COMP cultures when comparing day 7 against days 14 and 21 by 3.02-fold change ($p=0.0085$) and by 7.66-fold change ($p<0.0001$). And comparing day 14 and 21 by 2.53-fold change ($p<0.0001$).

		Sox9	***Ihh***	***Col2a1a***	***Col10a1***	***Col1a1***	***Acan***
WT	Day7	↑	↓	↑	↓	↓	↑
	Day14	↑	↑	↑	↑	↓	↑
	Day21	↑	↑	↑	↑	↓	↑
T585M	Day7	↑	↓	↔	↓	↓	↑
	Day14	↔	↓	↔	↑	↓	↓
	Day21	↓	↓	↓	↓	↔	↓

Table 10. Table summarising the outcome of the gene expression *of Sox9, Indian hedgehog (Ihh), collagen II (Col2a1), collagen X (Col10a1), collagen I (Col1a1) and aggrecan (Acan) after 21 days of culturing ATDC5 in a pellet culture compared to day 1 gene expression. N=3 and n=3.*

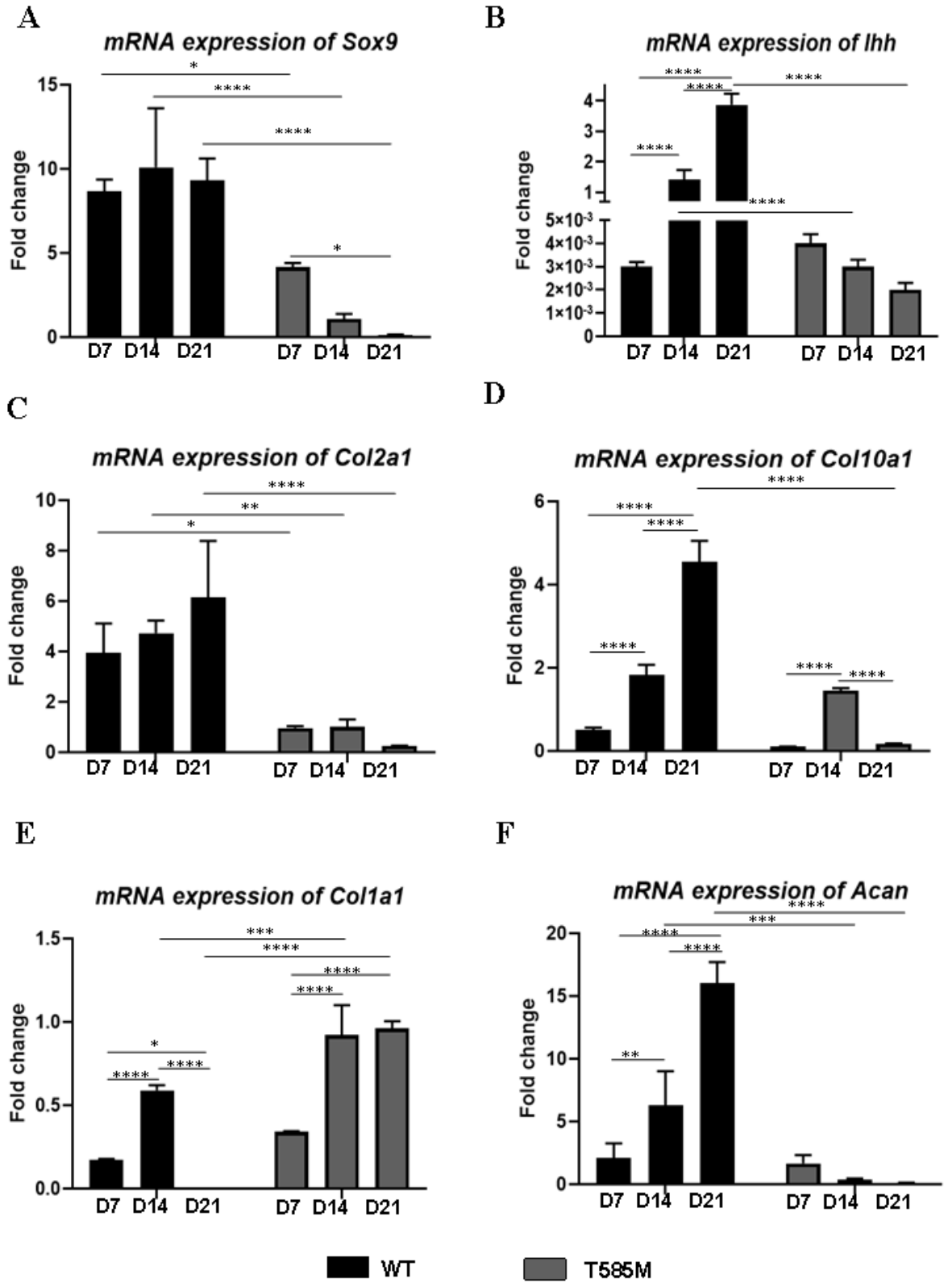

Figure 103. Gene expression after 21 days of culture. *Gene expression of Sox9* ***(A)****, Indian hedgehog (Ihh)* ***(B)****, type II collagen (Col2a1)* ***(C)****, type X collagen (Col10a1)* ***(D)****, type I collagen (Col1a1)* ***(E)****, aggrecan (Acan)* ***(F)*** *after 21 days of culturing ATDC5 in the pellet model expressing WT and T585M mutation. Quantification levels were normalised to the levels after seeding cells per ml before being differentiated (Day point 1). Two-way ANOVA statistical analysis where * p<0.05, **p<0.01, ***p<0.001, and ****p<0.0001. N=3 and n=3.*

7.3.10 Morphology in 3-dimensional 2% low gelling temperature agarose hydrogel seeded with ATDC5 cells expressing WT and p.T585M mutant COMP.

The effect of p.T585M COMP mutation on chondrogenesis was also studied in the 3-dimensional hydrogel model supplemented with growth factors, with and without dynamic compression. Interestingly, the hydrogels seeded with p.T585M COMP cells without compression collapsed at day 7-21 of the culture. Compressed mutant constructs also collapsed during histology processing at day 21 with compression and were discarded from the histological study.

Haematoxylin and eosin staining was used to study the morphology of the WT and MUT hydrogel constructs. As seen in the 2D and the pellet model, the mutant constructs showed a decrease in cell number after 14 days. Interestingly, the compressed WT model showed an increase in ECM deposition, with cells presenting a higher deposition of haematoxylin surrounding the cells and clusters (Figure 104).

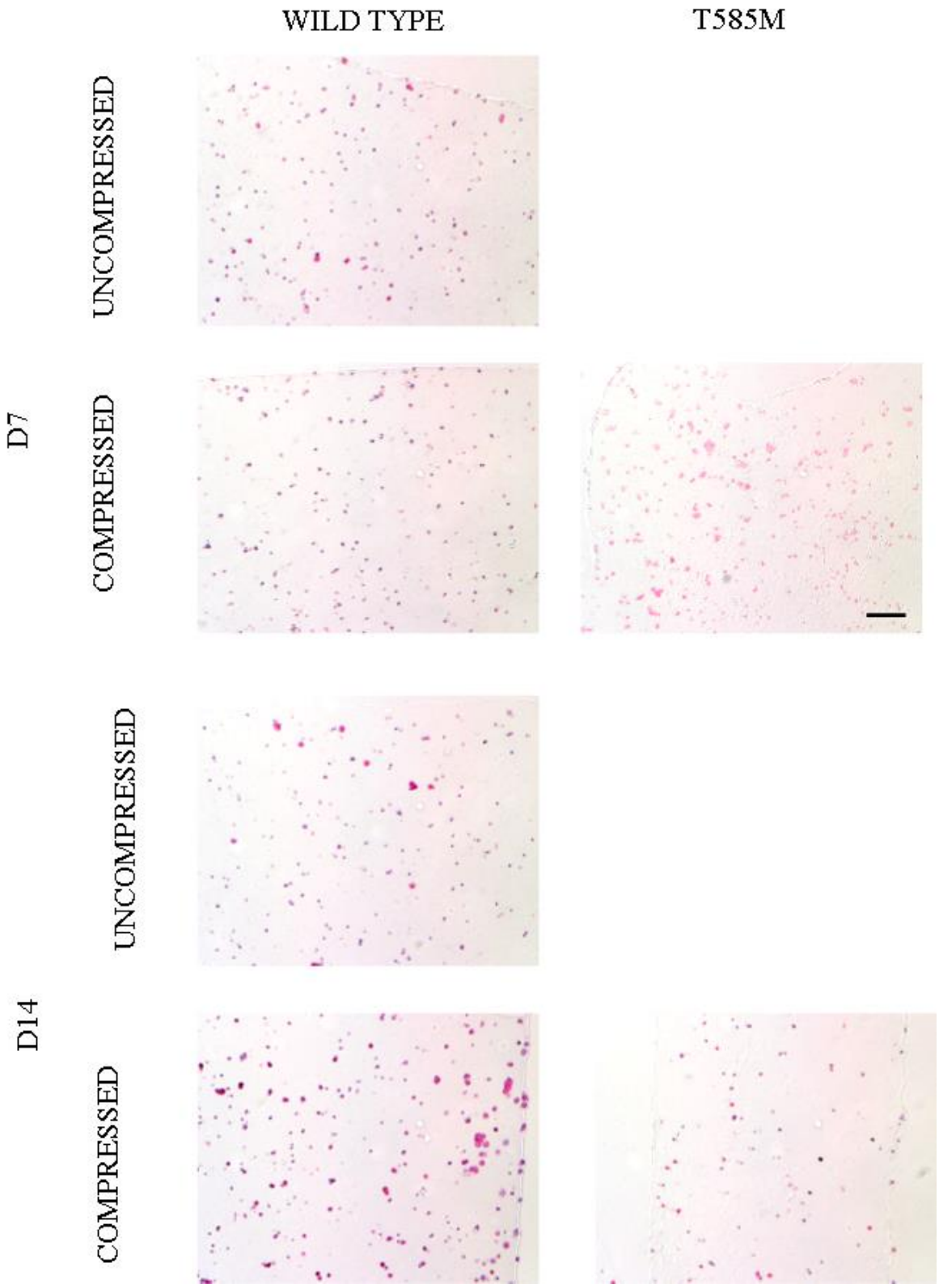

Figure 104. Histological analysis at days 7, 14 and 21. *Haematoxylin-eosin staining for cell morphology analysis for 3-dimensional culture in low gelling temperature agarose of ATDC5 expressing WT or T585M in no compressed and compressed models. Scale bar 100 µm. N=3 and n=3.*

7.3.11 The width and zonal stratification of 3-dimensional 2% low gelling temperature agarose constructs seeded with ATDC5 cells expressing WT and p.T585M mutant COMP

The area of the clusters within each layer was studied in the hydrogel constructs at the last viable day, day 14 (Figure 105.A). When comparing in-between conditions (WT vs p.T585M) for the middle and deep zone a significant decrease was observed in clusters area by 0.01509-fold change ($p<0.0001$) and 0.0062-fold change ($p<0.0001$) respectively. Comparing each zone for the same condition showed when seeding WT cells, a significant increase when comparing surface zone against middle and deep zones, by 3.64-fold change ($p=0.0267$) and by 3.37-fold change ($p<0.0001$) respectively. Comparing the middle against the deep zone a significant decrease was observed by 0.92-fold change ($p<0.0001$). The p.T585M cells model showed a significant decrease when comparing surface zone against middle and deep zones, by 0.05425-fold change ($p=0.0003$) and by 0.0206-fold change ($p<0.0001$) respectively.

The thickness of the scaffolds was also measured and compared (Figure 105.B). When comparing in-between conditions (WT vs p.T585M) for days 14 and 21 a significant decrease was observed by 0.715-fold change ($p=0.0005$) and 0.825-fold change ($p=0.0215$) respectively. Comparing for the same condition showed when seeding WT cells, a significant increase when comparing day 7 against days 14 and 21, by 2.028-fold change ($p<0.0001$) and by 1.90-fold change ($p<0.0001$) respectively. The p.T585M cells model also showed a significant increase when comparing days 7 against days 14 and 21, by 1.3259-fold change ($p=0.0133$) and by 1.43-fold change ($p=0.0023$) respectively.

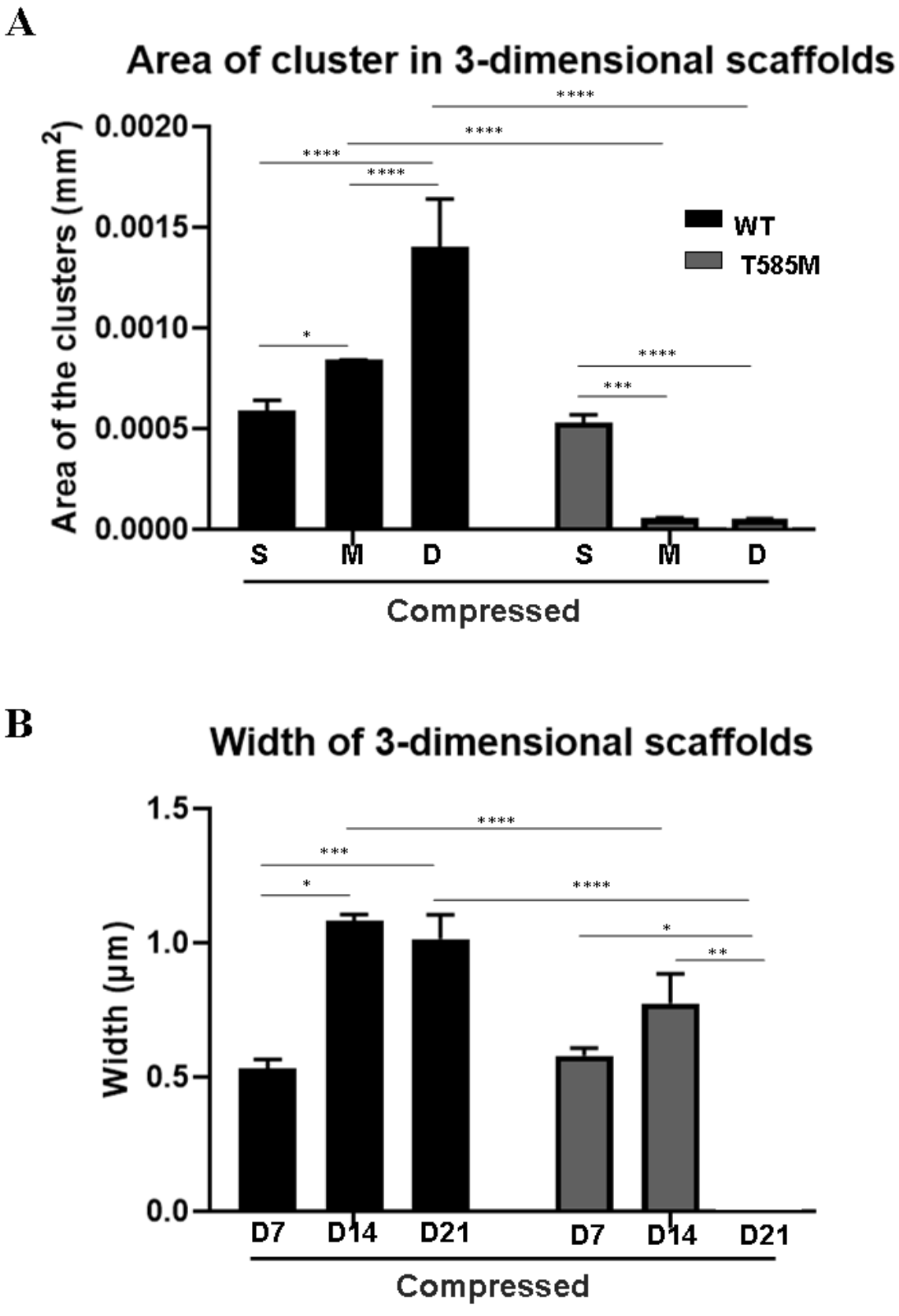

Figure 105. Analysis of width and area of clusters in WT and T585M models compressed. (A) *Area of clusters (mm^2) for each zone after 21 days when compressing was measured via ImageJ* ***(B)*** *Width (µm) was measured via ImageJ for all the conditions at each day point. Statistical analysis in both graphs was a two-way ANOVA statistical analysis where * p<0.05, **p<0.01, ***p<0.001, and ****p<0.0001. N=3 and n=3.*

7.3.12 Proteoglycan deposition in 3-dimensional 2% low gelling temperature agarose constructs seeded with ATDC5 cells expressing WT and p.T585M mutant COMP

Toluidine Blue and quantitative DMMB assay (Figure 106 and 107) were used to assess sGAG deposition in WT and p.T585M COMP hydrogels. Interestingly, WT constructs showed a higher Toluidine Blue staining, especially upon compression after 7 and 14 days, where the cells presented bright blue staining surrounding the clusters. In contrast, the amount of p.T585M COMP cells was diminished, and they did not show any evident deposition of pericellular sGAG matrix (Figure 104).

Comparing the sGAG deposition (Figure 107) within the uncompressed model showed for the WT condition a significant increase when comparing day 7 against days 14 and 21 by 1.49-fold change ($p=0.0168$) and by 3.912-fold change ($p<0.0001$) respectively and comparing day 14 against day 21 by 2.62-fold change ($p<0.0001$). When the same comparison was done in the p.T585M model, a significant decrease was observed at day 7 against days 14 and 21 by 0.327-fold change ($p=0.0247$) and by 0.235-fold change ($p=0.0102$) respectively. When compressing the constructs WT model showed a significant increase when comparing day 7 against days 14 and 21 by 2.32-fold change ($p<0.0001$) and by 3.00-fold change ($p<0.0001$) respectively and comparing day 14 against day 21 by 1.29-fold change ($p<0.0001$). T585M model construct compressed showed a significant decrease was observed at day 7 against days 14 and 21 by 0.365-fold change ($p=0.0133$) and by 0.21-fold change ($p=0.002$) respectively.

When comparison was across the condition for each day point, day 7 presented a significant increase when comparing the WT model uncompressed against compressed by 1.72-fold change ($p=0.0011$). Whereas comparing WT model against T585M model compressed showed a significant decrease by 0.468-fold change ($p<0.0001$). Day 14 presented a significant reduction when comparing WT against T585M uncompressing and compressing by 0.15-fold change ($p<0.0001$) and by 0.0735-fold change ($p<0.0001$) respectively. A significant increase was observed for the same day point when comparing the WT model uncompressed against compressed by 2.68-fold change ($p<0.0001$). Day 21 presented a significant reduction when comparing WT against T585M uncompressing and compressing by 0.041-fold change ($p<0.0001$) and by 0.032-fold change ($p<0.0001$) respectively. A significant increase was observed for the same day point when comparing the WT model uncompressed against compressed by 1.32-fold change ($p<0.0001$) (Figure 107).

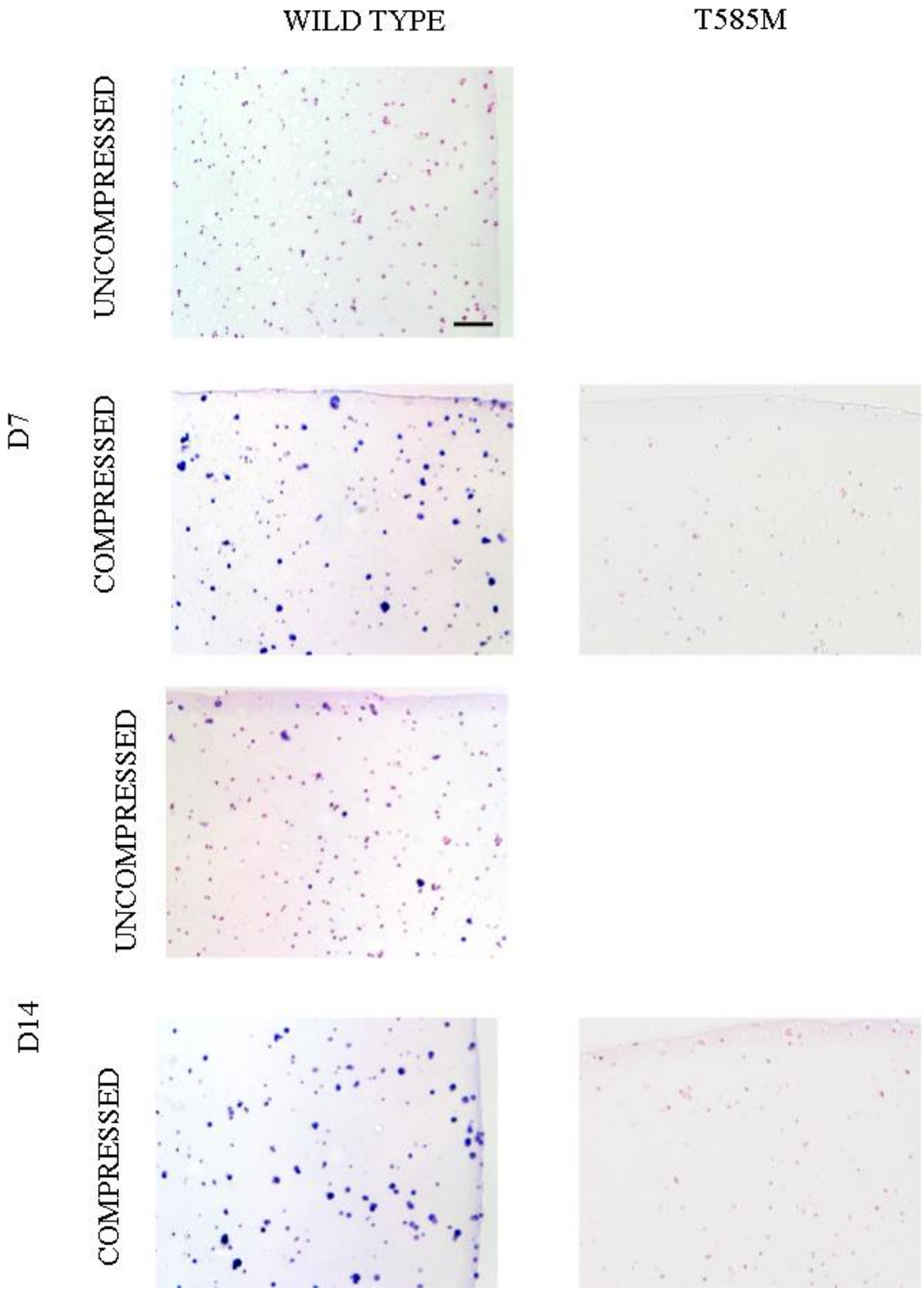

***Figure 106**. **GAG analysis at days 7, 14 and 21.** Toluidine blue staining for GAG analysis for 3-dimensional culture in low gelling temperature agarose of ATDC5 expressing WT or T585M in no compressed and compressed models. Scale bar 100 µm. N=3 and n=3.*

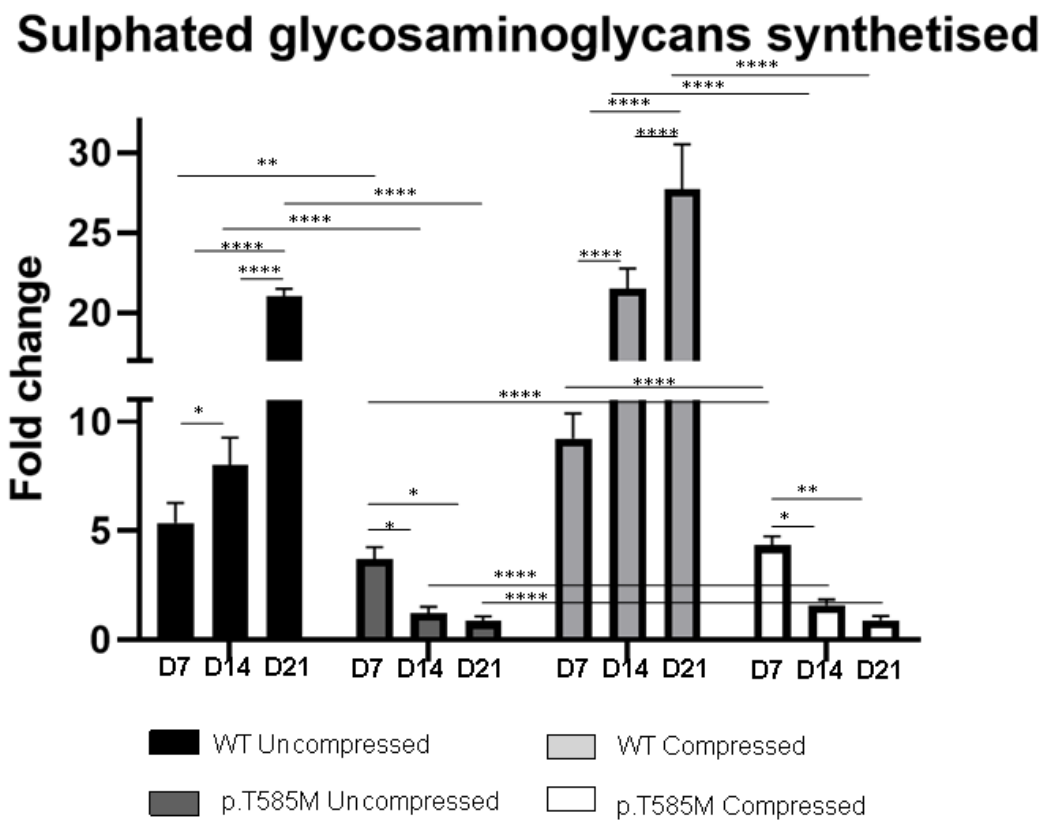

Figure 107. Analysis of sGAG deposition via quantification via DMMB assay after 21 days. *sGAG production was quantified in the WT and T585M models, being uncompressed* ***(A)*** *and compressed* ***(B)*** *after 7, 14, and 21 days. Three-way ANOVA statistical analysis where * p<0.05, **p<0.01, ***p<0.001, and ****p<0.0001. N=3 and n=3.*

7.3.13 Collagen deposition in 3-dimensional 2% low gelling temperature agarose constructs seeded with ATDC5 cells expressing WT and p.T585M mutant COMP

Picrosirus Red (Figure 106) and immunohistochemistry (Figure 107-108) were used to assess the quality of the ECM deposited in the engineered hydrogel constructs. Picrosirius Red (Figure 108) showed an ECM increase of deposition in the WT constructs, especially under compression after 14 days. For the mutant model, a decrease in cell number hindered the deposition of ECM specifically collagen, where no pericellular deposition was noted.

Immunohistochemistry was performed for type II collagen and type I collagen to study the quality of the ECM deposited by the engineered models (Figures 109 and 111). Type II collagen was detected in compressed WT constructs, either as an interterritorial matrix inside clusters of cells or as pericellular matrix deposition. Interestingly, collagen II deposition was barely detectable in WT uncompressed constructs, and in p.T585M COMP mutant hydrogels (Figure 109). Interestingly, type I collagen was undetectable in the WT constructs; however, after 14 days, the p.T585M COMP compressed samples showed pericellular deposition of type I collagen (Figure 110).

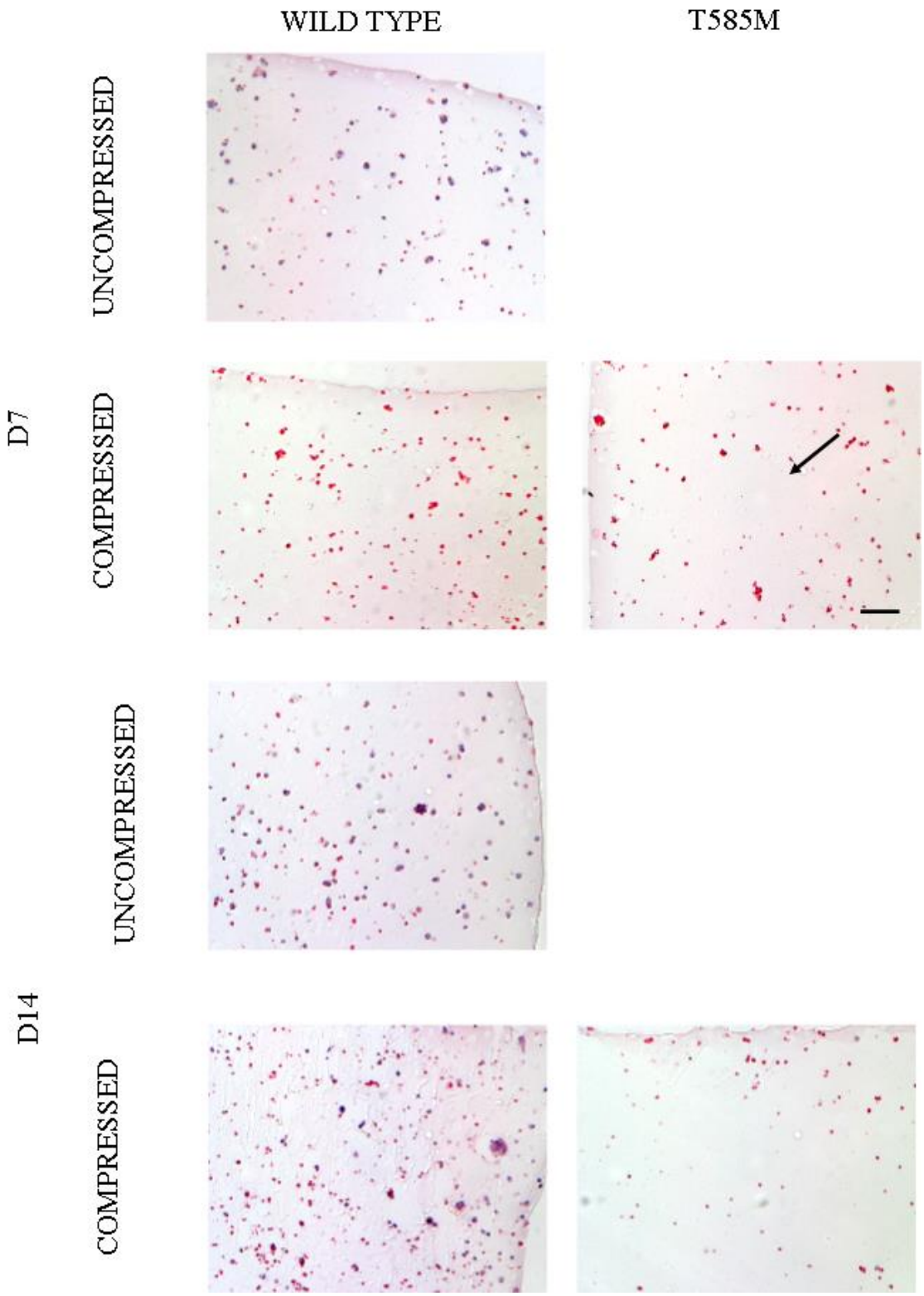

Figure 108. Collagen analysis at days 7, 14 and 21. *Picrosirius Red staining for collagen analysis for 3-dimensional culture in low gelling temperature agarose of ATDC5 expressing WT or T585M in no compressed and compressed models. Scale bar 100 µm. N=3 and n=3.*

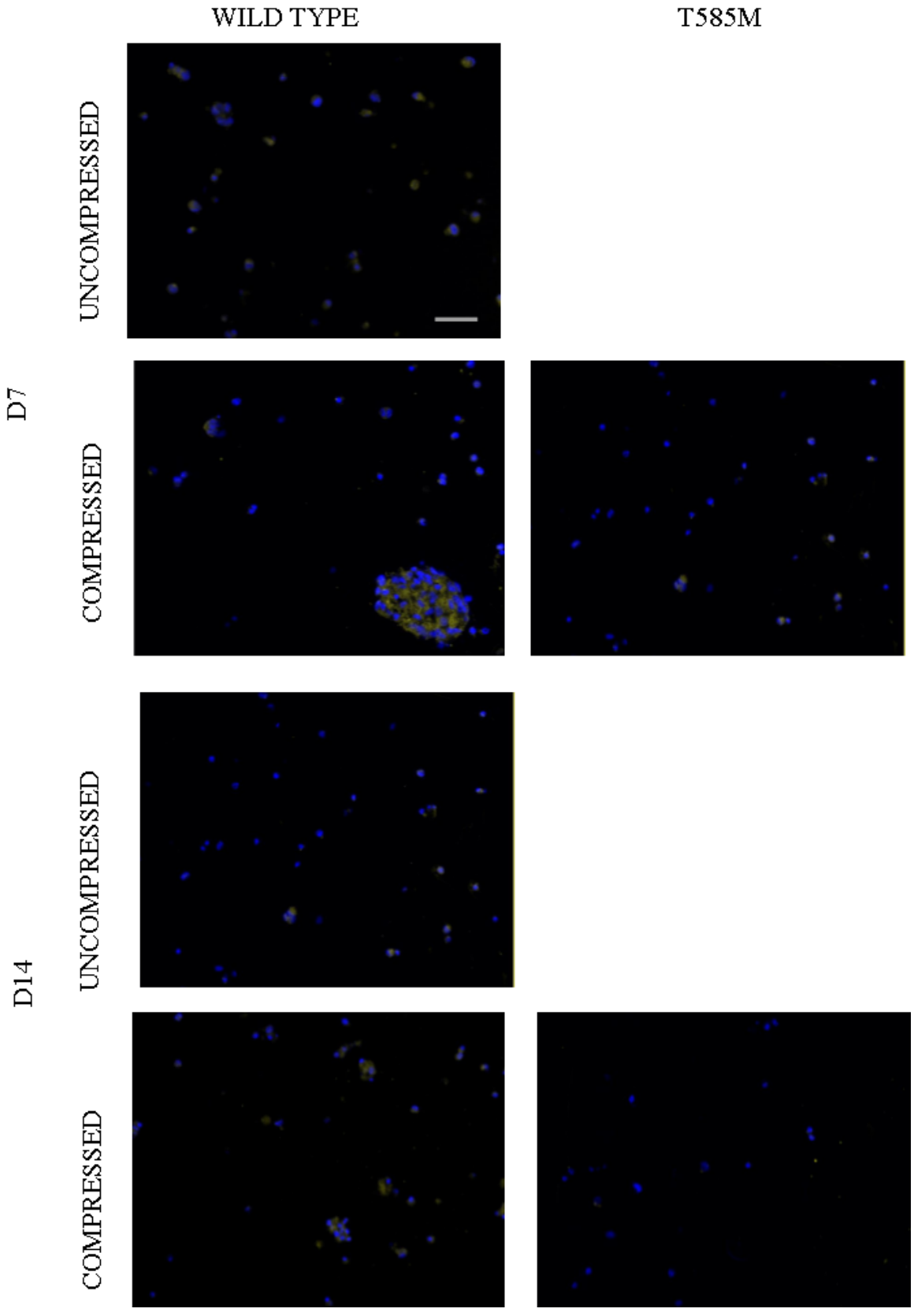

Figure 109. Immunohistochemistry for type II collagen in all conditions after 21 days. *3D hydrogel scaffolds seeded for 21 days were studied for immunohistological staining type II collagen in models expressing WT and T585M in. Scale bar = 200 µm. N=3 and n=3.*

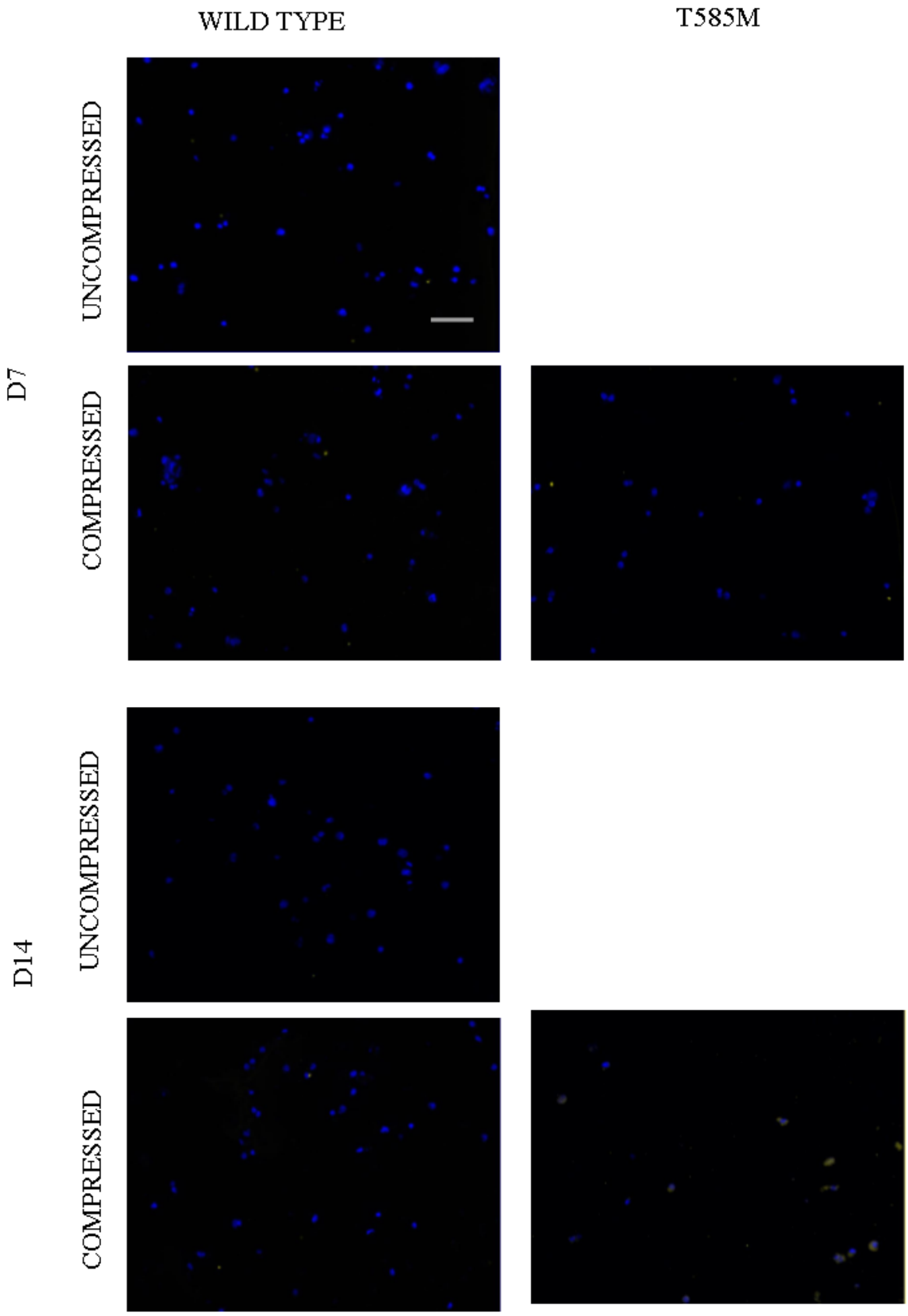

Figure 110. Immunohistochemistry for type I collagen in all conditions after 21 days. *3D hydrogel scaffolds seeded for 21 days were studied for type I collagen in a model expressing WT and T585M. Scale bar = 200 µm. N=3 and n=3.*

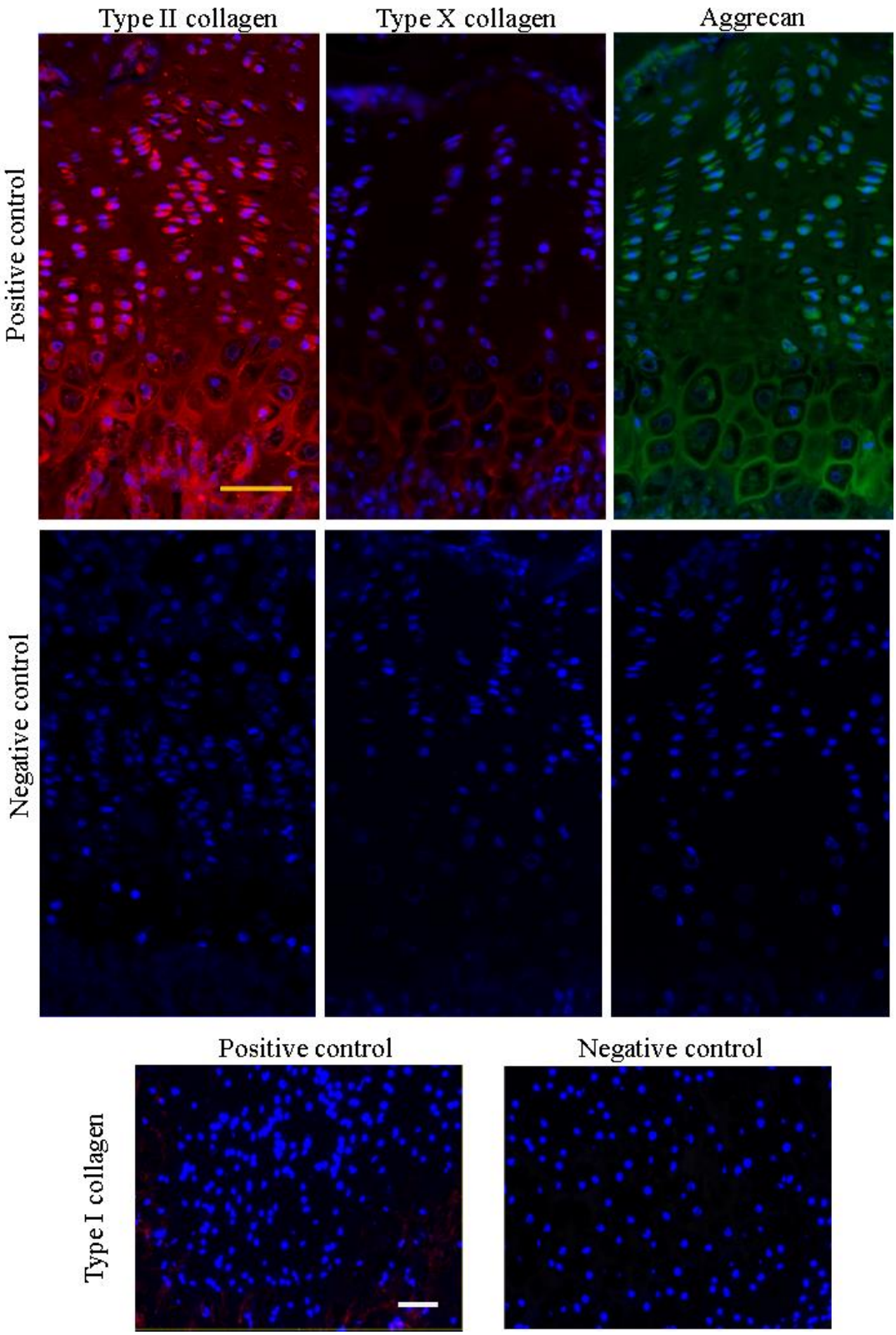

Figure 111. Positive and negative controls for type I, II and X collagen and aggrecan. *Positive and negative controls were done in 3-week-old mice femoral heads for type I, II and X collagen and aggrecan. Scale bar: 50 µm*

7.3.14 Cell apoptosis in 3-dimensional 2% low gelling temperature agarose hydrogel seeded with ATDC5 cells expressing WT and p.T585M mutant COMP

TUNEL assay was performed to assess cell apoptosis along with the day points, and its quantification was carried out via ImageJ (Figure 112 and 113). Positive apoptotic cells were normalised with the total cell number (DAPI positive). Quantification of the TUNEL images showed in the compressed p.T585M model a significant increase comparing day 7 against day 14 by 2.23-fold change ($p<0.0001$) (Figure 113). When comparing within the same day point but different condition a significant increase was observed at day 7 when comparing WT against p.T585M uncompressed by 1.2-fold change ($p=0.0015$), and when comparing uncompressed against compressed in the p.T585M condition by 1.82-fold change ($p<0.0001$). Day 14 presented a significant increase when comparing WT against p.T585M uncompressed and compressed by 1.835-fold change ($p<0.0001$), and by 2.3-fold change ($p<0.0001$) respectively. When comparing uncompressed against compressed in the p.T585M condition a significant increase was also noticed by 4.088-fold change ($p<0.0001$).

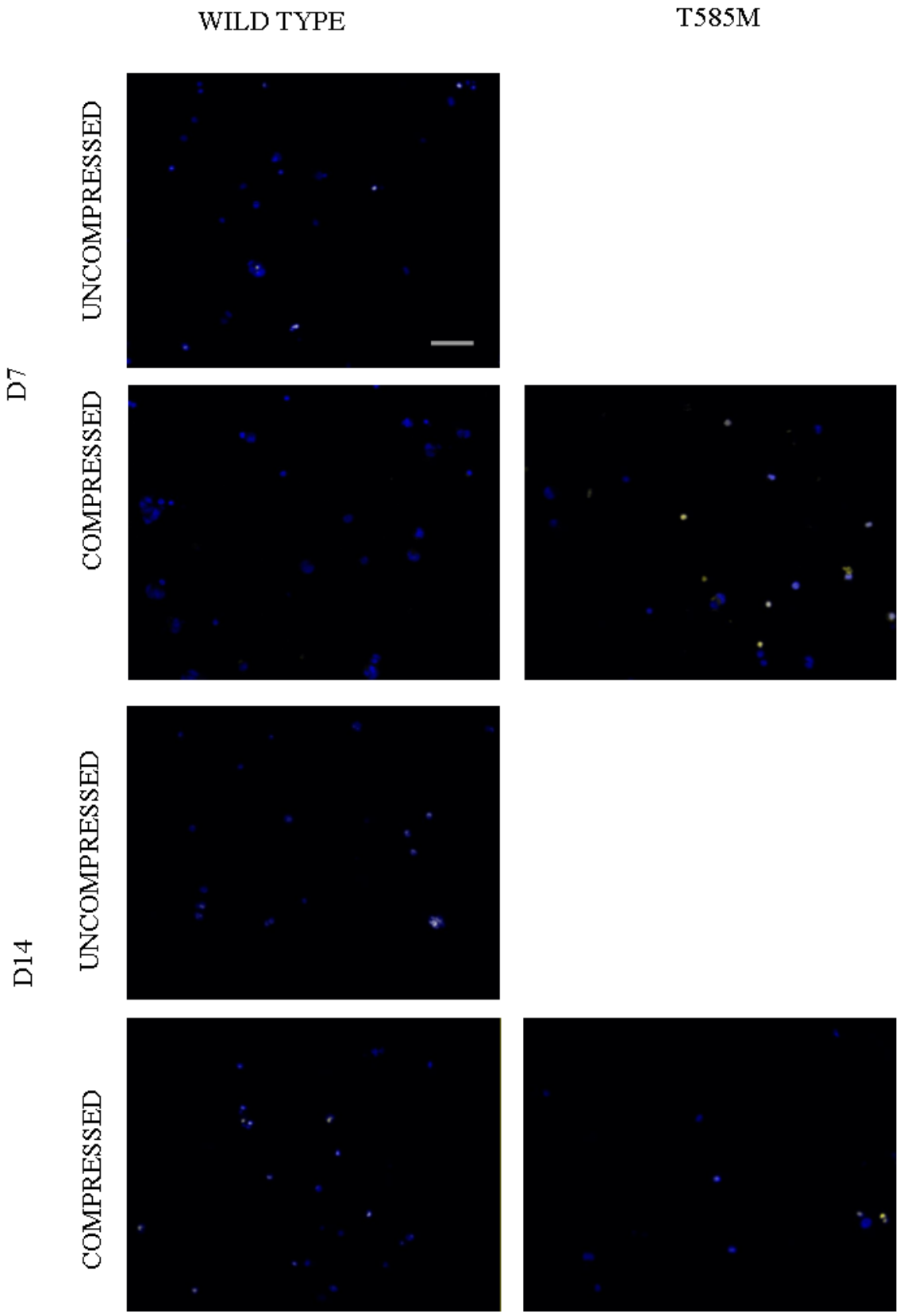

Figure 112. **Immunohistochemistry for cell apoptosis in all conditions after 21 days.** *3D hydrogels seeded for 21 days, compressed and no compressed, were analysed via TUNEL staining to study cell proliferation when expressing WT and T585M mutation. Scale bar = 200 µm. N=3 and n=3.*

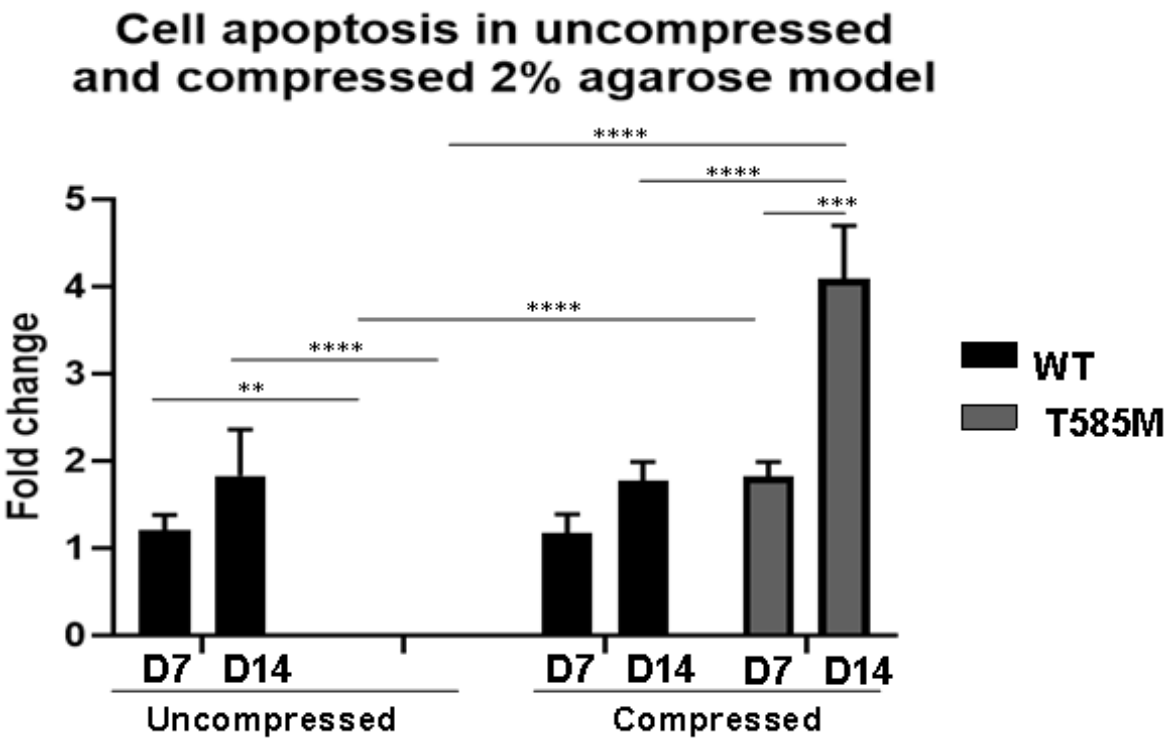

Figure 113. Cell apoptosis and numerical data and statistical analysis presented in graphs in the WT and T585M models uncompressed or compressed. *Quantification of cell apoptosis via ImageJ for all conditions along the 21 days compared to day 1. Three-way ANOVA statistical analysis where * p<0.05, **p<0.01, ***p<0.001, and ****p<0.0001. N=3 and n=3*

7.3.15 Cell proliferation and cell metabolic activity in 3-dimensional 2% low gelling temperature agarose constructs seeded with ATDC5 cells expressing WT and p.T585M mutant COMP

Cell proliferation was assessed using immunohistochemistry against Ki67 (Figure 114) and quantification of the percentage of proliferative cells (against all DAPI positive nuclei) was performed using ImageJ (Figure 115A). Quantification of the ki67 positive cells showed in the uncompressed WT model a significant decrease comparing day 7 against day 14 by 0.71-fold change ($p=0.0047$). When comparing within the same day point but different condition a significant increase was observed at day 7 when comparing WT against p.T585M uncompressed by 1.99-fold change ($p<0.0001$). A significant decrease was observed at day 7 when comparing uncompressed against compressed for the p.T585M condition by 0.78-fold change ($p=0.0002$) and WT against p.T585M model when compressing by 0.43-fold change ($p<0.0001$). Day 14 presented a significant increase when comparing WT against p.T585M uncompressed by 1.43-fold change ($p<0.0001$), and a significant decrease when compressing both models by 0.38-fold change ($p<0.0001$) respectively. When comparing uncompressed against compressed in the p.T585M condition a significant decrease was also noticed by 0.65-fold change ($p=0.0015$) (Figure 115A).

Cell metabolic activity was analysed for both WT and p.T585M COMP constructs with and without compression using MTT assay (Figure 115B). Comparing the cell metabolic activity within the uncompressed model showed for the WT condition a significant increase when comparing day 7 against days 14 and 21 by 2.84-fold change ($p<0.0001$) and by 2.811-fold change ($p<0.0001$) respectively. When compressing the constructs WT model showed a significant increase when comparing day 7 against days 14 and 21 by 2.707-fold change ($p<0.0001$) and by 2.94-fold change ($p<0.0001$) respectively. T585M model construct compressed showed a significant increase was observed at day 7 against day 21 by 1.21-fold change ($p=0.0017$).

When comparison was across the condition for each day point (Figure 115B), day 7 presented a significant decrease when comparing WT against p.T585M model uncompressed and compressed by 0.334-fold change ($p=0.0015$) and by 0.49-fold change ($p=0.0026$) respectively. Day 14 presented a significant reduction when comparing WT against T585M uncompressing and compressing by 0.11-fold change ($p<0.0001$) and by 0.115-fold change ($p<0.0001$) respectively. A significant increase was observed for the same day point when comparing the WT model uncompressed against compressed by 1.19-fold change ($p=0.0102$). Day 21 presented a significant increase when comparing WT against T585M uncompressing and compressing by 5.48-fold change ($p<0.0001$) and by 7.18-fold change ($p<0.0001$) respectively. A significant increase was observed for the same day point when comparing the WT model uncompressed against compressed by 1.31-fold change ($p<0.0001$).

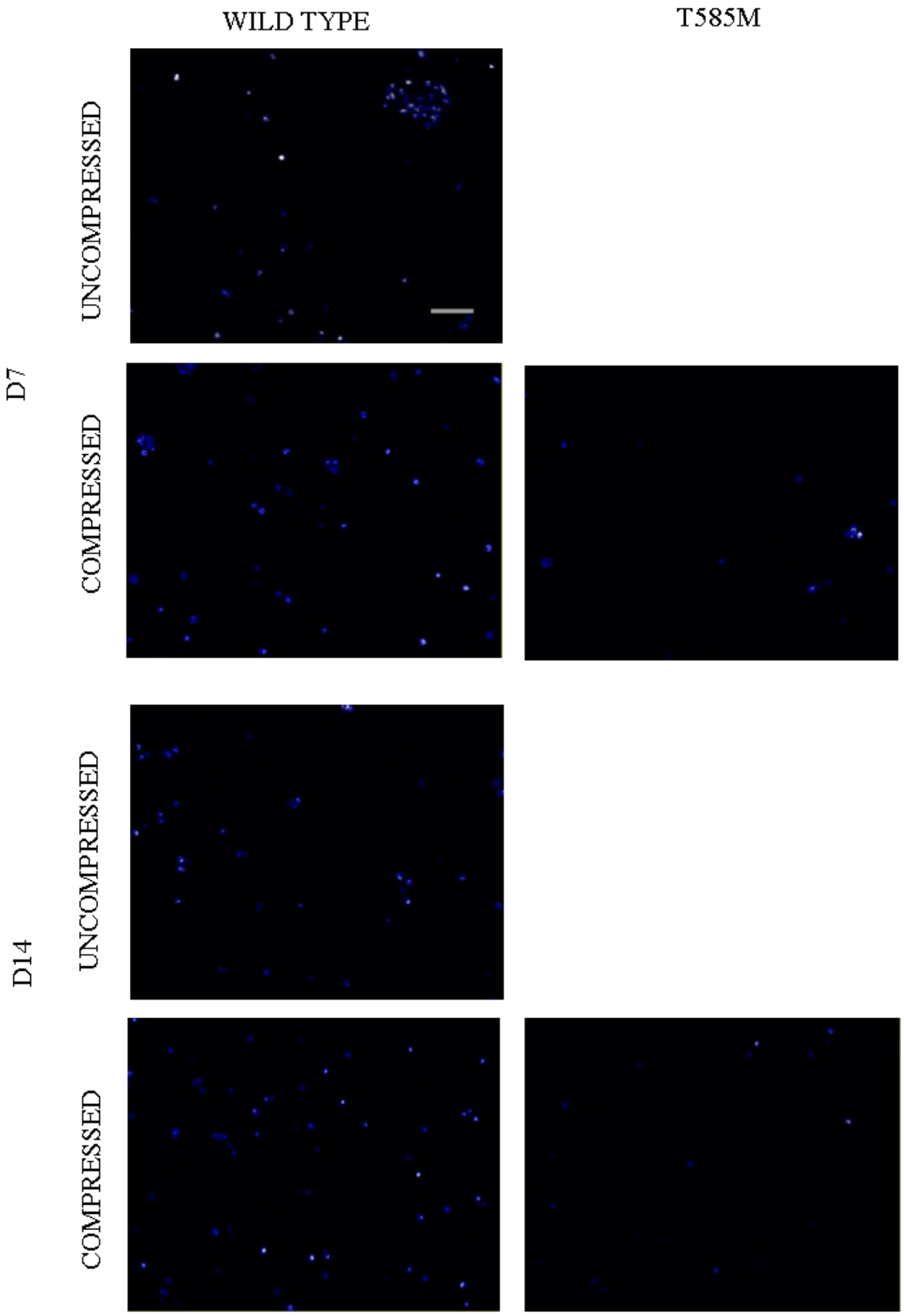

Figure 114. Immunohistochemistry for cell proliferation in all conditions after 21 days. *3D hydrogels seeded for 21 days, compressed and no compressed, were analysed via ki67 staining to study cell proliferation when expressing WT and T585M mutation. Scale bar = 200 µm. N=3 and n=3.*

A

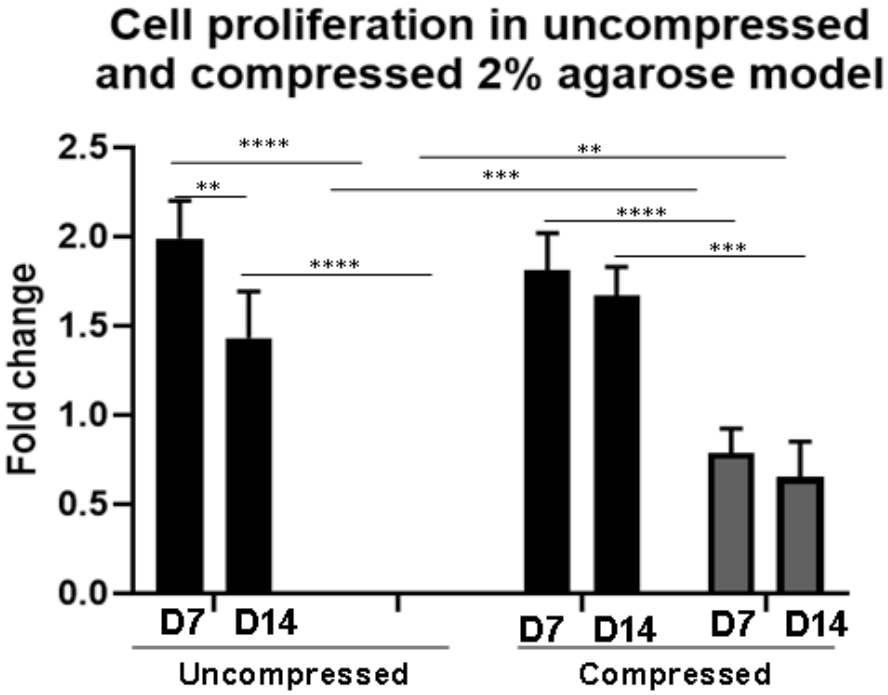

B

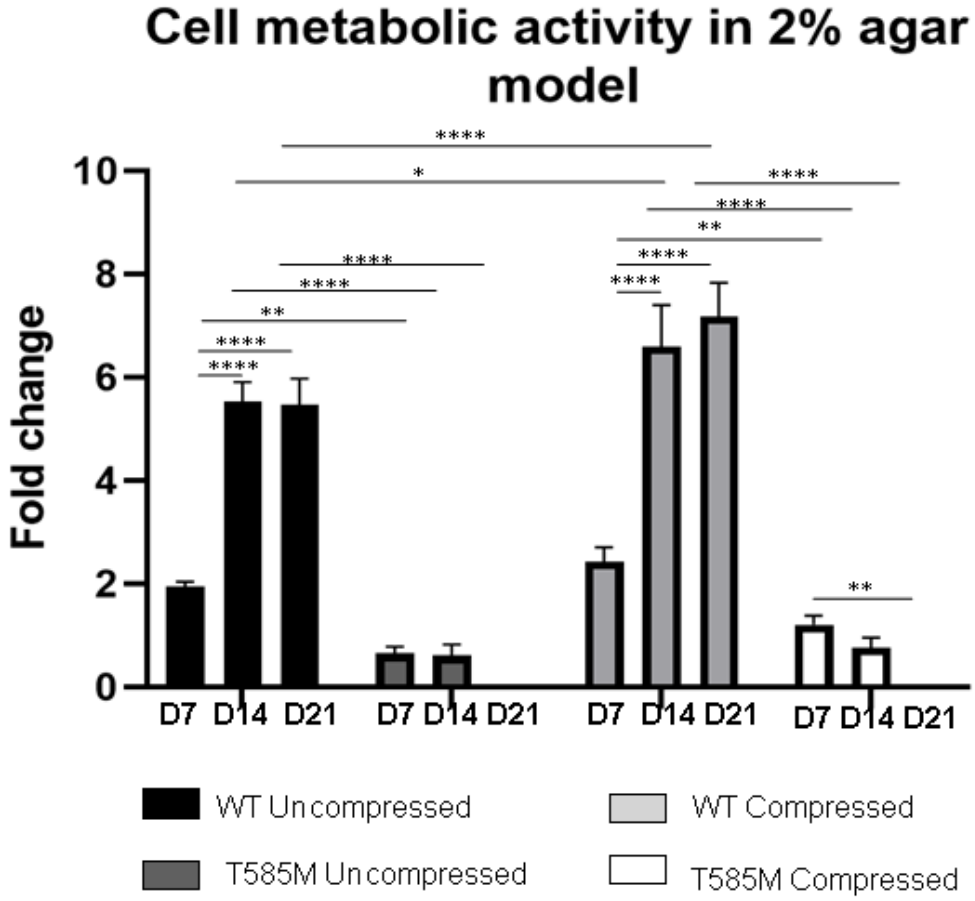

Figure 115. Cell proliferation and cell metabolic activity in WT and T585M models compressed and uncompressed. *Quantification of cell proliferation via ImageJ for all conditions along the 21 days compared to day 1 (A). Cell metabolic activity was analysed via MTT after 21 days for WT and T585M models no compressing and compressing* ***(B)*** *Three-way ANOVA statistical analysis where * p<0.05, **p<0.01, ***p<0.001, and ****p<0.0001. N=3 and n=3.*

7.3.16 Gene expression in 3-dimensional 2% low gelling temperature agarose hydrogel seeded with ATDC5 cells expressing WT and p.T585M mutant COMP.

Gene expression of articular cartilage markers of chondrogenesis (*Sox9* and *Ihh*) and ECM (type II (*Col2a1*), I (*Col1a1*) and X (*Col10a1*) collagen, and aggrecan (*Acan*)) was quantified for both uncompressed and compressed models of WT and p.T585M COMP (Figures 116 and 117 and Table 11).

mRNA expression of *Sox9* (Figure 116A) in the uncompressed WT model showed a significant decrease in expression showed a significant decrease visible at day 14 when comparing WT-COMP against p.T585M-COMP by 0.004-fold change ($p=0.004$). When comparison was done for the same condition, but within different day points, a significant increase in gene expression was observed in WT-COMP cultures when comparing day 7 against day 14 by 19.122-fold change ($p=0.011$). In the compressed model, when comparing WT-COMP against p.T585M-COMP at days 7 and 21 a significant decrease of gene expression was observed by 0.078-fold change ($p<0.0001$) and by 0.014-fold change ($p=0.0243$) respectively. Comparing each condition for different day points showed a significant decrease in WT-COMP cultures comparing day 7 against days 14 and 21 by 0.346-fold change ($p=0.0005$) and by 0.465-fold change ($p=0.004$) respectively. Comparison between uncompressed against compressed model showed at day 7 for the WT-COMP condition a significant increase by 38.45-fold change ($p<0.0001$).

Ihh expression (Figure 116B) in the compressed model, when comparing WT-COMP against p.T585M-COMP at day 21 a significant decrease of gene expression was observed by 0.00011-fold change ($p<0.0001$). Comparing each condition for different day points showed in the WT model a significant increase comparing days 7 and 14 against 21 by 20.57-fold change ($p<0.0001$) and by 43.16-fold change ($p<0.0001$) respectively. Comparison between uncompressed against compressed model showed at day 21 for the WT-COMP condition a significant increase by 419.51-fold change ($p<0.0001$).

Following the chondrogenic gene expression, the ECM synthesis genes were assessed. Applying compression led to a significant decrease in *Col2a1* expression (Figure 116C) when comparing WT-COMP against p.T585M-COMP at day 21 was observed by 0.0000909-fold change ($p<0.0001$). Comparing each condition for different day points showed in the WT model a significant increase comparing days 7 and 14 against 21 by 95.09-fold change ($p<0.0001$) and by 15.79-fold change ($p<0.0001$) respectively. Comparison between uncompressed against compressed model showed at day 21 for the WT-COMP condition a significant increase by 346.43-fold change ($p<0.0001$).

Col10a1 expression (Figure 117A) without compression in the WT model showed a significant decrease in expression showed a significant decrease visible at day 21 when comparing WT-COMP against p.T585M-COMP by 0.00084-fold change ($p=0.0006$). When comparison was done for the same condition, but within different day points, a significant increase in gene expression was observed in WT-COMP cultures when comparing day 7 and day 14 against day 21 by 4.03-fold change ($p=0.005$) and by 5.89-fold change ($p=0.0022$) respectively. In the compressed model, when comparing WT-COMP against p.T585M-COMP at days 7, 14 and 21 a significant decrease of gene expression was observed by 0.08-fold change ($p=0.0063$), by 0.014-fold change ($p=0.0019$) and by 0.00048-fold change ($p<0.0001$) respectively. Comparing each condition for different day points showed a significant increase in WT-COMP cultures comparing day 7 and 14 against 21 by 3.83-fold change ($p<0.0001$) and by 3.6389-fold change ($p<0.0001$) respectively. Comparison between uncompressed against compressed model showed at days 7, 14 and 21 for the WT-COMP condition a significant increase by 3.48-fold change ($p=0.0413$), by 5.36-fold change ($p=0.0112$) and by 3.31-fold change ($p<0.0001$) respectively.

Interestingly, *Col1A1* mRNA expression (Figure 117B) in the uncompressed WT model showed a significant decrease in expression showed a significant decrease visible at day 14 and 21 when comparing WT-COMP against p.T585M-COMP by 0.00311-fold change ($p<0.0001$) and by 0.0022-fold change ($p<0.0001$) respectively. When comparison was done for the same condition, but within different day points, a significant increase in gene expression was observed in WT-COMP cultures when comparing day 7 against day 14 by 9.75-fold change ($p<0.0001$), however, a significant decrease was visible comparing day 14 with day 21, by 0.1-fold change ($p<0.0001$).

In the compressed model, when comparing WT-COMP against p.T585M-COMP at day 7 a significant decrease of gene expression was observed by 0.0022-fold change ($p<0.0001$). Comparing each condition for different day points showed a significant decrease in WT-COMP cultures comparing day 7 against days 14 and 21 by 0.0005-fold change ($p<0.0001$) and by 0.0692-fold change ($p<0.0001$) respectively. Despite this, when comparing day 14 against day 21 a significant decrease was visible, by 144.86-fold change ($p<0.0001$).

Comparison between uncompressed against compressed model showed for the WT-COMP condition a significant increase at day 7 by 9.14-fold change ($p<0.0001$), and a significant decrease at day 14 by 0.0004-fold change ($p<0.0001$).

Acan expression (Figure 117C) in the uncompressed when comparison was done within WT-COMP but within different day points, a significant increase in gene expression was observed when comparing day 7 against day 21 by 164.13-fold change ($p<0.0001$). In the compressed model, when comparing WT-COMP against p.T585M-COMP at day 21 a significant decrease of gene expression was observed by 0.0000078-fold change ($p<0.0001$). Comparing each condition for different day points showed a significant increase in WT-COMP cultures comparing days 7 and 14 against 21 by 208.83-fold change ($p<0.0001$) and by 30.98-fold change ($p<0.0001$) respectively. Comparison between uncompressed against compressed model showed at day 21 for the WT-COMP condition a significant increase by 20.35-fold change ($p<0.0001$).

			Sox9	***Ihh***	***Col2a1a***	***Col10a1***	***Col1a1***	***Acan***
Uncompressed	WT	Day7	↓	↑	↓	↑	↓	↓
		Day14	↑	↓	↑	↑	↑	↑
		Day21	↑	↓	↓	↑	↓	↑
	T585M	Day7	↓	↓	↓	↓	↓	↓
		Day14	↓	↓	↓	↓	↓	↓
		Day21	↓	↓	↓	↓	↓	↓
Compressed	WT	Day7	↑	↑	↓	↑	↑	↓
		Day14	↑	↔	↑	↑	↓	↑
		Day21	↑	↑	↑	↑	↓	↑
	T585M	Day7	↓	↓	↓	↓	↓	↓
		Day14	↓	↓	↓	↓	↓	↓
		Day21	↓	↓	↓	↓	↓	↓

Table 11. Table summarising the outcome of the gene expression *of Sox9, Indian hedgehog (Ihh), collagen II (Col2a1), collagen X (Col10a1), collagen I (Col1a1) and aggrecan (Acan) after 21 days of culturing ATDC5 in a 3-dimensional culture compressed and uncompressed compared to day 1 gene expression. N=3 and n=3.*

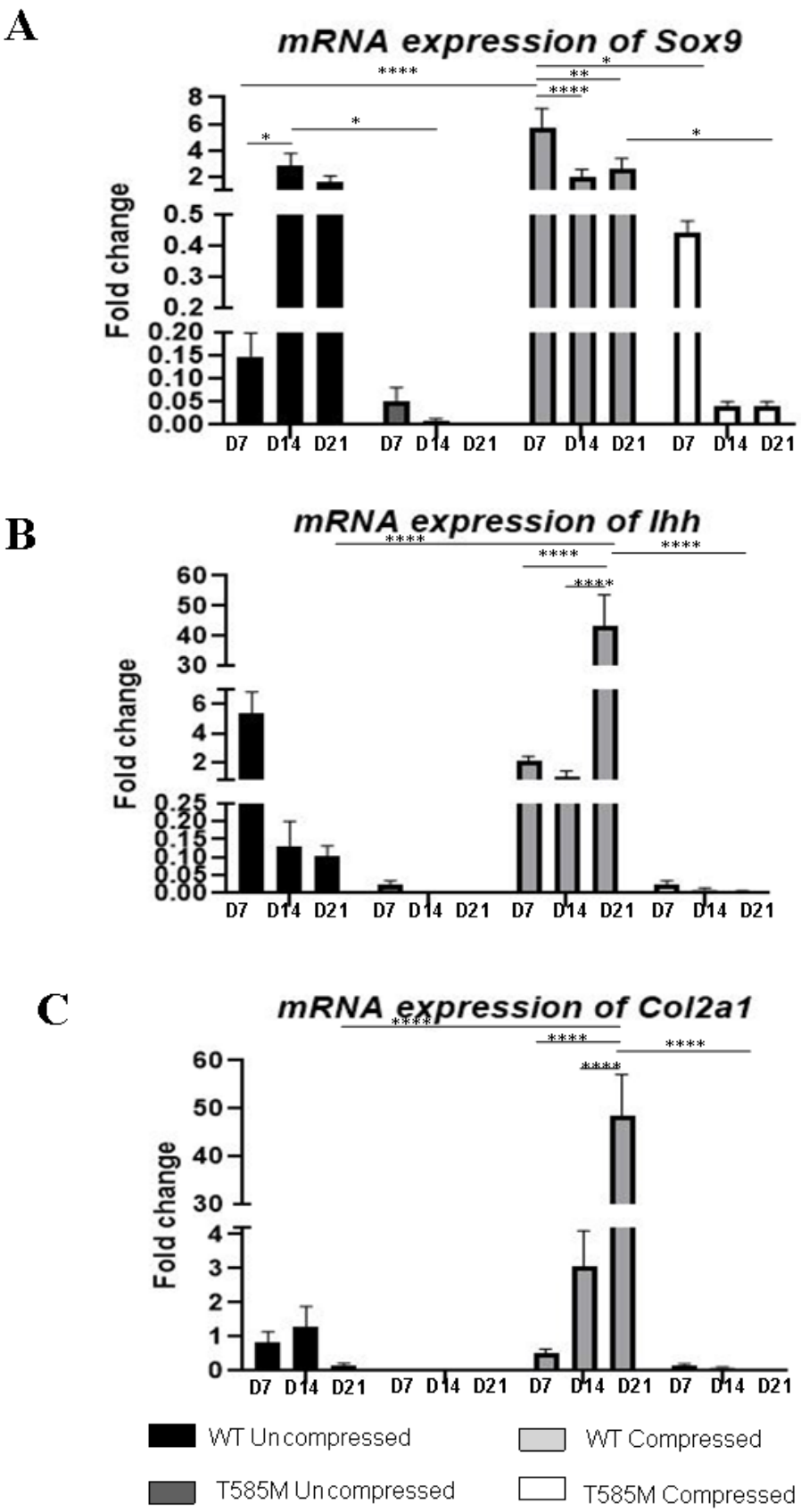

Figure 116. Gene expression after 21 days of culture. *Gene expression of Sox 9* ***(A)****, Indian hedgehog (Ihh)****(B)*** *and collagen II (Col2a1)* ***(C)*** *after 21 days of culturing ATDC5 in a 3D hydrogel scaffold expressing WT and p.T585M mutation with and without applying compression. Quantification levels were normalised to the levels after seeding cells per ml before being differentiated (Day point 1). Three-way ANOVA statistical analysis where * p<0.05, **p<0.01, ***p<0.001, and ****p<0.0001. N=3 and n=3.*

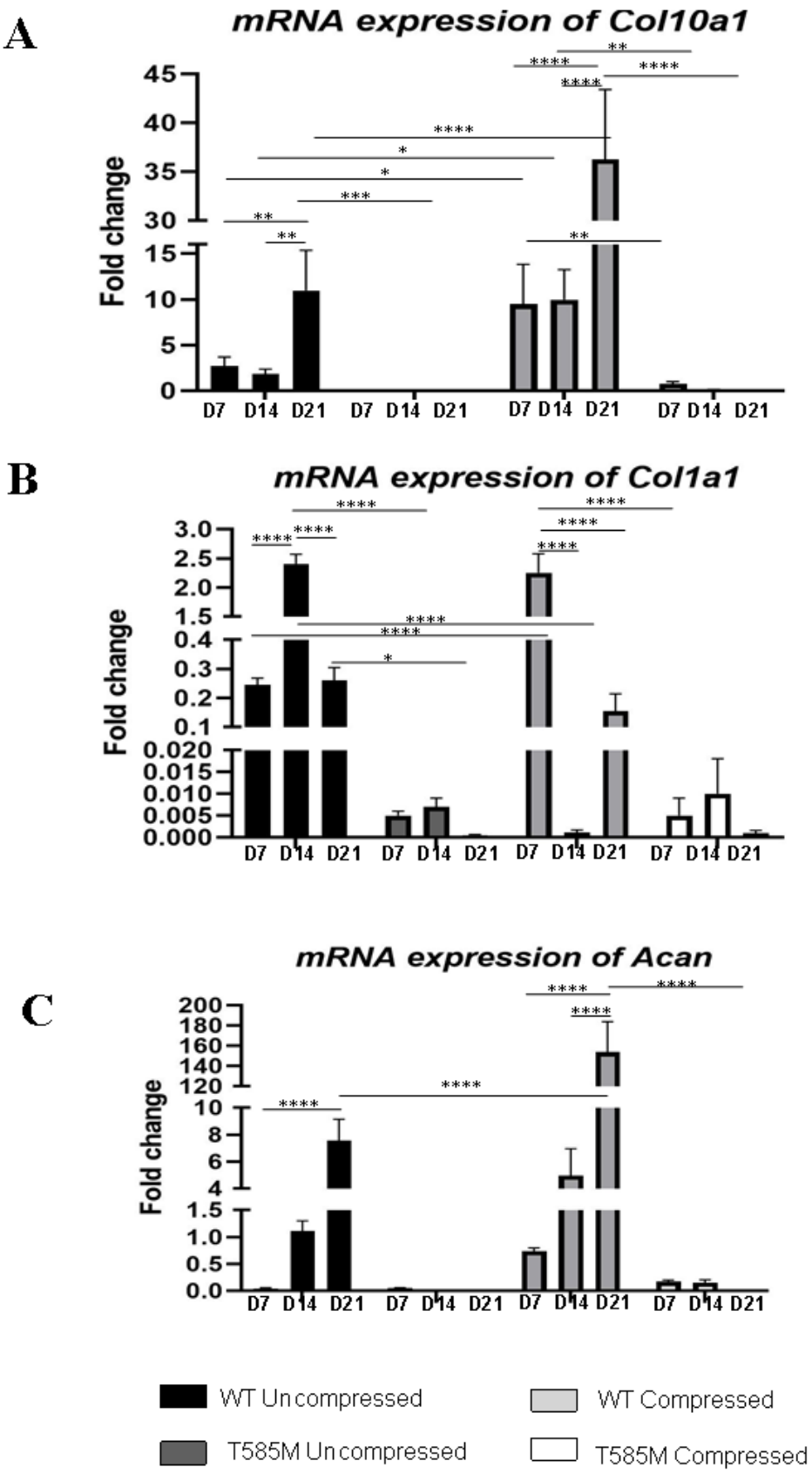

Figure 117. Gene expression after 21 days of culture. *Gene expression of collagen X (Col10a1)* ***(A)****, collagen I (Col1a1)* ***(B)*** *and aggrecan (Acan)* ***(C)*** *after 21 days of culturing ATDC5 in a 3D hydrogel scaffold expressing WT and p.T585M mutation with and without applying compression. Quantification levels were normalised to the levels after seeding cells per ml before being differentiated (Day point 1). Three-way ANOVA statistical analysis where * p<0.05, **p<0.01, ***p<0.001, and ****p<0.0001. N=3 and n=3.*

7.4 Discussion

Work presented in this chapter studied the physiological mechanism of the skeletal dysplasia resulting from mutations in the COMP gene using ATDC5 cells stably transfected with either a mutant or a wild type full-length cDNA COMP constructs. The chosen mutation, p.T585M COMP, has previously been studied in a mouse model and was chosen for this study to serve as a verification step for the 2-dimensional and 3-dimensional models (Pirog-Garcia *et al.*, 2007).

COMP mutations lead to an autosomal dominant skeletal dysplasia (Briggs and Chapman, 2002; Piróg et al., 2014), characterised by short limb dwarfism, abnormal shape or size of bones, joint laxity and early development of osteoarthritis (OA) (Briggs and Chapman, 2002; Coustry et al., 2018). Despite the mutant COMP pathological mechanism being validated, the wide range of functions of this protein and the extent of the mutations on cartilage, bones, or joints is still not fully deciphered (Coustry et al., 2018; Posey, Coustry and Hecht, 2018).

The main function of COMP protein is to serve as a link within the ECM by interacting with other main structural molecules as type II collagen or aggrecan (Chen et al., 2007; Halász et al., 2007). It was therefore hypothesised that building a mechanosensitive and/or stratified *in vitro* model of diseased cartilage could recapitulate these phenotypical changes and could replace the mouse model as means to study the progression of the disease.

The p.T585M COMP mutation does not cause retention of the protein in the endoplasmic reticulum (ER) and only a mild ER stress response; whereas mutations affecting T3, such as D469del, lead to high ER stress and activates APR and EOR pathways (Briggs, Bell and Piróg, 2017). The secretion of the mutated protein to the ECM in T585M, D605N and R718W mutations creating an abnormal environment has been hypothesised to be the cause of the cell apoptosis rather than the mutation itself (Robinson and Briggs, 2006; Piróg et al., 2014).

Overall, the data from the ATDC5 study suggests that the p.T585M mutation in the C-terminal domain of COMP results in an increase in cell apoptosis and abnormalities in the deposited ECM with a clear reduction of collagen and proteoglycans due to the cells death. An increase in cell apoptosis was also found in the patient's cells and the mouse model, relating to our results *in vitro* (Pirog-Garcia *et al.*, 2007).

7.4.1 2-dimensional monolayer model

In the monolayer (2-dimensional) ATDC5 cultures, an appearance of cell death was observed with lesser cells after 21 days of culture compared to the WT model and when initially cultured after 7 days. Quantification of sGAG deposition showed a significant decrease in mutant cultures compared to WT controls. This correlated with a significant decrease in aggrecan (*Acan*) gene expression which corresponds with what was previously seen in the other two models and the p.T585M COMP mouse model (Pirog-Garcia et al., 2007). Type II (*Col2a1*) and X (*Col10a1*) gene expression significantly decreased and type I (*Col1a1*) collagen was significantly increased in the p.T585M COMP ATDC5 cells during the chondrogenesis protocol compared to the WT COMP controls.

Mineralisation in the ATDC5 2-dimensional model analysed using Alizarin Red showed a significant decrease in calcium deposits in the p.T585M COMP model after 14 and 21 days compared to the WT cells. MED diseases are characterised by delayed mineralisation of the ossification centres (Jakkula et al., 2003). The high rates of cell apoptosis found in the 2-dimensional mutant model with the decrease of cell metabolic activity were similarly reported in the mouse expressing T585M mutation (Pirog-Garcia et al., 2007)

7.4.2 Pellet model

The pellet model showed a decrease in the gene expression of types II (Col2a1) and X (Col10a1) collagen in the mutant pellets with type II collagen undetected by immunohistochemistry in the mutant samples. Interestingly, collagen deposition was detected in the mutant pellets using Pircosirus Red staining, in particular at the surface and the centre of the pellet at days 14 and 21 which correlated with an increase in gene expression of type I collagen (Col1a1) and deposition visualised via immunohistochemistry of type I collagen. This deposition of type I collagen in the PCM was also seen in the 3-dimensional 2% agarose mutant model, and its increase is consistent with the development of OA, typical of mild MED/PSACH disease (Pirog-Garcia et al., 2007; Lahm et al., 2010; Coustry et al., 2018).

Type II (Col2a1) and X (Co10a1) collagen synthesis was equally increased along the days of culture in the WT pellets; in which, type X collagen was predominantly found in the centre of the pellet whereas type II collagen was distributed homogeneously in all layers. The pellet model collagen distribution mimics what can be found in articular cartilage tissue (Fox, Bedi and Rodeo, 2009). p.T585M model showed no deposition of type II or X collagen at any day point, proving the severity of the mutation regardless of not producing retention in the ER (Briggs, Bell and Piróg, 2017). Collagen deposition did not present a significant variation when

comparing wild type COMP expressing pellet model to untransfected pellet model, indicating that the overexpression of COMP did not affect the ECM deposition.

Examination of the proteoglycan deposition showed a significant reduction using toluidine blue staining and quantitative DMMB assay, particularly in the middle and deep zones of the mutant pellet, which correlated with the main areas of proteoglycan deposition in the wild type controls and native cartilage (Fox, Bedi and Rodeo, 2009). This was also visible in the 3-dimensional model and accordance with the p.T585M COMP mouse model (Pirog-Garcia et al., 2007).

Comparison between the proteoglycan deposited in wild type expressed pellet model against untransfected cells pellet model showed an increment in the deposition on untransfected cells. Untransfected cells pellet model deposited an increase of 39.29-fold change after 21 days of seeding, while, when expressing wild type COMP protein, the pellet model reached 27.78-fold change. Interestingly, COMP deposition in healthy cartilage is focused in the PCM of the middle zone, an area rich in sGAG, therefore, overexpression of COMP could have affected sGAG synthesis (Shen, Heinegård and Sommarin, 1995; Fox, Bedi and Rodeo, 2009).

Cell proliferation and cell metabolic activity were significantly reduced in the p.T585M COMP pellets when compared to the WT controls. Specifically, cell proliferation was analysed in the centre and surface of the pellet, showing higher expression in the surface, compared to the centre of the T585M expressed model. The reduction in cell proliferation was similar in the 3-dimensional 2% agarose mutant model and correlated with findings in the literature (Pirog-Garcia et al., 2007; Posey, Coustry and Hecht, 2018; Bell et al., 2019; Yip, Chan and Cheah, 2019).

Cell apoptosis in the mutant pellets was mainly present in the middle and centre layers of the pellet without presenting a spatial dysregulation. Interestingly, the pathway by which apoptosis is initiated by the mutant COMP postulated to be mediated by CHOP (DDIT3) (Pirog-Garcia et al., 2007). A study that crossed the p.T585M COMP mouse with a CHOP null mouse resulted in a decrease in apoptosis on the resting zone of the mutant growth plate (Piróg et al., 2014). The cell morphology is further affected in the course of the disease (Pirog-Garcia et al., 2007); however, the densely packed cells in the pellet model impeded distinguishing the cell morphology. Moreover, pellet constructs could not be subject to mechanical compression. It has been hypothesised that since the p.T585M COMP protein is secreted into the ECM, it may directly impede matrix deposition and mechanosensing, therefore, the mutation was next studied in a compressible hydrogel.

7.4.3 3-dimensional 2% agarose model

Interestingly, the 3-dimensional 2% agarose model was highly affected by the mutation, which led to the collapse of the scaffold after 2 weeks of culture. Despite the scaffold collapse, some data could still be collected on day 21. The collapse of the mutant scaffolds highlighted the important role of COMP in the ECM as matrix stabiliser and bridge molecule (Pirog-Garcia *et al.*, 2007).

Picrosirius Red, staining for collagen deposition showed a higher PCM deposition in the WT COMP model, compared to the p.T585M COMP constructs, which also presented visible cell apoptosis which was later confirmed by a cell apoptotic assay. The collagen deposition was verified using immunohistochemistry for type II and I collagen, showing that type II synthesis was increased throughout the WT-COMP culture, especially upon compression. Interestingly, the p.T585M COMP constructs did not show type II collagen deposition but type I collagen was present in the PCM of mutant ATDC5 cells after 2 weeks. Gene expression correlated with the deposition of type II collagen, which for WT cells increased dramatically upon compression. Similar was seen for the Col10a1 mRNA in the WT COMP ATDC5 constructs. In contrast, the p.T585M COMP samples showed a decrease in type II and X collagen production upon compression.

When comparing the WT-COMP model against the untransfected ATDC5 cells, a notable increment in the synthesis of collagen was visible in the untransfected ATDC5 cells model. Not only when performing the Picrosirius Red assay, with a more PCM deposition, but also when immunostaining for type II and X collagen. These results were reinforced with the RNA expression, in which when compressing untransfected ATDC5 cells type II collagen rise to 2500-fold change after 14 days, while the WT-COMP model only reached a maximum of 50-fold change after 21 days. On the other hand, type X collagen expression, increased to a 40-fold change in the WT-COMP model, while in the compressed untransfected ATDC5 cells model was a 300-fold change for the same day. Knowing the role of COMP, acting as an interactive protein in between the ECM proteins, overexpression of this protein could maybe impede or alter the normal deposition of other ECM components. Interestingly, a decrease in collagen fibril diameter was seen in a study in which COMP levels were elevated (Bastiaansen-Jenniskens *et al.*, 2010)

One of the functions of COMP is to moderate the collagen fibril assembly within the ECM. p.T585M COMP mutation does not lead to ER retention of mutant COMP. Therefore, its release

into the ECM could not only disrupt the interactions with other molecules but also affect the collagen fibrils arrangement (Robinson and Briggs, 2007; Piróg et al., 2014; Posey, Coustry and Hecht, 2018). This has been reported in other tissues such as tendons and ligament, where mutant collagen fibrils were thicker and fused, presenting a disorganised network and orientation, and variable fibre diameters (Pirog-Garcia et al., 2007). In addition to this, matrix and cartilage loss have been reported in the articular surface of ageing knee joints of mutant mice, which could reflect the early onset of OA (Pirog-Garcia et al., 2007). Interestingly, a putative collagen-binding site is located near the position 585 of COMP (in between residues 579 and 595) possibly disrupting the interaction of the protein with collagen (Holden et al., 2001).

Type X collagen (Col10a1) gene expression was also highly reduced in the mutant constructs. Moreover, immunohistochemistry showed type I collagen synthesis in the PCM of the mutant constructs. As previously mentioned, p.T585M COMP mutation leads to early-onset OA (Pirog-Garcia et al., 2007; Posey, Coustry and Hecht, 2018), and type I collagen increase is observed in the development of OA (Lahm et al., 2010).

Apart from variations in collagen, differences in proteoglycan synthesis and deposition were also noted. Toluidine blue staining showed a decrease in GAG deposition in the PCM of mutant constructs, this correlated with a decrease in the area of the cluster in the middle and deep zones of the constructs, where proteoglycans are the main ECM component. These results were further confirmed using DMMB assay, where sGAG content was significantly reduced n both compressed and uncompressed mutant samples compared to WT controls. These results were supported as well with a reduction in the aggrecan (Acan) gene expression in the mutant model when compressing and no compressing for all-day points. Our findings are consistent with the p.T585M COMP mouse model that also showed a reduction of sGAG in the growth plate cartilage (Pirog-Garcia et al., 2007).

Similarly, to previously found with collagen deposition, when comparing the wild type against the untransfected compressed models, sGAG synthesis was higher in the untransfected model, suggesting again that COMP over-expression affected the deposition of sGAG. In healthy cartilage, COMP is usually located in the superficial layers and the middle layers territorially. Since the middle layer main composition is proteoglycans, an increment in the expression of COMP could compromise sGAG deposition (Shen, Heinegård and Sommarin, 1995; Fox, Bedi and Rodeo, 2009).

Aside from a loss of ECM proteins, a progressive increase in cell apoptosis and a reduction in cell proliferation was observed in both compressed and uncompressed mutant models. Cell metabolic activity measured using the MTT assay and cell proliferation assessed by immunohistochemistry against Ki67 were significantly decreased in mutant constructs compared to WT controls. The reduction in cell proliferation has also been reported in the p.T585M COMP mouse model (Pirog-Garcia et al., 2007). This decrease in cell proliferation has been shown in all mouse models with rER stress as part of the disease mechanism (Pirog-Garcia et al., 2007; Posey, Coustry and Hecht, 2018; Bell et al., 2019; Yip, Chan and Cheah, 2019). The 2% agarose model showed spatially dysregulated apoptosis in the p.T585M COMP model, which was significantly increased compared to the WT model, both compressed and uncompressed. This spatial dysregulation apoptosis was also visible in the T585M COMP mutant mice (Piróg et al., 2014). Our mutant hydrogel model recapitulated previous findings in the mouse model, with an unstable matrix, increased apoptosis and decreased proliferation and GAG. Cells presenting the p.T585M mutation in our study did no show mechanoresponsiveness. This could be vital for further studies looking at disease pathways and diseases in which mechanosensing is affected.

All p.T585M COMP ATDC5 models recapitulated the phenotype of the disease, with abnormal ECM deposition, an increase in cell apoptosis and a decrease in cell proliferation. These data suggest that 3-dimensional 2% agarose and pellet models could be employed to study and discover possible targets to treat rare skeletal diseases and reduce the use of animal sin research in the future. Suggestions on targeting the ER stress such as chemical chaperones, in order to mitigate the damage of the mutated protein, are already applied in other rER stress-related diseases such as type II diabetes and cystic fibrosis (Briggs, Bell and Piróg, 2017). Other studies suggest anti-inflammatory and antioxidant compounds (Posey, Alcorn and Hecht, 2014). Suitable and reproducible *in vitro* models could enable high throughput screening of drug libraries to combat or mitigate the disease phenotype without the need for gene editing.

Chapter 8. Discussion

8. Discussion

Articular cartilage studies are often hindered by the difficulty in obtaining human material and the use of costly animal models. Tissue engineering is opening possibilities to develop models of cartilage that facilitate *in vitro* studies. This project aimed to mimic *in vitro* articular cartilage to study the progression and replicability of Pseudoachondroplasia (PSACH), a skeletal dysplasia in cartilage, in an *in vitro* model and use its applicability to get further insight into potential treatments. The pellet and 3D model could be applied in the study of other skeletal diseases and exploring therapies or cartilage ageing.

PSACH is an autosomal dominant disease, with an incidence of 1 in 20,000 birth, that results from mutations in the gene encoding COMP and characterises by short-limbed dwarfism, brachydactyly, deformity of legs and laxity of joints and ligaments (Briggs and Chapman, 2002; Tufan *et al.*, 2007). Through the literature regarding PSACH mutations, it has been suggested that *in vitro* models are inadequate to study the pathways involved in the development of PSACH (Suleman *et al.*, 2012). COMP expression has been proved to be upregulated by cyclic compressions, being considered a mechanosensitive gene (Giannoni *et al.*, 2003). Therefore, 2-dimensional models could result in insufficient recapitulating the disease.

Interestingly, when seeding the p.T585M expressed cells into 2-dimensional, a marked high cell apoptosis was visible. The significant cell death not only impeded the cells from depositing PCM or ECM but also affected the RNA expression, where levels were practically null after 21 days of seeding.

Pellets expressing p.T585M COMP recapitulated more closely the development of the disease was changed in the ECM were visible. This model allowed to measure the progressive loss of sGAG, especially in the centre of the pellet, after 14 days. Collagen also suffered alterations in its deposition, where type II and X collagen synthesis was drastically reduced in the pellets after 7 days of seeding, as oppose to the increment of type I collagen in the centre of the pellet at day 14 and towards outer layers of the pellet after 21 days. Cell apoptosis was noted to increase in the centre of the pellet after only 7 days of seeding and was drastically raised after 14 and 21, mimicking what is found *in vivo.*

Similarly, to what was found in the pellet, the 3-dimensional hydrogel model showed that, without compression, the cells did not produce enough PCM and the hydrogel was not able to sustain itself, disintegrating. When compressing, the p.T585M COMP, as previously

mentioned, a significant decrease in sGAG deposition was notable after only 7 days of seed. Types II and X collagen, similarly to the pellet model, presented a lack of deposition, whereas type I collagen appeared synthesised pericellularly after 14 days of seeding. Comparison of the wild type expressing model when compressed and uncompressing showed a significantly higher gene expression in *Ihh*, *Col2a1*, *Col10a1* and *Acan.*

Previous drugs and therapeutic approaches including, ER stress-reducing drugs, such as valproate, lithium and phenyl butyric acid, decreased intracellular COMP retention, chondrocyte cell apoptosis and markers for inflammation, despite this, resulted in reduced limb length in mice (Posey *et al.,* 2014). Antioxidant therapy administered along with nonsteroidal anti-inflammatory drugs (NSAIDs), showed that mice treated with aspirin, ibuprofen, resveratrol, turmeric or CoQ10 for 4 weeks showed less cell apoptosis, restoring the cell proliferation, and reducing COMP retention (Posey *et al.,* 2014). Another approach used is antisense oligonucleotides (ASO), which have proven to reduce the mutant copy up to 38%, although the wild-type copies up to 60%, however, a significant reduction in inflammation, chondrocyte death and pathology was visible (Posey *et al.,* 2014). Regardless of the potential of these approaches, much is yet to be done, especially in those mutations affecting CDT-COMP, this is why our 3D and pellet model could be key in a future study of treatments in human cartilage disorders, especially those affecting mechanosensitive genes.

As previously mentioned, the low cost and short culture periods make both 3-dimensional models easier to use in the understanding of the development of the disease. Only in 14 days both models started to show a progression of the disease, with variation in the ECM composition and deposition and increased cell apoptosis. Especially the compressed hydrogel model, with the applied compressive forces similar to the ones occurring in the articular cartilage naturally, offer a vision of the mechanical properties deteriorates along with the progression of the disease. Despite the pellet model not being compressed in this study, it could be embedded into low gelling temperature agarose and be subject to compression as well, for the study of the mechanosensitive properties in a stratified tissue. Both 3-dimensional pellets and hydrogel models could be used as well to provide insight into how treatments work against the disease, as previously mentioned, exploring different alternatives and studying how this component delays the progression of the PSACH. Finally, we acknowledge that *in vitro* models will not reach the complexity found in vivo models. However, they can be applied as an initial assessment to better understand and study different treatments before moving onto costly and time-consuming animal models.

This study showed that the tissue-engineered pellet and 3D models not only summarise the already known cell apoptosis and visible changes in the infrastructure of the ECM when expressing p.T585M but also allowed us for the very first time to see its effects in a novel mechanosensitive compressed *in vitro* model. These models, especially the mechanocompressed one, hold great potential to study different treatments in CDT-COMP mutations. Usually, mutations affecting the T3 domain, where COMP is retained, as opposed to CDT-COMP mutations where COMP is release into the ECM, are the ones typically study. Most of the treatments, such as antioxidants or anti-inflammatories, test the retention of COMP, however, it would be interesting to test these treatments in CDT-COMP mutations.

Chapter 9. Conferences and publications

9.1 Conferences:

2017: Poster presentation of “Designing a 3-dimensional in vitro model of articular cartilage for the study of cartilage-related diseases” at the International Skeletal Dysplasia Society (ISDS) conference in Belgium

2016: Poster presentation of “3D modelling of zonal stratified cartilage tissue” at the British Society Matrix Biology (BSMB) conference in the UK

9.2 Publications:

2016: Poster publication of the abstract “3D modelling of zonal stratified cartilage tissue” at the International Journal of Experimental Pathology

2016: Chapter in an online book SM Group about “Tissue Engineering Approaches for the Study and Therapeutic Intervention in Osteoarthritis”

.

Chapter 10. Bibliography

10 Bibliography

Akiyama, H. *et al.* (2000) 'Differential expressions of BMP family genes during chondrogenic differentiation of mouse ATDC5 cells', *Cell Structure and Function*, 25(3), pp. 195–204. doi: 10.1247/csf.25.195.

Akizuki, S. *et al.* (1986) 'Tensile properties of human knee joint cartilage: I. Influence of ionic conditions, weight bearing, and fibrillation on the tensile modulus', *Journal of orthopaedic research* 4(4), pp 379-392.

Akkiraju, H. and Nohe, A. (2015) 'Role of Chondrocytes in Cartilage Formation, Progression of Osteoarthritis and Cartilage Regeneration', *Journal of Developmental Biology*. Multidisciplinary Digital Publishing Institute, 3(4), pp. 177–192. doi: 10.3390/jdb3040177.

Al-Sabah, A. *et al.* (2016) 'Importance of reference gene selection for articular cartilage mechanobiology studies', *Osteoarthritis and Cartilage*. W.B. Saunders Ltd, 24(4), pp. 719–730. doi: 10.1016/j.joca.2015.11.007.

Alharbi, A. R. *et al.* (2016) 'Highly Hydrophilic Electrospun Polyacrylonitrile/ Polyvinypyrro-lidone Nanofibers Incorporated with Gentamicin as Filter Medium for Dam Water and Wastewater Treatment', *Journal of Membrane and Separation Technology*, 5(2), pp. 38–56.

Alini, M. *et al.* (2003) 'The potential and limitations of a cell-seeded collagen/hyaluronan scaffold to engineer an intervertebral disc-like matrix.', *Spine*, 28(5), pp. 446–54; discussion 453. doi: 10.1097/01.BRS.0000048672.34459.31.

Altaf, F. M. *et al.* (2006) 'Ascorbate-enhanced chondrogenesis of ATDC5 cells.', *European cells & materials*, 12, pp. 64–9; discussion 69-70. Available at: http://www.ncbi.nlm.nih.gov/pubmed/17096313 (Accessed: 8 November 2019).

Anderson, D. E. and Johnstone, B. (2017) 'Dynamic mechanical compression of chondrocytes for tissue engineering: A critical review', *Frontiers in Bioengineering and Biotechnology*. Frontiers Media S.A., 5(76). doi: 10.3389/fbioe.2017.00076.

Andrade, A. C. *et al.* (2007) 'Wnt gene expression in the post-natal growth plate: Regulation with chondrocyte differentiation', *Bone*, 40(5), pp. 1361–1369. doi: 10.1016/j.bone.2007.01.005.

Andrzejewska, A., Lukomska, B. and Janowski, M. (2019) 'Concise Review: Mesenchymal

Stem Cells: From Roots to Boost', *STEM CELLS*. John Wiley & Sons, Ltd, 37(7), pp. 855–864. doi: 10.1002/stem.3016.

Archer, C. W., Rooney, P. and Wolpert, L. (1982) 'Cell shape and cartilage differentiation of early chick limb bud cells in culture', *Cell Differentiation*, 11(4), pp. 245–251. doi: 10.1016/0045-6039(82)90072-0.

Armiento, A. R., Alini, M. and Stoddart, M. J. (2019) 'Articular fibrocartilage - Why does hyaline cartilage fail to repair?', *Advanced Drug Delivery Reviews*. Elsevier B.V., 146, pp. 289–305. doi: 10.1016/j.addr.2018.12.015.

Armstrong, C.G. and Mow, V.C. (1982) 'Variations in the intrinsic mechanical properties of human articular cartilage with age, degeneration, and water content', *Journal of bone and joint surgery*, 64(1), pp 88-94.

Asadi, N. *et al.* (2018) 'Nanocomposite hydrogels for cartilage tissue engineering: a review', *Artificial Cells, Nanomedicine and Biotechnology*. Taylor and Francis Ltd., pp. 465–471. doi: 10.1080/21691401.2017.1345924.

Asahina, I., Sampath, T. K. and Hauschka, P. V. (1996) 'Human Osteogenic Protein-1 Induces Chondroblastic, Osteoblastic, and/or Adipocytic Differentiation of Clonal Murine Target Cells', *Experimental Cell Research*. Academic Press, 222(1), pp. 38–47. doi: 10.1006/excr.1996.0005.

Aspberg, A and Aspberg, Anders (2016) 'Cartilage Proteoglycans', *Physiology and Development*. Springer International Publishing, 1, pp. 3–14. doi: 10.1007/978-3-319-29568-8_1.

Ateshian, G. A. *et al.* (1997) 'Finite deformation biphasic material properties of bovine articular cartilage from confined compression experiments', *Journal of Biomechanics*. Elsevier, 30(11–12), pp. 1157–1164. doi: 10.1016/S0021-9290(97)85606-0.

Athanasiou, K.A. *et al.* (1994) 'Comparative study of the intrinsic mechanical properties of the human acetabular and femoral head cartilage', *Journal of orthopaedic* research, 12(3), pp 340-349.

Athanasiou, K. A. *et al.* (2015) 'Harnessing biomechanics to develop cartilage regeneration strategies.', *Journal of biomechanical engineering*, 137(2), p. 020901. doi: 10.1115/1.4028825.

Atsumi, T. *et al.* (1990) 'A chondrogenic cell line derived from a differentiating culture of AT805 teratocarcinoma cells', *Cell Differentiation and Development*, 30(2), pp. 109–116.

doi: 10.1016/0922-3371(90)90079-C.

Baek, K. *et al.* (2016) 'Gene Transfection for Stem Cell Therapy', *Current Stem Cell Reports*. Springer International Publishing, pp. 52–61. doi: 10.1007/s40778-016-0029-5.

Bas, A. *et al.* (2004) 'Utility of the housekeeping genes 18S rRNA, β-actin and glyceraldehyde-3-phosphate-dehydrogenase for normalization in real-time quantitative reverse transcriptase-polymerase chain reaction analysis of gene expression in human T lymphocytes', *Scandinavian Journal of Immunology*. Scand J Immunol, 59(6), pp. 566–573. doi: 10.1111/j.0300-9475.2004.01440.x.

Basic, N. *et al.* (1996) 'TGF-beta and basement membrane matrigel stimulate the chondrogenic phenotype in osteoblastic cells derived from fetal rat calvaria.', *Journal of bone and mineral research : the official journal of the American Society for Bone and Mineral Research*, 11(3), pp. 384–91. doi: 10.1002/jbmr.5650110312.

Bastiaansen-Jenniskens, Y. M. *et al.* (2010) 'Elevated levels of cartilage oligomeric matrix protein during in vitro cartilage matrix generation decrease collagen fibril diameter', *Cartilage*. SAGE Publications, 1(3), pp. 200–210. doi: 10.1177/1947603510361238.

Becerra, J. *et al.* (2010) 'Articular cartilage: structure and regeneration.', *Tissue engineering. Part B, Reviews*, 16(6), pp. 617–27. doi: 10.1089/ten.TEB.2010.0191.

Beekman, B. *et al.* (1997) 'Synthesis of Collagen by Bovine Chondrocytes Cultured in Alginate; Posttranslational Modifications and Cell–Matrix Interaction', *Experimental Cell Research*. Academic Press, 237(1), pp. 135–141. doi: 10.1006/EXCR.1997.3771.

Beighton, P. *et al.* (1992) 'International classification of osteochondrodysplasias', *European Journal of Pediatrics*. Springer-Verlag, 151(6), pp. 407–415. doi: 10.1007/BF01959352.

Bellus, G. A. *et al.* (1995) 'Achondroplasia is defined by recurrent G380R mutations of FGFR3.', *American Journal of Human Genetics*. Elsevier, 56(2), p. 368. Available at: https://www.ncbi.nlm.nih.gov/pmc/articles/PMC1801129/ (Accessed: 14 October 2019).

Bencherif, S. A., Braschler, T. M. and Renaud, P. (2013) 'Advances in the design of macroporous polymer scaffolds for potential applications in dentistry', *Journal of Periodontal and Implant Science*, 43(6), pp. 251–261. doi: 10.5051/jpis.2013.43.6.251.

Benya, P. D. and Shaffer, J. D. (1982) 'Dedifferentiated chondrocytes reexpress the differentiated collagen phenotype when cultured in agarose gels', *Cell*, 30(1), pp. 215–224. doi: 10.1016/0092-8674(82)90027-7.

Bernstein, P. *et al.* (2009) ‘Pellet culture elicits superior chondrogenic redifferentiation than alginate-based systems’, *Biotechnology Progress*, 25(4), pp. 1146–1152. doi: 10.1002/btpr.186.

Bhat, S., Tripathi, A. and Kumar, A. (2011) ‘Supermacroprous chitosan–agarose–gelatin cryogels: *in vitro* characterization and *in vivo* assessment for cartilage tissue engineering’, *Journal of The Royal Society Interface*. Royal Society, 8(57), pp. 540–554. doi: 10.1098/rsif.2010.0455.

Bhattacharjee, M. *et al.* (2015) ‘Tissue engineering strategies to study cartilage development, degeneration and regeneration’, *Advanced Drug Delivery Reviews*, 84, pp. 107–122. doi: 10.1016/j.addr.2014.08.010.

Bhosale, A. M. and Richardson, J. B. (2008) ‘Articular cartilage: structure, injuries and review of management’, *Br Med Bull*. 2008/08/05, 87, pp. 77–95. doi: 10.1093/bmb/ldn025.

Bhumiratana, S. *et al.* (2014) ‘Large, stratified, and mechanically functional human cartilage grown in vitro by mesenchymal condensation.’, *Proceedings of the National Academy of Sciences of the United States of America*, 111(19), pp. 6940–5. doi: 10.1073/pnas.1324050111.

Bhumiratana, S. and Vunjak-Novakovic, G. (2015) ‘Engineering physiologically stiff and stratified human cartilage by fusing condensed mesenchymal stem cells’, *Methods*. Academic Press Inc., 84, pp. 109–114. doi: 10.1016/j.ymeth.2015.03.016.

Bi, W. *et al.* (1999) ‘Sox9 is required for cartilage formation’, *Nature Genetics*, 22(1), pp. 85–89. doi: 10.1038/8792.

Bi, W. *et al.* (2001). “Haploinsufficiency of Sox9 Results in Defective Cartilage Primordia and Premature Skeletal Mineralization.” Proceedings of the National Academy of Sciences of the United States of America 98 (12): 6698–6703. https://doi.org/10.1073/pnas.111092198

Bian, L. *et al.* (2009) ‘Influence of Temporary Chondroitinase ABC-Induced Glycosaminoglycan Suppression on Maturation of Tissue-Engineered Cartilage’, *Tissue Engineering Part A*, 15(8), pp. 2065–2072. doi: 10.1089/ten.tea.2008.0495.

Bian, L. *et al.* (2011) ‘Enhanced MSC chondrogenesis following delivery of TGF-β3 from alginate microspheres within hyaluronic acid hydrogels in vitro and in vivo’, *Biomaterials*, 32, pp. 6425–6434. doi: 10.1016/j.biomaterials.2011.05.033.

Blumbach, K. *et al.* (2009) ‘Combined role of type IX collagen and cartilage oligomeric

matrix protein in cartilage matrix assembly: Cartilage oligomeric matrix protein counteracts type IX collagen-induced limitation of cartilage collagen fibril growth in mouse chondrocyte cultures', *Arthritis and Rheumatism*. Arthritis Rheum, 60(12), pp. 3676–3685. doi: 10.1002/art.24979.

Bohme, K. *et al.* (1992) 'Induction of proliferation or hypertrophy of chondrocytes in serum-free culture: The role of insulin-like growth factor-I, insulin, or thyroxine', *Journal of Cell Biology*. J Cell Biol, 116(4), pp. 1035–1042. doi: 10.1083/jcb.116.4.1035.

Bonadies, I. (2018) 'Electrospun Nanofibers as 3D-Structures for Nanomedicine', *Nanomedicine*, 1(1), p. 1001. Available at: https://meddocsonline.org/journal-of-nanomedicine/electrospun-nanofibers-as-3d-structures-for-nanomedicine.html (Accessed: 16 June 2020).

Bonnevie, E. D. *et al.* (2015) 'Elastoviscous Transitions of Articular Cartilage Reveal a Mechanism of Synergy between Lubricin and Hyaluronic Acid', *PLOS ONE*. Edited by H. A. Awad. Public Library of Science, 10(11), p. e0143415. doi: 10.1371/journal.pone.0143415.

Bosnakovski, D. *et al.* (2004) 'Chondrogenic differentiation of bovine bone marrow mesenchymal stem cells in pellet cultural system', *Experimental Hematology*, 32(5), pp. 502–509. doi: 10.1016/j.exphem.2004.02.009.

Bougault, C. *et al.* (2008) 'Molecular analysis of chondrocytes cultured in agarose in response to dynamic compression', *BMC Biotechnolog*, 8(71). doi: 10.1186/1472-6750-8-71.

Bougault, C. *et al.* (2009) 'Investigating conversion of mechanical force into biochemical signaling in three-dimensional chondrocyte cultures', *Nature Protocols*, 4(6), pp. 928–938. doi: 10.1038/nprot.2009.63.

Briggs, M. D. *et al.* (1995) 'Pseudoachondroplasia and multiple epiphyseal dysplasia due to mutations in the cartilage oligomeric matrix protein gene', *Nature Genetics*, 10(3), pp. 330–336. doi: 10.1038/ng0795-330.

Briggs, M. D. *et al.* (1998) 'Diverse mutations in the gene for cartilage oligomeric matrix protein in the pseudoachondroplasia-multiple epiphyseal dysplasia disease spectrum.', *American journal of human genetics*. Elsevier, 62(2), pp. 311–9. doi: 10.1086/301713.

Briggs, M. D. *et al.* (2014) 'Genotype to phenotype correlations in cartilage oligomeric matrix protein associated chondrodysplasias', *European Journal of Human Genetics*, 22, pp. 1278–1282. doi: 10.1038/ejhg.2014.30.

Briggs, M. D., Bell, P. A. and Pirog, K. A. (2015) 'The utility of mouse models to provide information regarding the pathomolecular mechanisms in human genetic skeletal diseases: The emerging role of endoplasmic reticulum stress (Review)', *International Journal of Molecular Medicine*. Spandidos Publications, 35(6), pp. 1483–1492. doi: 10.3892/ijmm.2015.2158.

Briggs, M. D., Bell, P. and Piróg, K. A. (2017) 'Pseudoachondroplasia and multiple epiphyseal dysplasia: Molecular genetics, disease mechanisms and therapeutic targets', in Grässel, S. and Aszódi, A. (eds) *Cartilage: Pathophysiology*. Springer International Publishing, pp. 135–153. doi: 10.1007/978-3-319-45803-8_7.

Briggs, M. D. and Chapman, K. L. (2002) 'Pseudoachondroplasia and multiple epiphyseal dysplasia: Mutation review, molecular interactions, and genotype to phenotype correlations', *Human Mutation*. John Wiley & Sons, Ltd, 19(5), pp. 465–478. doi: 10.1002/humu.10066.

Brittberg, M. *et al.* (1994) 'Treatment of deep cartilage defects in the knee with autologous chondrocyte transplantation.', *The New England journal of medicine*, 331(14), pp. 889–95. doi: 10.1056/NEJM199410063311401.

Brix, M. O. *et al.* (2014) 'Treatment of Full-Thickness Chondral Defects With Hyalograft C in the Knee: Long-term Results.', *The American journal of sports medicine*, 42(6), pp. 1426–32. doi: 10.1177/0363546514526695.

Brunet, L. J. *et al.* (1998) 'Noggin, Cartilage Morphogenesis, and Joint Formation in the Mammalian Skeleton', *Science*, 280(5368), pp. 1455–1457. doi: 10.1126/science.280.5368.1455.

Budde, B. *et al.* (2005) 'Altered Integration of Matrilin-3 into Cartilage Extracellular Matrix in the Absence of Collagen IX', *Molecular and Cellular Biology*. American Society for Microbiology, 25(23), pp. 10465–10478. doi: 10.1128/mcb.25.23.10465-10478.2005.

Bulman, M.P. *et al*. (2000) 'Mutations in the Human Delta Homologue, DLL3, Cause Axial Skeletal Defects in Spondylocostal Dysostosis. ' *Nature Genetics* 24 (4): 438–41. https://doi.org/10.1038/74307

Caron, M. M. J. *et al.* (2012) 'Redifferentiation of dedifferentiated human articular chondrocytes: Comparison of 2D and 3D cultures', *Osteoarthritis and Cartilage*, 20(10), pp. 1170–1178. doi: 10.1016/j.joca.2012.06.016.

Caron, M. M. J. *et al.* (2013) 'Hypertrophic differentiation during chondrogenic

differentiation of progenitor cells is stimulated by BMP-2 but suppressed by BMP-7', *Osteoarthritis and Cartilage*, 21(4), pp. 604–613. doi: 10.1016/j.joca.2013.01.009.

Di Cesare, P. E. *et al.* (2002) 'Matrix-matrix interaction of cartilage oligomeric matrix protein and fibronectin', *Matrix Biology*. Matrix Biol, 21(5), pp. 461–470. doi: 10.1016/S0945-053X(02)00015-X.

Chapman, K. L. *et al.* (2001) 'Mutations in the region encoding the von Willebrand factor A domain of matrilin-3 are associated with multiple epiphyseal dysplasia', *Nature Genetics*, 28(4), pp. 393–396. doi: 10.1038/ng573.

Chen, C. *et al.* (2016) 'Skeleton Genetics: a comprehensive database for genes and mutations related to genetic skeletal disorders', *Database: The Journal of Biological Databases and Curation*. Oxford University Press, 2016. doi: 10.1093/DATABASE/BAW127.

Chen, D., Li, S. and Li, T.-F. (2015) 'BMPs and Wnts in Bone and Cartilage Regeneration', in *A Tissue Regeneration Approach to Bone and Cartilage Repair*. Springer, pp. 17–37. doi: 10.1007/978-3-319-13266-2_2.

Chen, F. H. *et al.* (2005) 'Cartilage oligomeric matrix protein/thrombospondin 5 supports chondrocyte attachment through interaction with integrins.', *The Journal of biological chemistry*. American Society for Biochemistry and Molecular Biology, 280(38), pp. 32655–61. doi: 10.1074/jbc.M504778200.

Chen, F. H. *et al.* (2007) 'Interaction of cartilage oligomeric matrix protein/thrombospondin 5 with aggrecan', *Journal of Biological Chemistry*. J Biol Chem, 282(34), pp. 24591–24598. doi: 10.1074/jbc.M611390200.

Chen, H.-C. *et al.* (2008) 'Inverse association of general joint hypermobility with hand and knee osteoarthritis and serum cartilage oligomeric matrix protein levels.', *Arthritis and rheumatism*. NIH Public Access, 58(12), pp. 3854–64. doi: 10.1002/art.24319.

Chen, H. *et al.* (2000) 'Cartilage oligomeric matrix protein is a calcium-binding protein, and a mutation in its type 3 repeats causes conformational changes', *Journal of Biological Chemistry*. J Biol Chem, 275(34), pp. 26538–26544. doi: 10.1074/jbc.M909780199.

Chen, T.-L. L. *et al.* (2008) 'COMP mutations: Domain-dependent relationship between abnormal chondrocyte trafficking and clinical PSACH and MED phenotypes', *Journal of Cellular Biochemistry*. John Wiley & Sons, Ltd, 103(3), pp. 778–787. doi: 10.1002/jcb.21445.

Chen, T. *et al.* (2004) 'Cell-type specific trafficking of expressed mutant COMP in a cell

culture model for PSACH.', *Matrix biology : journal of the International Society for Matrix Biology*, 23(7), pp. 433–444. doi: 10.1016/J.MATBIO.2004.09.005.

Cho, Y. S. *et al.* (2014) 'A novel technique for scaffold fabrication: SLUP (salt leaching using powder)', *Current Applied Physics*, 14(3), pp. 371–377. doi: 10.1016/j.cap.2013.12.013.

Choi, N.-Y. *et al.* (2010) 'Gel-type autologous chondrocyte (Chondron TM) implantation for treatment of articular cartilage defects of the knee', *BMC Musculoskeletal Disorders*. BioMed Central, 11(1), p. 103. doi: 10.1186/1471-2474-11-103.

Chung, C. and Burdick, J. A. (2008) 'Engineering cartilage tissue.', *Advanced drug delivery reviews*, 60(2), pp. 243–62. doi: 10.1016/j.addr.2007.08.027.

Clemmons, D. R. (2004) 'The relative roles of growth hormone and IGF-1 in controlling insulin sensitivity.', *The Journal of clinical investigation*, 113(1), pp. 25–7. doi: 10.1172/JCI20660.

Coustry, F. *et al.* (2012) 'D469del-COMP retention in chondrocytes stimulates caspase-independent necroptosis.', *The American journal of pathology*. American Society for Investigative Pathology, 180(2), pp. 738–48. doi: 10.1016/j.ajpath.2011.10.033.

Coustry, F. *et al.* (2018) 'Mutant cartilage oligomeric matrix protein (COMP) compromises bone integrity, joint function and the balance between adipogenesis and osteogenesis', *Matrix Biology*. Elsevier B.V., 67, pp. 75–89. doi: 10.1016/j.matbio.2017.12.014.

Dahlin, R. L. *et al.* (2014) 'TGF-β3-induced chondrogenesis in co-cultures of chondrocytes and mesenchymal stem cells on biodegradable scaffolds', *Biomaterials*, 35(1), pp. 123–132. doi: 10.1016/j.biomaterials.2013.09.086.

Dashtdar, H. *et al.* (2016) 'Ultra-structural changes and expression of chondrogenic and hypertrophic genes during chondrogenic differentiation of mesenchymal stromal cells in alginate beads', *PeerJ*. PeerJ Inc., 2016(3). doi: 10.7717/peerj.1650.

Delezoide, A. L. *et al.* (1998) 'Spatio-temporal expression of FGFR 1, 2 and 3 genes during human embryo-fetal ossification.', *Mechanisms of development*, 77(1), pp. 19–30. doi: 10.1016/s0925-4773(98)00133-6.

Deliormanlı, A. M. and Atmaca, H. (2018) 'Biological Response of Osteoblastic and Chondrogenic Cells to Graphene-Containing PCL/Bioactive Glass Bilayered Scaffolds for Osteochondral Tissue Engineering Applications', *Applied Biochemistry and Biotechnology*. Humana Press Inc., 186(4), pp. 972–989. doi: 10.1007/s12010-018-2758-7.

Délot, E. *et al.* (1999) ‘Trinucleotide expansion mutations in the cartilage oligomeric matrix protein (COMP) gene’, *Human Molecular Genetics*, 8(1), pp. 123–128. doi: 10.1093/hmg/8.1.123.

Denef, N. *et al.* (2000) ‘Hedgehog induces opposite changes in turnover and subcellular localization of patched and smoothened.’, *Cell*, 102(4), pp. 521–31. doi: 10.1016/s0092-8674(00)00056-8.

Denker, H. W. (2006) ‘Potentiality of embryonic stem cell: An ethical problem even with alternative stem cell sources’, *Journal of Medical Ethics*. BMJ Publishing Group, 32(11), pp. 665–671. doi: 10.1136/jme.2005.014738.

Dickinson, S. C. *et al.* (2003) ‘Cleavage of cartilage oligomeric matrix protein (thrombospondin-5) by matrix metalloproteinases and a disintegrin and metalloproteinase with thrombospondin motifs’, *Matrix Biology*. Elsevier, 22(3), pp. 267–278. doi: 10.1016/S0945-053X(03)00034-9.

Dinser, R. *et al.* (2002) ‘Pseudoachondroplasia is caused through both intra- and extracellular pathogenic pathways’, *The Journal of Clinical Investigation*. American Society for Clinical Investigation, 110(4), p. 505. doi: 10.1172/JCI14386.

Doran, P. M. (2015) ‘Cartilage Tissue Engineering: What Have We Learned in Practice?’ In *Methods in Molecular Biology*, 1340:3–21. Humana Press Inc. https://doi.org/10.1007/978-1-4939-2938-2_1

Duance, V. C. (1983) ‘Surface of articular cartilage: Immunohistological studies’, *Cell Biochemistry and Function*. Cell Biochem Funct, 1(3), pp. 143–144. doi: 10.1002/cbf.290010304.

Duarte Campos, D. F. *et al.* (2012) ‘Supporting Biomaterials for Articular Cartilage Repair.’, *Cartilage*, 3(3), pp. 205–21. doi: 10.1177/1947603512444722.

Ducy, P. *et al.* (1997) ‘Osf2/Cbfa1: a transcriptional activator of osteoblast differentiation.’, *Cell*, 89(5), pp. 747–54. doi: 10.1016/s0092-8674(00)80257-3.

Duke, J. *et al.* (2003) ‘Apoptosis staining in cultured pseudoachondroplasia chondrocytes’, *APOPTOSIS*. Kluwer Academic Publishers, 8(2), pp. 191–197. doi: 10.1023/A:1022926811397.

Durant, T. J. S. *et al.* (2014) ‘Mesenchymal stem cell response to growth factor treatment and low oxygen tension in 3-dimensional construct environment.’, *Muscles, ligaments and*

tendons journal, 4(1), pp. 46–51. Available at: http://www.ncbi.nlm.nih.gov/pubmed/24932447 (Accessed: 8 June 2016).

Duval, K. *et al.* (2017) 'Modeling physiological events in 2D vs. 3D cell culture', *Physiology*. American Physiological Society, pp. 266–277. doi: 10.1152/physiol.00036.2016.

Dzobo, K. *et al.* (2018). 'Advances in Regenerative Medicine and Tissue Engineering: Innovation and Transformation of Medicine*', Stem Cells International*, 2018, pp 24 https://doi.org/10.1155/2018/2495848

Edwards, S. L. *et al.* (2011) 'Modeling tissue growth within nonwoven scaffolds pores.', *Tissue engineering. Part C, Methods*, 17(2), pp. 123–30. doi: 10.1089/ten.TEC.2010.0182.

Elder, B. D. and Athanasiou, K. A. (2009) 'Hydrostatic pressure in articular cartilage tissue engineering: From chondrocytes to tissue regeneration', *Tissue Engineering - Part B: Reviews*, 15(1), pp. 43–53. doi: 10.1089/ten.teb.2008.0435.

Enomoto, H. *et al.* (2000) 'Cbfa1 Is a Positive Regulatory Factor in Chondrocyte Maturation', *Journal of Biological Chemistry*, 275(12), pp. 8695–8702. doi: 10.1074/jbc.275.12.8695.

Epstein, D. J., *et al.* (1991) 'Splotch (Sp2H), a Mutation Affecting Development of the Mouse Neural Tube, Shows a Deletion within the Paired Homeodomain of Pax-3.' Cell 67 (4): 767–74. https://doi.org/10.1016/0092-8674(91)90071-6.

Eyre, D. (2002) 'Collagen of articular cartilage.', *Arthritis Research*, 4(1), p. 30. doi: 10.1186/ar380.

Fernández-Iglesias, Á. *et al.* (2020) 'A simple method based on confocal microscopy and thick sections recognizes seven subphases in growth plate chondrocytes', *Scientific Reports*. Nature Research, 10(1), pp. 1–10. doi: 10.1038/s41598-020-63978-6.

Fischer, A. H. *et al.* (2008) 'Hematoxylin and Eosin Staining of Tissue and Cell Sections', *Cold Spring Harbor Protocols*, 2008(6), p. pdb.prot4986-pdb.prot4986. doi: 10.1101/pdb.prot4986.

Fitzgerald, J. *et al.* (2008) 'Evidence for articular cartilage regeneration in MRL/MpJ mice', *Osteoarthritis and Cartilage*, 16(11), pp. 1319–1326. doi: 10.1016/j.joca.2008.03.014.

Flexcell (2015) *FLEXCELL ® INTERNATIONAL CORPORATION BioPress ™ Culture Plates*.

Fox, A. J. S., Bedi, A. and Rodeo, S. A. (2009) 'The Basic Science of Articular Cartilage:

Structure, Composition, and Function', *Sports Health*. Sage CA: Los Angeles, CA: SAGE Publications, 1(6), pp. 461–468. doi: 10.1177/1941738109350438.

Fox, A. J. S., Bedi, A. and Rodeo, S. A. (2012) 'The Basic Science of Human Knee Menisci: Structure, Composition, and Function', *Sports Health: A Multidisciplinary Approach*, 4(4), pp. 340–351. doi: 10.1177/1941738111429419.

Frenkel, S. R. and Di Cesare, P. E. (2004) 'Scaffolds for Articular Cartilage Repair', *Annals of Biomedical Engineering*, 32(1), pp. 26–34. doi: 10.1023/B:ABME.0000007788.41804.0d.

Friedenstein, A. J. (1976) 'Precursor cells of mechanocytes.', *International review of cytology*, 47, pp. 327–59. doi: 10.1016/s0074-7696(08)60092-3.

Furth, M. E. and Atala, A. (2013) 'Tissue Engineering: Future Perspectives', in *Principles of Tissue Engineering: Fourth Edition*. Elsevier Inc., pp. 83–123. doi: 10.1016/B978-0-12-398358-9.00006-9.

Gadjanski, I. *et al.* (2013) 'Supplementation of exogenous adenosine 5'-triphosphate enhances mechanical properties of 3D cell-agarose constructs for cartilage tissue engineering.', *Tissue engineering. Part A*, 19(19–20), pp. 2188–200. doi: 10.1089/ten.TEA.2012.0352.

García-Carvajal, Z. *et al.* (2013) 'Cartilage Tissue Engineering: The Role of Extracellular Matrix (ECM) and Novel Strategies', in *Regenerative Medicine and Tissue Engineering*. InTech. doi: 10.5772/55917.

Gentili, C. and Cancedda, R. (2009) 'Cartilage and Bone Extracellular Matrix', *Current Pharmaceutical Design*, 15(12), pp. 1334–1348. doi: 10.2174/138161209787846739.

Gerber, H.-P. *et al.* (1999) 'VEGF couples hypertrophic cartilage remodeling, ossification and angiogenesis during endochondral bone formation', *Nature Medicine*, 5(6), pp. 623–628. doi: 10.1038/9467.

Giannoni, P. *et al.* (2003) 'The mechanosensitivity of cartilage oligomeric matrix protein (COMP)', *Biorheology*. IOS Press, 40, pp. 101–109.

Goldring, M. B. (2012) 'Chondrogenesis, chondrocyte differentiation, and articular cartilage metabolism in health and osteoarthritis.', *Therapeutic advances in musculoskeletal disease*, 4(4), pp. 269–85. doi: 10.1177/1759720X12448454.

Gorth, D. and J Webster, T. (2011) *Biomaterials for Artificial Organs*, *Biomaterials for Artificial Organs*. doi: 10.1533/9780857090843.2.270.

Graeter, L. J. *et al.* (2014) *Elsevier's medical laboratory science examination review*.

Gregory, K. E. *et al.* (1999) 'Abnormal Collagen Assembly, though Normal Phenotype, in Alginate Bead Cultures of Chick Embryo Chondrocytes', *Experimental Cell Research*, 246(1), pp. 98–107. doi: 10.1006/excr.1998.4291.

Gunetti, M. *et al.* (2012) 'Validation of analytical methods in GMP: The disposable Fast Read 102® device, an alternative practical approach for cell counting', *Journal of Translational Medicine*, 10(1). doi: 10.1186/1479-5876-10-112.

Hall, B., Limaye, A. and Kulkarni, A. B. (2009) 'Overview: Generation of Gene Knockout Mice', *Current Protocols in Cell Biology*. doi: 10.1002/0471143030.cb1912s44.

Han, F. *et al.* (2005) 'Transforming growth factor-beta1 (TGF-beta1) regulates ATDC5 chondrogenic differentiation and fibronectin isoform expression.', *Journal of cellular biochemistry*, 95(4), pp. 750–62. doi: 10.1002/jcb.20427.

Han, L., Grodzinsky, A. J. and Ortiz, C. (2011) 'Nanomechanics of the Cartilage Extracellular Matrix', *Annu. Rev. Mater. Res*, 41, pp. 133–68. doi: 10.1146/annurev-matsci-062910-100431.

Han, Y. *et al.* (2016) 'Leptin induces osteocalcin expression in ATDC5 cells through activation of the MAPK-ERK1/2 signaling pathway', *Oncotarget*. Impact Journals LLC, 7(39), pp. 64021–64029. doi: 10.18632/oncotarget.11578.

Han, Y. and Lefebvre, V. (2008) 'L-Sox5 and Sox6 Drive Expression of the Aggrecan Gene in Cartilage by Securing Binding of Sox9 to a Far-Upstream Enhancer', *Molecular and Cellular Biology*, 28(16), pp. 4999–5013. doi: 10.1128/MCB.00695-08.

Hangody, L. *et al.* (1998) 'Mosaicplasty for the treatment of articular cartilage defects: application in clinical practice.', *Orthopedics*, 21(7), pp. 751–6. Available at: http://www.ncbi.nlm.nih.gov/pubmed/9672912 (Accessed: 26 May 2016).

Hashimoto, Y. *et al.* (2003) 'Mutation (D472Y) in the Type 3 Repeat Domain of Cartilage Oligomeric Matrix Protein Affects Its Early Vesicle Trafficking in Endoplasmic Reticulum and Induces Apoptosis', *The American Journal of Pathology*, 163(1), pp. 101–110. doi: 10.1016/S0002-9440(10)63634-6.

Haugh, M. G., Murphy, C. M. and O'Brien, F. J. (2010) 'Novel freeze-drying methods to produce a range of collagen-glycosaminoglycan scaffolds with tailored mean pore sizes.', *Tissue engineering. Part C, Methods*, 16(5), pp. 887–94. doi: 10.1089/ten.TEC.2009.0422.

Hecht, J. T. *et al.* (1995) 'Mutations in exon 17B of cartilage oligomeric matrix protein (COMP) cause pseudoachondroplasia', *Nature Genetics*. Nature Publishing Group, 10(3), pp. 325–329. doi: 10.1038/ng0795-325.

Hecht, J. T. *et al.* (1998) 'Retention of cartilage oligomeric matrix protein (COMP) and cell death in redifferentiated pseudoachondroplasia chondrocytes', *Matrix Biology*. Elsevier, 17(8–9), pp. 625–633. doi: 10.1016/S0945-053X(98)90113-5.

Hecht, J. T. *et al.* (2001) 'Calreticulin, PDI, Grp94 and BiP chaperone proteins are associated with retained COMP in pseudoachondroplasia chondrocytes.', *Matrix biology : journal of the International Society for Matrix Biology*, 20(4), pp. 251–62. Available at: http://www.ncbi.nlm.nih.gov/pubmed/11470401 (Accessed: 16 October 2019).

Hecht, J. T. *et al.* (2004) 'Chondrocyte cell death and intracellular distribution of COMP and type IX collagen in the pseudoachondroplasia growth plate', *Journal of Orthopaedic Research*, 22(4), pp. 759–767. doi: 10.1016/j.orthres.2003.11.010.

Heo, D. N. *et al.* (2011) 'Development of nanofiber coated indomethacin-eluting stent for tracheal regeneration', in *Journal of Nanoscience and Nanotechnology*, pp. 5711–5716. doi: 10.1166/jnn.2011.4495.

Hoch, E., Tovar, G. E. M. and Borchers, K. (2016) 'Biopolymer-based hydrogels for cartilage tissue engineering', *Bioinspired, Biomimetic and Nanobiomaterials*, 5(2), pp. 51–66. doi: 10.1680/jbibn.15.00017.

Holden, P. *et al.* (2001) 'Cartilage oligomeric matrix protein interacts with type IX collagen, and disruptions to these interactions identify a pathogenetic mechanism in a bone dysplasia family.', *The Journal of biological chemistry*, 276(8), pp. 6046–55. doi: 10.1074/jbc.M009507200.

Holden, P. *et al.* (2005) 'Secretion of Cartilage Oligomeric Matrix Protein Is Affected by the Signal Peptide', *Journal of Biological Chemistry*, 280(17), pp. 17172–17179. doi: 10.1074/jbc.M411716200.

Hongisto, V. *et al.* (2013) 'High-Throughput 3D Screening Reveals Differences in Drug Sensitivities between Culture Models of JIMT1 Breast Cancer Cells', *PLoS ONE*. Edited by M. A. Deli. Public Library of Science, 8(10), p. e77232. doi: 10.1371/journal.pone.0077232.

Horton, W. A. (2003) 'Skeletal development: insights from targeting the mouse genome.', *Lancet (London, England)*, 362(9383), pp. 560–9. doi: 10.1016/S0140-6736(03)14119-0.

Hsieh-Bonassera, N. D. *et al.* (2009) 'Expansion and redifferentiation of chondrocytes from osteoarthritic cartilage: Cells for human cartilage tissue engineering', *Tissue Engineering - Part A*. Mary Ann Liebert Inc., 15(11), pp. 3513–3523. doi: 10.1089/ten.tea.2008.0628.

Huang, B. J., Hu, J. C. and Athanasiou, K. A. (2016) 'Cell-based tissue engineering strategies used in the clinical repair of articular cartilage', *Biomaterials*, 98, pp. 1–22. doi: 10.1016/j.biomaterials.2016.04.018.

Huang, C.-Y. C. *et al.* (2004) 'Chondrogenesis of human bone marrow-derived mesenchymal stem cells in agarose culture.', *The anatomical record. Part A, Discoveries in molecular, cellular, and evolutionary biology*. United States, 278(1), pp. 428–436. doi: 10.1002/ar.a.20010.

Huang, X. *et al.* (2018) 'Co-treatment of TGF-β3 and BMP7 is superior in stimulating chondrocyte redifferentiation in both hypoxia and normoxia compared to single treatments', *Scientific Reports*. Nature Publishing Group, 8(1). doi: 10.1038/s41598-018-27602-y.

Hughes, C. S., Postovit, L. M. and Lajoie, G. A. (2010) 'Matrigel: A complex protein mixture required for optimal growth of cell culture', *PROTEOMICS*. WILEY-VCH Verlag, 10(9), pp. 1886–1890. doi: 10.1002/pmic.200900758.

Ikegami, D. *et al.* (2011) 'Sox9 sustains chondrocyte survival and hypertrophy in part through Pik3ca-Akt pathways', *Development*, 138(8), pp. 1507–1519. doi: 10.1242/dev.057802.

Iwamoto, M. *et al.* (2013) 'Toward regeneration of articular cartilage.', *Birth defects research. Part C, Embryo today : reviews*, 99(3), pp. 192–202. doi: 10.1002/bdrc.21042.

J, M., J, R. and JT, H. (1996) 'Natural History Study of Pseudoachondroplasia', *American journal of medical genetics*. Am J Med Genet, 63(2), pp. 406–410. doi: 10.1002/(SICI)1096-8628(19960517)63:2<406::AID-AJMG16>3.0.CO;2-O.

Jacek, P. *et al.* (2018) 'Scaffolds for Chondrogenic Cells Cultivation Prepared from Bacterial Cellulose with Relaxed Fibers Structure Induced Genetically', *Nanomaterials*. MDPI AG, 8(12), p. 1066. doi: 10.3390/nano8121066.

Jackson, G. C. *et al.* (2012) 'Pseudoachondroplasia and multiple epiphyseal dysplasia: A 7-year comprehensive analysis of the known disease genes identify novel and recurrent mutations and provides an accurate assessment of their relative contribution', *Human Mutation*, 33(1), pp. 144–157. doi: 10.1002/humu.21611.

Janik, H. and Marzec, M. (2015) 'A review: Fabrication of porous polyurethane scaffolds',

Materials Science and Engineering: C, 48, pp. 586–591. doi: 10.1016/j.msec.2014.12.037.

Jeong, G.-B. (2015) 'Thrombospondin-1 and Inhibition of Tumor Growth', *Korean Journal of Physical Anthropology*. Korean Association of Physical Anthropologists (KAMJE), 28(4), p. 175. doi: 10.11637/kjpa.2015.28.4.175.

Jiang, X. *et al.* (2002) 'Tissue Origins and Interactions in the Mammalian Skull Vault', *Developmental Biology*, 241(1), pp. 106–116. doi: 10.1006/dbio.2001.0487.

Jin, M. *et al.* (2003) 'Combined effects of dynamic tissue shear deformation and insulin-like growth factor I on chondrocyte biosynthesis in cartilage explants', *Archives of Biochemistry and Biophysics*, 414(2), pp. 223–231. doi: 10.1016/S0003-9861(03)00195-4.

Jin, M. and Grodzinsky, A. J. (2001) 'Effect of Electrostatic Interactions between Glycosaminoglycans on the Shear Stiffness of Cartilage: A Molecular Model and Experiments', *Macromolecules*, 34(23), pp. 8330–8339. doi: 10.1021/ma0106604.

Johansson, N. *et al.* (1997) 'Collagenase-3 (MMP-13) is expressed by hypertrophic chondrocytes, periosteal cells, and osteoblasts during human fetal bone development', *Developmental Dynamics*, 208(3), pp. 387–397. doi: 10.1002/(SICI)1097-0177(199703)208:3<387::AID-AJA9>3.0.CO;2-E.

Johnstone, B. *et al.* (2013) 'Tissue engineering for articular cartilage repair--the state of the art.', *European cells & materials*, 25, pp. 248–67. Available at: http://www.ncbi.nlm.nih.gov/pubmed/23636950 (Accessed: 14 April 2019).

Jokanović, V. *et al.* (2019) ' Scaffold in bone tissue engineering', *Stomatoloski glasnik Srbije*. Walter de Gruyter GmbH, 64(1), pp. 32–40. doi: 10.1515/sdj-2017-0004.

Jukes, J. M. *et al.* (2008) 'Critical Steps toward a tissue-engineered cartilage implant using embryonic stem cells.', *Tissue engineering. Part A*, 14(1), pp. 135–47. doi: 10.1089/ten.a.2006.0397.

Jung, Y. *et al.* (2008) 'Cartilage regeneration with highly-elastic three-dimensional scaffolds prepared from biodegradable poly(L-lactide-co-epsilon-caprolactone).', *Biomaterials*, 29(35), pp. 4630–6. doi: 10.1016/j.biomaterials.2008.08.031.

Junqueira, L. C. U., Bignolas, G. and Brentani, R. R. (1979) 'Picrosirius staining plus polarization microscopy, a specific method for collagen detection in tissue sections', *The Histochemical Journal*. Kluwer Academic Publishers, 11(4), pp. 447–455. doi: 10.1007/BF01002772.

Karaplis, A. C. *et al.* (1994) ‘Lethal skeletal dysplasia from targeted disruption of the parathyroid hormone-related peptide gene.’, *Genes & Development*, 8(3), pp. 277–289. doi: 10.1101/gad.8.3.277.

Karsenty, G., Kronenberg, H. M. and Settembre, C. (2009) ‘Genetic Control of Bone Formation’, *Annual Review of Cell and Developmental Biology*, 25(1), pp. 629–648. doi: 10.1146/annurev.cellbio.042308.113308.

Karuppaiah, K. *et al.* (2016) ‘FGF signaling in the osteoprogenitor lineage non-autonomously regulates postnatal chondrocyte proliferation and skeletal growth’, *Development (Cambridge)*. Company of Biologists Ltd, 143(10), pp. 1811–1822. doi: 10.1242/dev.131722.

Kelly, T. A. N. *et al.* (2006) ‘Spatial and temporal development of chondrocyte-seeded agarose constructs in free-swelling and dynamically loaded cultures’, *Journal of Biomechanics*. Elsevier, 39(8), pp. 1489–1497. doi: 10.1016/j.jbiomech.2005.03.031.

Kennedy, J. *et al.* (2005) ‘Novel and recurrent mutations in the C-terminal domain ofCOMP cluster in two distinct regions and result in a spectrum of phenotypes within the pseudoachondroplasia - multiple epiphyseal dysplasia disease group’, *Human Mutation*, 25(6), pp. 593–594. doi: 10.1002/humu.9342.

Kim, I. L., Mauck, R. L. and Burdick, J. A. (2011) ‘Hydrogel design for cartilage tissue engineering: A case study with hyaluronic acid’, *Biomaterials*, 32(34), pp. 8771–8782. doi: 10.1016/j.biomaterials.2011.08.073.

Kisiday, J. D. (2019) ‘Expansion of Chondrocytes for Cartilage Tissue Engineering: A Review of Chondrocyte Dedifferentiation and Redifferentiation as a Function of Growth in Expansion Culture’, *Regenerative Medicine Frontiers*, 2(1), p. e200002. doi: 10.20900/rmf20200002.

Klein, T. J. *et al.* (2009) ‘Tissue engineering of articular cartilage with biomimetic zones.’, *Tissue engineering. Part B, Reviews*, 15(2), pp. 143–57. doi: 10.1089/ten.TEB.2008.0563.

Klein, T. J. *et al.* (2003) ‘Tissue engineering of stratified articular cartilage from chondrocyte subpopulations’, *Osteoarthritis and Cartilage*, 11(8), pp. 595–602. doi: 10.1016/S1063-4584(03)00090-6.

Klika, V. *et al.* (2016) ‘An overview of multiphase cartilage mechanical modelling and its role in understanding function and pathology’, *Journal of the Mechanical Behavior of Biomedical Materials*. Elsevier Ltd, 62, pp. 139–157. doi: 10.1016/j.jmbbm.2016.04.032.

Knippenberg, M. *et al.* (2006) 'Osteogenesis versus chondrogenesis by BMP-2 and BMP-7 in adipose stem cells', *Biochemical and Biophysical Research Communications*, 342(3), pp. 902–908. doi: 10.1016/j.bbrc.2006.02.052.

Koelling, S. *et al.* (2006) 'Cartilage oligomeric matrix protein is involved in human limb development and in the pathogenesis of osteoarthritis.', *Arthritis Research & Therapy*, 8(3), p. R56. doi: 10.1186/ar1922.

Kohn, A. D. and Moon, R. T. (2005) 'Wnt and calcium signaling: β-Catenin-independent pathways', *Cell Calcium*, 38(3–4), pp. 439–446. doi: 10.1016/j.ceca.2005.06.022.

Komiya, Y. and Habas, R. (2008) 'Wnt signal transduction pathways', *Organogenesis*, 4(2), pp. 68–75. doi: 10.4161/org.4.2.5851.

Komori, T. (2015) 'The functions of Runx family transcription factors and Cbfb in skeletal development', *Oral Science International*. No longer published by Elsevier, 12(1), pp. 1–4. doi: 10.1016/S1348-8643(14)00032-9.

Kornak, U. and Mundlos, S. (2003) 'Genetic disorders of the skeleton: A developmental approach', *American Journal of Human Genetics*, 73(3), pp. 447–474. doi: 10.1086/377110.

Krakow, D. (2015) 'Skeletal dysplasias.', *Clinics in perinatology*. NIH Public Access, 42(2), pp. 301–19, viii. doi: 10.1016/j.clp.2015.03.003.

Kronenberg, H. M. *et al.* (1997) 'Parathyroid hormone-related protein and Indian hedgehog control the pace of cartilage differentiation.', *The Journal of endocrinology*, 154 Suppl, pp. S39-45. Available at: http://www.ncbi.nlm.nih.gov/pubmed/9379136 (Accessed: 14 October 2019).

Kronenberg, H. M. (2003) 'Developmental regulation of the growth plate', *Nature*, 423(6937), pp. 332–336. doi: 10.1038/nature01657.

Kuchipudi, S. V. *et al.* (2012) '18S rRNA is a reliable normalisation gene for real time PCR based on influenza virus infected cells', *Virology Journal*. BioMed Central, p. 230. doi: 10.1186/1743-422X-9-230.

Kudva, A., Luyten, F. and Patterson, J. (2018) 'In Vitro Screening of Molecularly Engineered Polyethylene Glycol Hydrogels for Cartilage Tissue Engineering using Periosteum-Derived and ATDC5 Cells', *International Journal of Molecular Sciences*, 19(11), p. 3341. doi: 10.3390/ijms19113341.

Kung, L. H. W. *et al.* (2015) 'Increased Classical Endoplasmic Reticulum Stress Is Sufficient

to Reduce Chondrocyte Proliferation Rate in the Growth Plate and Decrease Bone Growth', *PLOS ONE*. Edited by F. Ruggiero. Public Library of Science, 10(2), p. e0117016. doi: 10.1371/journal.pone.0117016.

Kuno, K. *et al.* (2000) 'ADAMTS-1 cleaves a cartilage proteoglycan, aggrecan.', *FEBS letters*, 478(3), pp. 241–5. doi: 10.1016/s0014-5793(00)01854-8.

Kvansakul, M., Adams, Josephine C and Hohenester, E. (2004) 'Structure of a thrombospondin C-terminal fragment reveals a novel calcium core in the type 3 repeats', *The EMBO journal*. 2004/03/11, 23(6), pp. 1223–1233. doi: 10.1038/sj.emboj.7600166.

Kvansakul, M., Adams, Josephine C. and Hohenester, E. (2004) 'Structure of a thrombospondin C-terminal fragment reveals a novel calcium core in the type 3 repeats', *EMBO Journal*, 23(6), pp. 1223–1233. doi: 10.1038/sj.emboj.7600166.

Lahm, A. *et al.* (2010) 'Changes in content and synthesis of collagen types and proteoglycans in osteoarthritis of the knee joint and comparison of quantitative analysis with Photoshop-based image analysis', *Archives of Orthopaedic and Trauma Surgery*. Arch Orthop Trauma Surg, 130(4), pp. 557–564. doi: 10.1007/s00402-009-0981-y.

Lai, W. M., Hou, J. S. and Mow, V. C. (1991) 'A triphasic theory for the swelling and deformation behaviors of articular cartilage', *Journal of Biomechanical Engineering*, 113(3), pp. 245–258. doi: 10.1115/1.2894880.

Lammi, P. E. et al. (2001) 'Strong hyaluronan expression in the full-thickness rat articular cartilage repair tissue', Histochemistry and Cell Biology, 115(4), pp. 301–308. doi: 10.1007/s004180100265.

Langer, R. and Vacanti, J. (1993) 'Tissue engineering', *Science*. American Association for the Advancement of Science, 260(5110), pp. 815–818. doi: 10.1126/science.8493529.

Le, B. Q. *et al.* (2015) 'High-Throughput Screening Assay for the Identification of Compounds Enhancing Collagenous Extracellular Matrix Production by ATDC5 Cells', *Tissue Engineering - Part C: Methods*. Mary Ann Liebert Inc., 21(7), pp. 726–736. doi: 10.1089/ten.tec.2014.0088.

Le, B. Q. *et al.* (2017) 'Micro-Topographies Promote Late Chondrogenic Differentiation Markers in the ATDC5 Cell Line', *Tissue Engineering Part A*, 23(9–10), pp. 458–469. doi: 10.1089/ten.tea.2016.0421.

Lee, C. *et al.* (2006) 'The Influence of Mechanical Stimuli on Articular Cartilage Tissue

Engineering', *Topics in Tissue Engineering*, 2(2).

Lee, E. C. *et al.* (2001) 'A highly efficient Escherichia coli-based chromosome engineering system adapted for recombinogenic targeting and subcloning of BAC DNA.', *Genomics*. United States, 73(1), pp. 56–65. doi: 10.1006/geno.2000.6451.

Lee, HS and Salter, D.M. (2015). 'Biomechanics of Cartilage and Osteoarthritis.' *Osteoarthritis - Progress in Basic Research and Treatment.* IntechOpen doi: 10.5772/60011.

Lee, J. K. *et al.* (2017) 'The self-assembling process and applications in tissue engineering', *Cold Spring Harbor Perspectives in Medicine*. Cold Spring Harbor Laboratory Press. doi: 10.1101/cshperspect.a025668.

Leung, V. Y. L. *et al.* (2011) 'SOX9 governs differentiation stage-specific gene expression in growth plate chondrocytes via direct concomitant transactivation and repression', *PLoS Genetics*. PLoS Genet, 7(11), p. e1002356. doi: 10.1371/journal.pgen.1002356.

Levenberg, S. *et al.* (2003) 'Differentiation of human embryonic stem cells on three-dimensional polymer scaffolds.', *Proceedings of the National Academy of Sciences of the United States of America*. National Acad Sciences, 100(22), pp. 12741–6. doi: 10.1073/pnas.1735463100.

Lewis, M. C. *et al.* (2016) 'Extracellular Matrix Deposition in Engineered Micromass Cartilage Pellet Cultures: Measurements and Modelling', *PLOS ONE*. Edited by D. Nikitovic-Tzanakaki. Public Library of Science, 11(2), p. e0147302. doi: 10.1371/journal.pone.0147302.

Li, R. *et al.* (2009) 'Effect of cell-based VEGF gene therapy on healing of a segmental bone defect', *Journal of Orthopaedic Research*, 27(1), pp. 8–14. doi: 10.1002/jor.20658.

Lima, E. G. *et al.* (2007) 'The beneficial effect of delayed compressive loading on tissue-engineered cartilage constructs cultured with TGF-beta3.', *Osteoarthritis and cartilage / OARS, Osteoarthritis Research Society*, 15(9), pp. 1025–33. doi: 10.1016/j.joca.2007.03.008.

Lima, E. G. *et al.* (2008) 'Physiologic deformational loading does not counteract the catabolic effects of interleukin-1 in long-term culture of chondrocyte-seeded agarose constructs.', *Journal of biomechanics*, 41(15), pp. 3253–9. doi: 10.1016/j.jbiomech.2008.06.015.

Liu, X. and Ma, P. X. (2009) 'Phase separation, pore structure, and properties of nanofibrous gelatin scaffolds.', *Biomaterials*, 30(25), pp. 4094–103. doi: 10.1016/j.biomaterials.2009.04.024.

Liverani, L. *et al.* (2019) ‘Porous Biomaterials and Scaffolds for Tissue Engineering’, in *Encyclopedia of Biomedical Engineering*. Elsevier, pp. 188–202. doi: 10.1016/b978-0-12-801238-3.99872-6.

Lodish, H. *et al.* (2000) ‘Collagen: The Fibrous Proteins of the Matrix’. W. H. Freeman.

Lu, T., Li, Y. and Chen, T. (2013) ‘Techniques for fabrication and construction of three-dimensional scaffolds for tissue engineering.’, *International journal of nanomedicine*, 8, pp. 337–50. doi: 10.2147/IJN.S38635.

Luan, L. and Liang, Z. (2018) ‘Tanshinone IIA protects murine chondrogenic ATDC5 cells from lipopolysaccharide-induced inflammatory injury by down-regulating microRNA-203a’, *Biomedicine and Pharmacotherapy*. Elsevier Masson SAS, 103, pp. 628–636. doi: 10.1016/j.biopha.2018.04.051.

Lübke, C. *et al.* (2005) ‘Growth characterization of neo porcine cartilage pellets and their use in an interactive culture model’, *Osteoarthritis and Cartilage*. W.B. Saunders, 13(6), pp. 478–487. doi: 10.1016/j.joca.2004.01.009.

De Luca, F. *et al.* (2001) ‘Regulation of Growth Plate Chondrogenesis by Bone Morphogenetic Protein-2’, *Endocrinology*, 142(1), pp. 430–436. doi: 10.1210/endo.142.1.7901.

Ma, B. *et al.* (2013) ‘WNT Signaling and Cartilage: Of Mice and Men’, *Calcified Tissue International*, 92(5), pp. 399–411. doi: 10.1007/s00223-012-9675-5.

Mabuchi, A. *et al.* (2003) ‘Novel types of COMP mutations and genotype-phenotype association in pseudoachondroplasia and multiple epiphyseal dysplasia’, *Human Genetics*. Hum Genet, 112(1), pp. 84–90. doi: 10.1007/s00439-002-0845-9.

Mackie, E. J., Tatarczuch, L. and Mirams, M. (2011) ‘The skeleton: a multi-functional complex organ. The growth plate chondrocyte and endochondral ossification’, *Journal of Endocrinology*, 211(2), pp. 109–121. doi: 10.1530/JOE-11-0048.

Maddox, B. K. *et al.* (1997) ‘The fate of cartilage oligomeric matrix protein is determined by the cell type in the case of a novel mutation in pseudoachondroplasia’, *Journal of Biological Chemistry*, 272(49), pp. 30993–30997. doi: 10.1074/jbc.272.49.30993.

Maddox, B. K. *et al.* (2000) ‘A Cartilage Oligomeric Matrix Protein Mutation Associated with Pseudoachondroplasia Changes the Structural and Functional Properties of the Type 3 Domain’, *Journal of Biological Chemistry*, 275(15), pp. 11412–11417. doi:

10.1074/jbc.275.15.11412.

Maes, C. *et al.* (2010) 'Osteoblast Precursors, but Not Mature Osteoblasts, Move into Developing and Fractured Bones along with Invading Blood Vessels', *Developmental Cell*, 19(2), pp. 329–344. doi: 10.1016/j.devcel.2010.07.010.

Magne, D. *et al.* (2003) 'Phosphate Is a Specific Signal for ATDC5 Chondrocyte Maturation and Apoptosis-Associated Mineralization: Possible Implication of Apoptosis in the Regulation of Endochondral Ossification', *Journal of Bone and Mineral Research*, 18(8), pp. 1430–1442. doi: 10.1359/jbmr.2003.18.8.1430.

Makris, E. A., Hu, J. C. and Athanasiou, K. A. (2013) 'Hypoxia-induced collagen crosslinking as a mechanism for enhancing mechanical properties of engineered articular cartilage', *Osteoarthritis and Cartilage*, 21(4), pp. 634–641. doi: 10.1016/j.joca.2013.01.007.

Malashkevich, V. N. *et al.* (1996) 'The Crystal Structure of a Five-Stranded Coiled Coil in COMP: A Prototype Ion Channel?', *Science*, 274(5288), pp. 761–765. doi: 10.1126/science.274.5288.761.

Malda, J. et al. (2013) 'Of Mice, Men and Elephants: The Relation between Articular Cartilage Thickness and Body Mass', PLoS ONE. Edited by J. P. R. O. Orgel, 8(2), p. e57683. doi: 10.1371/journal.pone.0057683.

Mann, H. H. *et al.* (2004) 'Interactions between the cartilage oligomeric matrix protein and matrilins. Implications for matrix assembly and the pathogenesis of chondrodysplasias.', *The Journal of biological chemistry*, 279(24), pp. 25294–8. doi: 10.1074/jbc.M403778200.

Manzano, S. *et al.* (2015) 'Altered swelling and ion fluxes in articular cartilage as a biomarker in osteoarthritis and joint immobilization: A computational analysis', *Journal of the Royal Society Interface*. Royal Society of London, 12(102). doi: 10.1098/rsif.2014.1090.

Mariani, F. V. and Martin, G. R. (2003) 'Deciphering skeletal patterning: clues from the limb', *Nature*, 423(6937), pp. 319–325. doi: 10.1038/nature01655.

Martin, G. R. (1975) 'Teratocarcinomas as a model system for the study of embryogenesis and neoplasia', *Cell*, pp. 229–243. doi: 10.1016/0092-8674(75)90098-7.

Martinez Sanchez, A. H. *et al.* (2017) 'Chondrogenic differentiation of ATDC5-cells under the influence of Mg and Mg alloy degradation', *Materials Science and Engineering C*. Elsevier Ltd, 72, pp. 378–388. doi: 10.1016/j.msec.2016.11.062.

Mao, A. S., and Mooney, D. J. (2015). ‘Regenerative medicine: Current therapies and future directions*’, Proceedings of the National Academy of Sciences of the United States of America*, *112*(47), pp14452–14459. https://doi.org/10.1073/pnas.1508520112

Mauck, R. L. *et al.* (2000) ‘Functional tissue engineering of articular cartilage through dynamic loading of chondrocyte-seeded agarose gels.’, *Journal of biomechanical engineering*, 122(3), pp. 252–60.

Mauck, R. L. *et al.* (2002) ‘Influence of seeding density and dynamic deformational loading on the developing structure/function relationships of chondrocyte-seeded agarose hydrogels’, *Annals of Biomedical Engineering*, 30(8), pp. 1046–1056. doi: 10.1114/1.1512676.

Mauck, R. L. *et al.* (2003) ‘Synergistic Action of Growth Factors and Dynamic Loading for Articular Cartilage Tissue Engineering’, *Tissue Engineering*, 9(4), pp. 597–611. doi: 10.1089/107632703768247304.

Mauck, R. L. *et al.* (2003) ‘The role of cell seeding density and nutrient supply for articular cartilage tissue engineering with deformational loading’, *Osteoarthritis and Cartilage*. W.B. Saunders Ltd, 11(12), pp. 879–890. doi: 10.1016/j.joca.2003.08.006.

Mauck, R. L. and Burdick, J. A. (2011) ‘Engineering Cartilage Tissue’, in *Tissue Engineering*. Berlin, Heidelberg: Springer Berlin Heidelberg, pp. 493–520. doi: 10.1007/978-3-642-02824-3_23.

McCoy, A. M. (2015) ‘Animal Models of Osteoarthritis: Comparisons and Key Considerations’, Veterinary Pathology, 52(5), pp. 803–818. doi: 10.1177/0300985815588611.

McNulty, M. A. et al. (2012) ‘Histopathology of naturally occurring and surgically induced osteoarthritis in mice’, Osteoarthritis and Cartilage, 20(8), pp. 949–956. doi: 10.1016/j.joca.2012.05.001.

Medvedeva, E. V. *et al.* (2018) ‘Repair of damaged articular cartilage: Current approaches and future directions’, *International Journal of Molecular Sciences*. MDPI AG, 19(8), p. 2366. doi: 10.3390/ijms19082366.

Merritt, T. M. *et al.* (2006) ‘Expression of mutant cartilage oligomeric matrix protein in human chondrocytes induces the pseudoachondroplasia phenotype’, *Journal of Orthopaedic Research*, 24(4), pp. 700–707. doi: 10.1002/jor.20100.

Merritt, T. M. *et al.* (2007) ‘Unique Matrix Structure in the Rough Endoplasmic Reticulum Cisternae of Pseudoachondroplasia Chondrocytes’, *The American Journal of Pathology*,

170(1), pp. 293–300. doi: 10.2353/ajpath.2007.060530.

Mesallati, Tariq *et al.* (2013) 'Scaffold architecture determines chondrocyte response to externally applied dynamic compression', *Biomech Model Mechanobiol*, 12, pp. 889–899. doi: 10.1007/s10237-012-0451-2.

Miosge, N. *et al.* (2004) 'Expression of collagen type I and type II in consecutive stages of human osteoarthritis', *Histochemistry and Cell Biology*, 122(3), pp. 229–236. doi: 10.1007/s00418-004-0697-6.

Misenheimer, T. M. and Mosher, D. F. (1995) 'Calcium ion binding to thrombospondin 1', *Journal of Biological Chemistry*, 270(4), pp. 1729–1733. doi: 10.1074/jbc.270.4.1729.

Mo, X. M. *et al.* (2004) 'Electrospun P(LLA-CL) nanofiber: a biomimetic extracellular matrix for smooth muscle cell and endothelial cell proliferation.', *Biomaterials*, 25(10), pp. 1883–90. Available at: http://www.ncbi.nlm.nih.gov/pubmed/14738852 (Accessed: 3 June 2016).

Montagne, K., Furukawa, K. S. and Ushida, T. (2019) 'Hydrostatic Pressurization of Dissociated ATDC5 Aggregates as an in Vitro Model of Mechanical Load-induced Chondrocyte Damage', *Alternatives to Animal Testing and Experimentation*. Japanese Society for Alternative to Animal Experiments, 24(2), pp. 75–82. doi: 10.11232/aatex.24.75.

Moreira-Teixeira, L. S. *et al.* (2011) 'Cartilage Tissue Engineering', *Endocr Dev. Basel*, 21, pp. 102–115.

Mörgelin, M. *et al.* (1992) 'Electron microscopy of native cartilage oligomeric matrix protein purified from the Swarm rat chondrosarcoma reveals a five-armed structure.', *The Journal of biological chemistry*, 267(9), pp. 6137–41. Available at: http://www.ncbi.nlm.nih.gov/pubmed/1556122 (Accessed: 21 October 2019).

Morimoto, R. and Obinata, A. (2011) 'Overexpression of Hematopoietically Expressed Homeoprotein Induces Nonapoptotic Cell Death in Mouse Prechondrogenic ATDC5 Cells', *Biological & Pharmaceutical Bulletin*. The Pharmaceutical Society of Japan, 34(10), pp. 1589–1595. doi: 10.1248/bpb.34.1589.

Moulisová, V. *et al.* (2017) 'Hybrid Protein-Glycosaminoglycan Hydrogels Promote Chondrogenic Stem Cell Differentiation', *ACS Omega*. American Chemical Society, 2(11), pp. 7609–7620. doi: 10.1021/acsomega.7b01303.

Moutos, F. T., Freed, L. E. and Guilak, F. (2007) 'A biomimetic three-dimensional woven composite scaffold for functional tissue engineering of cartilage.', *Nature materials*, 6(2), pp.

162–7. doi: 10.1038/nmat1822.

Moutos, F. T. and Guilak, F. (2008) ‘Composite scaffolds for cartilage tissue engineering.’, *Biorheology*, 45(3–4), pp. 501–12. Available at: http://www.ncbi.nlm.nih.gov/pubmed/18836249 (Accessed: 6 June 2016).

Mow, V. C., Ratcliffe, A. and Poole, A. R. (1992) ‘Cartilage and diarthrodial joints as paradigms for hierarchical materials and structures.’, *Biomaterials*, 13(2), pp. 67–97. Available at: http://www.ncbi.nlm.nih.gov/pubmed/1550898 (Accessed: 13 May 2016).

Müller, W. W. *et al.* (2015) ‘Geosynthetics in geoenvironmental engineering’, *Science and Technology of Advanced Materials*. IOP Publishing, 16(3), p. 034605. doi: 10.1088/1468-6996/16/3/034605.

Murphy, M. K. *et al.* (2015) ‘Engineering a fibrocartilage spectrum through modulation of aggregate redifferentiation.’, *Cell transplantation*, 24(2), pp. 235–45. doi: 10.3727/096368913X676204.

Newton, P. T. *et al.* (2012) ‘Chondrogenic ATDC5 cells: An optimised model for rapid and physiological matrix mineralisation’, *International Journal of Molecular Medicine*, 30(5), pp. 1187–1193. doi: 10.3892/ijmm.2012.1114.

Nguyen, L. H. et al. (2011) ‘Unique biomaterial compositions direct bone marrow stem cells into specific chondrocytic phenotypes corresponding to the various zones of articular cartilage’, Biomaterials, 32(5), pp. 1327–1338. doi: 10.1016/j.biomaterials.2010.10.009.

Nickien *et al.*, (2018). ‘Comparison Between In Vitro and In Vivo Cartilage Overloading Studies Based on a Systematic Literature Review*’, Journal of Orthopaedic Research*, 36(8), pp2076-2086

Nilsson, O. *et al.* (2007) ‘Gradients in bone morphogenetic protein-related gene expression across the growth plate’, *Journal of Endocrinology*, 193(1), pp. 75–84. doi: 10.1677/joe.1.07099.

Nishimura, R. *et al.* (2003) ‘The role of SMADS in BMP signaling’, *Frontiers in Bioscience*, 8(6), p. 1049. doi: 10.2741/1049.

Oji, G. S. *et al.* (2007) ‘Indian hedgehog signaling pathway differences between swarm rat chondrosarcoma and native rat chondrocytes.’, *The Iowa orthopaedic journal*. University of Iowa, 27, pp. 9–16. Available at: http://www.ncbi.nlm.nih.gov/pubmed/17907424 (Accessed: 14 October 2019).

Ondrésik, M., Oliveira, J. M. and Reis, R. L. (2017) ‘Knee Articular Cartilage’, in Oliveira, J. M. and Reis, R. L. (eds) *Regenerative Strategies for the Treatment of Knee Disabilities, Studies in Mechanobiology, Tissue Engineering and Biomaterials*. Springer International Publishing, pp. 3–20. doi: 10.1007/978-3-319-44785-8_1.

Ornitz, D. M. (2005) ‘FGF signaling in the developing endochondral skeleton’, *Cytokine & growth factor reviews*. NIH Public Access, 16(2), p. 205. doi: 10.1016/J.CYTOGFR.2005.02.003.

Oshima, Y. et al. (2004) ‘Fate of transplanted bone-marrow-derived mesenchymal cells during osteochondral repair using transgenic rats to simulate autologous transplantation’, Osteoarthritis and Cartilage, 12(10), pp. 811–817. doi: 10.1016/j.joca.2004.06.014.

Otto, F. *et al.* (1997) ‘Cbfa1, a candidate gene for cleidocranial dysplasia syndrome, is essential for osteoblast differentiation and bone development.’, *Cell*, 89(5), pp. 765–71. doi: 10.1016/s0092-8674(00)80259-7.

Ozbek, S., Engel, J. and Stetefeld, J. (2002) ‘Storage function of cartilage oligomeric matrix protein: the crystal structure of the coiled-coil domain in complex with vitamin D(3).’, *The EMBO journal*. European Molecular Biology Organization, 21(22), pp. 5960–8. doi: 10.1093/emboj/cdf628.

Park, J. S. *et al.* (2011) ‘The effect of matrix stiffness on the differentiation of mesenchymal stem cells in response to TGF-β’, *Biomaterials*. NIH Public Access, 32(16), pp. 3921–3930. doi: 10.1016/j.biomaterials.2011.02.019.

Pathi, S. *et al.* (1999) ‘Interaction of Ihh and BMP/Noggin Signaling during Cartilage Differentiation’, *Developmental Biology*, 209(2), pp. 239–253. doi: 10.1006/dbio.1998.9181.

Pattappa, G. *et al.* (2019) ‘Cells under pressure – the relationship between hydrostatic pressure and mesenchymal stem cell *chondrogenesis’, European Cells and Materials*, 37, pp 360-381

Pelttari, K., Steck, E. and Richter, W. (2008) ‘The use of mesenchymal stem cells for chondrogenesis’, *Injury*, 39(1 SUPPL.), pp. 58–65. doi: 10.1016/j.injury.2008.01.038.

Peng, G. *et al.* (2014) ‘Surface zone articular chondrocytes modulate the bulk and surface mechanical properties of the tissue-engineered cartilage.’, *Tissue engineering. Part A*, 20(23–24), pp. 3332–41. doi: 10.1089/ten.TEA.2014.0099.

Peng, X. X. *et al.* (2012) ‘Selection of suitable reference genes for normalization of

quantitative real-time PCR in cartilage tissue injury and repair in rabbits', *International Journal of Molecular Sciences*. MDPI AG, 13(11), pp. 14344–14355. doi: 10.3390/ijms131114344.

Percival, C. J. and Richtsmeier, J. T. (2013) 'Angiogenesis and intramembranous osteogenesis', *Developmental Dynamics*, 242(8), pp. 909–922. doi: 10.1002/dvdy.23992.

Perlman, R. L. (2016) 'Mouse Models of Human Disease: An Evolutionary Perspective', *Evolution, Medicine, and Public Health*. Oxford University Press (OUP), p. eow014. doi: 10.1093/emph/eow014.

Pfander, D. *et al.* (2004) 'Tenascin and aggrecan expression by articular chondrocytes is influenced by interleukin 1β: A possible explanation for the changes in matrix synthesis during osteoarthritis', *Annals of the Rheumatic Diseases*. BMJ Publishing Group Ltd, 63(3), pp. 240–244. doi: 10.1136/ard.2002.003749.

Phull, A. R. *et al.* (2016) 'Applications of Chondrocyte-Based Cartilage Engineering: An Overview', *BioMed Research International*. Hindawi Limited. doi: 10.1155/2016/1879837.

Pirog-Garcia, K. A. *et al.* (2007) 'Reduced cell proliferation and increased apoptosis are significant pathological mechanisms in a murine model of mild pseudoachondroplasia resulting from a mutation in the C-terminal domain of COMP', *Human Molecular Genetics*, 16(17), pp. 2072–2088. doi: 10.1093/hmg/ddm155.

Piróg, K. A. *et al.* (2014) 'Abnormal Chondrocyte Apoptosis in the Cartilage Growth Plate is Influenced by Genetic Background and Deletion of CHOP in a Targeted Mouse Model of Pseudoachondroplasia', *PLoS ONE*. Edited by D. I. Nurminsky, 9(2), p. e85145. doi: 10.1371/journal.pone.0085145.

Pizette, S. and Niswander, L. (2000) 'BMPs Are Required at Two Steps of Limb Chondrogenesis: Formation of Prechondrogenic Condensations and Their Differentiation into Chondrocytes', *Developmental Biology*, 219(2), pp. 237–249. doi: 10.1006/dbio.2000.9610.

Pombo-Suarez, M. *et al.* (2008) 'Reference genes for normalization of gene expression studies in human osteoarthritic articular cartilage', *BMC Molecular Biology*. BioMed Central, 9(1), p. 17. doi: 10.1186/1471-2199-9-17.

Poole, C. A., Flint, M. H. and Beaumont, B. W. (1984) 'Morphological and functional interrelationships of articular cartilage matrices.', *Journal of anatomy*. ENGLAND, 138 (Pt 1, pp. 113–138.

Posey, K L *et al.* (2008) ‘Model systems for studying skeletal dysplasias caused by TSP-5/COMP mutations.’, *Cellular and molecular life sciences : CMLS*. Switzerland, 65(5), pp. 687–699. doi: 10.1007/s00018-007-7485-0.

Posey, K. L. and Hecht, J. T. (2017) ‘Novel therapeutic interventions for pseudoachondroplasia’, Bone, 102, pp. 60–68. doi: 10.1016/j.bone.2017.03.045.

Posey, K. L. *et al.* (2008) ‘Thrombospondins: from structure to therapeutics’, *Cellular and Molecular Life Sciences*, 65(5), pp. 687–699. doi: 10.1007/s00018-007-7485-0.

Posey, K. L., Alcorn, J. L. and Hecht, J. T. (2014) ‘Pseudoachondroplasia/COMP — translating from the bench to the bedside’, *Matrix Biology*, 37, pp. 167–173. doi: 10.1016/j.matbio.2014.05.006.

Posey, K. L., Coustry, F. and Hecht, J. T. (2018) ‘Cartilage oligomeric matrix protein: COMPopathies and beyond’, *Matrix Biology*, 71–72, pp. 161–173. doi: 10.1016/j.matbio.2018.02.023.

Reppel, L. *et al.* (2015) ‘Chondrogenic induction of mesenchymal stromal/stem cells from Wharton’s jelly embedded in alginate hydrogel and without added growth factor: An alternative stem cell source for cartilage tissue engineering’, *Stem Cell Research and Therapy*. BioMed Central Ltd., 6(1), p. 260. doi: 10.1186/s13287-015-0263-2.

Responte, D. J. *et al.* (2012) ‘Biomechanics-driven chondrogenesis: from embryo to adult.’, *FASEB journal : official publication of the Federation of American Societies for Experimental Biology*, 26(9), pp. 3614–24. doi: 10.1096/fj.12-207241.

Rimoin, D. L. *et al.* (1994) ‘A large family with features of pseudoachondroplasia and multiple epiphyseal dysplasia: exclusion of seven candidate gene loci that encode proteins of the cartilage extracellular matrix’, *Human Genetics*. Springer-Verlag, 93(3), pp. 236–242. doi: 10.1007/BF00212015.

Rochefort, G. Y. *et al.* (2005) ‘Influence of hypoxia on the domiciliation of mesenchymal stem cells after infusion into rats: Possibilities of targeting pulmonary artery remodeling via cells therapies?’, *Respiratory Research*, 6(1), p. 125. doi: 10.1186/1465-9921-6-125.

Rochira, V. *et al.* (2001) ‘Role of estrogen on bone in the human male: insights from the natural models of congenital estrogen deficiency.’, *Molecular and cellular endocrinology*, 178(1–2), pp. 215–20. doi: 10.1016/s0303-7207(01)00446-4.

Rosenberg, K. *et al.* (1998) ‘Cartilage oligomeric matrix protein shows high affinity zinc-

dependent interaction with triple helical collagen.', *The Journal of biological chemistry*, 273(32), pp. 20397–403. doi: 10.1074/jbc.273.32.20397.

Roughley, P. J. (2006) 'The structure and function of cartilage proteoglycans', *European Cells and Materials*. doi: vol012a11 [pii].

Spranger, J. W., Brill, P. W., Hall, C., Superti-Furga, A., & Unger, S. (2018). Bone dysplasias: an atlas of genetic disorders of skeletal development. Oxford University Press, USA.

Sakata, R., Iwakura, T. and Reddi, A. H. (2015) 'Regeneration of articular cartilage surface: Morphogens, cells, and extracellular matrix scaffolds', Tissue Engineering - Part B: Reviews, 21(5), pp. 461–473. doi: 10.1089/ten.teb.2014.0661.

Sampat, S. R. *et al.* (2013) 'Applied osmotic loading for promoting development of engineered cartilage', *Journal of Biomechanics*, 46(15), pp. 2674–2681. doi: 10.1016/j.jbiomech.2013.07.043.

Sato, E. *et al.* (2014) 'High molecular weight hyaluronic acid increases the differentiation potential of the murine chondrocytic ATDC5 cell line', *Journal of Orthopaedic Research*. John Wiley and Sons Inc., 32(12), pp. 1619–1627. doi: 10.1002/jor.22691.

Scarfì, S. (2016) 'Use of bone morphogenetic proteins in mesenchymal stem cell stimulation of cartilage and bone repair.', *World journal of stem cells*, 8(1), pp. 1–12. doi: 10.4252/wjsc.v8.i1.1.

Schmitz, M. *et al.* (2006a) 'Disruption of extracellular matrix structure may cause pseudoachondroplasia phenotypes in the absence of impaired cartilage oligomeric matrix protein secretion.', *The Journal of biological chemistry*. American Society for Biochemistry and Molecular Biology, 281(43), pp. 32587–95. doi: 10.1074/jbc.M601976200.

Schmitz, M. *et al.* (2006b) 'Disruption of Extracellular Matrix Structure May Cause Pseudoachondroplasia Phenotypes in the Absence of Impaired Cartilage Oligomeric Matrix Protein Secretion', *Journal of Biological Chemistry*, 281(43), pp. 32587–32595. doi: 10.1074/jbc.M601976200.

Schmitz, M. *et al.* (2008) 'Transgenic mice expressing D469Δ mutated cartilage oligomeric matrix protein (COMP) show growth plate abnormalities and sternal malformations', *Matrix Biology*, 27(2), pp. 67–85. doi: 10.1016/j.matbio.2007.08.001.

Schnabel, M. *et al.* (2002) 'Dedifferentiation-associated changes in morphology and gene

expression in primary human articular chondrocytes in cell culture', *Osteoarthritis and Cartilage*. W.B. Saunders Ltd, 10(1), pp. 62–70. doi: 10.1053/joca.2001.0482.

Schneider, C. A., Rasband, W. S. and Eliceiri, K. W. (2012) 'NIH Image to ImageJ: 25 years of image analysis', *Nature Methods*. Nat Methods, pp. 671–675. doi: 10.1038/nmeth.2089.

Schuh, E. *et al.* (2010) 'Effect of matrix elasticity on the maintenance of the chondrogenic phenotype.', *Tissue engineering. Part A*, 16(4), pp. 1281–90. doi: 10.1089/ten.TEA.2009.0614.

Schumacher, B. L. *et al.* (1994) 'A novel proteoglycan synthesized and secreted by chondrocytes of the superficial zone of articular cartilage.', *Archives of biochemistry and biophysics*, 311(1), pp. 144–52. doi: 10.1006/abbi.1994.1219.

Seriwatanachai, D., Krishnamra, N. and Charoenphandhu, N. (2012) 'Chondroregulatory action of prolactin on proliferation and differentiation of mouse chondrogenic ATDC5 cells in 3-dimensional micromass cultures', *Biochemical and Biophysical Research Communications*. Academic Press, 420(1), pp. 108–113. doi: 10.1016/j.bbrc.2012.02.123.

Shahriari, D. *et al.* (2016) 'Characterizing the degradation of alginate hydrogel for use in multilumen scaffolds for spinal cord repair', *Journal of Biomedical Materials Research - Part A*. John Wiley and Sons Inc., 104(3), pp. 611–619. doi: 10.1002/jbm.a.35600.

Shen, B. *et al.* (2009) 'BMP-2 enhances TGF-β3-mediated chondrogenic differentiation of human bone marrow multipotent mesenchymal stromal cells in alginate bead culture', *Tissue Engineering - Part A*. Mary Ann Liebert Inc., 15(6), pp. 1311–1320. doi: 10.1089/ten.tea.2008.0132.

Shen, Z., Heinegård, D. and Sommarin, Y. (1995) 'Distribution and expression of cartilage oligomeric matrix protein and bone sialoprotein show marked changes during rat femoral head development', *Matrix Biology*. Matrix Biol, 14(9), pp. 773–781. doi: 10.1016/S0945-053X(05)80020-4.

Shim, K. S. (2015) 'Pubertal growth and epiphyseal fusion.', *Annals of pediatric endocrinology & metabolism*. Korean Society of Pediatric Endocrinology, 20(1), pp. 8–12. doi: 10.6065/apem.2015.20.1.8.

Shimizu, T. *et al.* (2006) 'Polysurgery of cell sheet grafts overcomes diffusion limits to produce thick, vascularized myocardial tissues.', *FASEB journal : official publication of the Federation of American Societies for Experimental Biology*, 20(6), pp. 708–10. doi:

10.1096/fj.05-4715fje.

Shintani, N., Siebenrock, K. A. and Hunziker, E. B. (2013) ‘TGF-ß1 Enhances the BMP-2-Induced Chondrogenesis of Bovine Synovial Explants and Arrests Downstream Differentiation at an Early Stage of Hypertrophy’, *PLoS ONE*. Edited by C. Zhang. Public Library of Science, 8(1), p. e53086. doi: 10.1371/journal.pone.0053086.

Shukunami C, Ohta Y, Sakuda M, H. Y. (1998) ‘Sequential progression of the differentiation program by bone morphogenetic protein-2 in chondrogenic cell line ATDC5. - PubMed - NCBI’, *Exp Cell Res*, 25(241), pp. 1–11.

Shukunami, C. *et al.* (1997) ‘Cellular hypertrophy and calcification of embryonal carcinoma-derived chondrogenic cell line ATDC5 in vitro’, *Journal of Bone and Mineral Research*, 12(8), pp. 1174–1188. doi: 10.1359/jbmr.1997.12.8.1174.

Silva, J. C. *et al.* (2020) ‘Glycosaminoglycan remodeling during chondrogenic differentiation of human bone marrow−/synovial-derived mesenchymal stem/stromal cells under normoxia and hypoxia’, *Glycoconjugate Journal*. Springer, 37(3), pp. 345–360. doi: 10.1007/s10719-020-09911-5.

Singh, B. *et al.* (2012) ‘Human pathogens utilize host extracellular matrix proteins laminin and collagen for adhesion and invasion of the host.’, *FEMS microbiology reviews*. The Oxford University Press, 36(6), pp. 1122–80. doi: 10.1111/j.1574-6976.2012.00340.x.

Sivan, S. S., Wachtel, E. and Roughley, P. (2014) ‘Structure, function, aging and turnover of aggrecan in the intervertebral disc’, *Biochimica et Biophysica Acta (BBA) - General Subjects*, 1840(10), pp. 3181–3189. doi: 10.1016/j.bbagen.2014.07.013.

Soille, P. and Vincent, L. M. (1990) ‘Determining watersheds in digital pictures via flooding simulations</title&gt’;, in Kunt, M. (ed.) *Visual Communications and Image Processing ’90: Fifth in a Series*. SPIE, pp. 240–250. doi: 10.1117/12.24211.

Song, B., Estrada, K. D. and Lyons, K. M. (2009) ‘Smad signaling in skeletal development and regeneration.’, *Cytokine & growth factor reviews*. NIH Public Access, 20(5–6), pp. 379–88. doi: 10.1016/j.cytogfr.2009.10.010.

Spitznagel, L. *et al.* (2004) ‘Characterization of a pseudoachondroplasia-associated mutation (His587 Arg) in the C-terminal, collagen-binding domain of cartilage oligomeric matrix protein (COMP)’, *Biochemical Journal*. Portland Press, 377(2), pp. 479–487. doi: 10.1042/bj20031179.

Staines, K. A. *et al.* (2013) 'Cartilage to bone transitions in health and disease.', *The Journal of endocrinology*. Bioscientifica Ltd., 219(1), pp. R1–R12. doi: 10.1530/JOE-13-0276.

Stracke, J. O. *et al.* (2000) 'Matrix metalloproteinases 19 and 20 cleave aggrecan and cartilage oligomeric matrix protein (COMP)', *FEBS Letters*. No longer published by Elsevier, 478(1–2), pp. 52–56. doi: 10.1016/S0014-5793(00)01819-6.

Sudhakar, C. K. *et al.* (2015) 'Nanomedicine and Tissue Engineering', in *Nanotechnology Applications for Tissue Engineering*. Elsevier Inc., pp. 1–19. doi: 10.1016/B978-0-323-32889-0.00001-7.

Suleman, F. *et al.* (2012) 'A novel form of chondrocyte stress is triggered by a COMP mutation causing pseudoachondroplasia', *Human Mutation*, 33(1), pp. 218–231. doi: 10.1002/humu.21631.

Superti-Furga, A. *et al.* (1999) 'Recessively inherited multiple epiphyseal dysplasia with normal stature, club foot, and double layered patella caused by a DTDST mutation.', *Journal of medical genetics*, 36(8), pp. 621–4. Available at: http://www.ncbi.nlm.nih.gov/pubmed/10465113 (Accessed: 18 October 2019).

Superti-Furga, A., Bonafé, L. and Rimoin, D. L. (2001) 'Molecular-pathogenetic classification of genetic disorders of the skeleton.', *American journal of medical genetics*, 106(4), pp. 282–93. Available at: http://www.ncbi.nlm.nih.gov/pubmed/11891680 (Accessed: 9 October 2019).

.Svensson, L. *et al.* (2002) 'Cartilage Oligomeric Matrix Protein-Deficient Mice Have Normal Skeletal Development', *Molecular and Cellular Biology*. American Society for Microbiology, 22(12), pp. 4366–4371. doi: 10.1128/mcb.22.12.4366-4371.2002.

Swaminathan, S. *et al.* (2001) 'Rapid engineering of bacterial artificial chromosomes using oligonucleotides.', *Genesis (New York, N.Y. : 2000)*. United States, 29(1), pp. 14–21.

Takahashi, K. and Yamanaka, S. (2006) 'Induction of pluripotent stem cells from mouse embryonic and adult fibroblast cultures by defined factors.', *Cell*, 126(4), pp. 663–76. doi: 10.1016/j.cell.2006.07.024.

Tamm, C. *et al.* (2016) 'Fast and Efficient Transfection of Mouse Embryonic Stem Cells Using Non-Viral Reagents', *Stem Cell Reviews and Reports*, 12(5), pp. 584–591. doi: 10.1007/s12015-016-9673-5.

Tan, K. *et al.* (2009) 'The crystal structure of the signature domain of cartilage oligomeric

matrix protein: implications for collagen, glycosaminoglycan and integrin binding.', *FASEB journal : official publication of the Federation of American Societies for Experimental Biology*. The Federation of American Societies for Experimental Biology, 23(8), pp. 2490–501. doi: 10.1096/fj.08-128090.

Tan, K. and Lawler, J. (2009) 'The interaction of Thrombospondins with extracellular matrix proteins', *Journal of Cell Communication and Signaling*, pp. 177–187. doi: 10.1007/s12079-009-0074-2.

Tare, R. *et al.* (2018) 'OC8 ATDC5: An Ideal Cell Line for Studying Chondrocyte Differentiation and Modelling Cartilage Formation', *Orthopaedic Proceedings*, 90. doi: 10.1302/0301-620X.90BSUPP_II.0900363B;REQUESTEDJOURNAL:JOURNAL:PROCS;JOURNAL:JOURNAL:PROCS;ISSUE:ISSUE:10.1302.

Tare, R S *et al.* (2005) 'ATDC5: an Ideal Cell Line for Development of Tissue Engineering Strategies Aimed at Cartilage Generation', *European Cells and Materials*, 10.

Tare, Rahul S. *et al.* (2005) 'Tissue engineering strategies for cartilage generation-Micromass and three dimensional cultures using human chondrocytes and a continuous cell line', *Biochemical and Biophysical Research Communications*, 333(2), pp. 609–621. doi: 10.1016/j.bbrc.2005.05.117.

Teeple, E. et al. (2013) 'Animal models of osteoarthritis: Challenges of model selection and analysis', AAPS Journal, 15(2), pp. 438–446. doi: 10.1208/s12248-013-9454-x.

Temu, T. M. *et al.* (2010) 'The mechanism of ascorbic acid-induced differentiation of ATDC5 chondrogenic cells', *American Journal of Physiology - Endocrinology and Metabolism*, 299(2). doi: 10.1152/ajpendo.00145.2010.

Tessmar, J., Holland, T. and Mikos, A. (2005) 'Salt Leaching for Polymer Scaffolds', in *Scaffolding In Tissue Engineering*. CRC Press, pp. 111–124. doi: 10.1201/9781420027563.pt2.

Thielen, N., van der Kraan, P. and van Caam, A. (2019) 'TGFβ/BMP Signaling Pathway in Cartilage Homeostasis', *Cells*. MDPI AG, 8(9), p. 969. doi: 10.3390/cells8090969.

Thomas, J. T. et al. (1996) 'A human chondrodysplasia due to a mutation in a TGF-β super-family member', Nature Genetics, 12(3), pp. 315–317. doi: 10.1038/ng0396-315.

Thompson, A. Y., Piez, K. A. and Seyedin, S. M. (1985) 'Chondrogenesis in agarose gel

culture. A model for chondrogenic induction, proliferation and differentiation', *Experimental Cell Research*, 157(2), pp. 483–494. doi: 10.1016/0014-4827(85)90133-8.

Thompson, C. L. *et al.* (2015) 'Hedgehog signalling does not stimulate cartilage catabolism and is inhibited by Interleukin-1β', *Arthritis Research and Therapy*. BioMed Central Ltd., 17(1), p. 373. doi: 10.1186/s13075-015-0891-z.

Thorpe, S. D. *et al.* (2008) *Dynamic compression can inhibit chondrogenesis of mesenchymal stem cells, Biochemical and Biophysical Research Communications*. doi: 10.1016/j.bbrc.2008.09.154.

Thorpe, S. D. *et al.* (2013) 'Modulating gradients in regulatory signals within mesenchymal stem cell seeded hydrogels: a novel strategy to engineer zonal articular cartilage', *PLoS One*. 2013/04/25, 8(4), p. e60764. doi: 10.1371/journal.pone.0060764.

Thur, J. *et al.* (2001) 'Mutations in Cartilage Oligomeric Matrix Protein Causing Pseudoachondroplasia and Multiple Epiphyseal Dysplasia Affect Binding of Calcium and Collagen I, II, and IX', *Journal of Biological Chemistry*, 276(9), pp. 6083–6092. doi: 10.1074/jbc.M009512200.

Tortelli, F. and Cancedda, R. (2009) 'Three-dimensional cultures of osteogenic and chondrogenic cells: A tissue engineering approach to mimic bone and cartilage in vitro', *European Cells and Materials*. AO Research Institute Davos, pp. 1–14. doi: 10.22203/eCM.v017a01.

Tsumaki, N. *et al.* (2000) 'Enhancer Analysis of the α 1(II) and α 2(XI) Collagen Genes in Transfected Chondrocytes and Transgenic Mice', in *Extracellular Matrix Protocols*. New Jersey: Humana Press, pp. 187–195. doi: 10.1385/1-59259-063-2:187.

Tsumaki, N. *et al.* (2002) 'Bone Morphogenetic Protein Signals Are Required for Cartilage Formation and Differently Regulate Joint Development During Skeletogenesis', *Journal of Bone and Mineral Research*, 17(5), pp. 898–906. doi: 10.1359/jbmr.2002.17.5.898.

Tsumaki, N. (2015) 'Cartilage Regeneration Using Induced Pluripotent Stem Cell Technologies', in *A Tissue Regeneration Approach to Bone and Cartilage Repair*. Springer, pp. 85–98. doi: 10.1007/978-3-319-13266-2_6.

Tuckermann, J. P. *et al.* (2000) 'Collagenase-3 (MMP-13) and Integral Membrane Protein 2a (Itm2a) are Marker Genes of Chondrogenic/Osteoblastic Cells in Bone Formation: Sequential Temporal, and Spatial Expression of Itm2a, Alkaline Phosphatase, MMP-13, and Osteocalcin

in the Mouse', *Journal of Bone and Mineral Research*, 15(7), pp. 1257–1265. doi: 10.1359/jbmr.2000.15.7.1257.

Tufan, A. C. *et al.* (2007) 'Serum or plasma cartilage oligomeric matrix protein concentration as a diagnostic marker in pseudoachondroplasia: differential diagnosis of a family', *European Journal of Human Genetics*. Nature Publishing Group, 15(10), pp. 1023–1028. doi: 10.1038/sj.ejhg.5201882.

Tur, K. (2009) 'Biomaterials and Tissue Engineering for Regenerative Repair of Articular Cartilage Defects', *Archives of Rheumatology*. Turkish League Against Rheumatism, 24(4), pp. 206–217.

Unger, S. and Hecht, J. T. (2001) 'Pseudoachondroplasia and multiple epiphyseal dysplasia: New etiologic developments.', *American journal of medical genetics*, 106(4), pp. 244–50. Available at: http://www.ncbi.nlm.nih.gov/pubmed/11891674 (Accessed: 16 October 2019).

Usami, Y. *et al.* (2016) 'Wnt signaling in cartilage development and diseases: lessons from animal studies', *Laboratory Investigation*, 96(2), pp. 186–196. doi: 10.1038/labinvest.2015.142.

Vinatier, C. and Guicheux, J. (2016) 'Cartilage tissue engineering: From biomaterials and stem cells to osteoarthritis treatments', *Annals of Physical and Rehabilitation Medicine*. Elsevier Masson SAS, 59(3), pp. 139–144. doi: 10.1016/j.rehab.2016.03.002.

Vranka, J. *et al.* (2001) 'Selective intracellular retention of extracellular matrix proteins and chaperones associated with pseudoachondroplasia', *Matrix Biology*, 20(7), pp. 439–450. doi: 10.1016/S0945-053X(01)00148-2.

Wang, C. *et al.* (2011) 'Effects of adeno-associated virus-2-mediated human BMP-7 gene transfection on the phenotype of nucleus pulposus cells', *Journal of Orthopaedic Research*. John Wiley & Sons, Ltd, 29(6), pp. 838–845. doi: 10.1002/jor.21310.

Wang, R. N. *et al.* (2014) 'Bone Morphogenetic Protein (BMP) signaling in development and human diseases', *Genes and Diseases*. Chongqing Medical University, 1(1), pp. 87–105. doi: 10.1016/j.gendis.2014.07.005.

Wang, W., Rigueur, D. and Lyons, K. M. (2014) 'TGFβ signaling in cartilage development and maintenance', *Birth Defects Research Part C - Embryo Today: Reviews*. Wiley-Liss Inc., 102(1), pp. 37–51. doi: 10.1002/bdrc.21058.

Watkins, J. *et al.* (2009) 'Connective tissues', *The Pocket Podiatry Guide: Functional*

Anatomy. Churchill Livingstone, pp. 107–156. doi: 10.1016/B978-0-7020-3032-1.00004-4.

Watts, A. E., Ackerman-Yost, J. C. and Nixon, A. J. (2013) 'A comparison of three-dimensional culture systems to evaluate in vitro chondrogenesis of equine bone marrow-derived mesenchymal stem cells', *Tissue Engineering - Part A*. Mary Ann Liebert Inc., 19(19–20), pp. 2275–2283. doi: 10.1089/ten.tea.2012.0479.

Wei, F. *et al.* (2012) 'Activation of Indian hedgehog promotes chondrocyte hypertrophy and upregulation of MMP-13 in human osteoarthritic cartilage', *Osteoarthritis and Cartilage*, 20(7), pp. 755–763. doi: 10.1016/j.joca.2012.03.010.

Weirich, C. *et al.* (2007) 'Expression of PSACH-associated mutant COMP in tendon fibroblasts leads to increased apoptotic cell death irrespective of the secretory characteristics of mutant COMP.', *Matrix biology : journal of the International Society for Matrix Biology*, 26(4), pp. 314–23. doi: 10.1016/j.matbio.2007.01.004.

Weiss, H. E. *et al.* (2012) 'A semi-autonomous model of endochondral ossification for developmental tissue engineering', *Tissue Engineering - Part A*. Mary Ann Liebert Inc., 18(13–14), pp. 1334–1343. doi: 10.1089/ten.tea.2011.0602.

Wilhelm, D. *et al.* (2020) 'ATDC5 cells as a model of cartilage extracellular matrix neosynthesis, maturation and assembly', *Journal of Proteomics*. Elsevier B.V., 219, p. 103718. doi: 10.1016/j.jprot.2020.103718.

Woodfield, T. B. F. et al. (2005) 'Polymer scaffolds fabricated with pore-size gradients as a model for studying the zonal organization within tissue-engineered cartilage constructs', Tissue Engineering, 11(9–10), pp. 1297–1311. doi: 10.1089/ten.2005.11.1297.

Wozney, J. *et al.* (1988) 'Novel regulators of bone formation: molecular clones and activities', *Science*, 242(4885), pp. 1528–1534. doi: 10.1126/science.3201241.

Wu, B. *et al.* (2017) 'Phosphate regulates chondrogenesis in a biphasic and maturation-dependent manner', *Differentiation*. Elsevier Ltd, 95, pp. 54–62. doi: 10.1016/j.diff.2017.04.002.

Wu, Y. *et al.* (2020) 'Hybrid Bioprinting of Zonally Stratified Human Articular Cartilage Using Scaffold-Free Tissue Strands as Building Blocks', *Advanced Healthcare Materials*, 9(22), p. 2001657. doi: 10.1002/adhm.202001657.

Wu, C.-L. *et al.* (2021) 'Single cell transcriptomic analysis of human pluripotent stem cell chondrogenesis', *Nature Communications*. Nature Research, 12(1), pp. 1–18. doi:

10.1038/s41467-020-20598-y.

Wu, T. *et al.* (2015) 'The lubrication effect of hyaluronic acid and chondroitin sulfate on the natural temporomandibular cartilage under torsional fretting wear', *Lubrication Science*, 27(1), pp. 29–44. doi: 10.1002/ls.1253.

Xie, F. *et al.* (2014) 'Regulation of TGF-β Superfamily Signaling by SMAD Mono-Ubiquitination', *Cells*. MDPI AG, 3(4), pp. 981–993. doi: 10.3390/cells3040981.

Xing, D. et al. (2016) 'Perspectives on Animal Models Utilized for the Research and Development of Regenerative Therapies for Articular Cartilage', Curr Mol Bio Rep, 2, pp. 90–100. doi: 10.1007/s40610-016-0038-2.

Xu, K. *et al.* (2007) 'Cartilage oligomeric matrix protein associates with Granulin-Epithelin Precursor (GEP) and potentiates GEP-stimulated chondrocyte proliferation', *Journal of Biological Chemistry*. J Biol Chem, 282(15), pp. 11347–11355. doi: 10.1074/jbc.M608744200.

Xu, R. *et al.* (2019) 'miR-20a suppresses chondrogenic differentiation of ATDC5 cells by regulating Atg7', *Scientific Reports*. Nature Publishing Group, 9(1). doi: 10.1038/s41598-019-45502-7.

Yao, Y. and Wang, Y. (2013) 'ATDC5: An excellent in vitro model cell line for skeletal development', *Journal of Cellular Biochemistry*, 114(6), pp. 1223–1229. doi: 10.1002/jcb.24467.

Yao, Y., Zhai, Z. and Wang, Y. (2014) 'Evaluation of Insulin Medium or Chondrogenic Medium on Proliferation and Chondrogenesis of ATDC5 Cells', *BioMed research international*, 2014(5), p. 569241. doi: 10.1155/2014/569241.

Ying, H. *et al.* (2019) 'Long non-coding RNA activated by transforming growth factor beta alleviates lipopolysaccharide-induced inflammatory injury via regulating microRNA-223 in ATDC5 cells', *International Immunopharmacology*. Elsevier B.V., 69, pp. 313–320. doi: 10.1016/j.intimp.2019.01.056.

Yuan, X. *et al.* (2017) 'The Roles of Endoplasmic Reticulum Stress in the Pathophysiological Development of Cartilage and Chondrocytes', *Current Pharmaceutical Design*, 23(11), pp. 1693–1704. doi: 10.2174/1381612822666161025152423.

Yuan, X., Serra, R. A. and Yang, S. (2015) 'Function and regulation of primary cilia and intraflagellar transport proteins in the skeleton.', *Annals of the New York Academy of*

Sciences, 1335, pp. 78–99. doi: 10.1111/nyas.12463.

Zelzer, E. and Olsen, B. R. (2003) 'The genetic basis for skeletal diseases', Nature, 423(6937), pp. 343–348. doi: 10.1038/nature01659.

Zhai, Z., Yao, Y. and Wang, Y. (2013) 'Importance of Suitable Reference Gene Selection for Quantitative RT-PCR during ATDC5 Cells Chondrocyte Differentiation', *PLoS ONE*, 8(5), p. 64786. doi: 10.1371/journal.pone.0064786.

Zhang, J., Yang, Z., Li, C., Dou, Y., Li, Y., Thote, T., Wang, D., *et al.* (2013) 'Cells behave distinctly within sponges and hydrogels due to differences of internal structure.', *Tissue engineering. Part A*, 19(19–20), pp. 2166–75. doi: 10.1089/ten.TEA.2012.0393.

Zhang, X., Blalock, D. and Wang, J. (2015) 'Classifications and Definitions of Normal Joints', *InTech*. doi: 10.5772/59977.

Zheng, Q. *et al.* (2003) 'Type X collagen gene regulation by Runx2 contributes directly to its hypertrophic chondrocyte–specific expression in vivo', *The Journal of Cell Biology*, 162(5), pp. 833–842. doi: 10.1083/jcb.200211089.

Zhou, J., Wei, X. and Wei, L. (2014) 'Indian Hedgehog, a critical modulator in osteoarthritis, could be a potential therapeutic target for attenuating cartilage degeneration disease.', *Connective tissue research*, 55(4), pp. 257–61. doi: 10.3109/03008207.2014.925885.

Zhou, S., Cui, Z. and Urban, J. P. G. (2004) 'Factors influencing the oxygen concentration gradient from the synovial surface of articular cartilage to the cartilage-bone interface: A modeling study', *Arthritis & Rheumatism*. Wiley Subscription Services, Inc., A Wiley Company, 50(12), pp. 3915–3924. doi: 10.1002/art.20675.

Zhu, Y. et al. (2015) 'The influence of Chm-I knockout on ectopic cartilage regeneration and homeostasis maintenance', Tissue Engineering - Part A, 21(3–4), pp. 782–792. doi: 10.1089/ten.tea.2014.0277.